Louisiana Transportation Research Center

Final Report 626

Evaluating Louisiana New Continuity Detail for Girder Bridges

by

Ayman M. Okeil, Ph.D., P.E. (FL)
Marco Canales, Ph.D.

LSU

4101 Gourrier Avenue | Baton Rouge, Louisiana 70808
(225) 767-9131 | (225) 767-9108 fax | www.ltrc.lsu.edu

TECHNICAL REPORT STANDARD PAGE

1. Title and Subtitle
Evaluating Louisiana New Continuity Detail for Girder Bridges

2. Author(s)
Ayman M. Okeil, Ph.D., P.E. (FL)
Marco Canales, M.Sc.

3. Performing Organization Name and Address
Department of Civil and Environmental Engineering
3255 P.F. Taylor Hall
Louisiana State University
Baton Rouge, LA 70803

4. Sponsoring Agency Name and Address
Louisiana Department of Transportation and Development
P.O. Box 94245
Baton Rouge, LA 70804-9245

5. Report No.
FHWA/LA.17/626

6. Report Date
December 2020

7. Performing Organization Code
LTRC Project Number: 14-1ST
SIO Number: 30001660

8. Type of Report and Period Covered
Final
04/2014 – 08/2019

9. No. of Pages
303

10. Supplementary Notes
Conducted in Cooperation with the U.S. Department of Transportation, Federal Highway Administration

11. Distribution Statement
Unrestricted. This document is available through the National Technical Information Service, Springfield, VA 21161.

12. Key Words
prestressed concrete; creep; continuous structures; bridges; live load

13. Abstract
This report summarizes results from an investigation of the behavior of link slabs as a means for achieving partial bridge continuity. Data collected over a period of three years from a structural health monitoring system installed in the Ouachita River Bridge was used to study link slab behavior. Multiple spans with various continuity details and support conditions were instrumented to investigate link slab performance.

Recorded data from the sensors was used to analyze and interpret various aspects of bridge behavior with special emphasis on link slabs. Girder end displacements, girder end rotations, crack widths in the link slab, as well as forces in the link slab were investigated. It was found that temperature gradient has a direct effect on link slab performance. The effects of temperature gradient were also dependent on support and continuity conditions of the segments employing the

link slab. The adopted crack control detail was not found to be effective in arresting transverse deck cracking. Furthermore, greater support restraint was found to lead to greater stresses in the link slab, and hence result in higher forces and wider transverse deck cracks in the link slab. Shorter continuous segments were found to experience wider transverse cracks in the link slabs, as well as higher tension forces.

The performance of the instrumented link slabs was found to be acceptable for construction of jointless bridge deck. Furthermore, it can be said that the performance of bridges employing link slabs is superior to fully continuous bridge spans, which has been shown to lead to higher stress concentrations at girder ends as was observed for the Audubon Bridge (see LTRC Projects 08-1ST and 12-1ST). Therefore, it is recommended that the link slab detail without the crack control detail be adopted as the standard detail for bridge connections to reduce the need for expansion joints.

Project Review Committee

Each research project will have an advisory committee appointed by the LTRC Director. The Project Review Committee is responsible for assisting the LTRC Administrator or Manager in the development of acceptable research problem statements, requests for proposals, review of research proposals, oversight of approved research projects, and implementation of findings.

LTRC appreciates the dedication of the following Project Review Committee Members in guiding this research study to fruition.

LTRC Administrator/Manager

Walid Alaywan, Ph.D., P.E.
Sr. Structures Research Manager

Members

Paul Fossier, P.E.
Jenny Fu, P.E.
Nick Fagerburg, P.E.
Mike Boudreaux, P.E.
Arturo Aguirré, P.E. FHWA

Directorate Implementation Sponsor

Christopher P. Knotts, P.E.
DOTD Chief Engineer

Evaluating Louisiana New Continuity Detail for Girder Bridges

By
Ayman M. Okeil, Ph.D., P.E. (FL)
Marco Canales, Ph.D.

Department of Civil and Environmental Engineering
3255-D Patrick F. Taylor Hall
Louisiana State University
Baton Rouge, LA 70803

LTRC Project No. 14-1ST
SIO No. 030-00-1660

conducted for
Louisiana Department of Transportation and Development
Louisiana Transportation Research Center

December 2020

Abstract

This report summarizes results from an investigation of the behavior of link slabs as a means for achieving partial bridge continuity. Monitoring data collected over a period of three years from a structural health monitoring system installed in the Ouachita River Bridge was used to study link slab behavior. Multiple spans with various continuity details and support conditions were instrumented to investigate link slab performance.

Recorded data from the sensors was used to analyze and interpret various aspects of bridge behavior with special emphasis on link slabs. Girder end displacements, girder end rotations, crack widths in the link slab, as well as forces in the link slab were investigated. It was found that temperature gradient has a direct effect on link slab performance. The effects of temperature gradient were also dependent on support and continuity conditions of the segments employing the link slab. The adopted crack control detail was not found to be effective in arresting transverse deck cracking. Furthermore, greater support restraint was found to lead to greater stresses in the link slab, and hence result in higher forces and wider transverse deck cracks in the link slab. Shorter continuous segments were found to experience wider transverse cracks in the link slabs, as well as higher tension forces.

The performance of the instrumented link slabs was found to be acceptable for construction of jointless bridge deck. Furthermore, it can be said that the performance of bridges employing link slabs is superior to fully continuous bridge spans, which has been shown to lead to higher stress concentrations at girder ends as was observed for the Audubon Bridge (see LTRC Projects 08-1ST and 12-1ST). Therefore, it is recommended that the link slab detail without the crack control detail be adopted as the standard detail for bridge connections to reduce the need for expansion joints.

Acknowledgments

The authors gratefully acknowledge the financial support provided by the Louisiana Transportation Research Center (LTRC) (LTRC Project No. 14-1ST) and the Louisiana Department of Transportation and Development (DOTD)

The authors also acknowledge the assistance of Ahmed Elshoura, graduate student in the Department of Civil and Environmental Engineering for assistance in conducting the live load tests of the Ouachita bridge and for assistance in mapping link slab cracking in the field.

The authors would also like to thank Jenny Fu (DOTD), bridge design administrator, for initiating the idea behind this project and for providing information pertinent to the project throughout its execution and to Paul Fossier (DOTD), former bridge design administrator, for supporting the effort.

Finally, special thanks are due to Dr. Walid Alaywan (LTRC), senior structures research engineer, for his support of this research.

Implementation Statement

This study demonstrates that the performance of the link slab is a feasible alternative for eliminating expansion joints in bridge construction. The Louisiana Department of Transportation and Development (DOTD) stands to directly benefit from this project by helping in establishing general policies for the design of multispan prestressed concrete girder bridges as follows:

1. The link slab detail currently adopted in the DOTD's *Bridge Design and Evaluation Manual* is adequate for the construction of new bridges and should be used over the NCHRP 519 positive moment continuity detail that was investigated in LTRC Project 08-1ST. The link slab detail is simpler to construct, which will lead to construction acceleration and lower potential for damage caused by leaks through expansion joints, while eliminating high positive restraint moments.
2. The transverse crack control detail (groove) at the center of link slab was not effective in arresting expected transverse cracks at the joint. Therefore, it is not deemed a necessary detail, especially that the crack widths are not alarming and do not require intervention.
3. Anchoring diaphragms in bent caps imposes higher strains on the link slab and may lead to wider crack widths. Therefore, it is recommended that such a detail not be used in link slab construction as long as other horizontal forces (e.g., braking and seismic) could be resisted by another mechanism of the bridge structure.

Table of Contents

List of Tables

List of Figures

Introduction

Bridge design efficiency is of great importance since it typically translates into faster construction, lower construction, and maintenance budgets. Therefore, it is of paramount importance to improve the detailing of one of the most widely used alternatives in bridge construction: the simple span bridge with expansion joints at both span ends; see Figure 1(a).

Figure 1. Different joint conditions used in Ouachita River Bridge

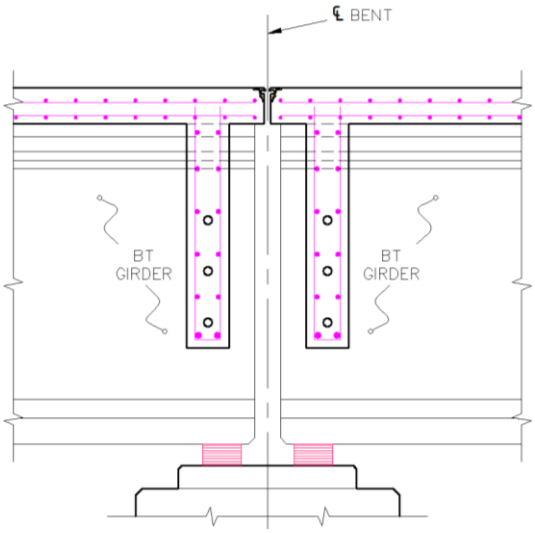

(a) Expansion Joint

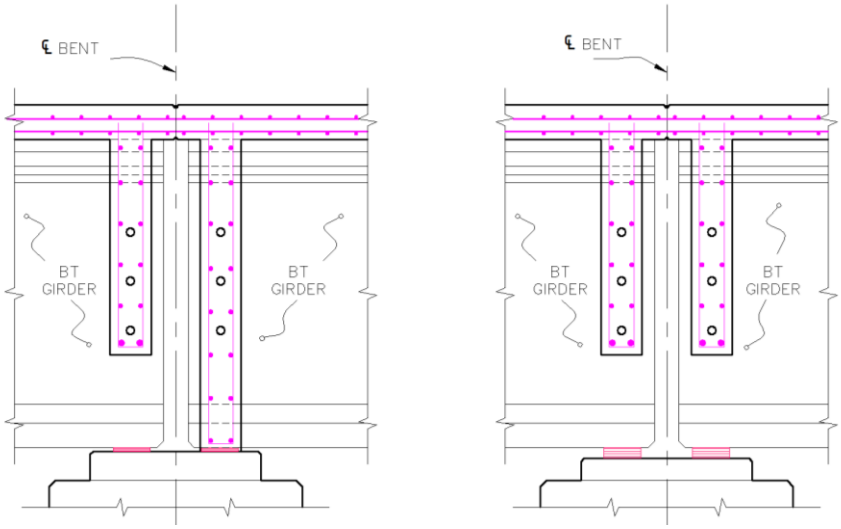

(b) Deck-Only Continuous Joint
(Fixed supports (left) – Expansion supports (right))

One of the most common details is the connection between adjacent spans. In addition to the explicit simple span construction, where girders from adjacent spans are completely independent of each other, engineers have attempted to introduce full continuity as well as partial continuity. Figure 2 shows the three possible continuity conditions between prestressed concrete girders from adjacent spans, namely, simple span construction, full continuity and partial continuity, which is typically achieved by casting a link slab to connect adjacent spans while the girders remain unattached; see Figure 1(b).

Figure 2. Typical continuity conditions in precast PSC girder bridges: (a) simply-supported, (b) fully continuous, and (c) partially continuous

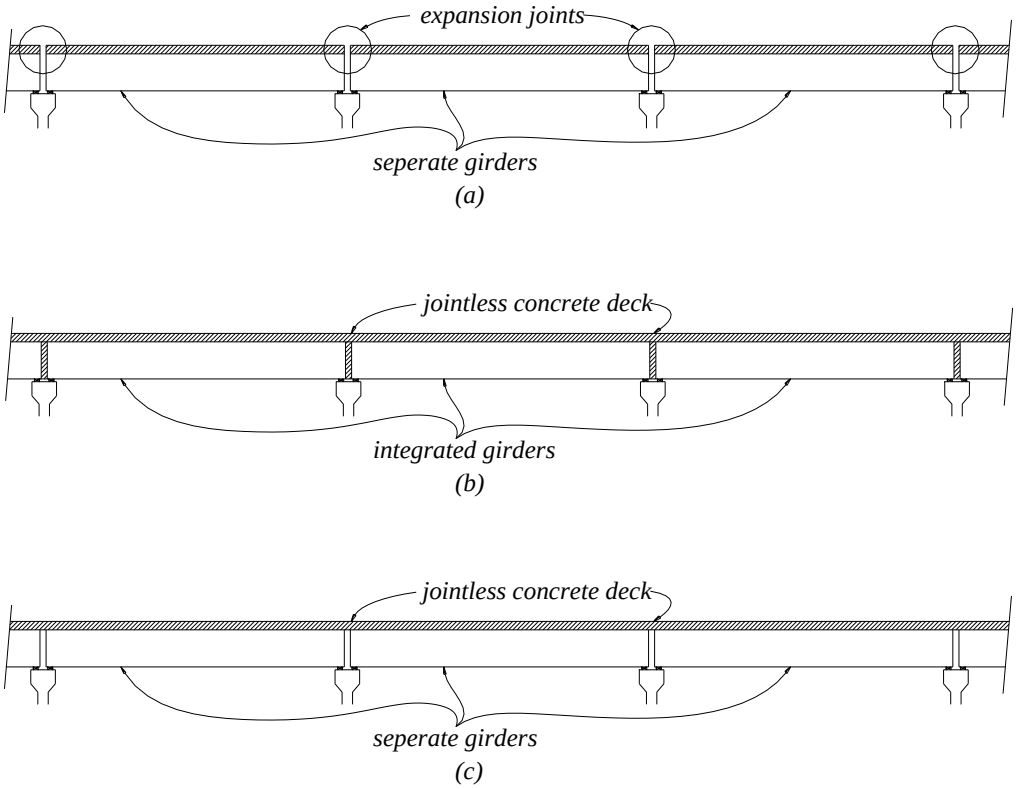

Jointless bridge decks have been of interest to structural engineers for a number of decades. By eliminating expansion joints from the construction process, the design can potentially become less costly both directly (by reducing the cost of the construction of the joints themselves) and indirectly (by reducing the cost of the additional maintenance and strengthening that can be necessary when the joints fail or cause damage to other elements in their vicinity) *[1; 2]*.

This report presents the findings from a project whose purpose was to investigate the performance of a recently constructed bridge that employed the link slab partial continuity

detail. A structural health monitoring system was installed on several segments of the 20-span bridge. Each of the instrumented segments was designed to provide insight about a different detail variation such as number of spans in a connected segment, crack control mitigation, and support configuration.

Literature Review

Precast prestressed concrete girder bridges are considered to be one of the more efficient designs, which is reflected by the statistics in the National Bridge Inventory (NBI) *[3]*. They offer many advantages over traditional designs, such as, ease of construction and durability. Prestressed concrete girders are usually precast of site and transported for erection before pouring composite decks on site. As a result, full continuity between the girders has generally been sacrificed for the sake of ease of construction. Traditionally bridge deck joints have gaps of 1-3 in. under operating conditions *[4]*. These gaps within the joints have the disadvantages of causing ride discomfort, debris accumulation, the need for maintenance as the gap can grow larger over time due to support settlement, shrinkage, and/or temperature change, concrete deterioration due to larger dynamic impact load from the tire hitting span adjacent to the gap; and leakage of rain water on the bridge substructure, which can cause corrosion to the substructure *[5]*. Even when strip seal joints are installed, they are usually worn down by vehicles and often break resulting in the need for continuous maintenance.

Bridge expansion joints are used to accommodate thermal movements in the deck and other short- and long-term deck movements caused by creep, shrinkage, moisture changes, vehicular traffic, and other loads. However, deck joints are costly to construct, install, and maintain. Deck drainage water, contaminated with chemicals, such as deicing salts and leaks through joints, can damage the bridge superstructure and the pier caps below. This can lead to the damage of vital bridge parts, such as internal reinforcement, girder ends, caps, and bearings. Accumulated debris in the joints may restrain deck expansion, causing increased pavement pressures in bridge decks. According to Au and Lam, expansion joints have not performed up to design expectations, in particular, during winter operations, which has compromised the durability of many of these structures *[6]*. Water leakage over time has caused premature corrosion damage at girder ends and in the supporting pier structures (see Figure 3). In addition, there is a high risk of span separation for multiple-simple-span bridges due to earthquakes or floods and water surges during hurricanes. Accordingly, there is a need for reducing or eliminating expansion joints in bridge decks for thousands of bridges in the United States that are constructed as simple spans *[7]*. To alleviate these problems, continuity details can be used to cover the gaps between every two adjacent deck ends. Such continuity with precast, prestressed girders permits the elimination of maintenance costs associated with bridge deck joints and deck drainage onto the substructures, in addition to improving the appearance and the riding qualities. Several projects have been executed, adopting different continuity details. In Louisiana, the new John James Audubon Bridge crossing the

Mississippi River to connect West Feliciana and Point Coupe parishes employs a detail recommended in NCHRP Report 519 *[8]*. This continuity detail is not included in the current design standard used in Louisiana, which required long-term monitoring of its performance and its impact on the whole bridge structure, especially stresses, girder ends rotation, and relative girder end movement.

Figure 3. Corrosion damage caused by chloride-contamination leaks in bridge deck expansion joints *[6]*

Okeil and El-Safty investigated partial continuity in bridge systems with jointless decks, i.e., link slab *[9]*. The study, which focused on the flexural design, shows that jointless deck systems can be efficiently used to eliminate or reduce the number of expansion joints by replacing them with a link-slab. Link-slabs are used on bridges with superstructures comprising of simply supported precast pretensioned concrete girders, for instance, super T-girders or I-girders, and cast-in-situ reinforced concrete deck slabs to achieve deck continuity. In some practices, link-slabs are usually cast after casting of the deck slabs to reduce the stresses in the link slab. Some researchers suggested that link-slab reinforcement should be deboned as well. Results presented in El-Safty and Okeil show that introducing link-slabs in typical bridges may reduce the live-load stress range by 4.7% to 19.9%, which can increase the fatigue life of the girders *[10]*. A modified three-moment equation was also proposed in the study to permit the development of a simplified procedure that can be used in a design environment. Saber and Aleti investigated the use of fiberglass-reinforced plastic (FRP) grid for reinforcement in link-slabs *[7]*. The technique would allow lower flexural stiffness of the link-slab approaching the behavior of a hinge. Okeil and Cai developed a monitoring system for evaluating the performance of a new NCHRP 519 continuity detail (for positive moment reinforcement to extend out of girder ends) *[11]*, which can be seen in Figure 4. Different sensor types (measuring strain, girder end rotation, relative movement,

and corresponding temperatures) were employed to monitor and interpret the structural performance of the detail. For example, mathematical formulation with the use of a modified three-moment equation, is an objective that can allow developing a design procedure.

Figure 4. Alternatives for positive moment reinforcement [7]

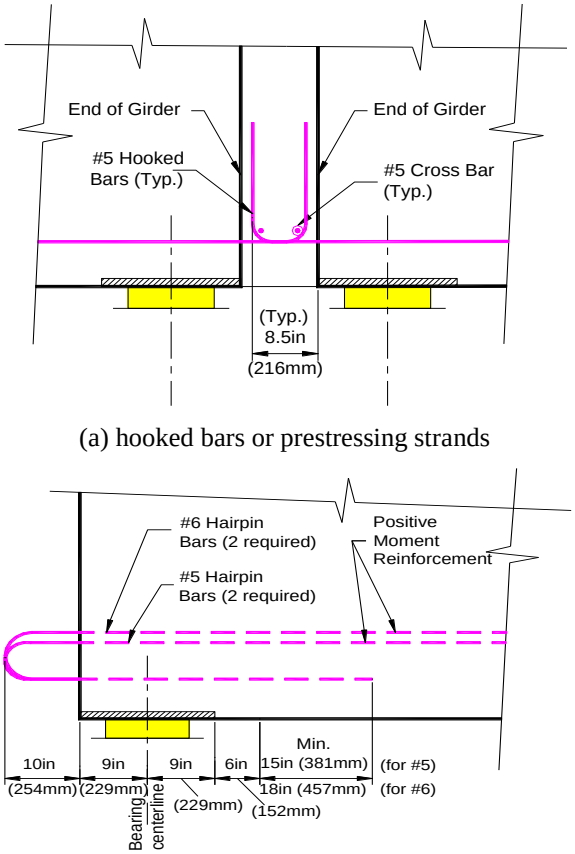

(a) hooked bars or prestressing strands

(b) hairpin bars

In Louisiana, the standard continuity diaphragm detail was different than the full continuity detail recommended by NCHRP Project 12-53. In the old Louisiana detail, a continuous deck was cast over the support while girder ends were debonded from the continuity diaphragm by providing an asphaltic material layer as can be seen in Figure 5. The debonding allowed movement of the girder ends from adjacent spans with respect to each other. Because of the existence of the diaphragm and continuous deck, the relative movement becomes more restrained at the top of the girder in comparison with the bottom.

Figure 5. Bond breaker at girder ends

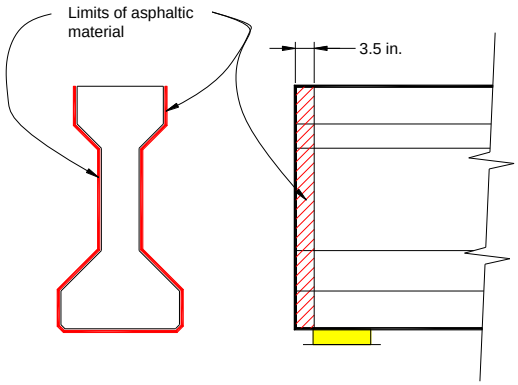

In 2008, the Louisiana Transportation Research Center (LTRC) funded a research project for long-term monitoring of a bridge constructed with a positive moment continuity detail with major differences from the continuity detail adopted in the *Louisiana DOTD Bridge Design Manual [12]*. The monitored segment is part of Bridge No. 61390613004101 from the John James Audubon Project, which was contracted as a design-build project. The monitored segment is a skewed segment that was built using bulb-T girders. The segment was chosen given that the skewed layouts and bulb-T girders were not part of the scope of the National Cooperative Highway Research Program (NCHRP) Project 12-53 that recommended the new continuity detail *[8]*. The project was extended in 2013 to continue observing the performance of the hairpin detailing used in the John James Audubon project.

For a period of over five years, a structural health monitoring system was used to collect data for these two research projects *[13]*. The study confirmed the ability of the continuity detailing to transfer forces from one girder to the adjacent girder; however, creep and thermal effects were identified as loading conditions that could lead to positive moments at the continuous girder ends. At girder ends, prestressing effects are almost nonexistent, which can lead to girder end cracking. Live load tests also revealed that the strains from the live load test were lower than long-term effects. Hossain et al. carried out a live-load test and developed a three-dimensional (3D) finite-element (FE) model of a three-span continuous prestressed–concrete girder bridge (skewed layout) with a new positive-moment continuity detail to convert the girders into a continuous superstructure using NCHRP recommended continuity detail *[14]*. The results show that live loads generated minimal positive moments, leading to single-digit microstrain levels at these continuity details. The FE was validated using the field results and was used to study the ability of the new detail to transfer forces between adjacent girders.

In 2013, DOTD began construction of the Ouachita River Bridge at Harrisonburg, Louisiana. This bridge would replace the existing Long-Allen Bridge, which is a two-lane 320 ft. riveted steel truss swing span structure, in order to greatly improve traffic flow in the region. The new bridge is a four-lane navigable river crossing bridge of 3,275 ft. total length, composed of 21 spans divided in two prestressed concrete girder approach spans, and one main three-span segment with steel girders. Both approach spans are divided into several deck-only continuous segments. Deck-only continuity refers to the continuity provided by a link slab, which is the only structural element that spans the gap between girder ends as can be seen in Figure 1(b). End diaphragms can be full-depth diaphragms or partial depth diaphragms. Full-depth diaphragms are typically used at fixed bearing locations with the idea of ensuring that horizontal forces are transferred to the substructure at that location. This project provided an opportunity for DOTD to study the performance of link slabs under different support, detailing, and span conditions, which triggered LTRC to fund Project 14-1ST. This report summarizes the findings of this project.

Objective

The main objective of this project was to investigate the performance of deck-only continuity under varying support and continuity conditions on the Ouachita River Bridge project. The performance is evaluated based on collected data from instrumented spans of varying support, detailing, and span conditions.

The goals of the project were to:

1. Collect, analyze, and interpret field monitoring data to further understand the behavior of the continuity and support detailing on the Ouachita River Bridge.
2. Conduct periodic site visits to perform visual inspections of monitored segments with special emphasis on monitoring girder crack development.
3. Provide DOTD with recommendations to assist in adoption in the *Bridge Design and Evaluation Manual.*

Scope

This study focused on one 4-span continuous segment, three 2-span continuous segments, and one simple-span segment within the Ouachita River Bridge at Harrisonburg, Louisiana. All segments were instrumented with embedded and surface mounted sensors. The instrumentation plan was designed to provide information about the performance of the deck-only continuity joint with different support conditions and link slab details.

The monitored segments characteristics and data recorded by the installed monitoring system were used to understand the influence that the support conditions and link slab details can have on the performance of link slab continuous bridge segments. The performance of the link slab was assessed under thermal as well as live-load effects.

Methodology

The performance of the link slab detail was evaluated for long-term effects using a structural health monitoring (SHM) that was installed on the Ouachita River Bridge in Harrisonburg, Louisiana. The following sections describe the main features of the SHM system. Visual inspections and analytical models used in this study are also described in this section.

Structural Health Monitoring

A structural health monitoring plan was devised for the bridge chosen by DOTD to conduct the assessment study. This section describes the details of the monitored bridge, instrumentation plan, data processing, and interpretation.

Ouachita Bridge Description

The Ouachita River Bridge at Harrisonburg, LA, aims to greatly improve traffic flow in the region by replacing a riveted steel truss swing span structure originally built in 1932, which can be seen in Figure 6. Figure 7 shows the existing bridge alignment and the new alignment.

Figure 8 shows the new bridge, which carries a roadway with two 12-ft. lanes and two 10-ft. shoulders. The total length is 3,275 ft. with a 79-ft. clearance with the river at pool stage. DOTD utilized the Ouachita River Bridge Project as a testbed to evaluate the performance of several variations of the link slab and continuity diaphragm details with the goal of understanding the behavior of link slabs and minimizing and controlling concrete deck cracking.

The western approach span has a total length of 1,080 ft., divided into one 540-ft. continuous deck unit with four 135-ft. spans linked via link slab, and two 270-ft. continuous decks each with two 135-ft. spans joined with a link slab as can be seen in

Figure 10. The main span is a three-span continuous steel girder segment with two 300-ft. spans and a central 380-ft. span. This segment, which can be seen in Figure 11, was not instrumented and is not part of the scope of this project. Finally, the eastern approach span shown in Figure 12 has a total length of 1,215 ft., consisting of four 270-ft. continuous decks each two 135-ft. spans linked via link slab, and a single simply supported 135 ft. span. The monitored segments are: (1) one 4-span 540-ft. continuous deck segment in the western

approach span, (2) three 2-span 270 ft. continuous deck segments, and (3) a single 135-ft. span on the eastern approach span. The girder span lengths for the monitored segments are all 135 ft.

Figure 6. Existing LA-8 bridge

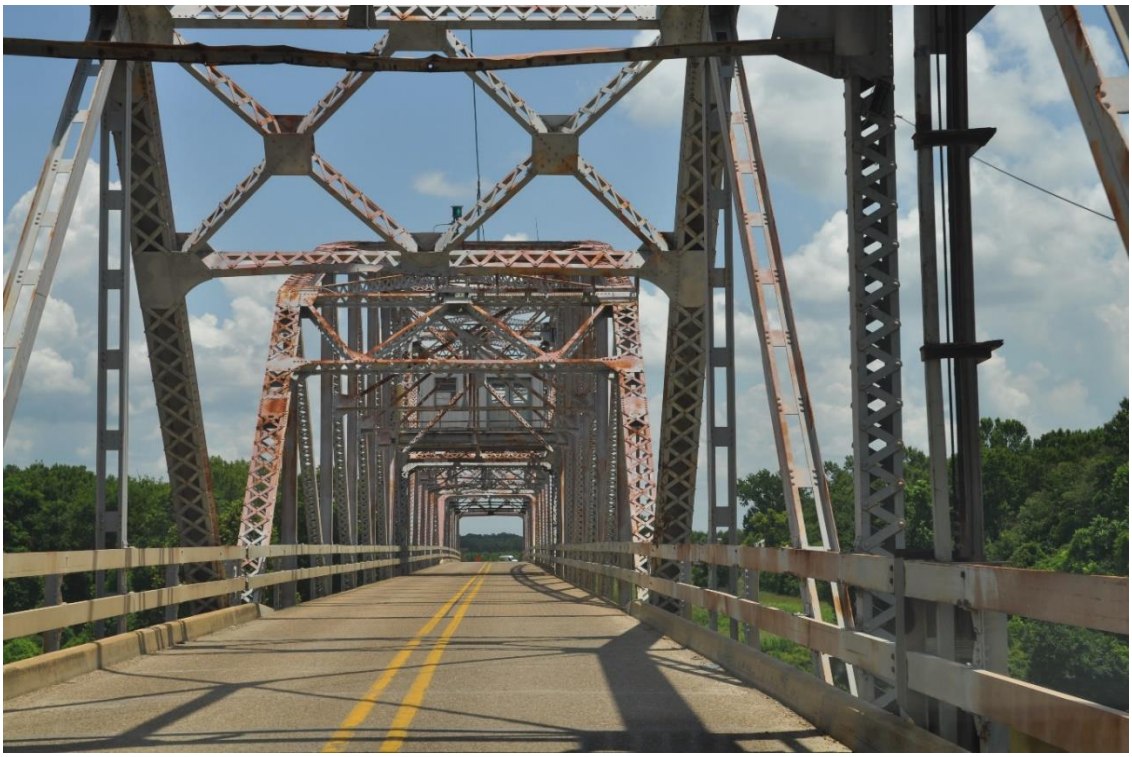

Figure 7. Long-Allen Bridge and Ouachita River Bridge at Harrisonburg alignment

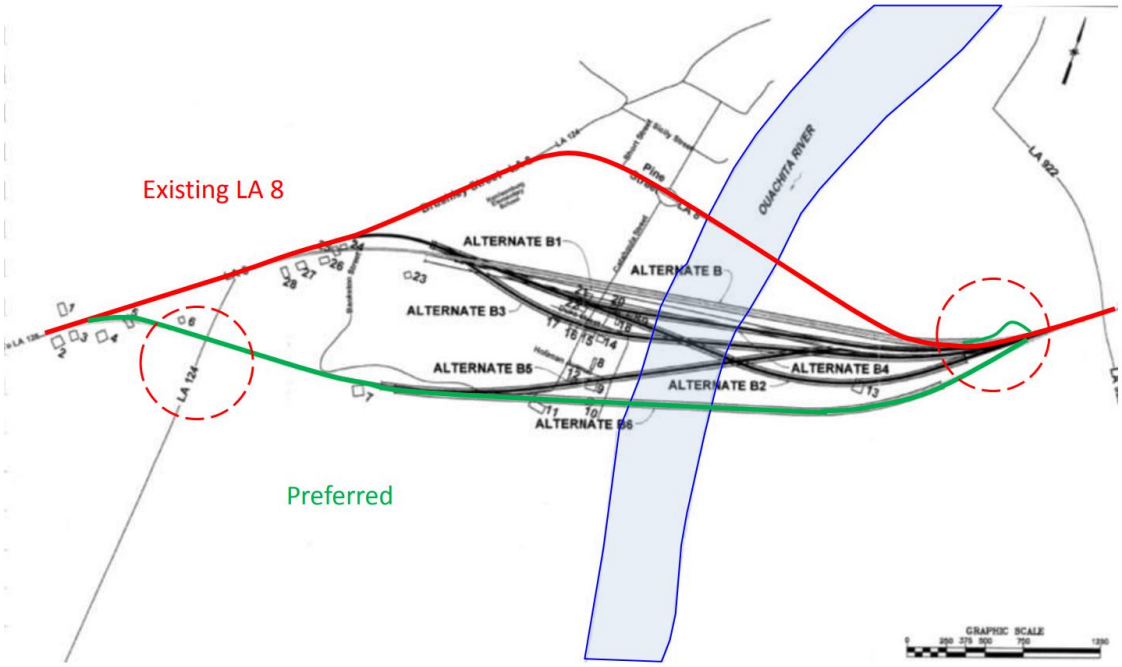

Figure 8. Ouachita River Bridge Project

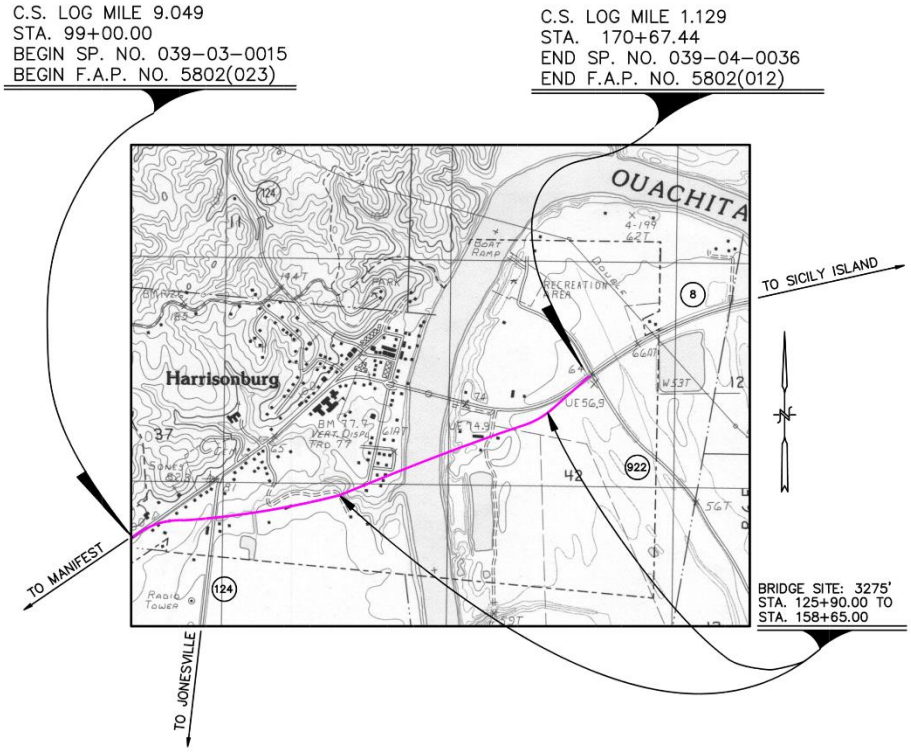

Figure 9. Ouachita River bridge view from East side looking at river crossing segment

Figure 10. Ouachita River Bridge western approach span

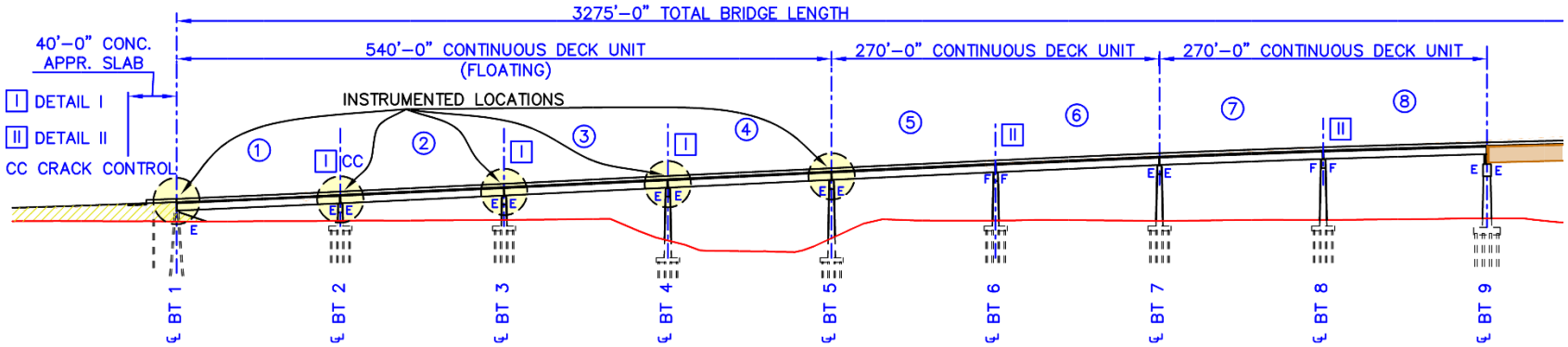

Figure 11. Ouachita River Bridge main span

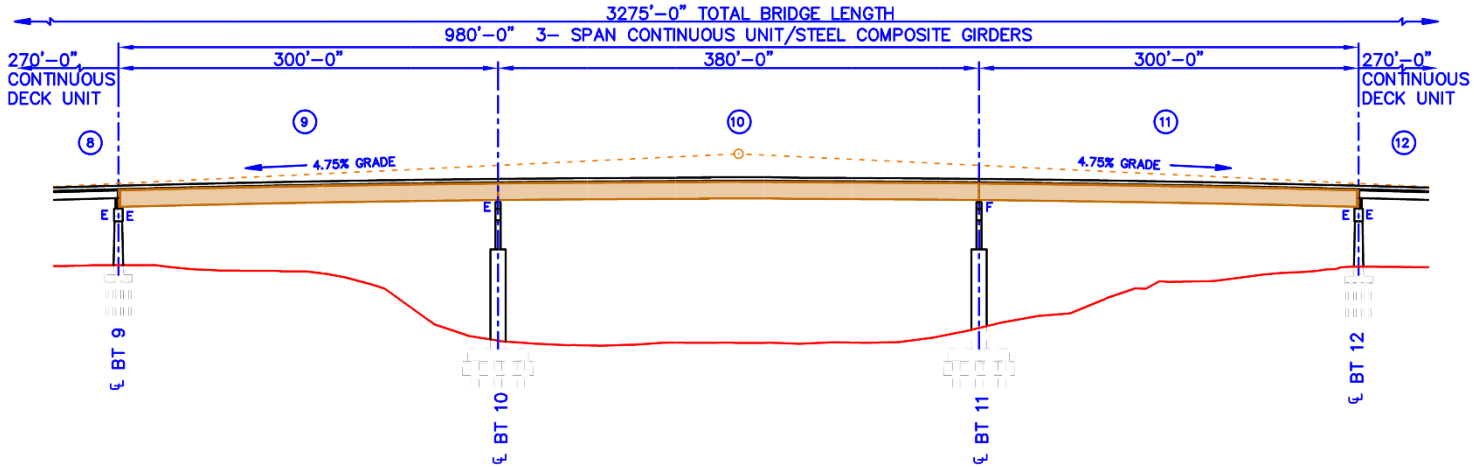

Figure 12. Ouachita River Bridge eastern approach span

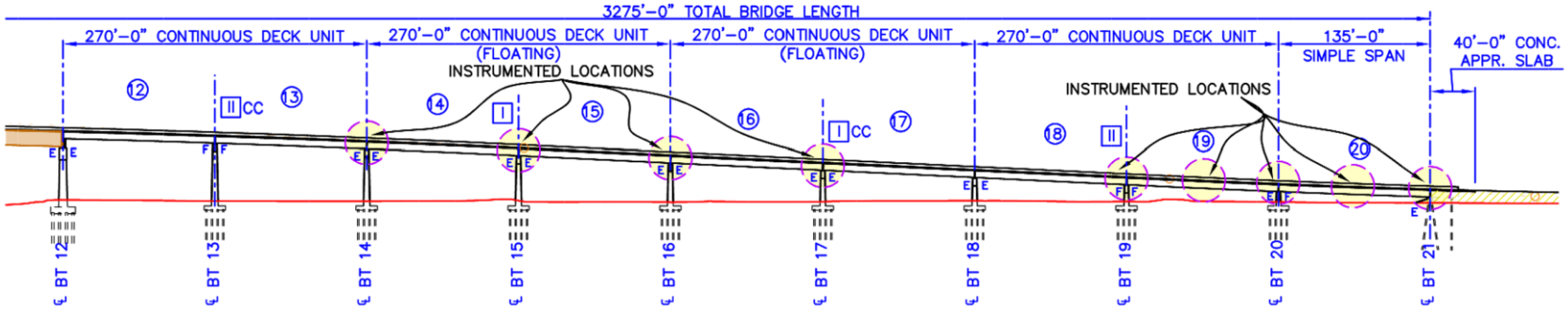

Figure 13. Typical cross section of the Ouachita River Bridge showing full and partial depth continuity diaphragms

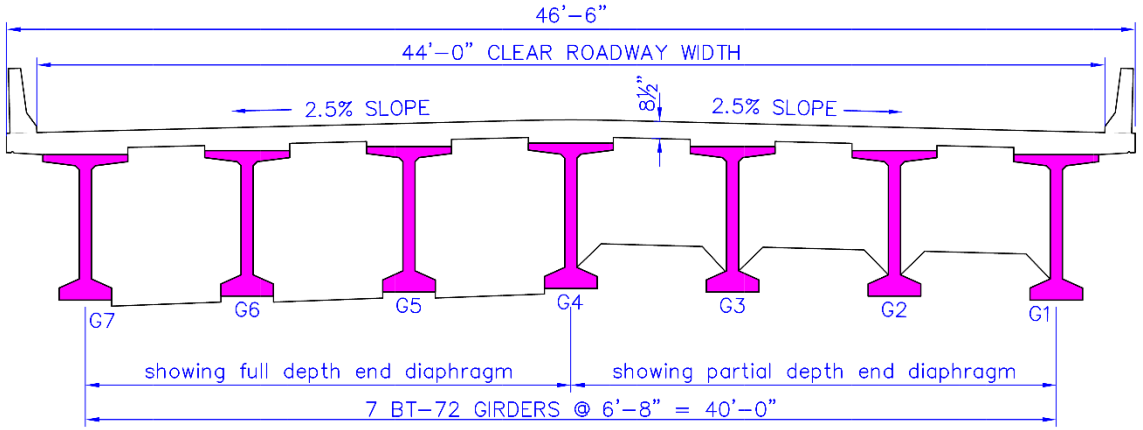

The typical cross section in the approach spans consists of an 8.5 in. reinforced concrete deck supported by 7 AASHTO Bulb-Tee (BT-72) precast prestressed concrete girders spaced 6’-8”. A cross section of the approach spans can be seen in Figure 13.

Two different support conditions were considered for different spans. The first considers the use of elastomeric bearing pads at the joints with no additional horizontal restriction to translation, this condition is referred to as an expansion support noted as (E) in Figure 10 through Figure 12. Figure 1(a) and Figure 1(b) (right) show this support condition for both non-continuous and continuous joint conditions, respectively. Figure 1(b) (left) and Figure 14 show another support condition where the reinforced concrete diaphragm is extended to the bent cap to restrain horizontal translation at non-continuous joint where girders are considered to be on fixed supports (F) based on the bearing pad choice.

Figure 14. Fixed support condition on a non-continuous joint

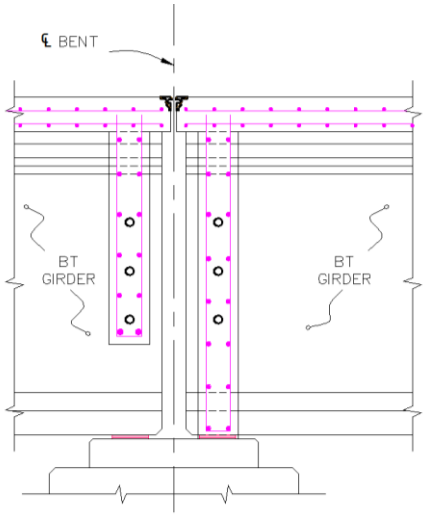

For the cases where link slabs were used; i.e., jointless deck, a crack control detail was provided for some link slabs to assess its efficiency in arresting transverse crack over the supports. The crack control detail (see Figure 15(a)) consisted of a 0.5 in. x 0.5 in. groove that was filled with a silicone sealant. Two meshes of steel reinforcement (top and bottom) were provided as can be seen in Figure 15(b). For the Ouachita Bridge, the longitudinal reinforcement consisted of #6 bars spaced at 7 in., which were 10-ft. long and were staggered by alternating a 2 ft.-6in. shift as shown to cover a total length of 15 ft. in the longitudinal direction. For some of the link slabs, stainless steel bars were used instead of typical black bars to assess if their performance will be different in the case of corrosion initiation. Finally, the link slab #6 bars (Figure 15(b)) were added to the

longitudinal deck reinforcement (#5 bars), which was continuous over the bents in some cases (Bents 2, 3, 4, 15, and 17) and were terminated 4 in. from the centerline of the bent in other cases (Bents 6, 8, 13, and 19).

Figure 15. Link slab details

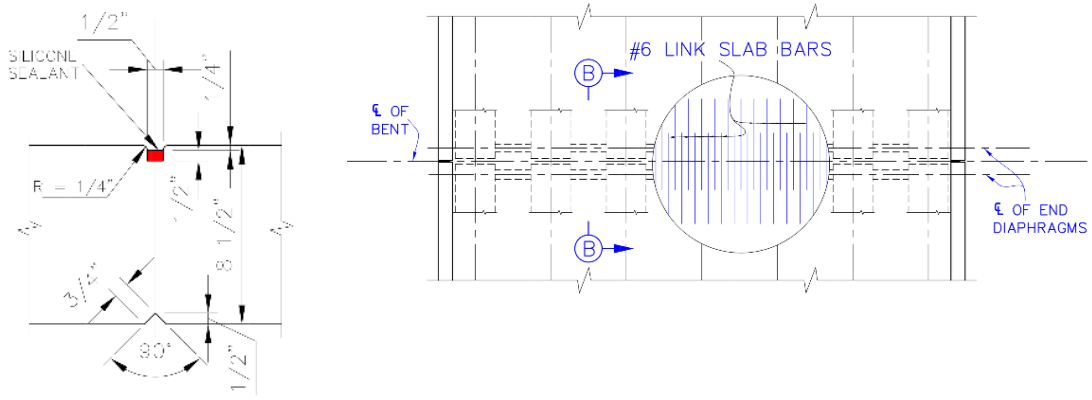

(a) Link slab crack control joint (CC)

(b) Additional link slab reinforcement (#6 @ 7 in. Top & Bottom)

Instrumentation Plan

The sensors and instrumentation chosen for the structural health monitoring system were designed to capture the following: (1) force in the top and (2) bottom link slab reinforcement, (2) differential displacements between the two adjacent girders at a joint, (3) displacement of the girder with respect to its supporting bent, (4) rotation of girder ends, (6) corresponding temperature for each of the recorded readings. Sensor placement was selected in order to obtain the necessary data at key locations within the structure and be able to effectively characterize link slab performance.

Six types of sensors were employed in the designed monitoring system, namely embedded sensors (sisterbars, strandmeters, and straingages) and surface-mounted sensors (gapmeters and titlmeters). All of the selected gages are based on the vibrating wire technology, which is known to be well suited for long-term monitoring as they do not suffer from drifting with age *[15; 16]*. Table 1 lists the type and number of each of the employed sensors. A total of 134 sensors were installed in three phases.

Phase 1: At precast girder fabrication – Embedded sensors within the precast prestressed girder were installed in the casting yard prior to the concrete casting. During this phase,

readings are taken at the time of installation, prior to, during, and after the concrete casting.

Phase 2: During deck construction – The sensors installed during this phase were the sensors embedded in the reinforced concrete deck. Similar to the sensors from Phase 1, these had initial readings recorded at the time of installation, prior to, during, and after the concrete casting.

Phase 3: After deck and diaphragm pouring – Surface mounted sensors were installed once casting of the concrete deck and diaphragms was complete.

Table 1. Types and number of sensors employed in this study

Sensor Type	Measurement	Location	Number
Sisterbars	Strain in reinforcing steel	Embedded	18
Strandmeters	Strain in reinforcing steel	Embedded	36
Straingages	Strain in reinforcing steel	Embedded	2
Gapmeters	Displacement	Surface mounted	64
Tiltmeters	Rotation	Surface mounted	12
Weather Stations	Temperature and humidity	Surface mounted	2
		Total:	**134**

Gapmeters were installed at girder bottom flanges between the bent cap and the girders, and at the bottom and top of girder webs between adjacent spans at Bents 1-5, 14, 16, 17, and 19-21 for girders G4 and G7. Tiltmeters were placed on the webs at girder ends at bents 14, 16, and 19-21 for girders G4 and G7. Strandmeters were placed within the concrete slab at the bottom and top of the link slab longitudinal reinforcement over girders G4 and G7, and in the slab between girders G4 and G5 for Bents 2-4, 15, 17, and 19. Sister bars were installed within the prestressed girders in the top and bottom flanges at midspan and within the slab, before each respective casting for girders G2, G4 and G7 for Spans 19 and 20. Strain gages were installed in the top and bottom flange of girder G7 in Span 20. Figure 16 shows the typical sensor arrangement at link slab joints, midpans, and end bents.

Sensor readout from all sensors installed in this (SHM) system happened in real time with an approximate interval between readings of 3 minutes. The sensors were wired to multiplexers, which were then connected to two separate data loggers — one for the east bank and another for the west bank. The detailed instrumentation plan and full list of installed sensors and their details is provided in Appendix A of this report.

Figure 16. Gapmeter, tiltmeter, and strandmeter placement

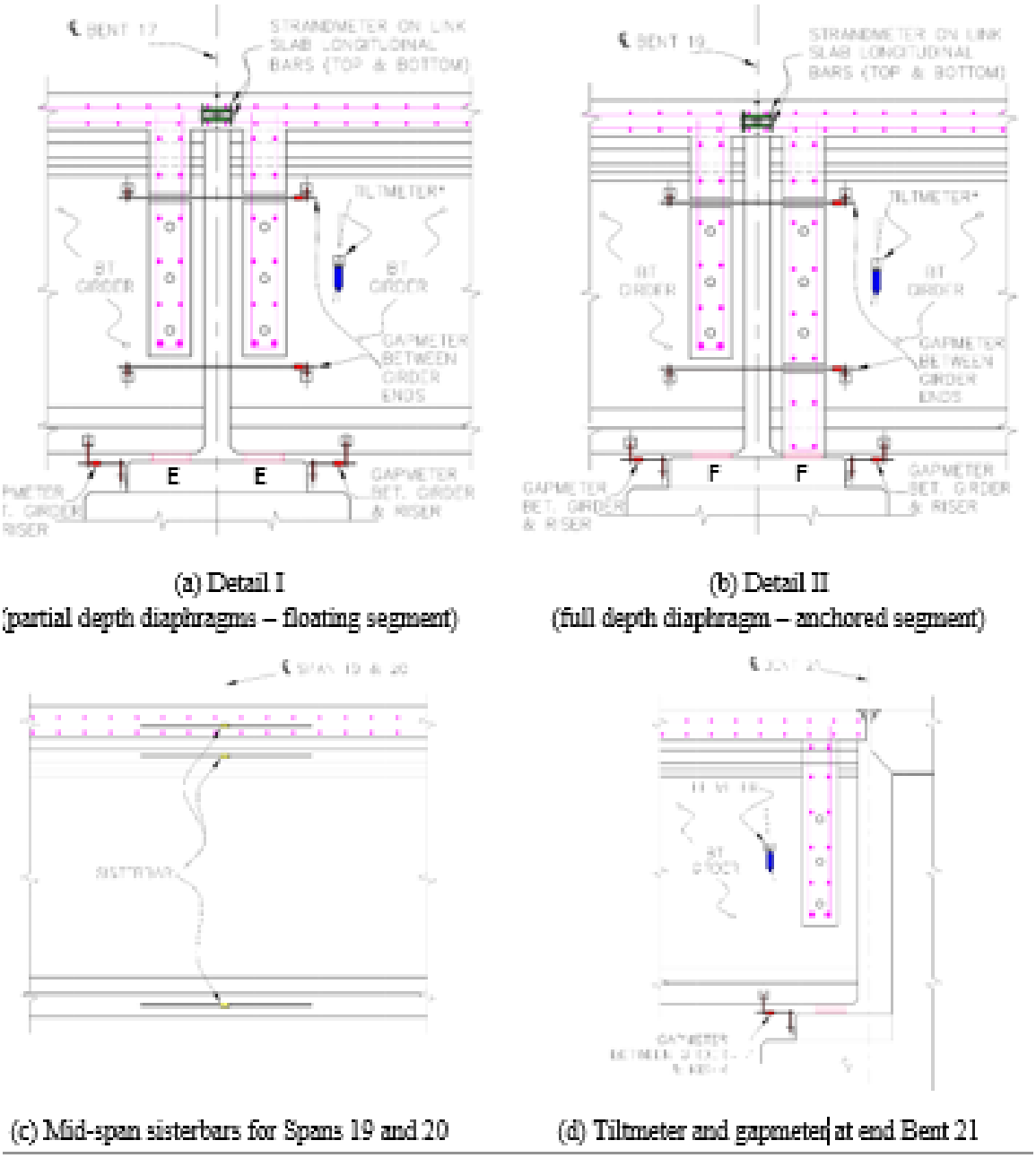

(a) Detail I
(partial depth diaphragms – floating segment)

(b) Detail II
(full depth diaphragm – anchored segment)

(c) Mid-span sisterbars for Spans 19 and 20

(d) Tiltmeter and gapmeter at end Bent 21

Data Collection

Data was logged to the system on a constant basis at approximately 3-minute intervals. The nature of the information collected varied throughout the period in which the SHM system was in use, but it all could be translated eventually into three types of information:

1. A Time Stamp – The time stamp recorded the reference time at which each of the readings was made, recording down to the second.
2. A Data Reading – Data readings for an early stage of the project logged the information collected as a frequency reading. The frequency reading could be converted into digits, another measurement unit for vibrating wire gages, and ultimately into engineering units. The conversion into engineering units could be referenced to any chosen baseline. Temperature corrections according to manufacturer recommendation was also applied. Later, as the data logging system was changed in the early days of 2017, the software in place was programed to perform automatic conversions and the readings were logged as engineering units directly. For some sensors, this was deemed to have a low accuracy for the purposes of this research and was later changed to log as a raw reading in digits.
3. A Temperature Reading – Similar to the data reading, the temperature was collected as a frequency reading in early collection, as degrees Fahrenheit in later logs, and ultimately changed to a digits reading to obtain maximum accuracy.

As mentioned earlier, the data collection system underwent several changes throughout its use. The changes were due to the different construction phases (casting yard vs. bridge site) and system buildup, which happened gradually as the bridge was erected. Also, temporary data loggers were initially used before the final system was completed. The next sections describe each phase of the data collection.

- Phase 0: The embedded sister bars within the prestressed concrete girders were the first sensors to be installed in the casting yard during girder fabrication. The initial data collected included information from the original 12 sister bars only. The information was recorded as frequency readings from each of these sensors. Data logging for this phase begins Jun 19, 2015, and ends Jul 30, 2015.
- Phase 1: The weather stations are installed shortly afterwards; these give readings every 15 minutes but are logged separately. Data logging for this phase began Jun 22, 2015, including only the weather stations. Beginning in Oct 24, 2015, additional sensors were included in these logs as the construction of the bridge progressed. First, 18 strandmeters in the west spans were installed and connected

to the loggers. Later on Feb 27, 2016, an additional 18 strandmeters, six additional sister bars in the slab, and two strain gages in the east spans were installed and connected to the logger. At that point, the total amount of sensors was 58 (18 sister bars, 36 strandmeters, 2 strain sages, and 2 weather stations). This phase uses multiple files to log data for different sensor types and collects the information in different formats. This phase extended until Jan 24, 2017, marking an overlap with the beginning of Phase 2 when the data logging system is changed.

- Phase 2: A new data logging system was employed on Jan 3, 2017, and while installation is completed information is logged in both systems. Sensor installation was done progressively of non-embedded sensors in both abutments over the following month. At this point the data collected was divided according to the sensors placement either in the east or west spans of the bridge. During this phase, sensor installation was completed, accounting for the full roster of 134 sensors (18 sister bars, 36 strandmeters, 2 strain gages, 12 tiltmeters, 64 gapmeters, and 2 weather stations). As stated earlier, sensor readings in this phase were initially recorded as engineering units, however, beginning on July 28, 2017 logs are made in digits in order to obtain increased accuracy. This data collection phase is ongoing.

Data Processing

The different data collection files and systems required a consolidation to be made in order to homogenize the information. Early collection files logged sensor data as frequency readouts, and later, as more sensors were included, the readings were logged as engineering units obtained through the preprogrammed conversion formulas for each sensor type as per the sensor manufacturer recommendations. The final format in which data collection was done involved logging the digit readings from each sensor in order to obtain the greatest level of accuracy. Digit readings are lower level readings that can be converted into engineering units, thus allowing control over the accuracy of the recorded values up to the resolution of each sensor.

Due to the variety of data readings recorded at different stages of the project and the fact that the number of sensors varied within each stage, a consolidation algorithm was developed to perform the initial data processing. This algorithm consisted of a series of scripts and functions that would read input data from the files saved by the different loggers throughout the project and generate a uniform output file using the sensor index

table and timestamps from each files. The index included information for each individual sensor and the files that contained its logs, complete with beginning date, end date, and data type collected. This index table would later be used to generate the output file through a function that would perform the corresponding conversions and temperature corrections necessary for each sensor type. Temperature corrections for each sensor differed based on sensor type and even for each type, it also differed based on each sensor's individual calibration coefficient that was provided by the manufacturer.

Temperature Data

Temperature data was logged on an individual basis for each of the installed sensors. The data in this report has all been corrected using the specified baselines in each section. The top-most strandmeters in the link slab were used to graph the temperature graphs in all link slab forces and crack width calculations. Temperature gradients were determined by using the average temperature from strandmeters in the link slab as the top most temperature reading, and the average reading from the gapmeters installed in each location as the bottom most reading.

Visual Inspections

Deck cracking was monitored in several bents at various points during the construction process over a period of approximately 15 months prior to being in service. Cracks were mapped visually and their widths were recorded using a crack comparator, and at later dates using a crack measuring scope. Crack widths, location, and lengths were logged at four different dates during construction, as well as during live load tests. The four dates when cracks were logged were Mar 24, 2016, May 18, 2016, Jan 23, 2017, and May 26, 2017. The cracks were monitored at Bents 2-4, 6, 12, 14, 16 and 18, which corresponded with link slab locations. These locations included some link slabs with the crack mitigation details discussed earlier and shown in Figure 15(a).

Live Load

A load test was conducted using two concrete trucks filled with coarse aggregates. The trucks axles were weighed right before the testing began using portable scales. The gross vehicle weight (GVW) for the two trucks used in the testing was 64.35 kip and 64.67 kip.

As can be seen in Figure 17 and Figure 18, they were positioned in a truck train (one on each span) and truck tandem (both trucks on the same span) configurations to cause a maximum negative and positive moment effects, respectively. The positions were repeated for each instrumented span and two positions of each configuration were used for each span targeting the middle of the bridge (Girder G4) and the exterior of the bridge (Girder G7). A total of 23 load cases were executed (11 positive and 12 negative), which are given in more detail in Appendix B.

The live load test was conducted over a period of approximately 7 hours beginning at 9 a.m. on July 11, 2017, and ending before 4pm of the same day. Data was logged separately for the live load test in order to disregard the hourly averages that are applied to the long-term data. Live load test data was recorded in 3-minute intervals for the entire set of sensors.

Figure 17. Positive moment truck position

(a) Side by side truck positioning

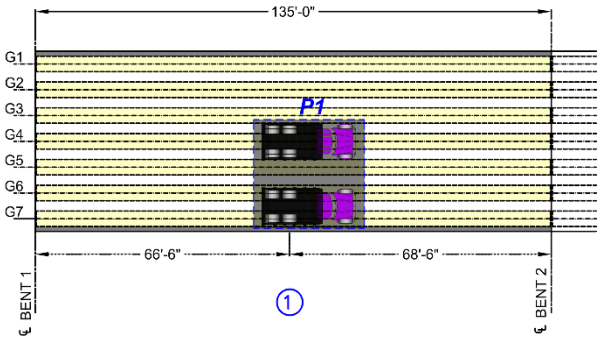

(b) Plan view of side by side truck positions

Figure 18. Negative moment truck position

(a) tandem truck positioning

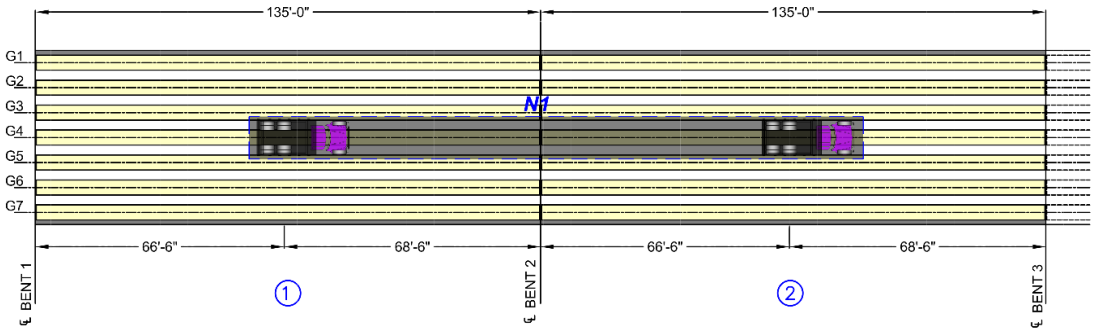

(b) Plan view of tandem truck position

Discussion of Results

In this section, results obtained from the monitored readings are presented. The results are either obtained directly from the sensor readings (e.g., temperature) or through manipulation of multiple sensor readings to obtain a certain behavioral aspect of the bridge (e.g., relative angle between girder ends). It should be noted that the results presented in this section are the key results pertinent to the scope of the project. Additional results and information can be found in the appendices.

Instrumented Segments and Spans

For presentation of results purposes, the instrumented bridge segments were classified in the following manner based on deck continuity conditions:

- Segment A – This segment is the longest jointless unit that has a 4-span continuous slab segment between Bents 1 and 5 and includes Spans 1 through Span 4. All supports for this segment were "Expansion" bearings, which is will be referred to as a *floating* segment in this report.
- Segment B – This segment is a 2-span continuous segment between Bents 14 and 16 and includes Span 14 and Span 15. This segment is also a floating segment.
- Segment C – This segment is a 2-span continuous segment between Bents 16 and 18 and includes Span 16 and Span 17. This segment is another floating segment.
- Segment D – This segment is a 2-span continuous segment between Bent 18 and Bent 20 and includes Span 18 and Span 19. This segment has a diaphragm cast into the middle support providing the span with anchored fixity at Bent 19.
- Segment E – This is a single-span segment between Bent 20 and Bent 21. This refers specifically to Span 20. This segment has a diaphragm cast into the western girder support providing the span with anchored fixity at one end.

These segments can be seen in Figure 19 through Figure 23.

Figure 19. Segment A

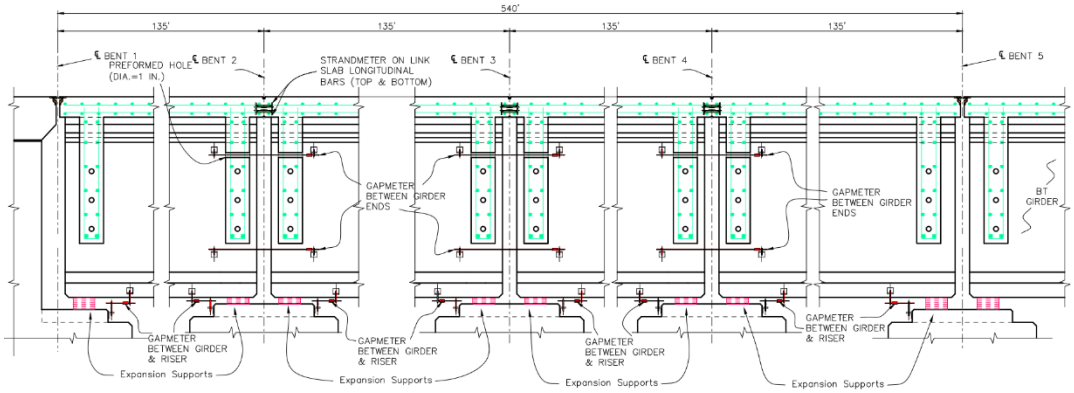

Figure 20. Segment B

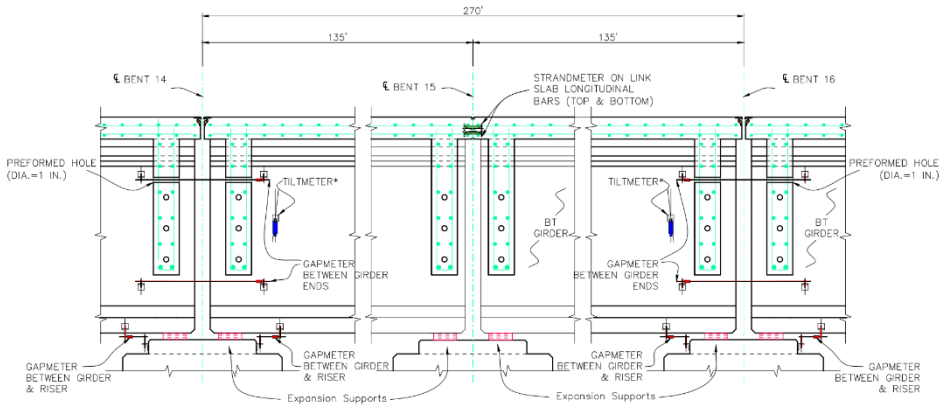

Figure 21. Segment C

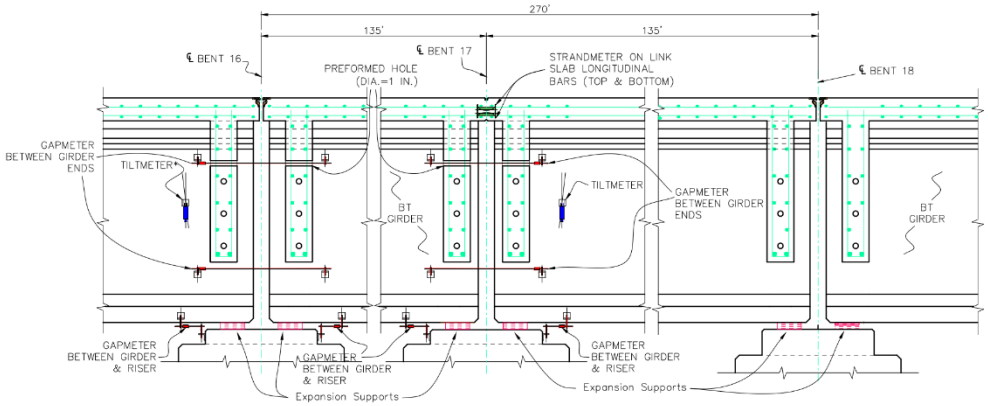

Figure 22. Segment D

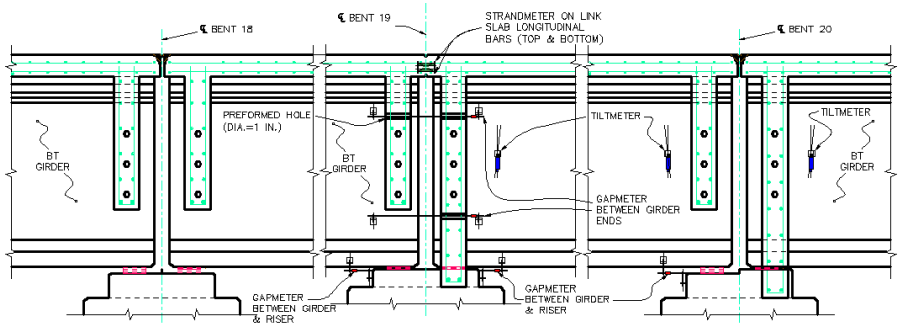

Figure 23. Segment E

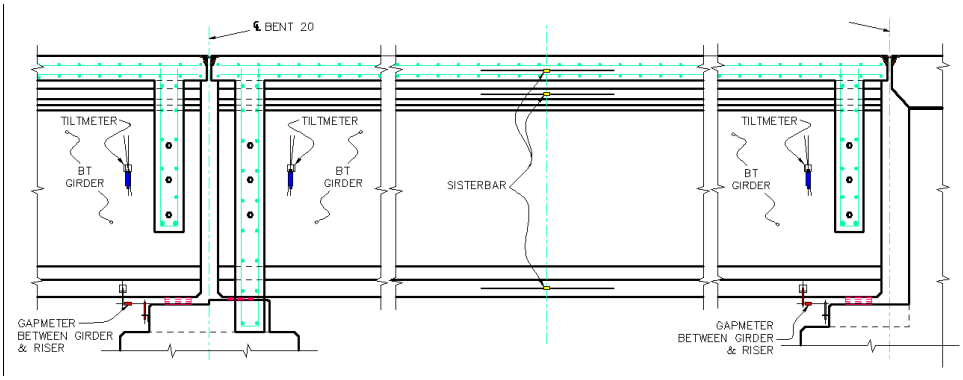

Girder End Displacement

The post-processed data was used to extract readings from the gapmeters installed to measure the relative movement between the girders and the risers on the bent caps supporting the girder in question. A special script was developed for the purpose where the readings from gapmeters at either end of a given segment and determine the total movement. The gapmeters that were considered for this correspond to those installed between the girder bottom flange and the riser as can be seen in Figure 16 (a) and (b).

Given that not every span has a gapmeter on each end of the girders, this calculation could not be done for every instrumented span or slab segment. Only Segments A and B have both gapmeters in place at the beginning and end of the segments, and only Spans 1, 2, 3, 4, 16, and 19 have both gapmeters in place to measure the girder end displacements at each span. Furthermore, the readings were not complete for the entire period of the project due to sensor malfunctions at several locations at different times. Since all gapmeters are surface mounted sensors, the cause of the malfunction could have been due

to many reasons (e.g., lightning strikes). Despite having multiple sensors with unusable data (i.e., out of range readings), further scrutiny of the entire records for these sensors shoed that sensor readings were still usable, which made it possible for comparisons to be drawn.

Figure 24 through Figure 27 show plots of the relative girder end displacements based on from the gapmeters installed at the beginning and end of each segment. It should be noted that the plotted deformations are the cumulative deformation recorded between both ends of each segment or span; i.e., Δ_{end} and Δ_{beg}

$$\Delta = \Delta_{end} + \Delta_{beg} \quad [1]$$

The plotted results are for a period of about two years from March 2017 to February 2019. It can be seen that seasonal and daily temperature changes are directly correlated to the plotted relative girder end movements. This is expected as seasonal changes cause a uniform elongation, or shortening, of the entire segment, which daily temperature changes are more affected by the temperature gradient, which causes girder camber leading to end rotations. In all cases, the girder end movements did not exceed 0.5 in. It can also be stated that floating segments experience smaller girder end movements (~ 0.2 in.) compared to anchored segments. This is true for all but one 2-span floating segment, which could be attributed to locking of girder bottom flanges with surrounding shear keys. The observed results indicate that anchoring diaphragms, whether by design or due to unforeseen locking, leads to more demands on the bearings.

Figure 24. Girder end displacement Span 19 Girder G7 in Segment D (fixed 2-span segment)

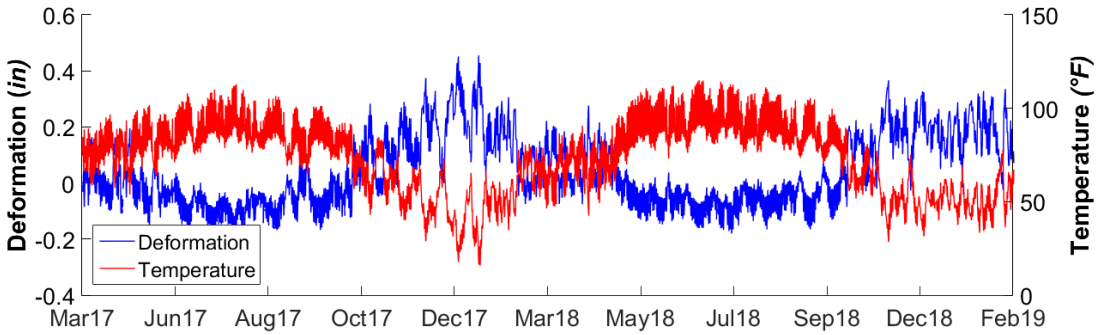

Figure 25. Girder end displacement Span 16 Girder G7 in Segment C (floating 2-span segment)

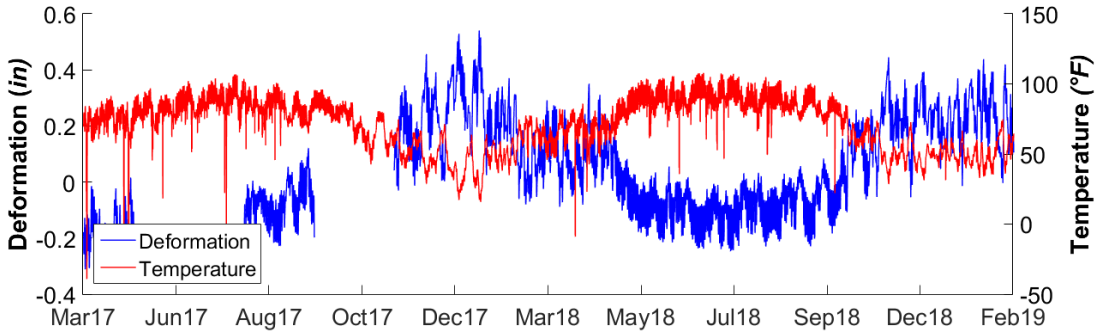

Figure 26. Girder end displacement Span 2 Girder G7 in Segment A (floating 4-span segment

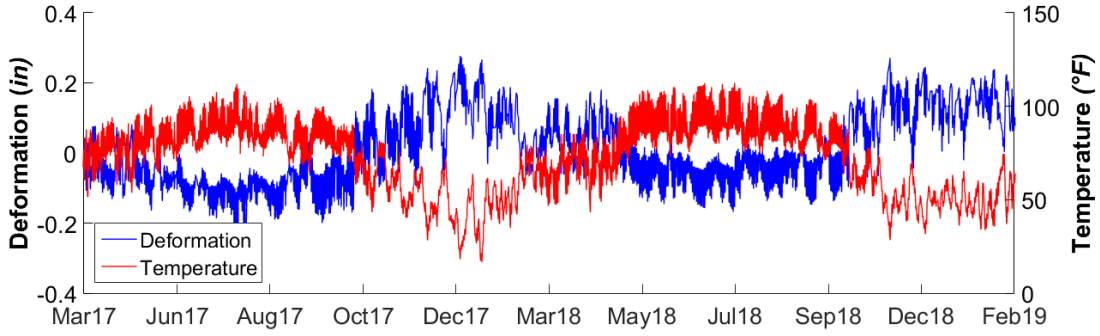

Figure 27. Girder end displacement Span 3 Girder G7 in Segment A (floating 4-span segment)

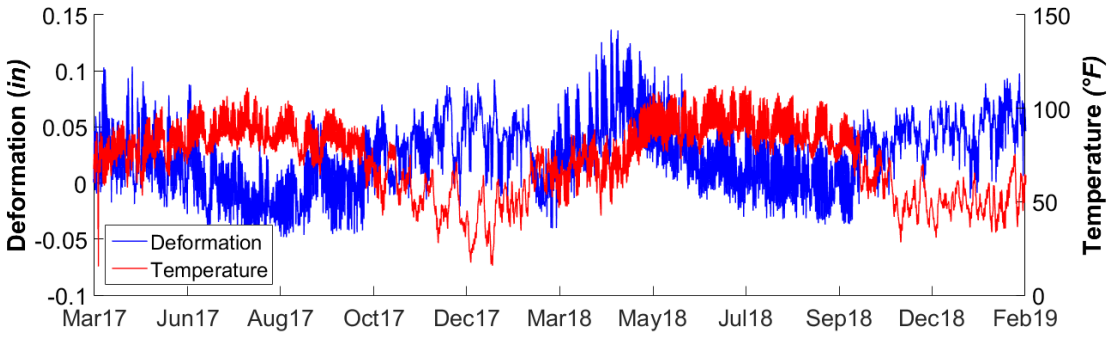

Relative Angle

Similar to the girder end displacement, it was possible to use the data logged from the gapmeters to estimate a relative angle between the girder ends at locations where gapmeters were installed. Information from gapmeters in four different positions in the bent were used along with numerical approximations to obtain a value for the relative

angle between the girder ends. The gapmeters that were considered in this analysis correspond to those installed at the top of the web, at the bottom of the web, and one at each face of the support between the girder and the riser, as can be seen in Figure 16. The gapmeters between the girder ends both give deformation readings that correspond to the sum of the displacements of both girder ends. The gapmeters between the girder and the riser give the displacement of each girder end with respect to the support. To obtain a value for the relative angle between the faces, the bisection method was used in order to obtain a numerical approximation as follows:

- First, the relative angle between the girder ends is assumed to be –2°. This angle corresponds to the minimum value that will be considered. This value was chosen given the fact that tiltmeters installed at girder ends never indicated a tilt above 1° or below -1°.
- Using the deformation from the bottom-most gapmeters (i.e., those between the girders and the risers shown in Figure 16) as a base point, the deformations at each of the other gapmeter positions is calculated for each girder using basic trigonometric relations. The process is then repeated assuming the maximum angle to be considered, which is 2° in this case.
- Considering that the sum of the deformations from each girder end should be equal to the gapmeter reading at that point, it is possible to estimate an error for each of the assumed angles. By observing the sign of the error, the new range of assumed angles can be selected using the midpoint and the corresponding extreme as the new minimum and maximums.

This process is followed iteratively until the calculated error is less than 0.03%, at which point the midpoint for the iteration is selected as the relative angle.

Figure 29 through Figure 33 show the relative angle between girder ends as calculated using the aforementioned procedure. It is clear that the relative angle between girder ends at bents with link slabs varies daily and seasonally following the ambient temperature variations (see Figure 28). The magnitude of the relative angle is limited, however, its effect on other bridge elements (e.g. bearings and shear keys) may still need to be assessed.

Figure 28. Average temperature readings from Bent 2 - Girder G7- Segment A (4-span floating segment)

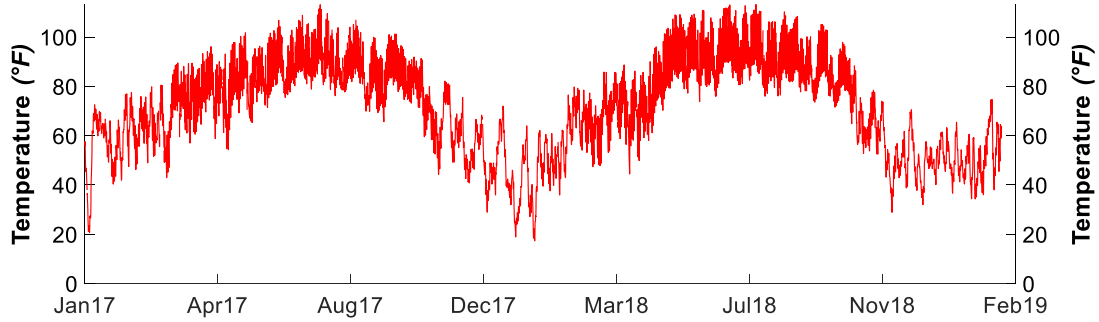

Figure 29. Relative angle at Bent 2 – Girder G7 –Segment A (4-span floating segment)

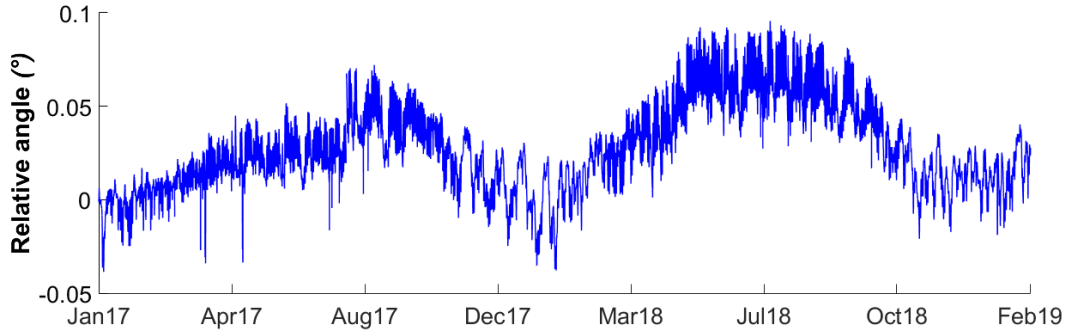

Figure 30. Relative angle at Girder G7 – Bent 3 – Segment A (4-span floating segment)

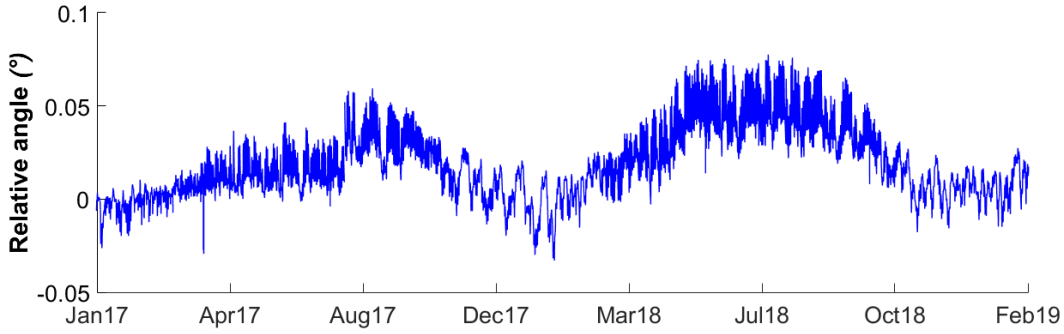

Figure 31. Relative angle at Girder G7 – Bent 4 – Segment A (4-span floating segment)

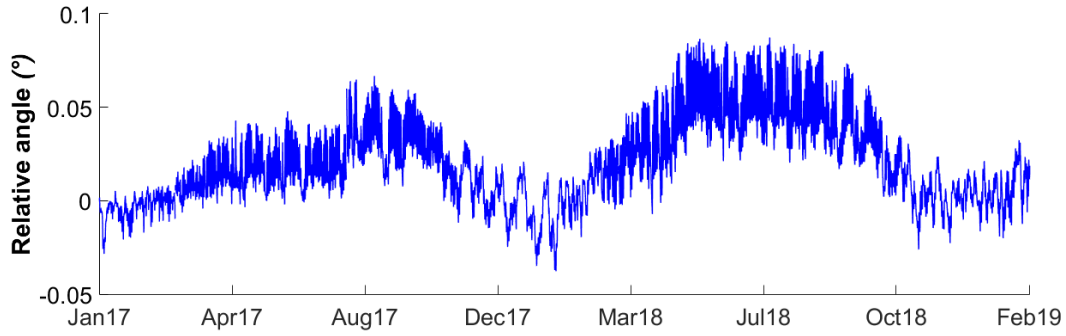

Figure 32. Relative angle at Bent 17 – Girder G7 –Segment C (2-span floating segment)

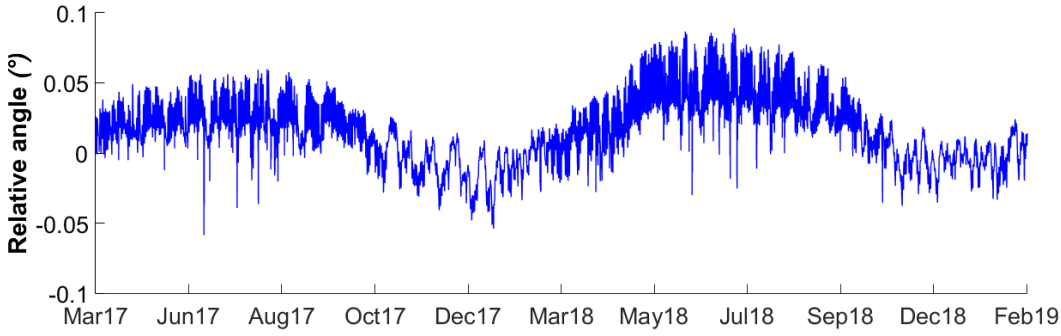

Figure 33. Relative angle at Bent 19 – Girder G7 –Segment D (2-span fixed segment)

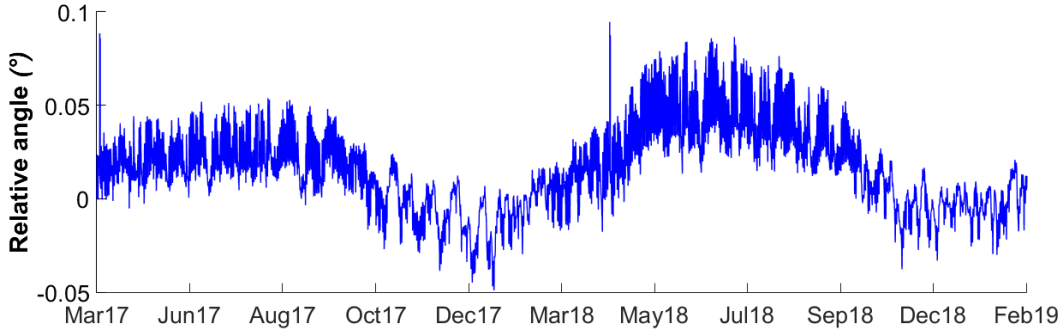

Link slab Force

Strandmeters installed on the link slab reinforcement were used to estimate the forces in the instrumented link slabs. In order to calculate the force in the link slab, the digits' readings from the strandmeters in the link slabs were converted into strains. It was assumed that link slabs are subjected to bending moments and axial forces, i.e., they are

not pure flexural members nor are they pure axial members. A script was developed that could determine the corresponding forces from the logged data readings by identifying the state of the strains from the sensors in the slab. Figure 34 shows the six main states considered in the force calculation.

Figure 34. Strain compatibility diagrams in the link slab

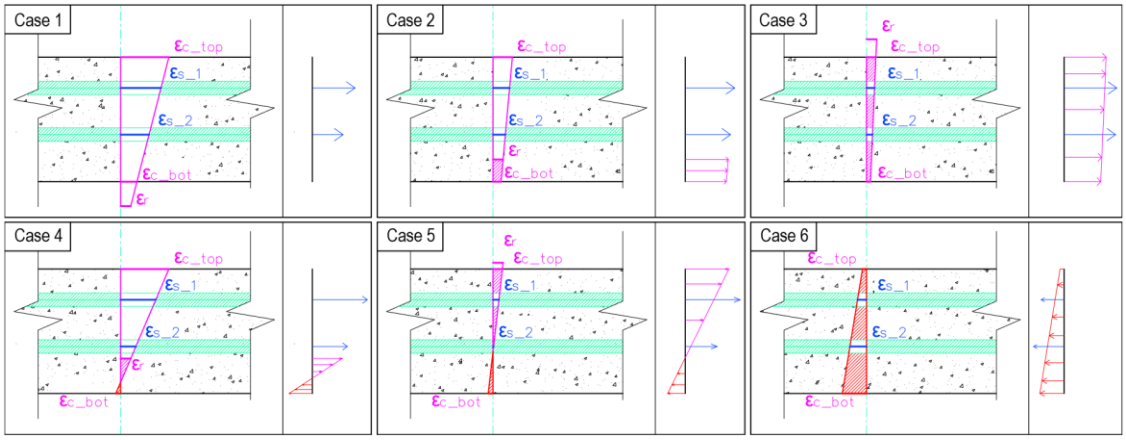

Contributions from concrete to the link slab force were taken into account. These contributions included compression, as well as tension when the strain in the concrete was below the rupture strain. However, when analyzing the obtained results, it was found that the values of the link slab force for different bents resulted in high magnitude forces. Upon close examination of the results, the majority of the link slab force was being generated by compression and tension forces within the concrete.

In view of the considerable cracking that had been previously observed, it was deemed necessary to revisit the considered conditions while determining the forces.

Figure 36 through Figure 40 show plots of the link slab forces based on the measured readings as interpreted using the aforementioned approach. Figure 35 shows the corresponding temperatures during the same monitoring period. The plots show that the link slab forces vary daily and are also affected by seasonal temperature changes. This can be attributed to the fact that seasonal temperature changes contribute to crack opening, or closure, which is superimposed on the temperature gradient effect that leads to relative girder end rotations as described in the previous section. The magnitude of the link slab forces can increase beyond what is expected for a link slab system. This may be attributed to the fact that shear keys provide additional stiffness that far exceeds the stiffness of bearing pads.

Figure 35. Temperature at Bent 2 – Girder G7 Segment A (4-span floating segment)

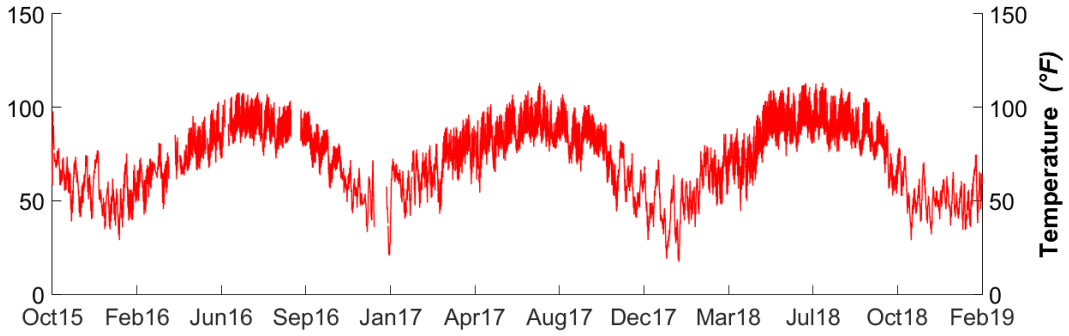

Figure 36. Link slab force at Bent 2 – Girder G7 – Segment A (4-span floating segment)

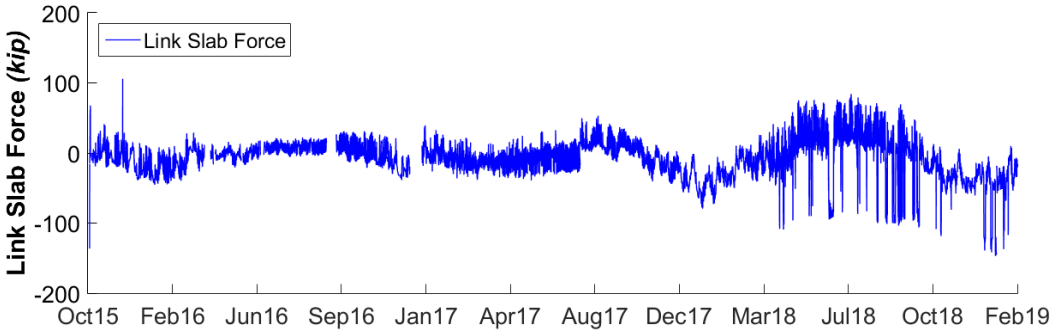

Figure 37. Link slab force at Bent 3 - Girder G7- Segment A (4-span floating segment)

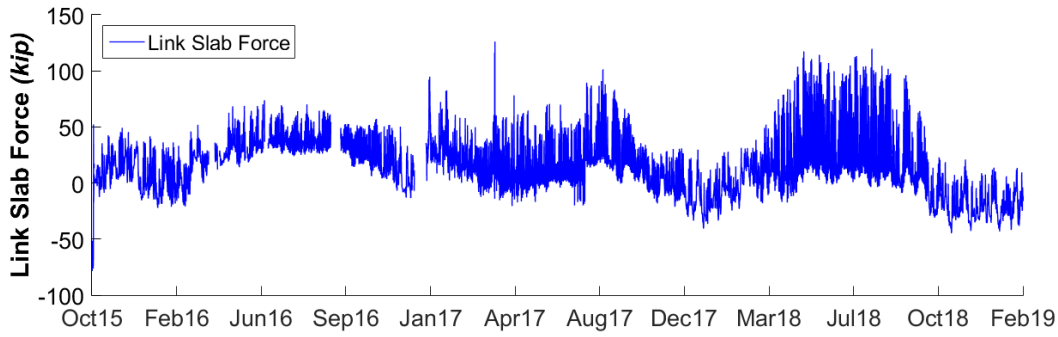

Figure 38. Link slab force at Bent 4 – Girder G7 – Segment A (4-span floating segment)

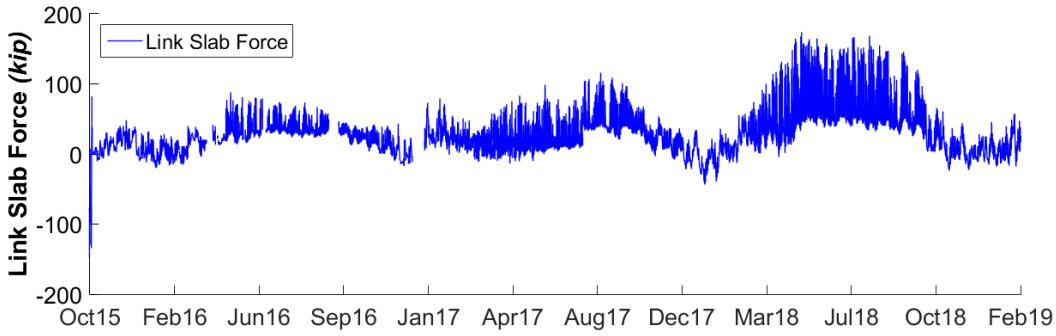

Figure 39. Link slab force at Bent 17 – Girder G7 –Segment C (2-span floating segment)

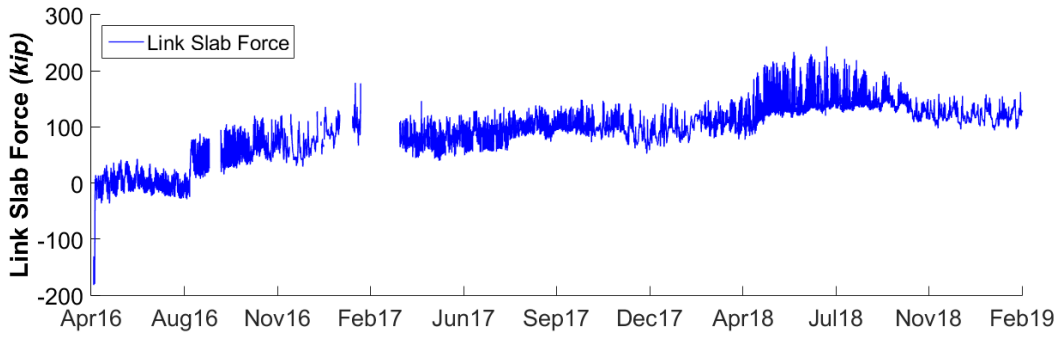

Figure 40. Link slab force at Bent 19 – Girder G7 –Segment D (2-span fixed support segment)

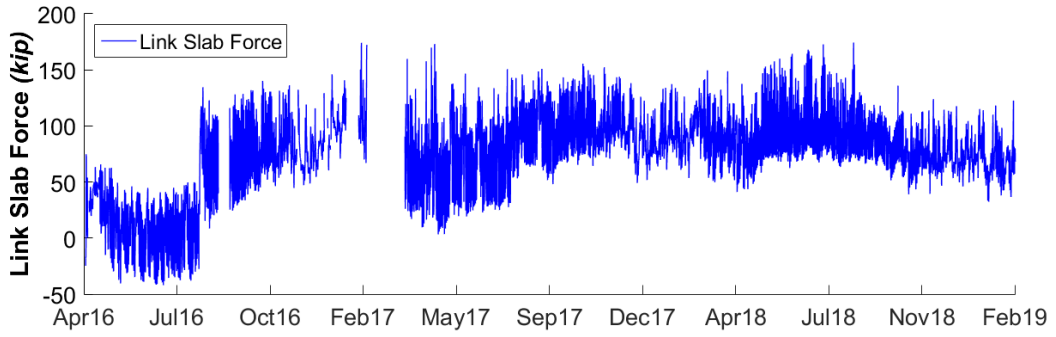

Crack Width

When a reinforced concrete section cracks, the concrete's contribution in tension should no longer be considered for the depth of the section that has cracked. Similarly, when a crack opens, compression stresses within the concrete will not develop until the crack has

closed completely. In order to account for the effects of cracking, the recorded strain readings from the strandmeters can be used in order to estimate stress for crack width and depth calculation.

Several different approaches were considered while determining the width of the crack in concrete structures. Approaches based on the Gergely-Lutz solution, such as ACI 318-89 and ACI 318-95 were considered. Additionally, approaches based on Beeby's solution and approaches based on Frosch's solution were also considered. However, the Gergely-Lutz, Beeby, and Frosch approaches were originally developed to be used principally on flexural members. Although the link slab will be subjected to a degree of flexure, it is also subjected to substantial axial forces simultaneously. After careful consideration, the approach used to estimate crack width was that developed by Broms and Lutz for use with tensile members *[17]*.

$$W_{max} = 0.138 f_s d_c \sqrt{1 + \left(\frac{s}{4d_c}\right)^2} \times 10^{-3} \qquad [2]$$

Where, d_c = the concrete cover for the reinforcing steel, f_s = the service stress in the reinforcing steel, s = the bar spacing.

Initial Cracking

In order to obtain an appropriate frame of reference, the crack width calculation was baselined to a point in time 12 hours after the pouring time for each slab, which was near midnight on the night after pouring for all slabs. This baseline calculation was independent of the standard baselining that was used for all other calculations.

Crack depth was determined by establishing the depth of the slab that had been subjected to a strain above the rupture strain, assuming a linear crack surface. Crack widths were logged for every time step, along with the depth cracked for both the bottom and top surfaces. And by comparing with previous time step results, it was possible to keep track of the cracking. Once the slab had cracked beyond a certain depth, any portion of the slab within the cracked area was disregarded in subsequent tension force calculations. A similar concept was applied in order to determine points of contact for compression within the crack.

Crack Reversal

The link slab steel reinforcement strains from the strandmeters were used to determine displacement relative to the crack width established in the previous section and based on using the crack spacing from the Broms-Lutz equation. This calculation was referred to as the crack reversal. Crack reversal was determined for every time step, and in the occasions when the reversal was greater than the logged crack width, contact between both concrete sides of the link slab was assumed. Once contact is identified, compression from the concrete section was then calculated considering only the depth of concrete that was within contact.

Disregarding tension from cracked sections and compressions from sections not within contact range considerably reduced the link slab forces, resulting in a link slab force much more dominated by forces in the steel. Figure 42 through Figure 46 show plots of the crack widths as estimated using the aforementioned approach. Figure 41 shows the corresponding temperatures during the same monitoring period. The plots show that cracking of the link slab occurs at an early stage of the life of the deck. Once the initial cracks tack place, the variations in the width of the cracks is closely related to daily temperature gradient variations.

Figure 41. Temperature at the link sab at Bent 2 – Girder G7 –Segment A (4-span floating segment)

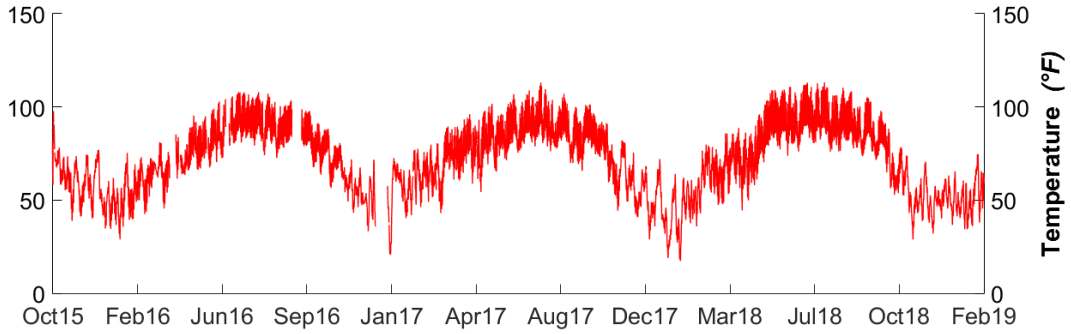

Figure 42. Crack width at the link sab at Bent 2 – Girder G7 –Segment A (4-span floating segment)

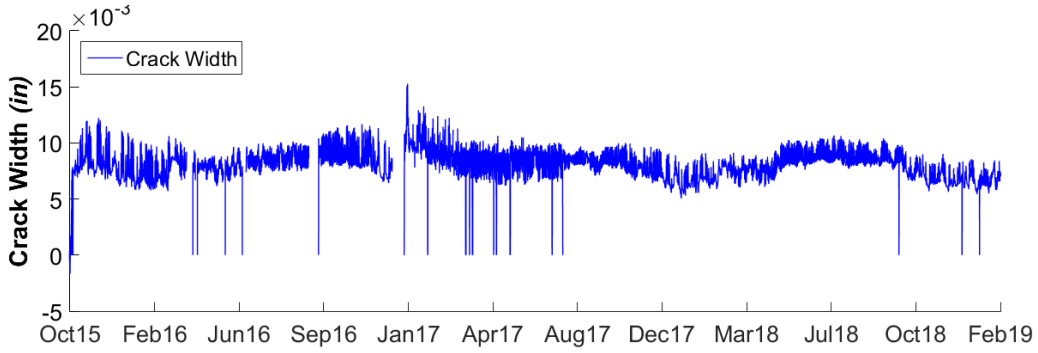

Figure 43. Crack width at the link sab at Bent 3 – Girder G7 –Segment A (4-span floating segment)

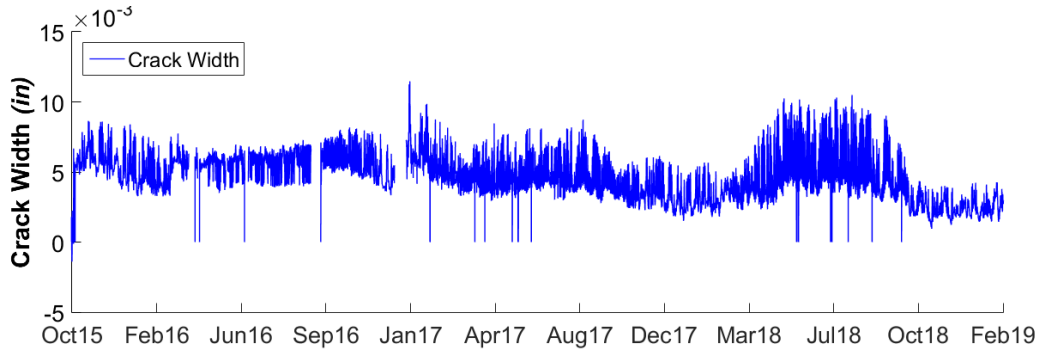

Figure 44. Crack width at the link sab at Bent 4 – Girder G7 –Segment A (4-span floating segment)

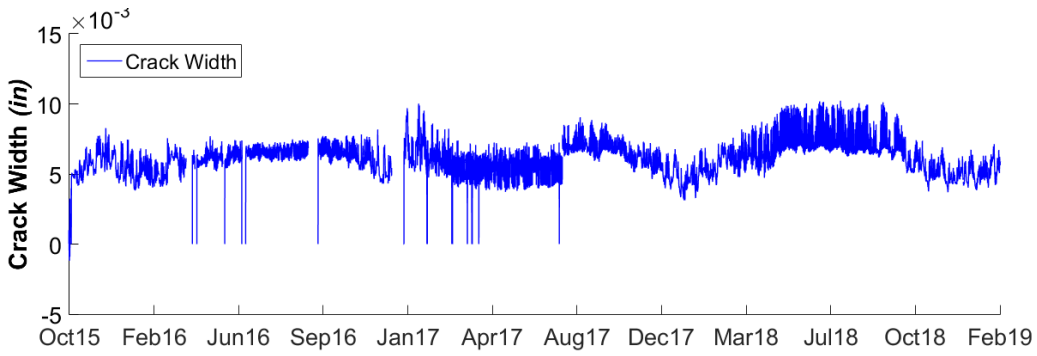

Figure 45. Crack width at the link sab at Bent 17 – Girder G7 –Segment C (2-span floating segment)

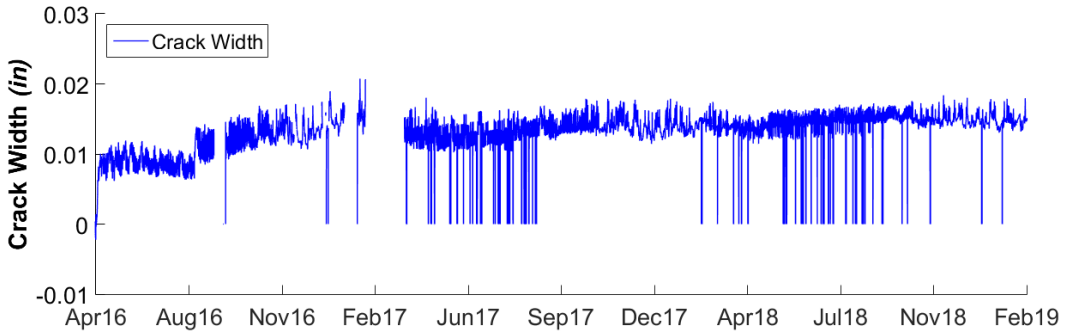

Figure 46. Crack width at the link sab at Bent 19 – Girder G7 –Segment D (2-span fixed support segment)

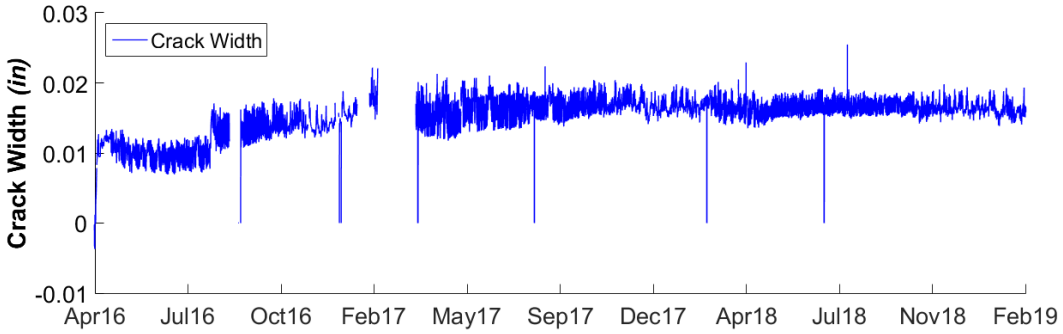

Live Load Tests

Recorded data for the live load testing was logged separately than the rest of the long-term data. This was necessary since data for long-term analysis was being averaged on an hourly basis. For the live load test, this would not have been viable given the short duration of the truck placement in testing positions (approximately 10 min).

The results from the live load testing were used to obtain plots of behioral aspects similar to those described earlier for the long-term testing. Strandmeter information was used to determine forces in the concrete and steel within the link slab.

Figure **47** shows a plot of the constiuting forces in the link slab from both reinforcement meshes, concrete in compression and concrete in tension (if applicable). This information was used to determine a resulting force within the link slab, which is the sum of these components as can be seen in Figure 48.

Figure 47. Live load forces in the link sab at Bent 3 – Girder G7 –Segment A (4-span floating segment)

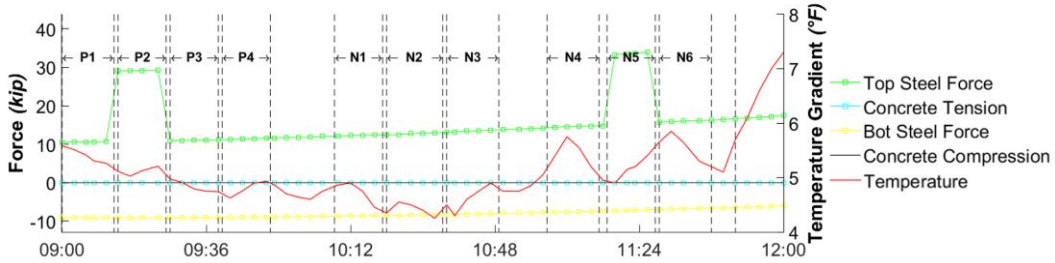

Figure 48. Live load forces in the link sab at Bent 3 – Girder G7 –Segment A (4-span floating segment)

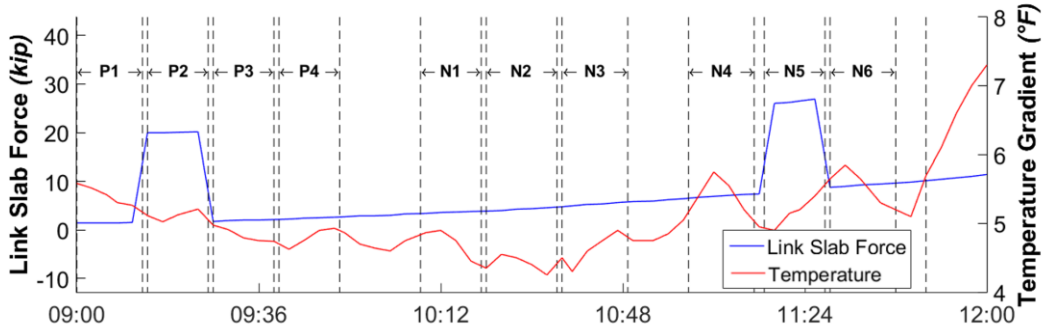

Information from gapmeter readings of displacements between girder bottom flanges and the supporting bent cap was used to obtain segment/girder end displacements using readings from gapmeters at either end of a specific segment or span, as in Figure 49. It can be seen that the shown plot indicates a direct influence of loading cases P1 and N4 at that location (Girder G7 – Span 1 – Segment A). It should be noted that these cases involve trucks positioned directly over Girder G7 in Span 1.

Figure 49. Girder end displacement at Span 1 – Girder G7 –Segment A (4-span floating segment)

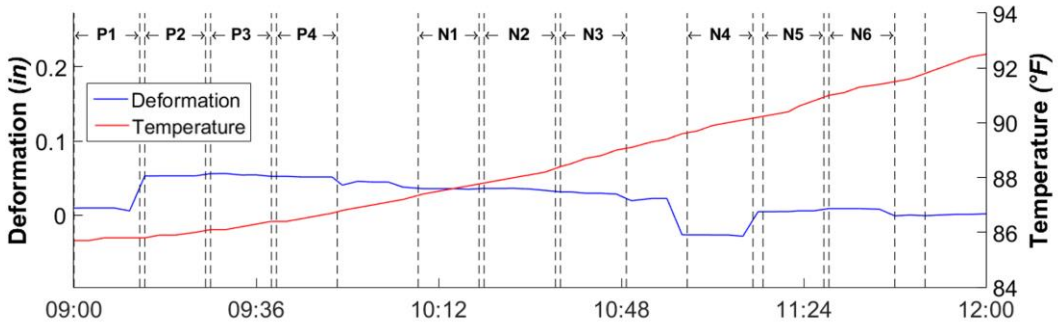

Gapmeter readings at specific bents logging displacements between girder ends as well as supports at the bent were used in order to determine the relative angle at a specific bent as can be seen in Figure 50. As described earlier, a combination of strandmeter and gapmeter data was used in order to obtain temperature gradient values. In Figure 50, the loading positions influencing Girder G7 relative angle at Bent 3 were loading cases P1, P2, N4, and N5. It should be noted that N5 caused a larger relative angle between the girder ends than the other the other cases.

Figure 50. Relative angle between girder ends at Bent 3 – Girder G7 –Segment A (4-span floating segment)

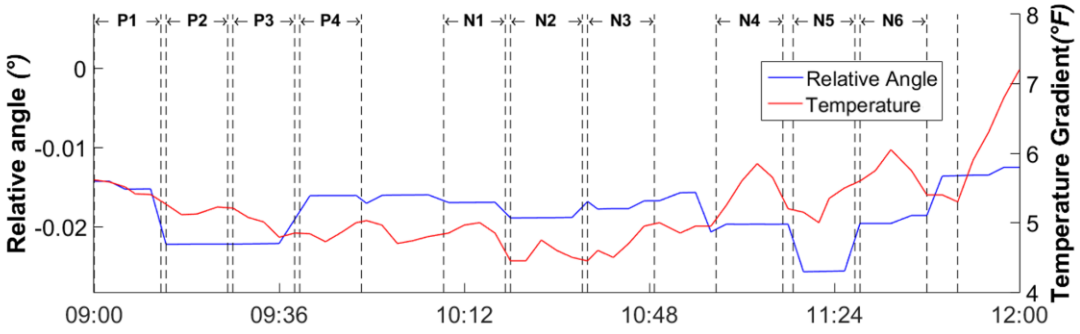

STAAD Verification

A STAAD model was developed for a specific bent, under specific temperature conditions, to better understand the observed results. The line model was developed with a focus on modeling the interaction between the girders, the slab, the link slab, and supports. Spring elements were used to model the supports and beam elements were used

to model a single girder and the link slab, albeit with end moment release for the link slab. The model can be seen in Figure 51.

Figure 51. Line element model used in STAAD

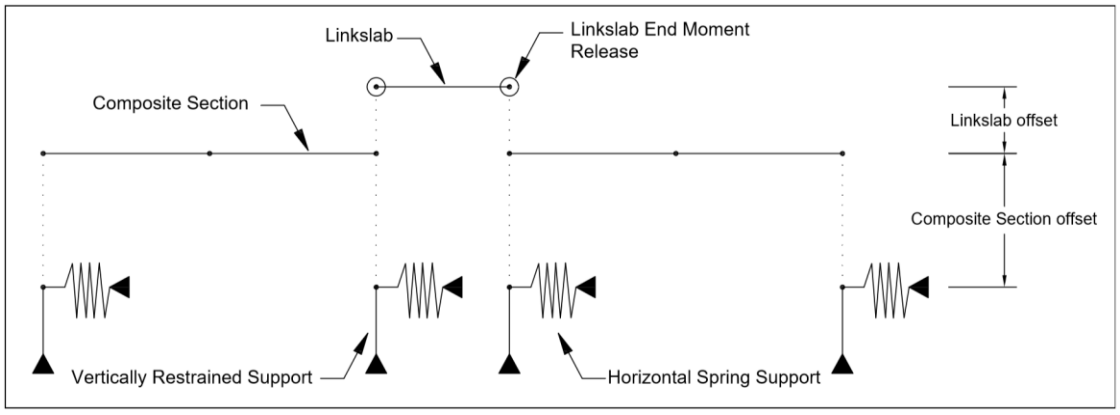

A time step was selected from the field monitoring data. Temperature gradient and uniform temperature information was pulled from the corresponding sensors at the selected bent, and loaded into STAAD using both built-in and custom loading. The effects of uniform temperature were loaded using the built-in loading within the software. Due to the nature of the composite section, it was not possible to use built-in loading for temperature gradient. Therefore, temperature gradient effects were custom loaded by determining the beam end moments for the specific temperature gradient conditions in the composite section using the recommendations within AASHTO LRFD Bridge Design Specifications.

Figure 52 shows the temperature gradient profile that was used in the calculation. Thermally induced stresses could then be calculated from basic principles *[18]*. Thermal gradients cause end curvature and subsequent moment that could be determined for each design case *[19; 20]*. Girder curvature is given by

$$\psi = \frac{\alpha_c}{I} \cdot \int \theta_{(y)} \cdot b_{(y)} \cdot (y - n)\, dy \qquad [3]$$

Where, α_c = the thermal expansion coefficient of concrete, $\theta_{(y)}$ = the temperature change, $b_{(y)}$ = the net section width at height y, n = the distance between the neutral axis and the arbitrary datum, and y = the height at which the net section width is considered. An equivalent end moment that would cause similar curvature can be expressed as follows.

$$M = E_c \int \alpha_c \theta_{(y)} b_{(y)} (y - n)\, dy \qquad [4]$$

Where, E_c = the modulus of elasticity of concrete. This moment was then applied to the girder ends within the STAAD model.

Figure 52. Temperature gradient profile

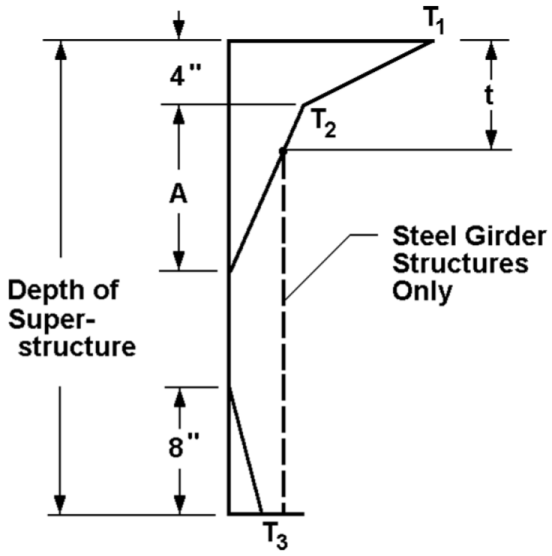

Upon comparison between the STAAD results and the data obtained from the structural health monitoring project an important difference could be observed. The forces at the link slab within the STAAD model were significantly lower than those calculated from the sensor data. However, it was also found that the girder ends in the STAAD model were having displacements much higher than the ones recorded in the SHM system.

The discrepancy between the idealized model and the actual bridge conditions may be due to differences in support conditions. To test this hypothesis, the support stiffnesses were fine-tuned within the STAAD model and it was found that the link slab force increased as the girder end displacements decreased accordingly. Results were calibrated on the basis of the displacement at the girder ends for the support directly below the link slab, and it was found that by increasing the support stiffness considerably both the girder end displacements and link slab force would coincide between the STAAD model and the SHM calculations.

During construction, the research team performed multiple inspections of the bridge. The condition of the gap between the girders' bottom flanges and the shear keys surrounding

them was as can be seen in Figure 53. This led to a hypothesis that debris accumulation in this gap may restrain girder end movements more than what is expected, or even lead to complete locking of the movement.

Figure 53. Conditions of the gap between the shear keys and the girder bottom flanges

Transverse Crack Observations

As is typical with cast-in-place decks, transverse cracks were observed at all link slab locations. Though certain crack mitigation strategies were employed at different bents (see Figure 15(a)), visible cracks were found to propagate transversely in parallel to the saw-cut silicone filled 0.5-in. grooves that were put in place at these bents. At certain points, cracks would disappear into the saw-cut groove, but then would reappear as transverse cracks running parallel to the groove approximately 3 to 6 in. away. In other words, the crack control detail was not efficient in arresting the cracks.

Though crack widths were affected by the support conditions at the girder ends, the prevalence of cracking in bents that had saw-cut grooves led to the conclusion that this particular strategy does not mitigate crack initiation. In light of this observation, it will not be a requirement in the new DOTD standard details. Figure 54 (a) shows one of the cracks next to a link slab saw cut. This pattern was typical for many of the link slabs where the crack control measure was employed. Figure 54 (b) shows the crack pattern at Bent 13 (fixed bearings and anchored diaphragm), and Bent 15 (expansion bearings with partial diaphragm and no crack control), 17 (expansion bearings with partial diaphragm with crack control detail), and 19 (similar to Bent 13). It can be seen that transverse cracks did not take place within the crack control groove as was intended. Cracks escaped

the groove for most of the deck width. Furthermore, it is clear that link slabs over bents with fixed supports (Bents 13 and 19), where one of the bents supporting girders' end diaphragms were anchored to the bent cap experienced wider cracks when compared to the much narrower crack widths in link slabs over bents that supported girders over expansion supports. Therefore, it can be stated that a greater degree of restraint at the bent was noted to affect crack width negatively. The difference between the observed crack width for Bents 15 and 17 in comparison to Bents 13 and 19 may also be attributed to the difference in longitudinal slab reinforcement (#5 bars) configuration (continuous for Bents 15 and 17 and terminated for Bents 13 and 19). However, a clear correlation between the two configurations and crack widths could not be established for the results shown in Figure 54 (b) and the observed crack widths on the western approach spans. Furthermore, there is no incentive to curtail reinforcement at that location were the link slab forces are at their highest.

Crack measurement logs were summarized according to the total crack area for each bent (Table 2), as well as the maximum logged crack width at each bent (Table 3). Crack widths were expected to vary with time as well as the current temperature at the time of measurement due to the movement of the girders connected to the link slabs. All the reported values took place on sunny days during day hours between 12:00 pm and 3:00 pm. It should be noted that some bents could not be logged at certain dates given the fact that the deck had not been poured at that particular date. An increase in total crack area was observed in most cases, with exceptions observed for the final log date at some of the bents with greater age.

Figure 54. Top view of transverse deck cracking at sample link slab locations

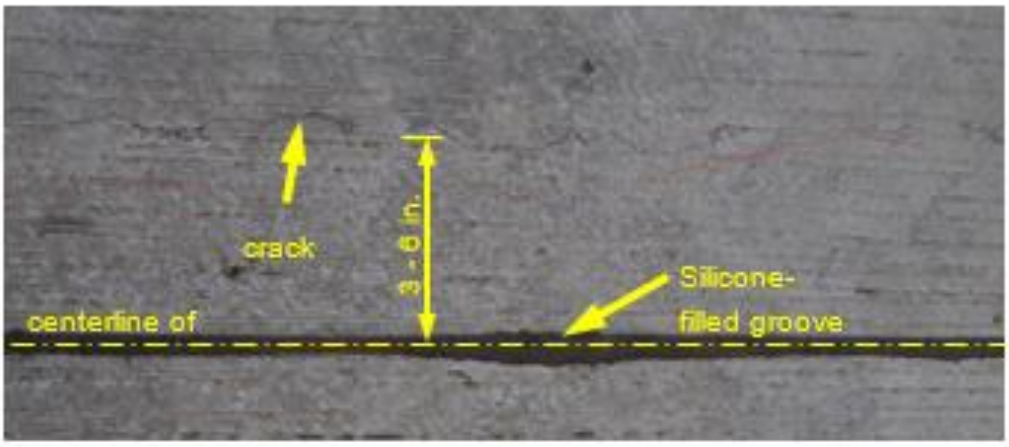

(a) picture of a typical link slab crack location

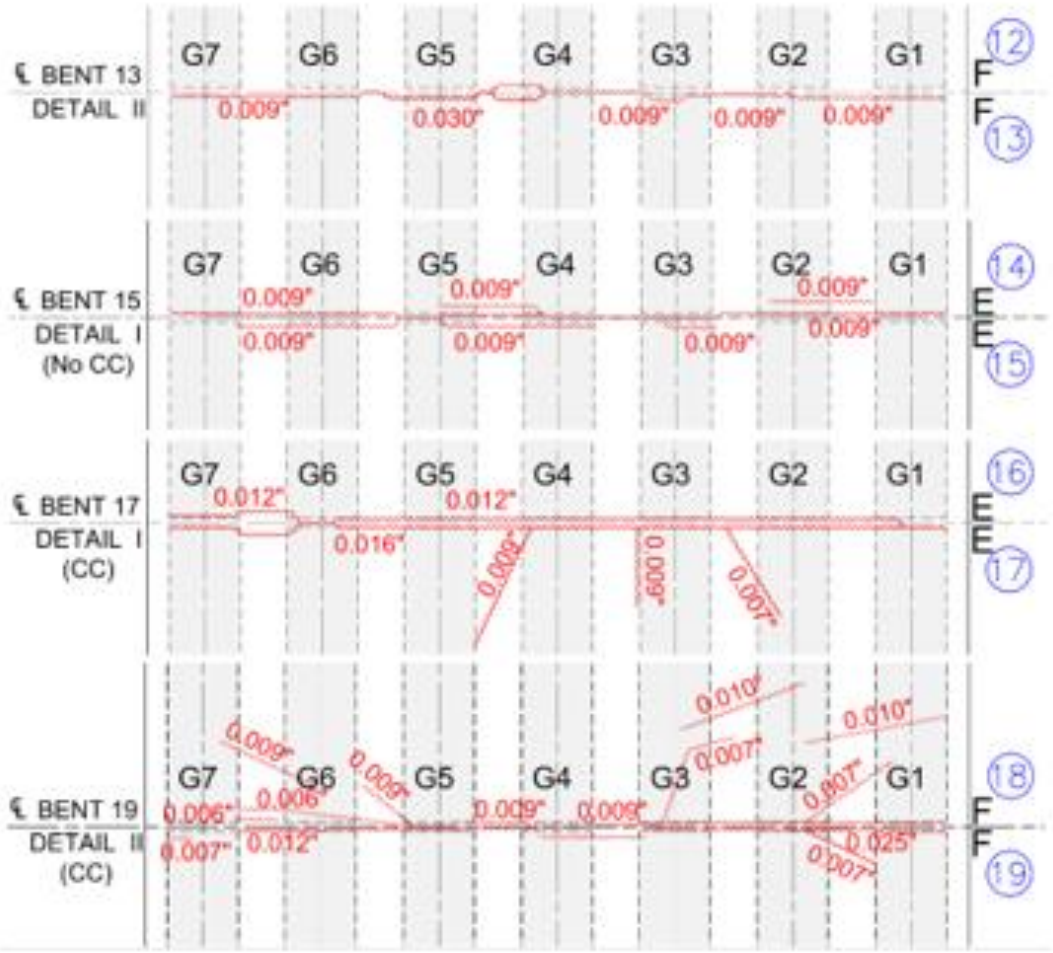

(b) link slab cracks at four bents with different support configurations

Table 2. Total cracking area

Total Crack Area (in^2)				
Bent	3/24/2016	05/18/2016	01/23/2017	05/26/2017
2	2.519	2.519	6.520	5.708
3	10.570	10.570	10.570	13.820
4	9.405	9.405	9.405	9.596
6	10.500	10.500	10.500	7.920
13	--	--	--	6.687
15	--	--	4.752	8.316
17	--	5.040	8.946	16.236
19	--	17.764	17.764	15.168

Table 3. Maximum crack width

Maximum Crack Width (in)				
Bent	3/24/2016	05/18/2016	01/23/2017	05/26/2017
2	0.020	0.020	0.020	0.035
3	0.020	0.020	0.020	0.020
4	0.015	0.015	0.015	0.020
6	0.025	0.025	0.025	0.016
13	--	--	--	0.030
15	--	--	0.009	0.009
17	--	0.009	0.009	0.016
19	--	0.030	0.030	0.030

In the following sections, the results from all approaches described in the Methodology section are discussed. It should be noted that the results presented herein are the key results that are pertinent to the objective of the project.

Thermal Conditions

Temperature readings varied greatly during the day for each of the corresponding sensors. Seasonal temperature changes also had a substantial impact in the measured response in all bents. As temperatures reached their peak or floor values during the corresponding summer and winter seasons, link slab forces, crack widths and girder end movements could be found to respond accordingly. Figure 55 shows the full range of temperature readings for the strandmeter installed on the top reinforcement of the link slab at Bent 2

Girder G7. This temperature pattern generally conformed with that of all other bents and logged sensors. As can be observed from Figure 55, the lowest recorded temperature readings occurred during the winter months, specifically during the month of January.

Figure 55. Full range of temperature readings for the link slab in Bent 2 Girder G7

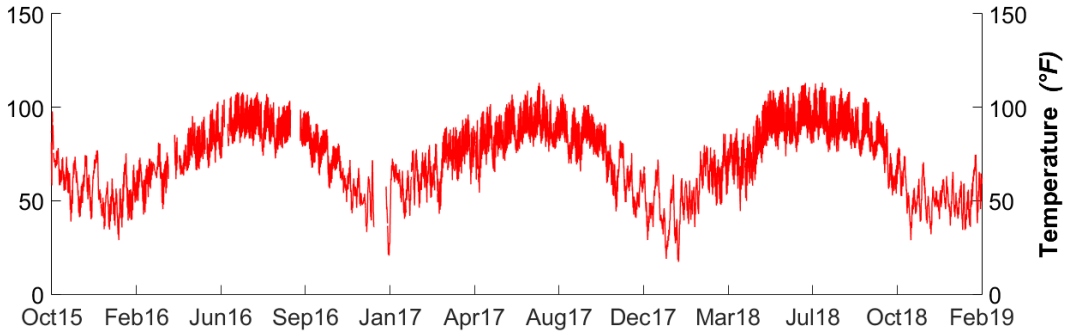

The greatest temperature readings were recorded during the summer months, specifically during the month of August, with temperatures peaking during the day in the afternoon, usually between 2 pm and 4 pm. Figure 56 (a) shows temperature readings over a 48-hour period at the beginning of the month of August 2017. Figure 56 (b) shows temperature readings over a 48-hour period in early January 2018. During the winter months it was found that temperature readings were generally at their lowest during the early hours of the morning between 7 and 9 am, and reaching their highest values any given day during the winter months in the afternoon, between 4 and 6 pm.

Figure 56. Temperature readings over a 48-hour period for the link slab in Bent 3 Girder G7

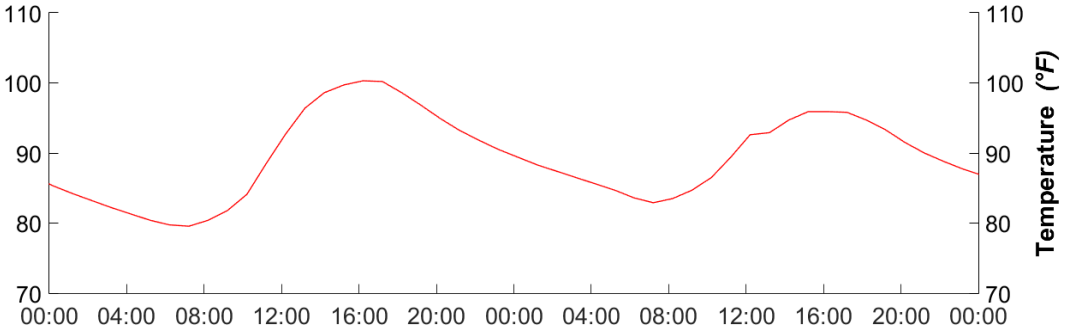

(a) Summer

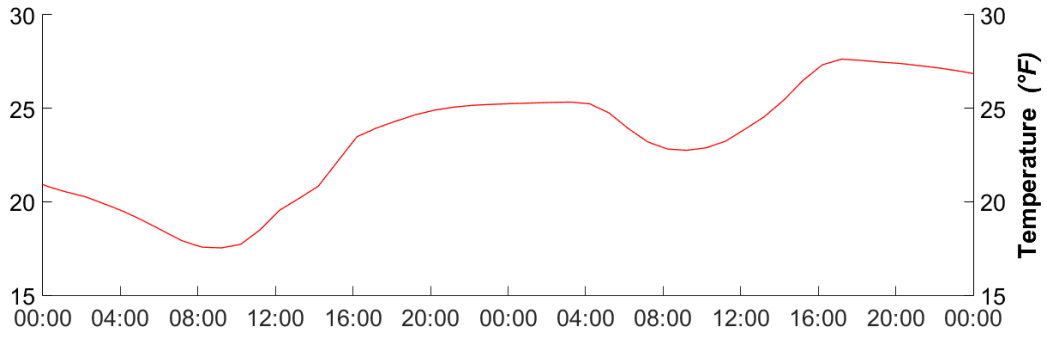

(b) Winter

The difference between temperature readings from the top sensor (strandmeter on the top reinforcement of the link slab) and the bottom sensor (gapmeter between bottom flange and bent cap) was considered a measure of the severity temperature gradient. It was found that the temperature gradient follows a similar trend as was observed in the previously mentioned temperature readings. As can be observed in Figure 57, peak temperature gradient readings were found during the summer in the month of July (with temperature gradients reaching peak values between 10° F and 20° F) and the lowest being negative values found in the month of December, which is an indication of a negative temperature gradients, i.e., causing downward girder camber (recorded during the winter months) with the lowest values occurring most notably during the month of December.

Figure 57. Temperature gradient readings for the link slab in Bent 3 Girder G7

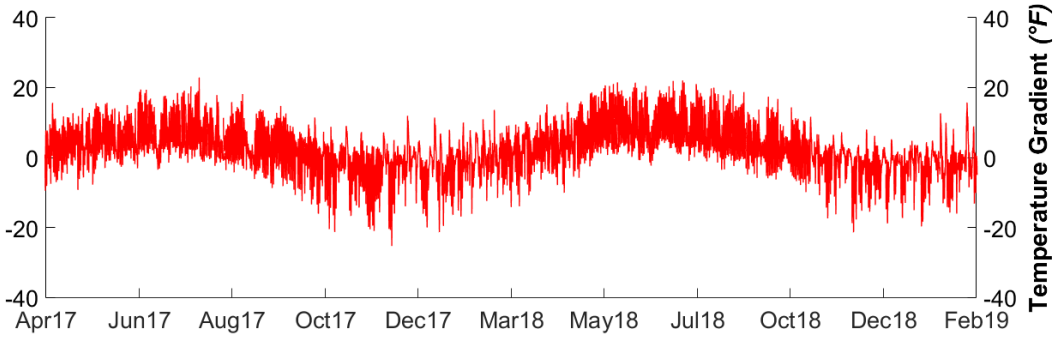

Figure 58 **(**a), in the summer temperature gradient variation during the day generally peaks in the evening, between 4 and 6 pm, with the values generally tapering off after this point. The lowest temperature gradient values in any given day during the summer months generally occurred in the morning hours around 9 am. As can be seen in Figure 58 **(**b), temperature gradient during winter months can fall within negative ranges with

the lowest values being within the range of -10°F and -20°F. The lowest recorded temperature gradient values during the winter months generally occur at midday, and the maximum values during a day range around 0°F in the winter, occurring generally at midnight. As will be seen in later sections, the impact of the temperature gradient as well as uniform temperature could be observed in all the recorded analyses and will be discussed in each respective section.

Figure 58. Temperature gradient readings over a 48-hour period for the link slab in Bent 3 Girder G7

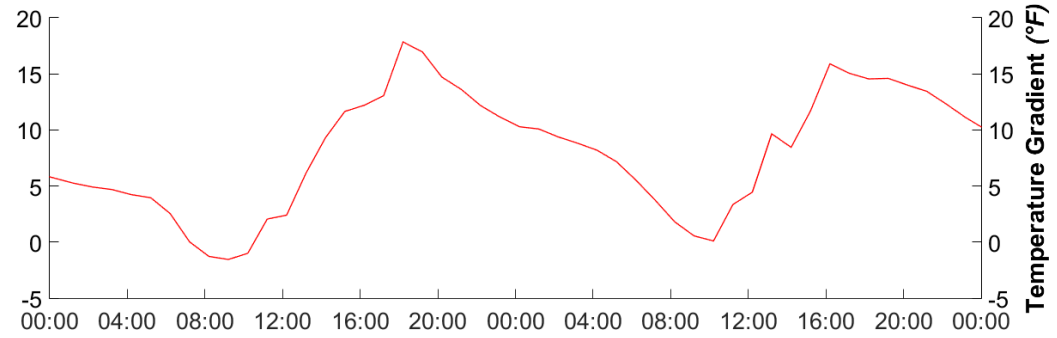

(a) Summer

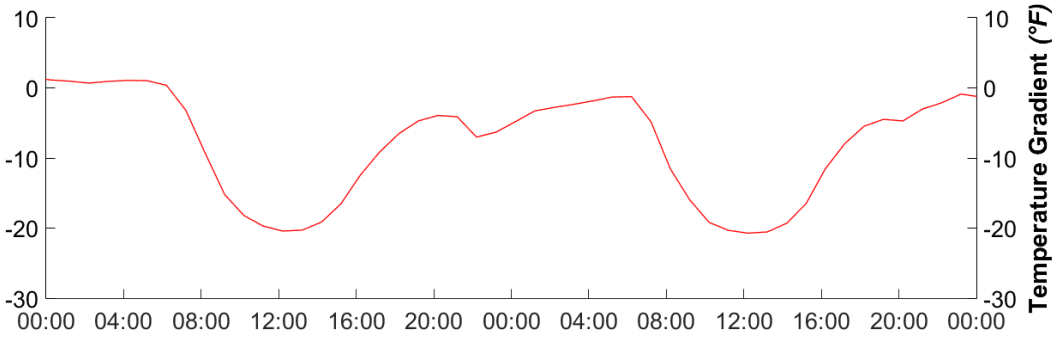

(b) Winter

Girder End Displacement

In the specific spans and segments where sensors were installed between the girders' bottom flanges and their supporting bent caps, girder ends displacement could be measured. As stated earlier, it was found that girder ends respond to temperature changes. Additionally, support conditions and continuity conditions also affected girder end movements. All values of girder end displacements shown in this section have been baselined to a point in time corresponding to the lowest temperature gradient in the

displayed period. To demonstrate the effect of temperature conditions on girder end displacements, a 24-hour period corresponding to August 1, 2017, over Girder G7 is chosen for the plots presented in this section.

When comparing the response within the 4-span segment (Figure 59) and a 2-span segment with similar support conditions (Figure 60) it can be observed that the continuity condition affected the response with large differences in the range of values recorded. As can be observed by comparing Figure 59 and Figure 60, the range of displacements in the 4 span continuous segment were much lower than those recorded within the 2-span segment.

Figure 59. Girder end displacement in Segment A (4-span floating segment) in Girder G7 over a 24-hour period

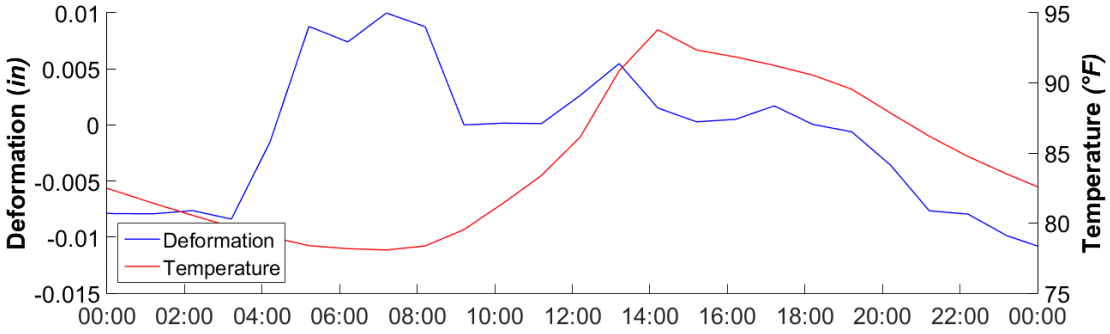

Figure 60. Girder end displacement in Segment B (2-span floating segment) in Girder G7 over a 24-hour period

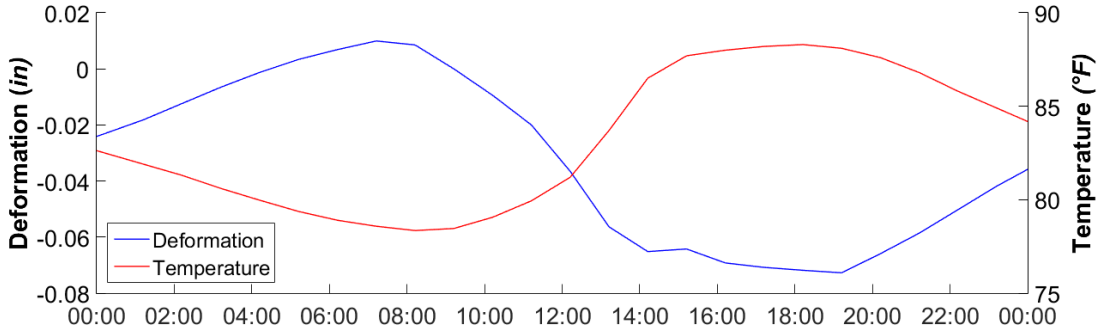

There is also a difference in the nature of the response. A clearer response pattern to temperature variation was observed in the 2-span segment than was observed in the 4-span segment. This difference is likely due to the continuity provided by the additional restraint caused by the existence of link slabs connecting 4 spans in comparison to the

relatively freer to move 2-span segment. It is important to note that the girder end displacement reflects only the sum of the displacements between the girder and the bent cap at the corresponding supports. The displacement at this level will be affected not only by variations in temperature gradient, but also those due to uniform temperature readings.

Figure 61 shows the girder end displacements of the first span in the 4-span segment, Figure 62 shows the girder end displacements of the second span in the same segment. There is an important difference in the response pattern observed, which is likely due to the difference in continuity at each end of the corresponding spans. The first span (Figure 61) has continuity in only one end; whereas, the second span (Figure 62) has a continuity at both ends. The span with the free end (Figure 61) displays much higher girder end displacements than the span with continuity at both ends (Figure 62).

Figure 61. Girder end displacement in Span 1 – Girder G7 – Segment A (4-span floating segment) over a 24-hour period

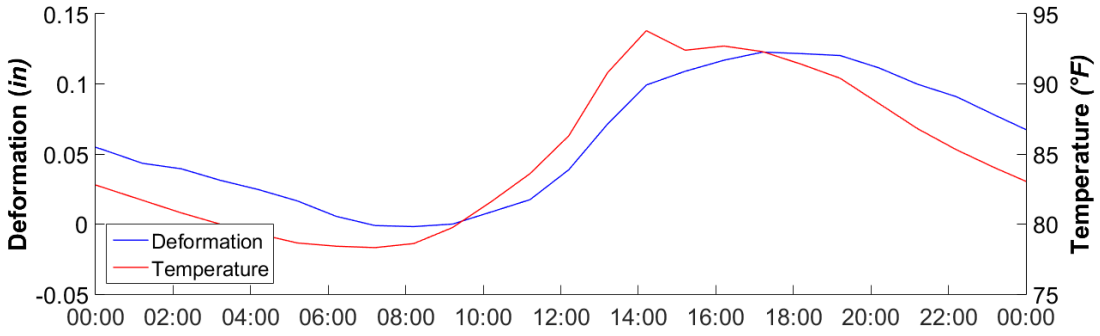

Figure 62. Girder end displacements in Span 2 – Girder G7 – Segment A (4-span floating segment) over a 24-hour period

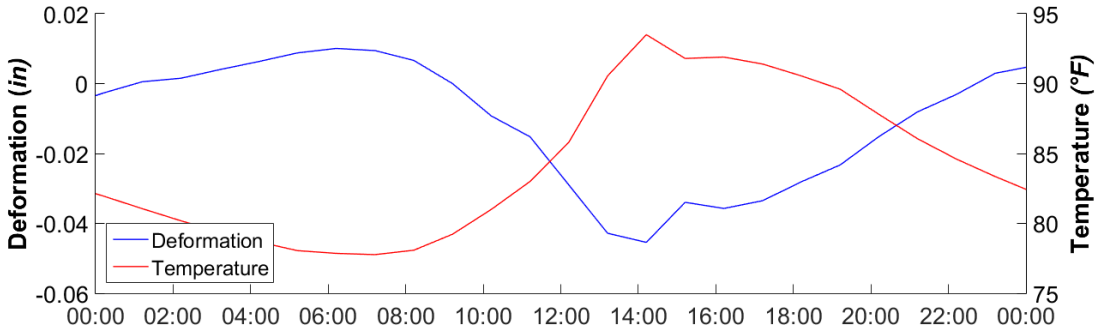

In Figure 63, the girder end displacement for one span of a 2-span segment with floating supports over a 24-hour period is plotted. In Figure 64, the girder end displacement for

one span of a 2-span segment with a fixed support over a 24-hour period is plotted. When comparing the results of Figure 64 to those of Figure 63, it can be seen that the range of displacements was lower, but did not present as dramatic a difference as was observed when comparing two spans in segments with very different continuity conditions such as that which can be observed between Figure 61 and Figure 63.

The fixed support in the 2-span segment whose girder end displacement is shown in Figure 64 is located at the continuity. From the observations in this comparison it can be inferred that a fixed support at the continuity will not affect the overall displacements that can occur at the extremes of the spans that conform the continuous segment as much as added continuity can.

Figure 63. Girder end displacement in Span 16 – Girder G7 –Segment C (2-span floating segment) over a 24-hour period

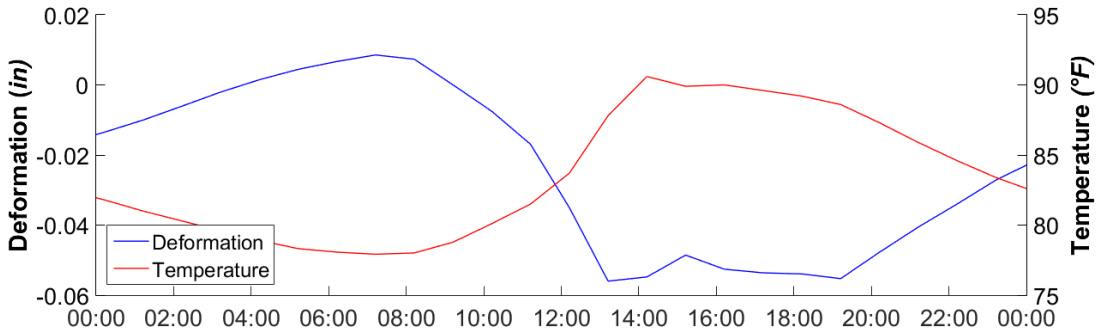

Figure 64. Girder end displacement in Span 19 – Girder G7 – Segment D (2-span fixed segment) over a 24-hour period

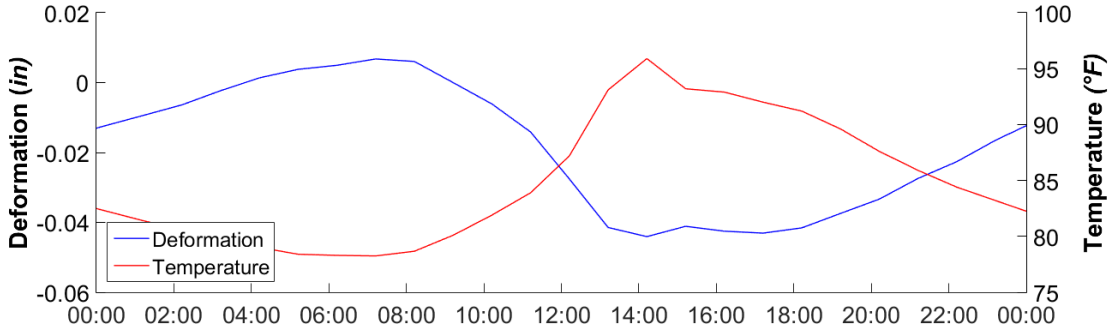

Relative Angle

Similar to how girder end displacements could be determined from the analysis of gapmeter data, this same data can be used to approximate girder end rotations as was discussed in the previous section of this report. Upon close observation of the relative angle's response certain relationships can be identified, which mainly confirm that girder rotations are directly affected by the change in temperature at the bridge site.

When comparing the relative angle at girder ends in the first bent in the 4-span segment, Figure 65, with that from the middle bent in the same segment, Figure 66, very small differences in magnitude can be observed. The relative angle response to the temperature gradient is similar in both cases, staying in phase with the variation of the temperature gradient. The minimum relative angle, or the point when the section is in its most vertical state, coincides with the lowest temperature gradient. Similarly, the highest relative angle coincides with the highest temperature gradient. The comparison of Figure 65 with Figure 67 also shows small variation from a difference in continuity conditions; however, it can be observed that smaller values of relative angle between girder ends can be observed in the bent that is part of the 4-span segment, Figure 65.

Figure 65. Relative angle at girder ends at Bent 2 – Girder G7 – Segment A (4-span floating segment) over a 24-hour period in the summer

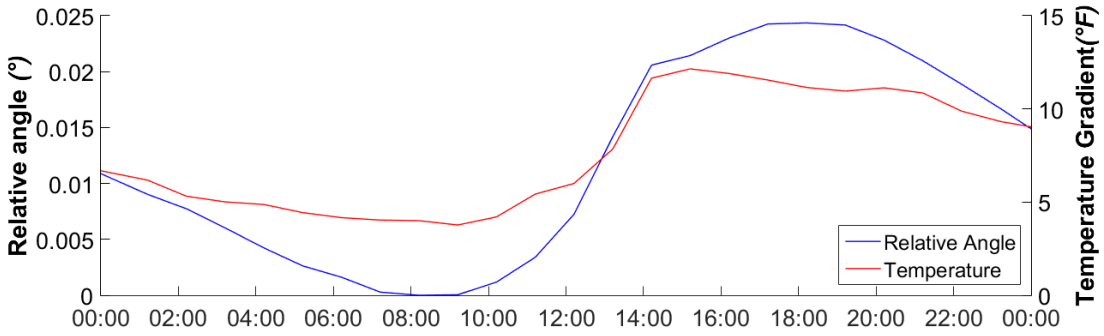

Figure 66. Relative angle at girder ends at Bent 3 – Girder G7 – Segment A (4-span floating segment) over a 24-hour period in the summer

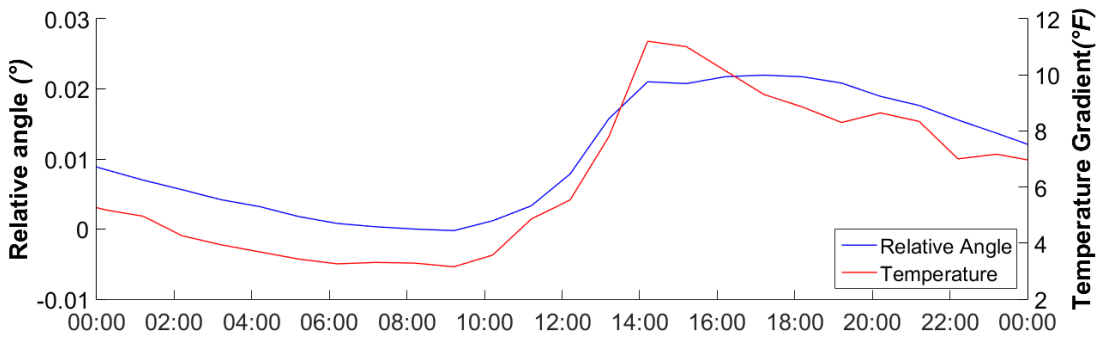

Figure 67. Relative angle at girder ends at Bent 17 – Girder G7 – Segment C (2-span floating segment) over a 24-hour period in the summer

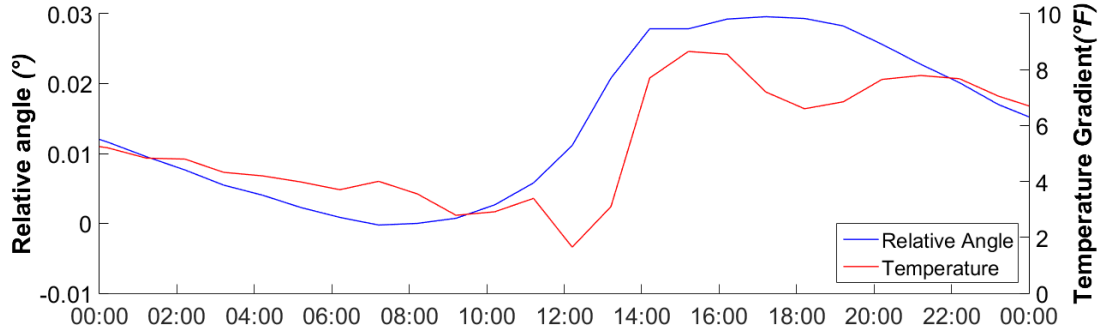

By comparing the results from the winter months (Figure 68 to Figure 70) with the summer months, it can be seen that the magnitude of relative angle has changed. Like in the summer, the relative angle behavior in the winter months is directly affected by changes in the temperature gradient. As before, the same observations can be made with respect to the effect that continuity can have on the relative angle by comparing these plots for winter months. Span segments with higher continuity provide more restriction to girder end rotation.

Figure 68. Relative angle at girder ends at Bent 2 – Girder G7 – Segment A (4-span floating segment) over a 24-hour period in the winter

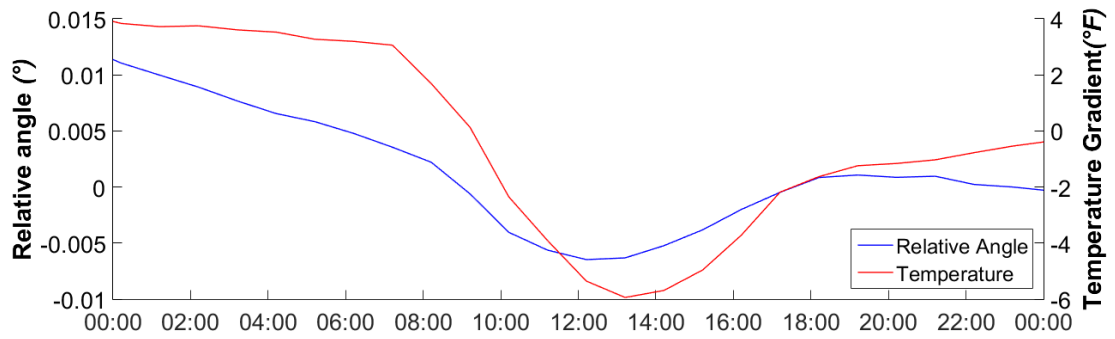

Figure 69. Relative angle at girder ends at Bent 3 – Girder G7 – Segment A (4-span floating segment) over a 24-hour period in the winter

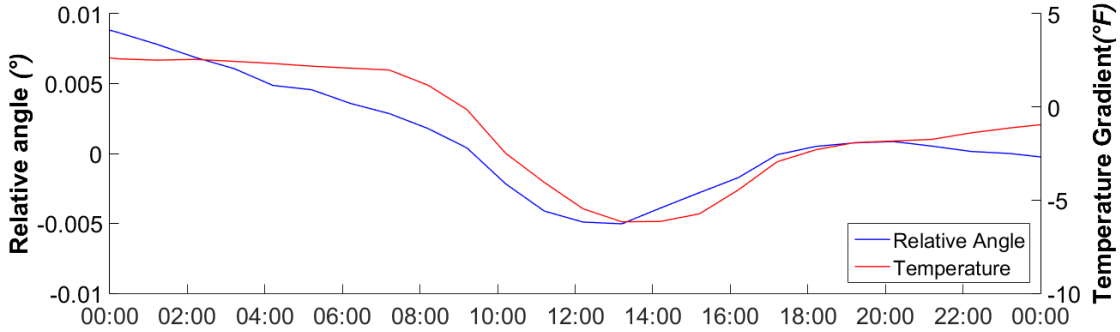

Figure 70. Relative angle at girder ends at Bent 17 – Girder G7 – Segment C (2-span floating segment) over a 24-hour period in the winter

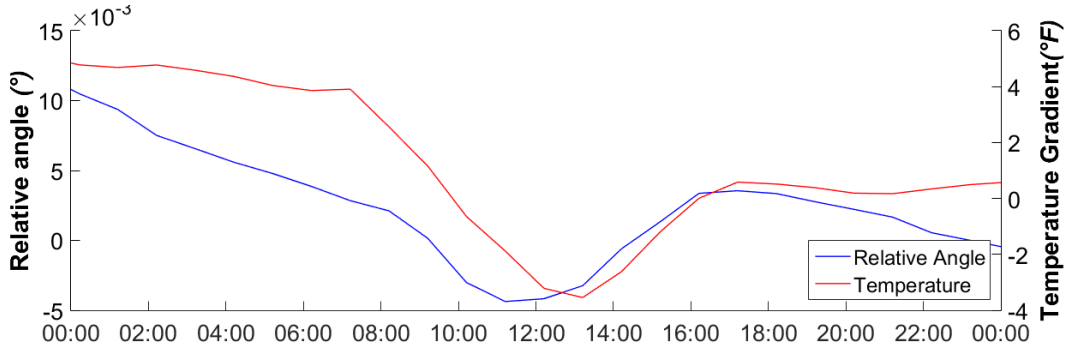

By comparing results from a bent with a fixed support as in Figure 71 with those from an equivalent 2-span segment with floating supports (as in Figure 67), a decrease in relative angle can be observed for the case with the fixed support. A similar relationship can be

observed for temperature gradient profiles during the winter months, as can be appreciated in Figure 70 and Figure 72.

This is due to the fact that providing fixity by anchoring end diaphragms in the supporting bent caps reduces one of the girder's ability to move and rotate. The more restrained girder is the one connected to the anchored end diaphragm. While this may seem like better outcome because of the reduction in movement, it is definitely associated with higher forces in the link slab as was evident by the larger crack widths in link slabs over these fixed supports.

Figure 71. Relative angle at the girder ends in the middle bent in a 2-span segment with a fixed support in Girder G7 over a 24-hour period in the summer

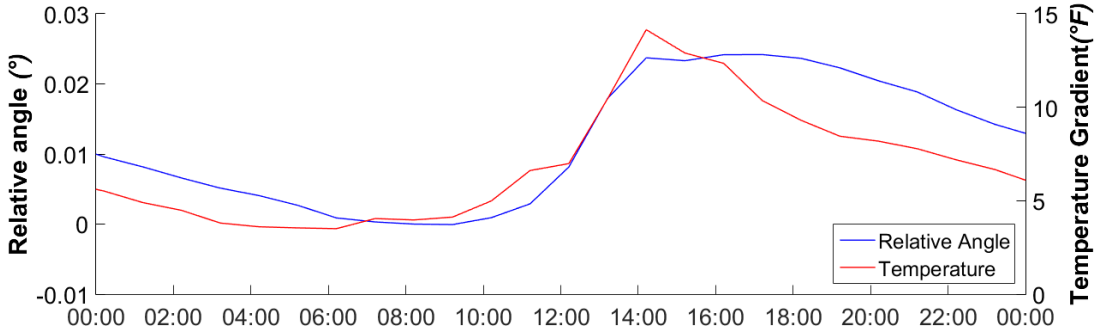

Figure 72. Relative angle at the girder ends in the middle bent in a 2-span segment with a fixed support in Girder G7 over a 24-hour period in the winter

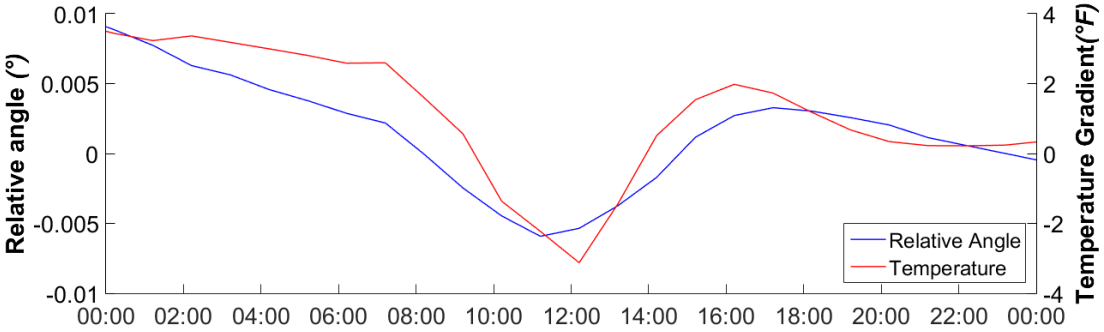

Crack Width

As was discussed earlier, the crack width can have a significant impact on link slab force calculation. Once the link slab has cracked, tension in the concrete can no longer be taken

into account, affecting link slab force calculation in tension. Furthermore, when the crack has formed it must close completely before compression in the concrete can be taken into account. Crack opening and closure occur daily with temperature changes. For these reasons, particular attention was given to crack width calculation. As was discussed in the previous sections, crack width was found to respond closely to variations in temperature, support conditions, as well as continuity conditions. It is important to note that crack widths in all of these figures refer to the cracks on the respective tension face, which will vary between the bottom and top of the slab based on the direction of the girder end rotation.

When comparing crack width calculations at two bents in segments with different continuity conditions (i.e., four spans vs. two spans such as can be observed between Figure 74 and Figure 75), a large difference can be seen in the magnitude of the expected crack width values. The bent with continuity on both sides (Figure 74) can be found to respond with narrower cracks than the segment with less restrained girders because of the lack of continuity beyond the two spans forming the considered segment (Figure 75).

Figure 73 and Figure 75 show crack width calculations at bents in spans with similar conditions at their individual ends but very different continuity conditions in their respective segments. Figure 73 refers to the first bent in a 4-span segment, and Figure 75 refers to the bent in a 2-span segment. The additional continuity from the 4-span segment affects the expected crack width displayed in Figure 73. By comparison, the reduced continuity from the 2-span segment in Figure 75 allows for wider cracks to form.

Figure 73. Crack width at Bent 2 – Girder G7 – Segment A (4-span floating segment) over a 24-hour period in the summer

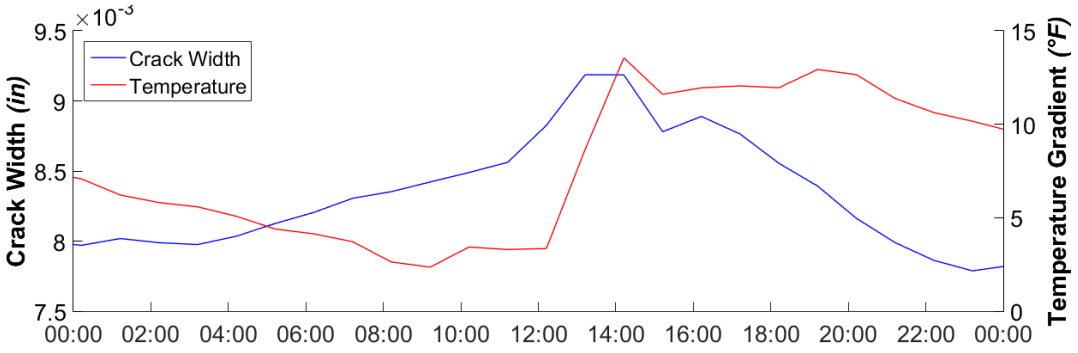

Figure 74. Crack width at Bent 3 – Girder G7 – Segment A (4-span floating segment) over a 24-hour period in the summer

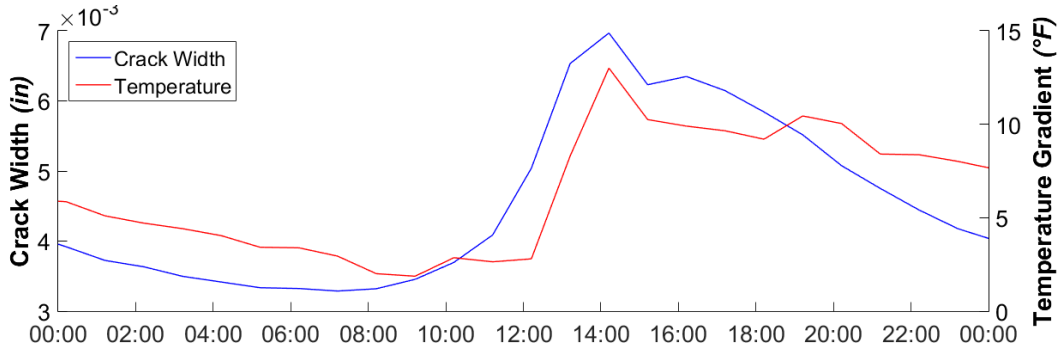

Figure 75. Crack width at Bent 17 – Girder G7 – Segment C (2-span floating segment) over a 24-hour period in the summer

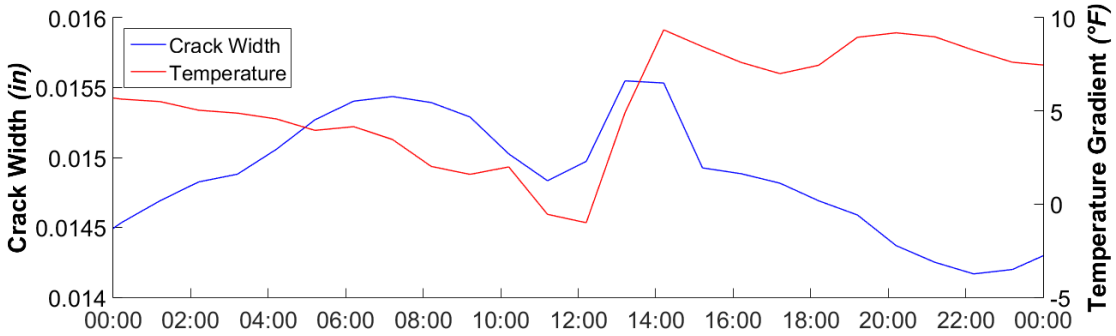

Similar to observation over summer, crack width response is directly affected by temperature variations during winter as well, albeit under a different response pattern. When observing the daily cracking fluctuations, it can be seen that a lower temperature gradient in the winter corresponds to a wider crack; whereas, in the summer, a lower temperature gradient corresponds to a narrower crack. This difference is likely due to the fact that the cracking is occurring in different faces of the slab in both seasons. During winter months, the temperature gradient profile tends to be negative for Girder G7. As a result, girders camber downward causing the link slab to be subjected to subjected negative moments, i.e., tensioned face of the link slab is likely to be the top. Conversely, the temperature gradient profile tends to be positive during the summer leading to upward girder camber, which subjects the link slab to positive moment, i.e., tensioned face of the slab is likely to be the bottom one. The observed crack widths are also affected by continuity conditions and restraints surrounding the link slab in question in the same way during both seasons.

When comparing two bents within a four-span segment, one with one free end and one continuous end (Figure 76) and one with both ends continuous (Figure 77), larger cracks are observed in the least restricted bent. Similarly, when comparing the middle bent from a 4-span segment (Figure 77) and the middle bent in a 2-span segment (Figure 78), a similar relationship can be identified, with larger cracks occurring in the 2-span segment.

Figure 76. Crack width at Bent 2 – Girder G7 – Segment A (4-span floating) over a 24-hour period in the winter

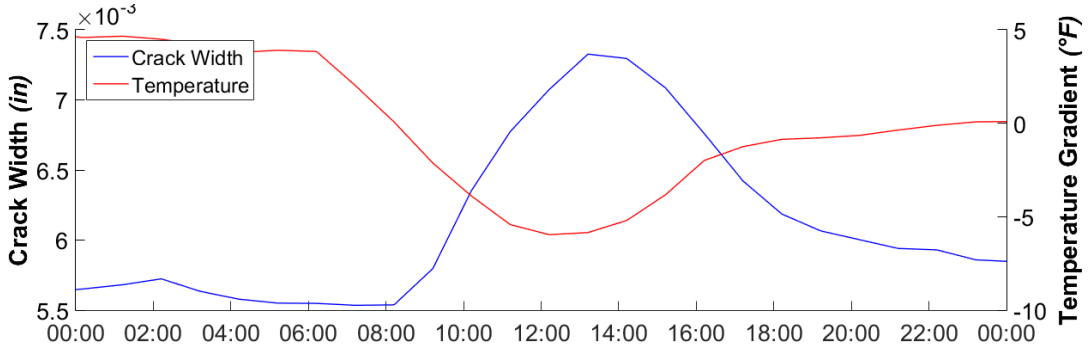

Figure 77. Crack width at Bent 3 – Girder G7 – Segment A (4-span floating) over a 24-hour period in the winter

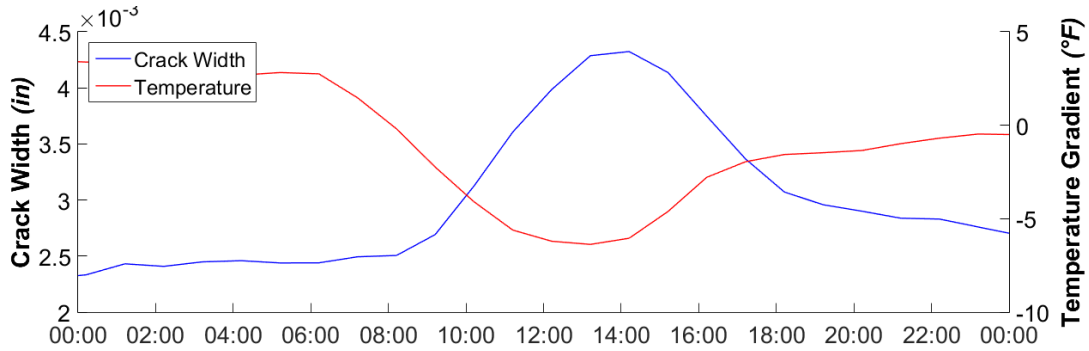

Figure 78. Crack width at Bent 17 – Girder G7 – Segment C (2-span floating segment) over a 24-hour period in the winter

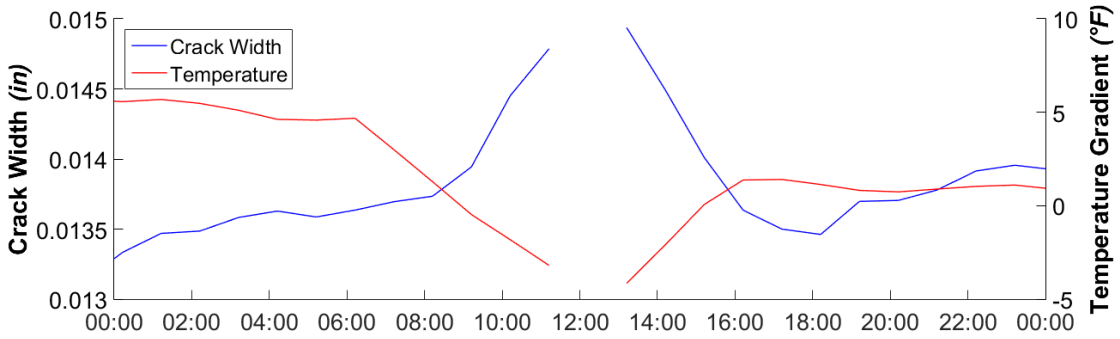

By comparing Figure 75 with Figure 79, it is possible to see the effect that a fixed support condition can have on cracking in the summer. The cracking is wider in the bent with the fixed support condition. This could likely be attributed to the increase in stiffness at the joint from the diaphragm in the fixed support. An increase in the stiffness at the joint would increase stress levels and produce wider cracks on the slab. The effect is also present in the winter, as can be observed by comparing Figure 78 with Figure 80.

Figure 79. Crack width at Bent 19 – Girder G7 – Segment D (2-span fixed segment) over a 24-hour period in the summer

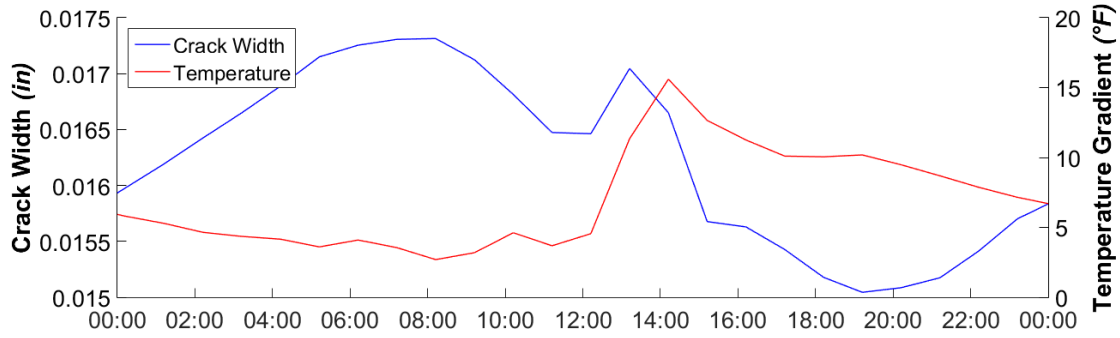

Figure 80. Crack width at Bent 19 – Girder G7 – Segement D (2-span fixed segment) over a 24-hour period in the winter

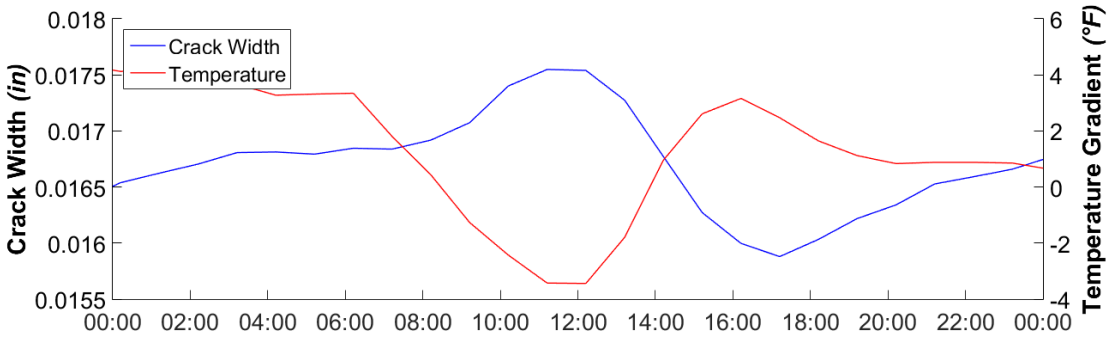

From the observations in this research, an increase to support stiffness will likely widen the cracks in the corresponding bent by concentrating stresses around the joint. Conversely, an increase in continuity reduces the possibility for cracking as more restrictions exist for the crack to open. In terms of temperature, it is clear that in all the cases crack formation responds very closely to temperature gradient.

Forces in the Link Slab

Internal Link Slab Force Components

Forces in the link slab were estimated using crack width information based on the approach described in the previous chapter for the different cross-sectional states illustrated in Figure 34. By obtaining the strains in the corresponding steel and forming a compatibility condition it becomes possible to determine the stress state in the link slab cross section, which can be converted into the respective forces. It should be noted that like in the previous section, all diagrams in this section were obtained by baselining the results to the lowest temperature gradient within the graphed period. In this manner, the values that are displayed represent the force variations that take place within that period.

Figure 81 and Figure 82 represent the first and middle bents respectively within the 4-span segment. By comparing these two figures, it is possible to see that both are responding with tension on the same face, the bottom one, with larger forces appearing in the middle bent. In this regard it can be appreciated that the increased restraint to the middle bent (Figure 82) is resulting in the concentration of higher forces than those in the bent with one continuous end on only one side (Figure 81). The same behavior is observed when comparing Figure 81 with Figure 83. Figure 81 shows a plot of the forces

in the link slab at the bent between a span with a free end and another with a continuous end within a 4-span segment. Similarly, Figure 83 represents the bent at the continuous end of a span with both a free end and a continuous end, but within a 2-span segment. In this comparison, it is possible to observe that the bent in the 4-span segment is receiving larger forces than the bent in the 2-span segment; sustaining the notion that greater continuity increases restraint, and therefore greater forces develop in the link slab. Though the forces in the steel indicate that the tensioned face of the slab remains the same, the main difference is that the neutral axis has moved downward in the 2-span segment resulting in a greater range of compression forces in the top steel. The movement of the neutral axis helps explain why despite seeing greater forces in the 2-span segment narrower cracking were observed.

Figure 81. Forces in the link slab at Bent 2 – Girder G7 – Segment A (4-span floating segment) over a 24-hour period in the summer

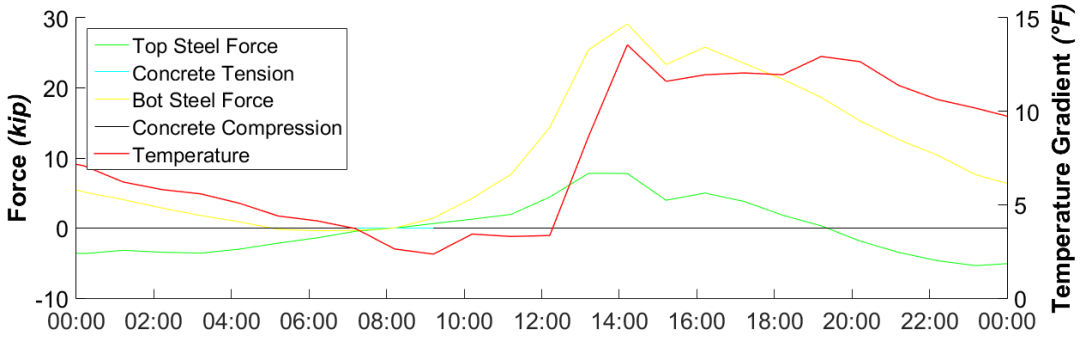

Figure 82. Forces in the link slab at Bent 3 – Girder G7 – Segment A (4-span floating segment) over a 24-hour period in the summer

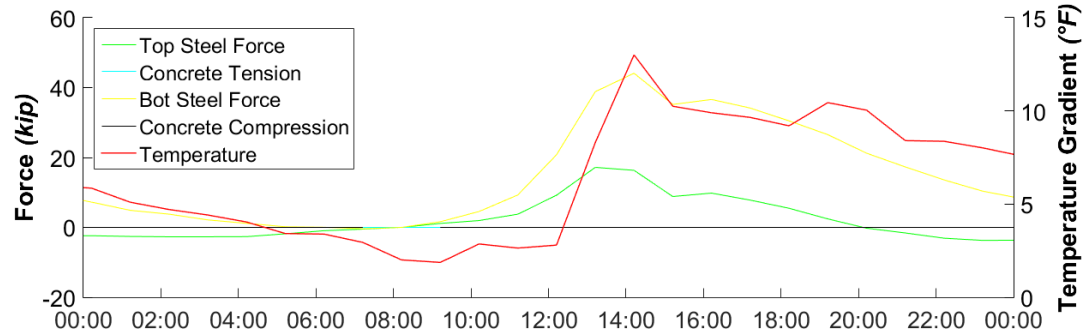

Figure 83. Forces in the link slab at Bent 17 – Girder G7 – Segment C (2-span floating segment) over a 24-hour period in the summer

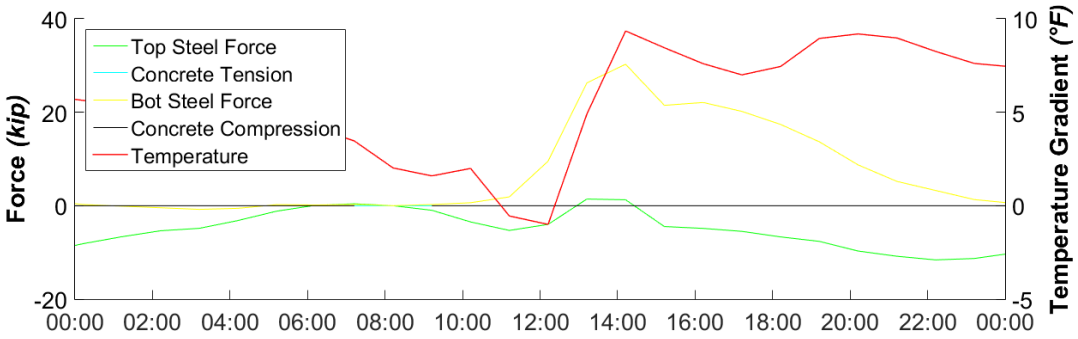

When comparing the results obtained for these same bents in the winter, it can be observed that the tension face has shifted to the top. Consequently, cracks are reversed with the largest crack width being at the top face of the slab, with the top steel having greater tension forces. Figure 84 shows the internal forces for a link slab at a bent between one span with a free end and one with continuous end, and Figure 85 shows the same values a link slab at a bent between two spans with continuous ends. Similar to what has been observed previously, comparing these two figures, it can be observed that the link slab adjacent to the span with the higher restraint (Figure 85) is also the link slab receiving the higher total force in the link slab, which is the summation of all internal forces. In this case, the concrete contribution to the link slab force is negligible and the top and bottom steel are the only parts resisting the applied force.

A comparison between the plots in Figure 84, representing a bent in a 4-span segment, and Figure 86, representing a bent in a 2-span segment furthers the notion of higher continuity leads to higher link slab forces as can be seen for the case of the link slab over the bent in the 4-span segment, Figure 84.

Figure 84. Forces in the link slab at Bent 2 – Girder G7 – Segment A (4-span floating segment) over a 24-hour period in the winter

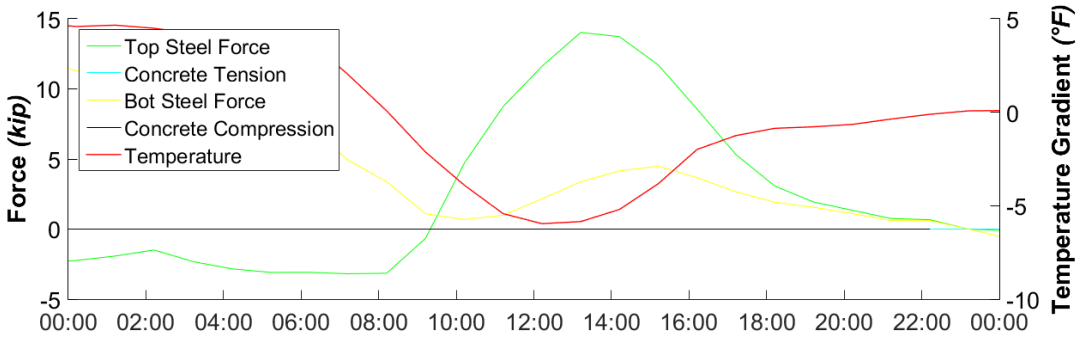

Figure 85. Forces in the link slab at Bent 3 – Girder G7 – Segment A (4-span floating segment) over a 24-hour period in the winter

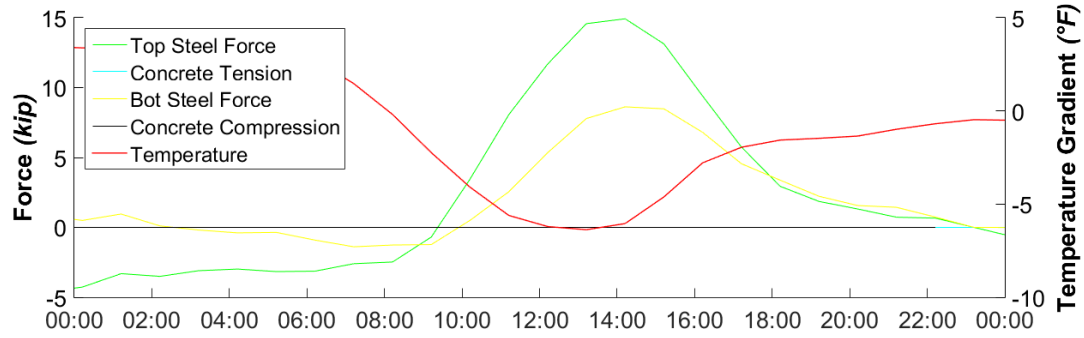

Figure 86. Forces in the link slab at Bent 17 – Girder G7 – Segment C (2-span floating segment) over a 24-hour period in the winter

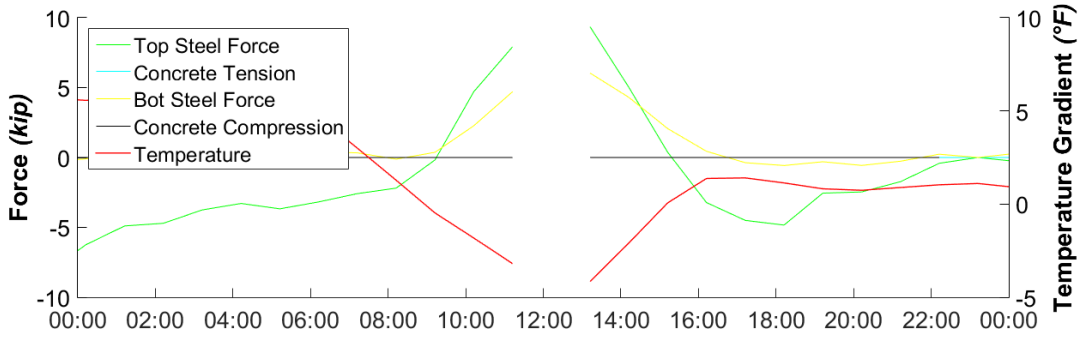

By comparing Figure 83, a link slab within a 2-span segment with floating supports, and Figure 87 for a link slab within a 2-span segment with a fixed support, it is possible to see that the latter is subjected to compressive forces. This implies that the tension face in the bent with the fixed support is opposite to the tension face in the bent with the floating

support. This behavior may be due to the additional stiffness and restraint provided by the anchored end diaphragm.

A similar behavior is observed during winter months. Figure 86 and Figure 88 show the internal forces for the same bents whose behavior during summer months was discussed earlier. In this case, the forces are similar for both support conditions, which suggests that there is a greater restriction in the floating support than is being assumed.

This notion is sustained by the verification done in STAAD. In order to obtain results that were compatible with the results obtained directly from the sensors, support stiffness had to be increased substantially in the STAAD model. This additional restriction could be coming from a point of contact or friction with the support. It should also be noted that this can also explain why there are higher tension forces in Figure 83 than in Figure 87.

Figure 87. Forces in the link slab at Bent 19 – Girder G7 – Segment D (2-span fixed segment) over a 24-hour period in the summer

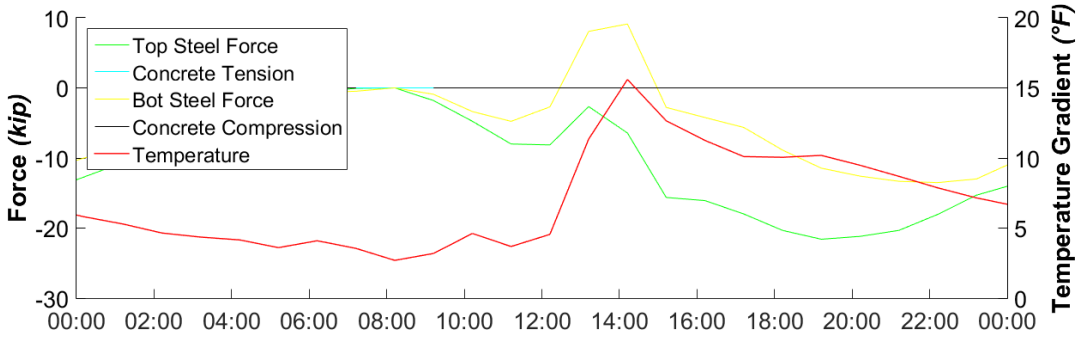

Figure 88. Forces in the link slab at Bent 19 – Girder G7 – Segment D (2-span fixed segment) over a 24-hour period in the winter

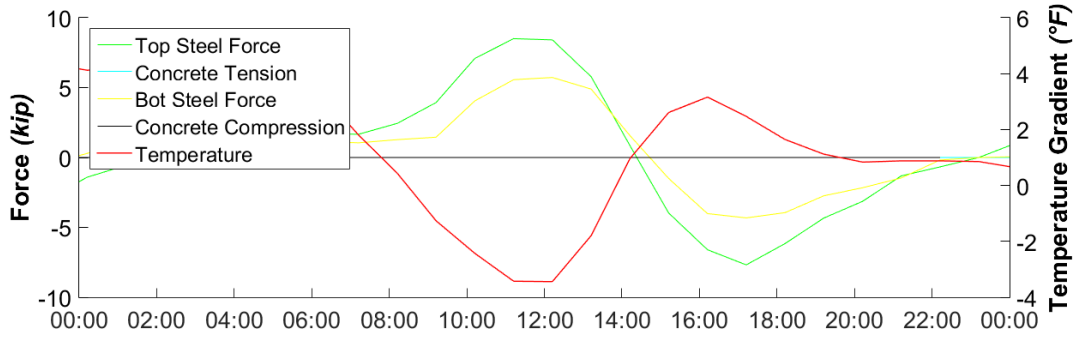

Total Link Slab Force

The total force in the link slab was obtained by algebraically summing the internal forces in the link slab taking into account the effects of cracking. As in the previous section, all the plots in this section are based on sensor data that was baselined to the point with the lowest temperature gradient within the specified period. This implies that the results for link slab force that are obtained represent the link slab force variation that takes place during a 24-hour period due to temperature gradient variations.

The magnitude of the total link slab force reinforced the observations of the previous section. Increased continuity results in higher forces and response to temperature gradient changes remains evident. Figure 89 represents a link slab with less continuity than the one represented in Figure 90 and therefore is subjected to smaller total link slab force. Similarly, Figure 89 and Figure 91 reveal that the latter, which represents the link slab with the least continuity, is subjected to lower force values.

Figure 89. Link slab force at Bent 2 – Girder G7 – Segment A (4-span floating segment) over a 24-hour period in the summer

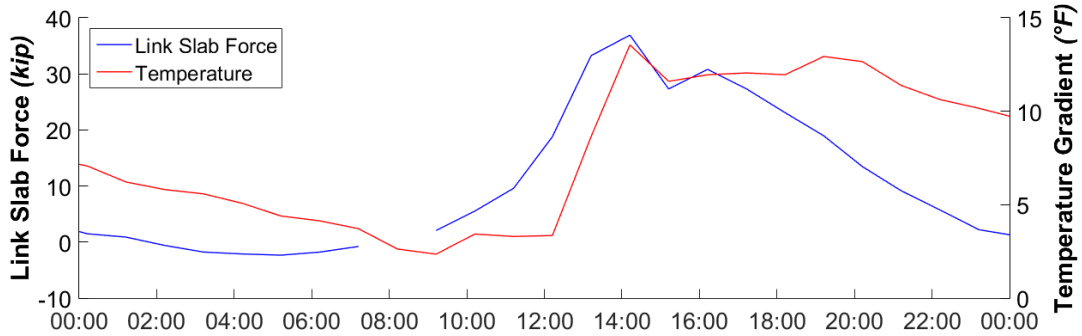

Figure 90. Link slab force at Bent 3 – Girder G7 – Segment A (4-span floating segment) over a 24-hour period in the summer

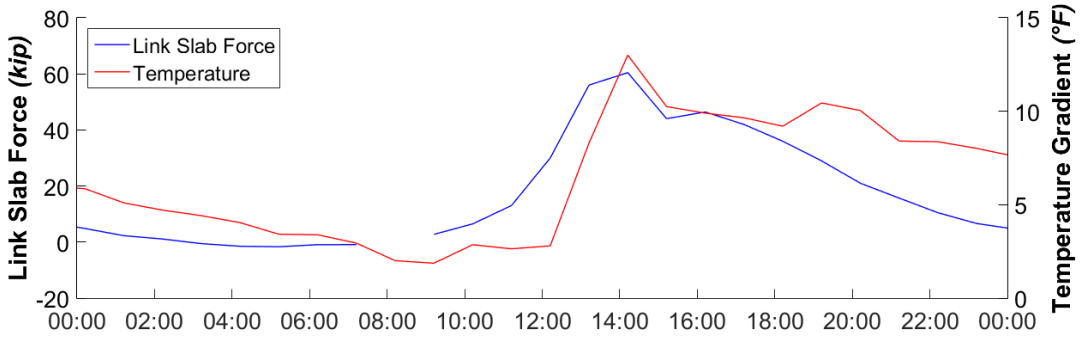

Figure 91. Link slab force at Bent 17 – Girder G7 – Segment C (2-span floating segment) over a 24-hour period in the summer

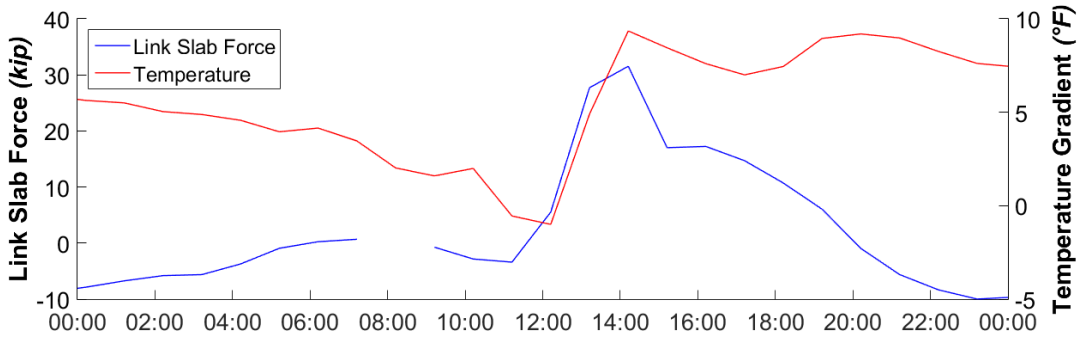

The winter data reinforces all the observations that have been made for summer months behavior. The tensioned face being reversed implies a response that looks different than that of the summer months. By comparing bents with varying degrees of continuity, it becomes evident that greater continuity implies greater forces, which can be seen by comparing the plots in Figure 92 through Figure 94.

Figure 92. Link slab force at Bent 2 – Girder G7 – Segment A (4-span floating segment) over a 24-hour period in the winter

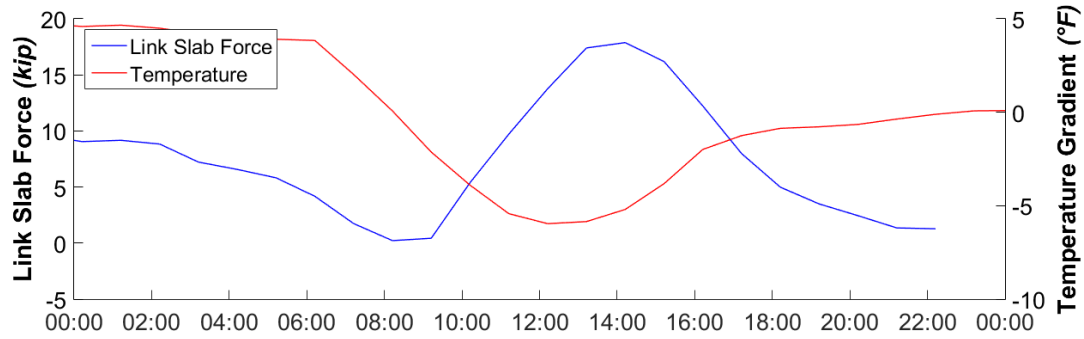

Figure 93. Link slab force at Bent 3 – Girder G7 – Segment A (4-span floating segment) over a 24-hour period in the winter

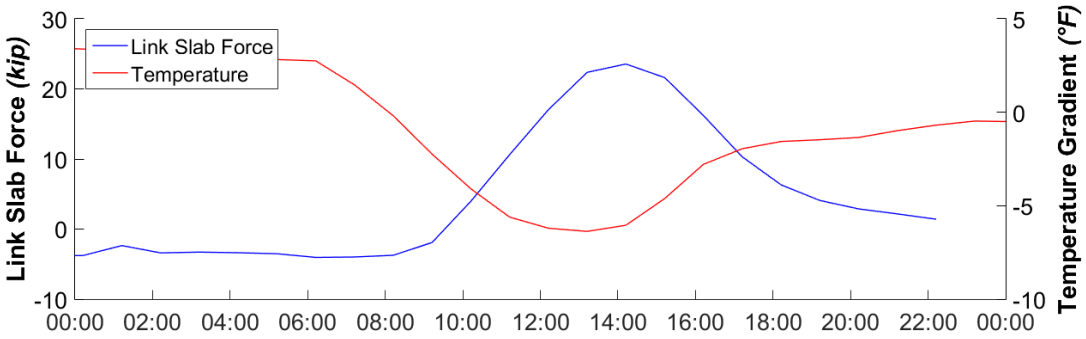

Figure 94. Link slab force at Bent 17 – Girder G7 – Segment C (2-span floating segment) over a 24-hour period in the winter

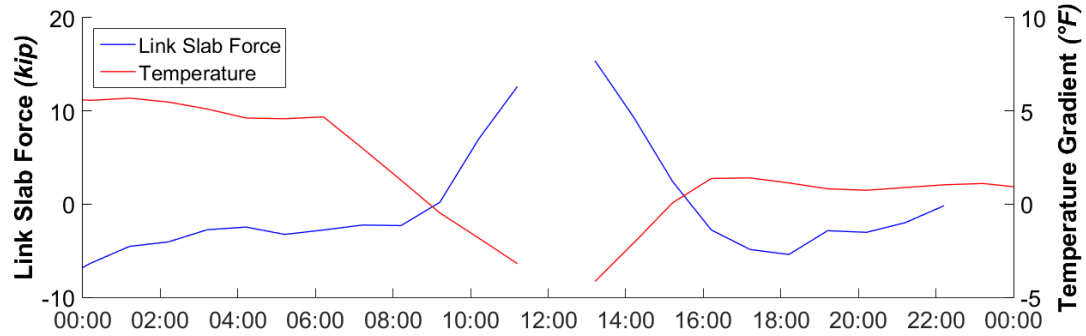

Accordingly, an increase in support restraint also results in higher forces. This can be observed from the comparison of the final two plots shown in Figure 95 and Figure 96 with the previous figures.

Figure 95. Link slab force at the center bent in a 2-span segment with a fixed support at Girder G7 over a 24-hour period in the summer

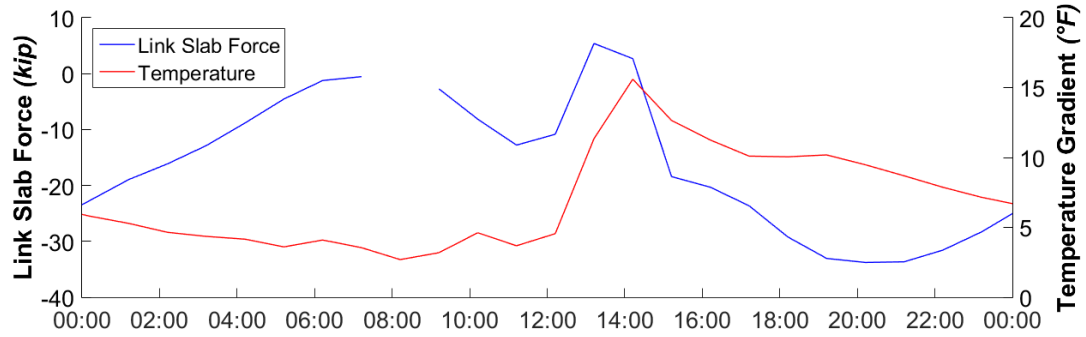

Figure 96. Link slab force at the center bent in a 2-span segment with a fixed support at Girder G7 over a 24-hour period in the winter.

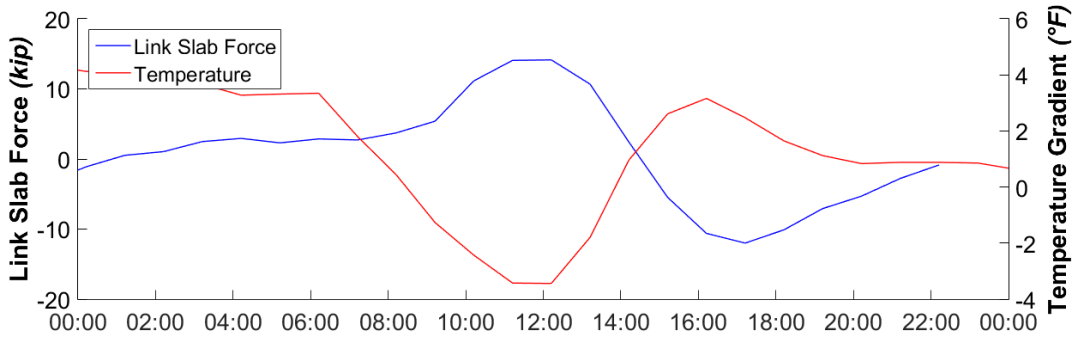

Conclusions

The conclusions from this study can be summarized as follows:

Girder End Displacement

Increasing the continuity of a segment will introduce additional restraint to displacement and deformation of girder ends in a similar way as support conditions. From the observations in this study, it was found that recorded girder end displacement values saw a greater effect from a change in continuity conditions than with a change in support conditions. As continuity increases, girder end displacement values become smaller. Most of the girder end displacement that will be taking place will be due to changes from temperature.

Crack Width

An increase in the restraint by support conditions results in an increase of crack widths on the tensioned face of the link slab. When comparing the crack widths that formed in bents with a fixed support condition, and those with expansion supports, greater crack widths were concentrated around those with a fixed support condition, this was observed both from visual inspections, as well as the analysis drawn from gapmeter measurements.

On the other hand, link slabs in the 4-span segment saw a decrease in crack width formation when compared to the bents in 2-span segments. Spans that formed part of a system with greater continuity saw less crack width formation than those with less continuity. This is probably because as the continuity increases stress will have more places to distribute to, with less continuity stress will concentrate in fewer places and therefore can cause wider cracks.

Crack width formation is affected directly by temperature gradient variations on a daily basis.

Link Slab Force

Recorded tension forces in the link slabs over expansion supports are, in many cases, greater than the bearing support can theoretically account for on its own resistance. This

indicates that there is an additional restriction at the girder end. This could be due to friction between the shear keys and the girder bottom flanges they surround due to debris accumulation in the gap between them. This was observed from the values of tension that can develop on the link slab, as well as by comparison with the STAAD model. In order for displacements in the STAAD model to match displacements recorded on the sensors, support conditions in the model had to be increased substantially.

Higher support restraint leads to greater link slab forces. As support conditions allow girder ends to rotate more freely, stresses in the link slab are relieved. As support conditions become more restrictive to girder end movements, forces in the link slab increase.

Relative Angle

The minimum relative angle, or the point when the girders are in their most vertical state; i.e., minimal girder end rotations, coincides with the lowest temperature gradient. Similarly, the highest recorded relative angle at the girder ends coincided with the highest temperature gradient, showing that temperature gradient is the most dominant factor of girder end rotation.

The relative angle was not greatly affected by a change in the continuity conditions, however the small changes that took place showed that as the continuity condition increased, the girder end rotation decreased.

Temperature

Every recorded and analyzed value from the collected data showed a clear influence from temperature changes on the recorded sensors' readings. Though temperature changes in both uniform and gradient form affected every measured value, the response seemed to be more closely matched with changes in the temperature gradient throughout the day.

Seasonal effects to temperature ranges caused changes in the stresses the link slabs are subjected to. Due to its particular temperature gradient, girder end rotations in the winter can be inverted when compared to from the summer, this was reflected in the forces that develop within the link slab, as well as the nature and position of the cracking.

Recommendations

Based on the findings of this project, the research team recommends the adoption of the link slab detail in construction of jointless bridge decks in Louisiana. Link slabs reduce the need for costly expansion joints (construction and maintenance). Link slab details are also easier to construct in comparison with full positive moment continuity details recommended in NCHRP Report 519. Furthermore, full continuity details attract large continuity moments, which have been observed (Project 08-1ST and Project 12-1ST) to cause girder end cracking.

Special consideration shall be given to support conditions in segments employing the link slab detail. The results presented in this report show that additional restraint to girder end movements leads to larger link slab forces and crack widths. It is not recommended that anchored end diaphragms be used with the link slab detail, which led to the largest observed crack widths and link slab forces. Furthermore, the use of shear keys can lead to unintentional restraint to girder end movement if it does not allow for longitudinal movement due to debris accumulation in the gap between the girder bottom flange and the surrounding shear key.

The link slab reinforcement used in the Ouachita River Bridge Project appears to be adequate and produce an acceptable link slab behavior. Regular inspection of the observed crack propagation and development are recommended to assess the adequacy of the link slab reinforcement over a longer time in service. Additional investigations are also needed to determine the maximum length that should be allowed for segments employing the link slab detail and the effect of braking forces on bearing pad movements in floating span configurations.

Acronyms, Abbreviations, and Symbols

Term	Description
DOTD	Louisiana Department of Transportation and Development
FHWA	Federal Highway Administration
ft.	foot (feet)
in.	inch(es)
LTRC	Louisiana Transportation Research Center
lb.	pound(s)
$b_{(y)}$	net section width at height y
d_c	concrete cover for the reinforcing steel
E_c	modulus of elasticity of concrete
f_s	service stress in the reinforcing steel
I	girder moment of inertia
n	distance between the neutral axis and the arbitrary datum
s	bar spacing
y	height at which the net section width is considered
w_{max}	maximum crack width
α_c	thermal expansion coefficient of concrete
Δ_{beg}	deformation recorded at beginning of span/segment
Δ	cumulative deformation recorded for a span/segment
Δ_{end}	deformation recorded at end of span/segment
$\theta_{(y)}$	temperature change
ψ	girder curvature

References

[1] Chang, L.-M. and Lee, Y.-J. "Evaluation of Performance of Bridge Deck Expansion Joints." *Journal of Performance of Constructed Facilities,* Vol. 16, No. 1, 2002, p. 3.

[2] Fincher, H. E. "Evaluation of Rubber Expansion Joints for Bridges." Report No. FHWA/IN/RTC-83/1, Washington, D.C., 1983.

[3] Federal Highway Administration. National Bridge Inventory (NBI). U.S. Department of Transportation. https://www.fhwa.dot.gov/bridge/nbi.cfm. Accessed 02/14/2019.

[4] LADOTD. Bridge Design Manual. Bridge Design Section, State of Louisiana, Department Of Transportation And Development, Baton Rouge, Louisiana, 2005.

[5] Saber, A., Roberts, F. L., Alaywan, W., and Toups, J. "Effectiveness of Continuity Diaphragm for Skewed Continuous Prestressed Concrete Girder Bridges." *PCI Journal*, Vol. 52, No. 2, 2007.

[6] Au, A. and Lam, C. "*Displacement Compatibility in Debonded Link Slab Design.*" Report No., Ontario, 2011

[7] Saber, A. and Aleti, A. R. "Behavior of FRP Link Slabs in Jointless Bridge Decks." *Advances in Civil Engineering*, 2012.

[8] Miller, R. A., Castrodale, R., Mirmiran, A., and Hastak, M. "Connection of Simple-Span Precast Concrete Girders for Continuity." NCHRP Report 519, Washington, D.C., 2004.

[9] Okeil, A. M. and El-Safty, A. K. "Partial Continuity in Bridge Girders with Jointless Decks." *Practice Periodical on Structural Design and Construction*, Vol. 10, No. 4, 2005, pp. 229-238.

[10] El-Safty, A. and Okeil, A. M. "Extending the Service Life of Bridges Using Continuous Decks." *PCI Journal*, Vol. 53, No. 6, 2008, pp. 96-111.

[11] Okeil, A. M. and Cai, S. C. S. "*A Monitoring System for Long-Term Performance of Positive Moment Continuity Detail in Prestressed Girder Bridges*." 88th Annual Meeting of the Transportation Research Board, National Academies, 2009.

[12] Louisiana Department of Transportation and Development, Bridge Design Section. *Bridge Design Manual*, Baton Rouge, LA, 2005.

[13] Okeil, A., Hossain, T., and Cai, C. S. "Field Monitoring of Positive Moment Continuity Detail in a Skewed Prestressed Concrete Bulb-Tee Girder Bridge." *PCI Journal*, 2013, pp. 80-90.

[14] Hossain, T., Okeil, A. M., and Cai, C. S. "Field Test and Finite-Element Modeling of a Three-Span Continuous-Girder Bridge." *Journal of Performance of Constructed Facilities*, Vol. 28, No. 1, 2014, pp. 136-148.

[15] Choquet, P., Juneau, F., DeBreuille, P. J., and Besette, J. "Reliability, Long-Term Stability and Gage Performance of Vibrating Wire Sensors with Reference to Case Histories." In 5th Symposium Field Measurements in Geomechanics, Singapore, 1999. pp. 49-54.

[16] Bordes, J. L. and DeBreuille, P. J. "Some Facts About Long-Term Reliability of Vibrating Wire Instruments." In Reliability of Geotechnical Instrumentation, National Research Council, Washington, D.C., USA, 1985. pp. 20-27.

[17] Broms, B. B. and Lutz, L. A. "Effects of Arrangement of Reinforcement on Crack Width and Spacing of Reinforced Concrete Members." *ACI Journal Proceedings,* Vol. 62, No. 11, 1965

[18] Ghimire, S. "Restraint Moments Due to Thermal Gradients in Continuous Prestressed Concrete Girder Bridges." Civil and Environmental Engineering, No. Master of Science in Civil Engineering (MSCE), Louisiana State University, 2014.

[19] Priestley, M. J. N. "Analysis of Temperature Gradient Effects." In RILEM-ACI Symposion on LTO of Structure, Budapest, 1984.

[20] Priestley, M. J. N. "Design of Concrete Bridges for Temperature Gradients." *Journal of American Concrete Institute*, Vol. 75, No. 5, 1978, pp. 209-217.

Appendix A

Structural Health Monitoring System

This appendix provides the complete details of the structural health monitoring system used in this project. The provided information includes the instrumentation plan and tabulated sensor details.

Figure A1. Instrumentation plan details – Spans 1 – 4

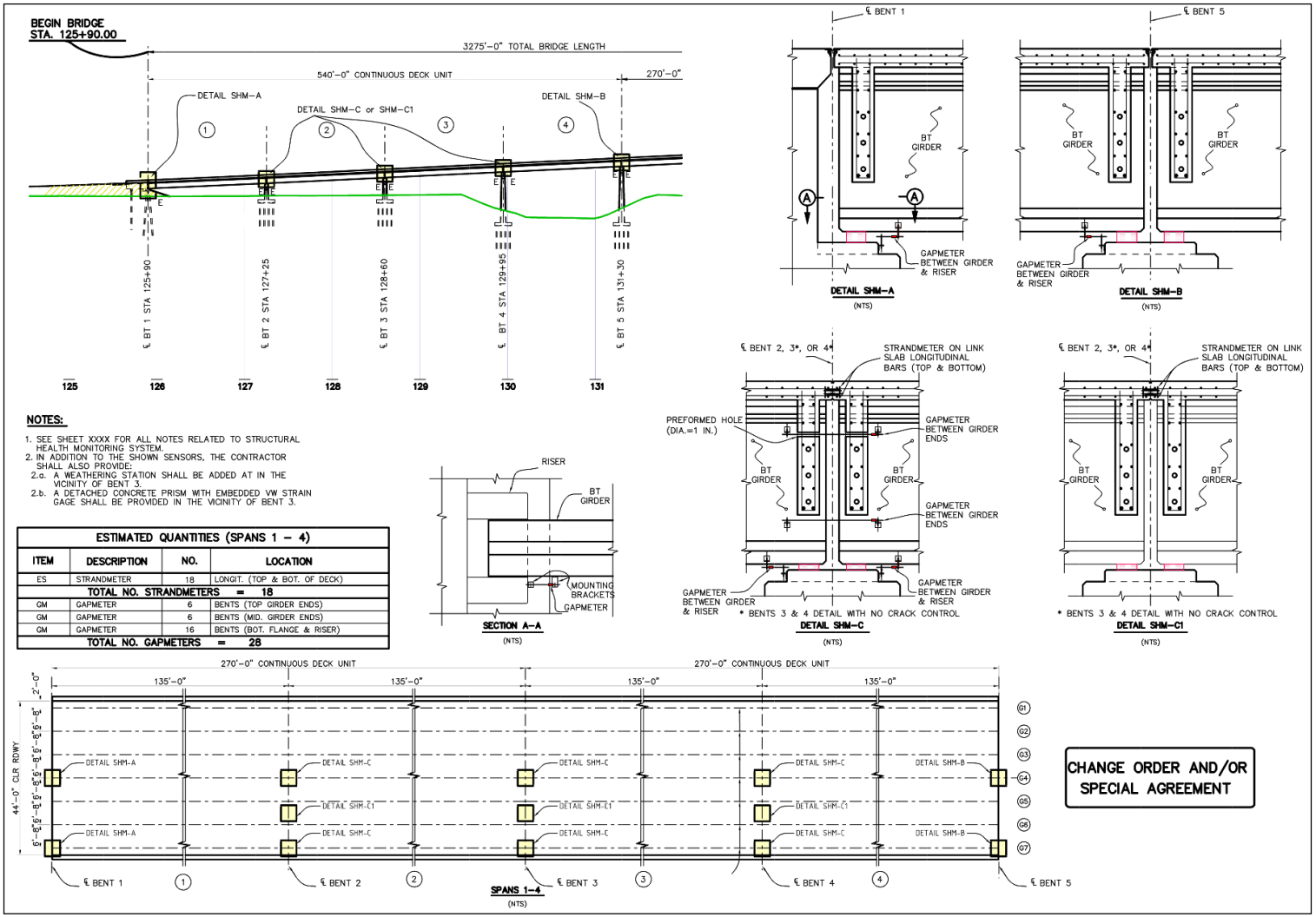

Figure A2. Instrumentation plan details – Spans 14 – 15

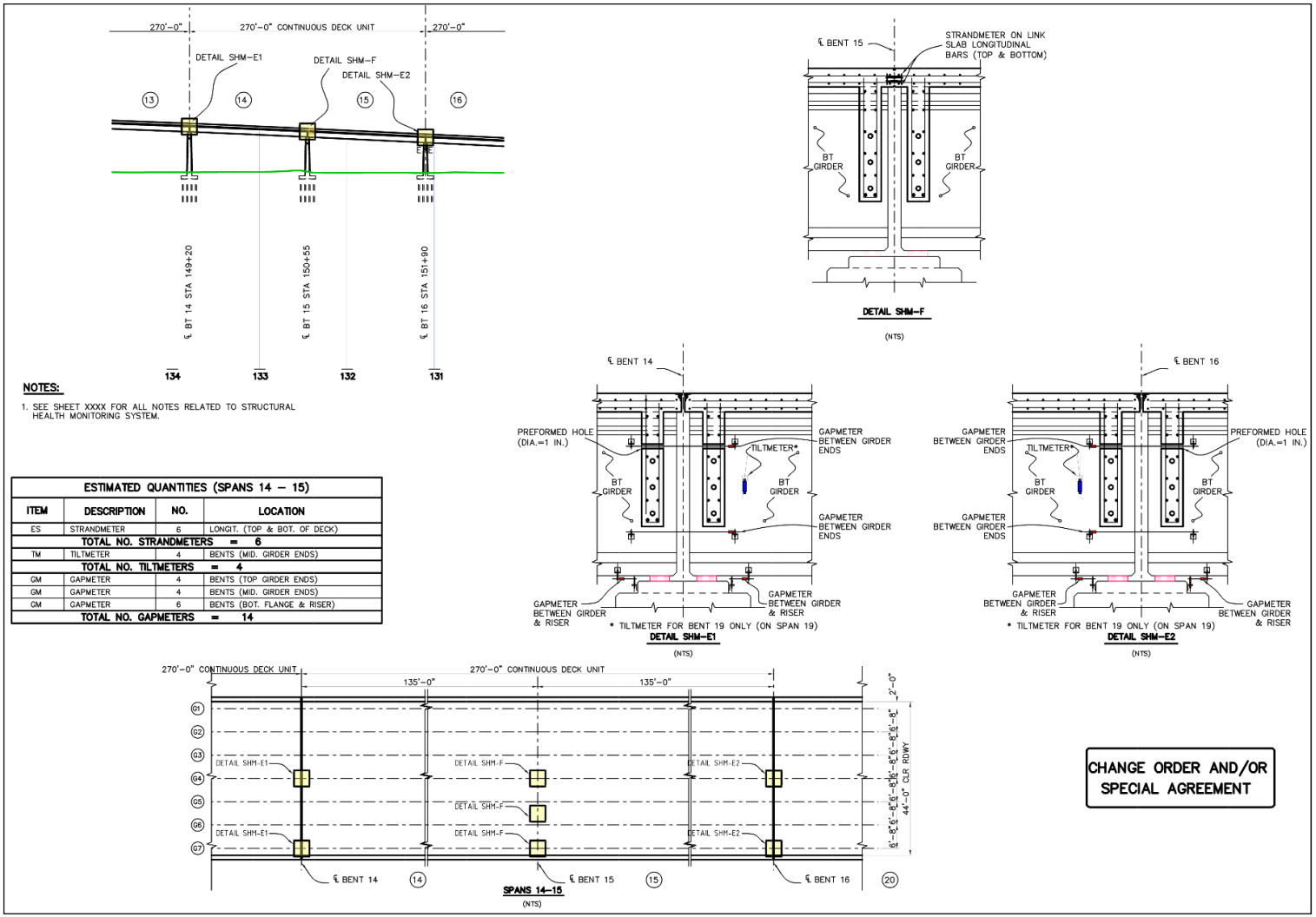

Figure A3. Instrumentation plan details – Spans 17 – 20

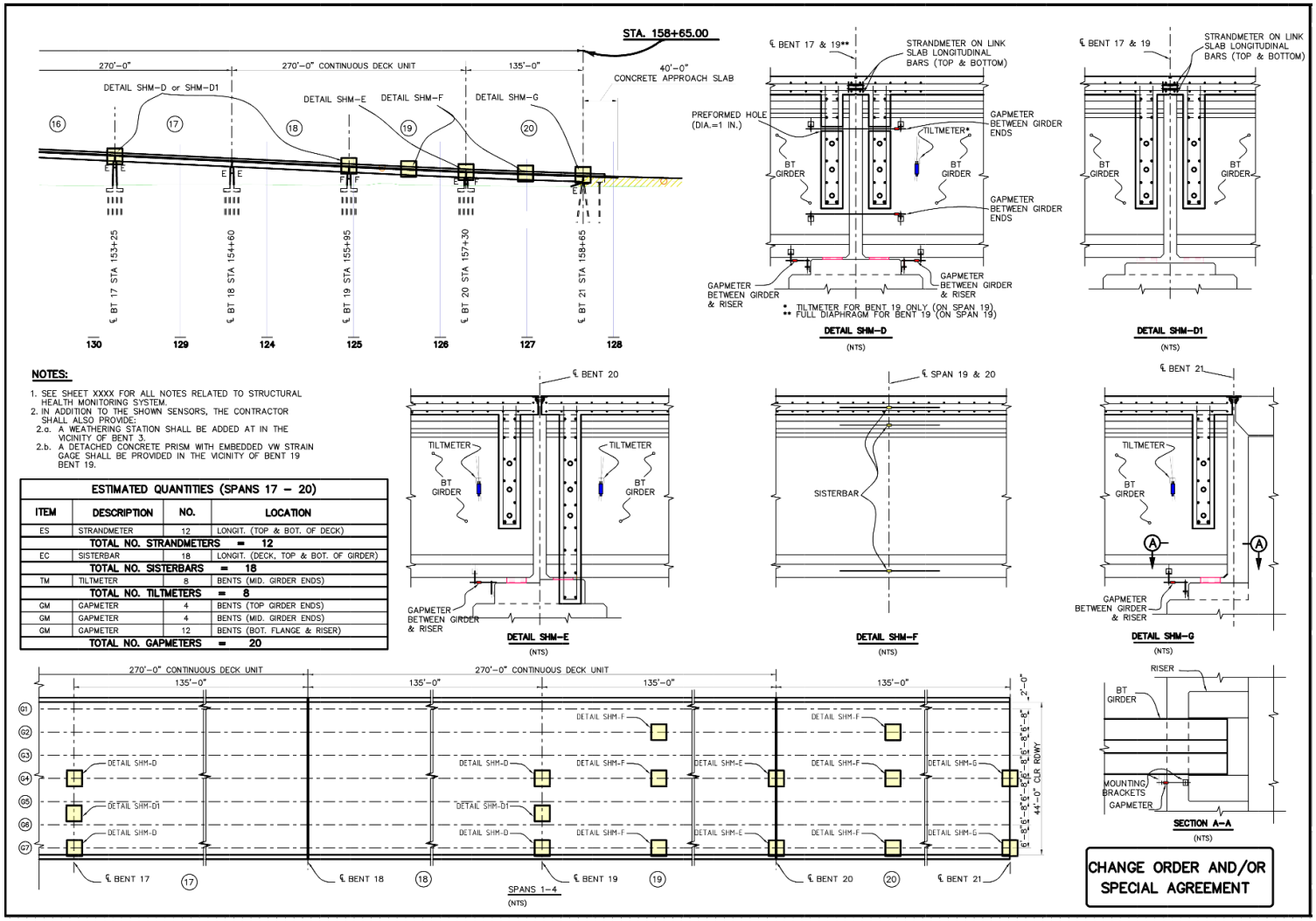

Table A1. Gapmeter installation table

Ouachita River Bridge - Crackmeters									
ID	DL.CH	Section	Girder	Location	Length (in.)	SN	Initial Reading	Temp (°C)	Temp (°F)
B1-G4-BFE	1	Bent 1	G4	Bottom Flange East	13	1606652	4054.8	17.2	63.0
B1-G7-BFE	2	Bent 1	G7	Bottom Flange East	13	1606654	4100.0	17.6	63.7
B2-G4-BFE	3	Bent 2	G4	Bottom Flange East	13	1606064	4174.4	11	51.8
B2-G4-BFW	4	Bent2	G4	Bottom Flange West	13	1606648	4058.1	14.7	58.5
B2-G4-BW	5	Bent 2	G4	Bottom of Web	48	1623403	5054.0	11.6	52.9
B2-G4-TW	6	Bent 2	G4	Top of Web	32	1529663	4718.0	13.6	56.5
B2-G7-BFE	7	Bent 2	G7	Bottom Flange East	13	1606649	4139.2	13.8	56.8
B2-G7-BFW	8	Bent 2	G7	Bottom Flange West	13	1606069	3974.6	14.3	57.7
B2-G7-BW	9	Bent 2	G7	Bottom of Web	48	1623405	5217.9	12.3	54.1
B2-G7-TW	10	Bent 2	G7	Top of Web	48	1529667	4932.0	11.5	52.7
B3-G4-BFE	17	Bent 3	G4	Bottom Flange East	13	1606068	4127.8	13.1	55.6
B3-G4-BFW	18	Bent 3	G4	Bottom Flange West	13	1606070	4079.6	14.8	58.6
B3-G4-BW	19	Bent 3	G4	Bottom of Web	32	1623413	4967.9	13.4	56.1
B3-G4-TW	20	Bent 3	G4	Top of Web	32	1529662	4935.3	13.5	56.3
B3-G7-BFE	21	Bent 3	G7	Bottom Flange East	13	1606656	4097.3	13.1	55.6
B3-G7-BFW	22	Bent 3	G7	Bottom Flange West	13	1606655	4039.8	12.6	54.7
B3-G7-BW	23	Bent 3	G7	Bottom of Web	48	1623411	5000.9	15.1	59.2
B3-G7-TW	24	Bent 3	G7	Top of Web	32	1529655	4706.2	14.3	57.7
B4-G4-BFE	32	Bent 4	G4	Bottom Flange East	13	1606647	4134.8	13	55.4
B4-G4-BFW	33	Bent 4	G4	Bottom Flange West	13	1606651	4066.9	16	60.8
B4-G4-BW	34	Bent 4	G4	Bottom of Web	48	1623404	5105.2	14.9	58.8
B4-G4-TW	35	Bent 4	G4	Top of Web	32	1529658	4352.1	14.7	58.5
B4-G7-BFE	36	Bent 4	G7	Bottom Flange East	13	1606653	4045.8	15.7	60.3
B4-G7-BFW	37	Bent 4	G7	Bottom Flange West	13	1606650	4114.7	13.5	56.3
B4-G7-BW	38	Bent 4	G7	Bottom of Web	48	1623414	2548.8	14.2	57.6
B4-G7-TW	39	Bent 4	G7	Top of Web	48	1529656	4808.1	13.4	56.1
B5-G4-BFW	46	Bent 5	G4	Bottom Flange West	13	1606062	3013.0	11.7	53.1
B5-G7-BFW	47	Bent 5	G7	Bottom Flange West	13	1606063	3045.2	12.1	53.8
B14-G4-BFE	48	Bent 14	G4	Bottom Flange East	13	1531827	3962.2	8.89	48.0
B14-G4-BFW	49	Bent 14	G4	Bottom Flange West	13	1531830	3698.0	8.6	47.5
B14-G4-BW	50	Bent 14	G4	Bottom of Web	32	1623407	5080.3	9.6	49.3
B14-G4-TW	51	Bent 14	G4	Top of Web	48	1529687	2502.8	9	48.2
B14-G7-BFE	52	Bent 14	G7	Bottom Flange East	13	1531829	3698.0	8.6	47.5
B14-G7-BFW	53	Bent 14	G7	Bottom Flange West	13	1531835	3835.9	9.9	49.8

B14-G7-BW	54	Bent 14	G7	Bottom of Web	32	1623410	5312.9	10.3	50.5
B14-G7-TW	55	Bent 14	G7	Top of Web	32	1529654	4686.0	10.5	50.9
B16-G4-BFE	64	Bent 16	G4	Bottom Flange East	13	1606065	3672.2	19.7	67.5
B16-G4-BFW	65	Bent 16	G4	Bottom Flange West	13	1531836	4448.8	20.2	68.4
B16-G4-BW	66	Bent 16	G4	Bottom of Web	32	16223412	5602.5	20.1	68.2
B16-G4-TW	67	Bent 16	G4	Top of Web	32	1529664	6255.8	19.8	67.6
B16-G7-BFE	68	Bent 16	G7	Bottom Flange East	13	1606066	3447.0	20.6	69.1
B16-G7-BFW	69	Bent 16	G7	Bottom Flange West	13	1606067	2340.6	20.6	69.1
B16-G7-BW	70	Bent 16	G7	Bottom of Web	32	1623409	4862.0	23.5	74.3
B16-G7-TW	71	Bent 16	G7	Top of Web	32	1529666	5083.0	22.8	73.0
B17-G4-BFE	74	Bent 17	G4	Bottom Flange East	13	1531826	3843.5	16.5	61.7
B17-G4-BFW	75	Bent 17	G4	Bottom Flange West	13	1531832	4109.8	17.3	63.1
B17-G4-BW	76	Bent 17	G4	Bottom of Web	48	1623406	4853.9	21.1	70.0
B17-G4-TW	77	Bent 17	G4	Top of Web	48	1609428	4970.6	21.3	70.3
B17-G7-BFE	78	Bent 17	G7	Bottom Flange East	13	1609417	4124.0	17.9	64.2
B17-G7-BFW	79	Bent 17	G7	Bottom Flange West	13	1529665	4780.1	21.7	71.1
B17-G7-BW	80	Bent 17	G7	Bottom of Web	32	1623402	4866.4	22.6	72.7
B17-G7-TW	81	Bent 17	G7	Top of Web	32	1609429	4144.7	21.7	71.1
B19-G4-BFE	88	Bent 19	G4	Bottom Flange East	13	1609423	4020.7	19.4	66.9
B19-G4-BFW	89	Bent 19	G4	Bottom Flange West	13	1531828	3945.3	19.7	67.5
B19-G4-BW	90	Bent 19	G4	Bottom of Web	32	1706436	5028.0	18	64.4
B19-G4-TW	91	Bent 19	G4	Top of Web	48	1609424	5299.2	15.7	60.3
B19-G7-BFE	92	Bent 19	G7	Bottom Flange East	13	1609431	4979.1	20	68.0
B19-G7-BFW	93	Bent 19	G7	Bottom Flange West	13	1906646	3833.1	30.4	86.7
B19-G7-BW	94	Bent 19	G7	Bottom of Web	32	1623408	5155.3	20.6	69.1
B19-G7-TW	95	Bent 19	G7	Top of Web	32	1609425	4830.5	20.2	68.4
B20-G4-BFW	115	Bent 20	G4	Bottom Flange East	13	1529888	3960.4	19.1	66.4
B20-G7-BFW	116	Bent 20	G7	Bottom Flange West	13	1531833	4150.0	19.8	67.6
B21-G4-BFW	133	Bent 21	G4	Bottom Flange West	13	1531831	3981.8	12.8	55.0
B21-G7-BFW	134	Bent 21	G7	Bottom Flange West	13	1531834	4094.8	14	57.2

Table A2. Tiltmeter installation table

Ouachita River Bridge - Tiltmeters									
ID	Gauge Type	DL.CH	Section	Girder	Location	SN	Initial Reading	Temp (°C)	Temp (°F)
B14-G4-CWE	Tiltmeter	56	Bent 14	G4	Center of Web East	1612763	7420	18.3	64.9
B14-G7-CWE	Tiltmeter	57	Bent 14	G7	Center of Web East	1612758	6046	18.3	64.9
B16-G4-CWE	Tiltmeter	72	Bent 16	G4	Center of Web East	1612761	7704	20.4	68.7
B16-G7-CWE	Tiltmeter	73	Bent 16	G7	Center of Web East	1612762	7798	21.2	70.2
B19-G4-CWE	Tiltmeter	96	Bent 19	G4	Center of Web East	1612759	7441.2	9.5	49.1
B19-G7-CWE	Tiltmeter	97	Bent 19	G7	Center of Web East	1601265	7172.9	10.3	50.5
B20-G4-CWE	Tiltmeter	117	Bent 20	G4	Center of Web East	1612767	7555.6	20.3	68.5
B20-G4-CWW	Tiltmeter	118	Bent 20	G4	Center of Web West	1612765	7001.5	21.3	70.3
B20-G7-CWE	Tiltmeter	119	Bent 20	G7	Center of Web East	1612768	7504.2	21.7	71.1
B20-G7-CWW	Tiltmeter	120	Bent 20	G7	Center of Web West	1612760	7427.1	22.1	71.8
B21-G4-CWW	Tiltmeter	135	Bent 21	G4	Center of Web West	1612766	7438	21.9	71.4
B21-G7-CWW	Tiltmeter	136	Bent 21	G7	Center of Web West	1612764	3960.4	19.1	66.4

Table A3. Sisterbar installation table

Ouachita River Bridge - Sisterbars									
ID	Gauge Type	DL.CH	Section	Girder	Location	SN	Initial Reading	Temp (°C)	Temp (°F)
S19-G2-TF_A	Sisterbar	104	Span 19	G2	Top Flange	1513274	5675.8	17.2	63.0
S19-G2-BF_A	Sisterbar	105	Span 19	G2	Bottom Flange	1513276	3314.1	17.5	63.5
S19-G2-S	Sisterbar	106	Span 19	G2	Slab	1513275	6783.1	17.3	63.1
S19-G4-TF_A	Sisterbar	107	Span 19	G4	Top Flange	1513277	5812.9	17.4	63.3
S19-G4-BF_A	Sisterbar	108	Span 19	G4	Bottom Flange	1513275	3762.5	17.5	63.5
S19-G4-S	Sisterbar	109	Span 19	G4	Slab	1513273	7504	17.9	64.2
S19-G7-TF_A	Sisterbar	110	Span 19	G7	Top Flange	1535109	5781.7	18.2	64.8
S19-G7-BF_A	Sisterbar	111	Span 19	G7	Bottom Flange	1535112	3300.5	18.1	64.6
S19-G7-S	Sisterbar	112	Span 19	G7	Slab	1535110	7130.4	18.4	65.1
S20-G2-TF	Sisterbar	122	Span 20	G2	Top Flange	1513267	6720	33.9	93.0
S20-G2-BF	Sisterbar	123	Span 20	G2	Bottom Flange	1513268	7000.6	34.1	93.4
S20-G2-S	Sisterbar	124	Span 20	G2	Slab	1535111	6804.4	26.8	80.3
S20-G4-TF_A	Sisterbar	125	Span 20	G4	Top Flange	1513272	6672.1	33.9	93.0
S20-G4-BF_A	Sisterbar	126	Span 20	G4	Bottom Flange	1513271	7092.5	34	93.2
S20-G4-S	Sisterbar	127	Span 20	G4	Slab	1535113	7532.9	30.7	87.2
S20-G7-TF_A	Sisterbar	110	Span 19	G7	Top Flange	1513269	6777	27.7	81.9
209-G7-BF_A	Sisterbar	111	Span 19	G7	Bottom Flange	1513270	7117	26.6	79.9
S20-G7-S	Sisterbar	130	Span 20	G7	Slab	1535114	7016.8	29.4	85.0

Table A4. Strandmeter installation table

Ouachita River Bridge - Strandmeters									
ID	Gauge Type	DL.CH	Section	Girder	Location	SN	Initial Reading	Temp (°C)	Temp (°F)
B2-G4-BS	Strandmeter	11	Bent 2	G4	Bot. of Slab	1521977	2932	38.1	100.6
B2-G4-TS	Strandmeter	12	Bent 2	G4	Top of Slab	1521982	3150	38.5	101.3
B2-S5.5-BS	Strandmeter	13	Bent 2	Slab b/t G4 & G5	Bot. of Slab	1521979	3227	39.4	102.9
B2-S5.5-TS	Strandmeter	14	Bent 2	Slab b/t G4 & G5	Top of Slab	1503423	3160	38.4	101.1
B2-G7-BS	Strandmeter	15	Bent 2	G7	Bot. of Slab	1503416	3003	38.9	102.0
B2-G7-TS	Strandmeter	16	Bent 2	G7	Top of Slab	1503420	3206	37.6	99.7
B3-G4-BS	Strandmeter	25	Bent 3	G4	Bot. of Slab	1503425	3118.7	25.5	77.9
B3-G4-TS	Strandmeter	26	Bent 3	G4	Top of Slab	1503424	2998	25.2	77.4
B3-S5.5-BS	Strandmeter	27	Bent 3	Slab b/t G4 & G5	Bot. of Slab	1503419	3071	25.6	78.1
B3-S5.5-TS	Strandmeter	28	Bent 3	Slab b/t G4 & G5	Top of Slab	1503417	3117	25.4	77.7
B3-G7-BS	Strandmeter	29	Bent 3	G7	Bot. of Slab	1521981	3339	25.1	77.2
B3-G7-TS	Strandmeter	30	Bent 3	G7	Top of Slab	1503418	2998.2	24.7	76.5
B4-G4-BS	Strandmeter	40	Bent 4	G4	Bot. of Slab	1503421	2945.2	25.8	78.4
B4-G4-TS	Strandmeter	41	Bent 4	G4	Top of Slab	1503421	3096.7	25.7	78.3
B4-S5.5-BS	Strandmeter	42	Bent 4	Slab b/t G4 & G5	Bot. of Slab	1503422	2844	25.9	78.6
B4-S5.5-TS	Strandmeter	43	Bent 4	Slab b/t G4 & G5	Top of Slab	1521983	3680	25.8	78.4
B4-G7-BS	Strandmeter	44	Bent 4	G7	Bot. of Slab	1521975	3155.7	25.9	78.6
B4-G7-TS	Strandmeter	45	Bent 4	G7	Top of Slab	1521980	3594.2	25.8	78.4
B15-G4-BS	Strandmeter	58	Bent 15	G4	Bot. of Slab	1536841	3364.1	18.5	65.3
B15-G4-TS	Strandmeter	59	Bent 15	G4	Top of Slab	1536840	2938.4	18.4	65.1
B15-S5.5-BS	Strandmeter	60	Bent 15	Slab b/t G4 & G5	Bot. of Slab	1536845	2911.1	19.4	66.9
B15-S5.5-TS	Strandmeter	61	Bent 15	Slab b/t G4 & G5	Top of Slab	1536844	3123.6	19.5	67.1
B15-G7-BS	Strandmeter	62	Bent 15	G7	Bot. of Slab	1536842	3095	19.5	67.1
B15-G7-TS	Strandmeter	63	Bent 15	G7	Top of Slab	1536843	2989	19.5	67.1
B17-G4-BS	Strandmeter	82	Bent 17	G4	Bot. of Slab	1530070	3234.6	23.2	73.8
B17-G4-TS	Strandmeter	83	Bent 17	G4	Top of Slab	1530067	3329.6	23.2	73.8
B17-S5.5-BS	Strandmeter	84	Bent 17	Slab b/t G4 & G5	Bot. of Slab	1530065	3000.8	25.3	77.5
B17-S5.5-TS	Strandmeter	85	Bent 17	Slab b/t G4 & G5	Top of Slab	1530072	2931.1	27.4	81.3
B17-G7-BS	Strandmeter	86	Bent 17	G7	Bot. of Slab	1530069	2965.3	33.7	92.7
B17-G7-TS	Strandmeter	87	Bent 17	G7	Top of Slab	1530068	3492.3	32	89.6
B19-G4-BS	Strandmeter	98	Bent 19	G4	Bot. of Slab	1530071	3149.6	17.3	63.1
B19-G4-TS	Strandmeter	99	Bent 19	G4	Top of Slab	1530066	3351	16.8	62.2
B19-S5.5-BS	Strandmeter	100	Bent 19	Slab b/t G4 & G5	Bot. of Slab	1521978	3084.2	23	73.4
B19-S5.5-TS	Strandmeter	101	Bent 19	Slab b/t G4 & G5	Top of Slab	1521976	3332.5	20.6	69.1
B19-G7-BS	Strandmeter	102	Bent 19	G7	Bot. of Slab	1530063	3307.6	23.4	74.1
B19-G7-TS	Strandmeter	103	Bent 19	G7	Top of Slab	1530064	2961.7	23.1	73.6

Table A5. Strain Gage installation table

Ouachita River Bridge – Strain Gages									
ID	Gauge Type	DL.CH	Section	Girder	Location	SN	Initial Reading	Temp (°C)	Temp (°F)
B3-STRAIN	Strain	31	Bent 3	N/A	N/A	N/A	3566.7	27.1	80.8
B20-STRAIN	Strain	121	Bent 20	N/A	N/A	N/A	3631.9	27.6	81.7
S20-G7-TF_B	Strain	128	Span 20	G7	Top Flange	N/A	5539.4	11.9	53.4
S20-G7-BF_B	Strain	129	Span 20	G7	Bottom Flange	N/A	3857.2	12.1	53.8

Appendix B

Live Load Test Trucks and Positions

This appendix provides the details of the axle weights for the two trucks used in the live load testing of the Ouachita Bridge and the positive and negative moment positioning of the trucks.

Figure B1. Dimensions and wheel loads for live load test trucks

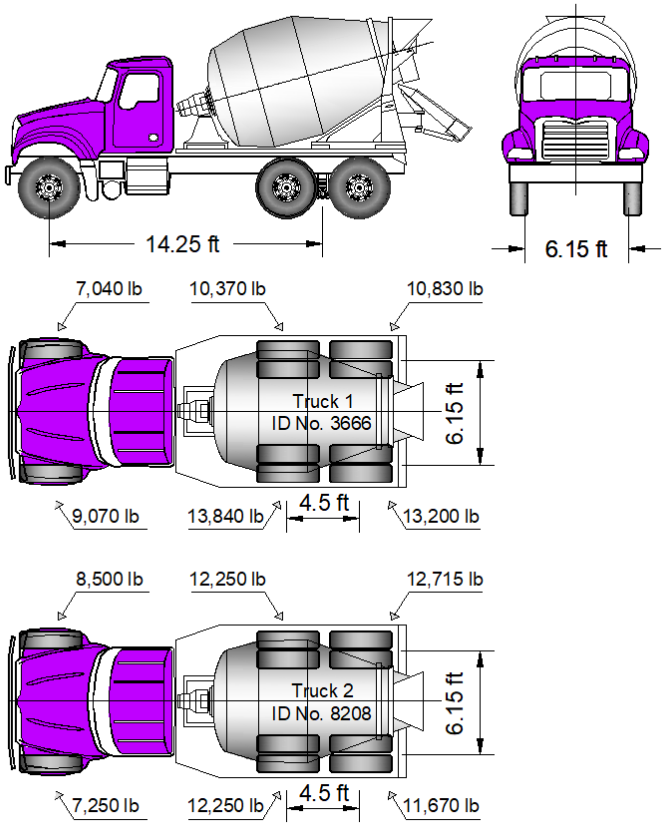

Figure B2. Positive moment positions for west approach spans

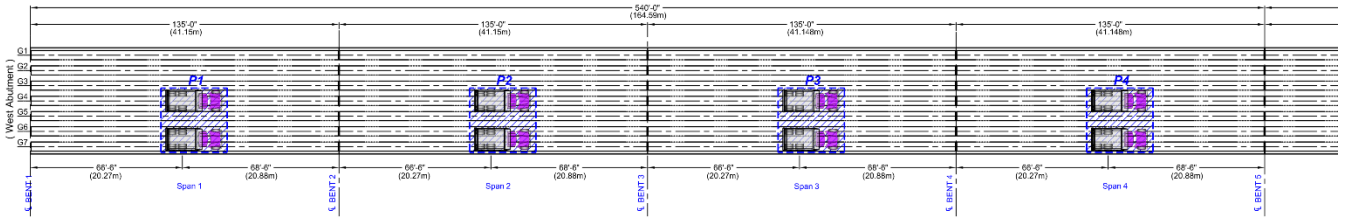

Figure B3. Positive moment positions for east approach spans

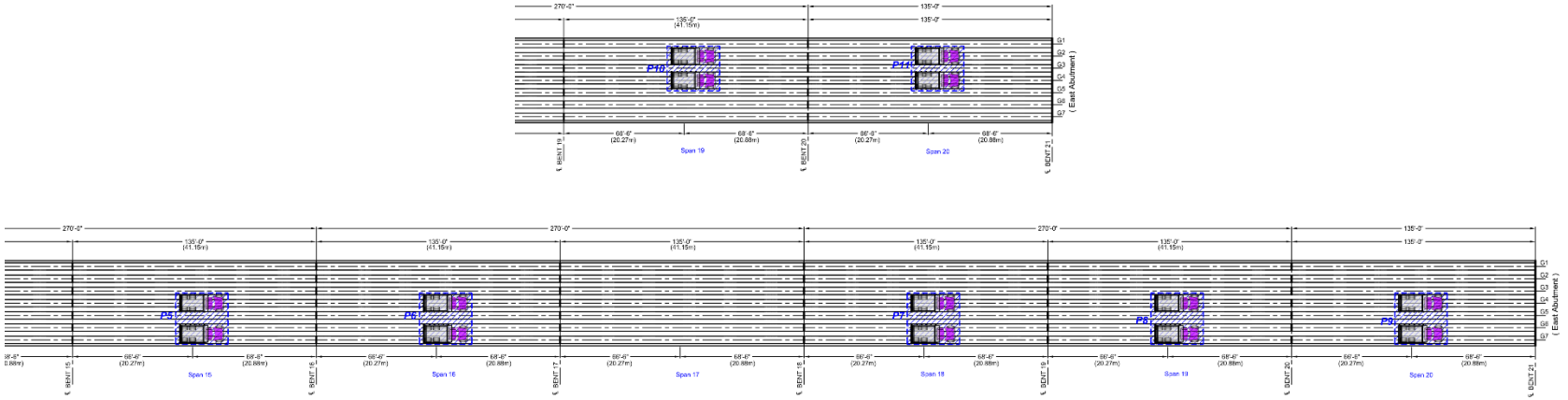

Figure B4. Negative moment positions for west approach spans

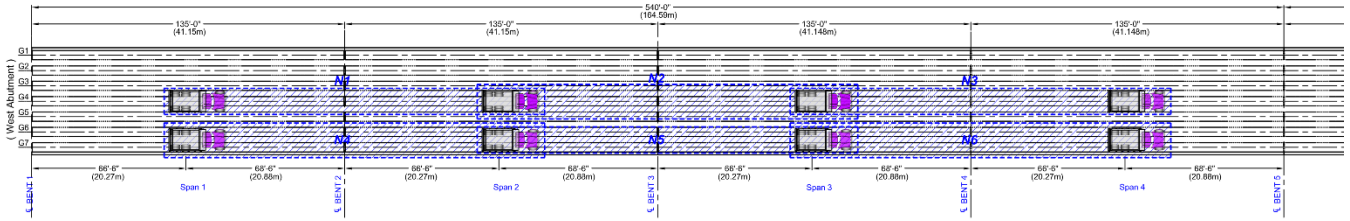

Figure B5. Negative moment positions for east approach spans

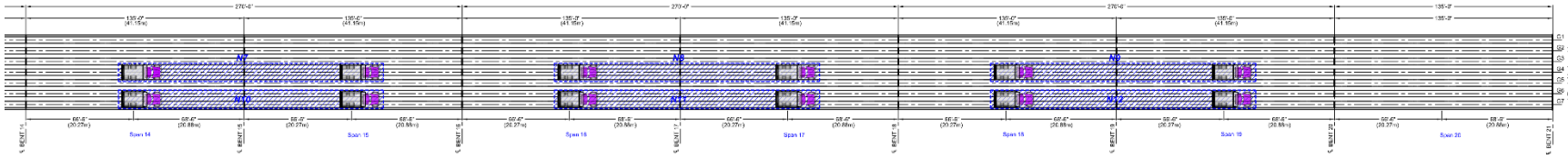

Figure B6. Positive live load positions P1 and P2

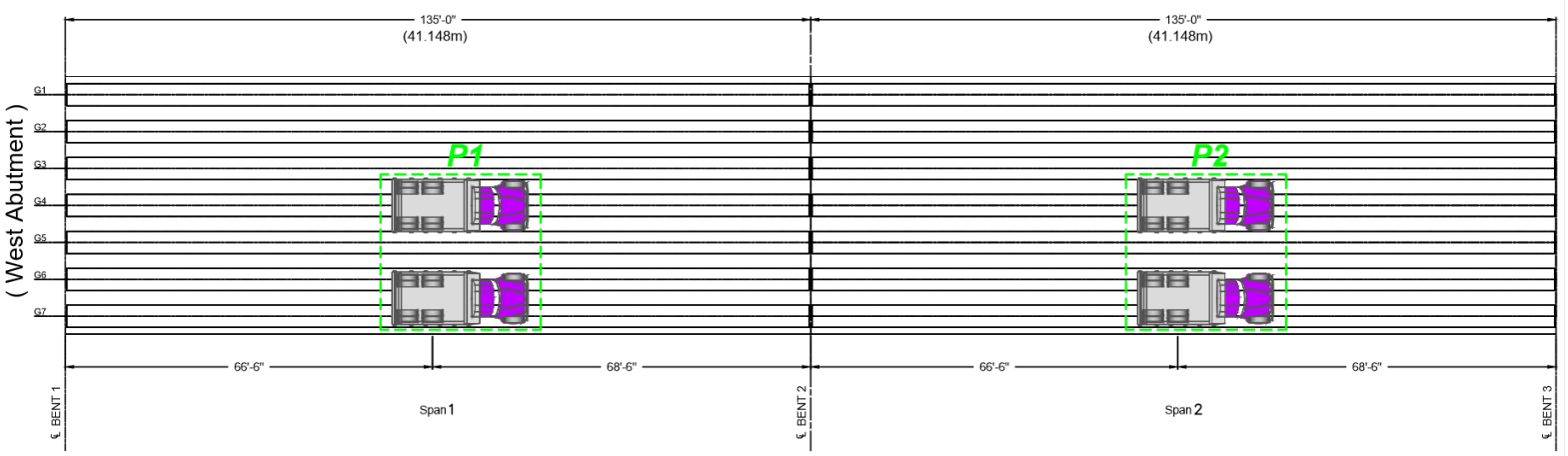

Figure B7. Positive live load positions P3 and P4

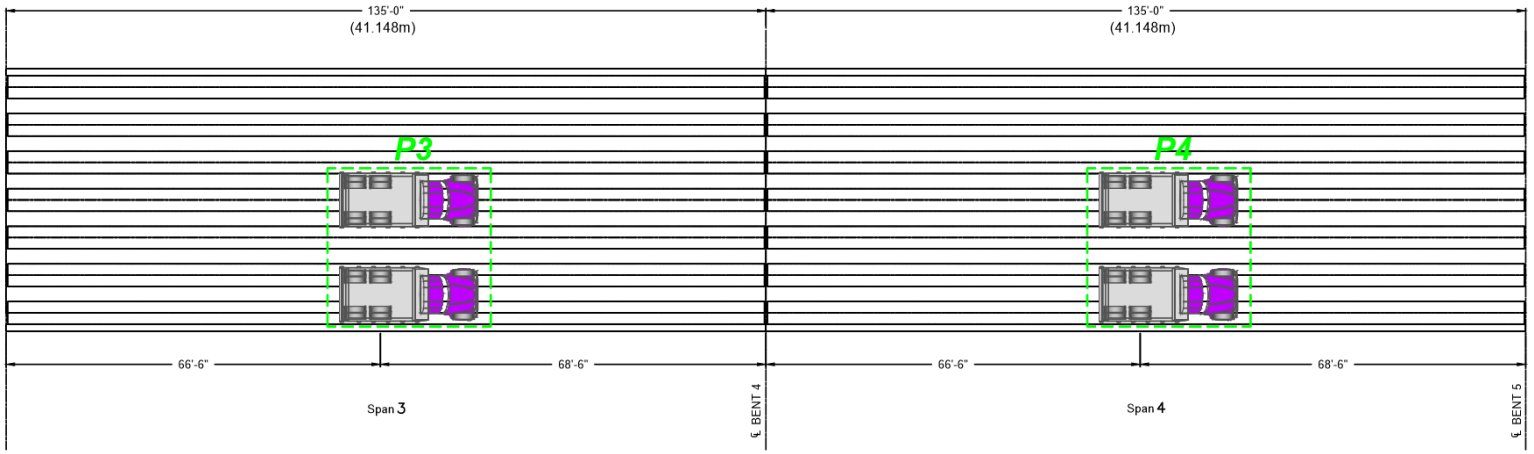

Figure B8. Positive live load positions P5 and P6

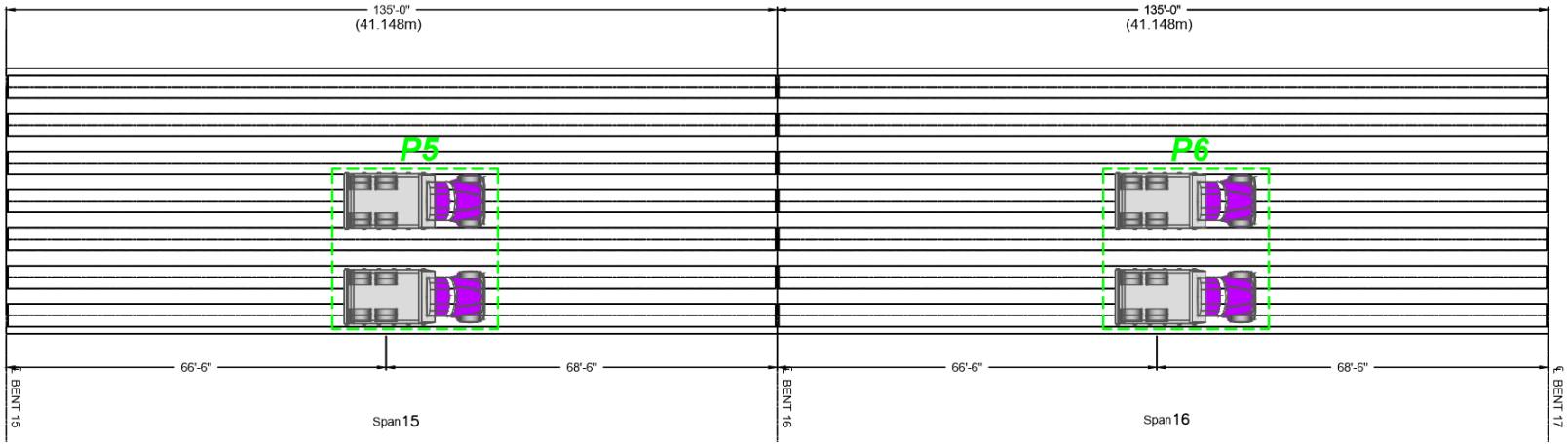

Figure B9. Positive live load positions P7 and P8

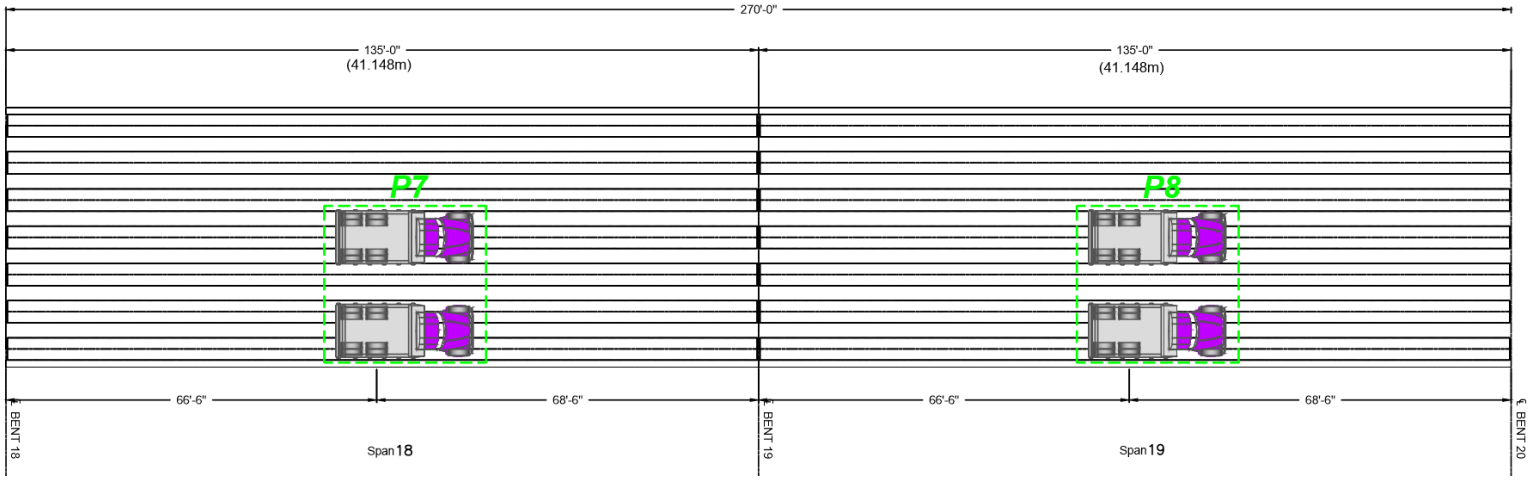

Figure B10. Positive live load position P9

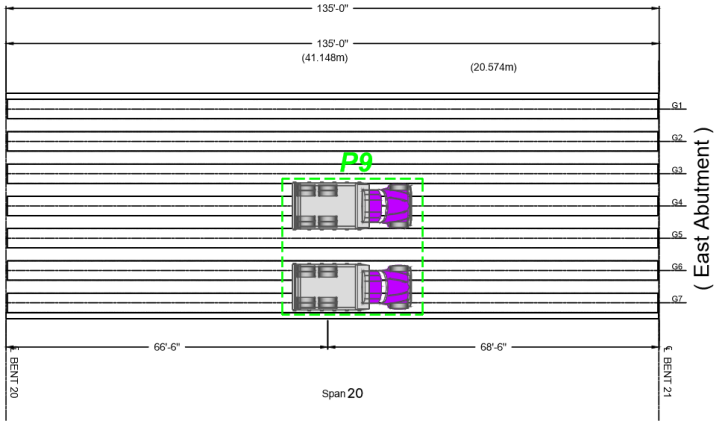

Figure B11. Positive live load positions P10 and P11

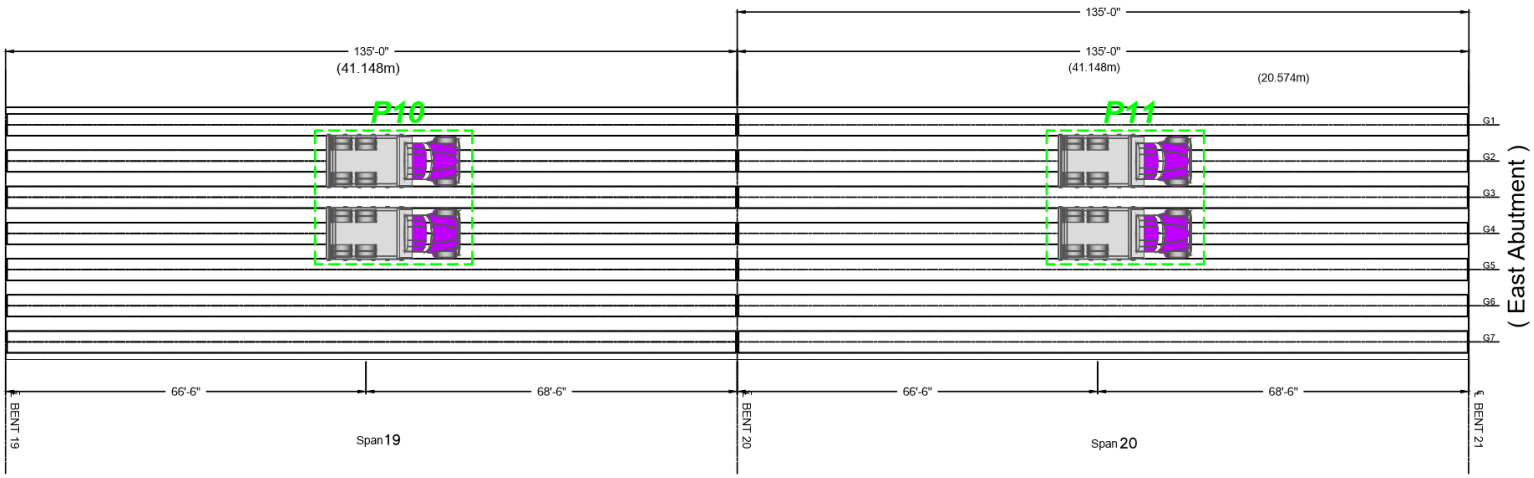

Figure B12. Negative live load positions N1 and N4

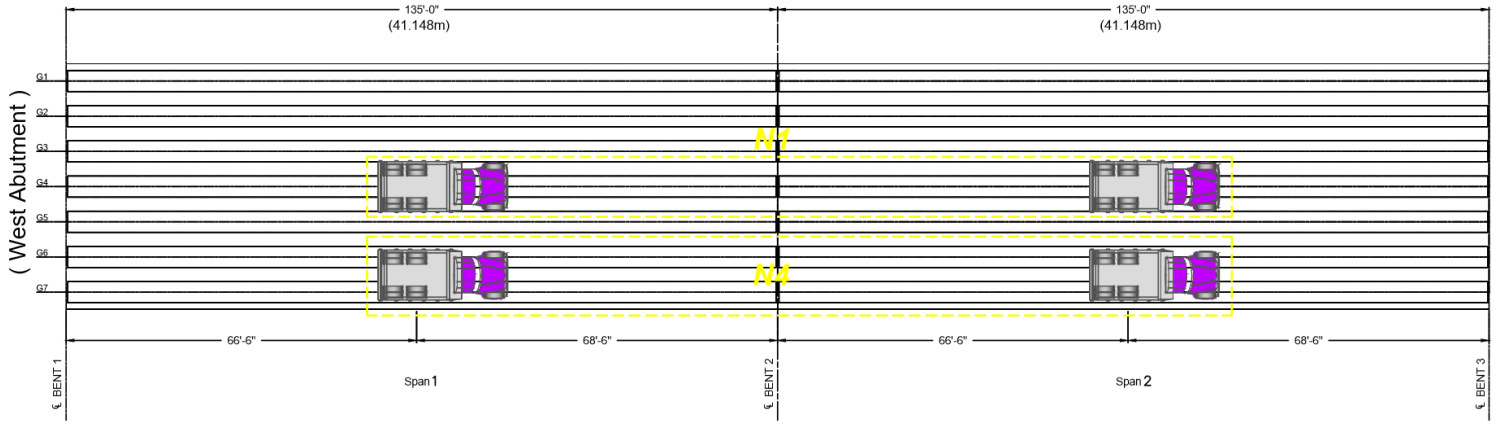

Figure B13. Negative live load positions N2 and N5

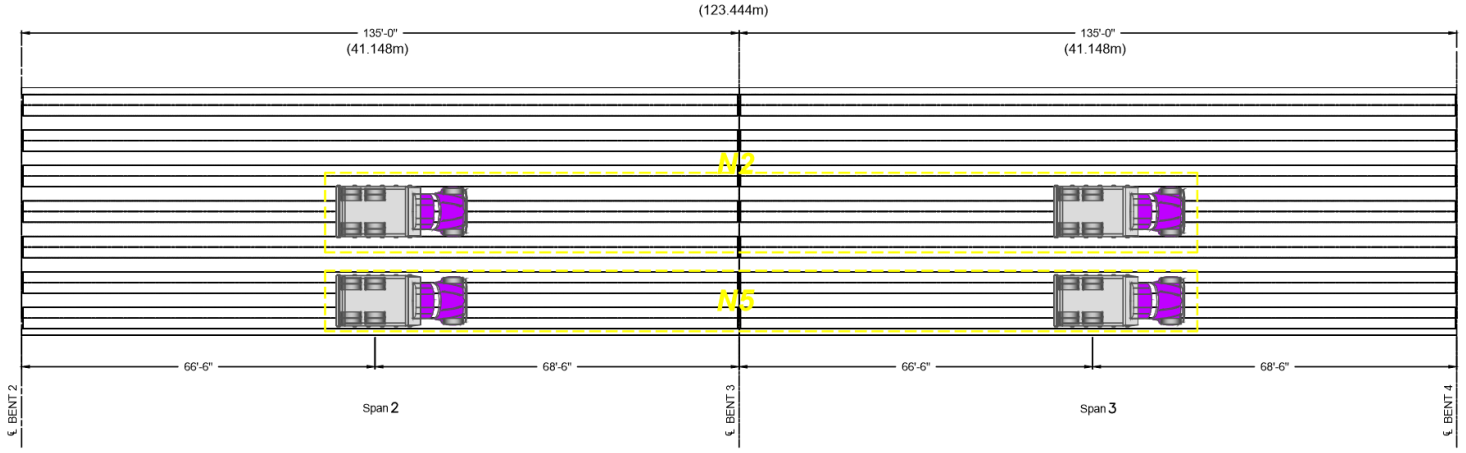

Figure B14. Negative live load positions N3 and N6

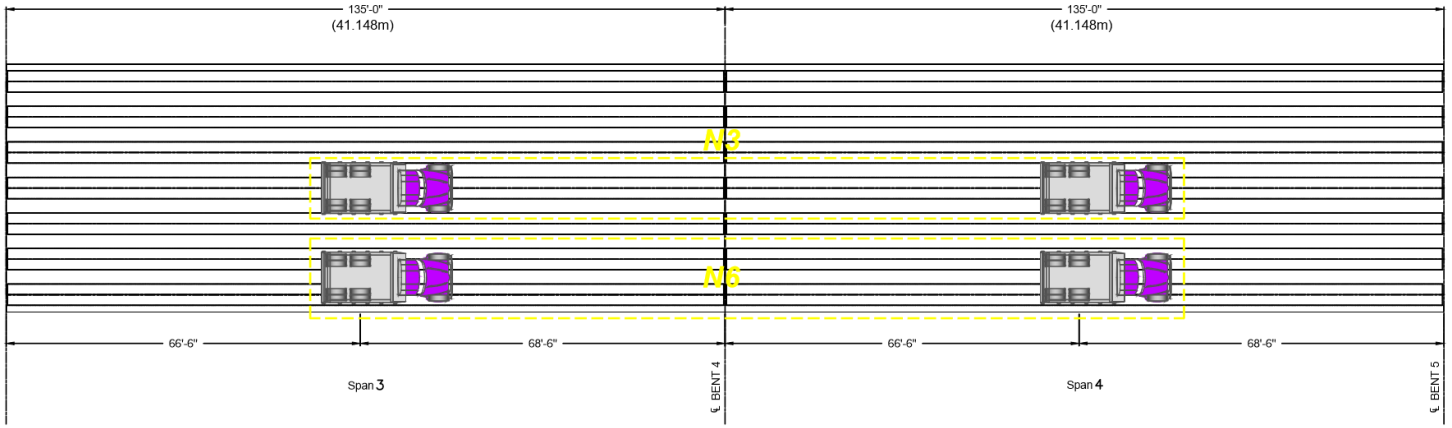

Figure B15. Negative live load positions N7 and N10

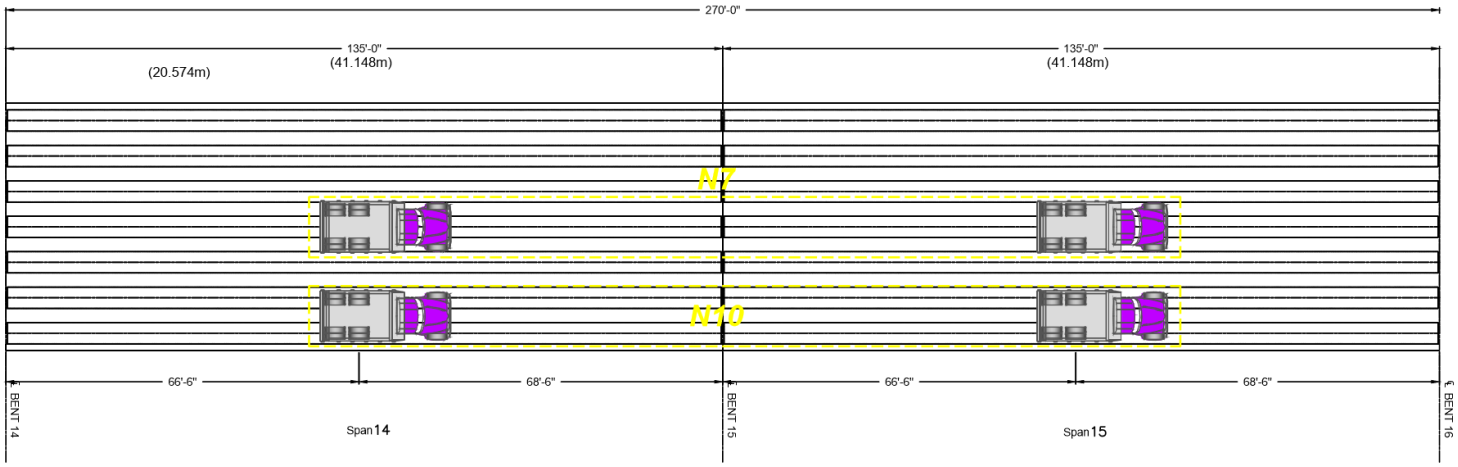

Figure B16. Negative live load positions N8 and N11

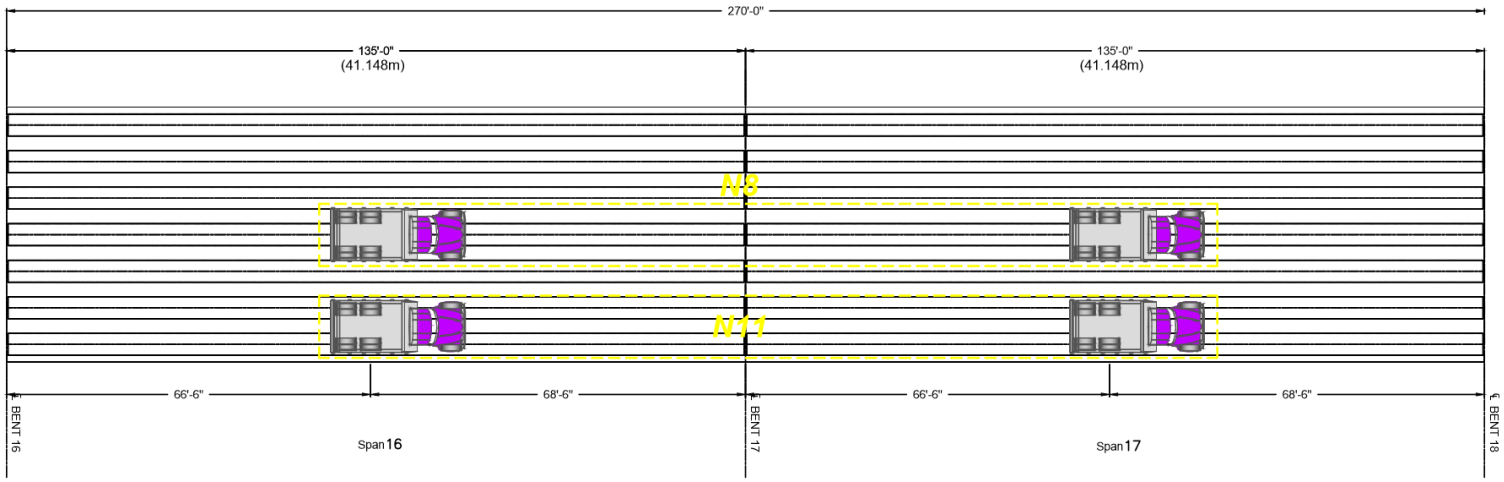

Figure B17. Negative live load positions N9 and N12

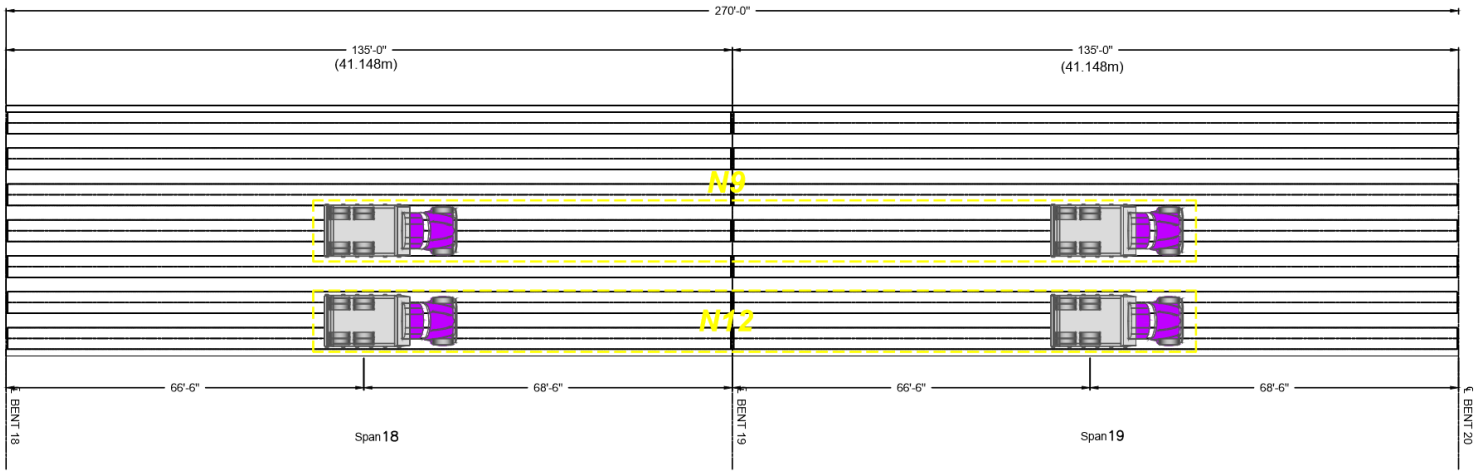

Appendix C

Recorded Readings from All Sensors

The following plots are a documentation of all sensor readings obtained since the beginning of installation of embedded sensors in casting yard on June 18, 2008, as part of Project LTRC 08-1ST through the end of the current project (LTRC 12-1ST) on December 31, 2013. No data was collected during the period between the end of Project LTRC 08-1ST on December 10, 2010 and the reinstatement of the monitoring system for the current project on February 2012, hence the gap that appears in the plots for all sensors. It should be noted that surface mounted sensors were installed at the bridge site, and therefore, their plots cover the period from January 9, 2009, through December 2013.

Note: Three plots are provided for each sensor. The first is the temperature reading obtained from the vibrating wire gage readings. The second and third are plots of the relative uncorrected and relative temperature corrected sensor readings (e.g., strain, gap, and slope).

S19_G2_S – Sisterbar on the slab at Girder 2 in Segment D

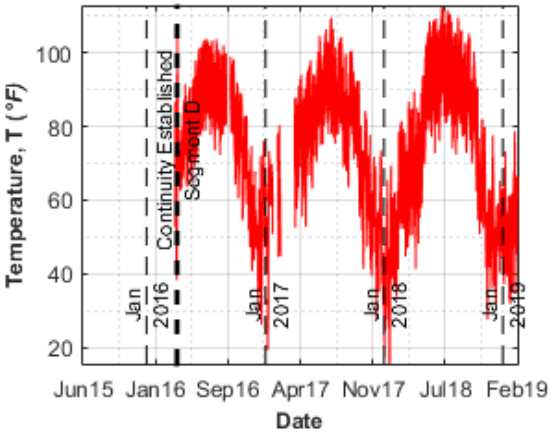

a) Temperature reading of the sensor

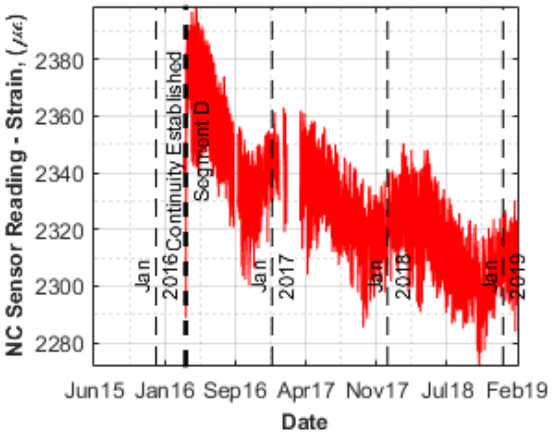

b) Sensor reading without temperature correction

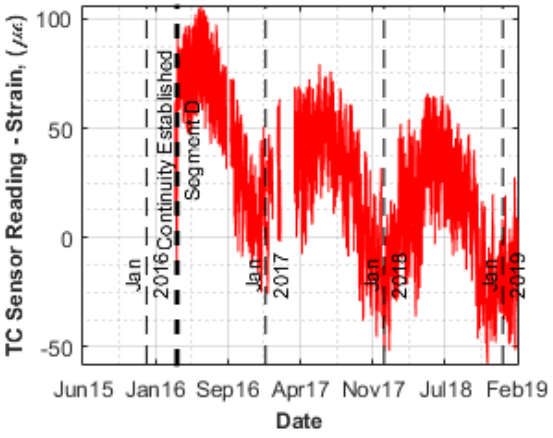

c) Sensor reading after temperature correction

S19_G2_TF_A – Sisterbar on the top flange at Girder 2 in Segment D

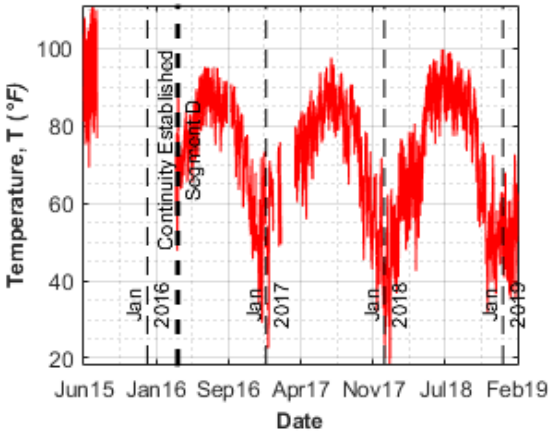

a) Temperature reading of the sensor

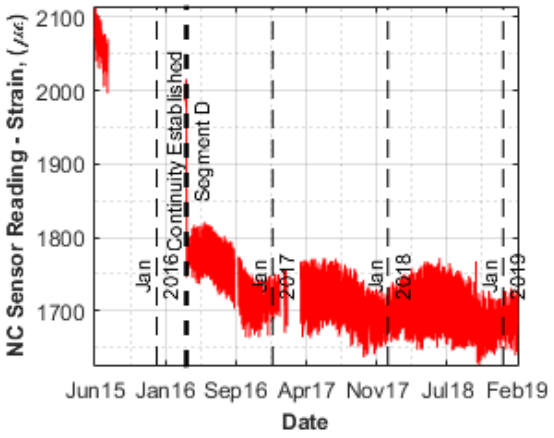

b) Sensor reading without temperature correction

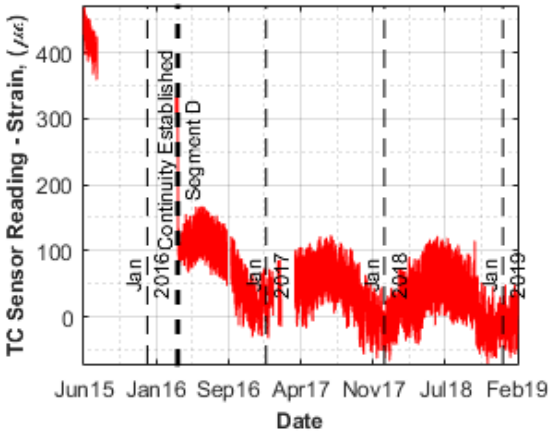

c) Sensor reading after temperature correction

S19_G2_BF_A – Sisterbar on the bottom flange at Girder 2 in Segment D

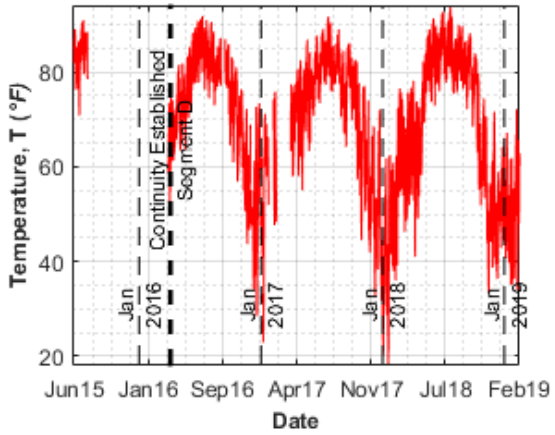

a) Temperature reading of the sensor

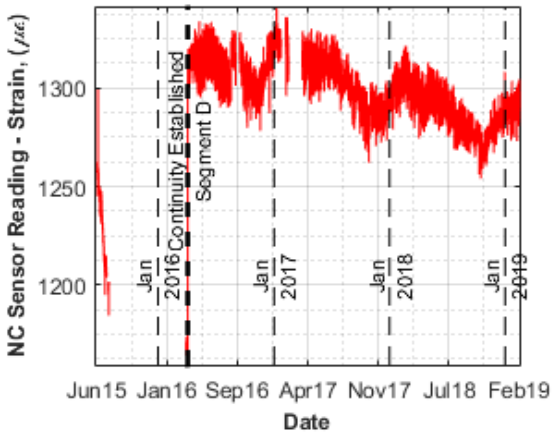

b) Sensor reading without temperature correction

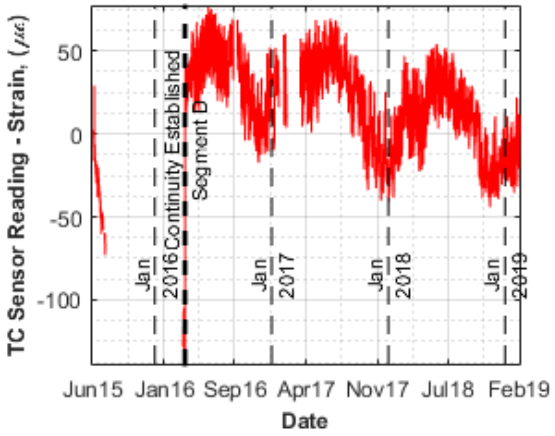

c) Sensor reading after temperature correction

S19_G4_S – Sisterbar on the slab at Girder 4 in Segment D

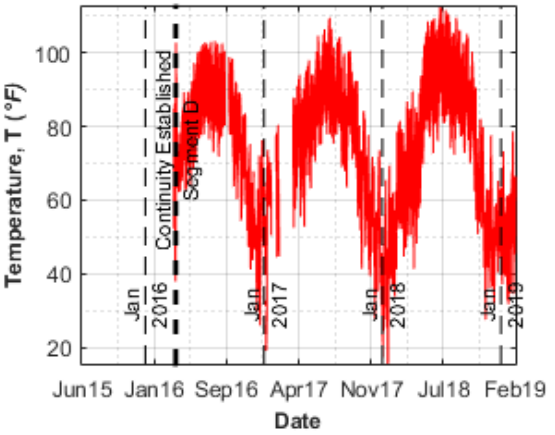

a) Temperature reading of the sensor

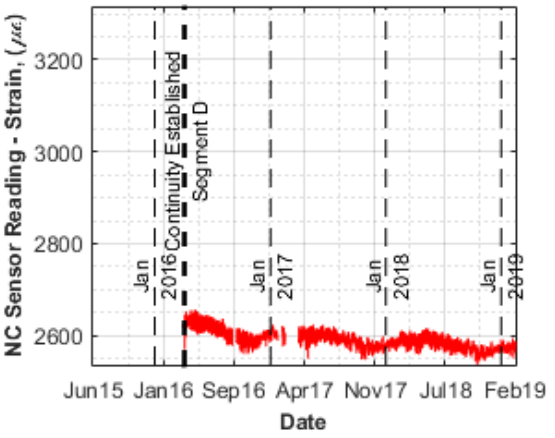

b) Sensor reading without temperature correction

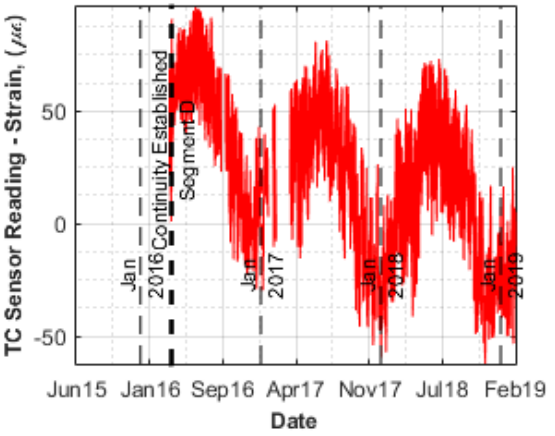

c) Sensor reading after temperature correction

S19_G4_TF – Sisterbar on the top flange at Girder 4 in Segment D

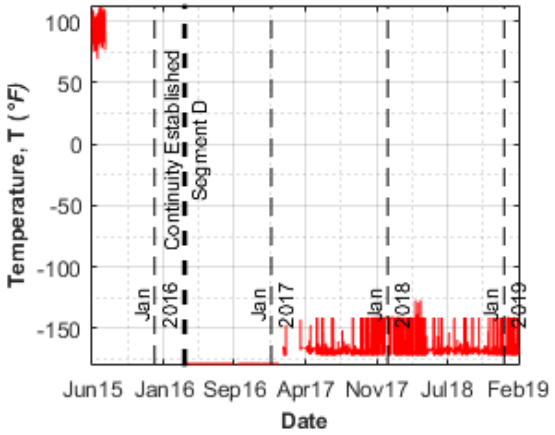

a) Temperature reading of the sensor

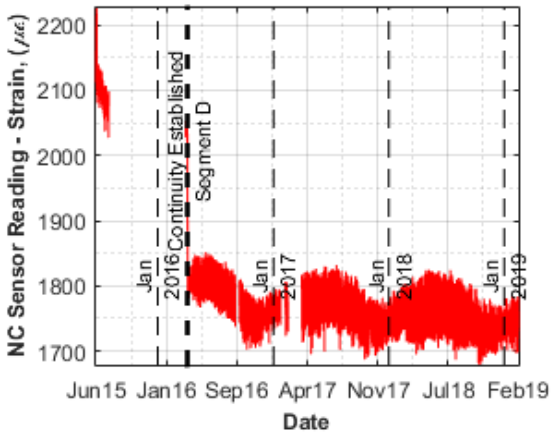

b) Sensor reading without temperature correction

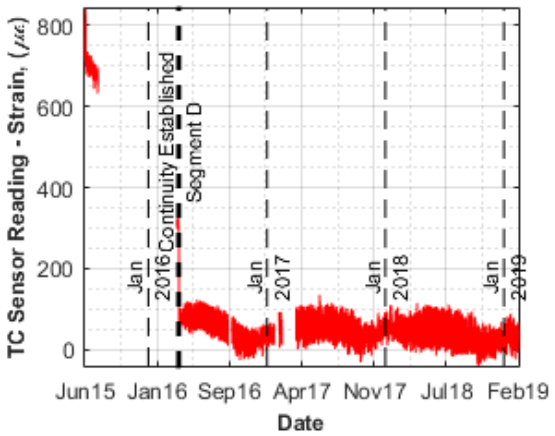

c) Sensor reading after temperature correction

S19_G4_BF – Sisterbar on the bottom flange at Girder 4 in Segment D

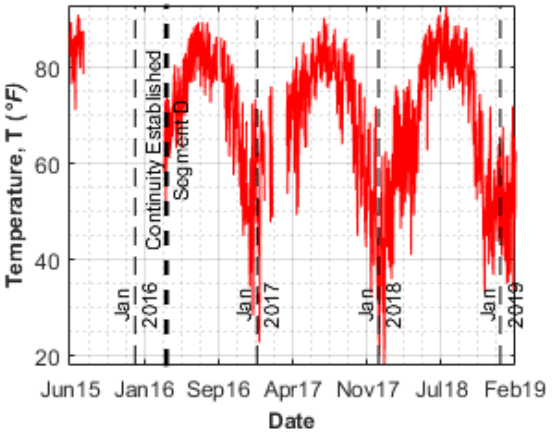

a) Temperature reading of the sensor

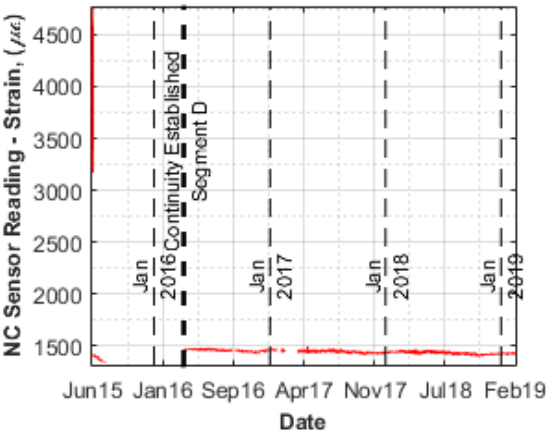

b) Sensor reading without temperature correction

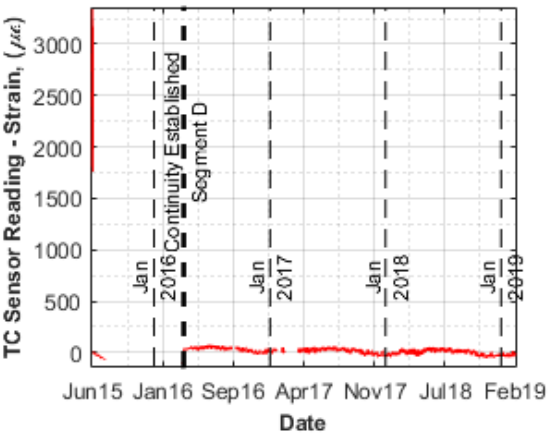

c) Sensor reading after temperature correction

S19_G7_S – Sisterbar on the slab at Girder 7 in Segment D

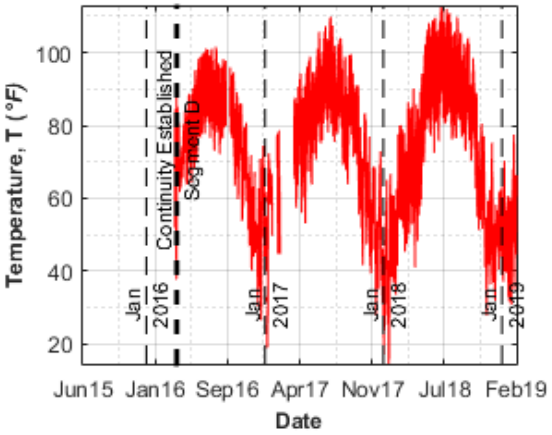

a) Temperature reading of the sensor

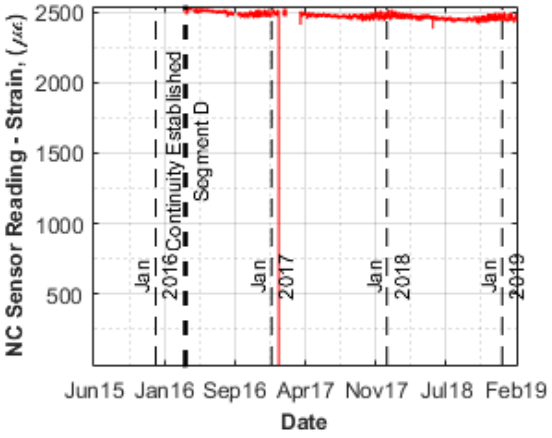

b) Sensor reading without temperature correction

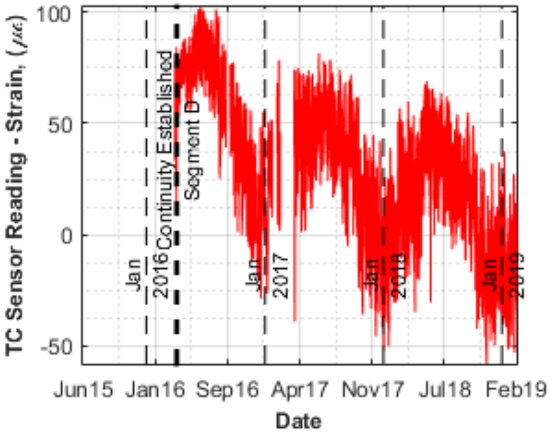

c) Sensor reading after temperature correction

S19_G7_TF – Sisterbar on the top flange at Girder 7 in Segment D

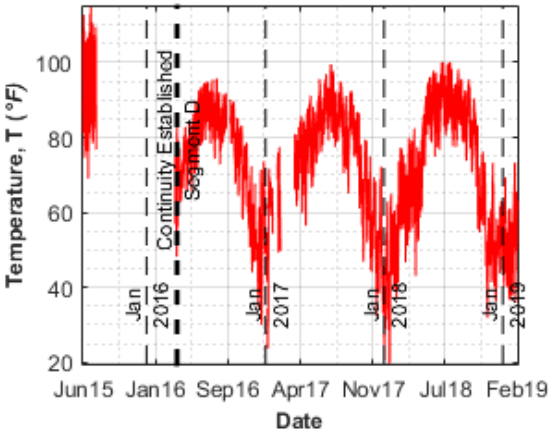

a) Temperature reading of the sensor

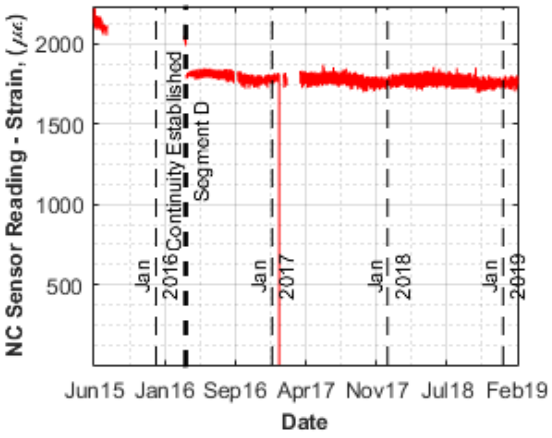

b) Sensor reading without temperature correction

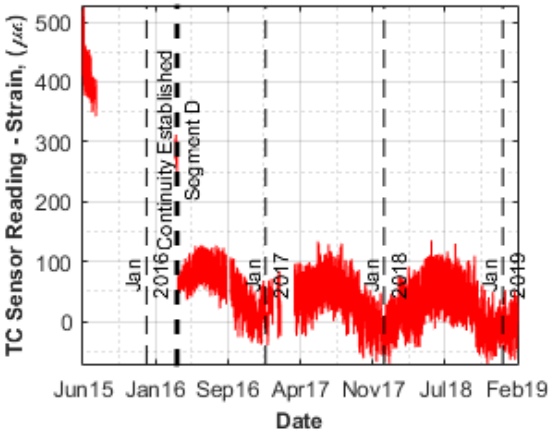

c) Sensor reading after temperature correction

S19_G7_BF – Sisterbar on the bottom flange at Girder 7 in Segment D

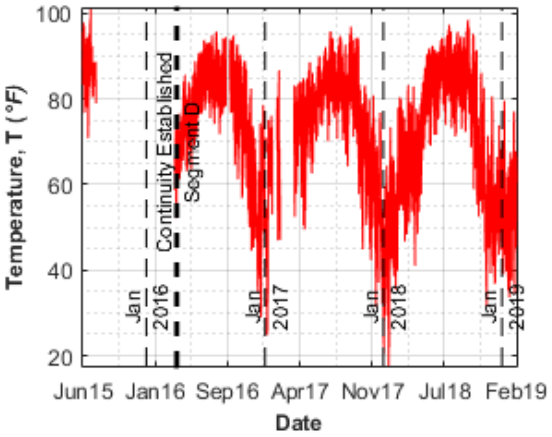

a) Temperature reading of the sensor

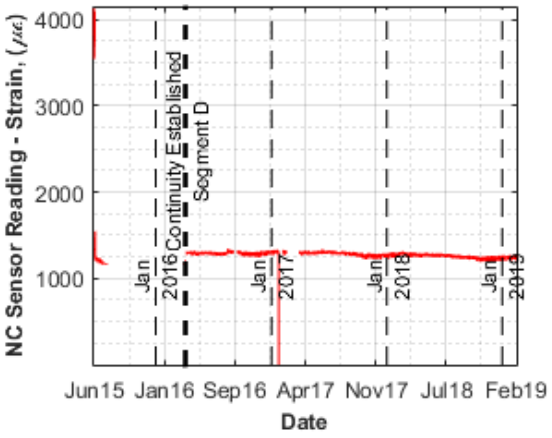

b) Sensor reading without temperature correction

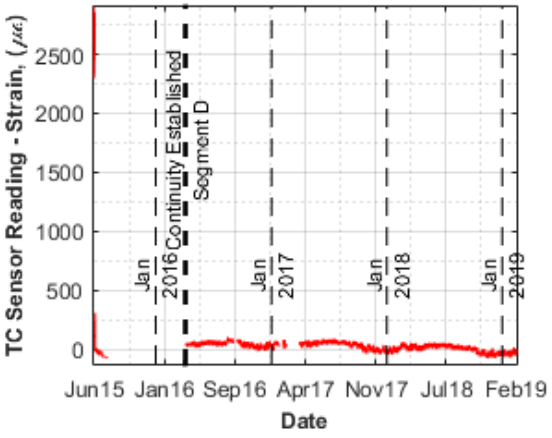

c) Sensor reading after temperature correction

B19_G4_BFE – Gapmeter on the riser in the east at Bent 19 Girder 4 in Segment D

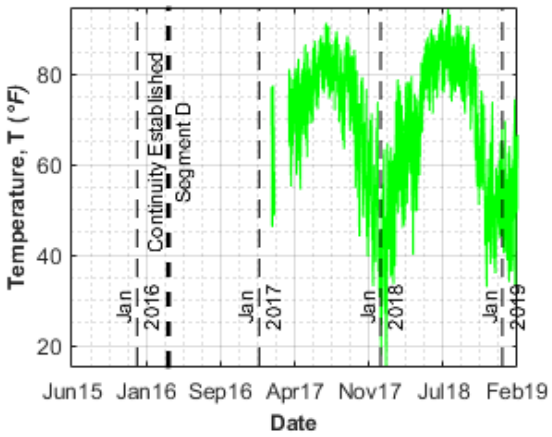

a) Temperature reading of the sensor

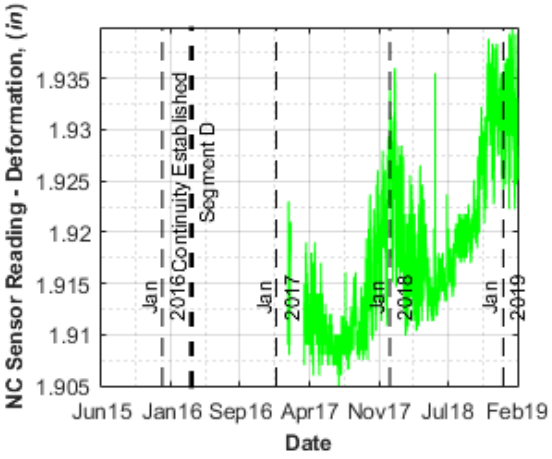

b) Sensor reading without temperature correction

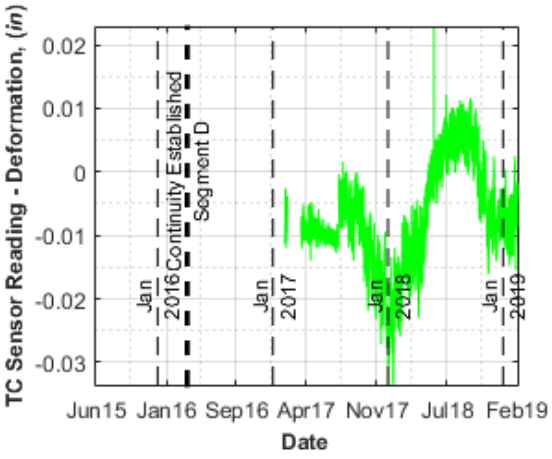

c) Sensor reading after temperature correction

B19_G4_BFW – Sisterbar on the riser in the west at Bent 19 Girder 4 in Segment D

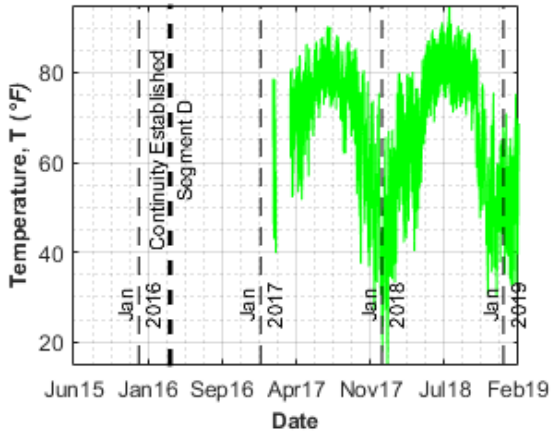

a) Temperature reading of the sensor

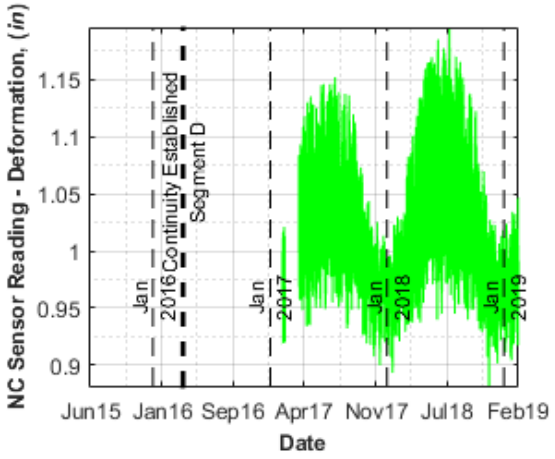

b) Sensor reading without temperature correction

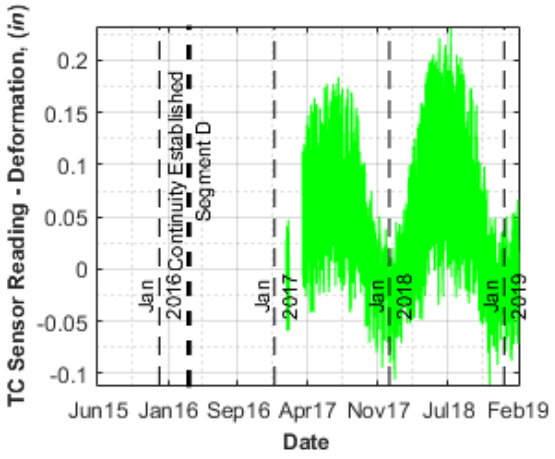

c) Sensor reading after temperature correction

B19_G4_BW – Gapmeter on the bottom of the web at Bent 19 Girder 4 in Segment D

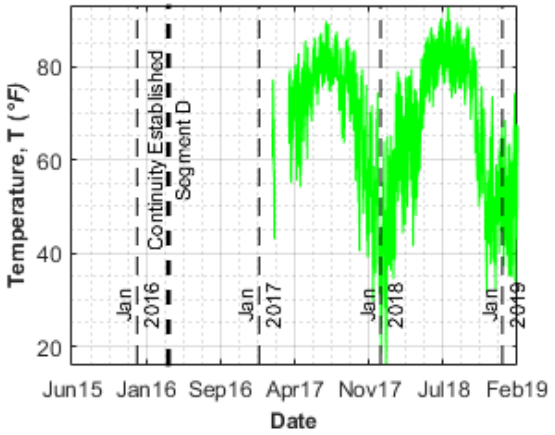

a) Temperature reading of the sensor

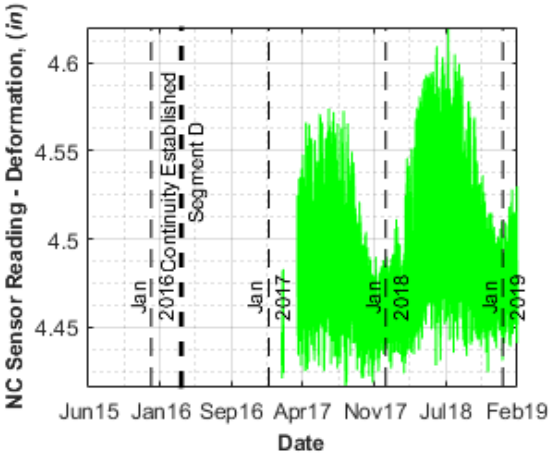

b) Sensor reading without temperature correction

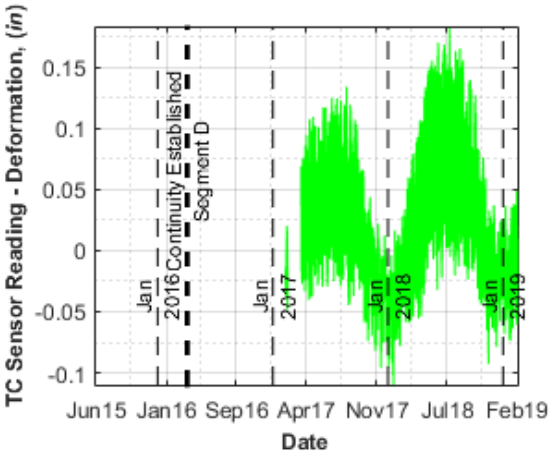

c) Sensor reading after temperature correction

B19_G4_TW – Sisterbar on the top of the web at Bent 19 Girder 4 in Segment D

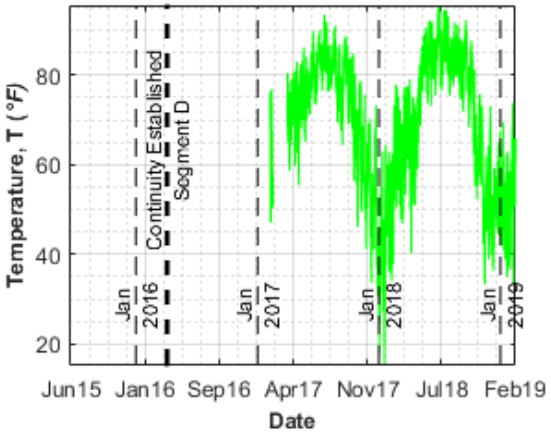

a) Temperature reading of the sensor

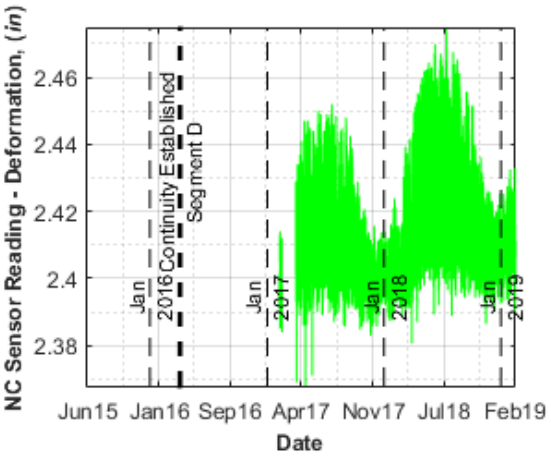

b) Sensor reading without temperature correction

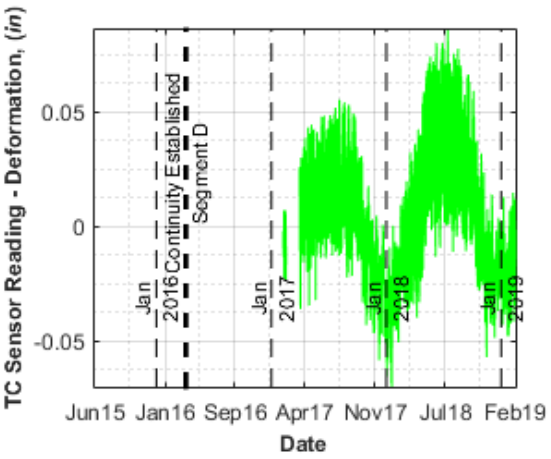

c) Sensor reading after temperature correction

B19_G7_BFE – Gapmeter on the riser in the east at Bent 19 Girder 7 in Segment D

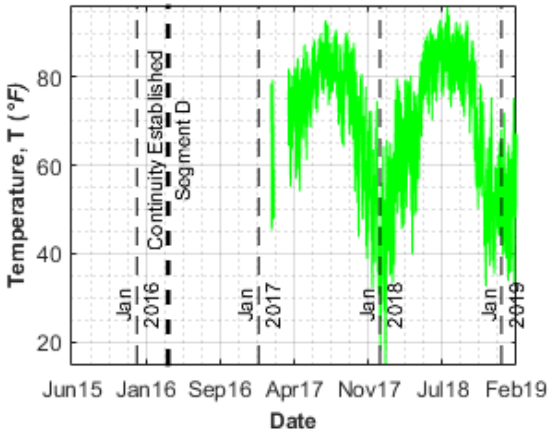

a) Temperature reading of the sensor

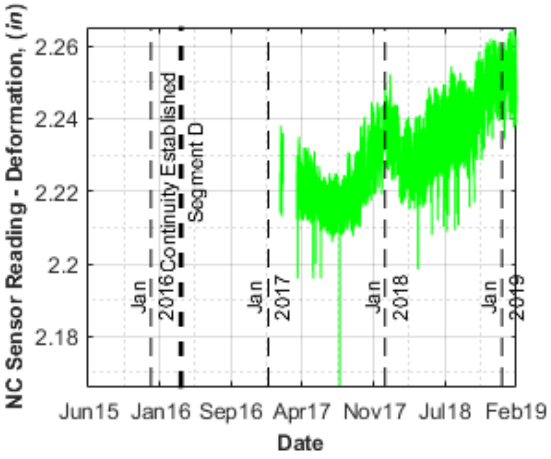

b) Sensor reading without temperature correction

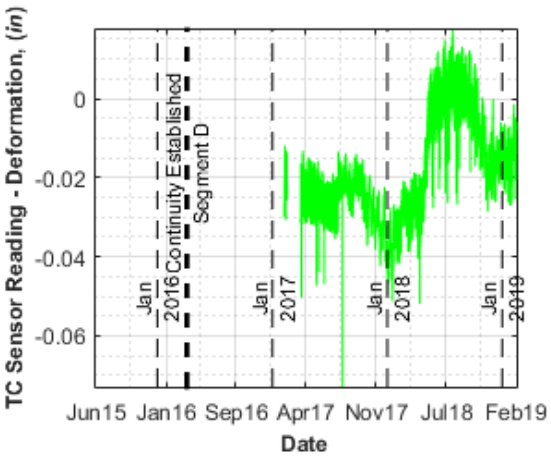

c) Sensor reading after temperature correction

B19_G7_BFW – Gapmeter on the riser in the west at Bent 19 Girder 7 in Segment D

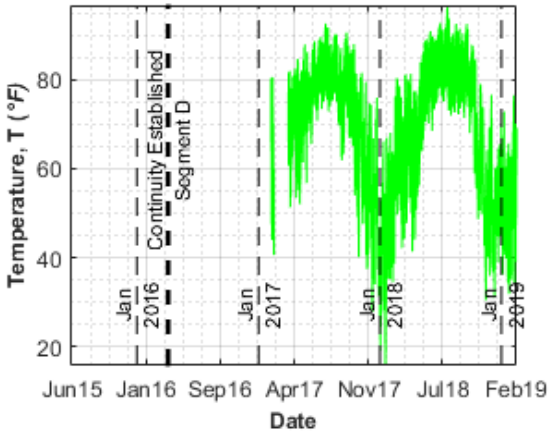

a) Temperature reading of the sensor

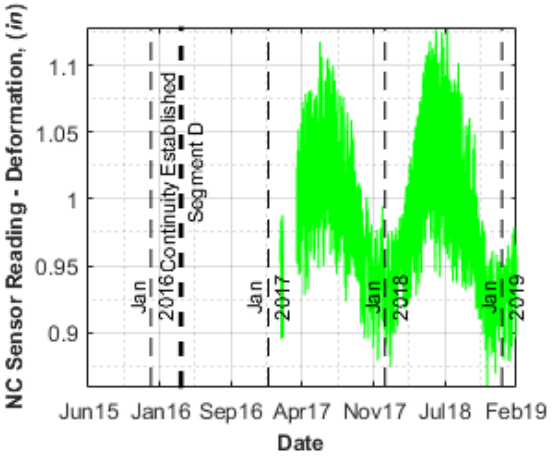

b) Sensor reading without temperature correction

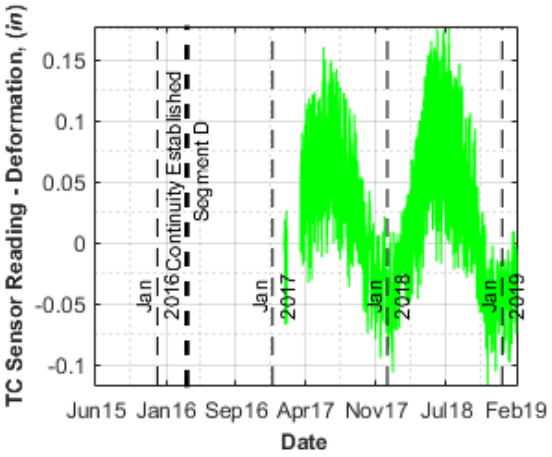

c) Sensor reading after temperature correction

B19_G7_BW – Gapmeter on the bottom of the web at Bent 19 Girder 7 in Segment D

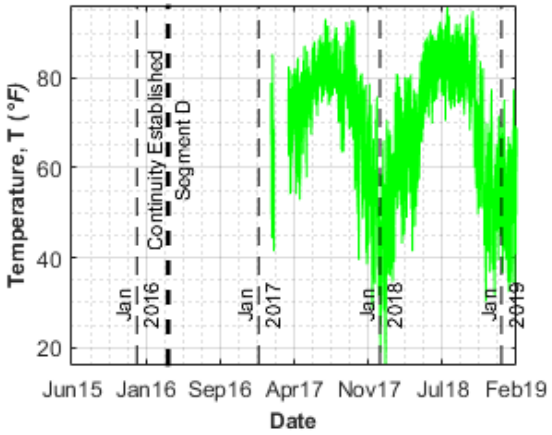

a) Temperature reading of the sensor

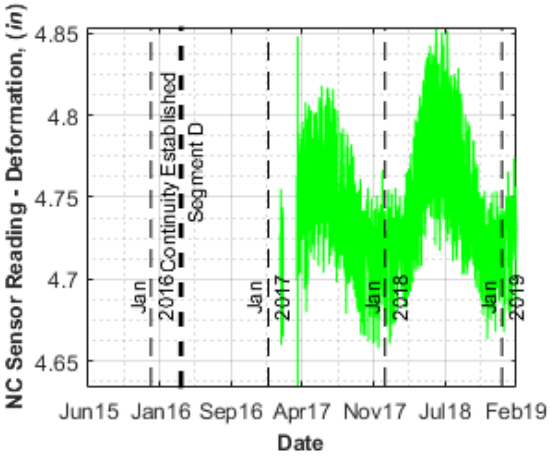

b) Sensor reading without temperature correction

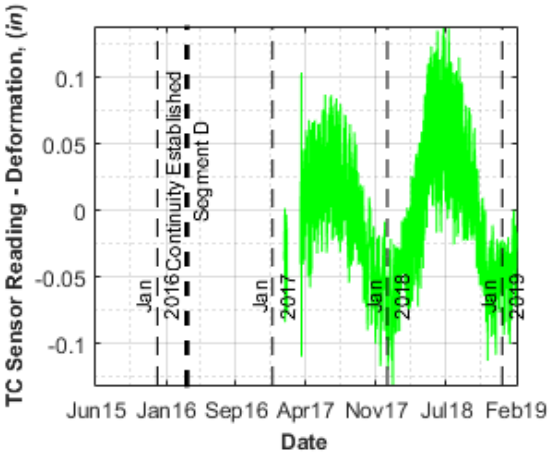

c) Sensor reading after temperature correction

B19_G7_TW – Gapmeter on the top of the web at Bent 19 Girder 7 in Segment D

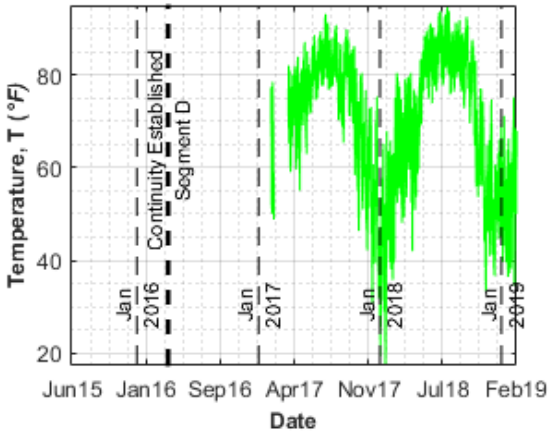

a) Temperature reading of the sensor

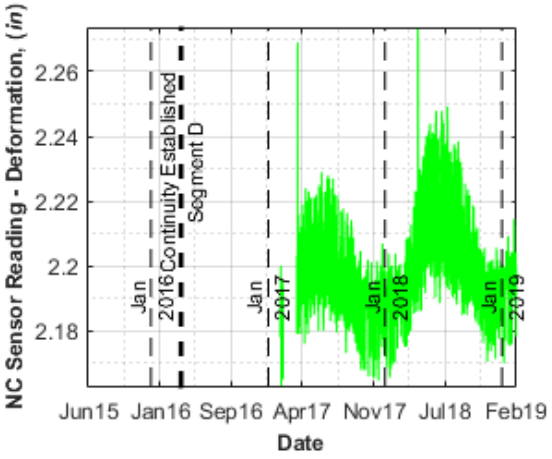

b) Sensor reading without temperature correction

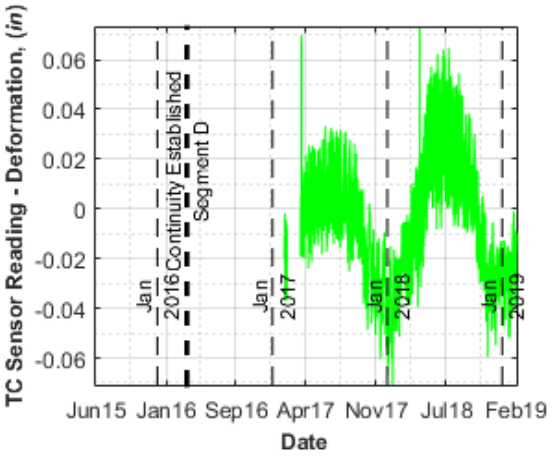

c) Sensor reading after temperature correction

B19_G4_CWE – Tiltmeter on the web on the east at Bent 19 Girder 4 in Segment D

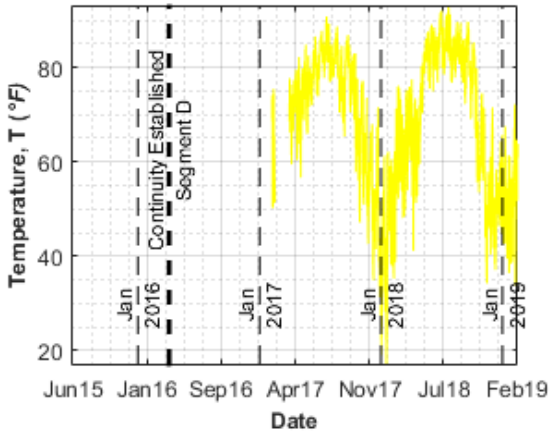

a) Temperature reading of the sensor

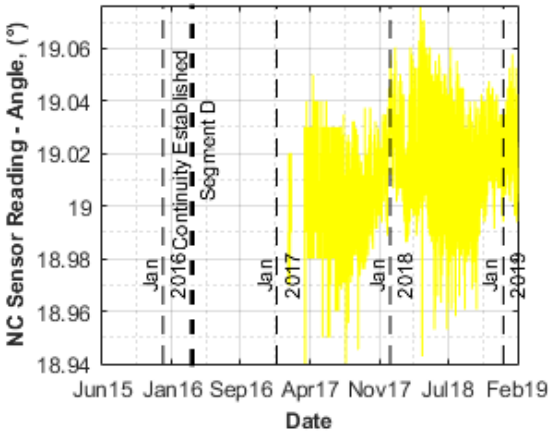

b) Sensor reading without temperature correction

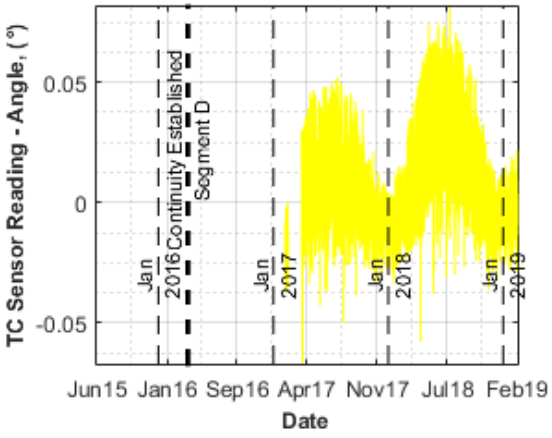

c) Sensor reading after temperature correction

B19_G7_CWE – Tiltmeter on the web on the east at Bent 19 Girder 7 in Segment D

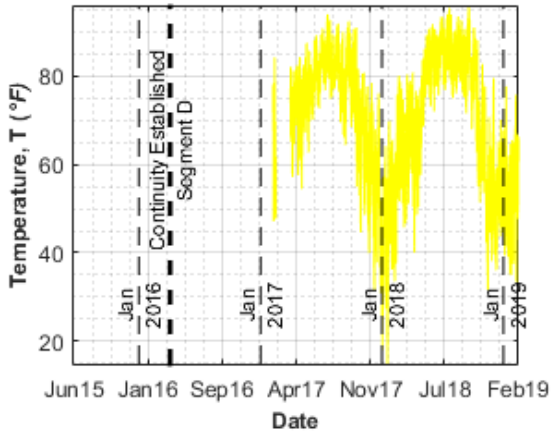

a) Temperature reading of the sensor

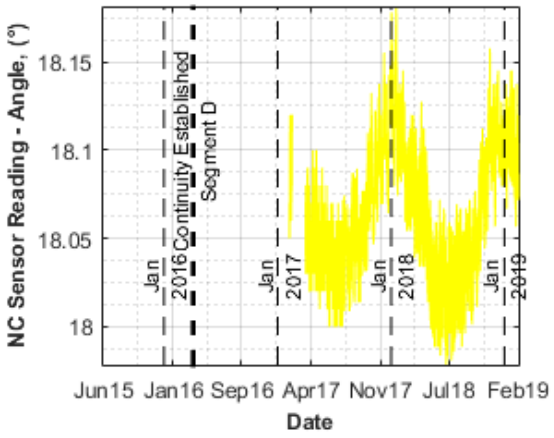

b) Sensor reading without temperature correction

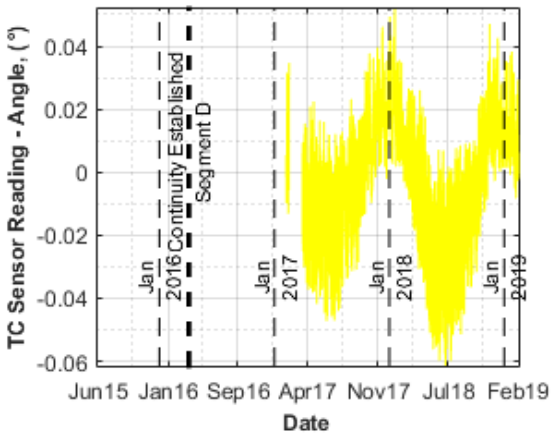

c) Sensor reading after temperature correction

B19_G4_BS –Strandmeter on the link slab at Bent 19 Girder 4 in Segment D

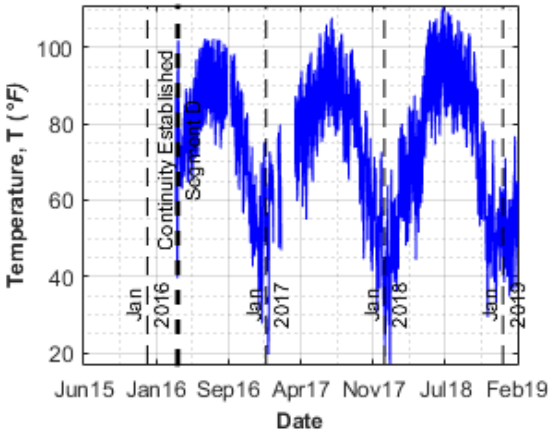

a) Temperature reading of the sensor

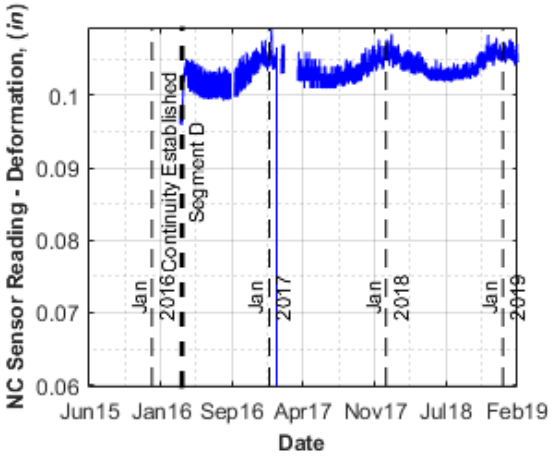

b) Sensor reading without temperature correction

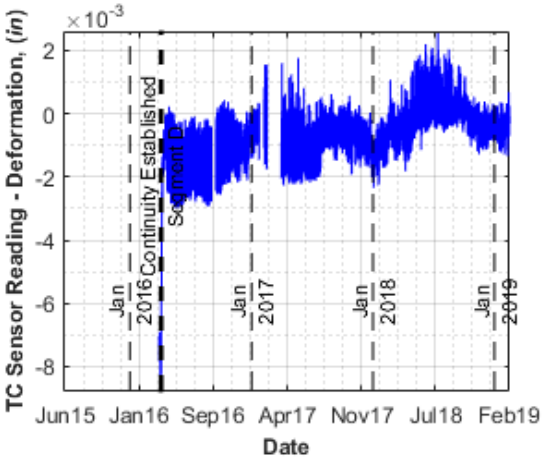

c) Sensor reading after temperature correction

B19_G4_TS – Strandmeter on the link slab at Bent 19 Girder 4 in Segment D

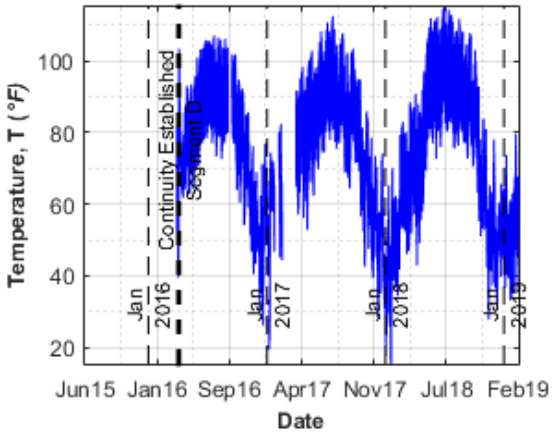

a) Temperature reading of the sensor

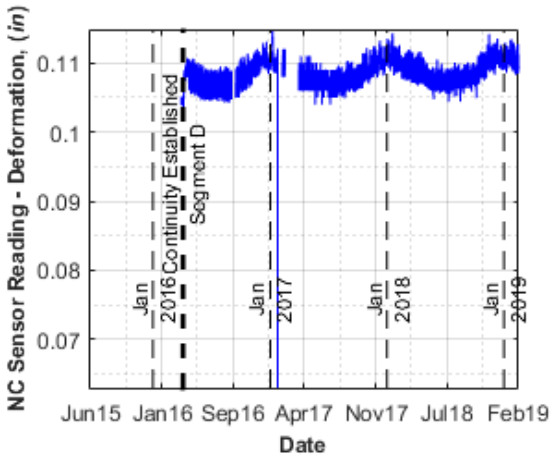

b) Sensor reading without temperature correction

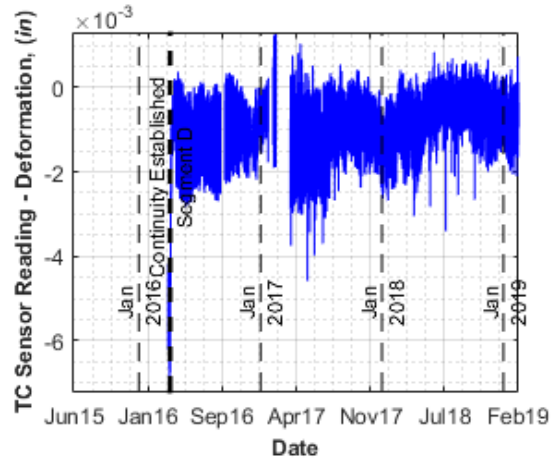

c) Sensor reading after temperature correction

B19_S5_5_BS –Strandmeter on the link slab at Bent 19 between Girder 4 and 5 in Segment D

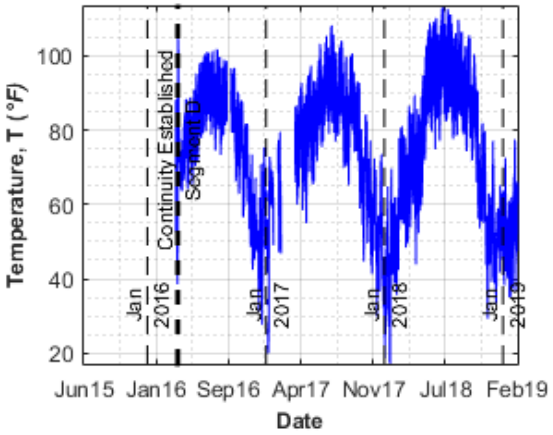

a) Temperature reading of the sensor

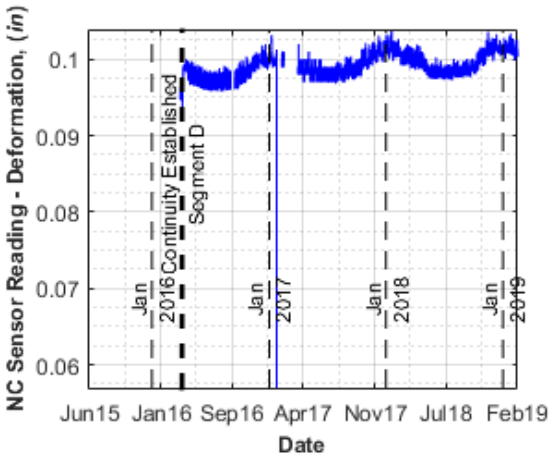

b) Sensor reading without temperature correction

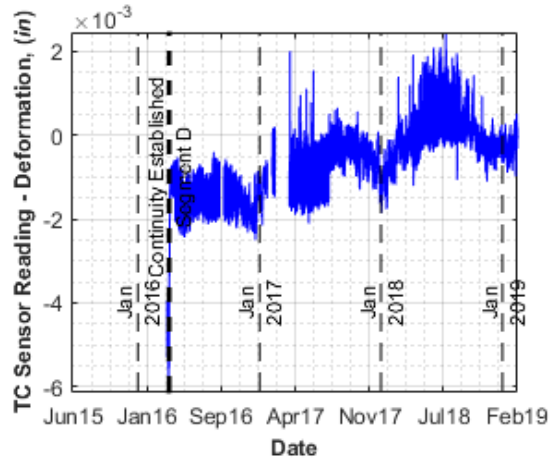

c) Sensor reading after temperature correction

B19_S5_5_TS – Strandmeter on the link slab at Bent 19 between Girder 4 and 5 in Segment D

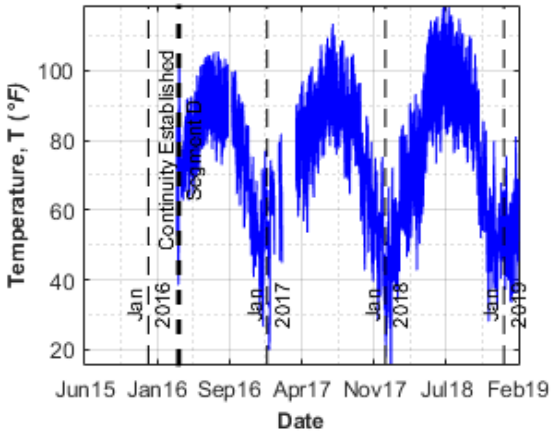

a) Temperature reading of the sensor

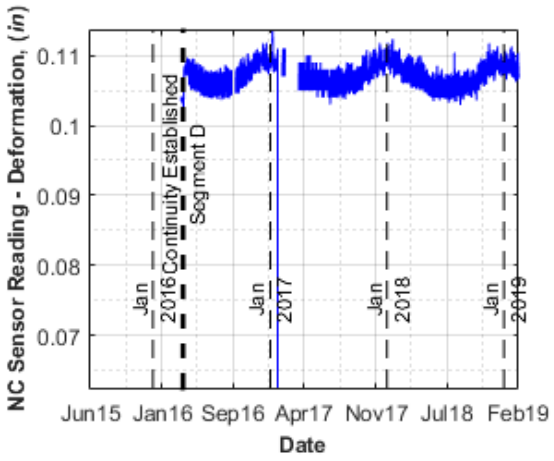

b) Sensor reading without temperature correction

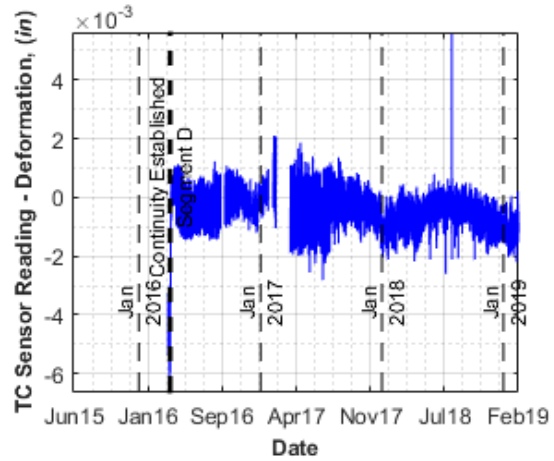

c) Sensor reading after temperature correction

B19_G7_BS –Strandmeter on the link slab at Bent 19 Girder 7 in Segment D

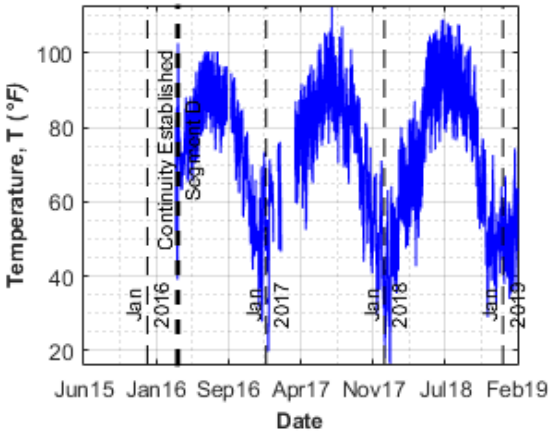

a) Temperature reading of the sensor

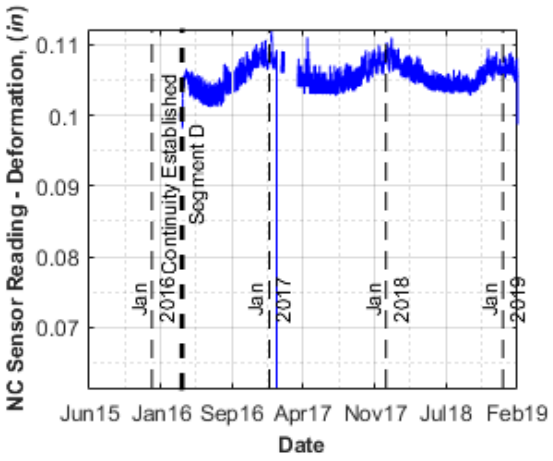

b) Sensor reading without temperature correction

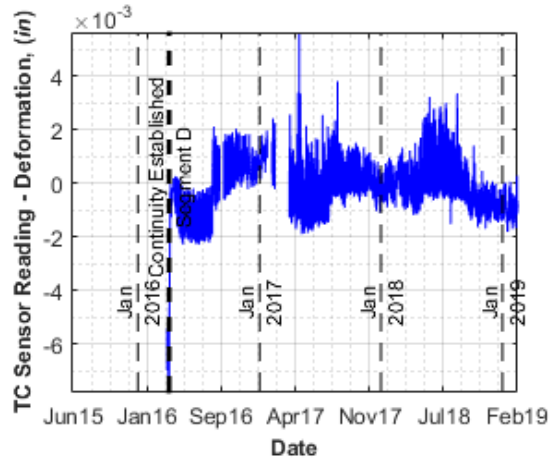

c) Sensor reading after temperature correction

B19_G7_TS –Strandmeter on the link slab at Bent 19 Girder 7 in Segment D

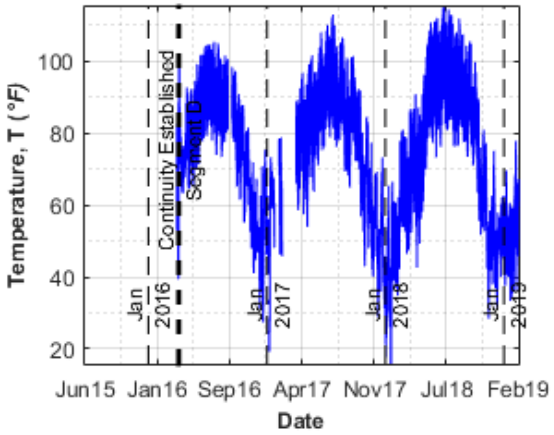

a) Temperature reading of the sensor

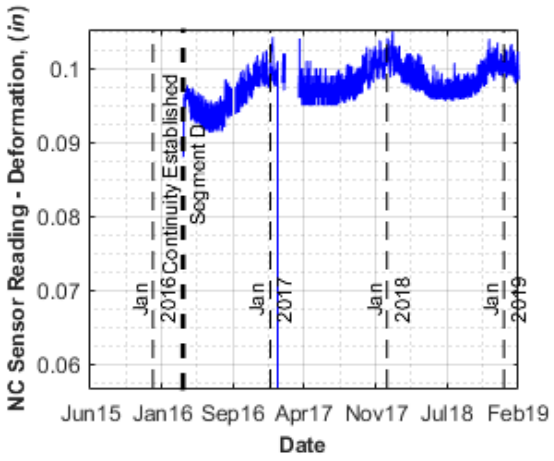

b) Sensor reading without temperature correction

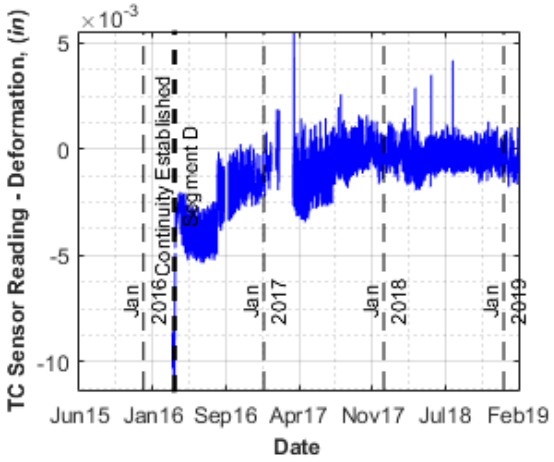

c) Sensor reading after temperature correction

B17_G4_BFE – Gapmeter on the riser in the east at Bent 17 Girder 4 in Segment C

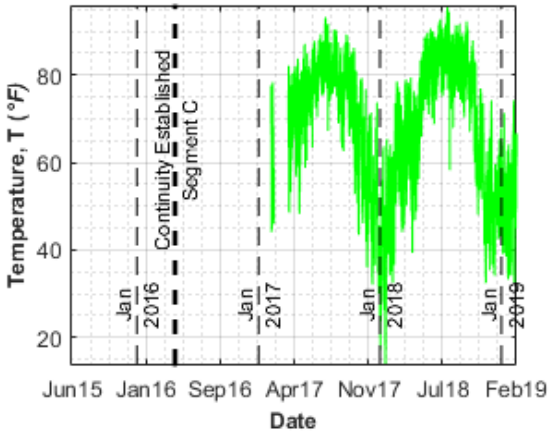

a) Temperature reading of the sensor

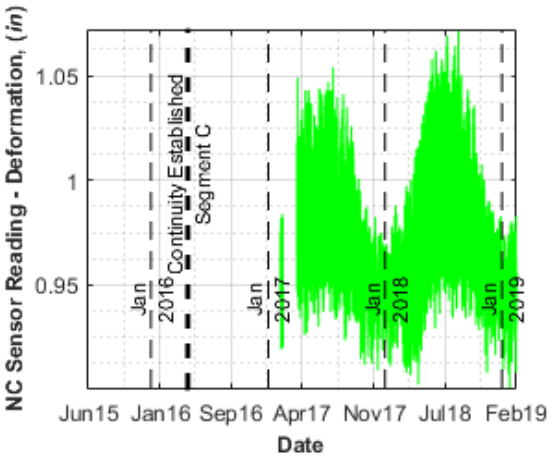

b) Sensor reading without temperature correction

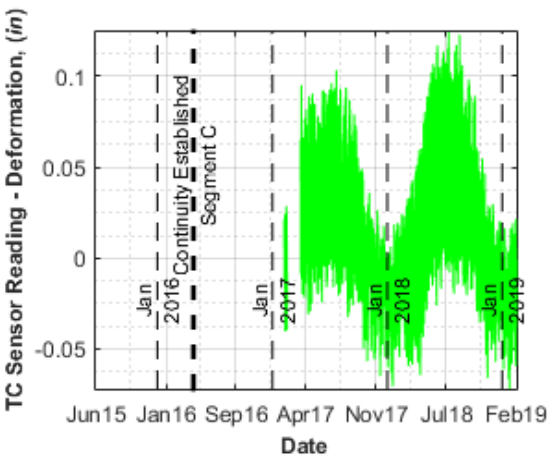

c) Sensor reading after temperature correction

B17_G4_BFW–Gapmeter on the riser in the west at Bent 17 Girder 4 in Segment C

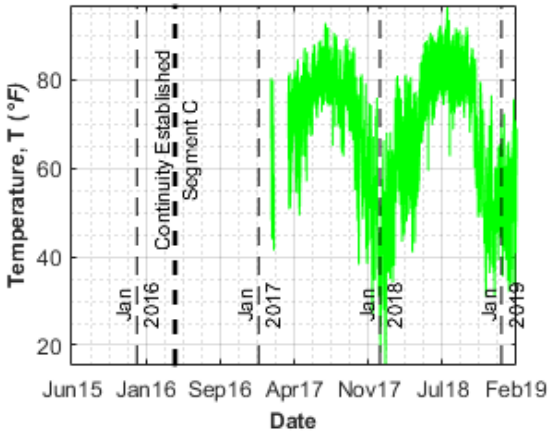

a) Temperature reading of the sensor

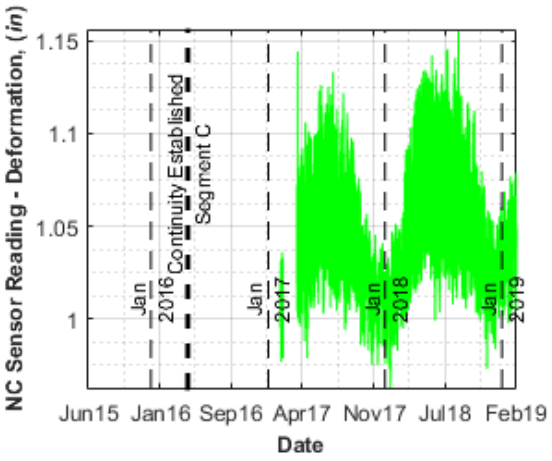

b) Sensor reading without temperature correction

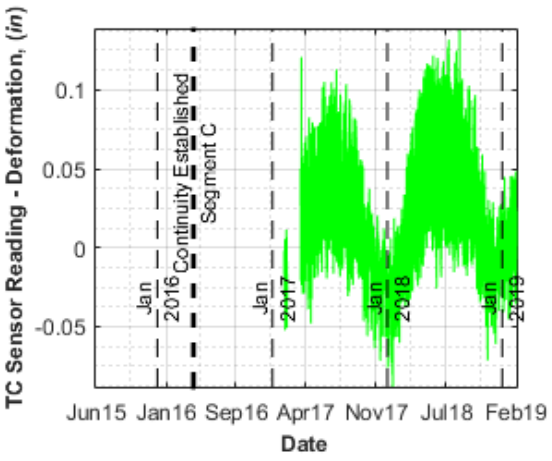

c) Sensor reading after temperature correction

B17_G4_BW – Gapmeter on the bottom of the web at Bent 17 Girder 4 in Segment C

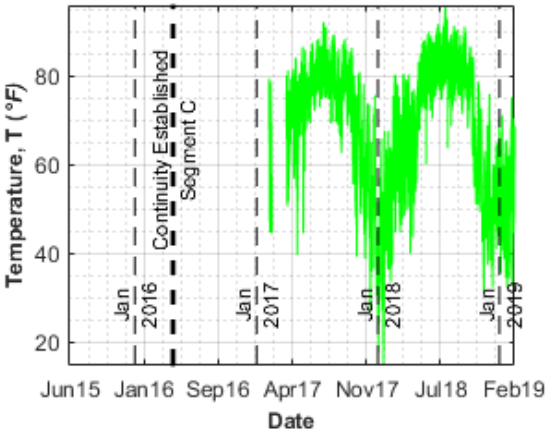

a) Temperature reading of the sensor

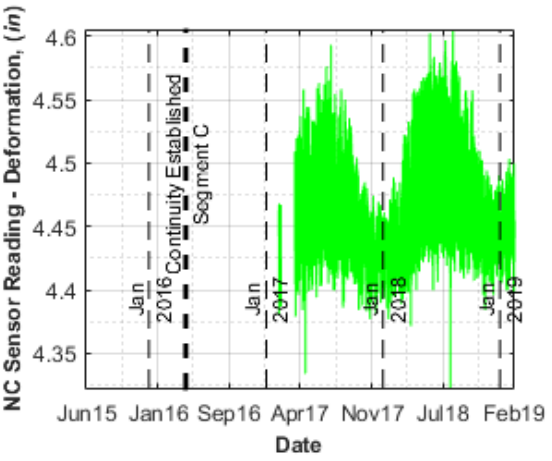

b) Sensor reading without temperature correction

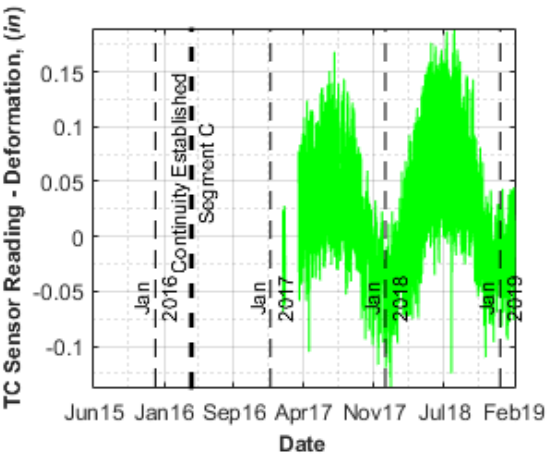

c) Sensor reading after temperature correction

B17_G4_TW– Gapmeter on the top of the web at Bent 17 Girder 4 in Segment C

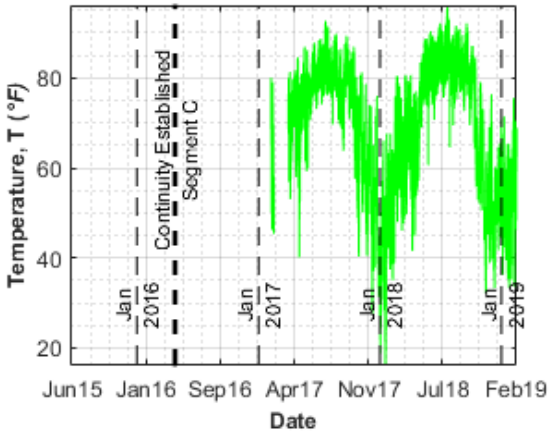

a) Temperature reading of the sensor

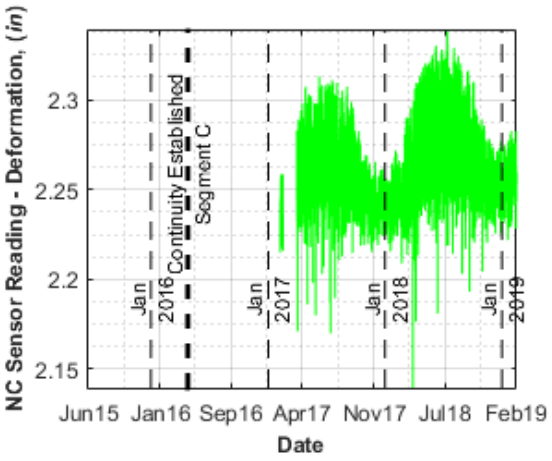

b) Sensor reading without temperature correction

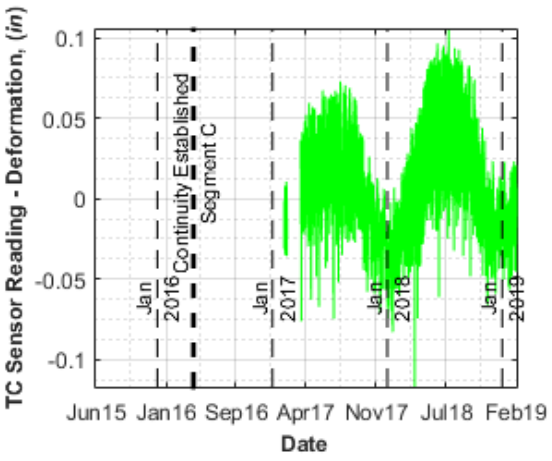

c) Sensor reading after temperature correction

B17_G7_BFE – Gapmeter on the riser in the east at Bent 17 Girder 7 in Segment C

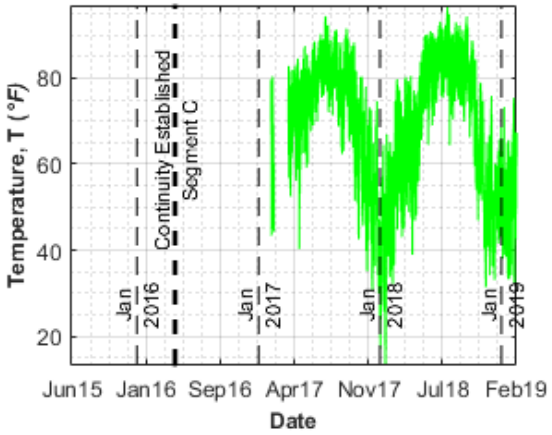

a) Temperature reading of the sensor

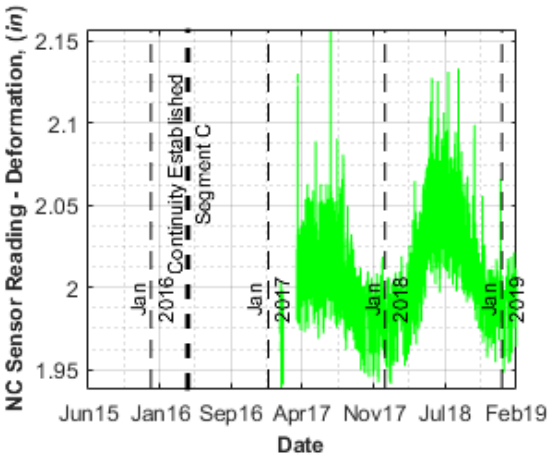

b) Sensor reading without temperature correction

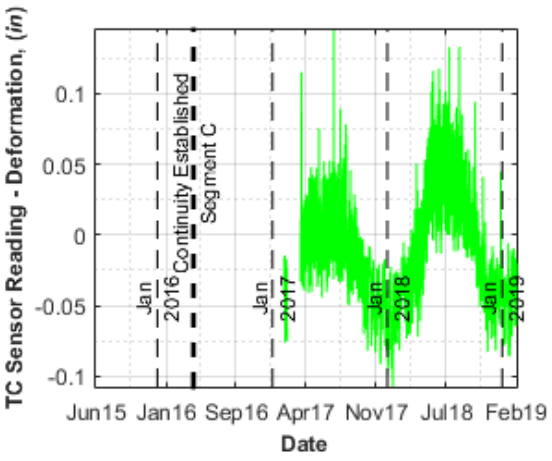

c) Sensor reading after temperature correction

B17_G7_BFW – Gapmeter on the riser in the west at Bent 17 Girder 7 in Segment C

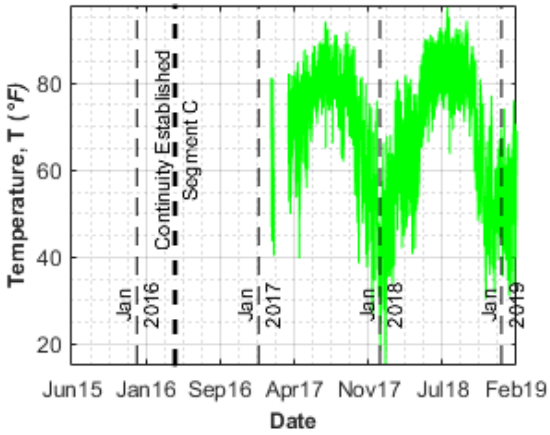

a) Temperature reading of the sensor

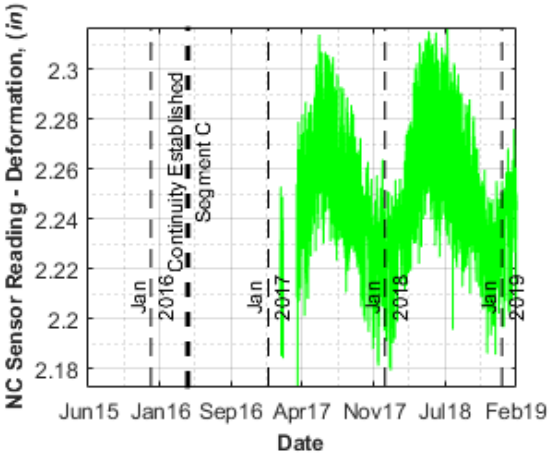

b) Sensor reading without temperature correction

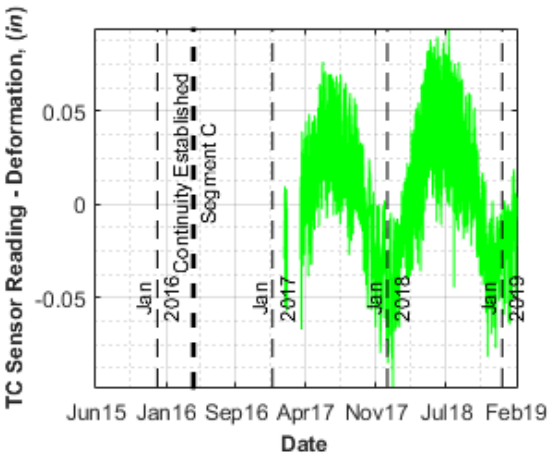

c) Sensor reading after temperature correction

B17_G7_BW – Gapmeter on the bottom of the web at Bent 17 Girder 7 in Segment C

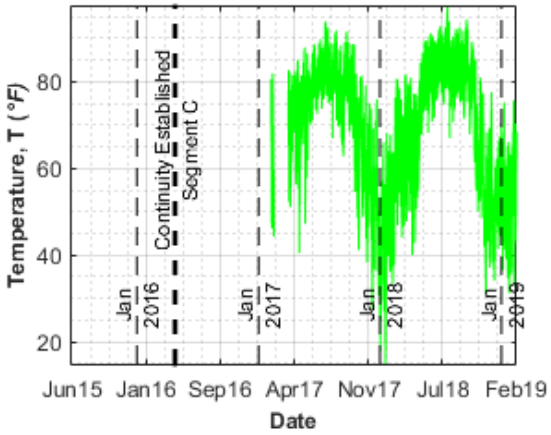

a) Temperature reading of the sensor

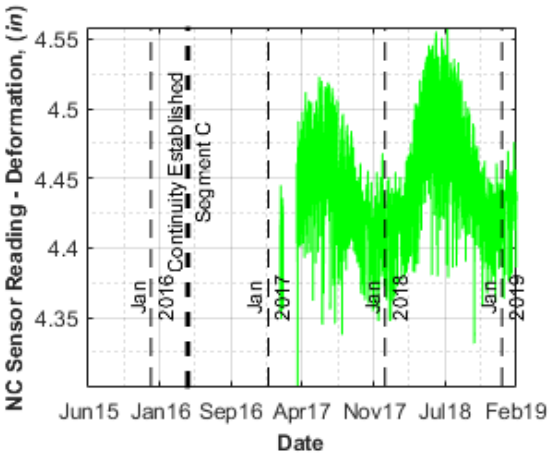

b) Sensor reading without temperature correction

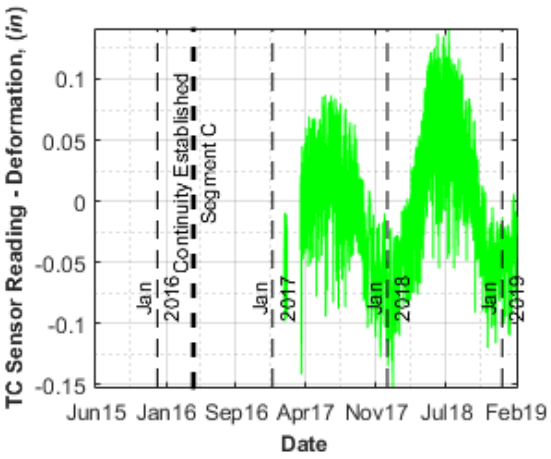

c) Sensor reading after temperature correction

B17_G7_TW – Gapmeter on the top of the web at Bent 17 Girder 7 in Segment C

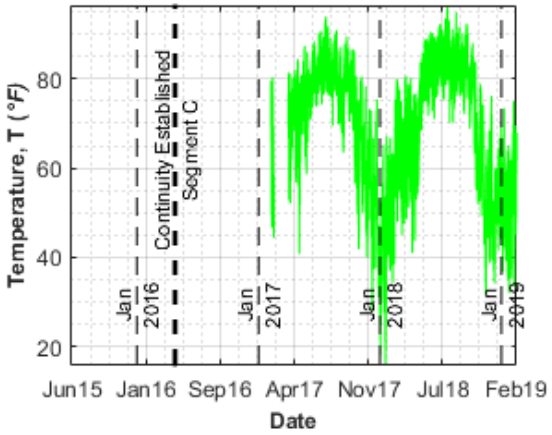

a) Temperature reading of the sensor

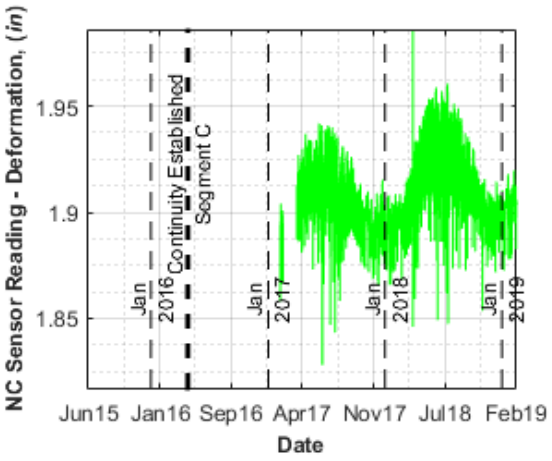

b) Sensor reading without temperature correction

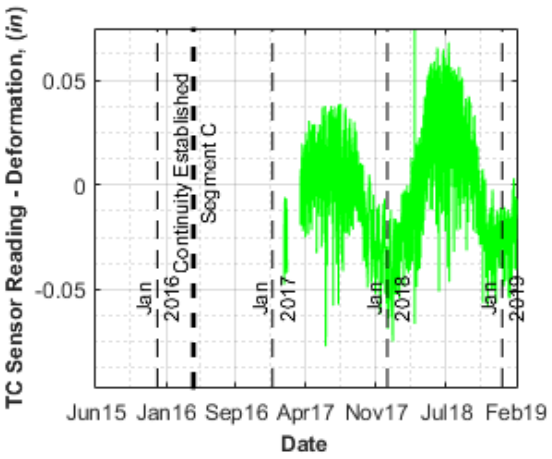

c) Sensor reading after temperature correction

B17_G4_BS – Strandmeter on the link slab at Bent 17 Girder 4 in Segment C

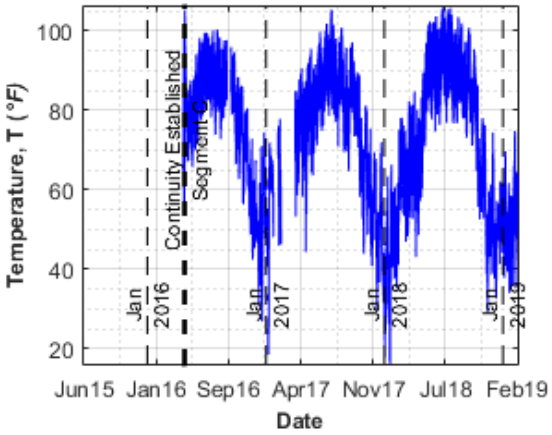

a) Temperature reading of the sensor

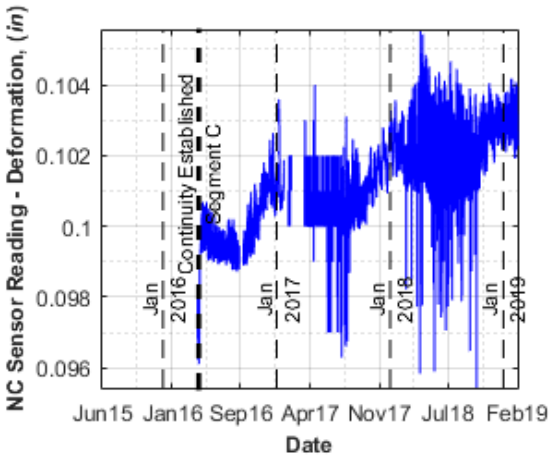

b) Sensor reading without temperature correction

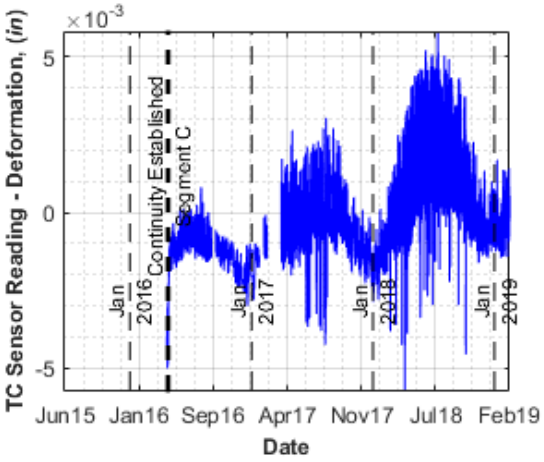

c) Sensor reading after temperature correction

B17_G4_TS – Strandmeter on the link slab at Bent 17 Girder 4 in Segment C

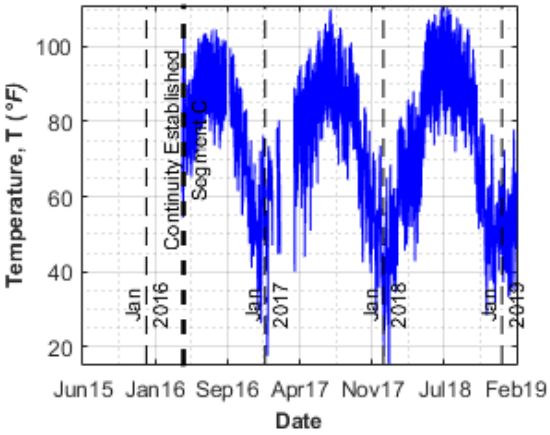

a) Temperature reading of the sensor

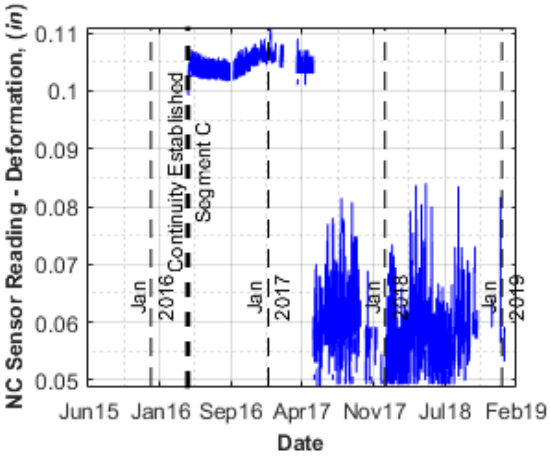

b) Sensor reading without temperature correction

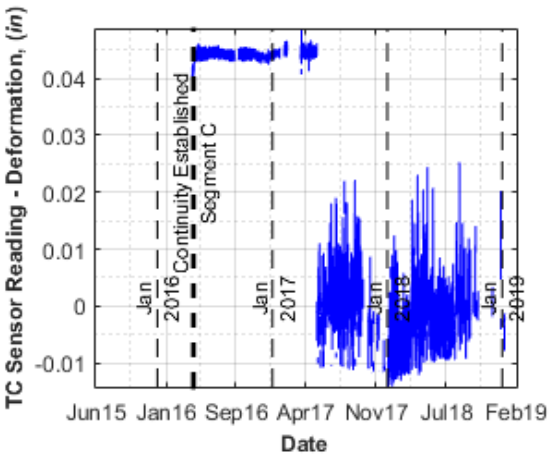

c) Sensor reading after temperature correction

B17_S5_5_BS – Strandmeter on the link slab at Bent 17 between Girder 4 and 5 in Segment C

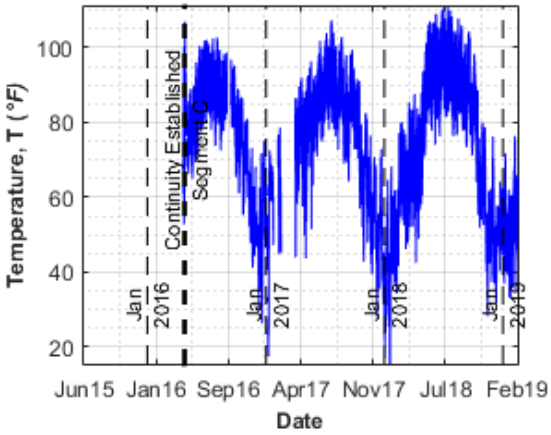

a) Temperature reading of the sensor

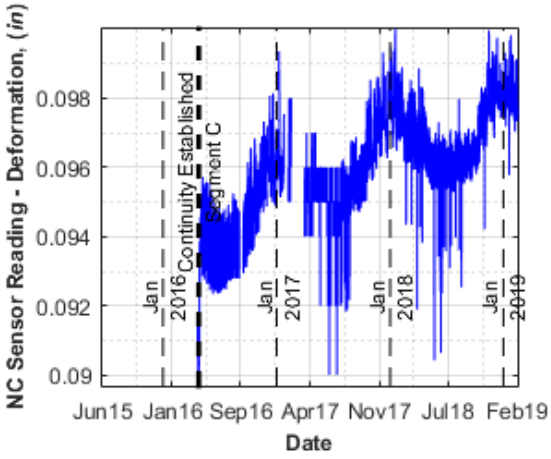

b) Sensor reading without temperature correction

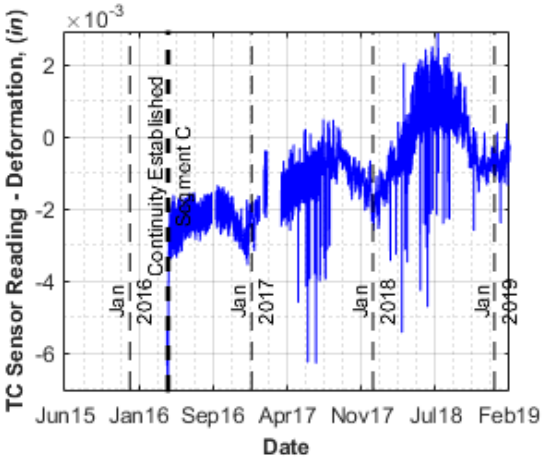

c) Sensor reading after temperature correction

B17_S5_5_TS – Strandmeter on the link slab at Bent 17 between Girder 4 and 5 in Segment C

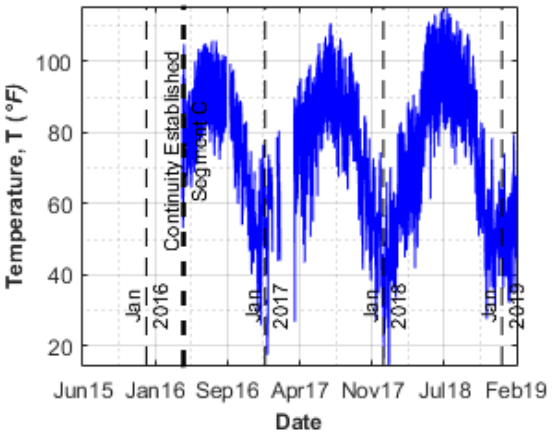

a) Temperature reading of the sensor

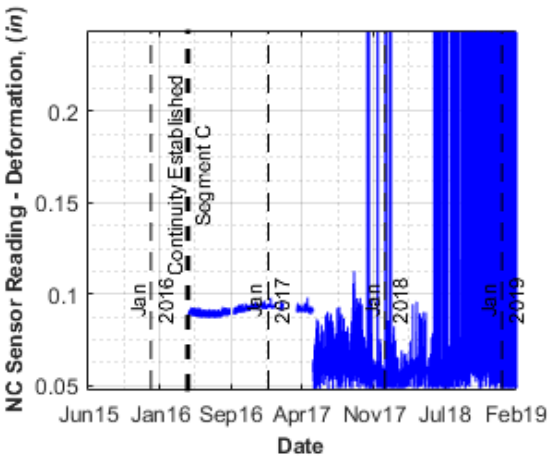

b) Sensor reading without temperature correction

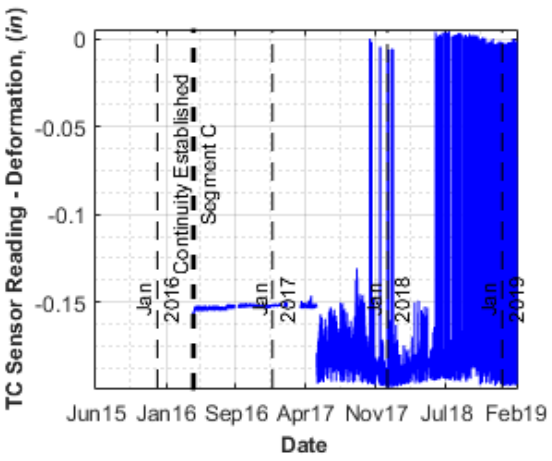

c) Sensor reading after temperature correction

B17_G7_BS – Strandmeter on the link slab at Bent 17 Girder 7 in Segment C

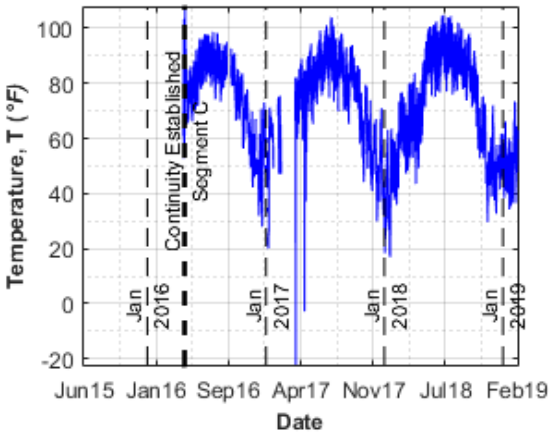

a) Temperature reading of the sensor

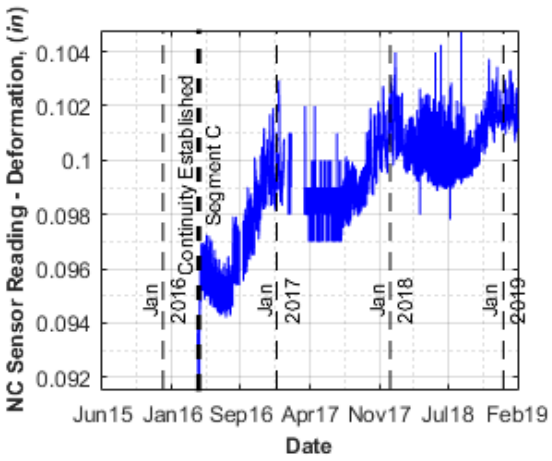

b) Sensor reading without temperature correction

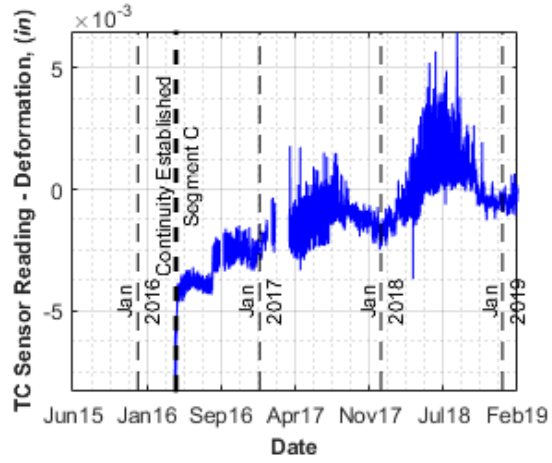

c) Sensor reading after temperature correction

B17_G7_TS – Strandmeter on the link slab at Bent 17 Girder 7 in Segment C

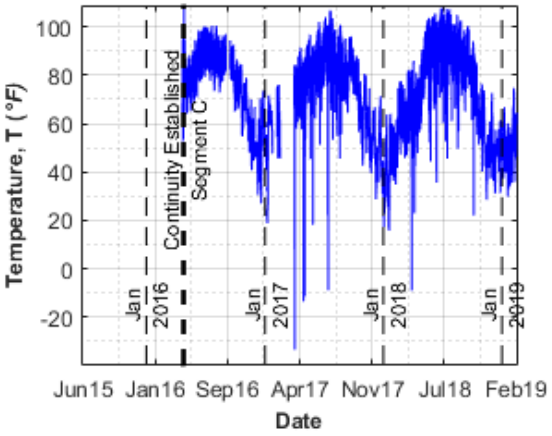

a) Temperature reading of the sensor

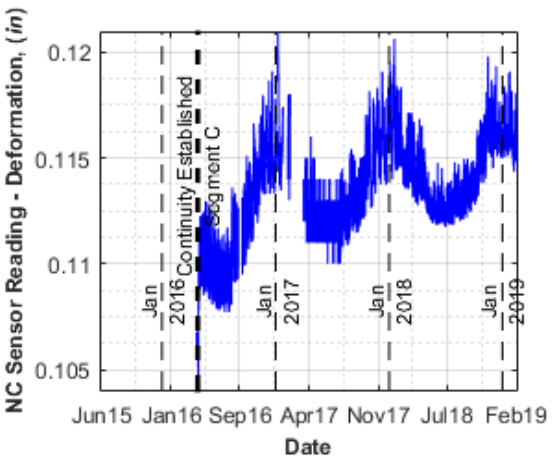

b) Sensor reading without temperature correction

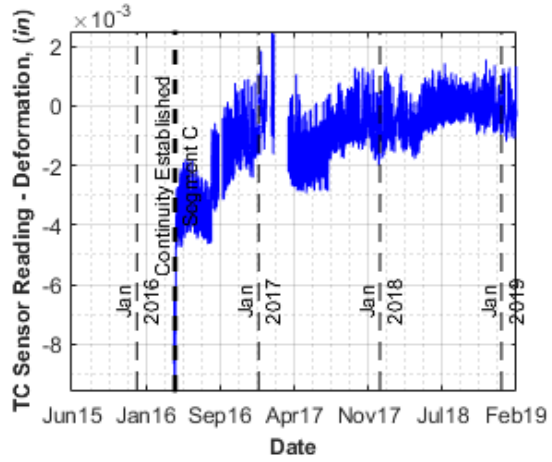

c) Sensor reading after temperature correction

B16_G4_BFE – Gapmeter on the riser in the east at Bent 16 Girder 4 in Segment C

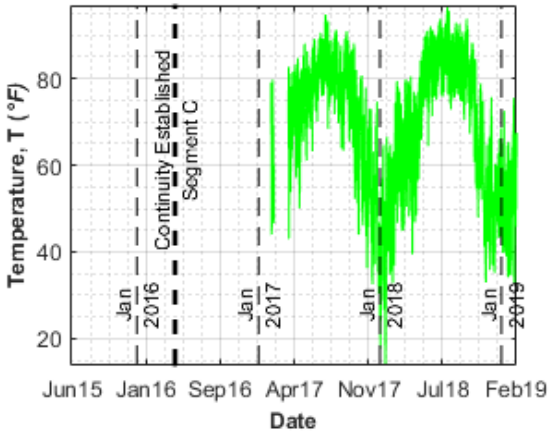

a) Temperature reading of the sensor

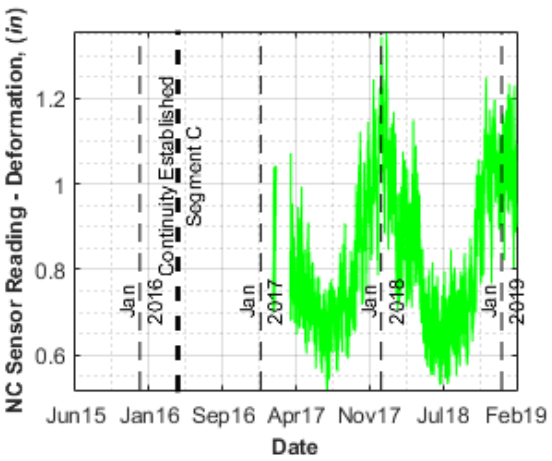

b) Sensor reading without temperature correction

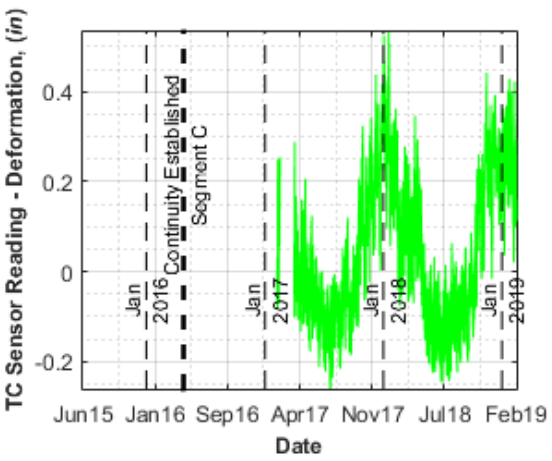

c) Sensor reading after temperature correction

B16_G4_BFW – Gapmeter on the riser in the west at Bent 16 Girder 4 in Segment B

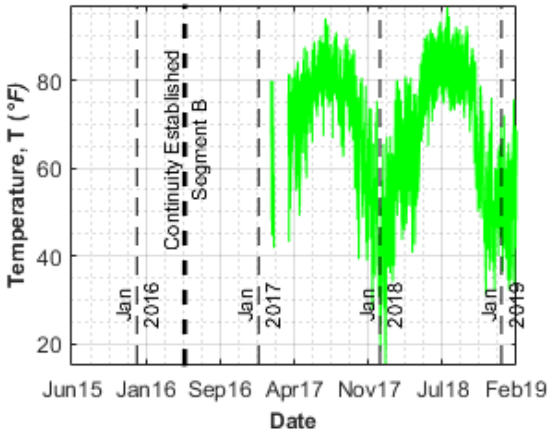

a) Temperature reading of the sensor

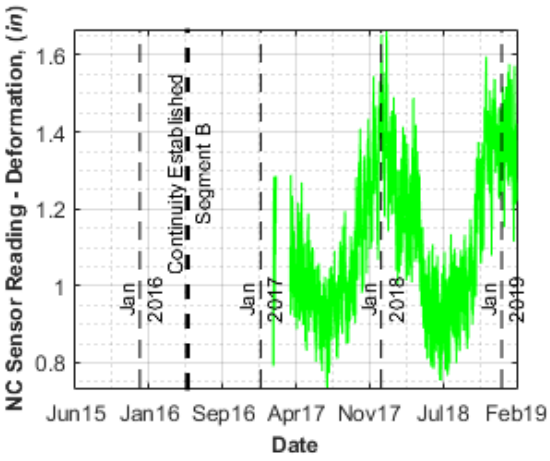

b) Sensor reading without temperature correction

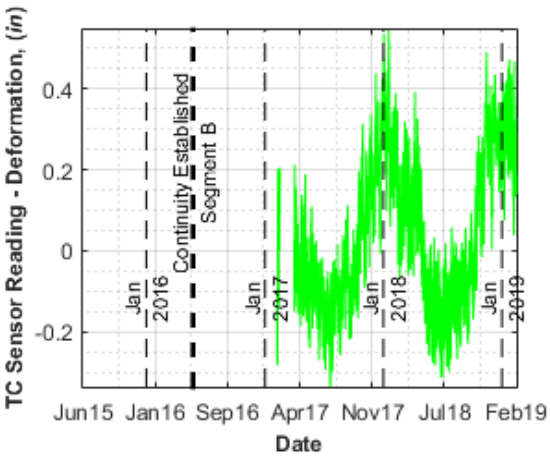

c) Sensor reading after temperature correction

B16_G4_BW – Gapmeter on the bottom of the web at Bent 16 Girder 4 in Segment B

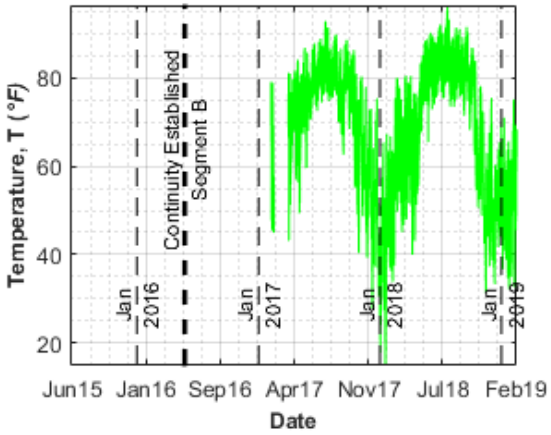

a) Temperature reading of the sensor

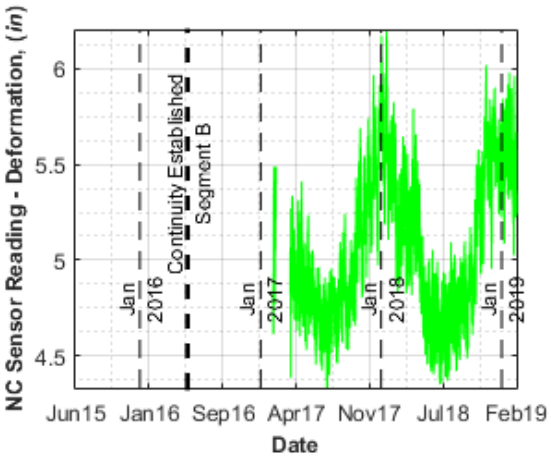

b) Sensor reading without temperature correction

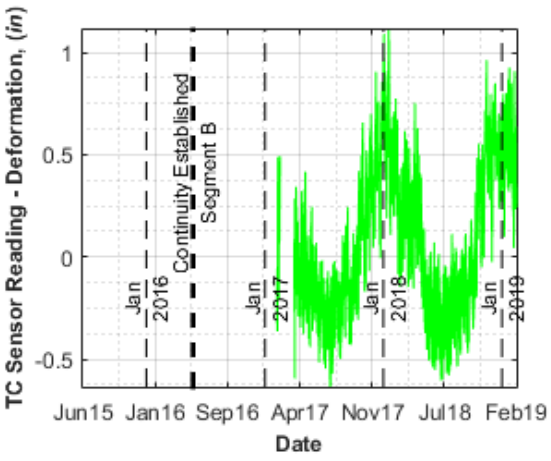

c) Sensor reading after temperature correction

B16_G4_TW – Gapmeter on the top of the web at Bent 16 Girder 4 in Segment B

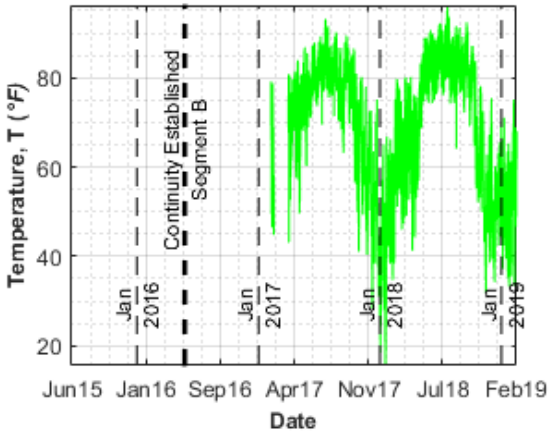

a) Temperature reading of the sensor

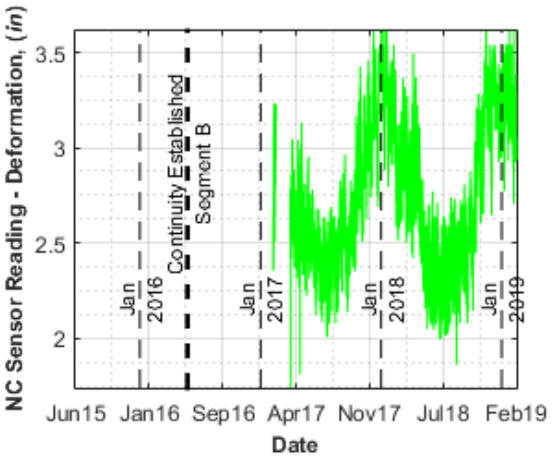

b) Sensor reading without temperature correction

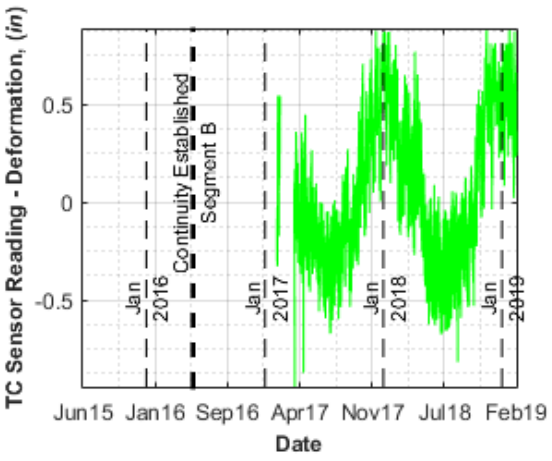

c) Sensor reading after temperature correction

B16_G7_BFE – Gapmeter on the riser in the east at Bent 16 Girder 7 in Segment C

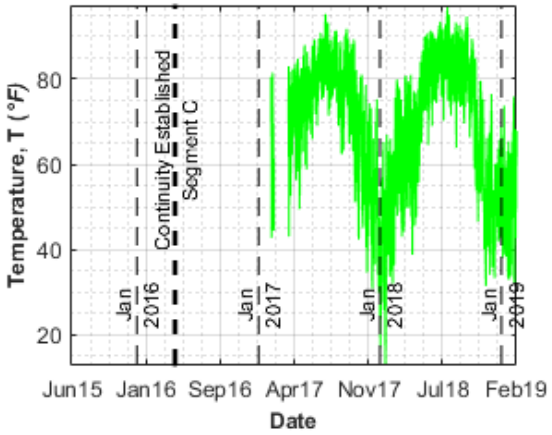

a) Temperature reading of the sensor

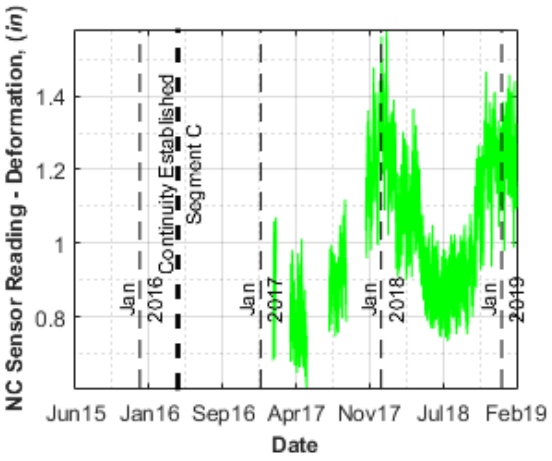

b) Sensor reading without temperature correction

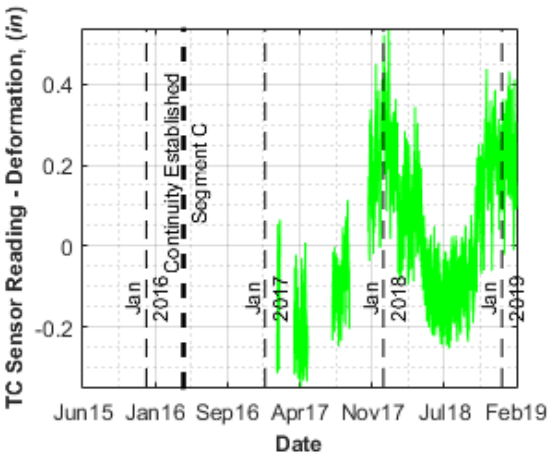

c) Sensor reading after temperature correction

B16_G7_BFW – Gapmeter on the riser in the west at Bent 16 Girder 7 in Segment B

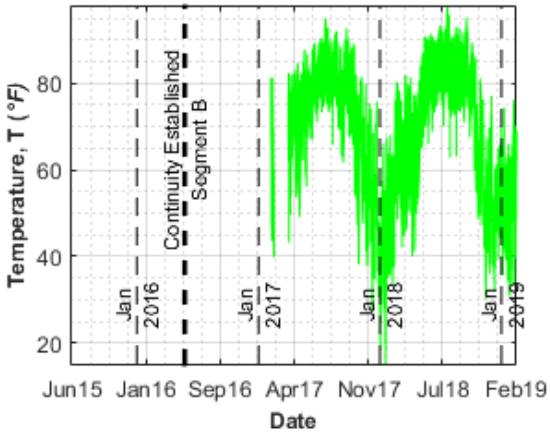

a) Temperature reading of the sensor

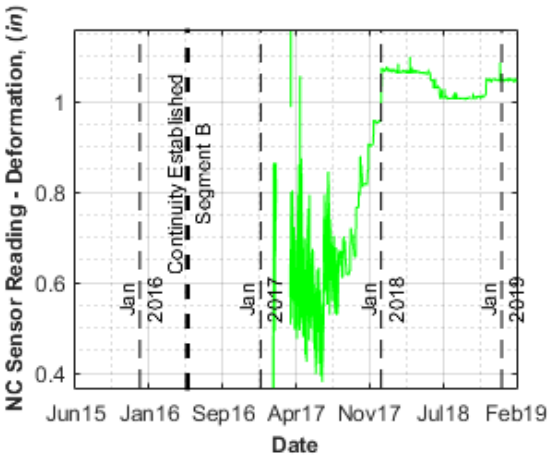

b) Sensor reading without temperature correction

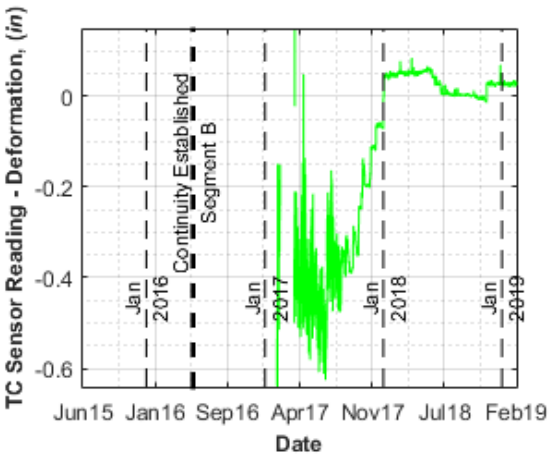

c) Sensor reading after temperature correction

B16_G7_BW – Gapmeter on the bottom of the web at Bent 16 Girder 7 in Segment B

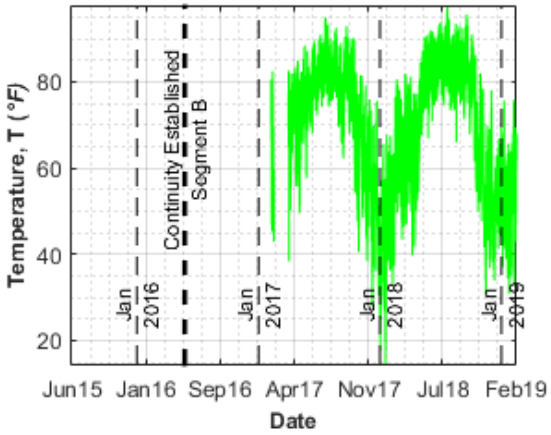

a) Temperature reading of the sensor

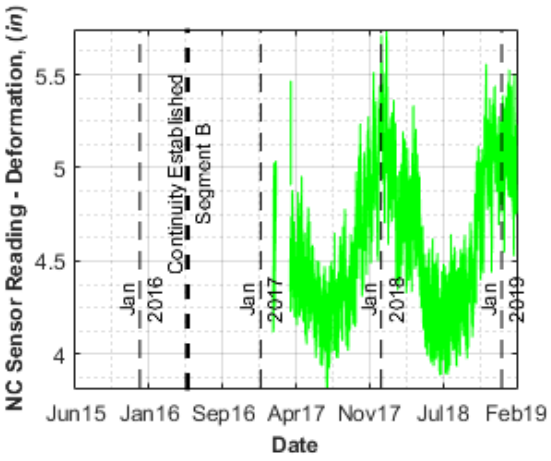

b) Sensor reading without temperature correction

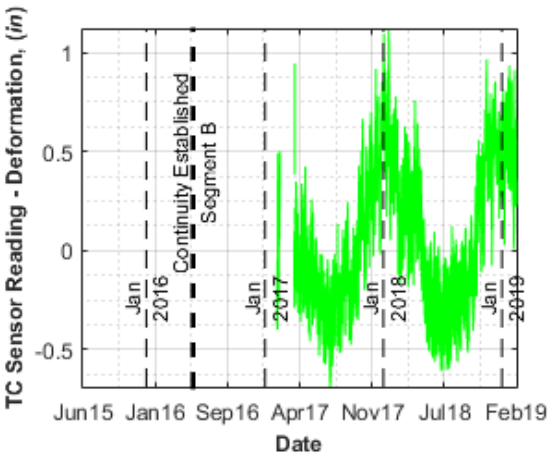

c) Sensor reading after temperature correction

B16_G7_TW – Gapmeter on the bottom of the web at Bent 16 Girder 7 in Segment B

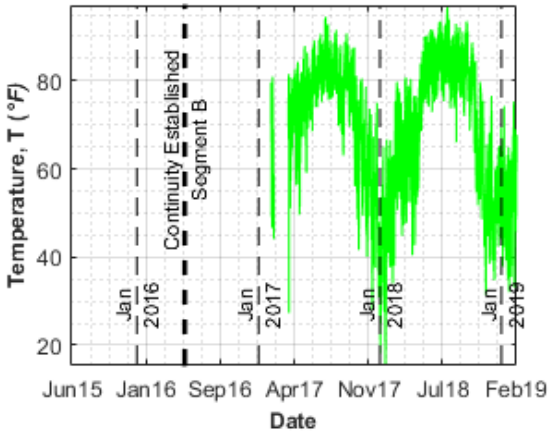

a) Temperature reading of the sensor

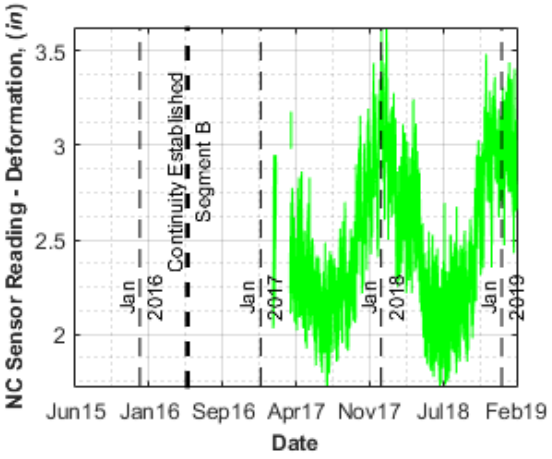

b) Sensor reading without temperature correction

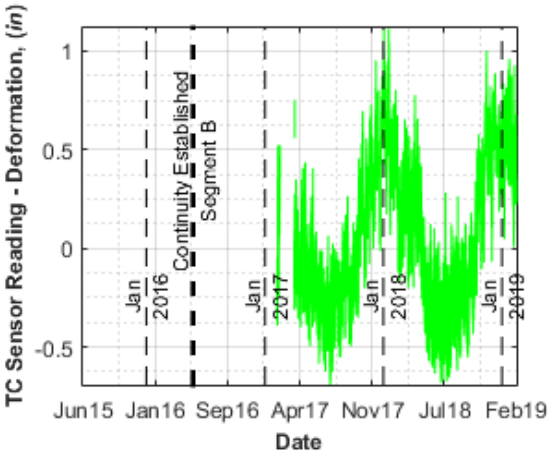

c) Sensor reading after temperature correction

B16_G4_CWE – Tiltmeter on the web on the east at Bent 16 Girder 4 in Segment C

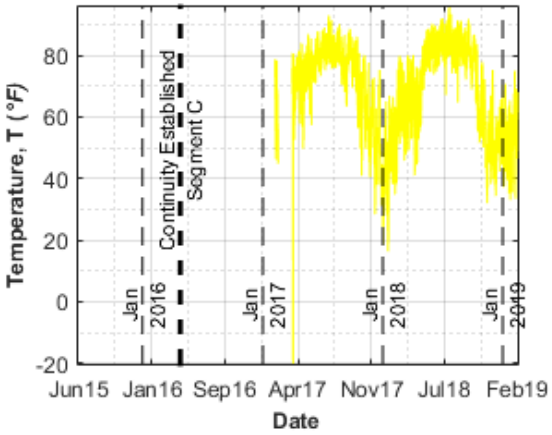

a) Temperature reading of the sensor

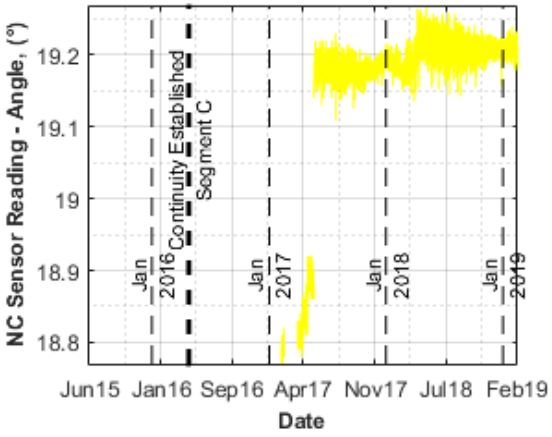

b) Sensor reading without temperature correction

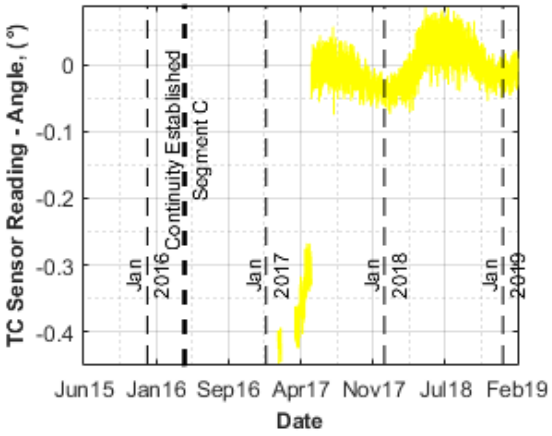

c) Sensor reading after temperature correction

B16_G7_CWE – Tiltmeter on the web on the east at Bent 16 Girder 7 in Segment C

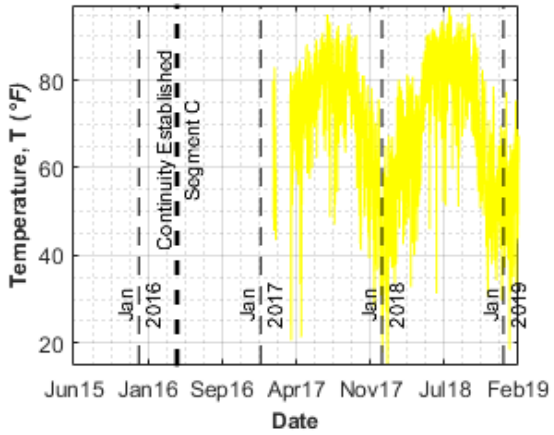

a) Temperature reading of the sensor

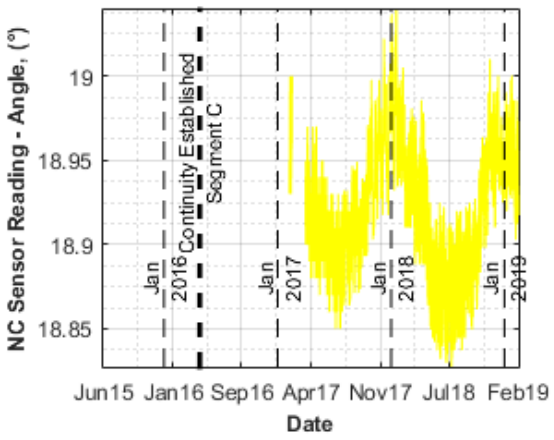

b) Sensor reading without temperature correction

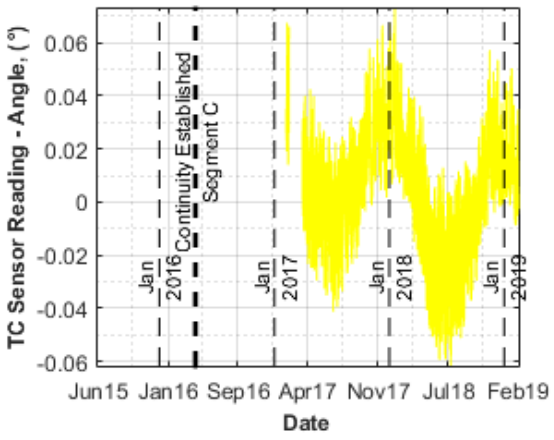

c) Sensor reading after temperature correction

B15_G4_BS – Strandmeter on the link slab at Bent 15 Girder 4 in Segment B

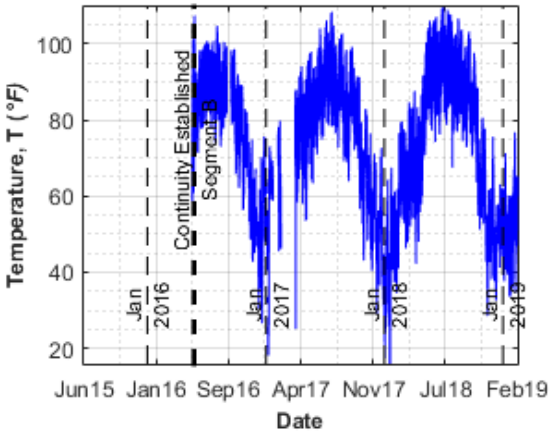

a) Temperature reading of the sensor

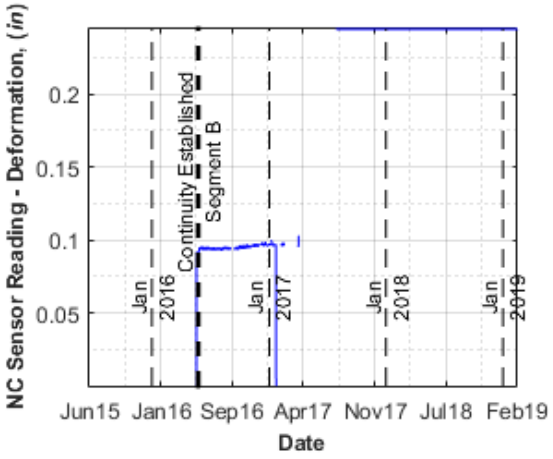

b) Sensor reading without temperature correction

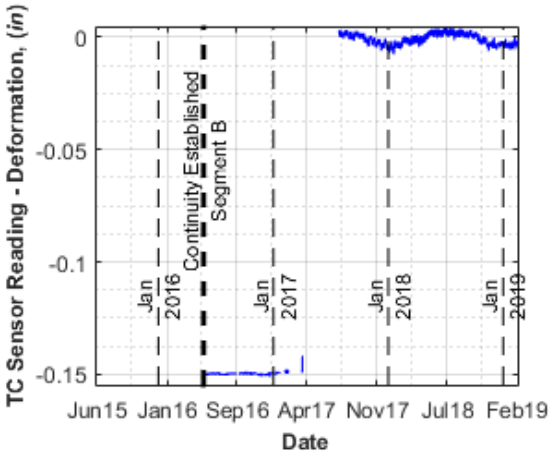

c) Sensor reading after temperature correction

B15_G4_TS – Strandmeter on the link slab at Bent 15 Girder 4 in Segment B

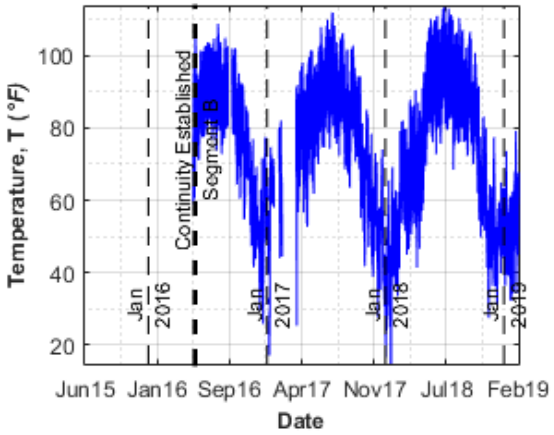

a) Temperature reading of the sensor

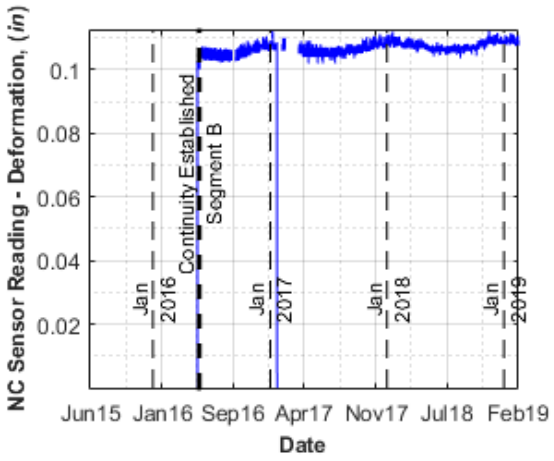

b) Sensor reading without temperature correction

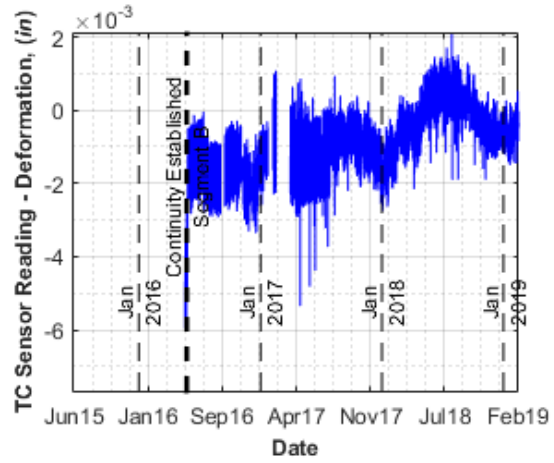

c) Sensor reading after temperature correction

B15_S5_5_BS – Strandmeter on the link slab at Bent 15 between Girder 4 and 5 in Segment B

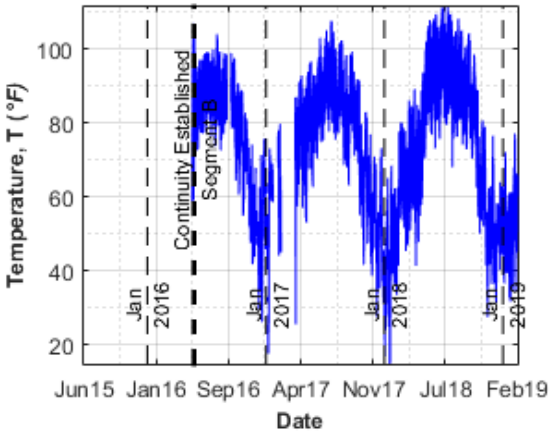

a) Temperature reading of the sensor

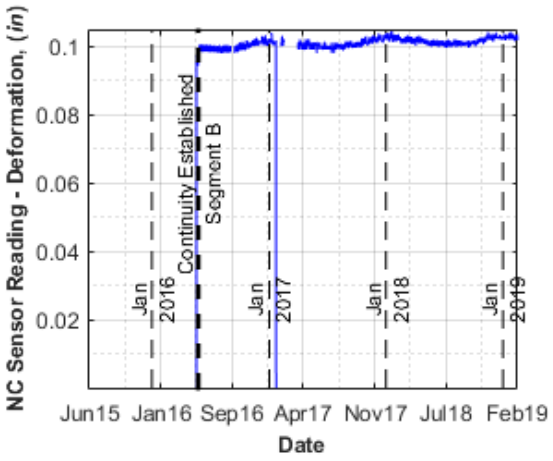

b) Sensor reading without temperature correction

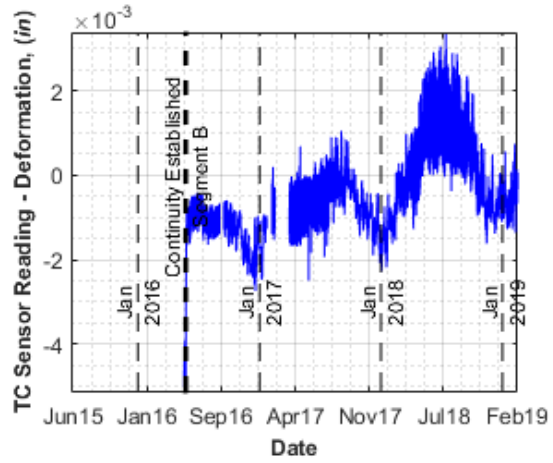

c) Sensor reading after temperature correction

B15_S5_5_TS – Strandmeter on the link slab at Bent 15 between Girder 4 and 5 in Segment B

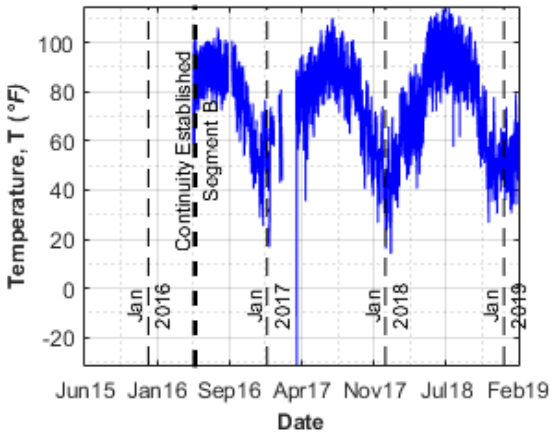

a) Temperature reading of the sensor

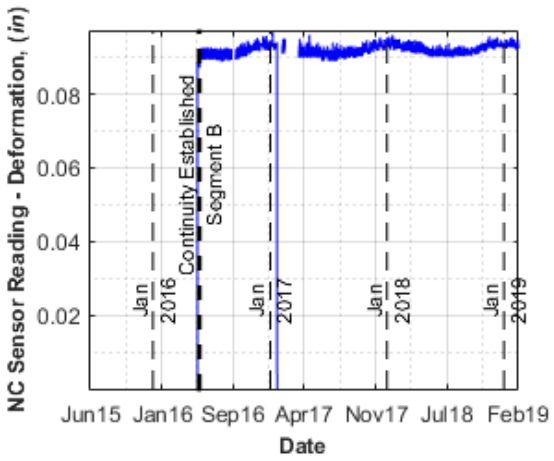

b) Sensor reading without temperature correction

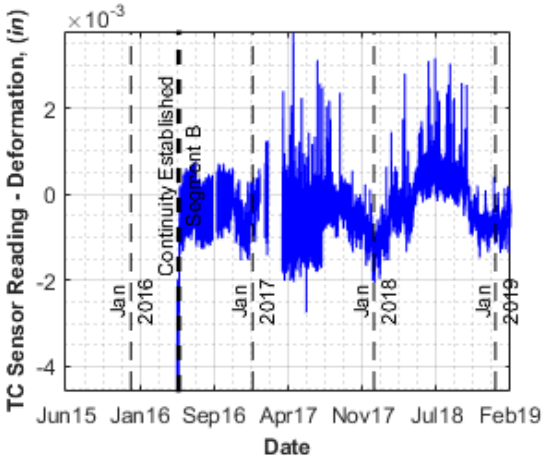

c) Sensor reading after temperature correction

B15_G7_BS – Strandmeter on the link slab at Bent 15 Girder 7 in Segment B

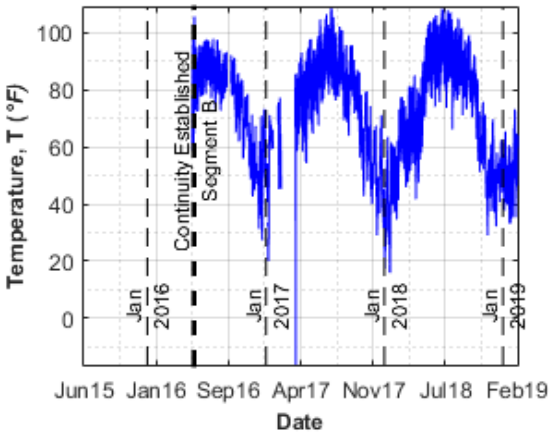

a) Temperature reading of the sensor

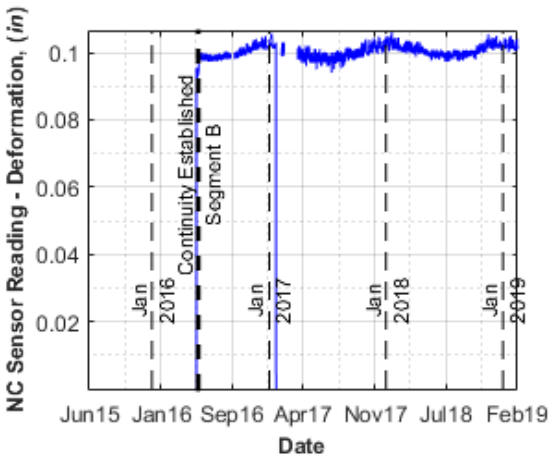

b) Sensor reading without temperature correction

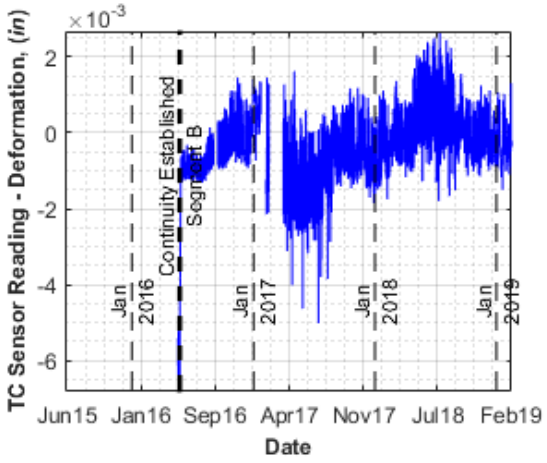

c) Sensor reading after temperature correction

B15_G7_TS – Strandmeter on the link slab at Bent 15 Girder 7 in Segment B

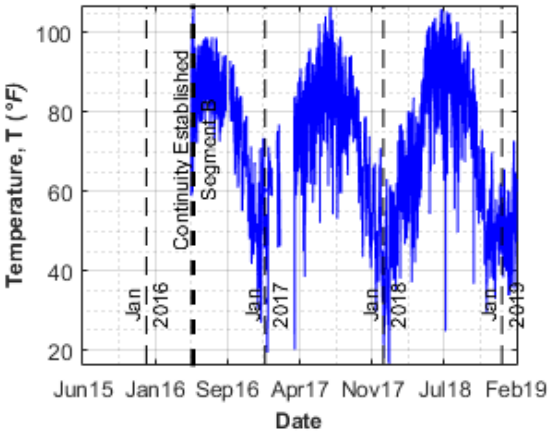

a) Temperature reading of the sensor

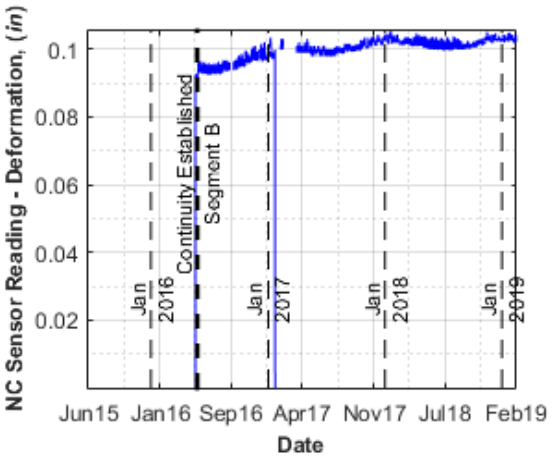

b) Sensor reading without temperature correction

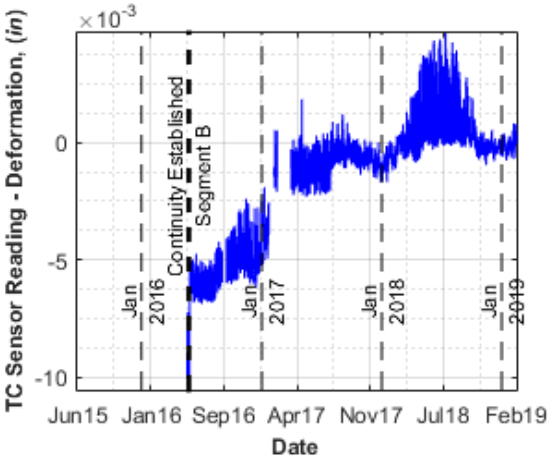

c) Sensor reading after temperature correction

B14_G4_BFE – Gapmeter on the riser in the east at Bent 14 Girder 4 in Segment B

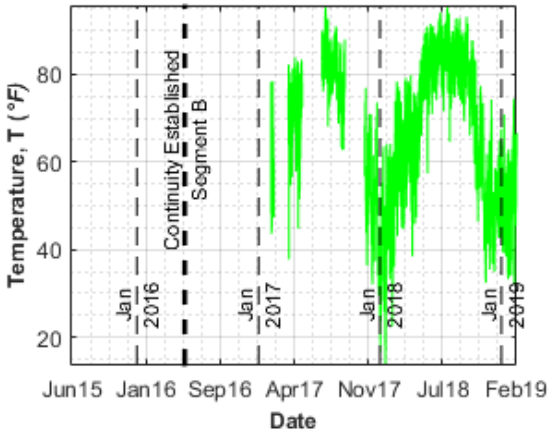

a) Temperature reading of the sensor

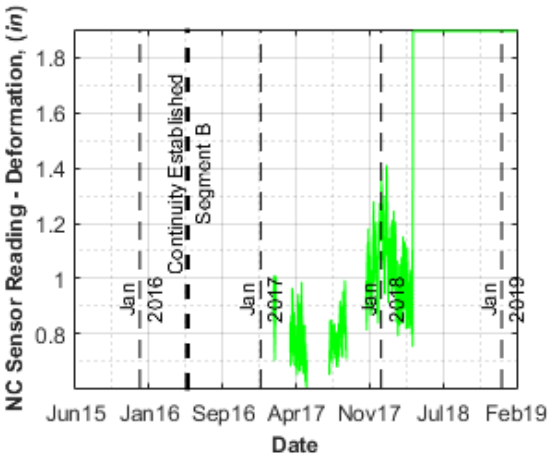

b) Sensor reading without temperature correction

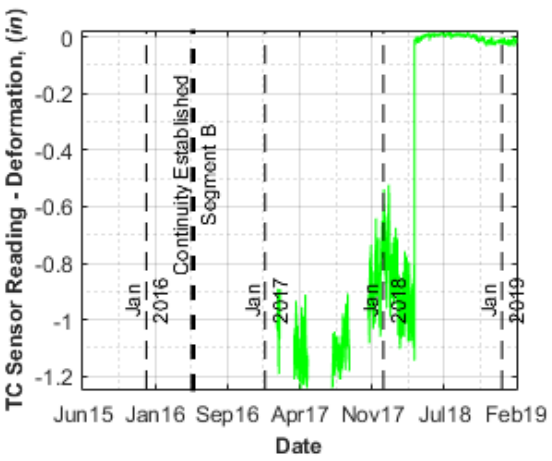

c) Sensor reading after temperature correction

B14_G4_BFW – Gapmeter on the riser in the west at Bent 14 Girder 4 in Segment B

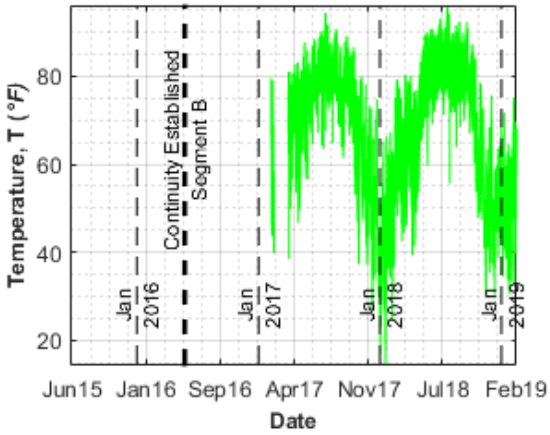

a) Temperature reading of the sensor

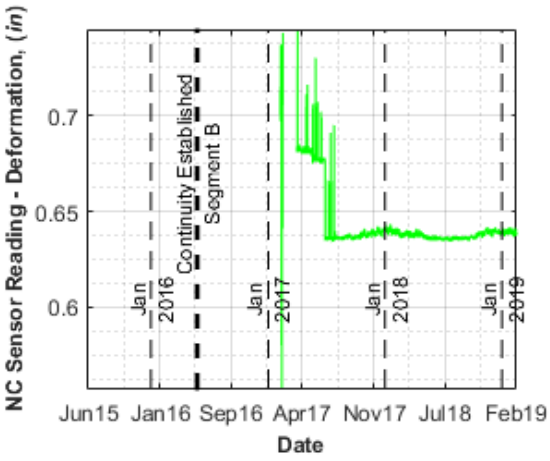

b) Sensor reading without temperature correction

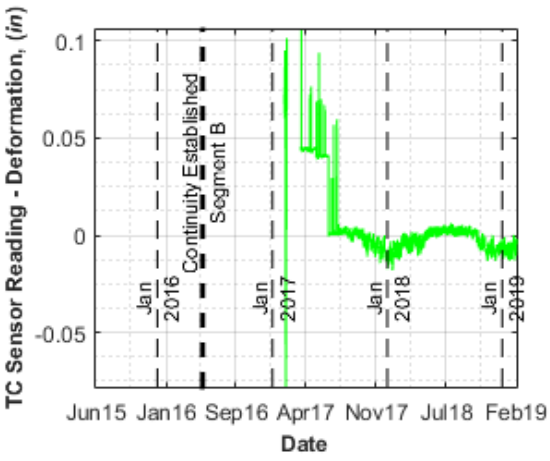

c) Sensor reading after temperature correction

B14_G4_BW – Gapmeter on the bottom of the web at Bent 14 Girder 4 in Segment B

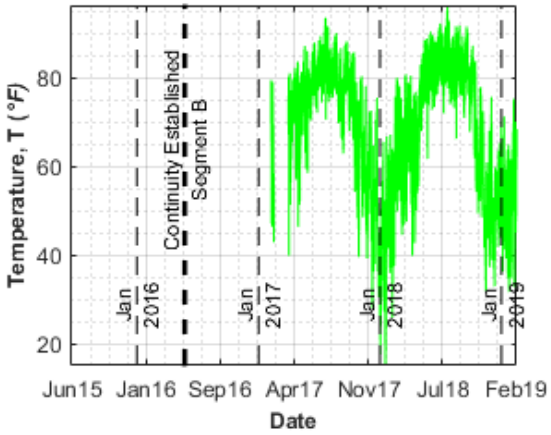

a) Temperature reading of the sensor

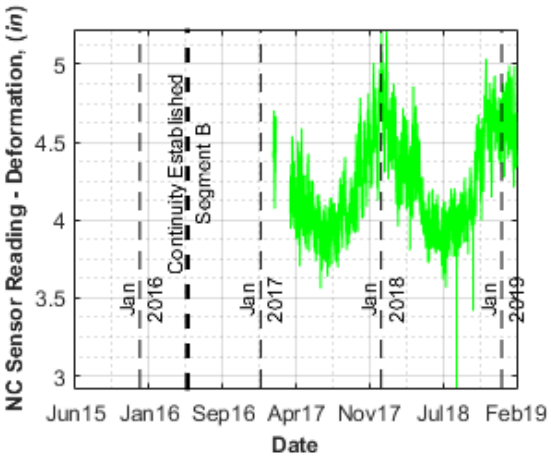

b) Sensor reading without temperature correction

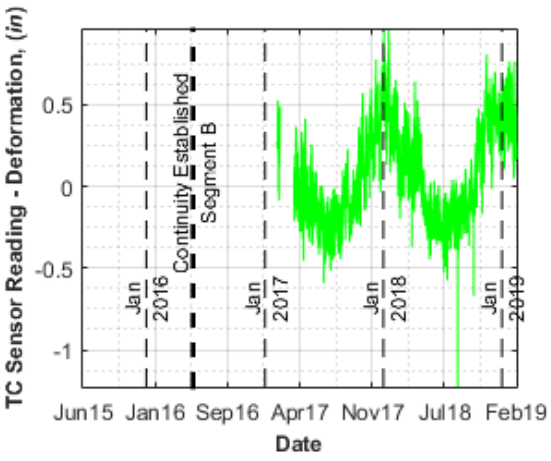

c) Sensor reading after temperature correction

B14_G4_TW – Gapmeter on the top of the web at Bent 14 Girder 4 in Segment B

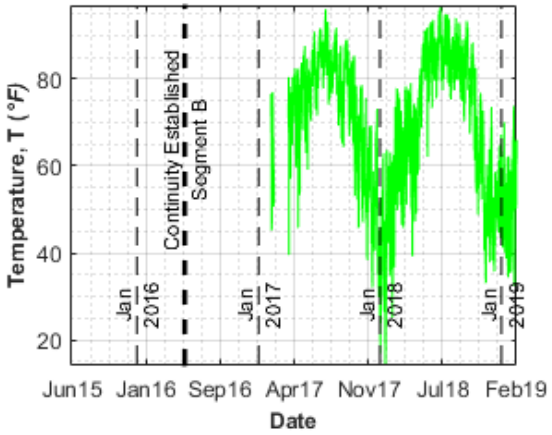

a) Temperature reading of the sensor

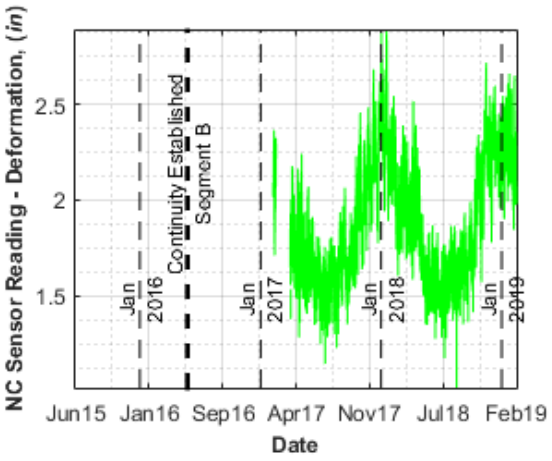

b) Sensor reading without temperature correction

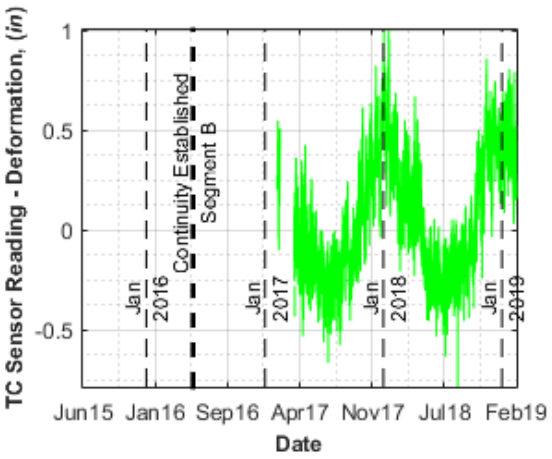

c) Sensor reading after temperature correction

B14_G7_BFE – Gapmeter on the riser in the east at Bent 14 Girder 7 in Segment B

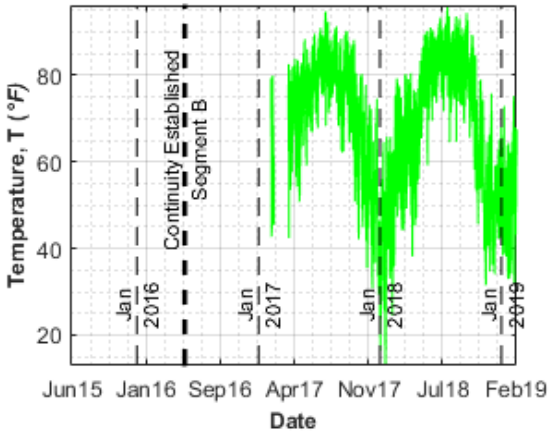

a) Temperature reading of the sensor

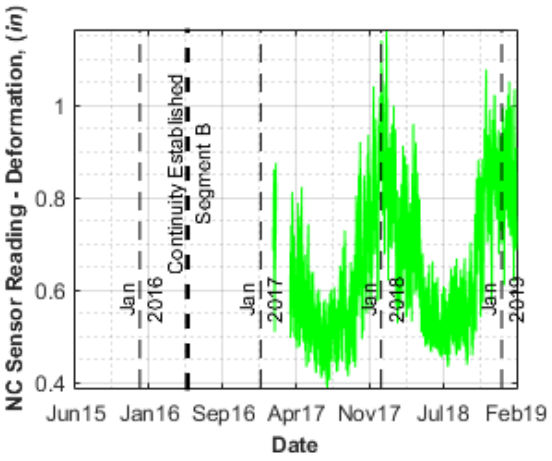

b) Sensor reading without temperature correction

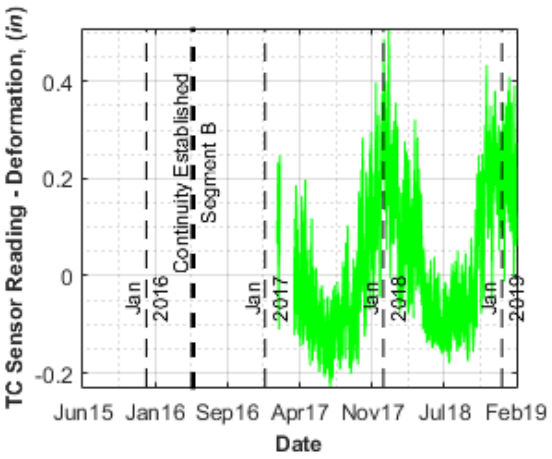

c) Sensor reading after temperature correction

B14_G7_BFW – Gapmeter on the riser in the west at Bent 14 Girder 7 in Segment B

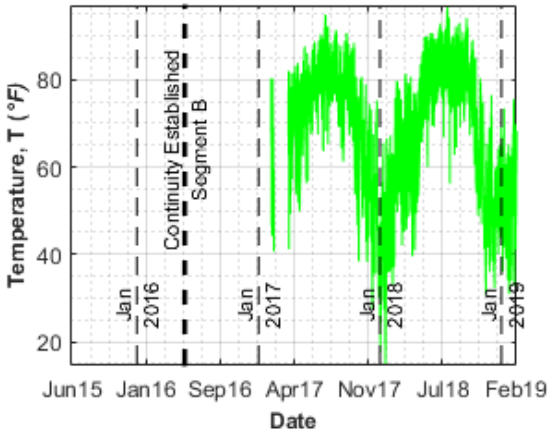

a) Temperature reading of the sensor

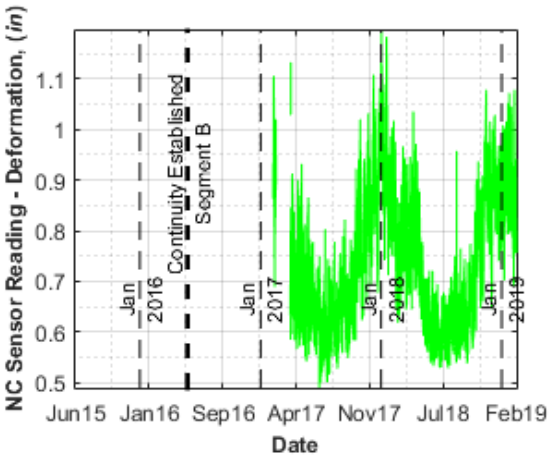

b) Sensor reading without temperature correction

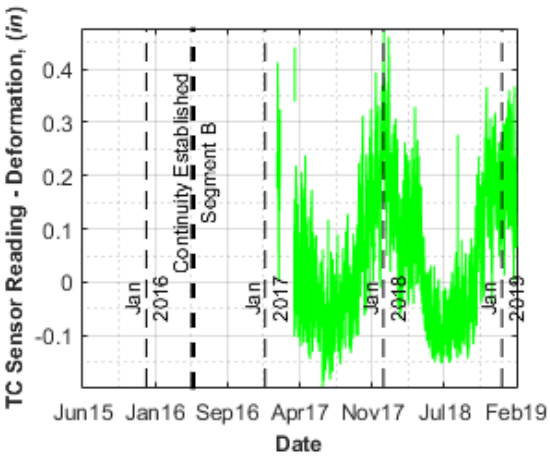

c) Sensor reading after temperature correction

B14_G7_BW – Gapmeter on the bottom of the web at Bent 14 Girder 7 in Segment B

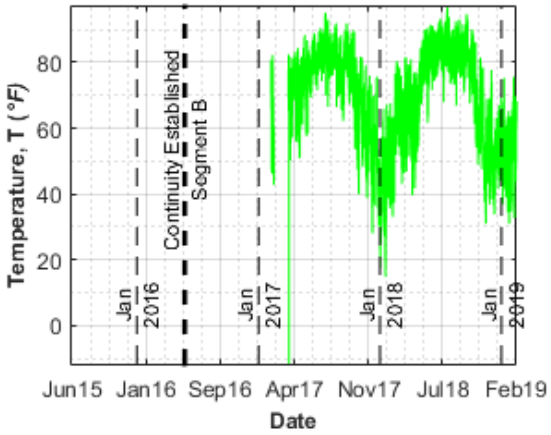

a) Temperature reading of the sensor

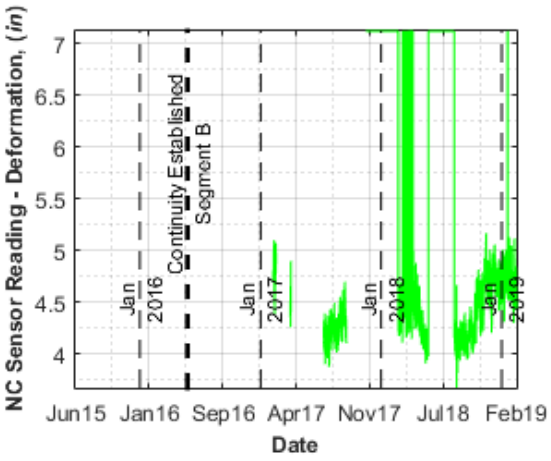

b) Sensor reading without temperature correction

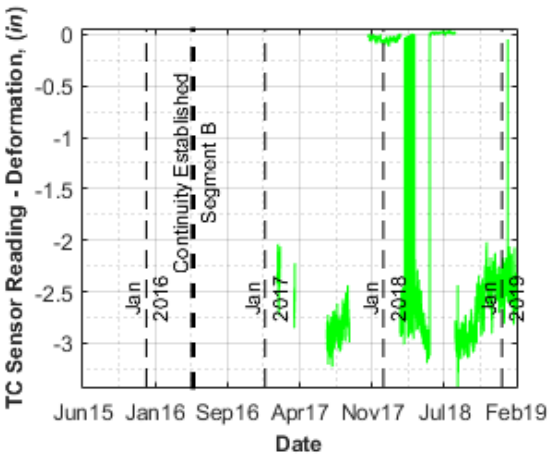

c) Sensor reading after temperature correction

B14_G7_TW – Gapmeter on the top of the web at Bent 14 Girder 7 in Segment B

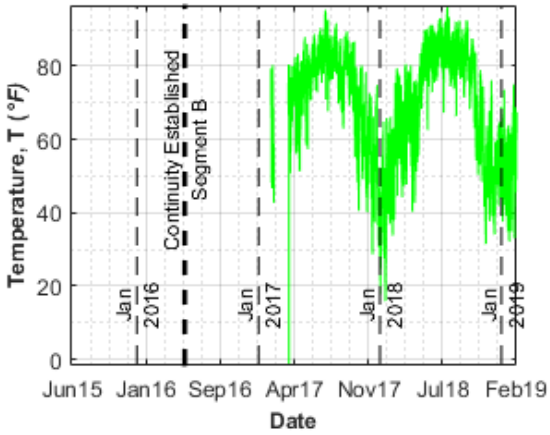

a) Temperature reading of the sensor

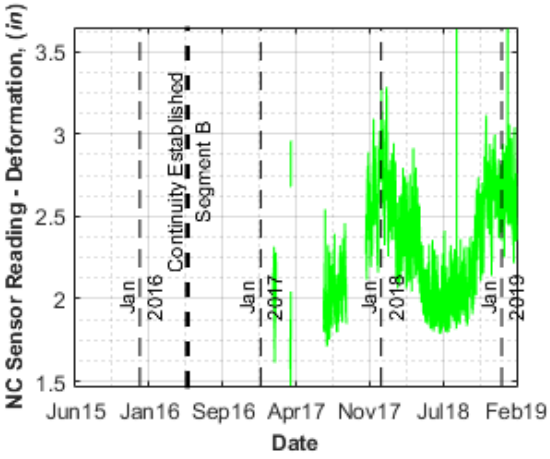

b) Sensor reading without temperature correction

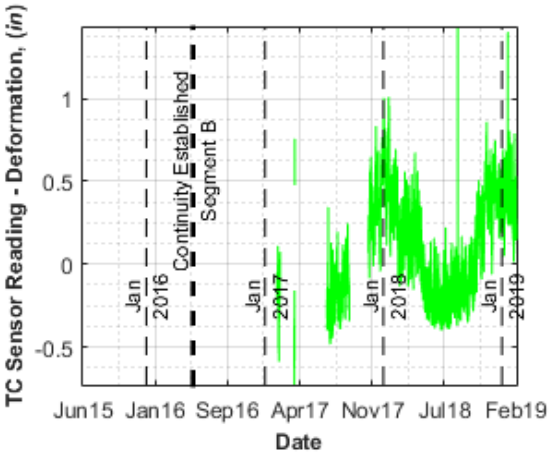

c) Sensor reading after temperature correction

B14_G4_CWE – Tiltmeter on the web on the east at Bent 14 Girder 4 in Segment B

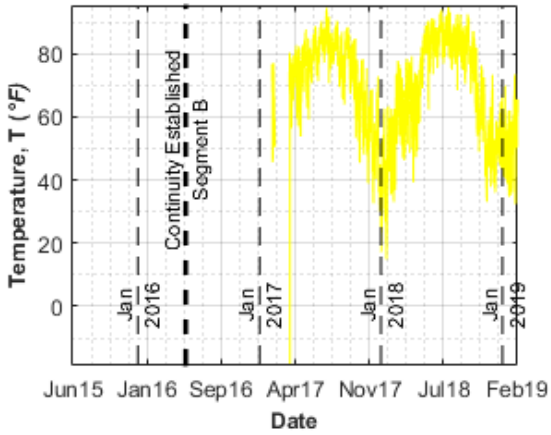

a) Temperature reading of the sensor

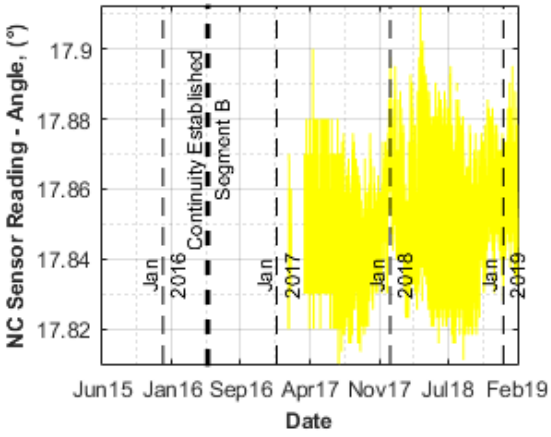

b) Sensor reading without temperature correction

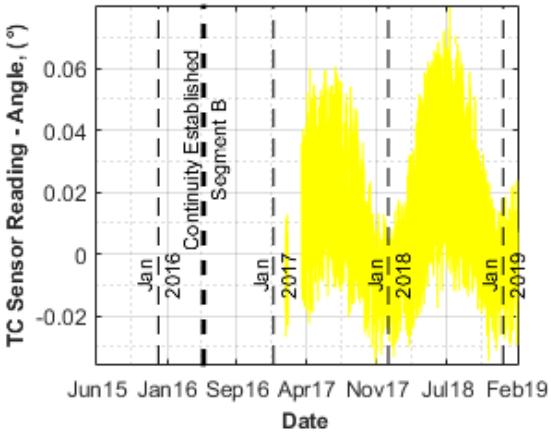

c) Sensor reading after temperature correction

B14_G7_CWE – Tiltmeter on the web on the east at Bent 14 Girder 7 in Segment B

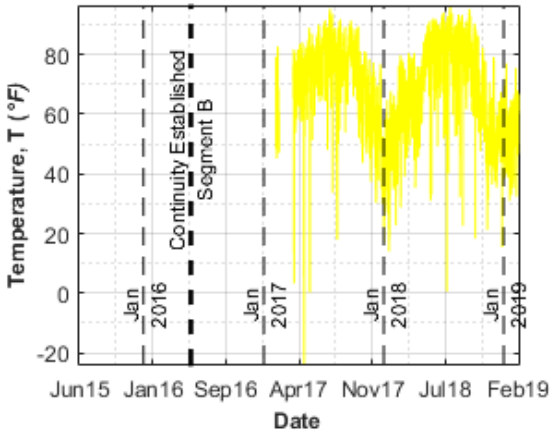

a) Temperature reading of the sensor

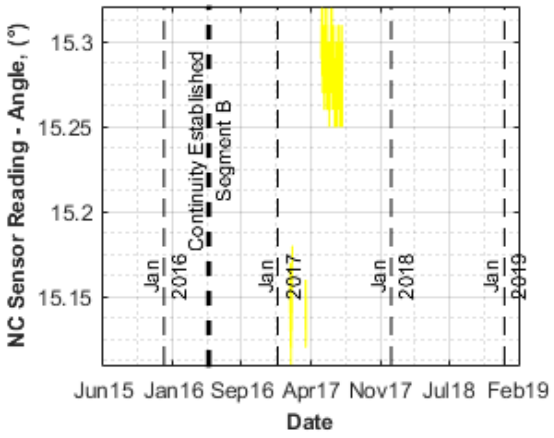

b) Sensor reading without temperature correction

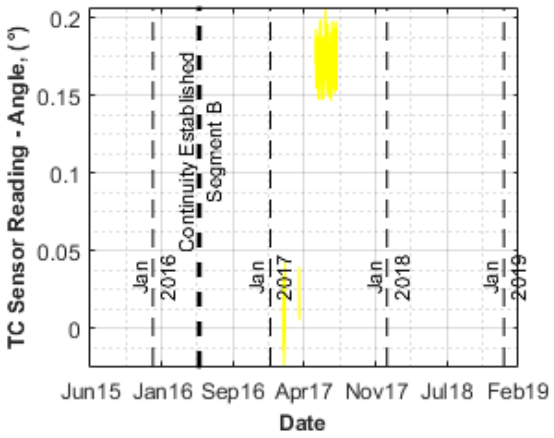

c) Sensor reading after temperature correction

B20_G4_BFW – Gapmeter on the riser in the west at Bent 20 Girder 4 in Segment D

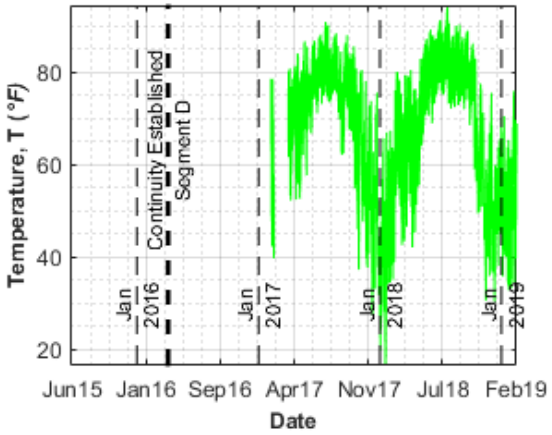

a) Temperature reading of the sensor

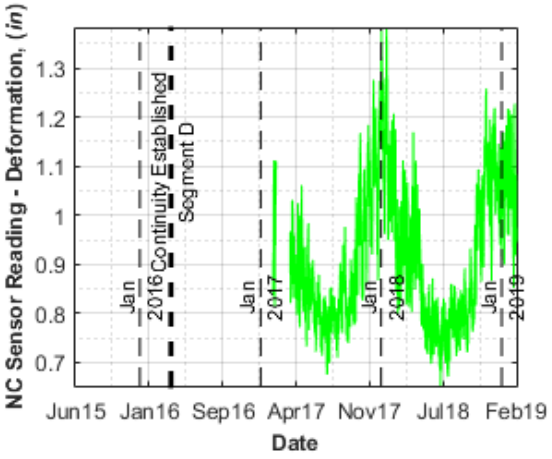

b) Sensor reading without temperature correction

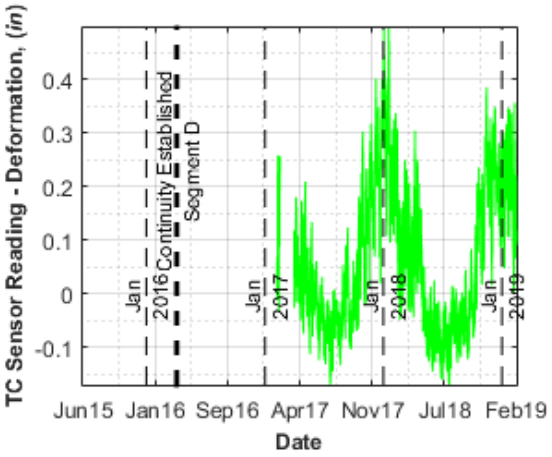

c) Sensor reading after temperature correction

B20_G7_BFW – Gapmeter on the riser in the west at Bent 20 Girder 7 in Segment D

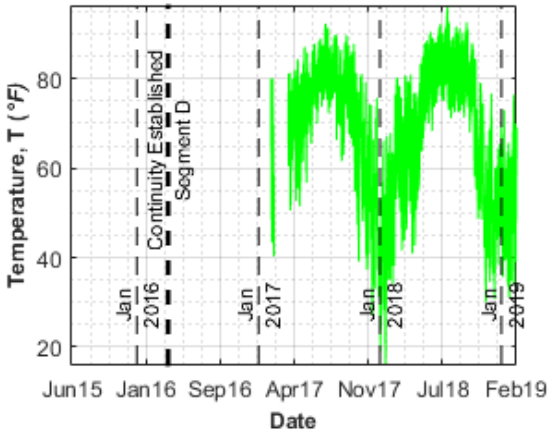

a) Temperature reading of the sensor

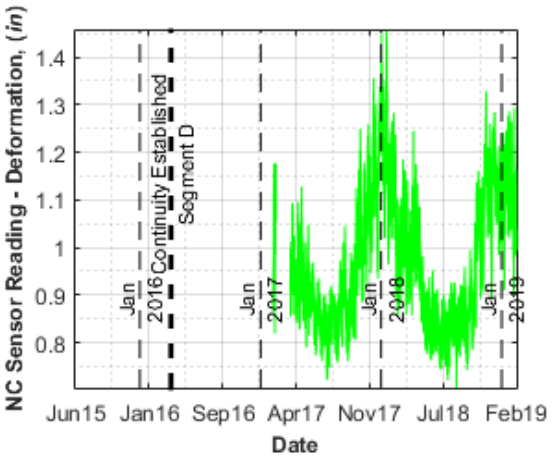

b) Sensor reading without temperature correction

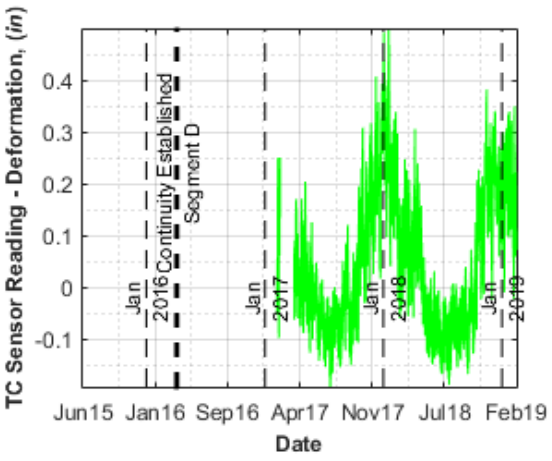

c) Sensor reading after temperature correction

B20_G4_CWE – Tiltmeter on the web on the east at Bent 20 Girder 4 in Segment E

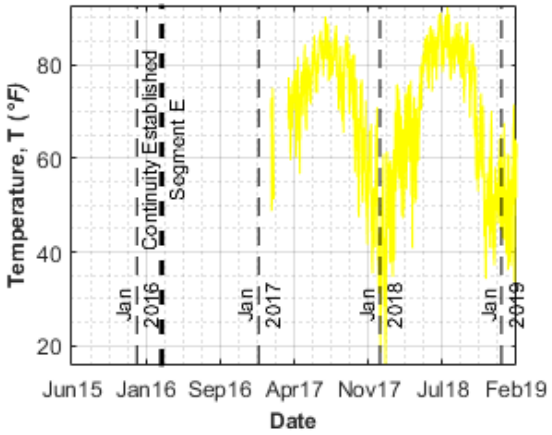

a) Temperature reading of the sensor

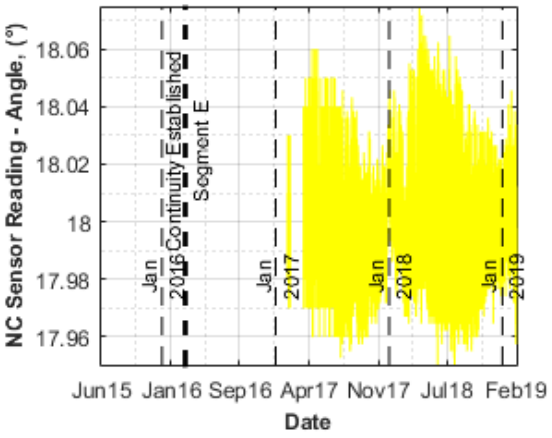

b) Sensor reading without temperature correction

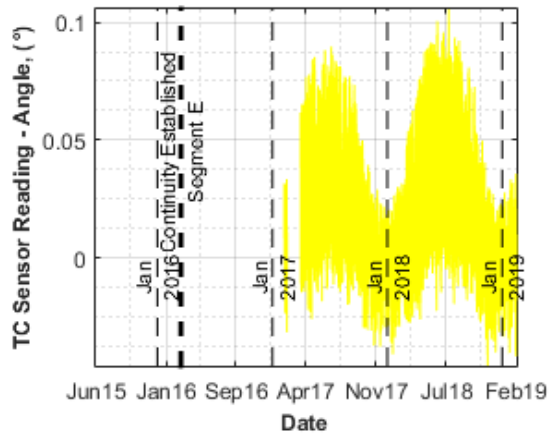

c) Sensor reading after temperature correction

B20_G4_CWW – Tiltmeter on the web on the west at Bent 20 Girder 4 in Segment D

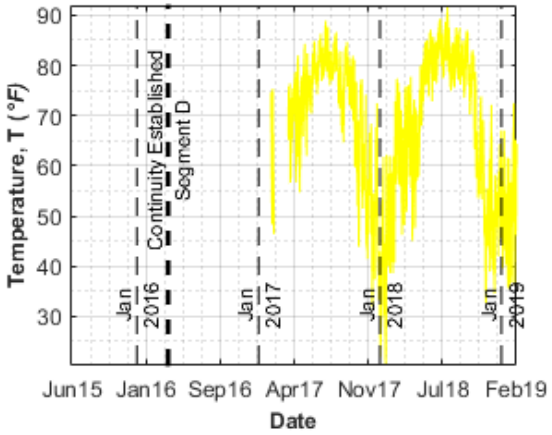

a) Temperature reading of the sensor

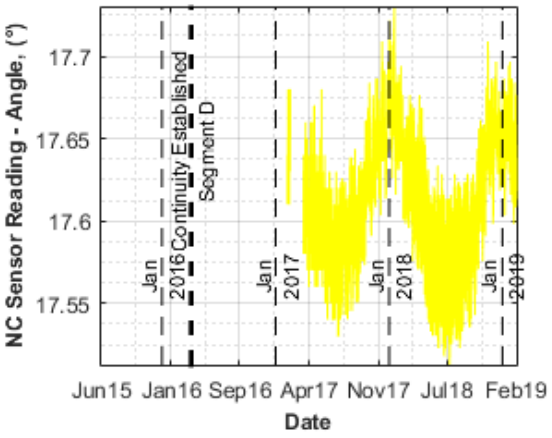

b) Sensor reading without temperature correction

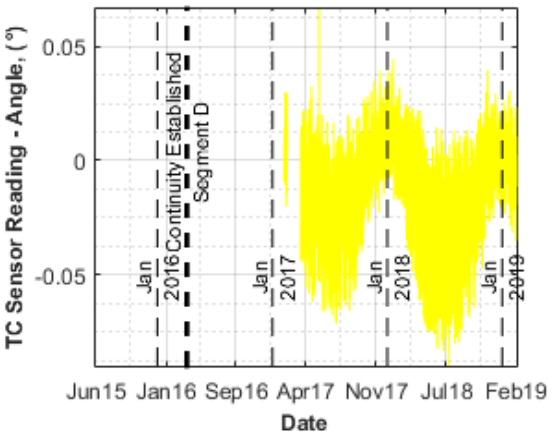

c) Sensor reading after temperature correction

B20_G7_CWE – Tiltmeter on the web on the east at Bent 20 Girder 7 in Segment E

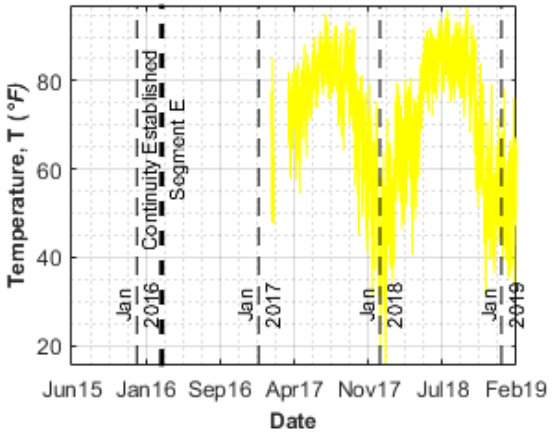

a) Temperature reading of the sensor

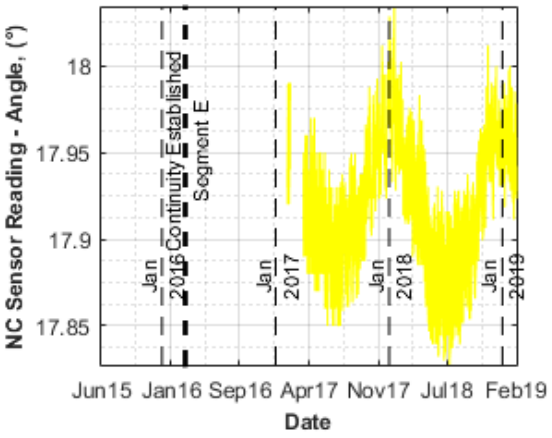

b) Sensor reading without temperature correction

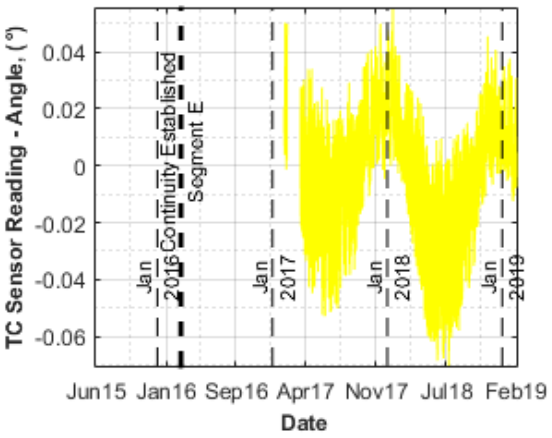

c) Sensor reading after temperature correction

B20_G7_CWW – Tiltmeter on the web on the west at Bent 20 Girder 7 in Segment D

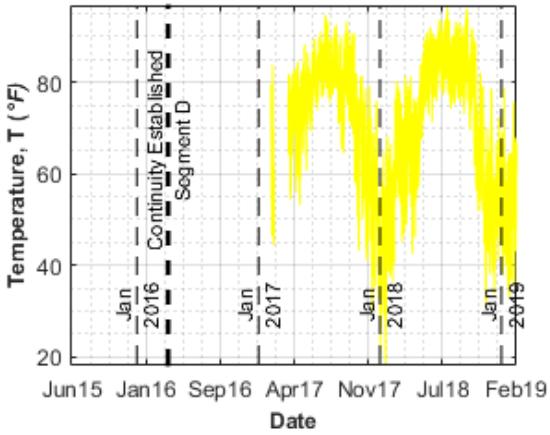

a) Temperature reading of the sensor

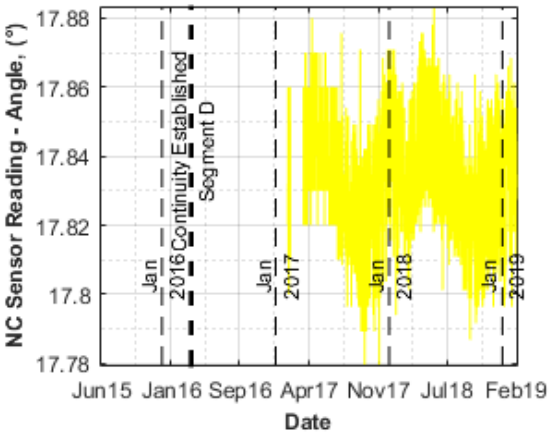

b) Sensor reading without temperature correction

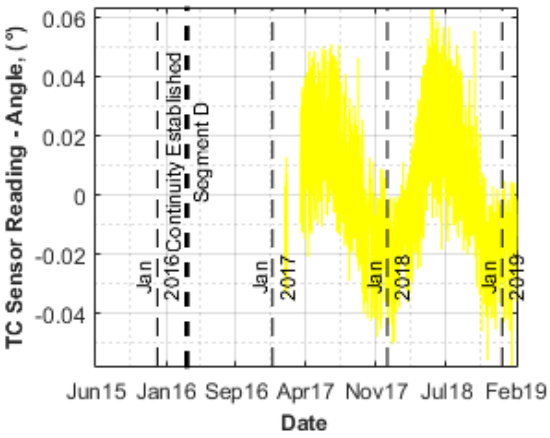

c) Sensor reading after temperature correction

B20_STRAIN – Strain gage in Segment E

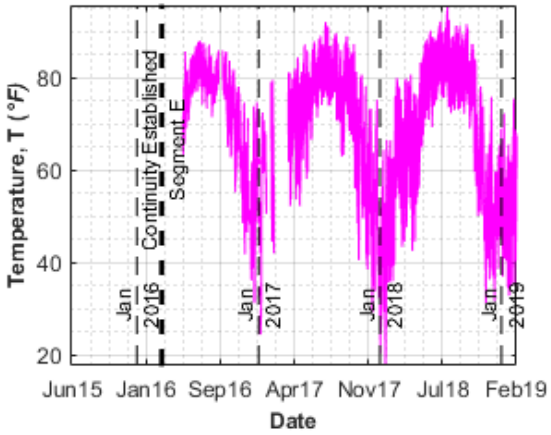

a) Temperature reading of the sensor

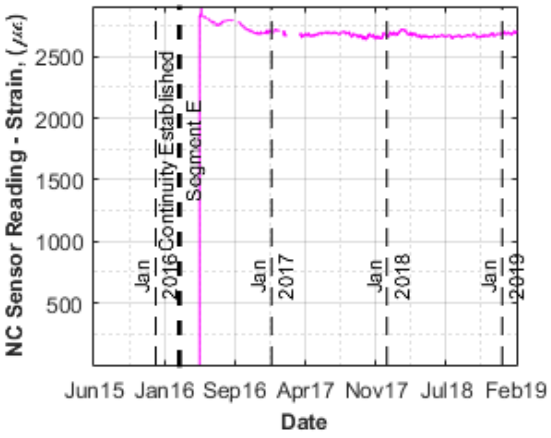

b) Sensor reading without temperature correction

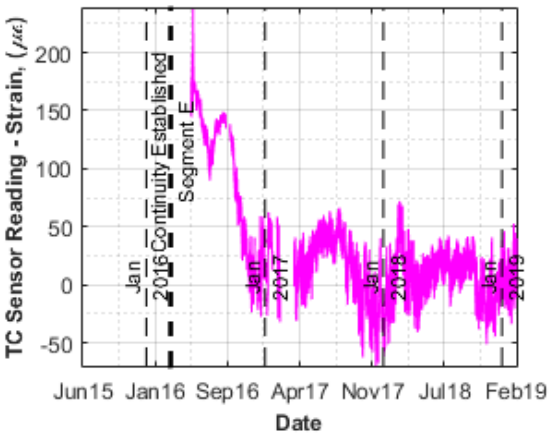

c) Sensor reading after temperature correction

S20_G2_S – Sisterbar on the slab at Girder 2 in Segment E

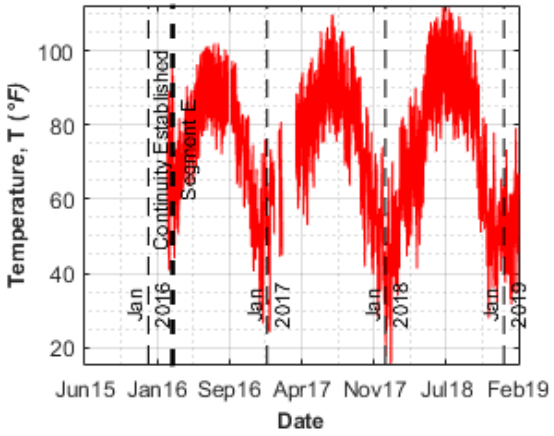

a) Temperature reading of the sensor

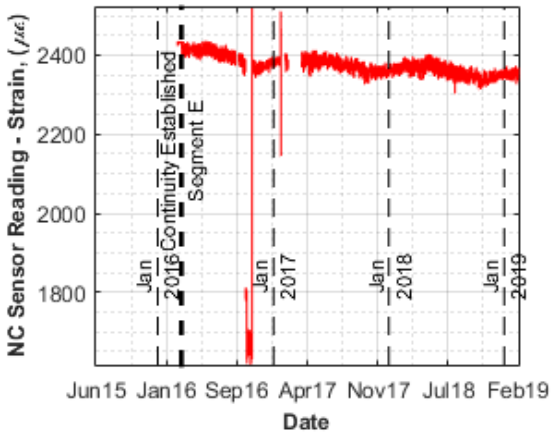

b) Sensor reading without temperature correction

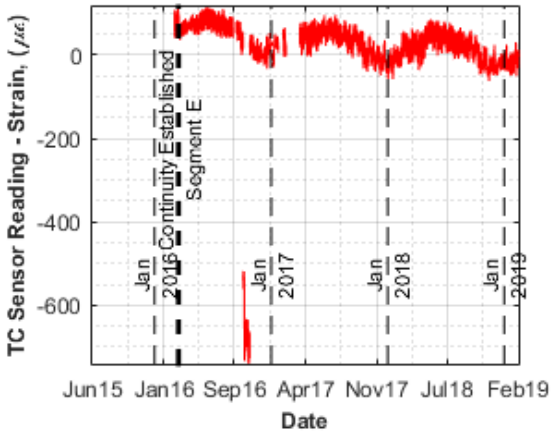

c) Sensor reading after temperature correction

S20_G2_TF_A – Sisterbar on the top flange at Girder 2 in Segment E

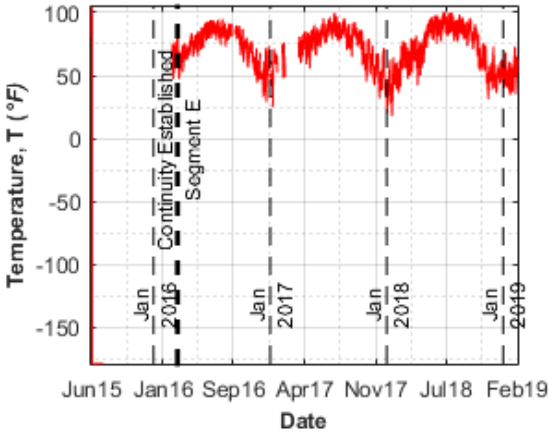

a) Temperature reading of the sensor

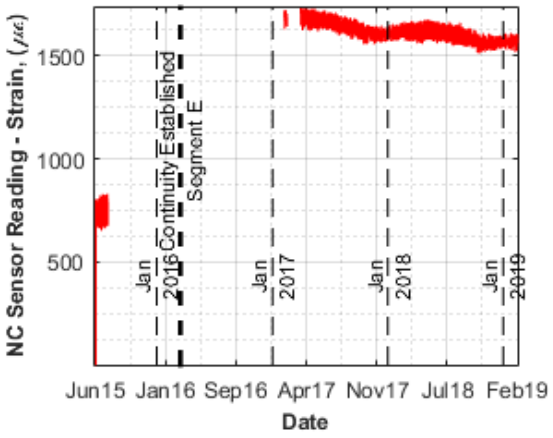

b) Sensor reading without temperature correction

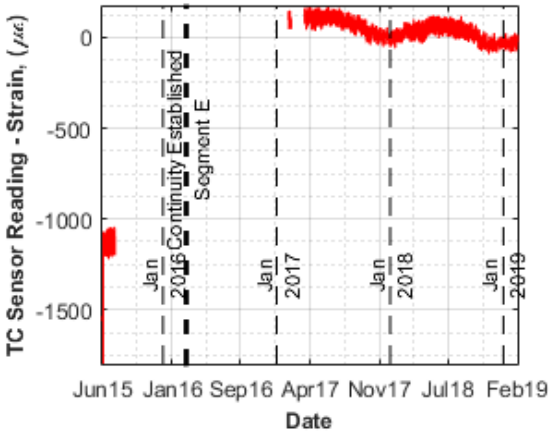

c) Sensor reading after temperature correction

S20_G2_BF_A – Sisterbar on the bottom flange at Girder 2 in Segment E

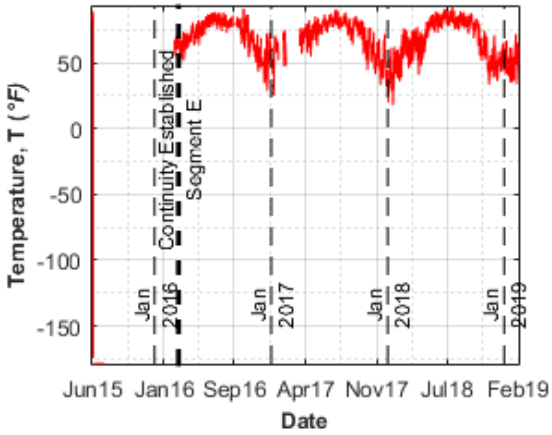

a) Temperature reading of the sensor

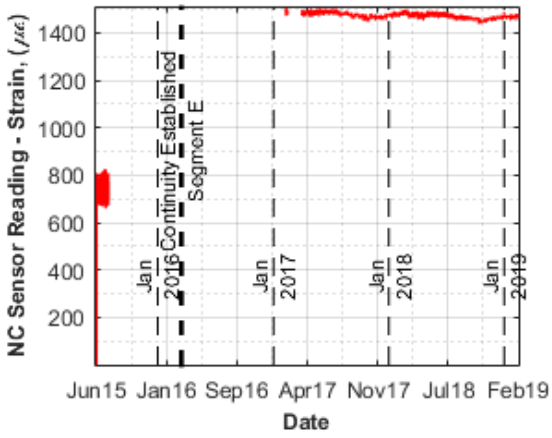

b) Sensor reading without temperature correction

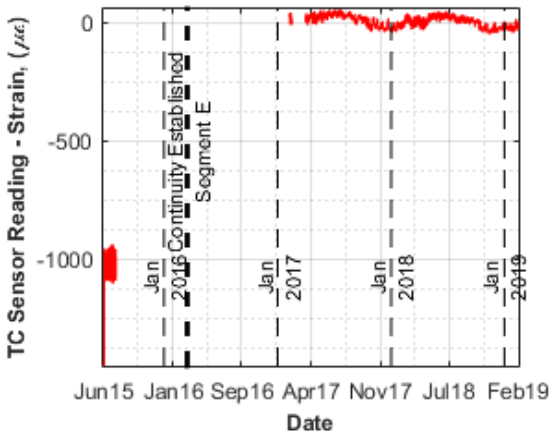

c) Sensor reading after temperature correction

S20_G4_S – Sisterbar on the slab at Girder 4 in Segment E

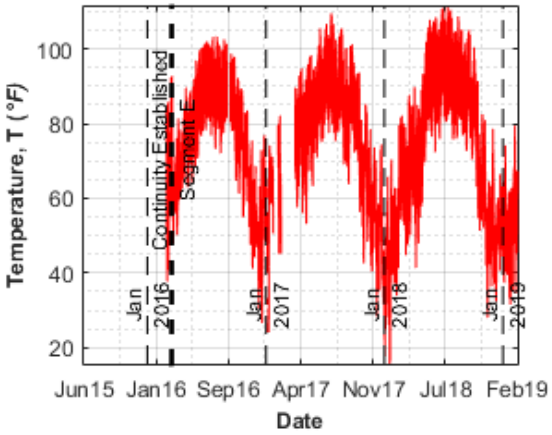

a) Temperature reading of the sensor

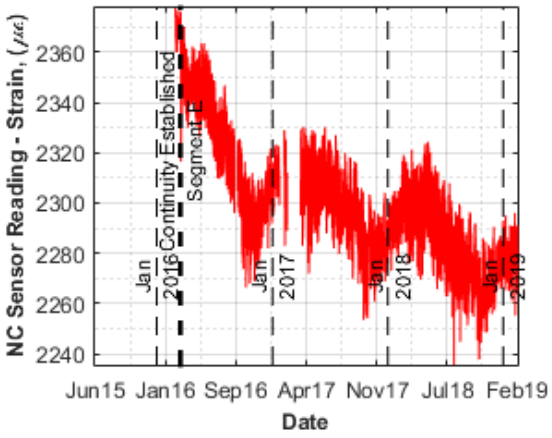

b) Sensor reading without temperature correction

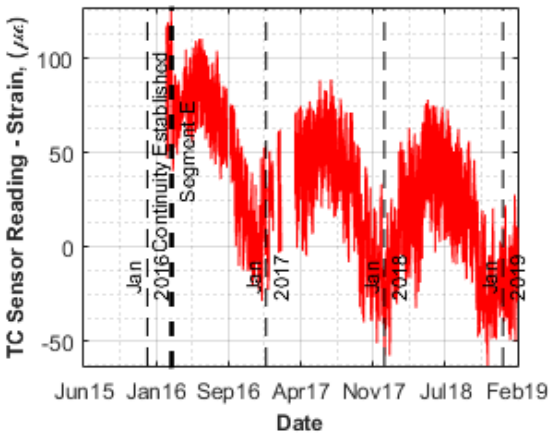

c) Sensor reading after temperature correction

S20_G4_TF – Sisterbar on the top flange at Girder 4 in Segment E

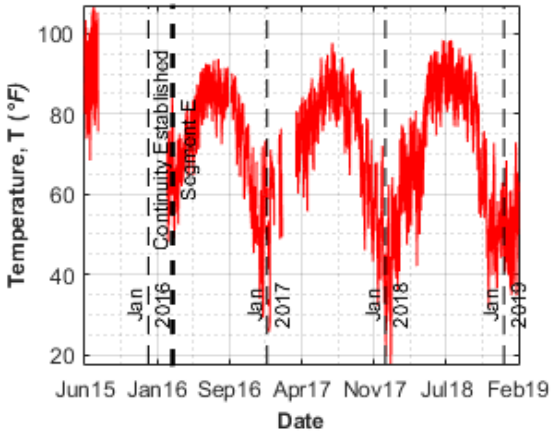

a) Temperature reading of the sensor

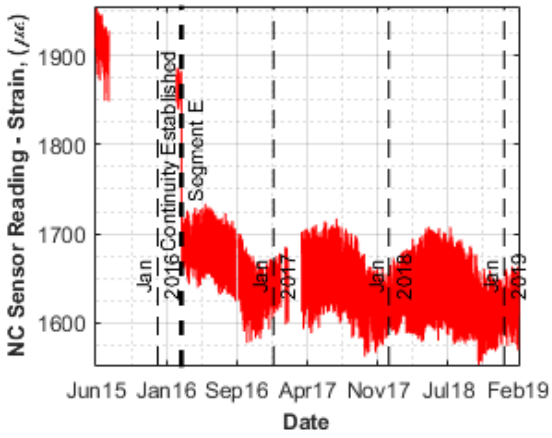

b) Sensor reading without temperature correction

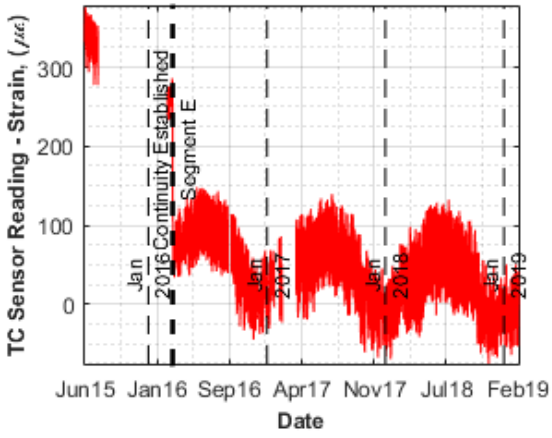

c) Sensor reading after temperature correction

S20_G4_BF – Sisterbar on the bottom flange at Girder 4 in Segment E

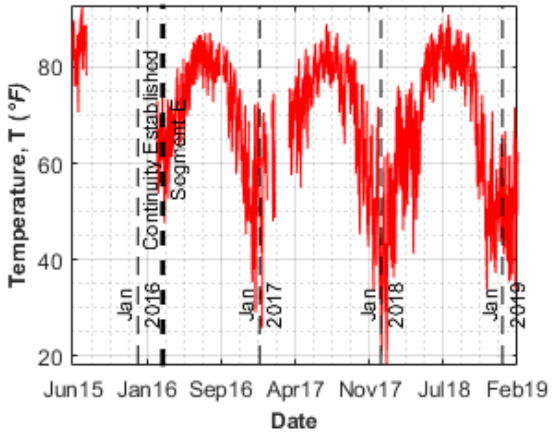

a) Temperature reading of the sensor

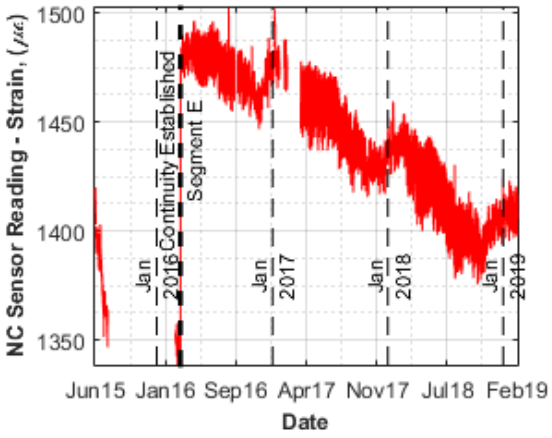

b) Sensor reading without temperature correction

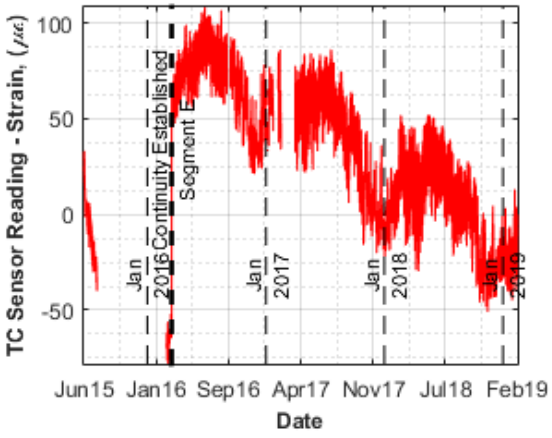

c) Sensor reading after temperature correction

S20_G7_S – Sisterbar on the slab at Girder 7 in Segment E

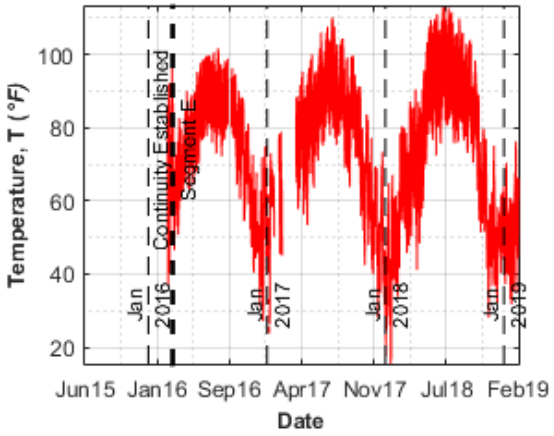

a) Temperature reading of the sensor

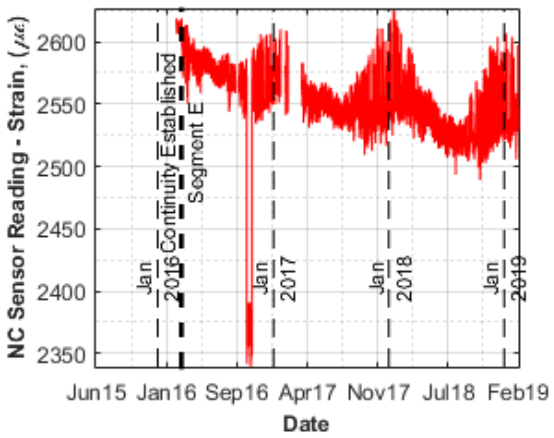

b) Sensor reading without temperature correction

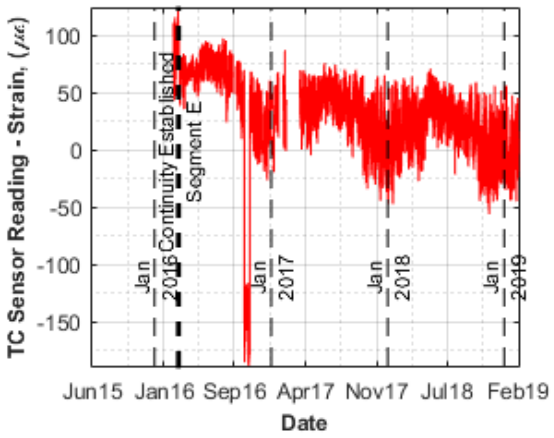

c) Sensor reading after temperature correction

S20_G7_TF – Sisterbar on the top flange at Girder 7 in Segment E

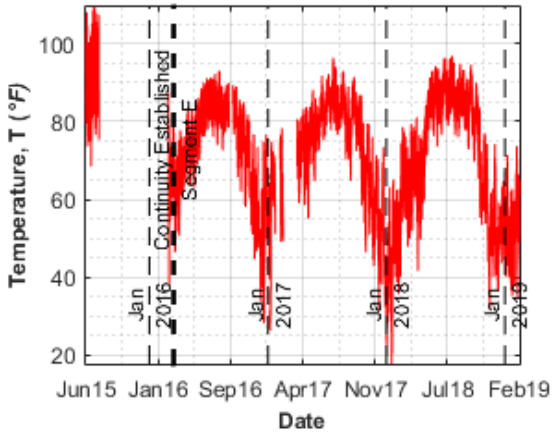

a) Temperature reading of the sensor

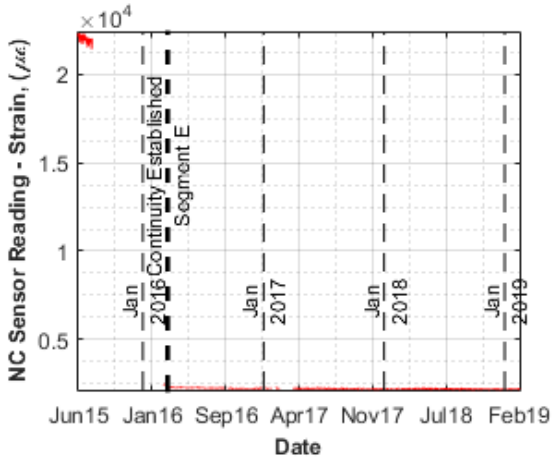

b) Sensor reading without temperature correction

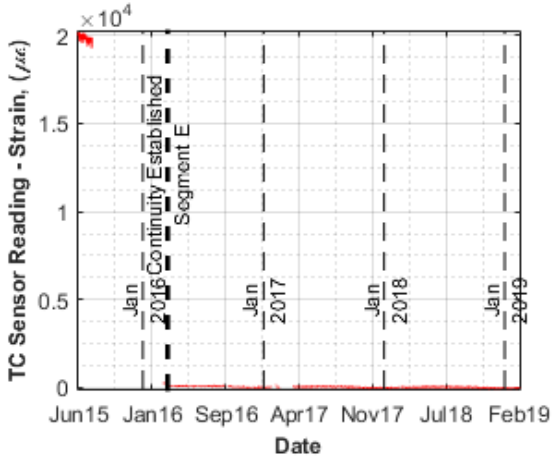

c) Sensor reading after temperature correction

S20_G7_BF – Sisterbar on the bottom flange at Girder 7 in Segment E

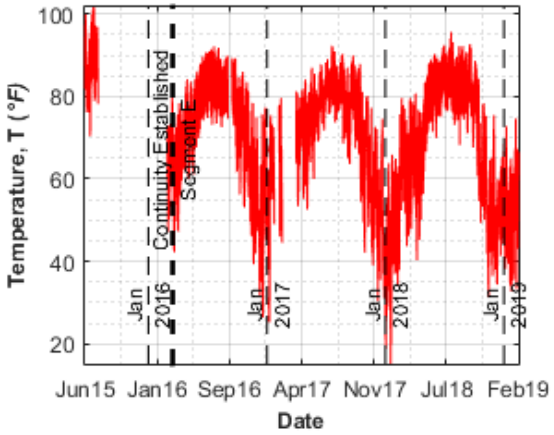

a) Temperature reading of the sensor

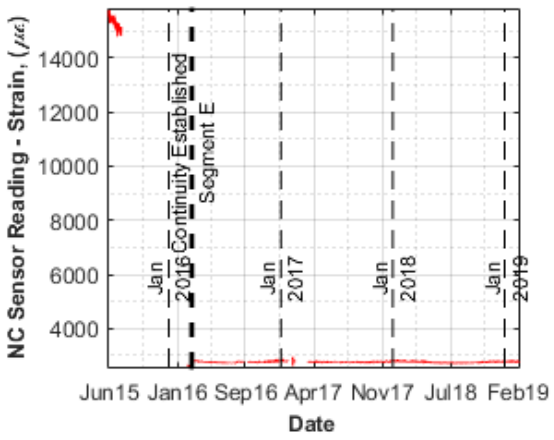

b) Sensor reading without temperature correction

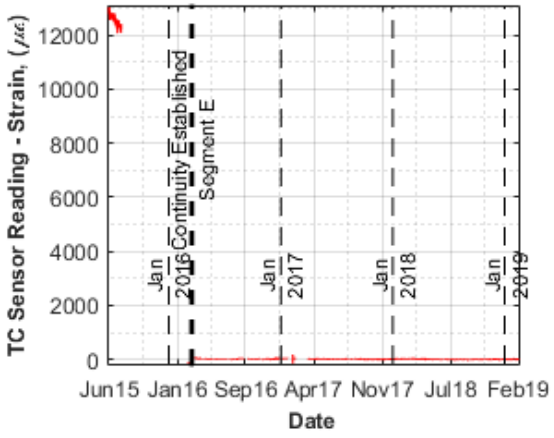

c) Sensor reading after temperature correction

B21_G4_BFW – Gapmeter on the riser in the west at Bent 21 Girder 4 in Segment E

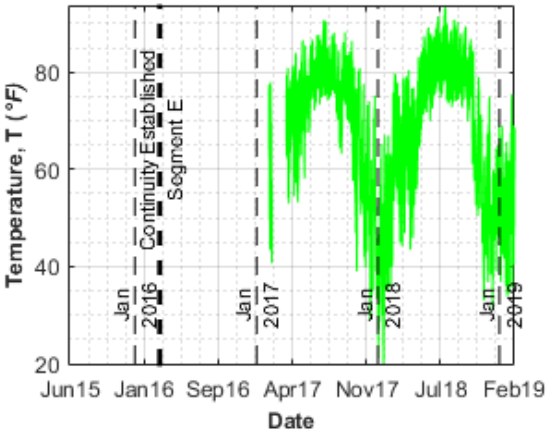

a) Temperature reading of the sensor

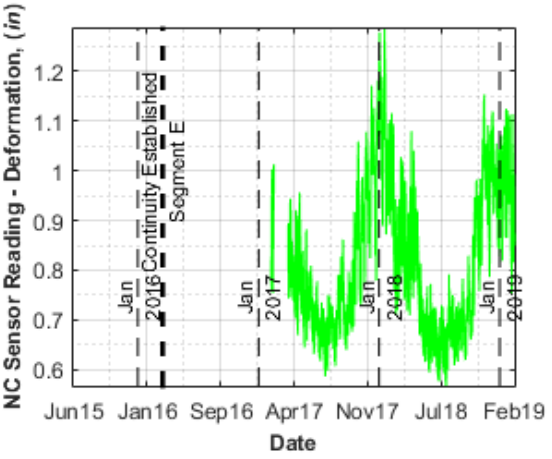

b) Sensor reading without temperature correction

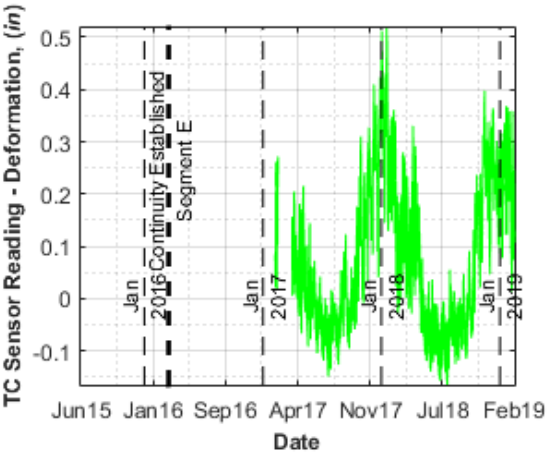

c) Sensor reading after temperature correction

B21_G7_BFW – Gapmeter on the riser in the west at Bent 21 Girder 7 in Segment E

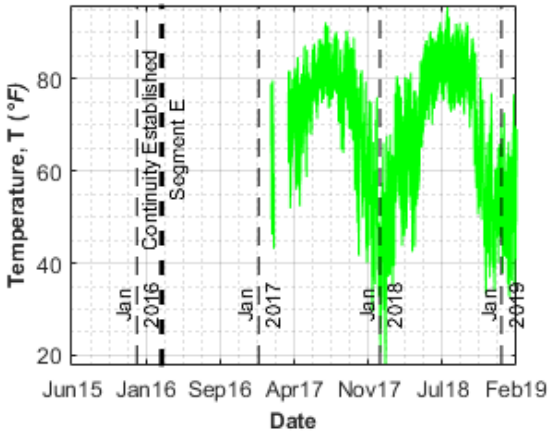

a) Temperature reading of the sensor

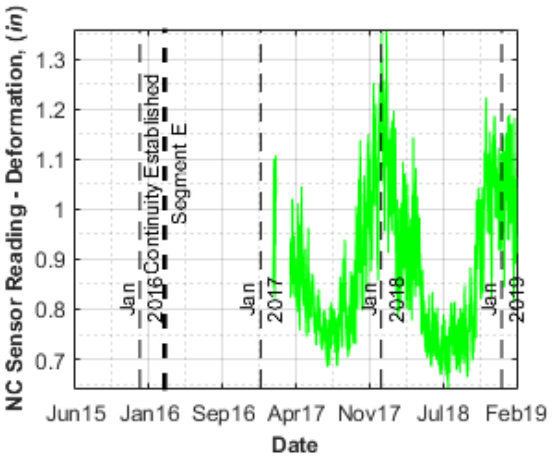

b) Sensor reading without temperature correction

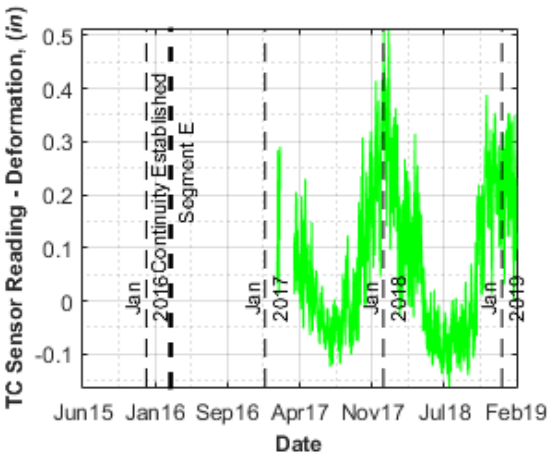

c) Sensor reading after temperature correction

B21_G4_CWW – Tiltmeter on the web on the west at Bent 21 Girder 4 in Segment E

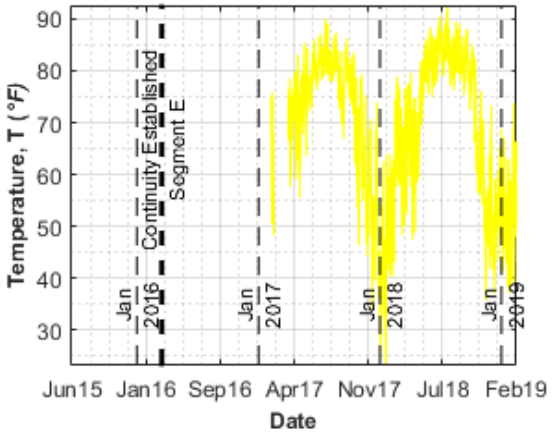

a) Temperature reading of the sensor

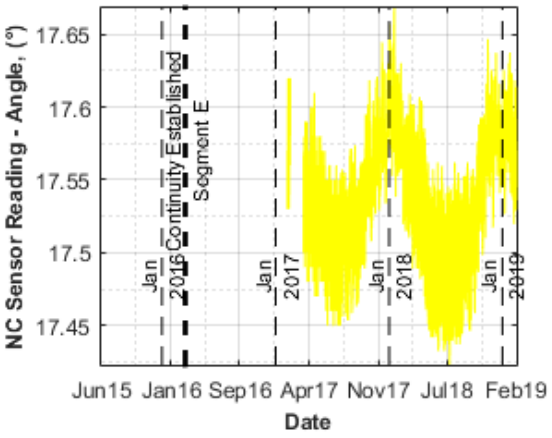

b) Sensor reading without temperature correction

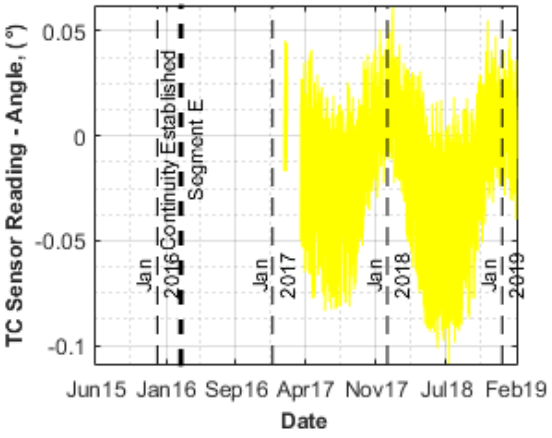

c) Sensor reading after temperature correction

B21_G7_CWW – Tiltmeter on the web on the west at Bent 21 Girder 7 in Segment E

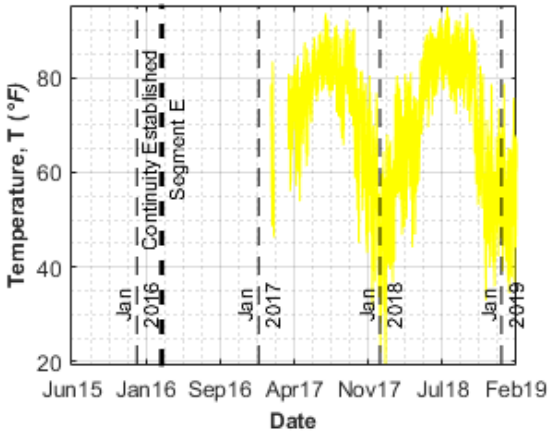

a) Temperature reading of the sensor

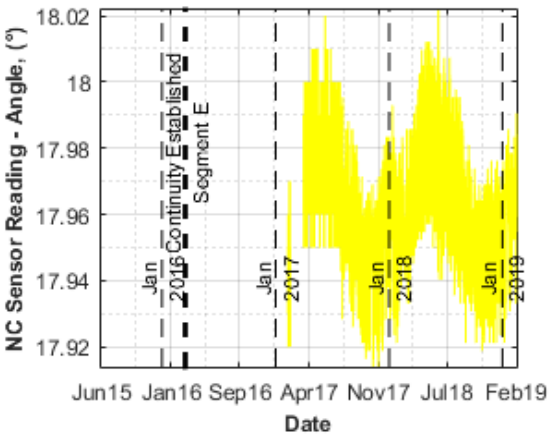

b) Sensor reading without temperature correction

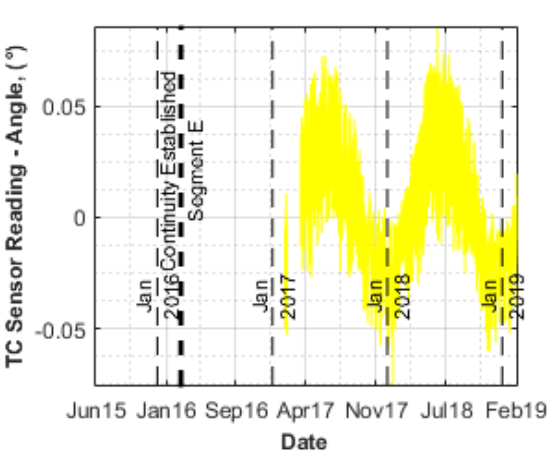

c) Sensor reading after temperature correction

B3_G4_BFE – Gapmeter on the riser in the east at Bent 3 Girder 4 in Segment A

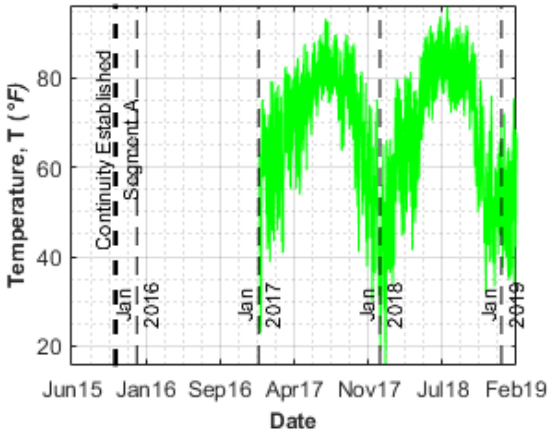

a) Temperature reading of the sensor

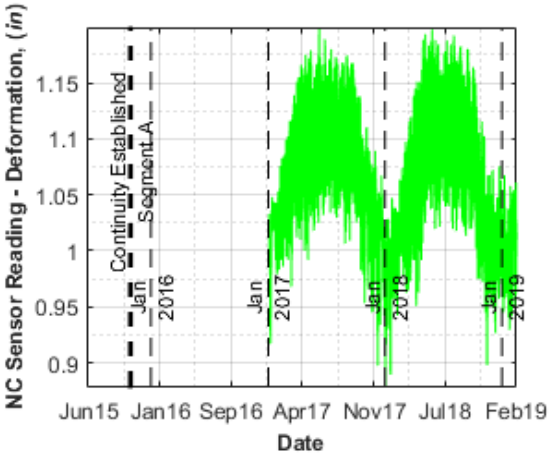

b) Sensor reading without temperature correction

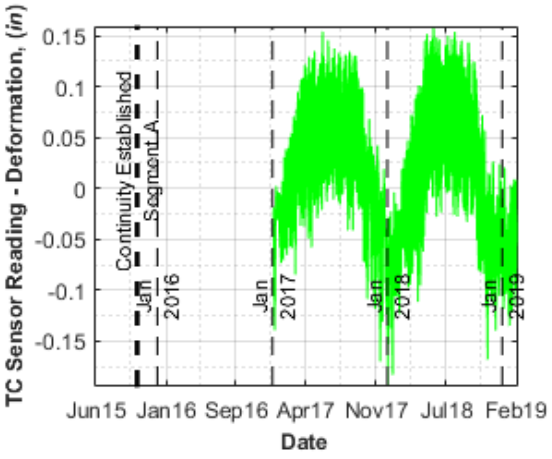

c) Sensor reading after temperature correction

B3_G4_BFW – Gapmeter on the riser in the west at Bent 3 Girder 4 in Segment A

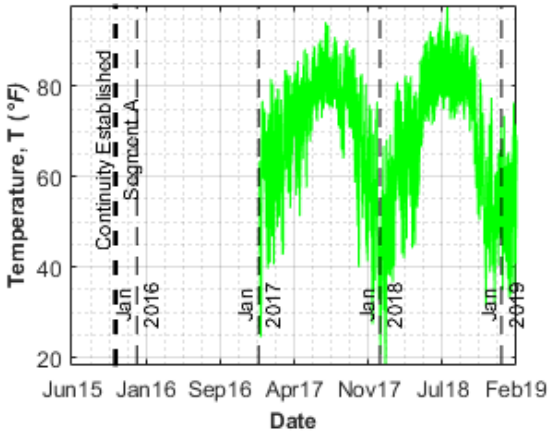

a) Temperature reading of the sensor

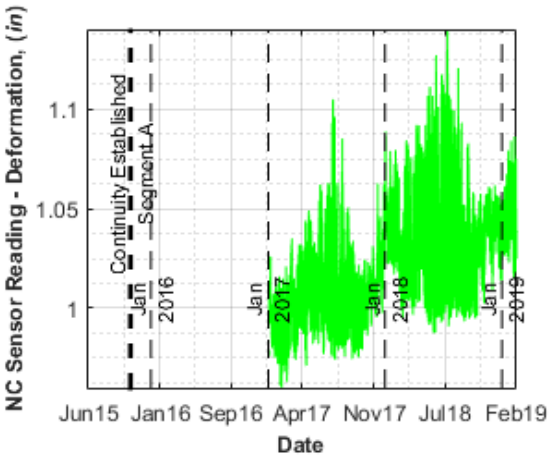

b) Sensor reading without temperature correction

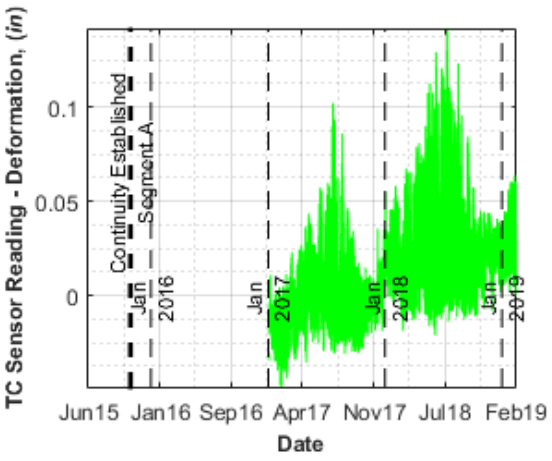

c) Sensor reading after temperature correction

B3_G4_BW – Gapmeter on the bottom of the web at Bent 3 Girder 4 in Segment A

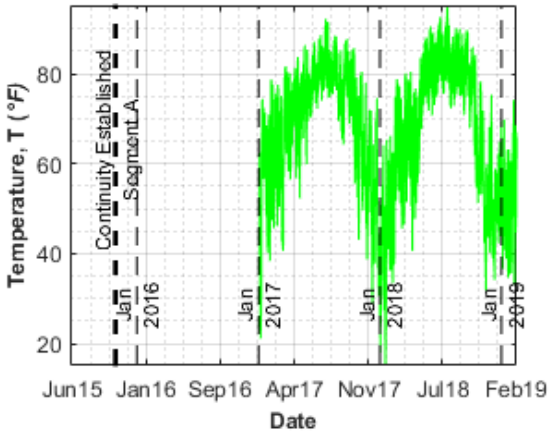

a) Temperature reading of the sensor

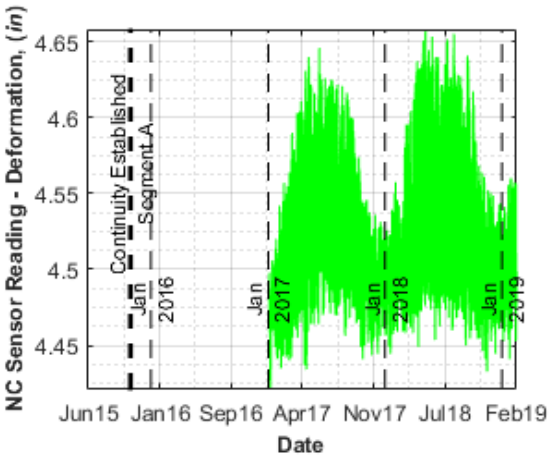

b) Sensor reading without temperature correction

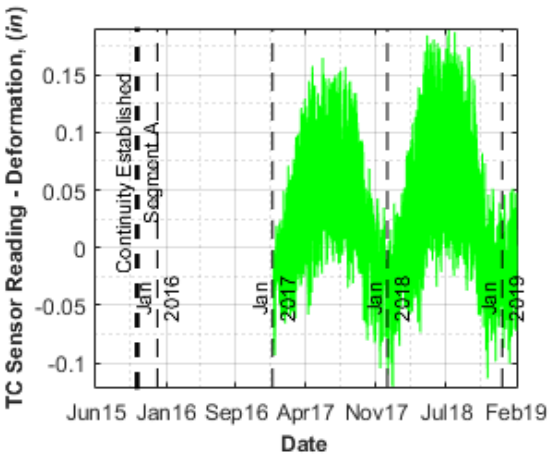

c) Sensor reading after temperature correction

B3_G4_TW – Gapmeter on the top of the web at Bent 3 Girder 4 in Segment A

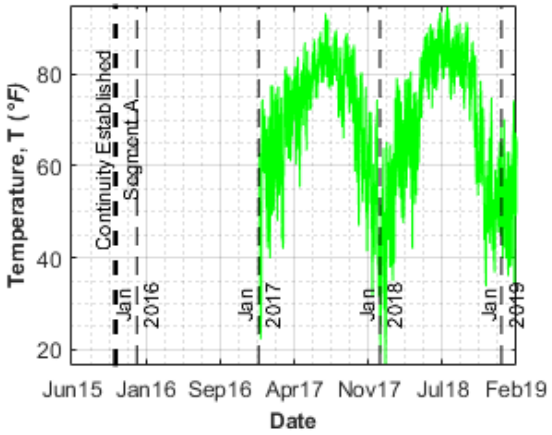

a) Temperature reading of the sensor

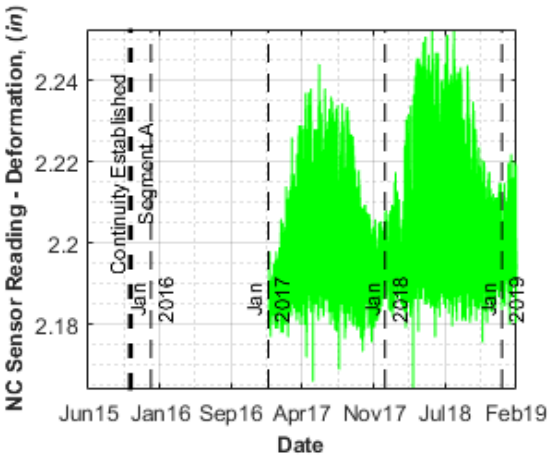

b) Sensor reading without temperature correction

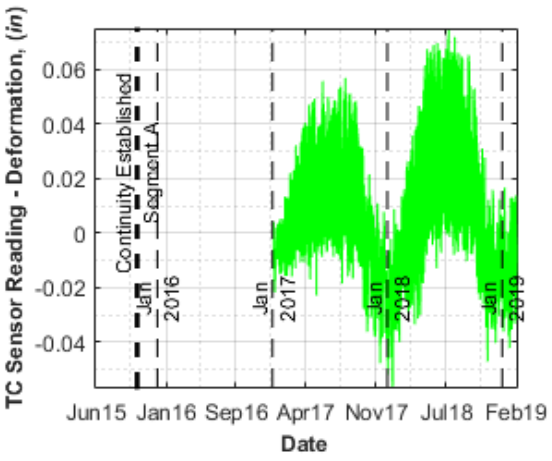

c) Sensor reading after temperature correction

B3_G7_BFE – Gapmeter on the riser in the east at Bent 3 Girder 7 in Segment A

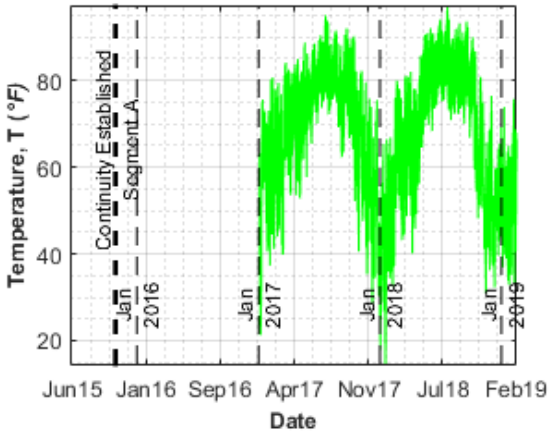

a) Temperature reading of the sensor

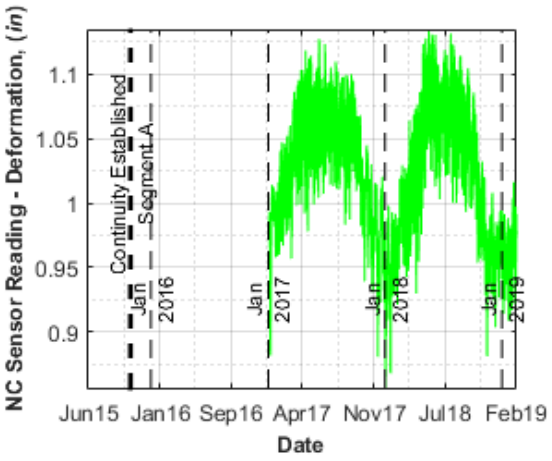

b) Sensor reading without temperature correction

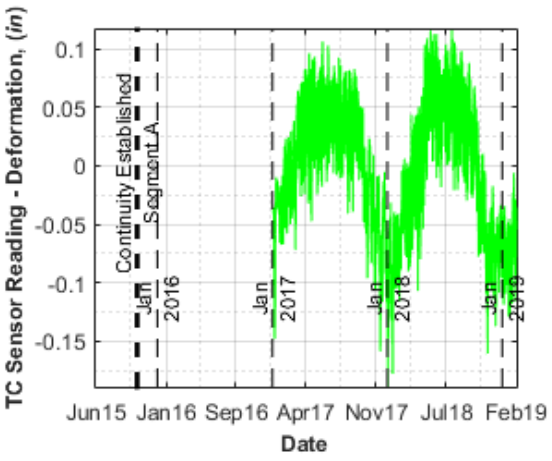

c) Sensor reading after temperature correction

B3_G7_BFW – Gapmeter on the riser in the west at Bent 3 Girder 7 in Segment A

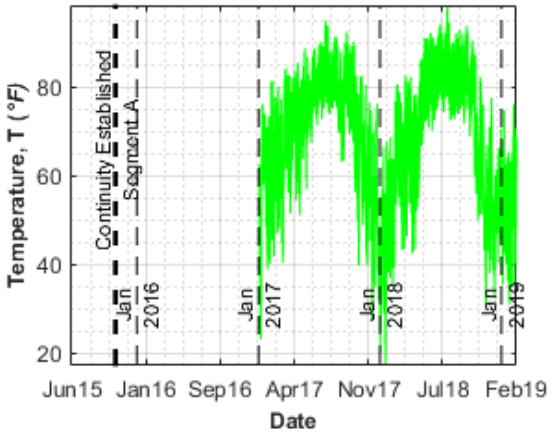

a) Temperature reading of the sensor

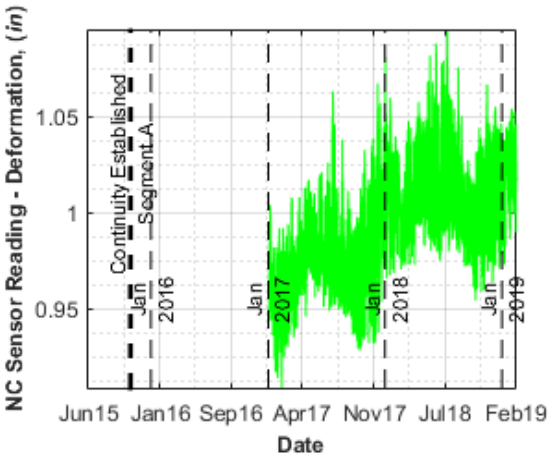

b) Sensor reading without temperature correction

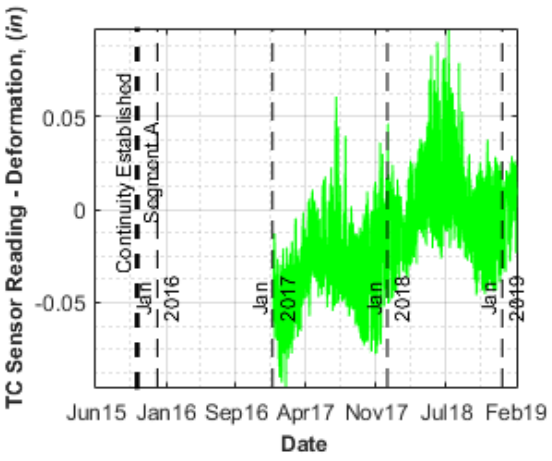

c) Sensor reading after temperature correction

B3_G7_BW – Gapmeter on the bottom of the web at Bent 3 Girder 7 in Segment A

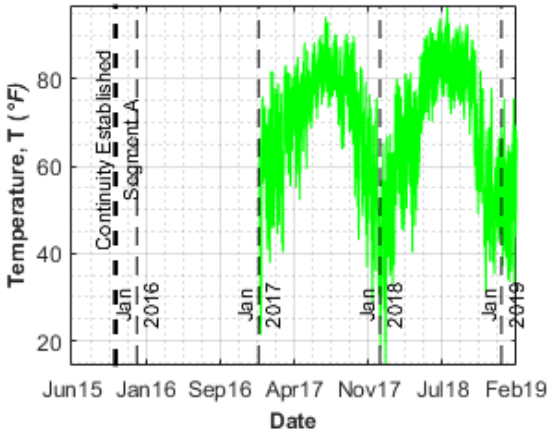

a) Temperature reading of the sensor

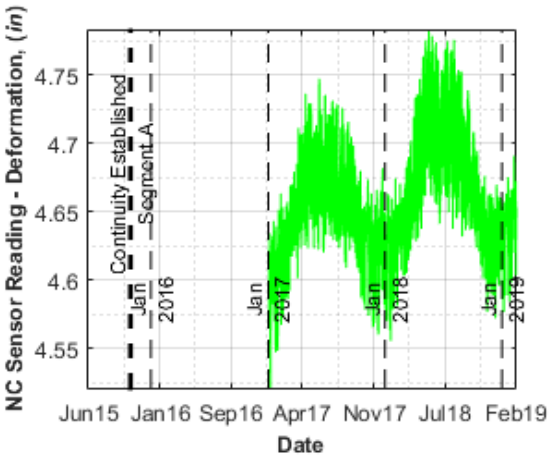

b) Sensor reading without temperature correction

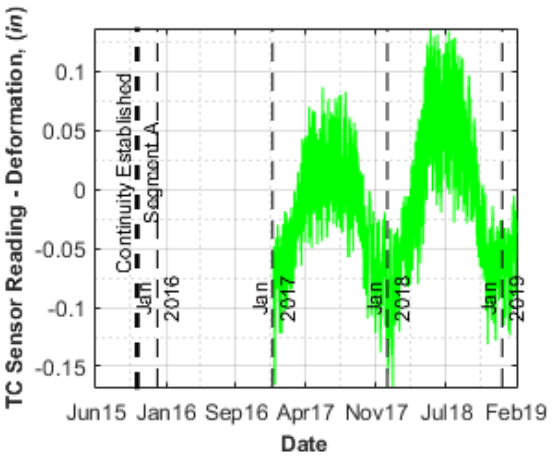

c) Sensor reading after temperature correction

B3_G7_TW – Gapmeter on the top of the web at Bent 3 Girder 7 in Segment A

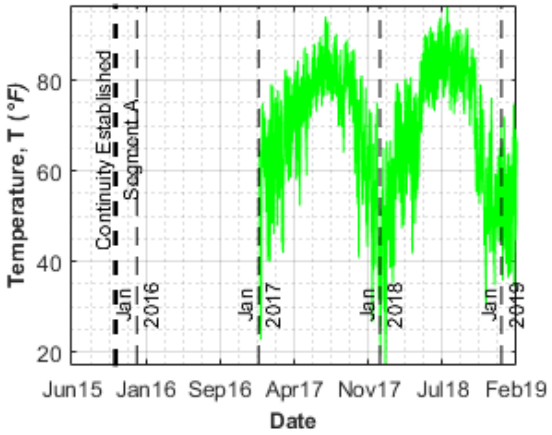

a) Temperature reading of the sensor

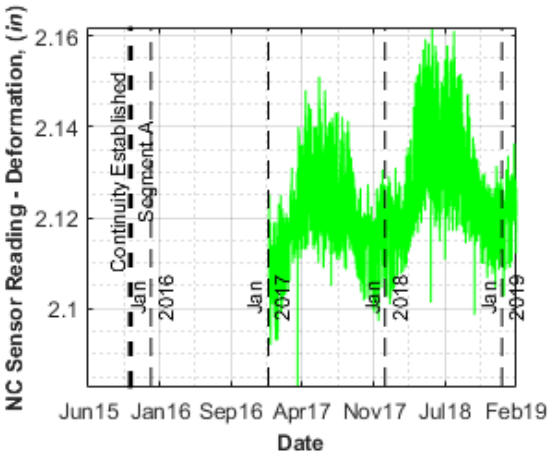

b) Sensor reading without temperature correction

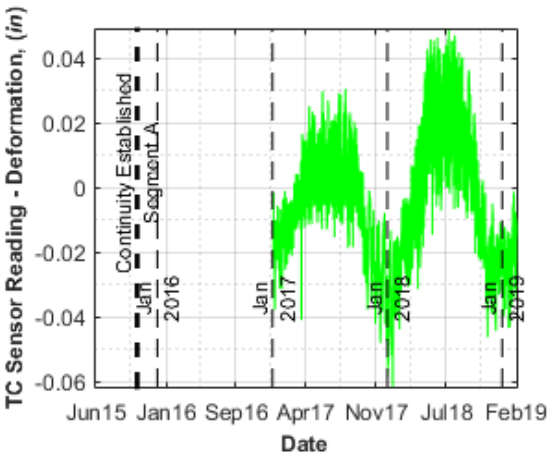

c) Sensor reading after temperature correction

B3_G4_BS – Strandmeter on the link slab at Bent 3 Girder 4 in Segment A

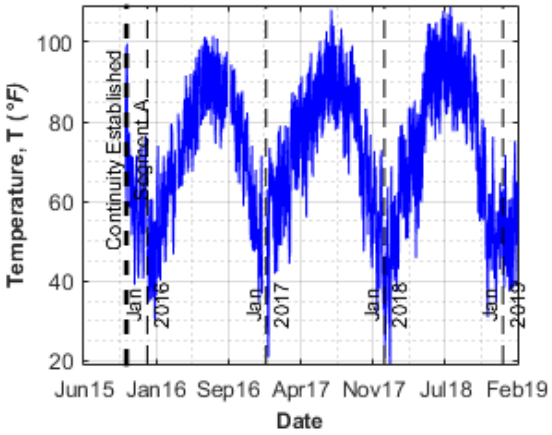

a) Temperature reading of the sensor

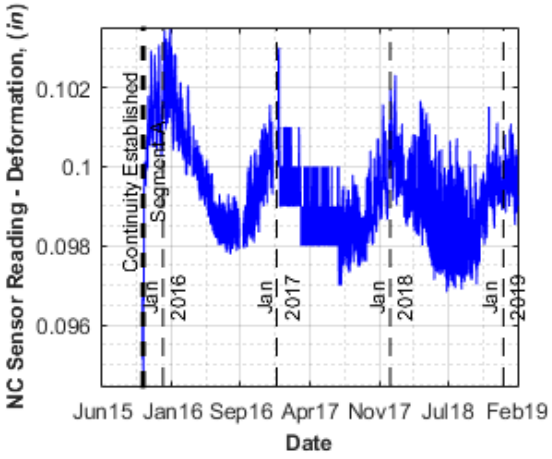

b) Sensor reading without temperature correction

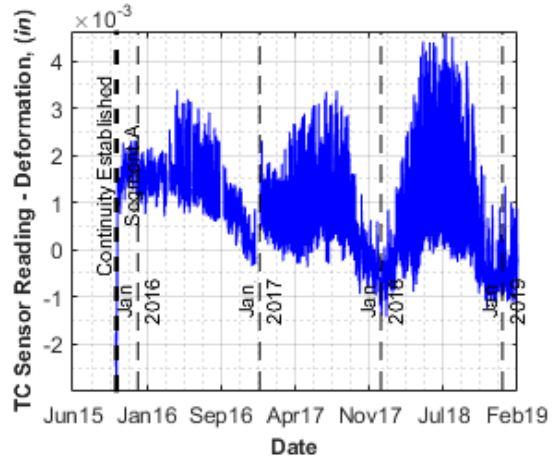

c) Sensor reading after temperature correction

B3_G4_TS – Strandmeter on the link slab at Bent 3 Girder 4 in Segment A

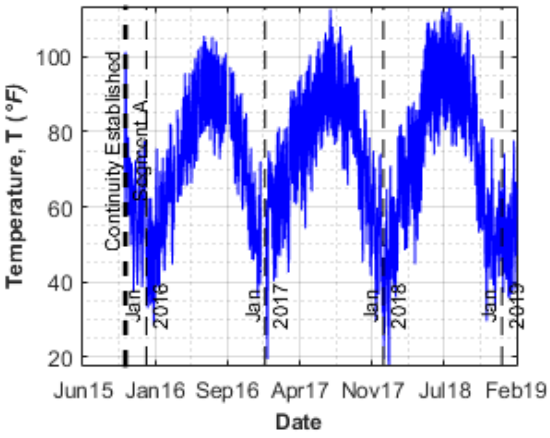

a) Temperature reading of the sensor

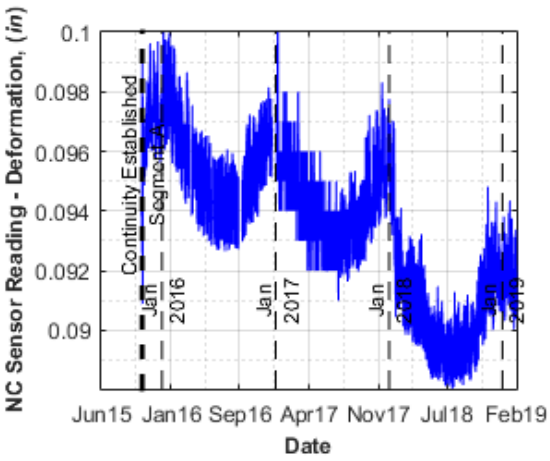

b) Sensor reading without temperature correction

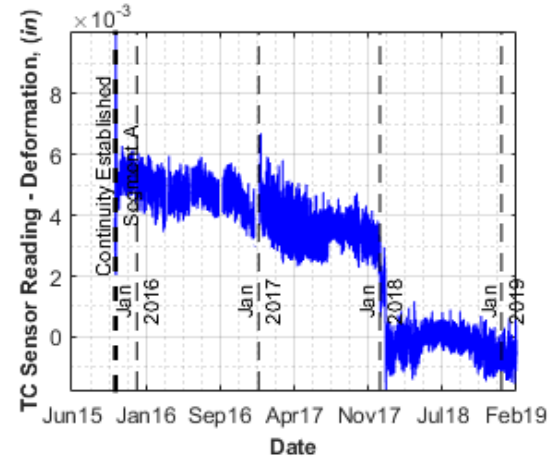

c) Sensor reading after temperature correction

B3_S5_5_BS – Strandmeter on the link slab at Bent 3 between Girder 4 and 5 in Segment A

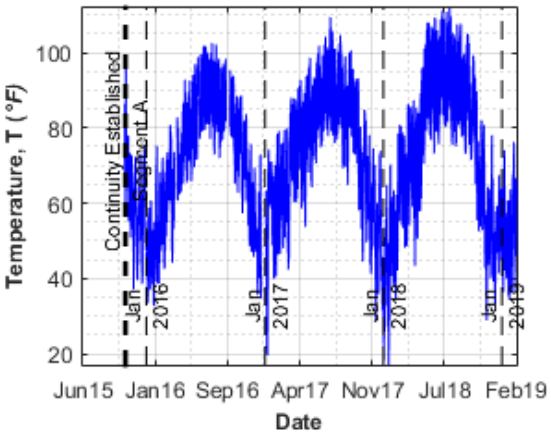

a) Temperature reading of the sensor

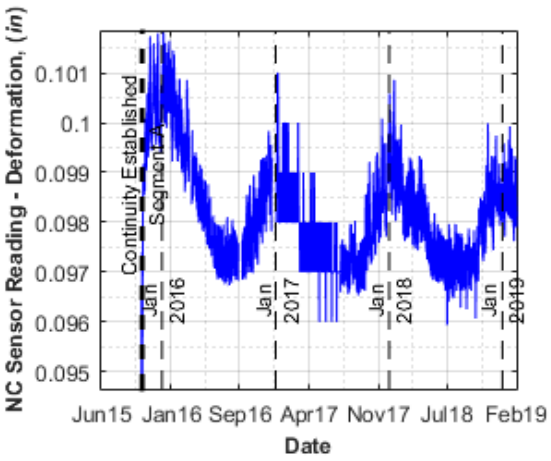

b) Sensor reading without temperature correction

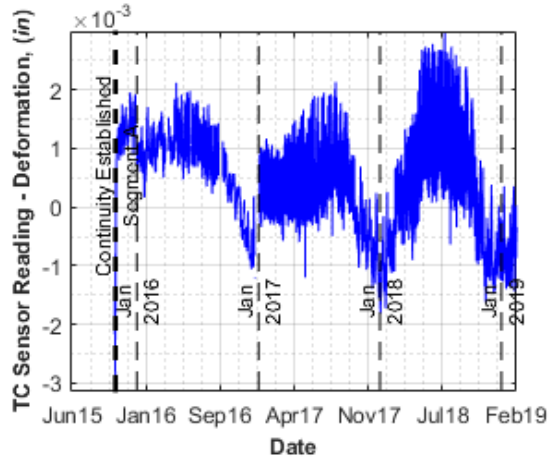

c) Sensor reading after temperature correction

B3_S5_5_TS – Strandmeter on the link slab at Bent 3 between Girder 4 and 5 in Segment A

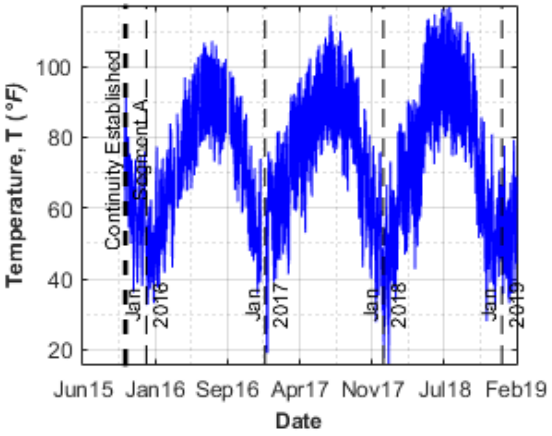

a) Temperature reading of the sensor

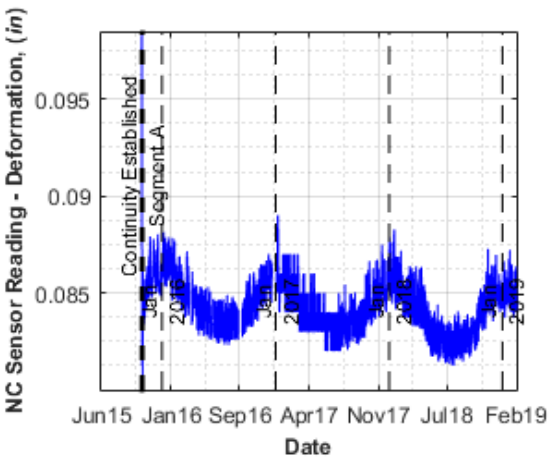

b) Sensor reading without temperature correction

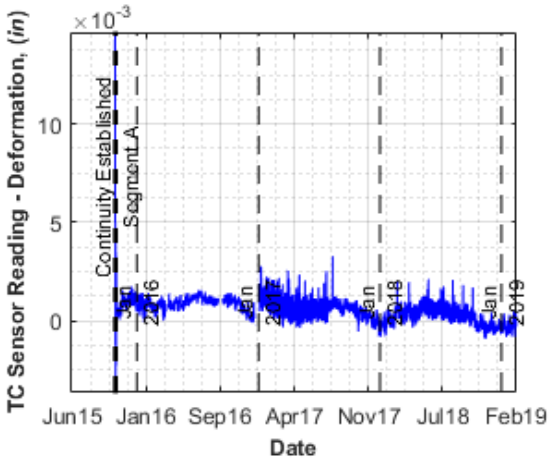

c) Sensor reading after temperature correction

B3_G7_BS – Strandmeter on the link slab at Bent 3 Girder 7 in Segment A

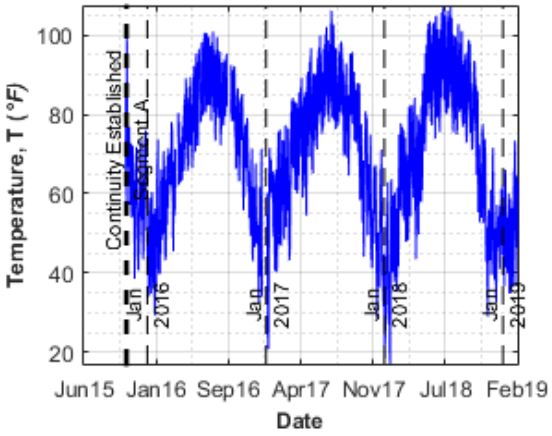

a) Temperature reading of the sensor

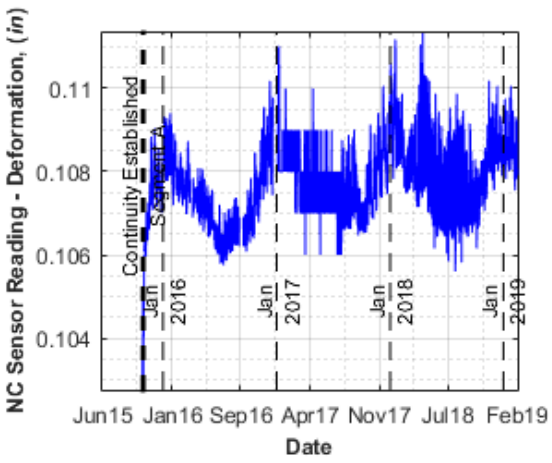

b) Sensor reading without temperature correction

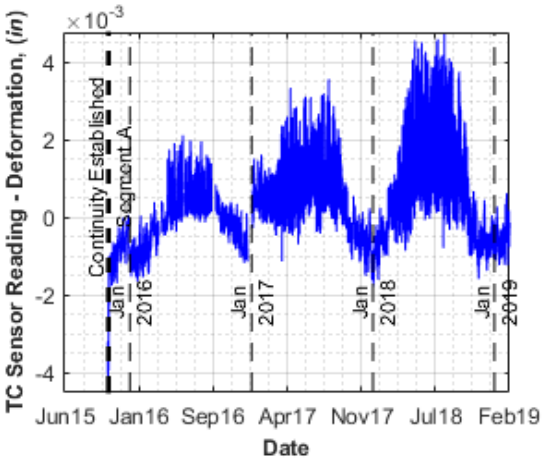

c) Sensor reading after temperature correction

B3_G7_TS – Strandmeter on the link slab at Bent 3 Girder 7 in Segment A

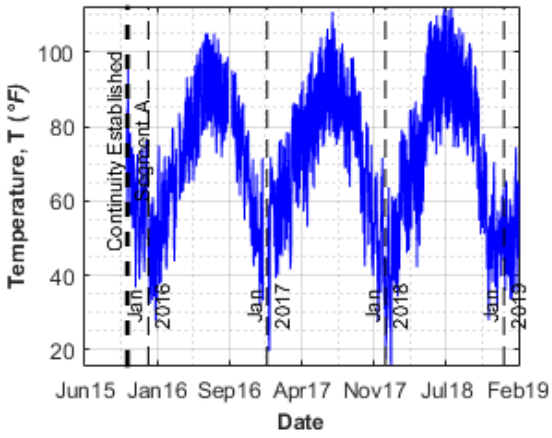

a) Temperature reading of the sensor

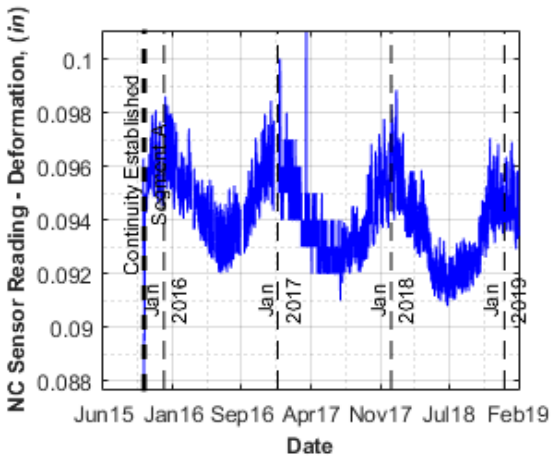

b) Sensor reading without temperature correction

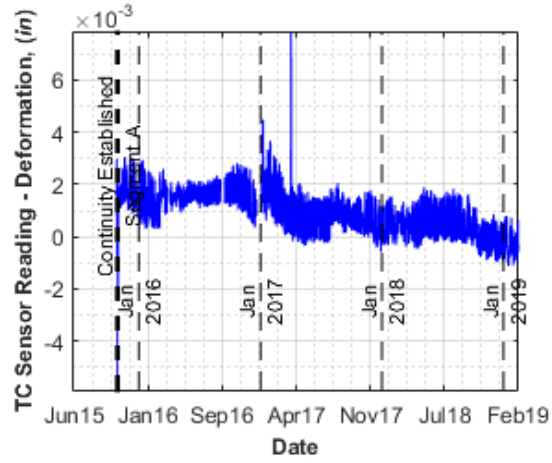

c) Sensor reading after temperature correction

B3_STRAIN – Strain gage in Segment A

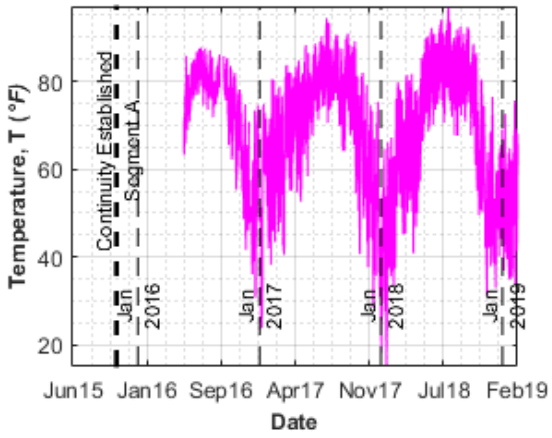

a) Temperature reading of the sensor

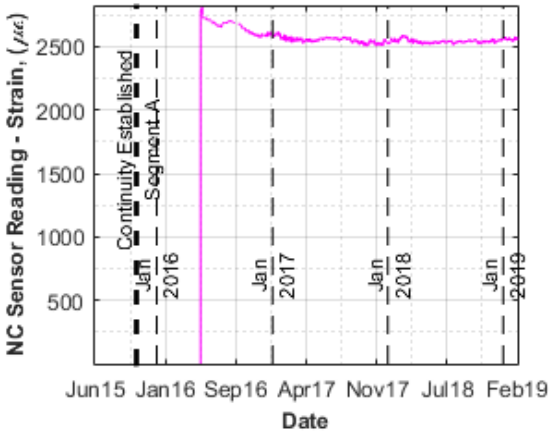

b) Sensor reading without temperature correction

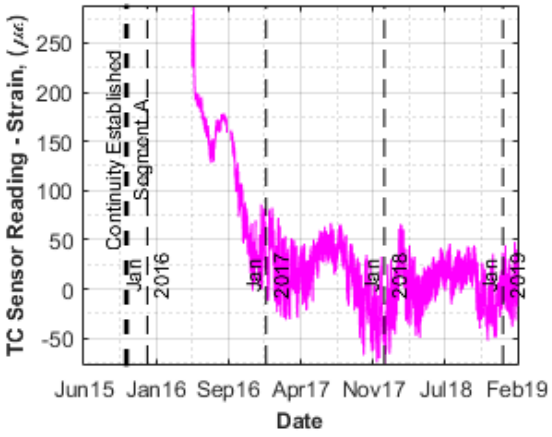

c) Sensor reading after temperature correction

B2_G4_BFE – Gapmeter on the riser in the east at Bent 2 Girder 4 in Segment A

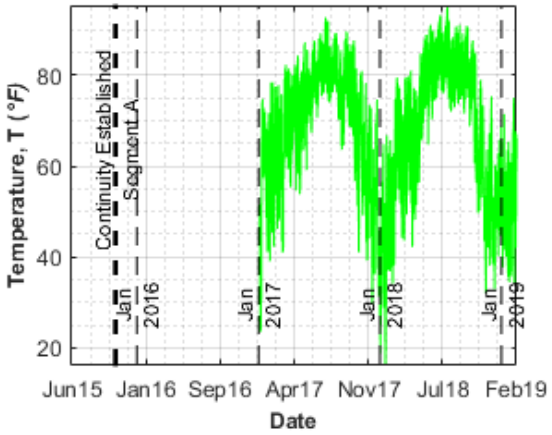

a) Temperature reading of the sensor

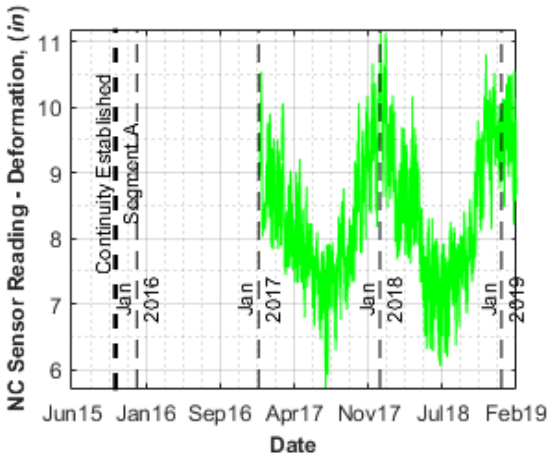

b) Sensor reading without temperature correction

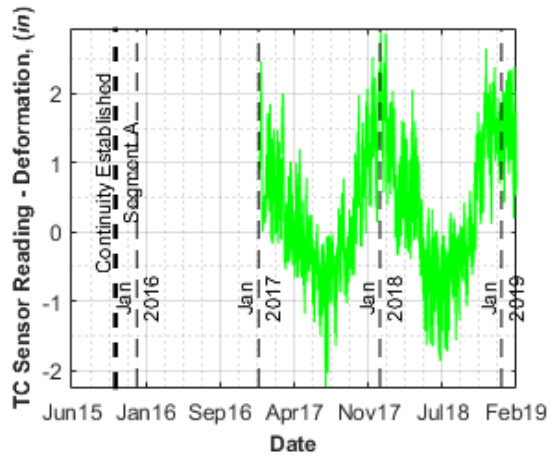

c) Sensor reading after temperature correction

B2_G4_BFW – Gapmeter on the riser in the west at Bent 2 Girder 4 in Segment A

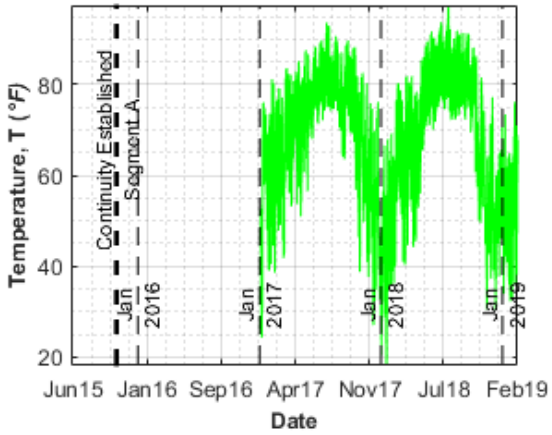

a) Temperature reading of the sensor

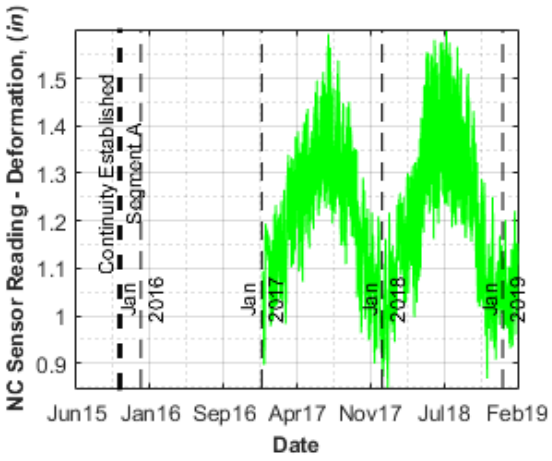

b) Sensor reading without temperature correction

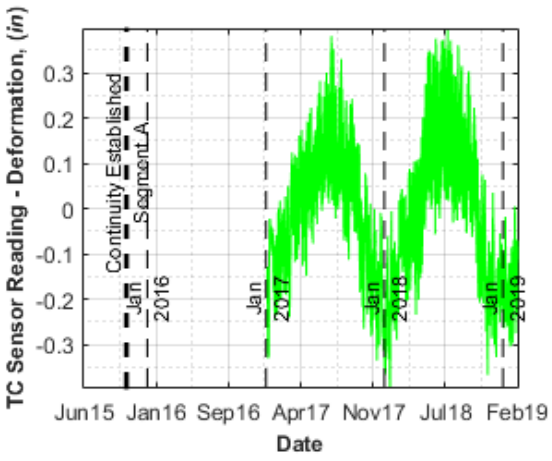

c) Sensor reading after temperature correction

B2_G4_BW – Gapmeter on the bottom of the web at Bent 2 Girder 4 in Segment A

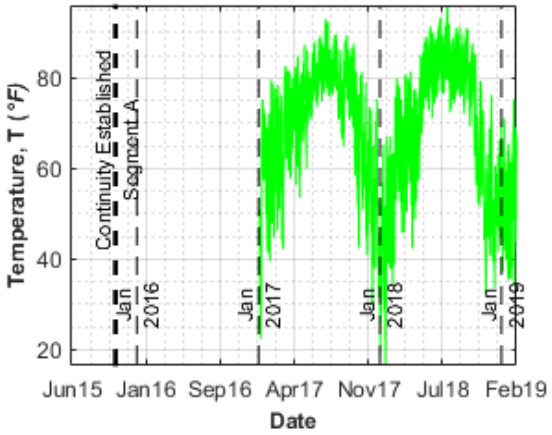

a) Temperature reading of the sensor

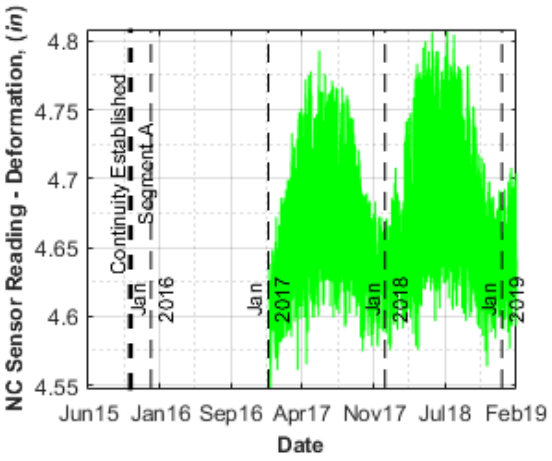

b) Sensor reading without temperature correction

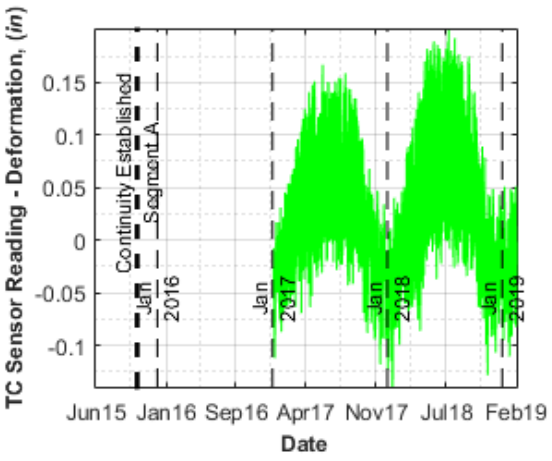

c) Sensor reading after temperature correction

B2_G4_TW – Gapmeter on the top of the web at Bent 2 Girder 4 in Segment A

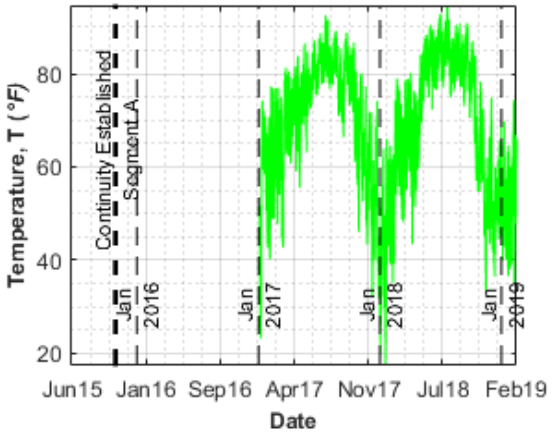

a) Temperature reading of the sensor

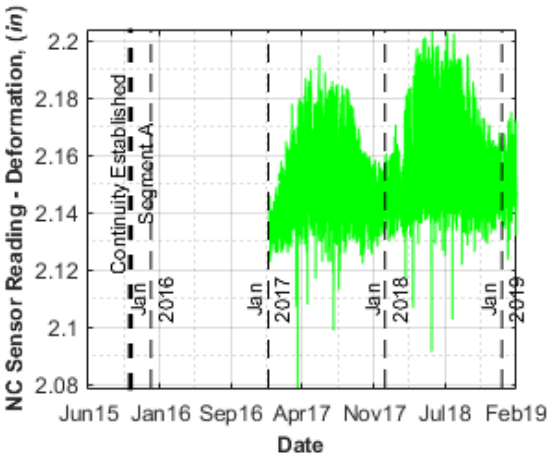

b) Sensor reading without temperature correction

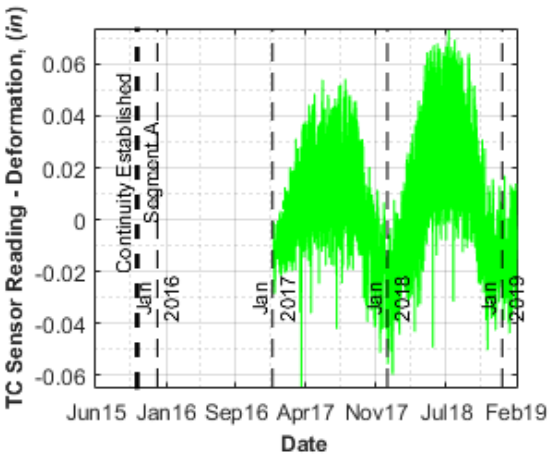

c) Sensor reading after temperature correction

B2_G7_BFE – Gapmeter on the riser in the east at Bent 2 Girder 7 in Segment A

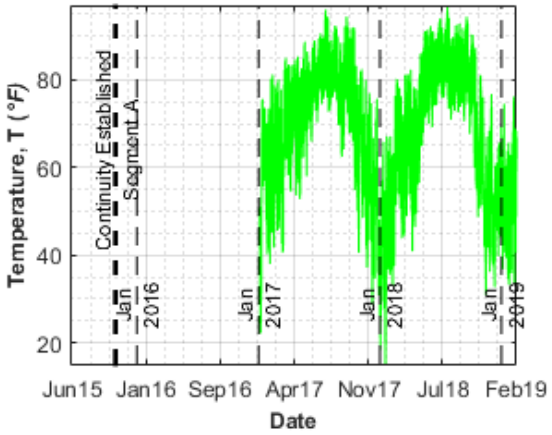

a) Temperature reading of the sensor

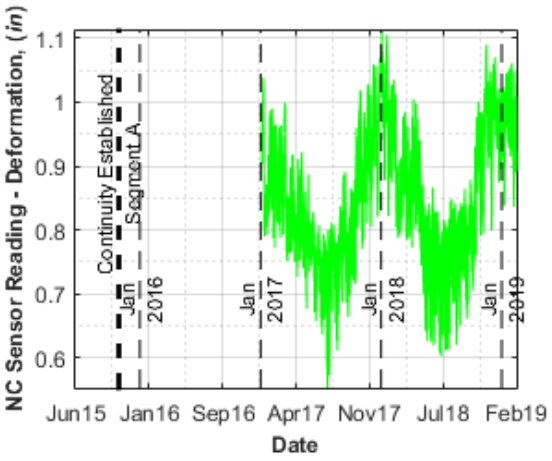

b) Sensor reading without temperature correction

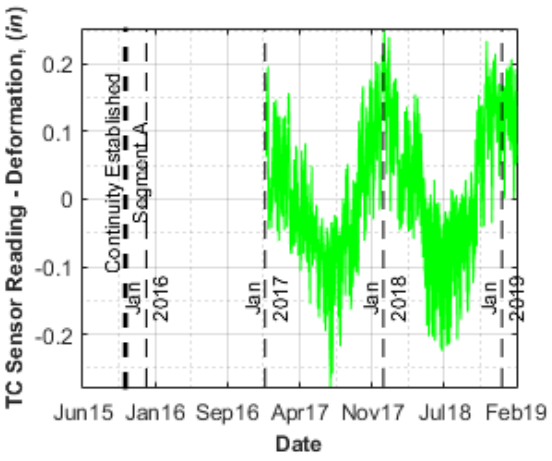

c) Sensor reading after temperature correction

B2_G7_BFW – Gapmeter on the riser in the west at Bent 2 Girder 7 in Segment A

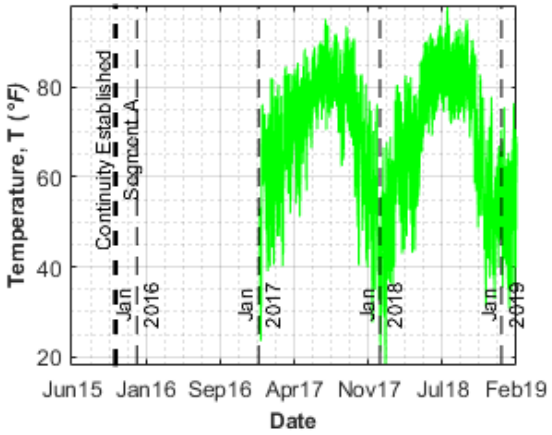

a) Temperature reading of the sensor

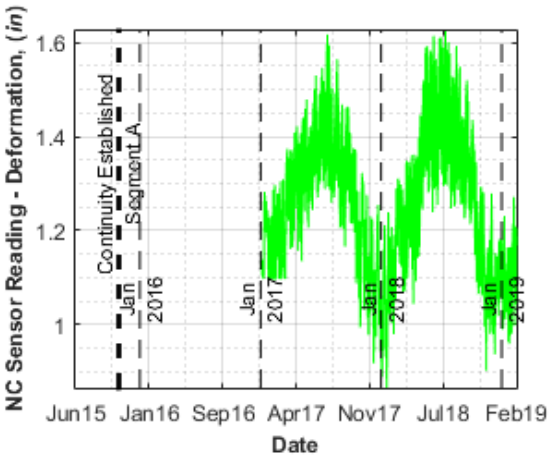

b) Sensor reading without temperature correction

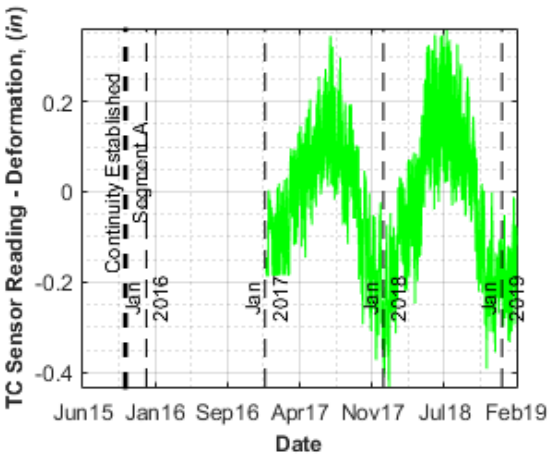

c) Sensor reading after temperature correction

B2_G7_BW – Gapmeter on the bottom of the web at Bent 2 Girder 7 in Segment A

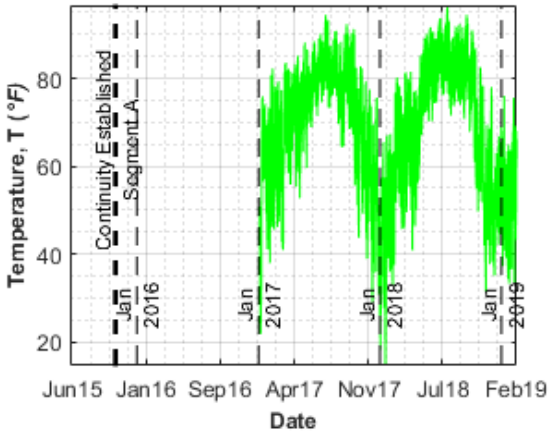

a) Temperature reading of the sensor

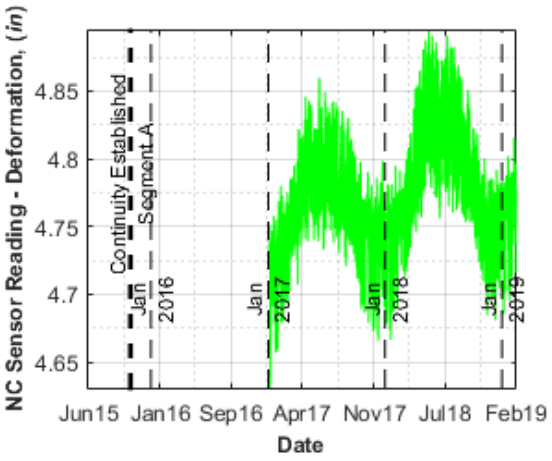

b) Sensor reading without temperature correction

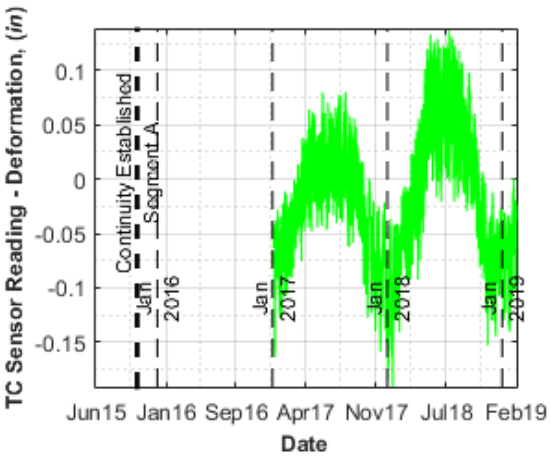

c) Sensor reading after temperature correction

B2_G7_TW – Gapmeter on the top of the web at Bent 2 Girder 7 in Segment A

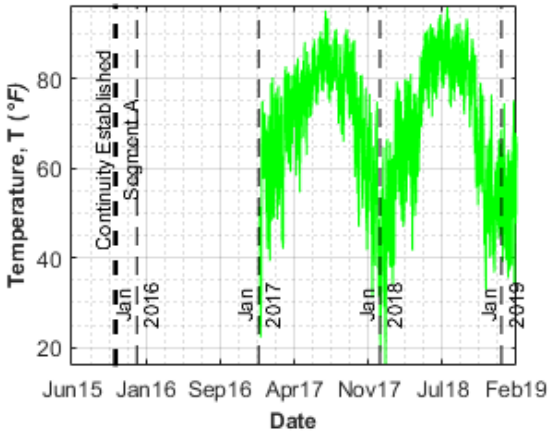

a) Temperature reading of the sensor

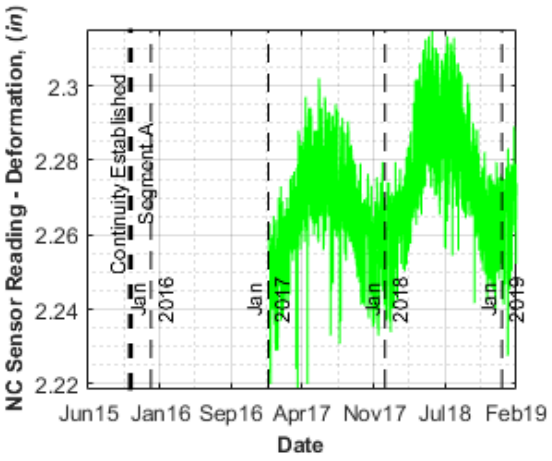

b) Sensor reading without temperature correction

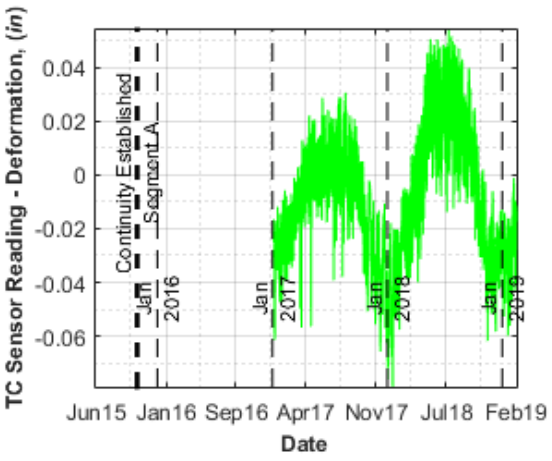

c) Sensor reading after temperature correction

B2_G4_BS – Strandmeter on the link slab at Bent 2 Girder 4 in Segment A

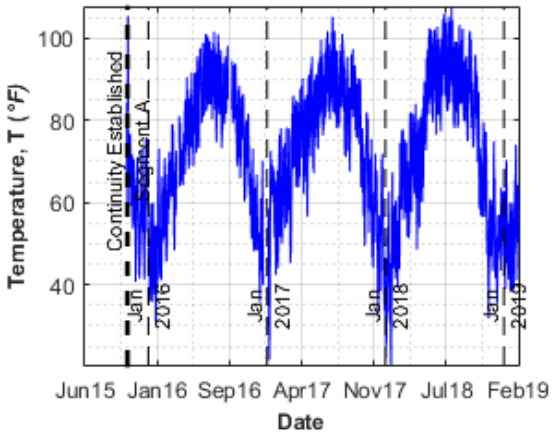

a) Temperature reading of the sensor

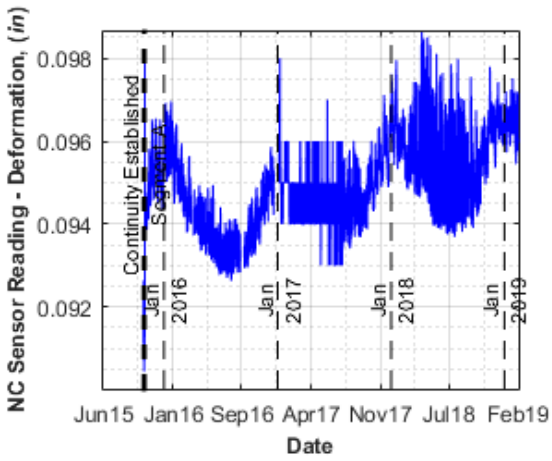

b) Sensor reading without temperature correction

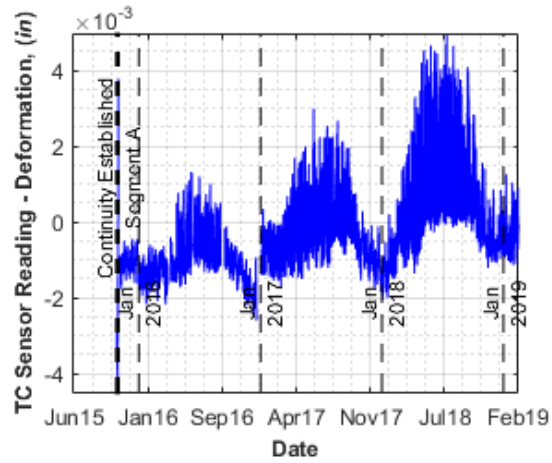

c) Sensor reading after temperature correction

B2_G4_TS – Strandmeter on the link slab at Bent 2 Girder 4 in Segment A

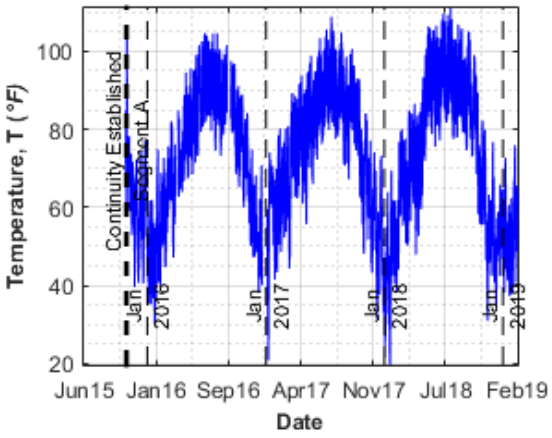

a) Temperature reading of the sensor

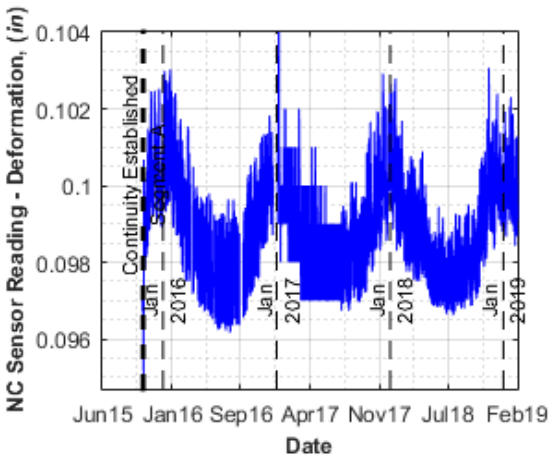

b) Sensor reading without temperature correction

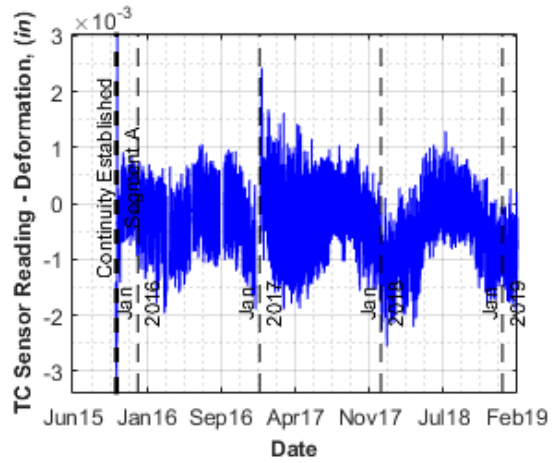

c) Sensor reading after temperature correction

B2_S5_5_BS – Strandmeter on the link slab at Bent 2 between Girder 4 and 5 in Segment A

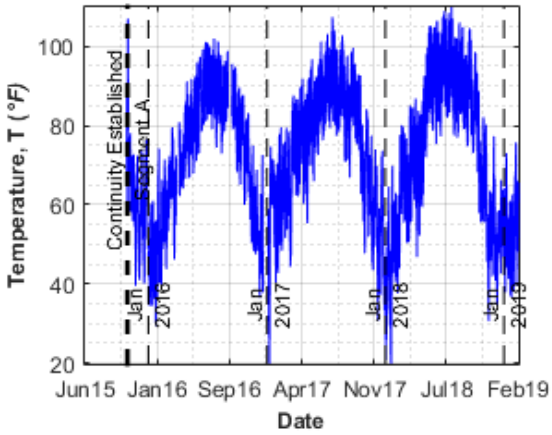

a) Temperature reading of the sensor

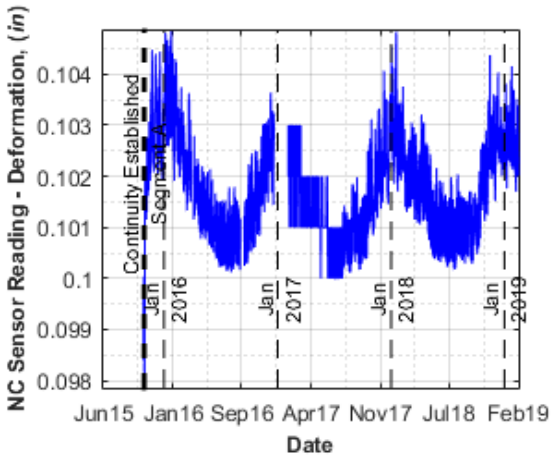

b) Sensor reading without temperature correction

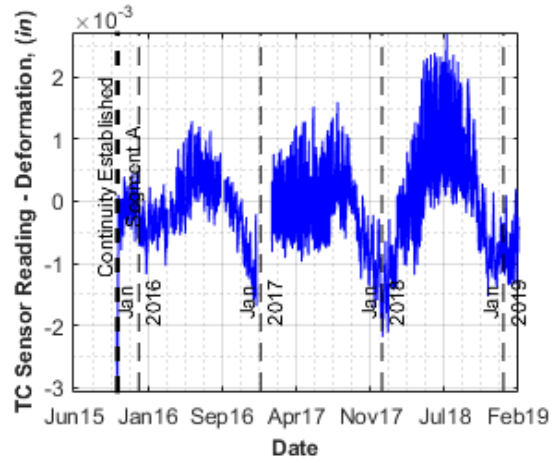

c) Sensor reading after temperature correction

B2_S5_5_TS – Strandmeter on the link slab at Bent 2 between Girder 4 and 5 in Segment A

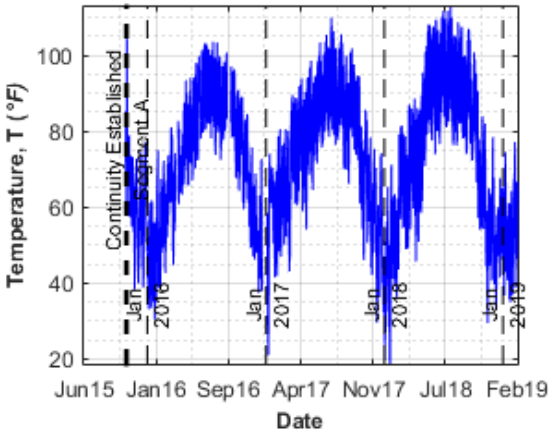

a) Temperature reading of the sensor

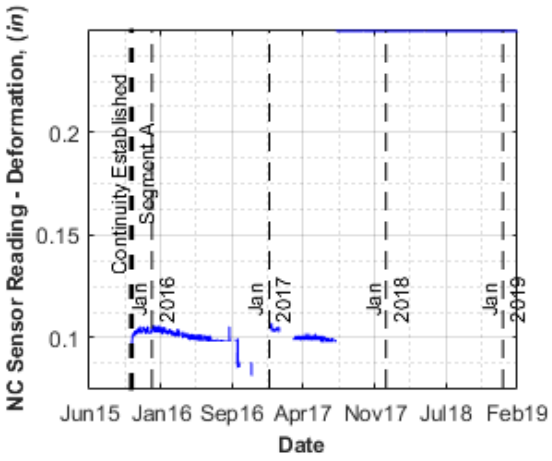

b) Sensor reading without temperature correction

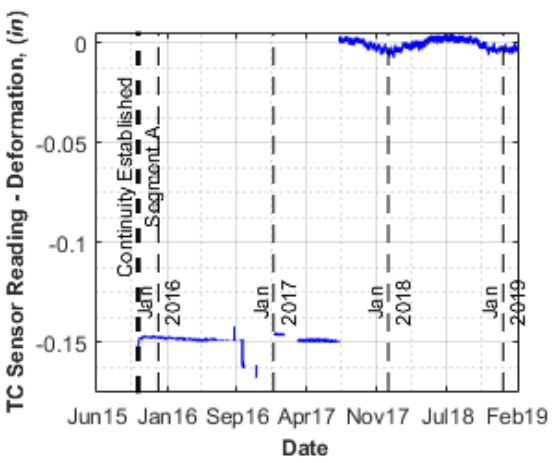

c) Sensor reading after temperature correction

B2_G7_BS – Strandmeter on the link slab at Bent 2 Girder 7 in Segment A

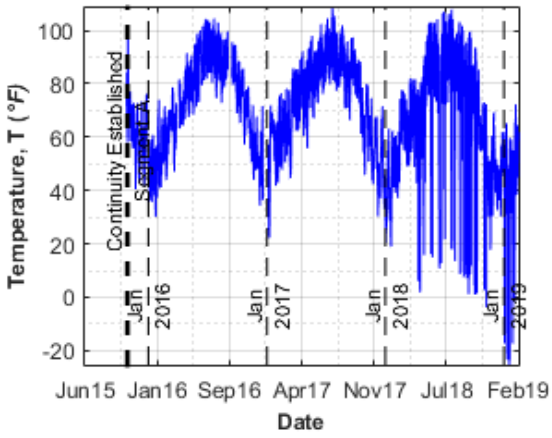

a) Temperature reading of the sensor

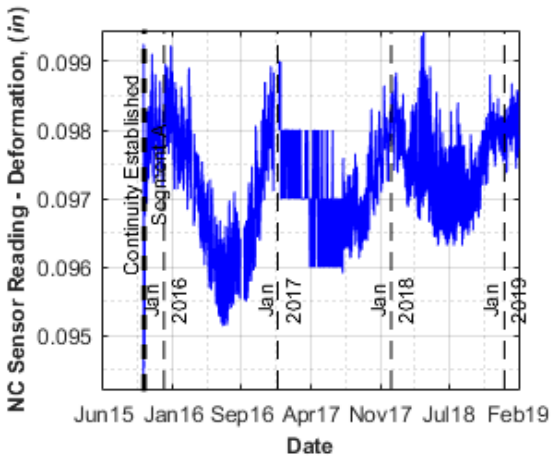

b) Sensor reading without temperature correction

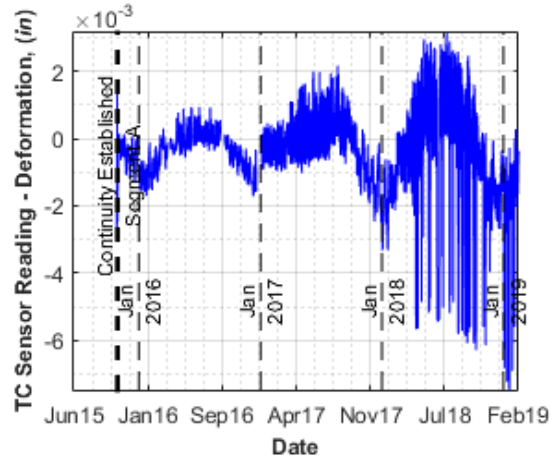

c) Sensor reading after temperature correction

B2_G7_TS – Strandmeter on the link slab at Bent 2 Girder 7 in Segment A

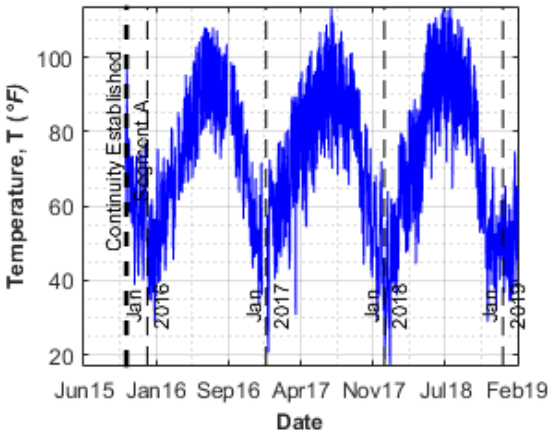

a) Temperature reading of the sensor

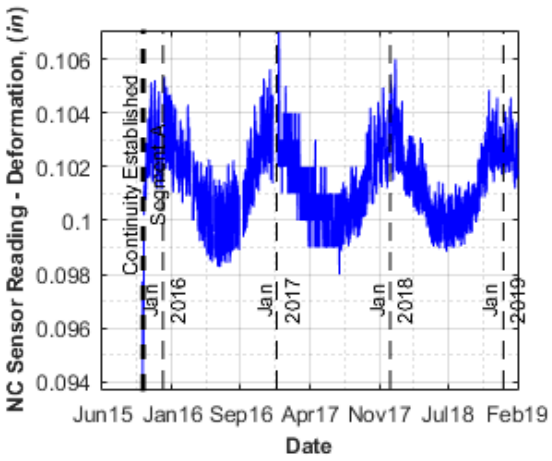

b) Sensor reading without temperature correction

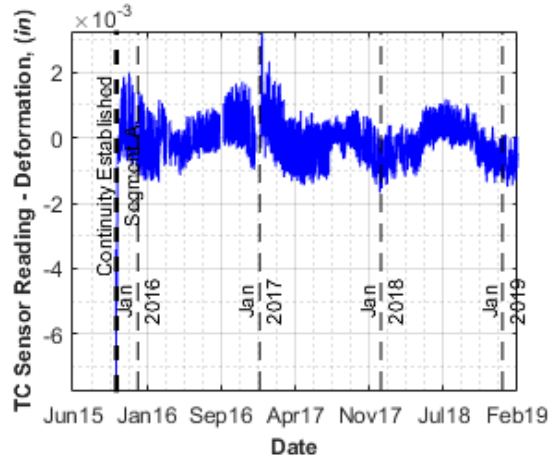

c) Sensor reading after temperature correction

B1_G4_BFE – Gapmeter on the riser in the east at Bent 1 Girder 4 in Segment A

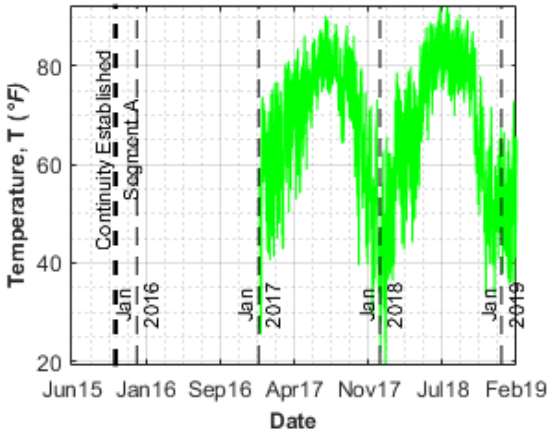

a) Temperature reading of the sensor

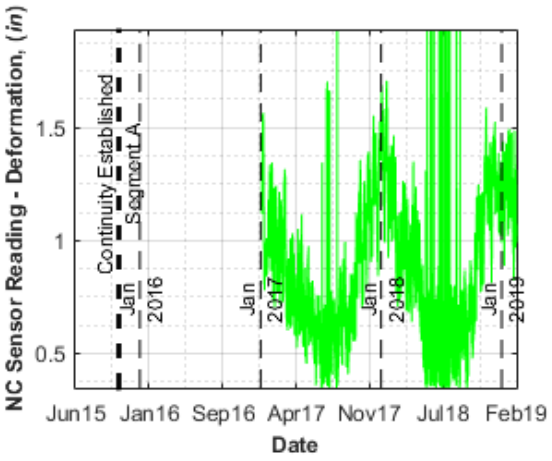

b) Sensor reading without temperature correction

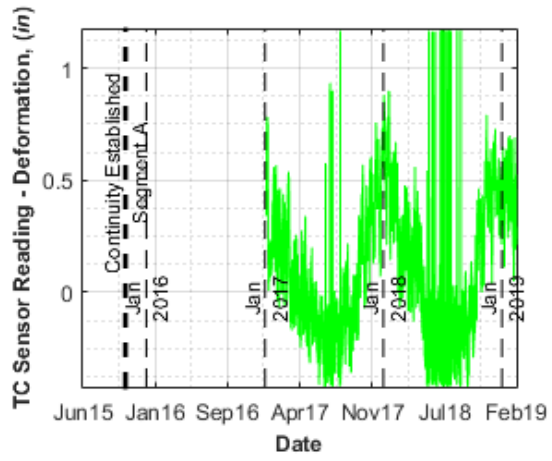

c) Sensor reading after temperature correction

B1_G7_BFE – Gapmeter on the riser in the east at Bent 1 Girder 7 in Segment A

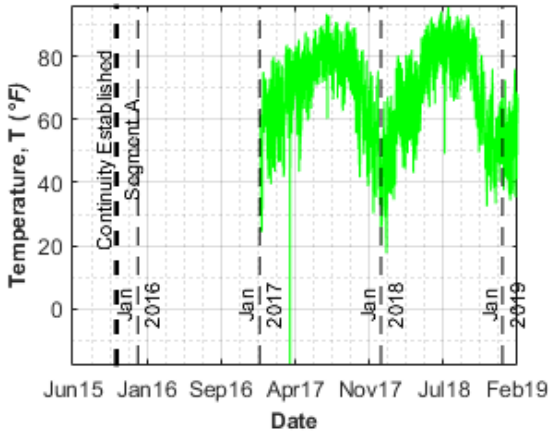

a) Temperature reading of the sensor

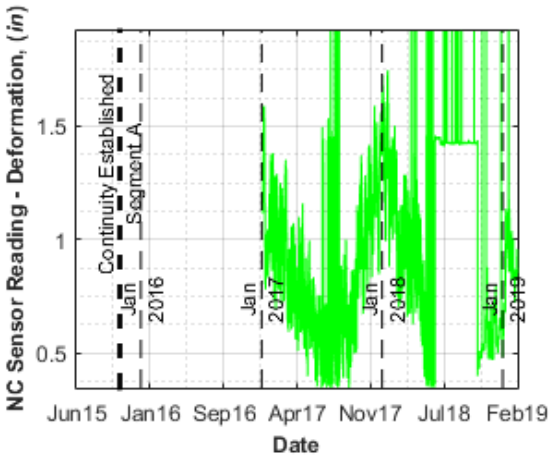

b) Sensor reading without temperature correction

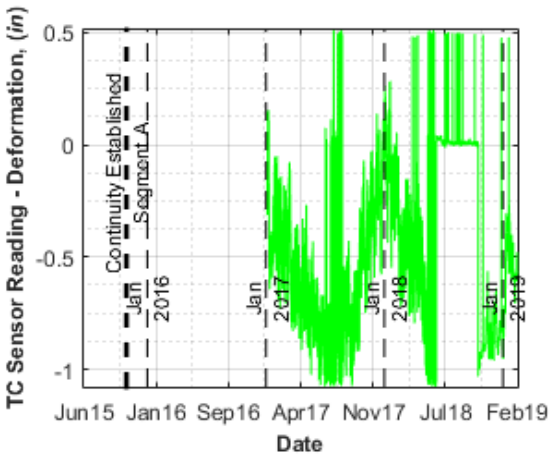

c) Sensor reading after temperature correction

B4_G4_BFE – Gapmeter on the riser in the east at Bent 4 Girder 4 in Segment A

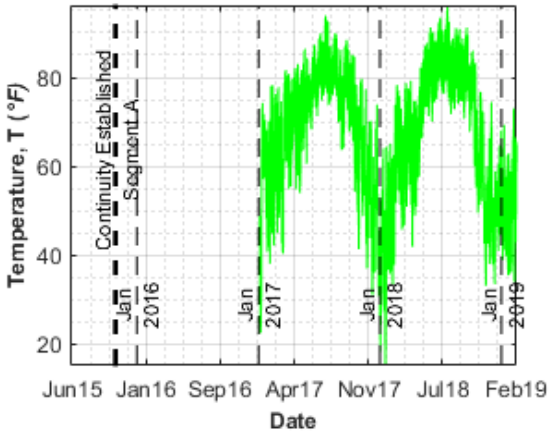

a) Temperature reading of the sensor

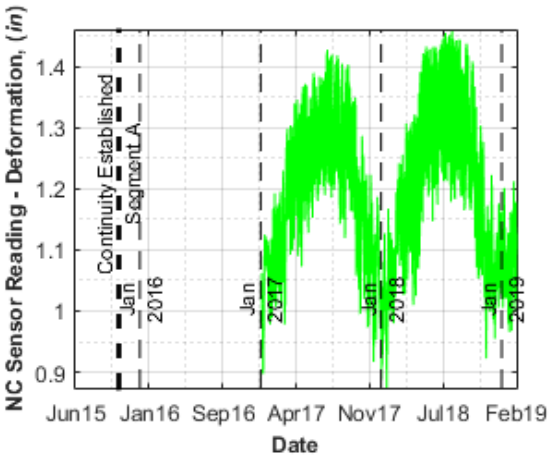

b) Sensor reading without temperature correction

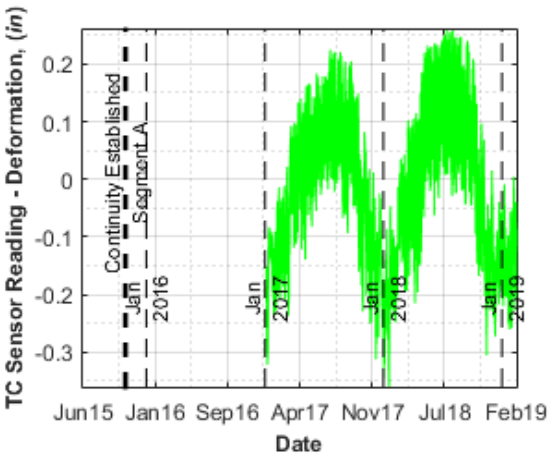

c) Sensor reading after temperature correction

B4_G4_BFW – Gapmeter on the riser in the west at Bent 4 Girder 4 in Segment A

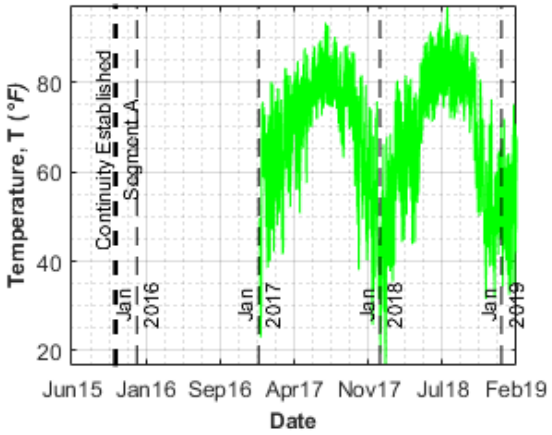

a) Temperature reading of the sensor

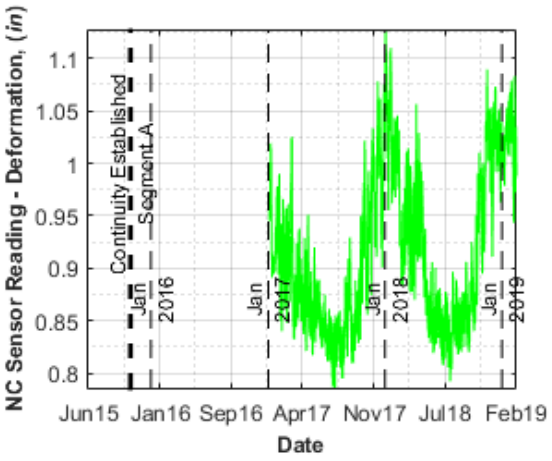

b) Sensor reading without temperature correction

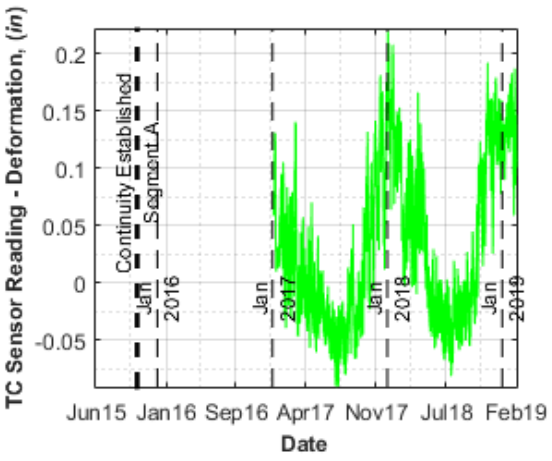

c) Sensor reading after temperature correction

B4_G4_BW – Gapmeter on the bottom of the web at Bent 4 Girder 4 in Segment A

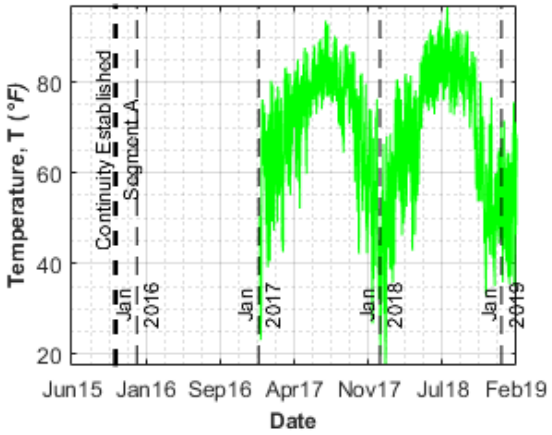

a) Temperature reading of the sensor

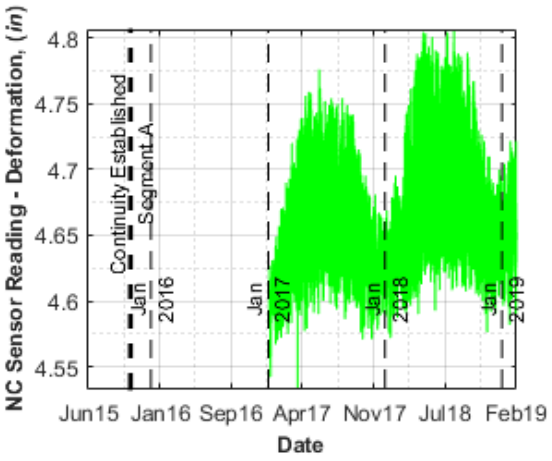

b) Sensor reading without temperature correction

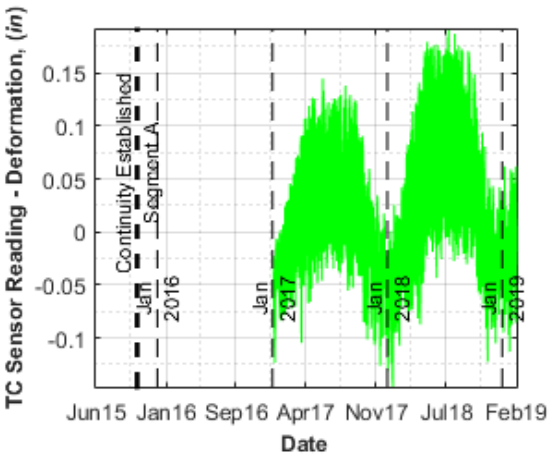

c) Sensor reading after temperature correction

B4_G4_TW – Gapmeter on the top of the web at Bent 4 Girder 4 in Segment A

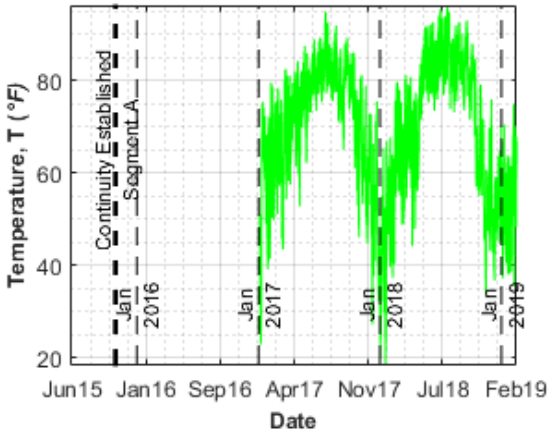

a) Temperature reading of the sensor

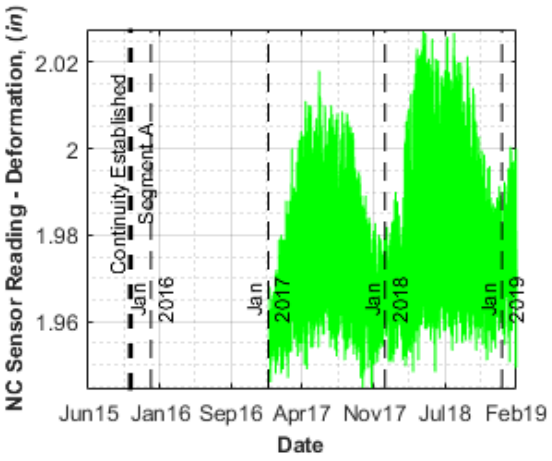

b) Sensor reading without temperature correction

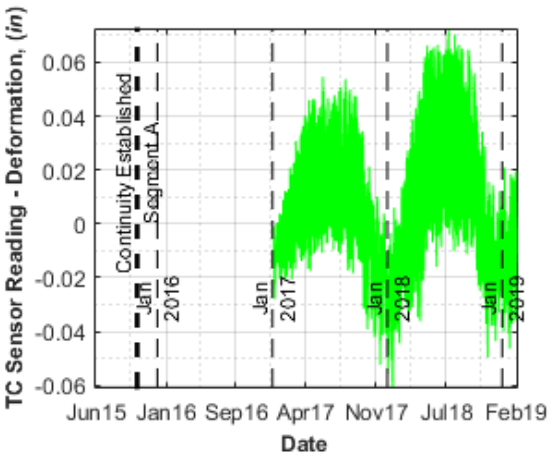

c) Sensor reading after temperature correction

B4_G7_BFE – Gapmeter on the riser in the east at Bent 4 Girder 7 in Segment A

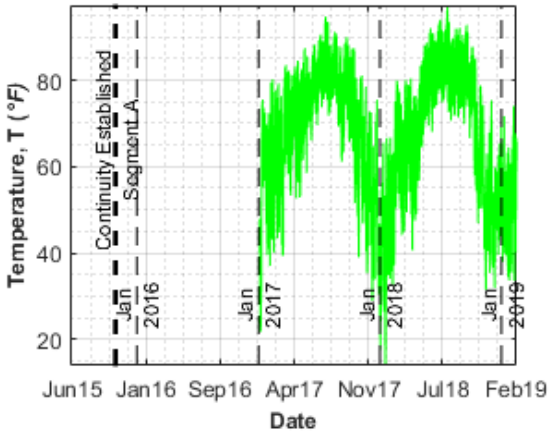

a) Temperature reading of the sensor

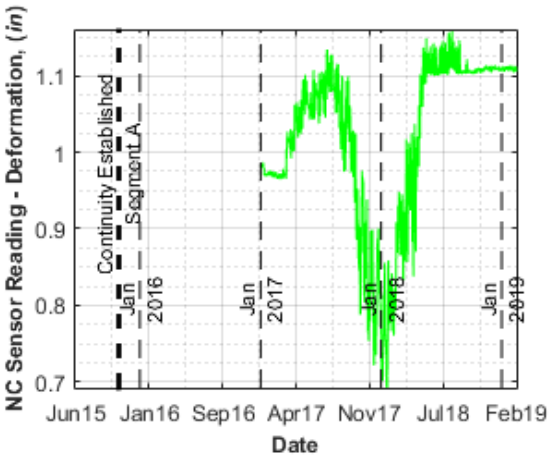

b) Sensor reading without temperature correction

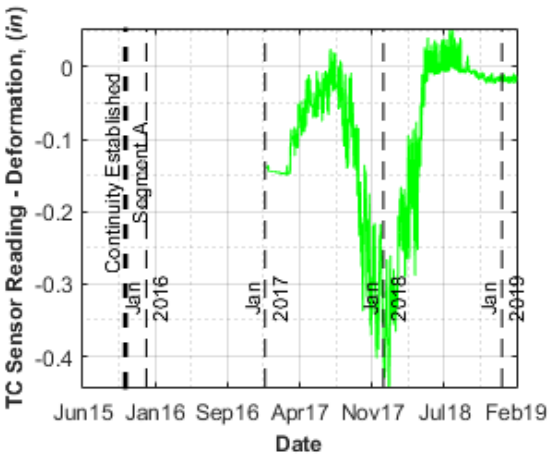

c) Sensor reading after temperature correction

B4_G7_BFW – Gapmeter on the riser in the west at Bent 4 Girder 7 in Segment A

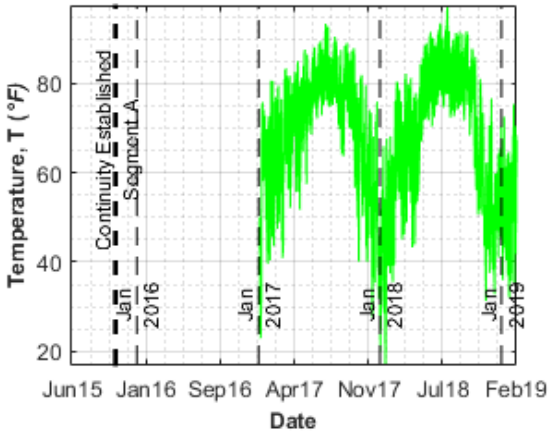

a) Temperature reading of the sensor

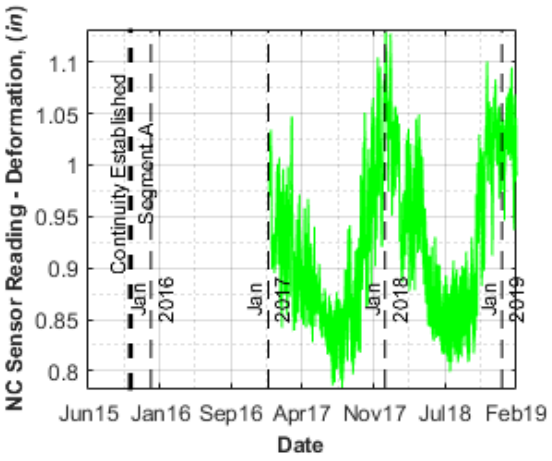

b) Sensor reading without temperature correction

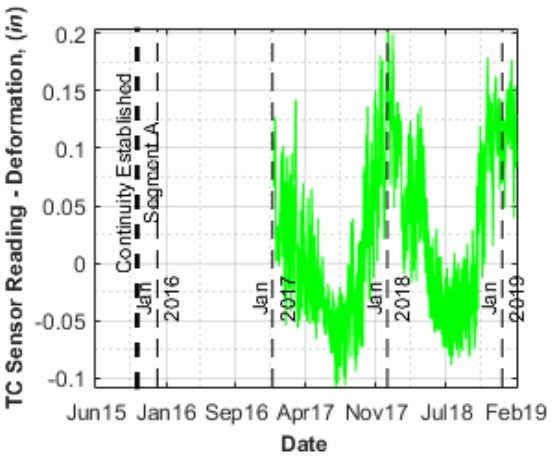

c) Sensor reading after temperature correction

B4_G7_BW – Gapmeter on the bottom of the web at Bent 4 Girder 7 in Segment A

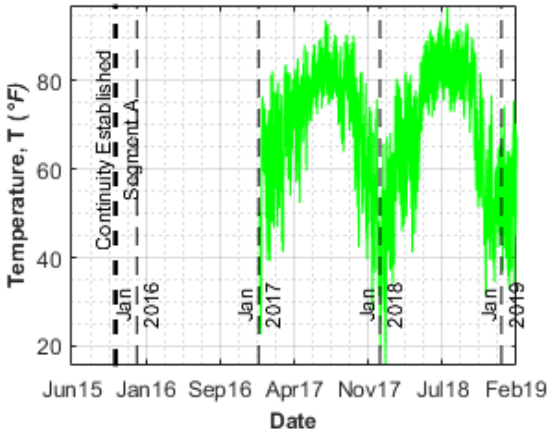

a) Temperature reading of the sensor

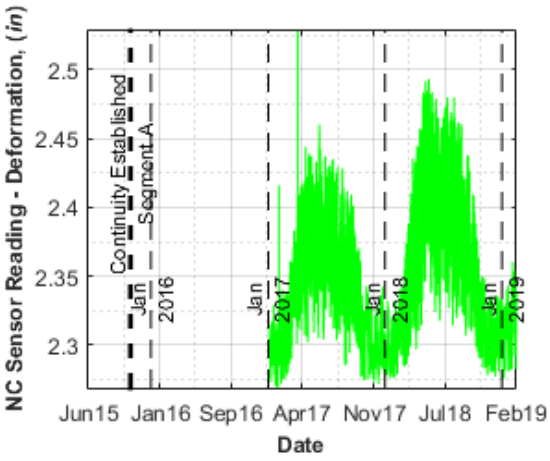

b) Sensor reading without temperature correction

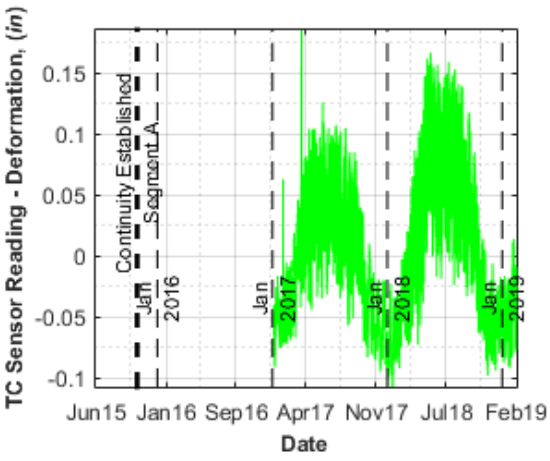

c) Sensor reading after temperature correction

B4_G7_TW – Gapmeter on the top of the web at Bent 4 Girder 7 in Segment A

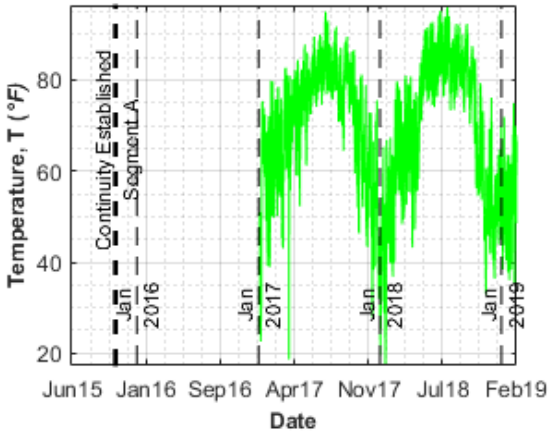

a) Temperature reading of the sensor

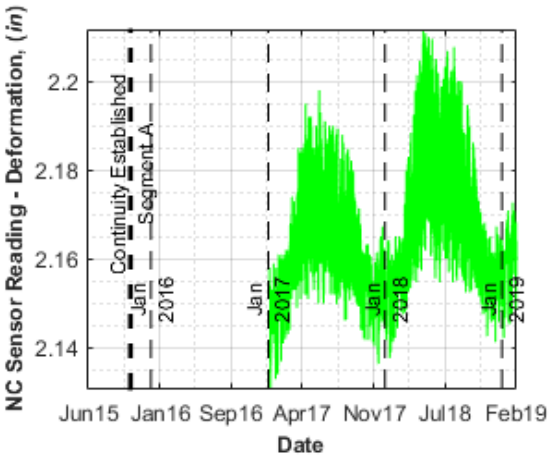

b) Sensor reading without temperature correction

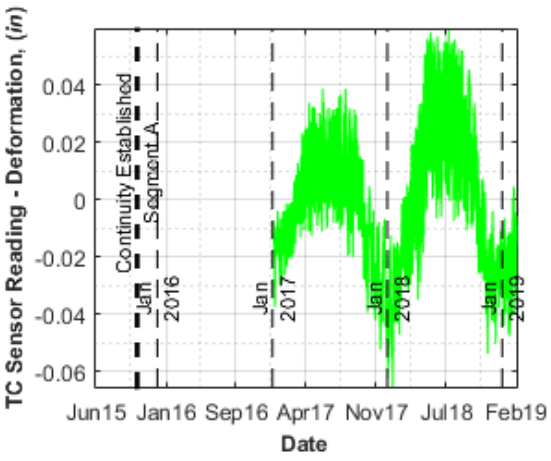

c) Sensor reading after temperature correction

B4_G4_BS – Strandmeter on the link slab at Bent 4 Girder 4 in Segment A

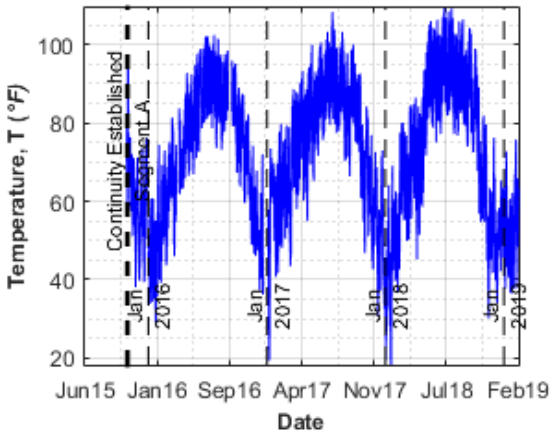

a) Temperature reading of the sensor

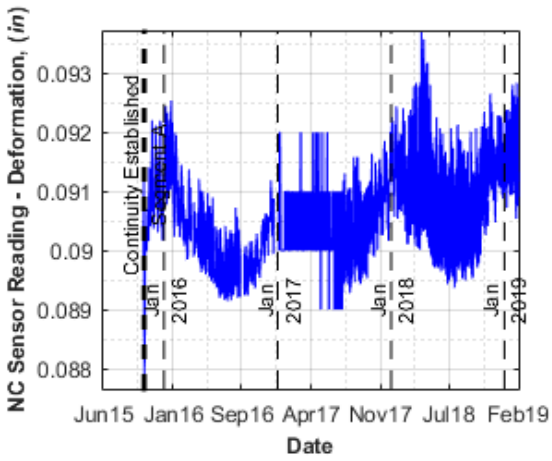

b) Sensor reading without temperature correction

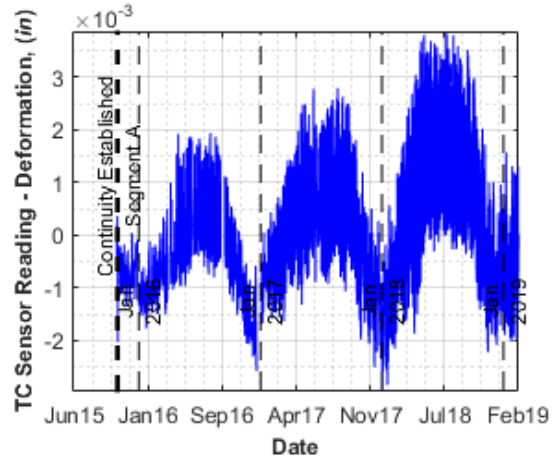

c) Sensor reading after temperature correction

B4_G4_TS – Strandmeter on the link slab at Bent 4 Girder 4 in Segment A

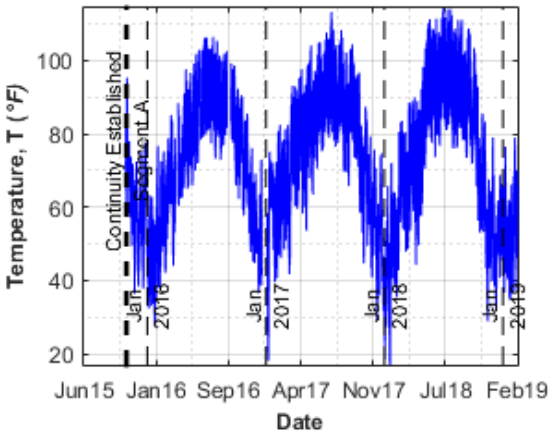

a) Temperature reading of the sensor

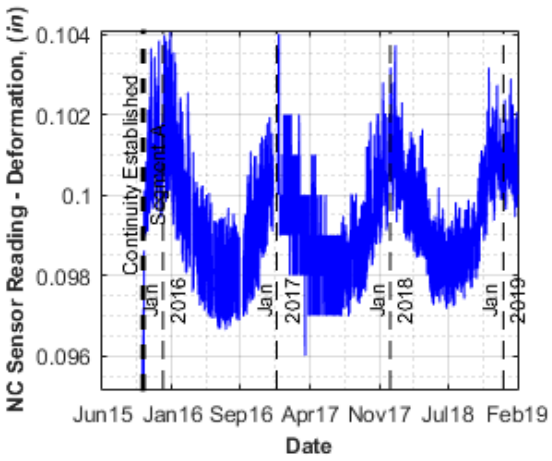

b) Sensor reading without temperature correction

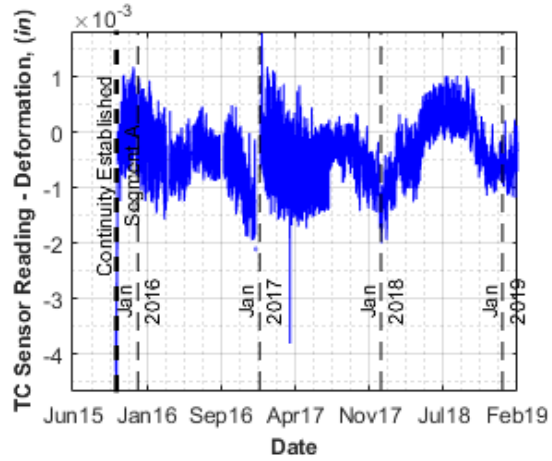

c) Sensor reading after temperature correction

B4_S5_5_BS – Strandmeter on the link slab at Bent 4 between Girder 4 and 5 in Segment A

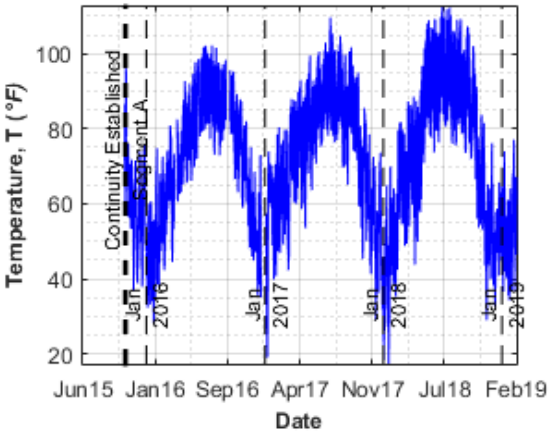

a) Temperature reading of the sensor

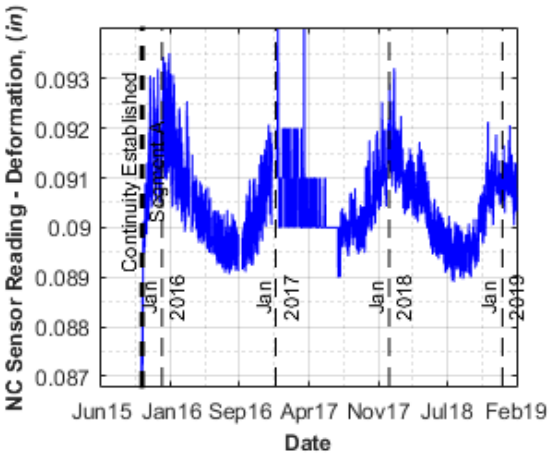

b) Sensor reading without temperature correction

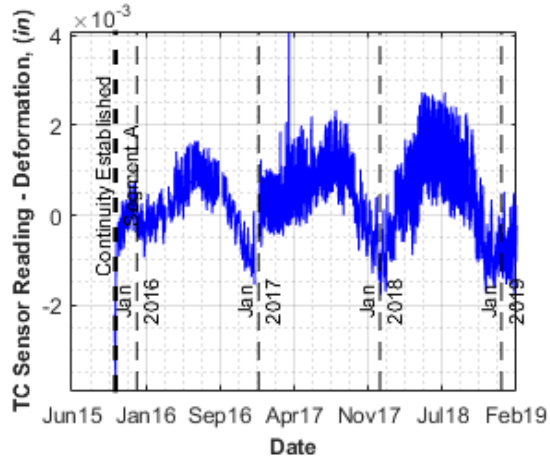

c) Sensor reading after temperature correction

B4_S5_5_TS – Strandmeter on the link slab at Bent 4 between Girder 4 and 5 in Segment A

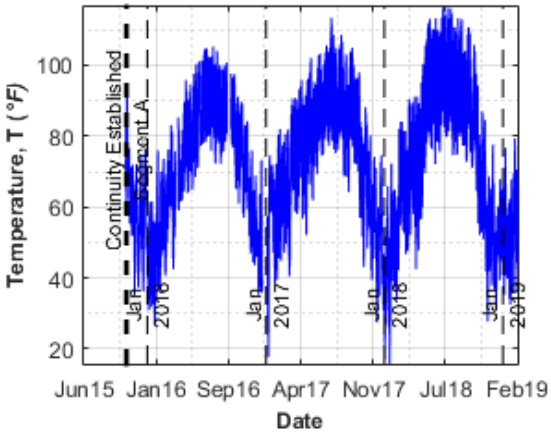

a) Temperature reading of the sensor

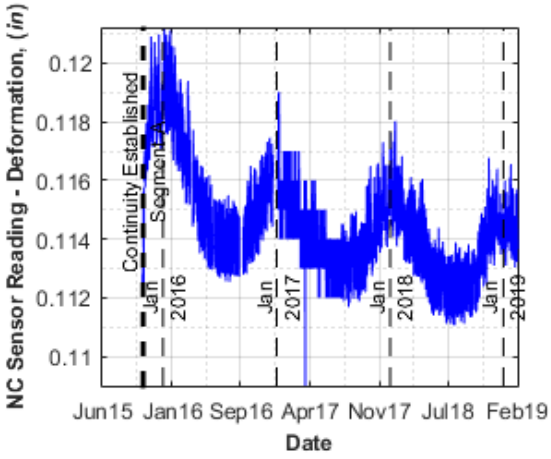

b) Sensor reading without temperature correction

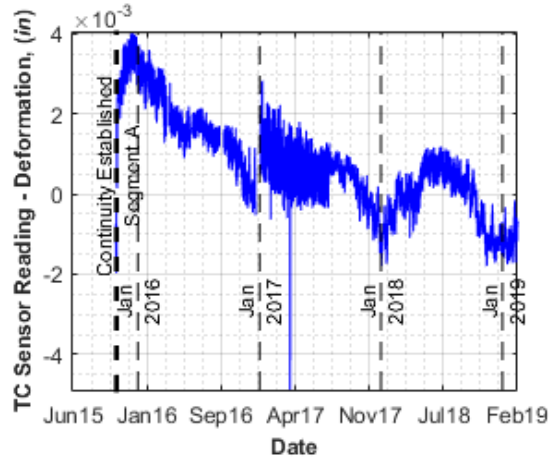

c) Sensor reading after temperature correction

B4_G7_BS – Strandmeter on the link slab at Bent 4 Girder 7 in Segment A

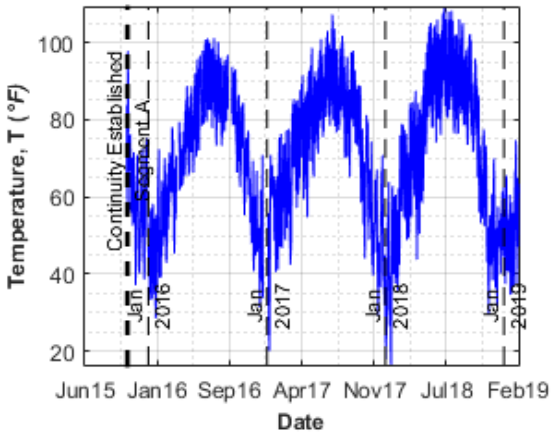

a) Temperature reading of the sensor

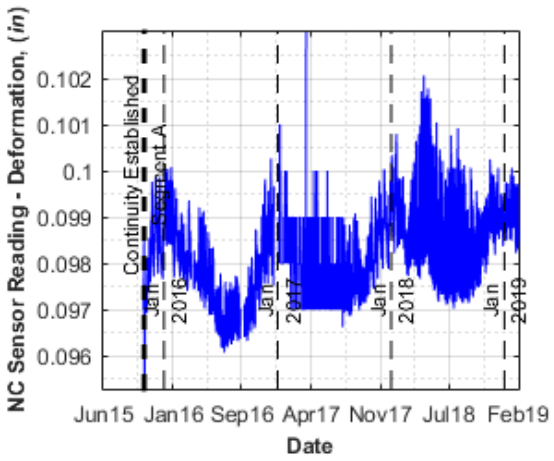

b) Sensor reading without temperature correction

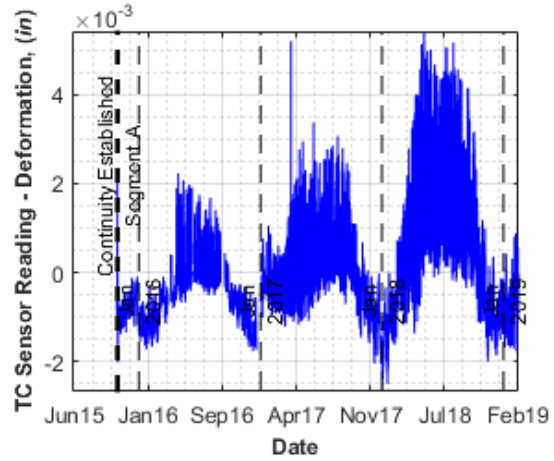

c) Sensor reading after temperature correction

B4_G7_TS – Strandmeter on the link slab at Bent 4 Girder 7 in Segment A

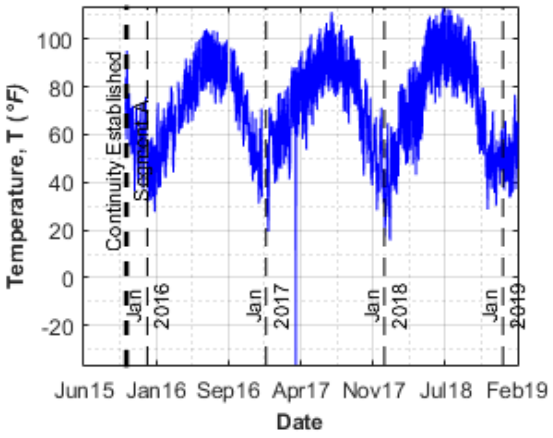

a) Temperature reading of the sensor

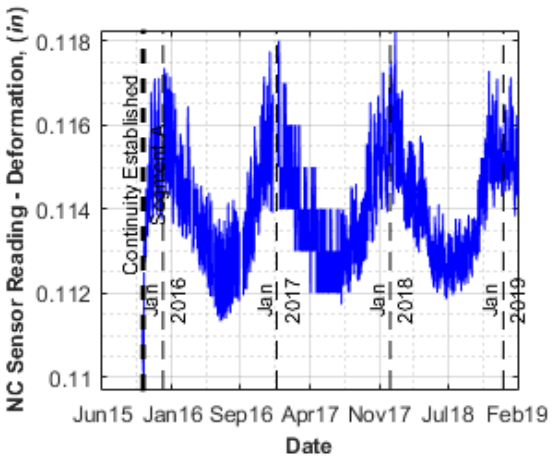

b) Sensor reading without temperature correction

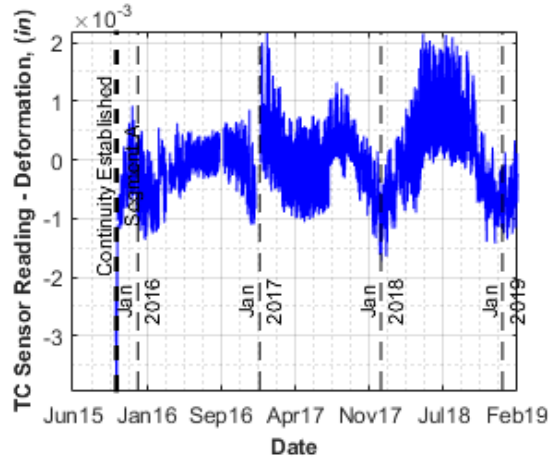

c) Sensor reading after temperature correction

B5_G4_BFW – Gapmeter on the riser in the west at Bent 5 Girder 4 in Segment A

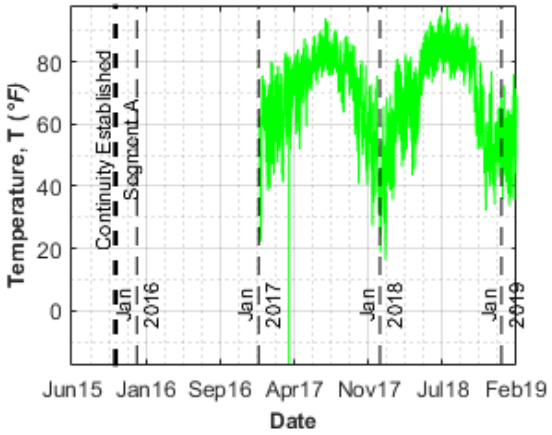

a) Temperature reading of the sensor

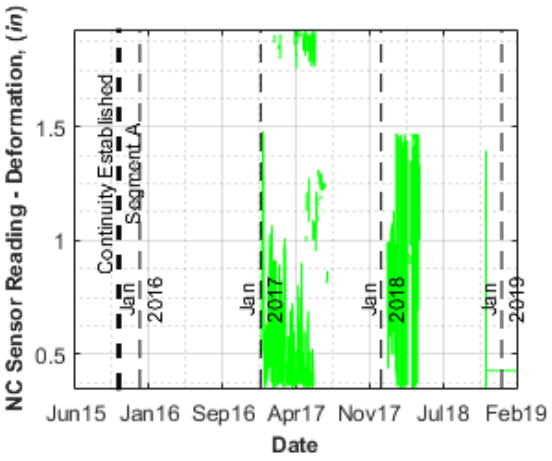

b) Sensor reading without temperature correction

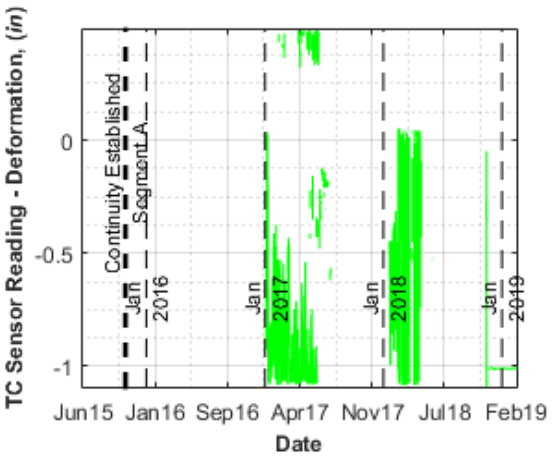

c) Sensor reading after temperature correction

B5_G7_BFW – Gapmeter on the riser in the west at Bent 5 Girder 7 in Segment A

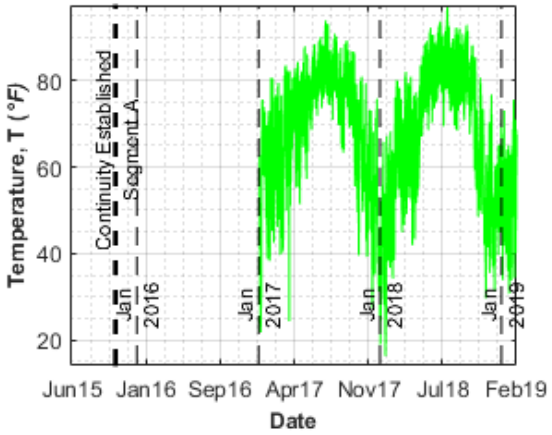

a) Temperature reading of the sensor

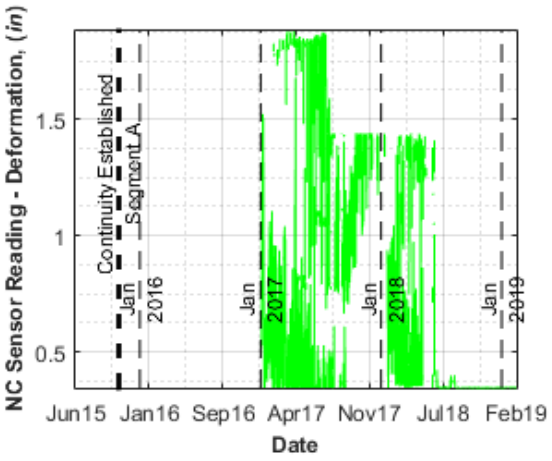

b) Sensor reading without temperature correction

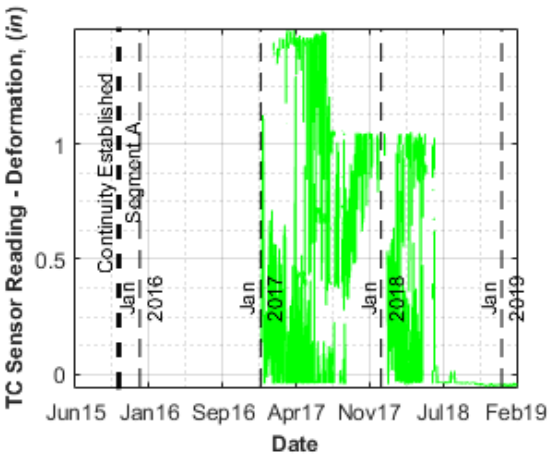

c) Sensor reading after temperature correction

Calculated Crack Width

Crack Width	Period: Full Range
Beginning: Pour Date	End: Feb 15 2019
Temperature	

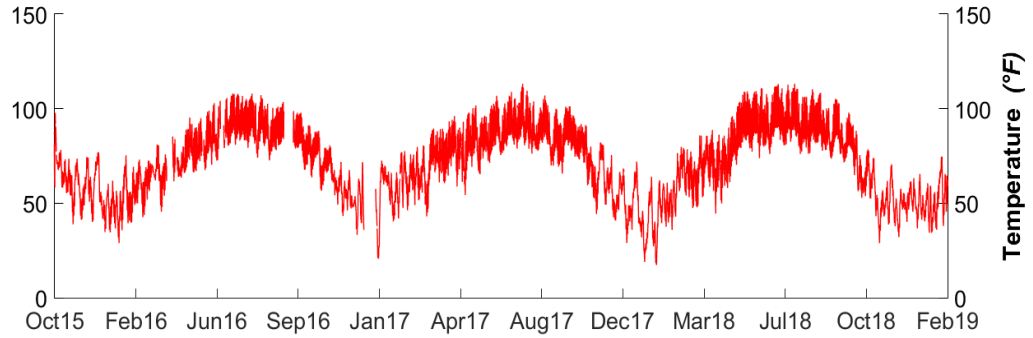

Girder 7	Baseline : 12 Hrs after pour date
Bent 2	Case: Expansion support (4 span)

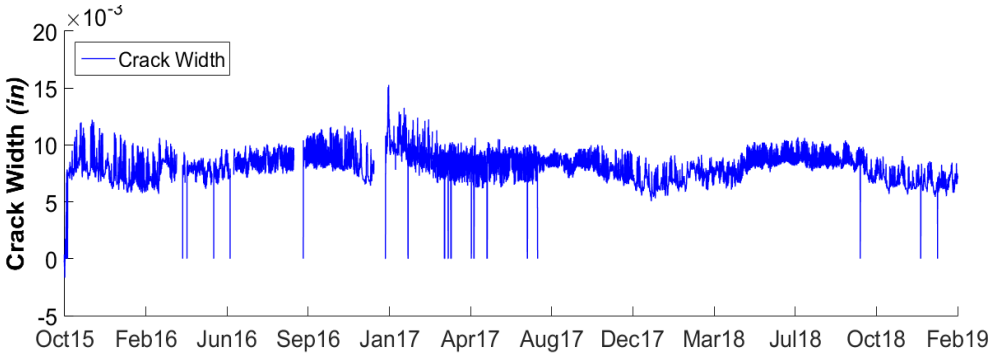

Bent 3	Case: Expansion support (4 span)

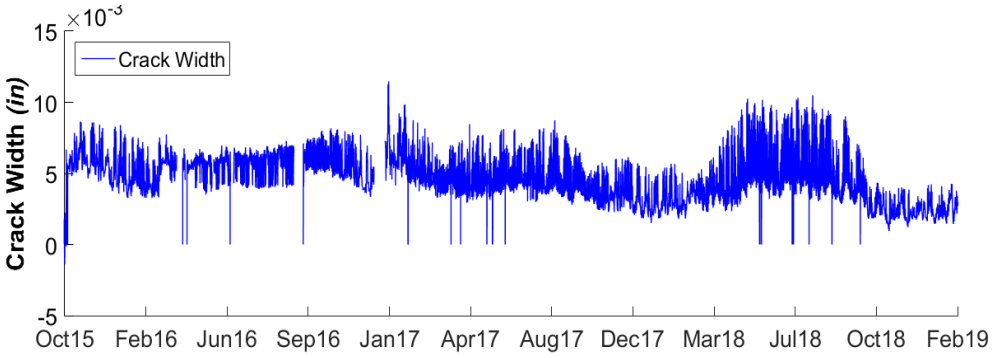

Crack Width	Period: Full Range
Bent 4	**Case: Expansion support (4 span)**

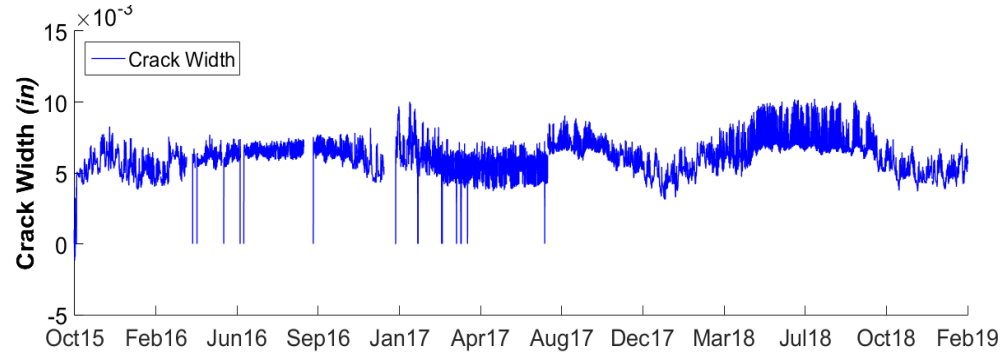

Bent 15	Case: Expansion support (2 span)

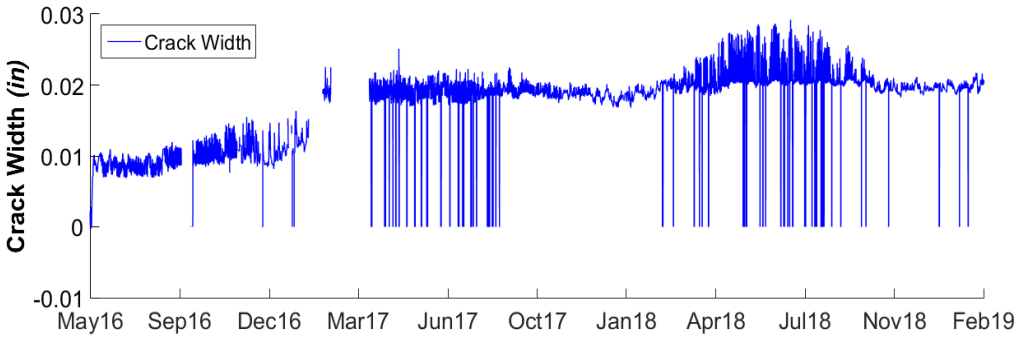

Bent 17	Case: Expansion support (2 span)

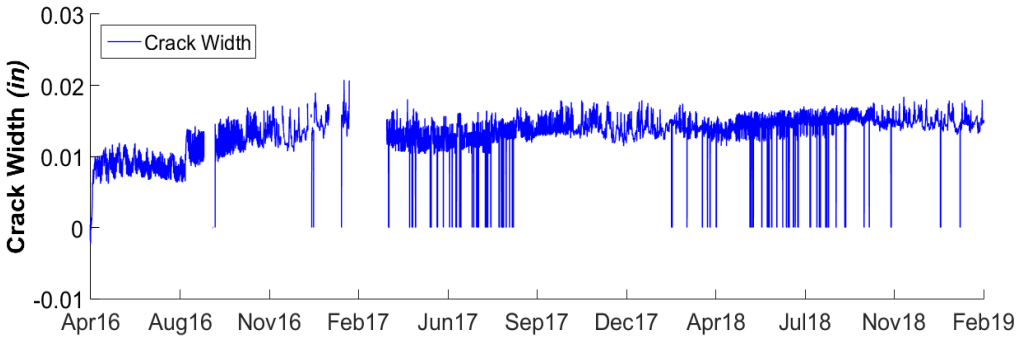

Bent 19	Case: Fixed support (2 span)

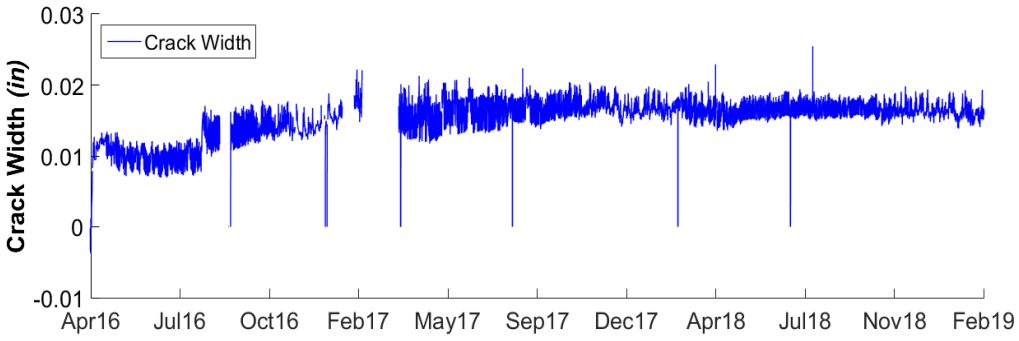

Girder 4	Baseline: 12 Hrs after pour date
Bent 2	**Case: Expansion support (4 span)**

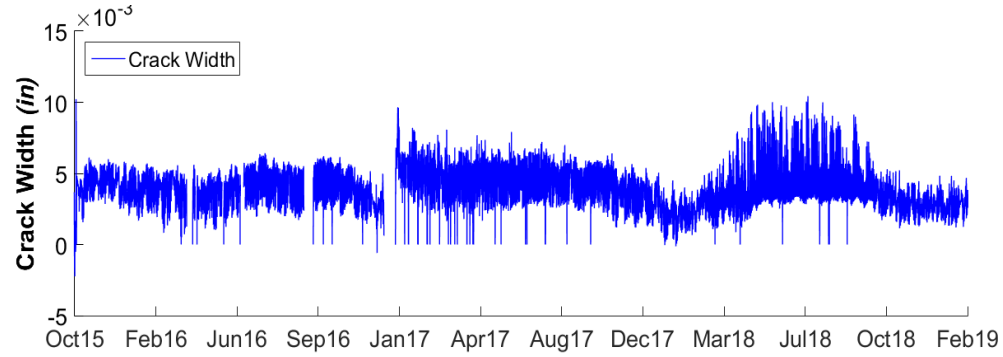

Bent 3	Case: Expansion support (4 span)

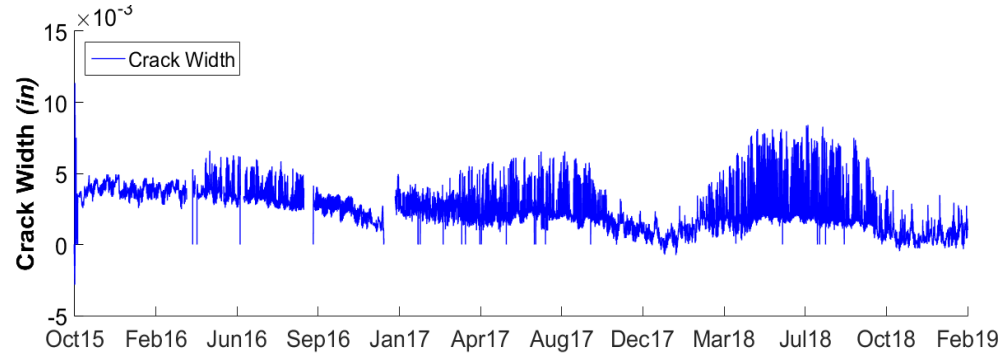

Bent 4	Case: Expansion support (4 span)

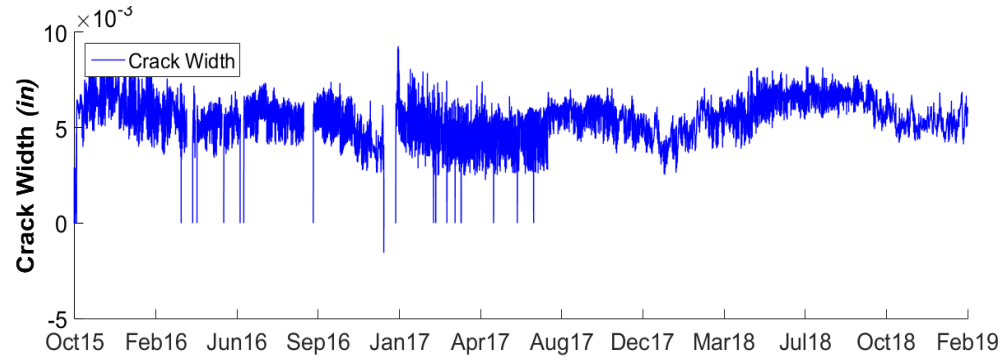

Bent 15	Case: Expansion support (2 span)

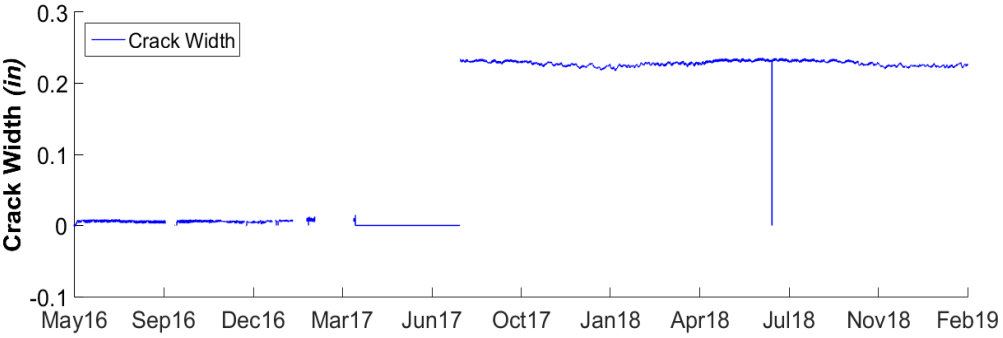

Girder 4	Baseline: 12 Hrs after pour date
Bent 17	**Case: Expansion support (2 span)**

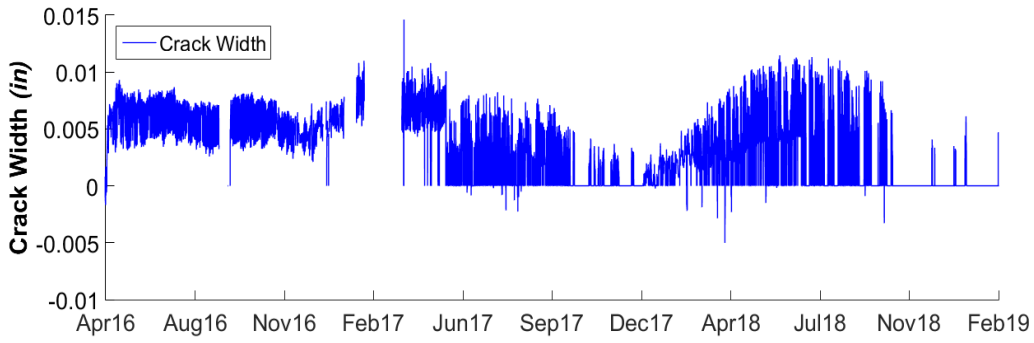

Bent 19	Case: Fixed support (2 span)

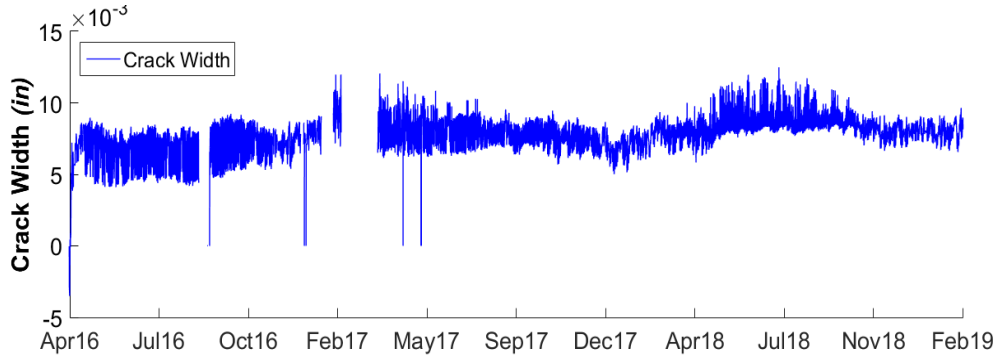

Crack width	**Period: 30 days**
Beginning: Jan 1 2018 0:00	**End: Jan 31 2018 0:00**
Girder 7	**Baseline : 12 hours after pouring**
Bent 2	**Case: Expansion support (4 span)**

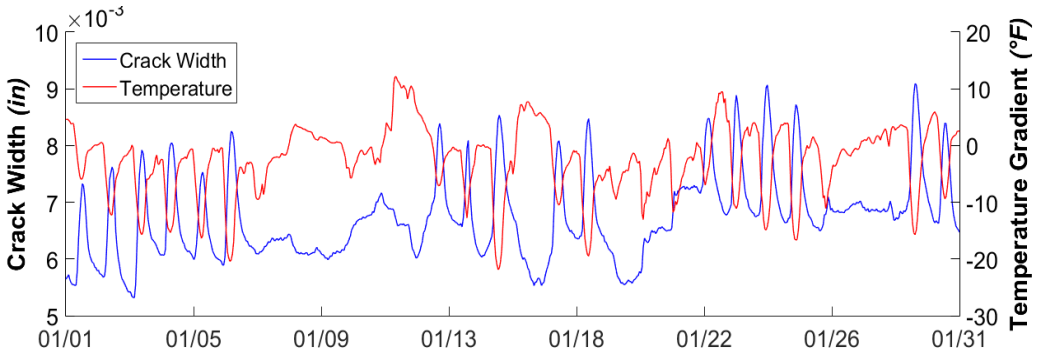

Bent 3	**Case: Expansion support (4 span)**

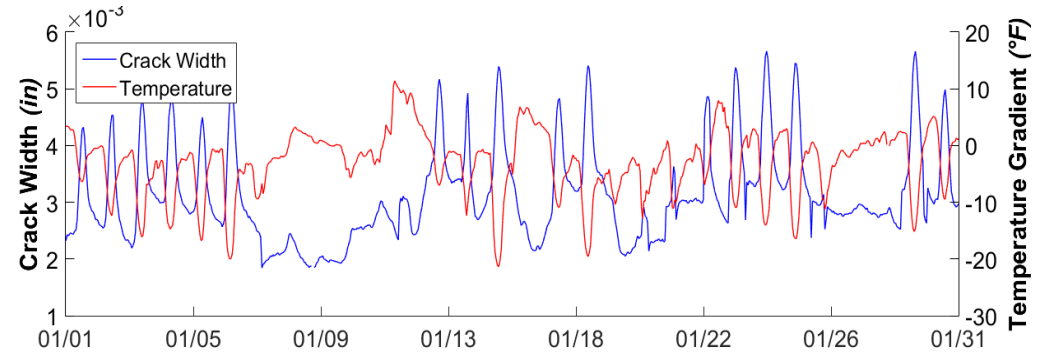

Bent 4	**Case: Expansion support (4 span)**

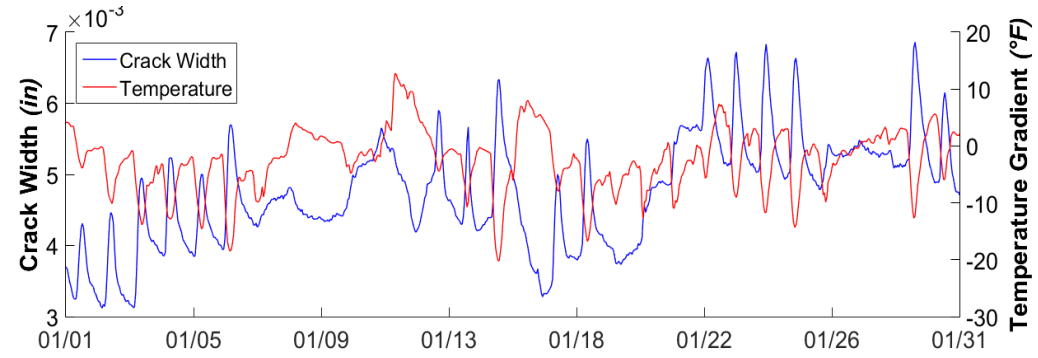

Crack width	Period: 30 days
Bent 15	**Case: Expansion support (2 span)**

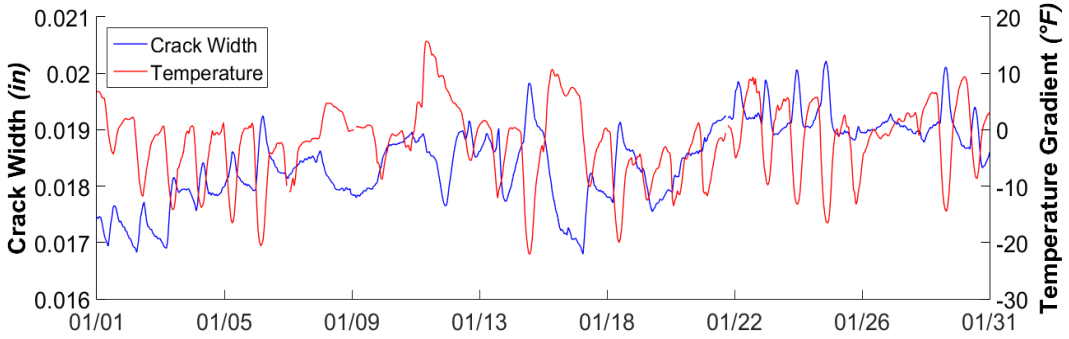

Bent 17	Case: Expansion support (2 span)

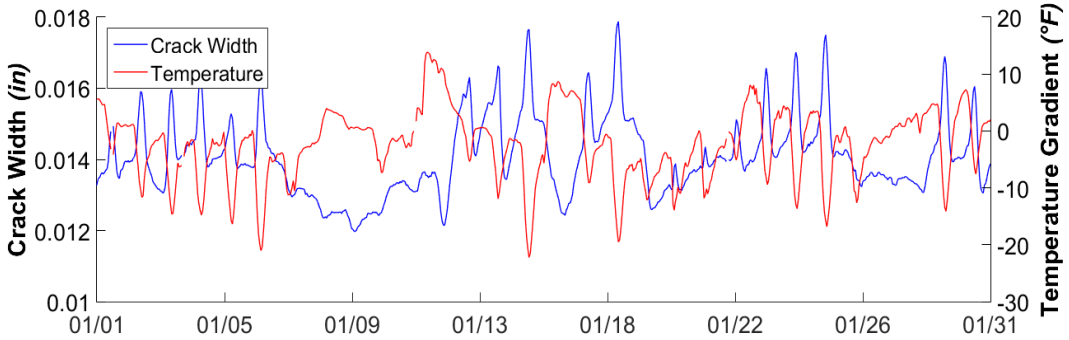

Bent 19	Case: Fixed support (2 span)

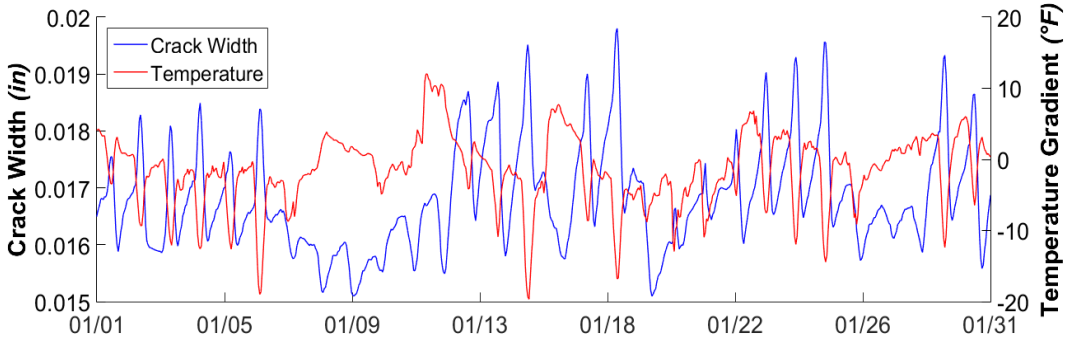

Girder 4	Baseline: Jan 2 2018 00:00
Bent 2	**Case: Expansion support (4 span)**

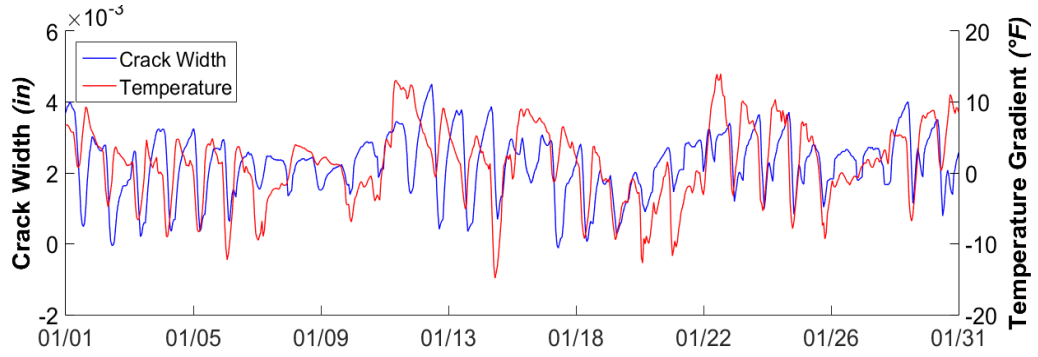

Bent 3	Case: Expansion support (4 span)

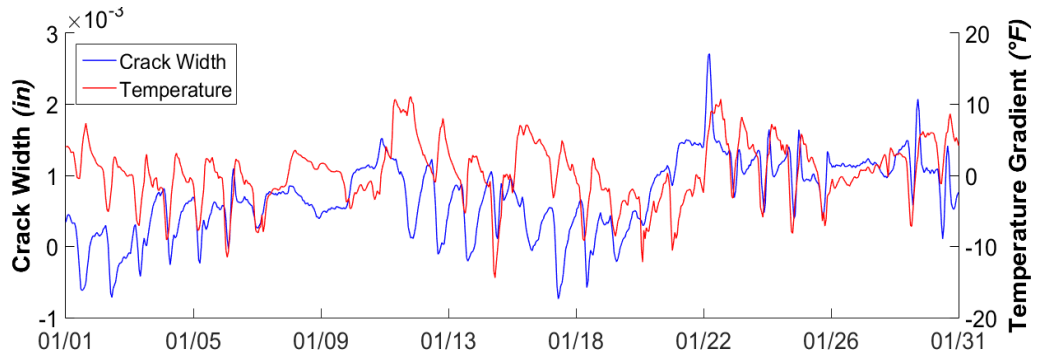

Bent 4	Case: Expansion support (4 span)

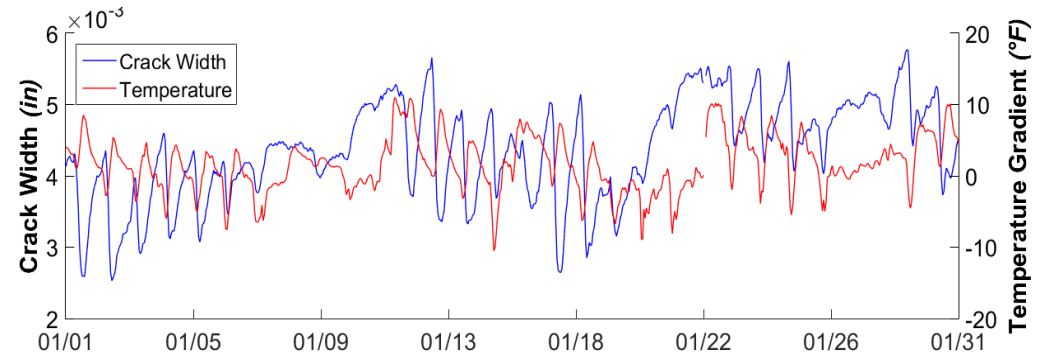

Bent 15	Case: Expansion support (2 span)

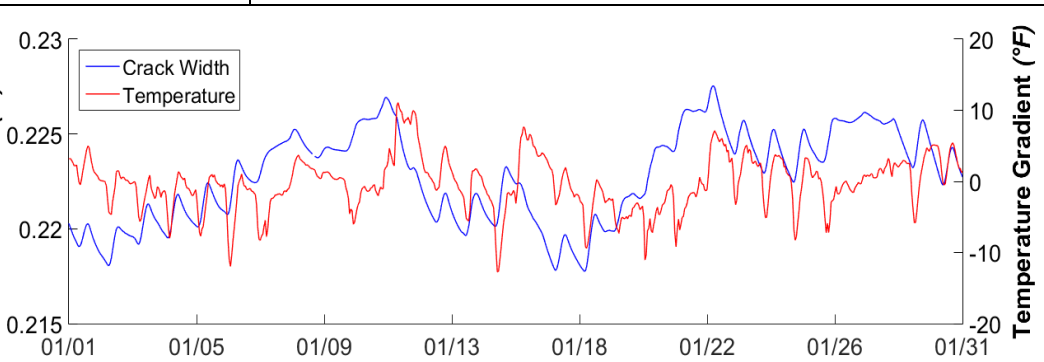

Girder 4	Baseline: Jan 2 2018 00:00
Bent 17	**Case: Expansion support (2 span)**

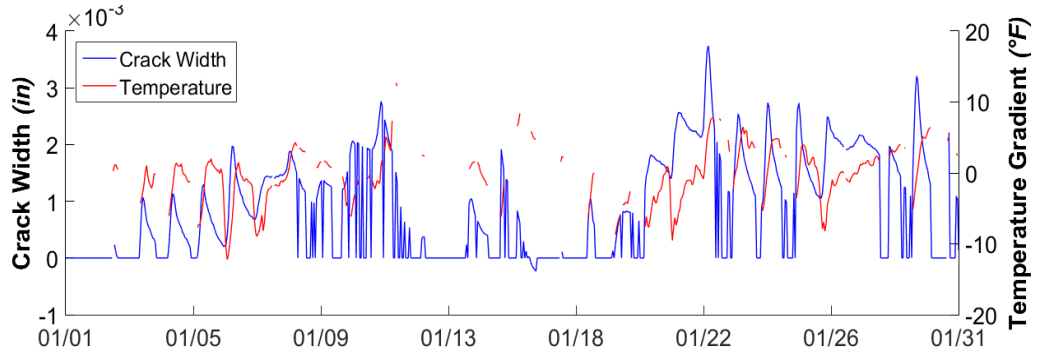

Bent 19	Case: Fixed support (2 span)

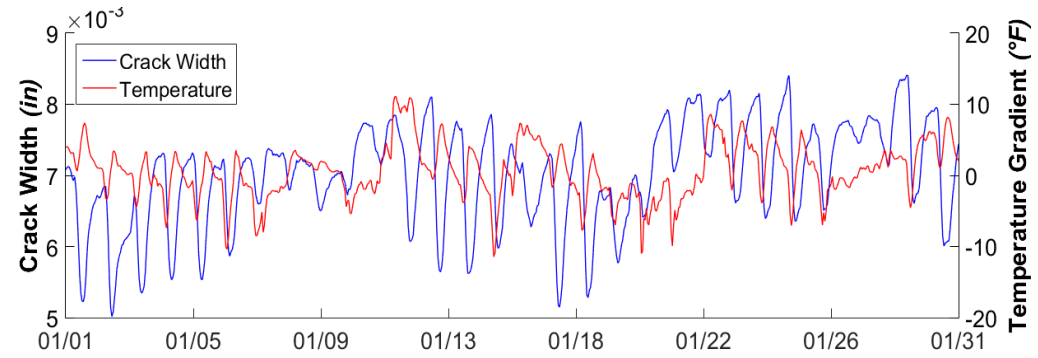

Crack width	Period: 24 hrs
Beginning: Aug 1 2018 0:00	End: Aug 31 2018 0:00
Girder 7	Baseline : Aug 1 2018 9:00
Bent 2	Case: Expansion support (4 span)

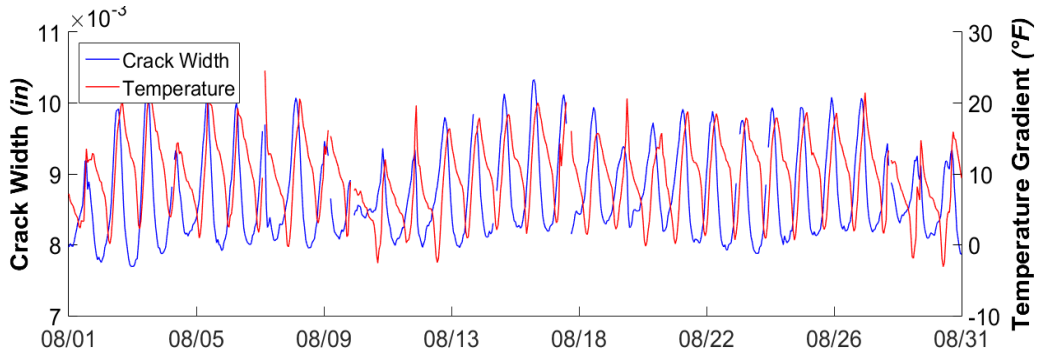

Bent 3	Case: Expansion support (4 span)

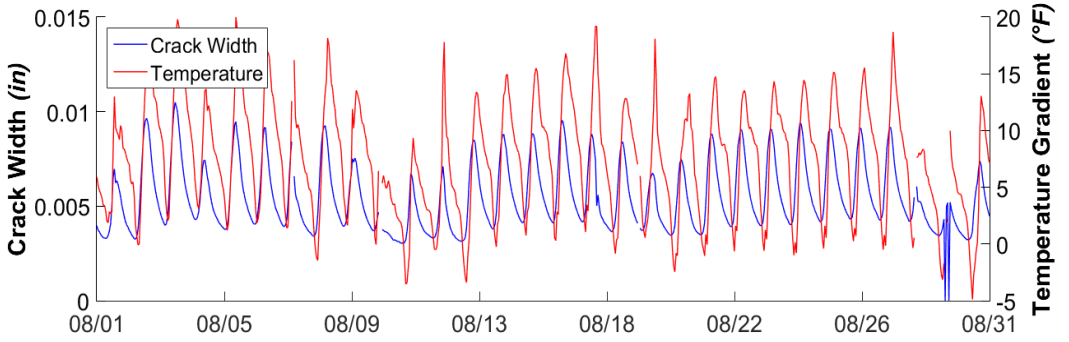

Bent 4	Case: Expansion support (4 span)

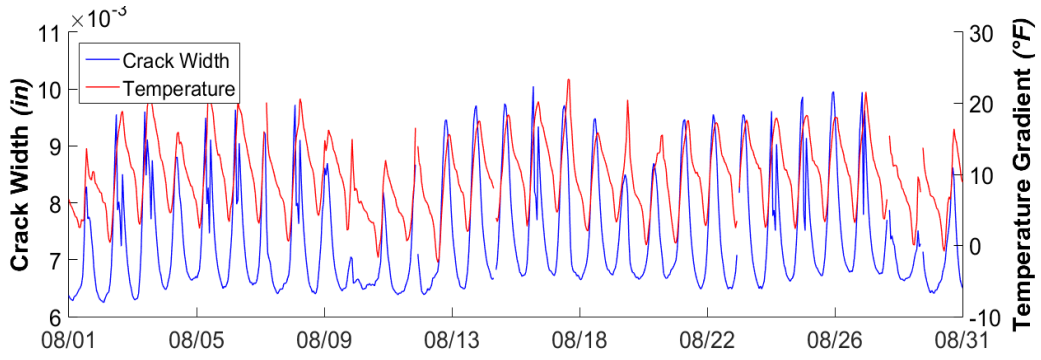

Crack width	Period: 24 hrs
Bent 15	**Case: Expansion support (2 span)**

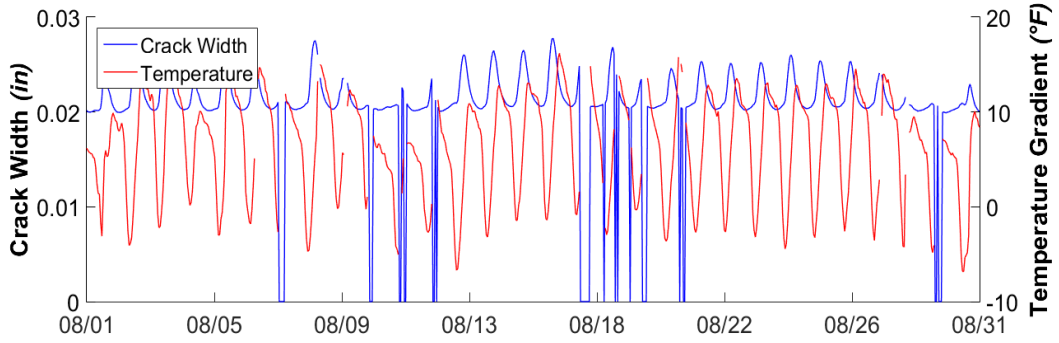

Bent 17	Case: Expansion support (2 span)

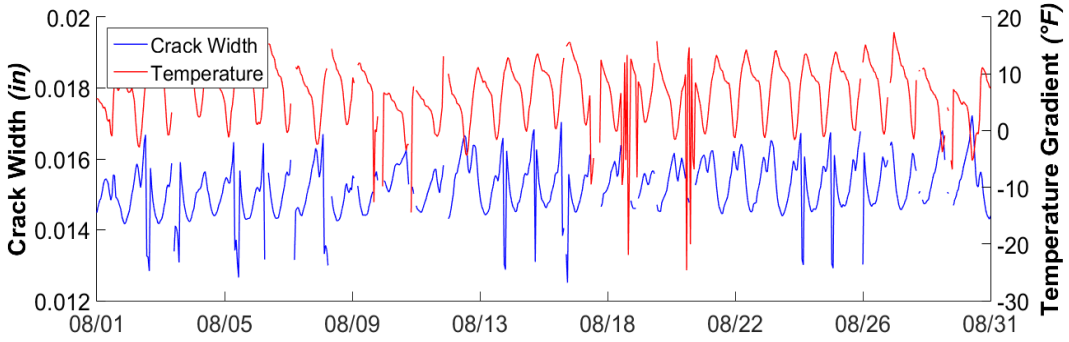

Bent 19	Case: Fixed support (2 span)

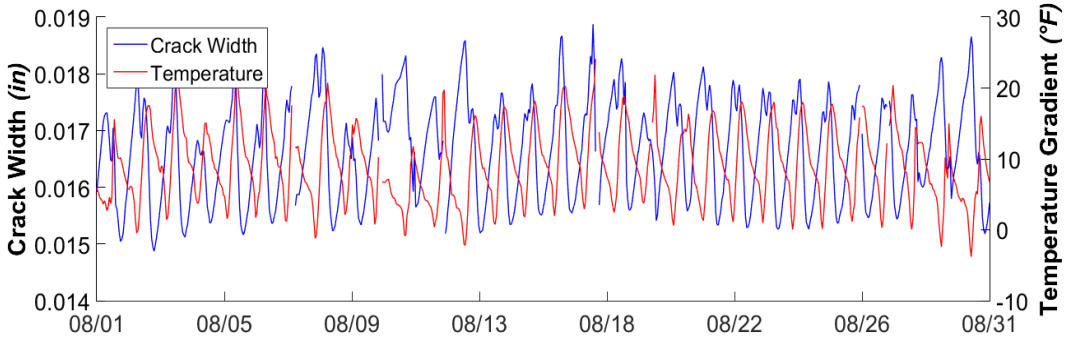

Girder 4	Baseline: Aug 1 2018 9:00
Bent 2	**Case: Expansion support (4 span)**

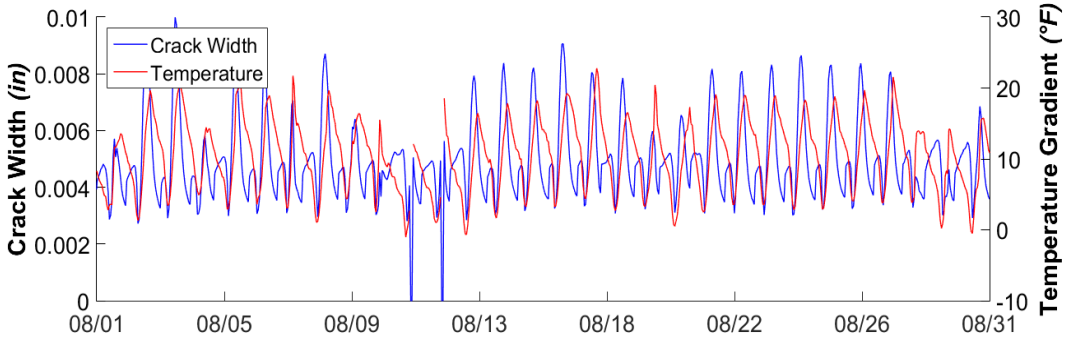

Bent 3	Case: Expansion support (4 span)

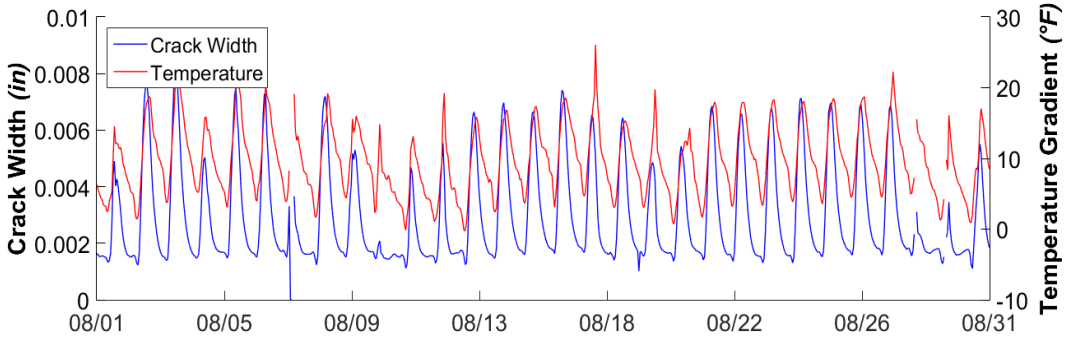

Bent 4	Case: Expansion support (4 span)

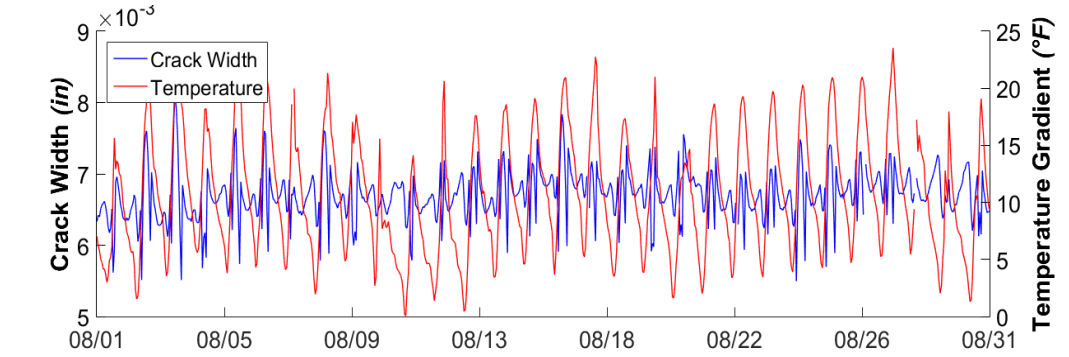

Bent 15	Case: Expansion support (2 span)

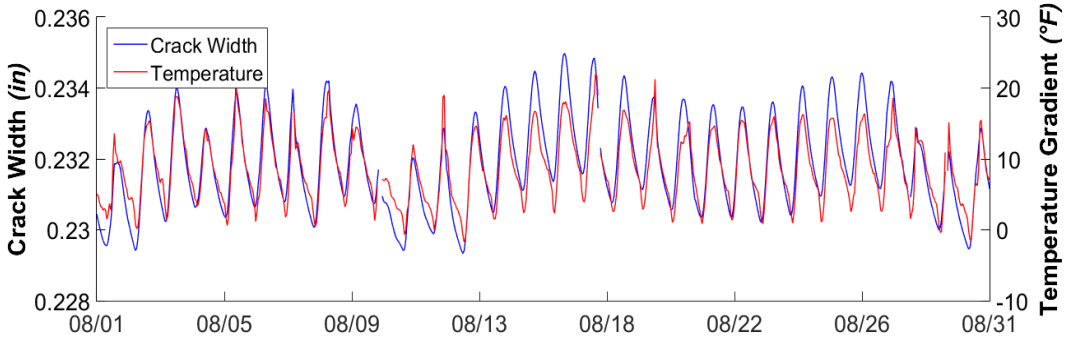

Girder 4	Baseline: Aug 1 2018 9:00
Bent 17	**Case: Expansion support (2 span)**

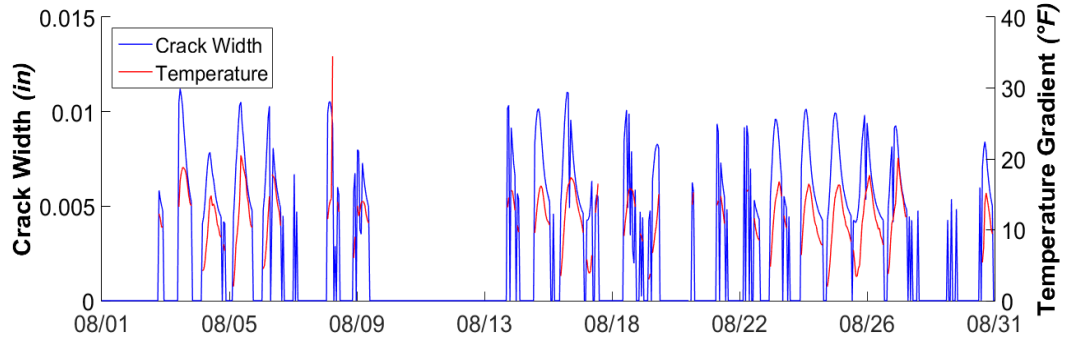

Bent 19	Case: Fixed support (2 span)

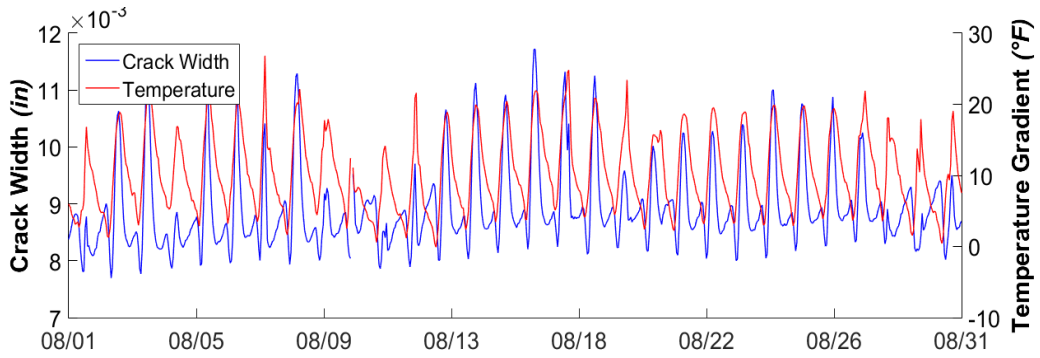

Crack width	Period: 24 hrs
Beginning: Jan 1 2018 0:00	End: Jan 2 2018 0:00
Girder 7	Baseline : 12 hours after pouring
Bent 2	Case: Expansion support (4 span)

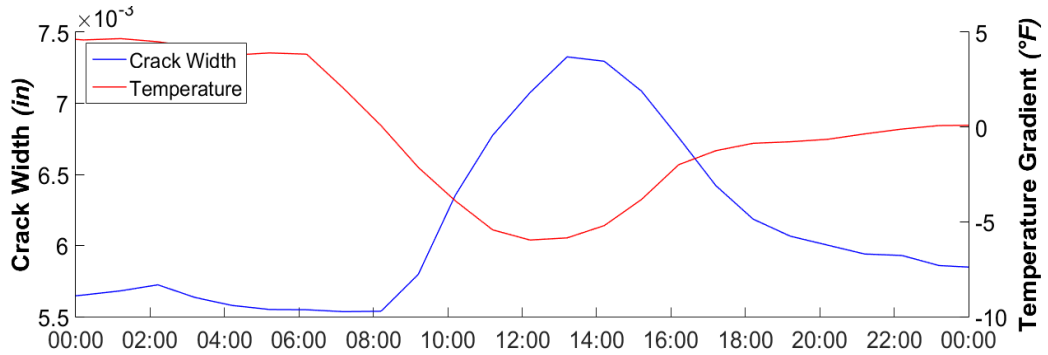

Bent 3	Case: Expansion support (4 span)

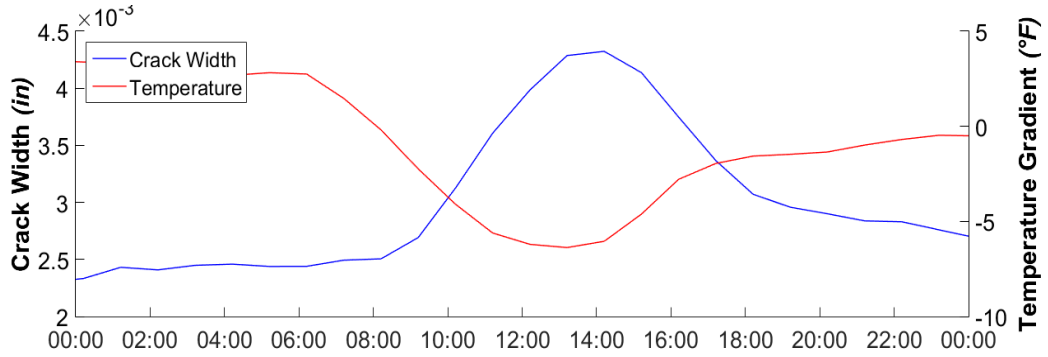

Bent 4	Case: Expansion support (4 span)

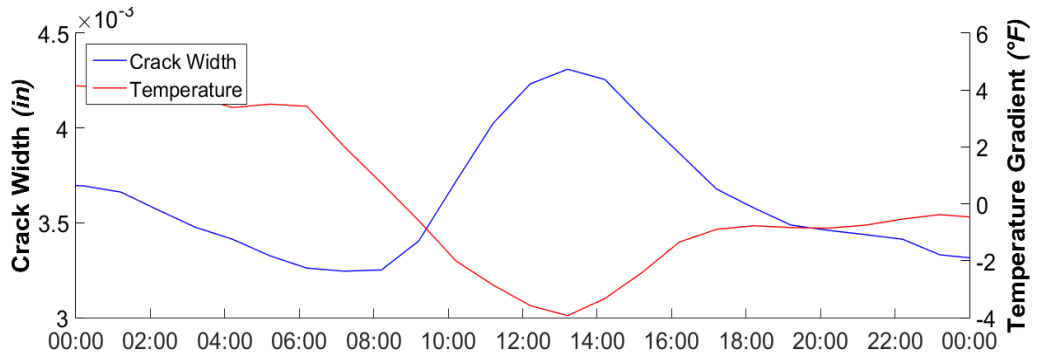

Crack width	Period: 24 hrs
Bent 15	**Case: Expansion support (2 span)**

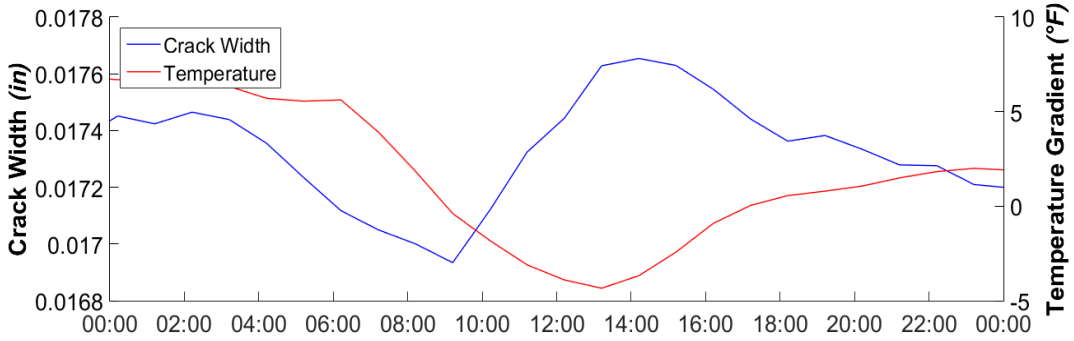

Bent 17	Case: Expansion support (2 span)

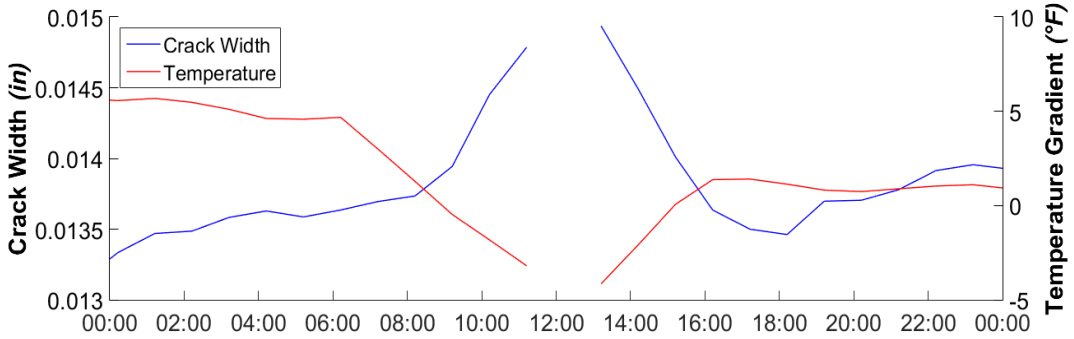

Bent 19	Case: Fixed support (2 span)

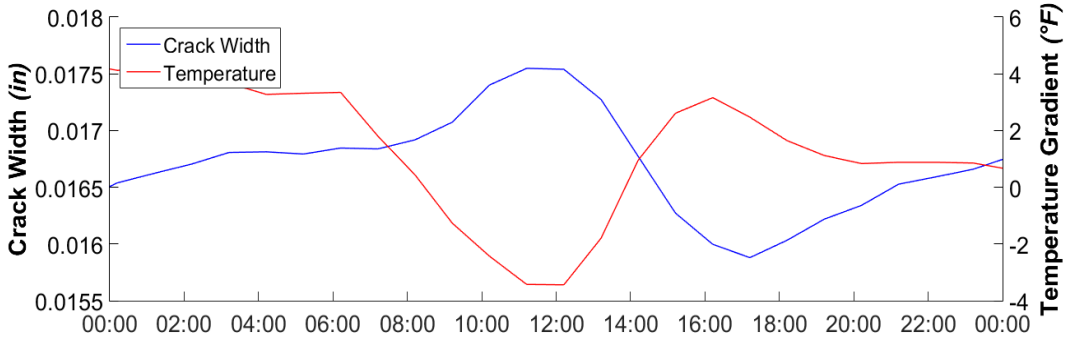

Girder 4	Baseline: 12 hours after pouring
Bent 2	**Case: Expansion support (4 span)**

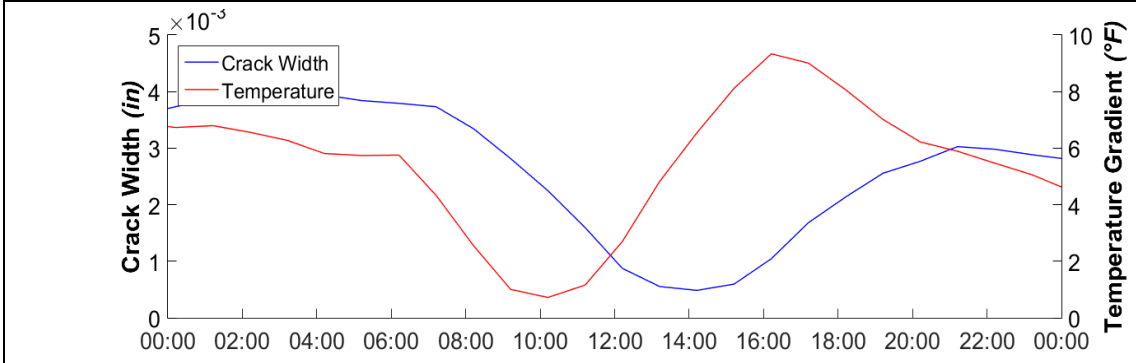

Bent 3	Case: Expansion support (4 span)

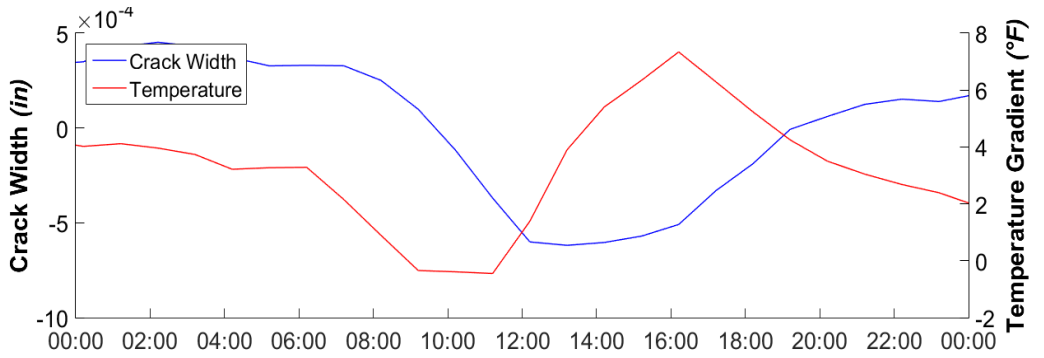

Bent 4	Case: Expansion support (4 span)

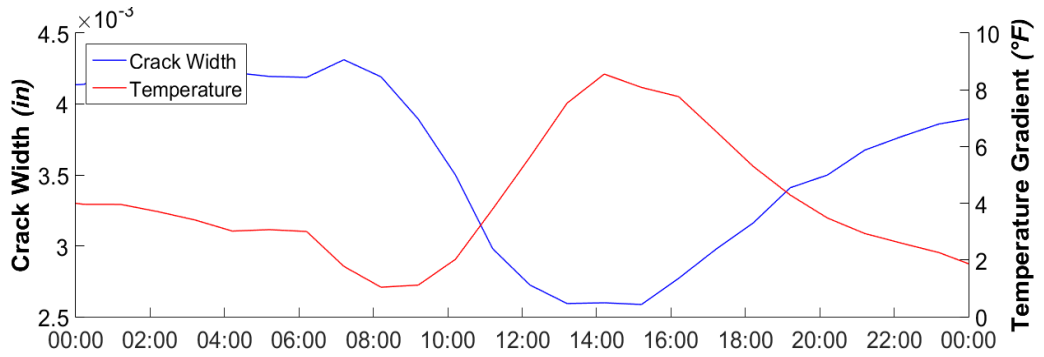

Bent 15	Case: Expansion support (2 span)

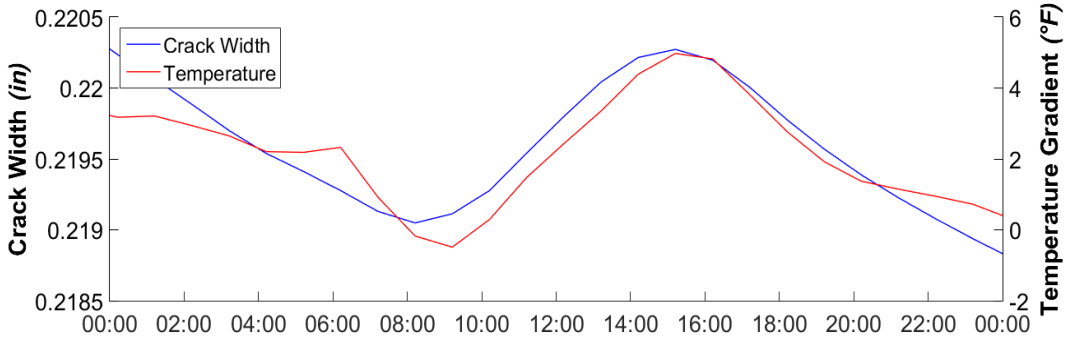

Girder 4	Baseline: 12 hours after pouring
Bent 17	**Case: Expansion support (2 span)**

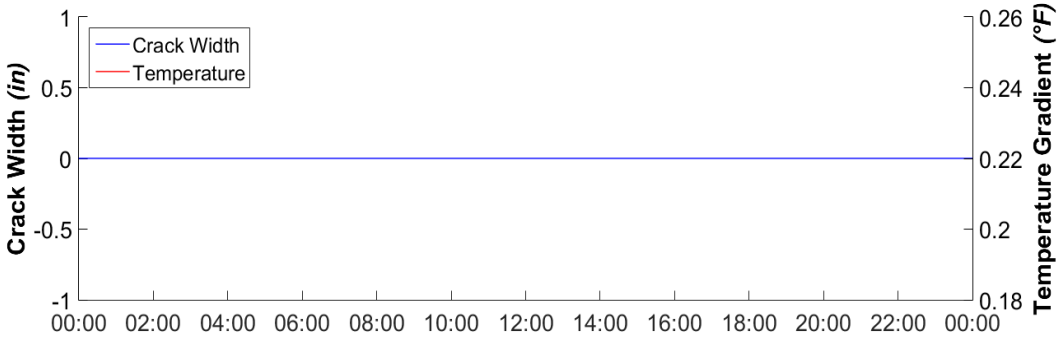

Bent 19	Case: Fixed support (2 span)

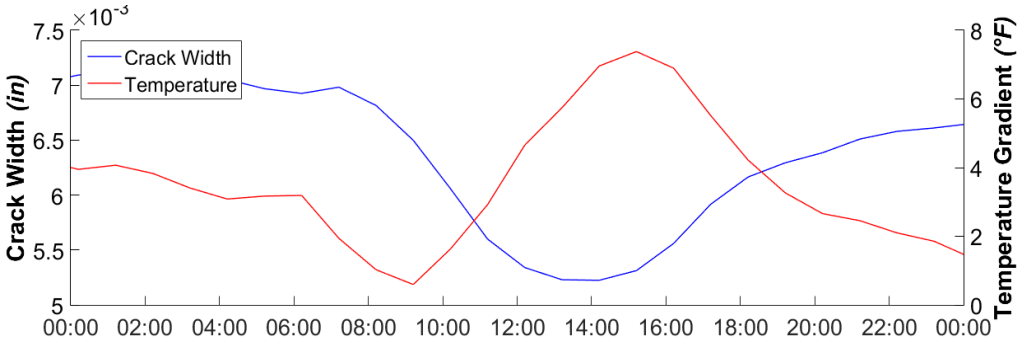

Crack width	**Period: 24 hrs**
Beginning: Aug 1 2018 0:00	**End: Aug 2 2018 0:00**
Girder 7	**Baseline : 12 hours after pouring**
Bent 2	**Case: Expansion support (4 span)**

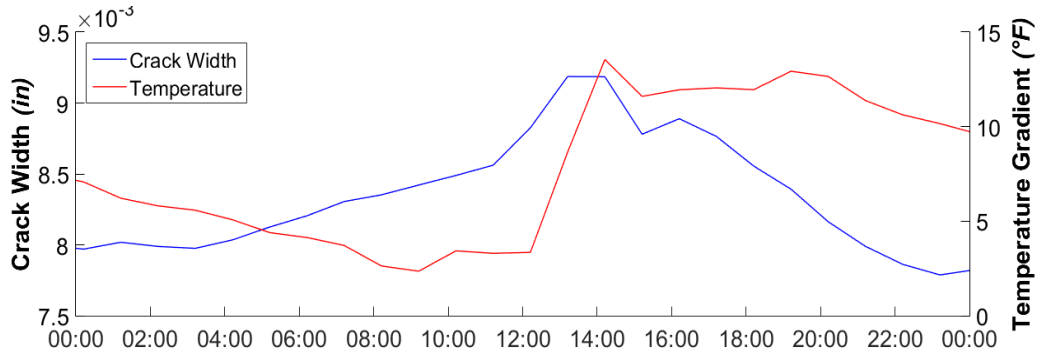

Bent 3	**Case: Expansion support (4 span)**

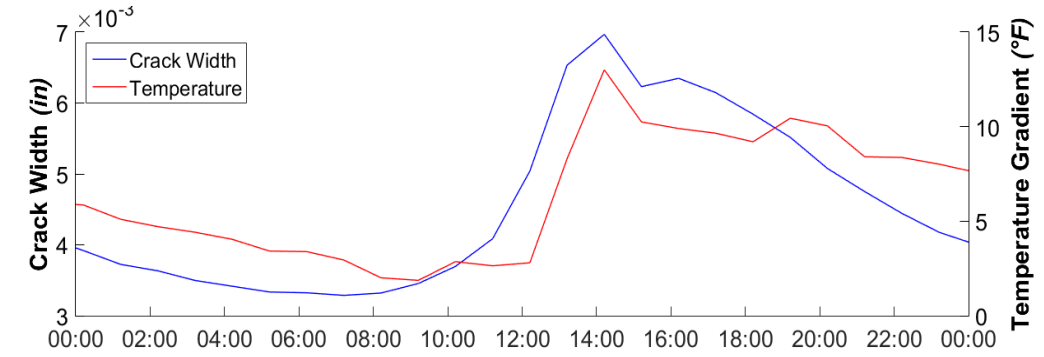

Bent 4	**Case: Expansion support (4 span)**

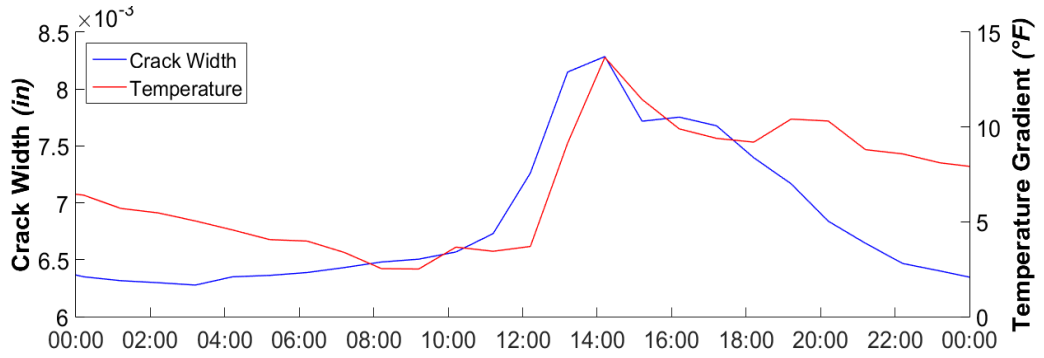

Crack width	Period: 24 hrs
Bent 15	**Case: Expansion support (2 span)**

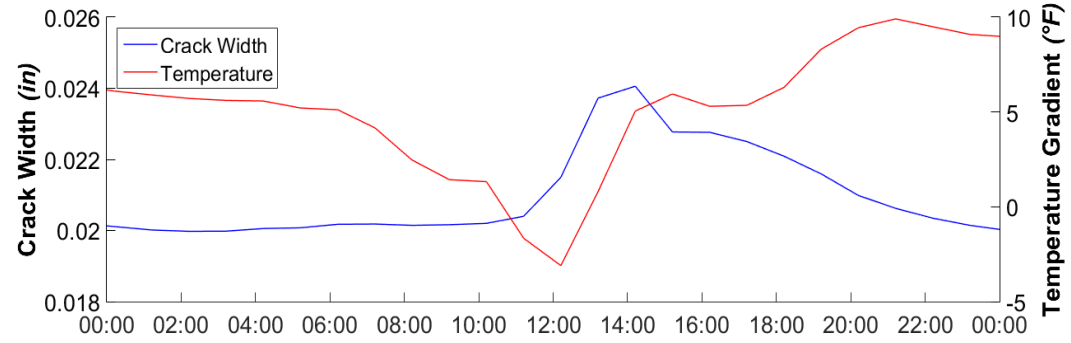

Bent 17	Case: Expansion support (2 span)

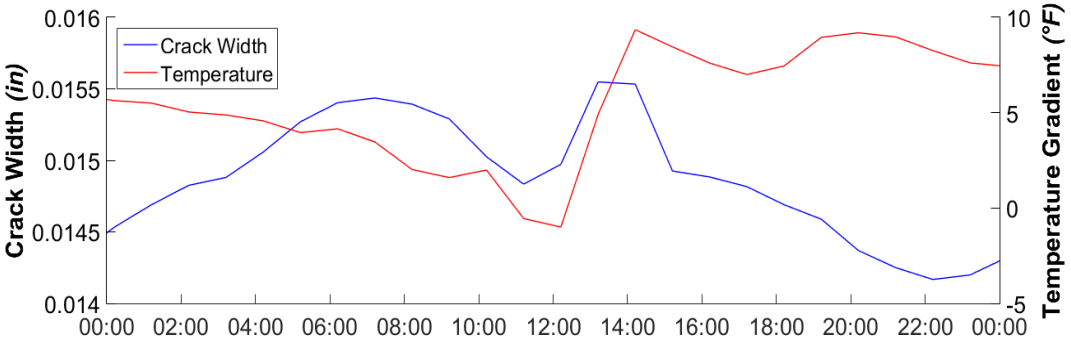

Bent 19	Case: Fixed support (2 span)

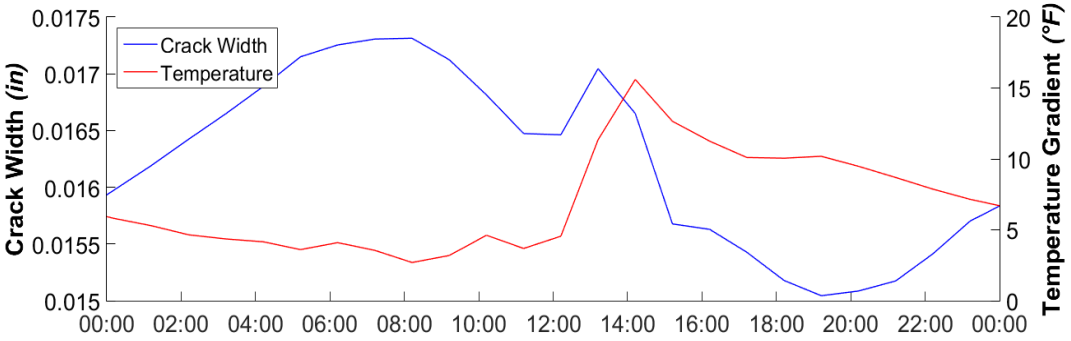

Girder 4	Baseline: 12 hours after pouring
Bent 2	**Case: Expansion support (4 span)**

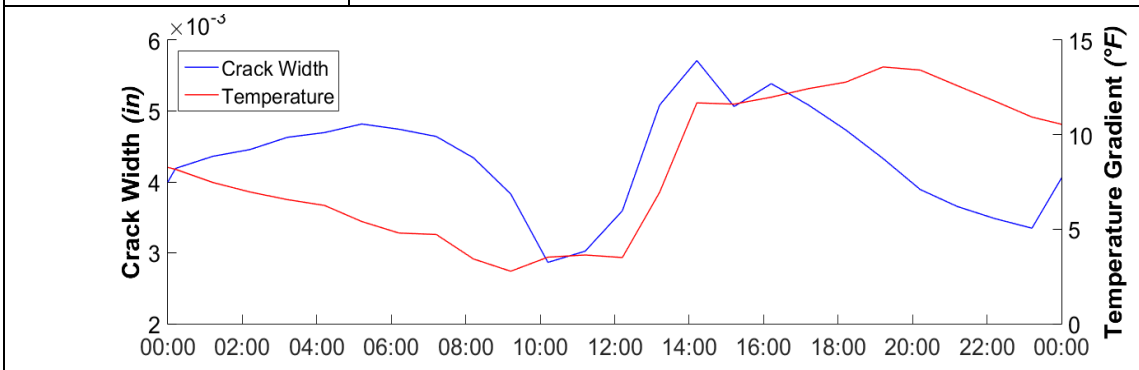

Bent 3	Case: Expansion support (4 span)

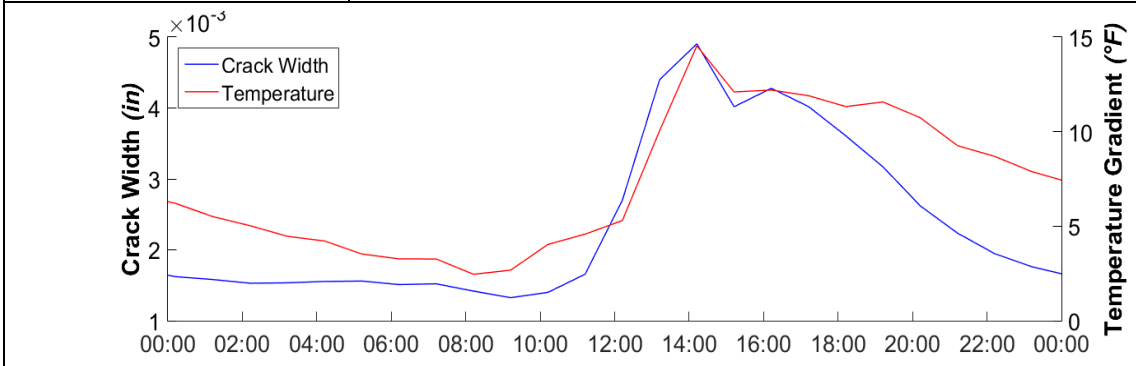

Bent 4	Case: Expansion support (4 span)

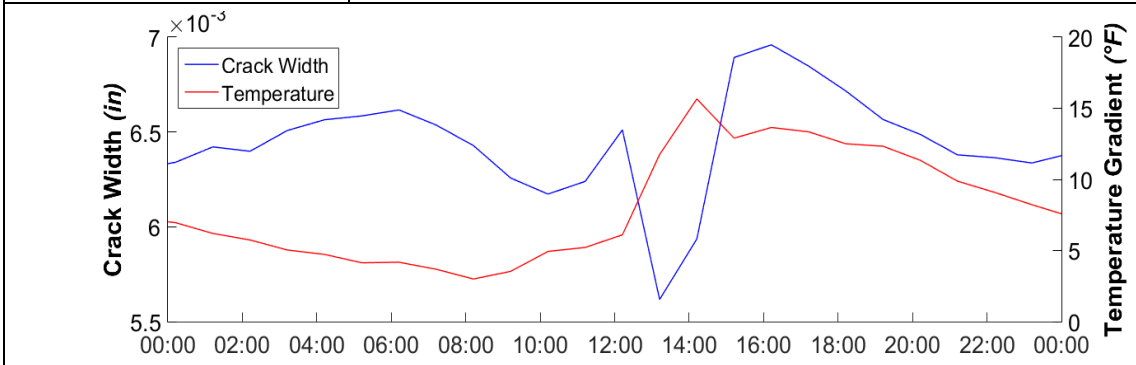

Bent 15	Case: Expansion support (2 span)

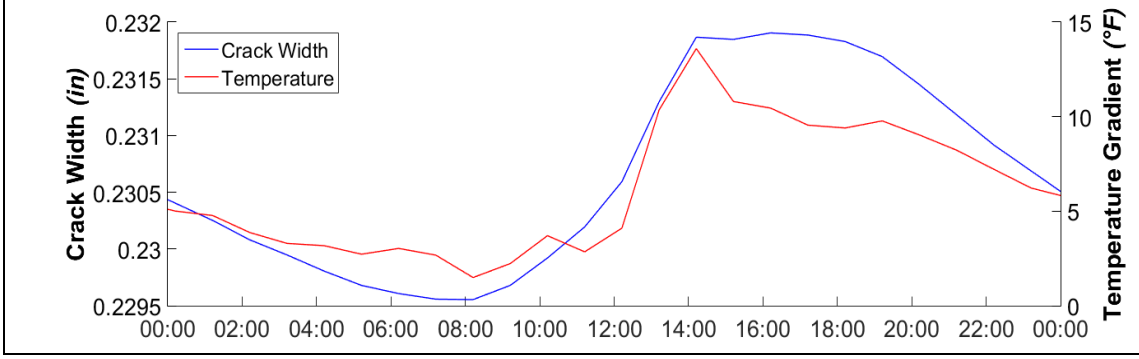

Girder 4	Baseline: 12 hours after pouring
Bent 17	**Case: Expansion support (2 span)**

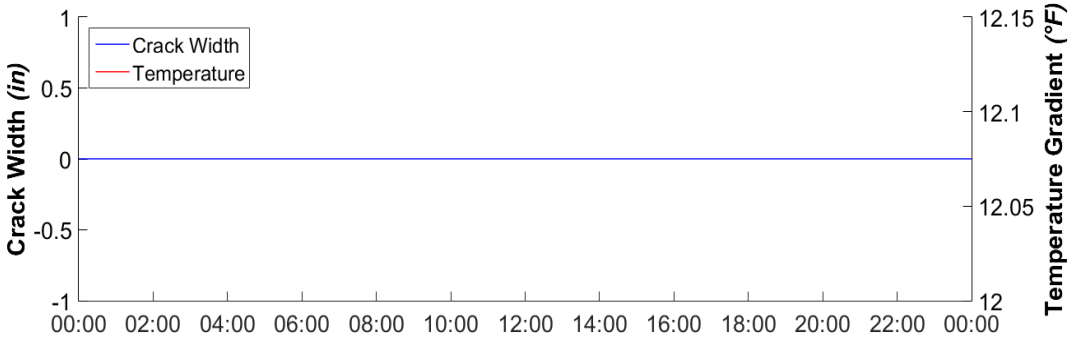

Bent 19	Case: Fixed support (2 span)

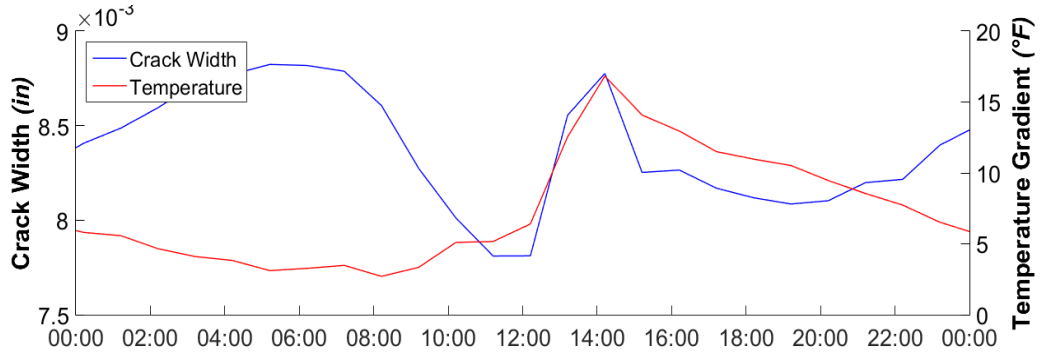

Girder End Displacement

Girder End Displacement	Period: Full Range
Beginning: sensor installation	End: Feb 15 2019
Girder 7	Baseline : Aug 1 2018 9:00
Segment A	Case: 4-span segment

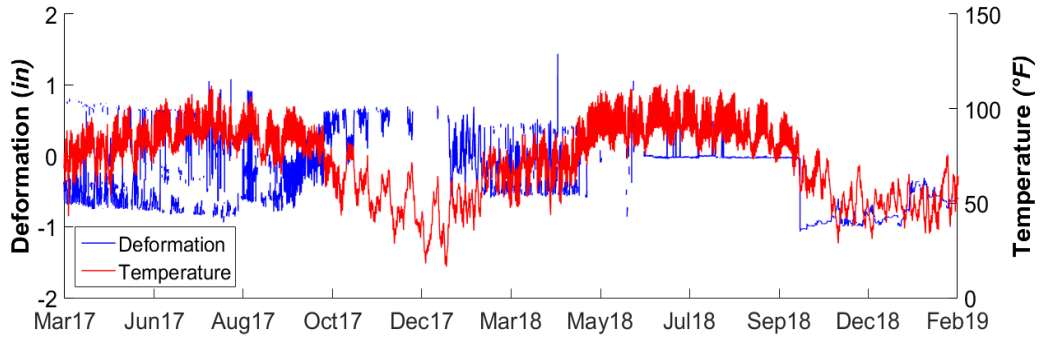

Segment B	Case: 2-span segment

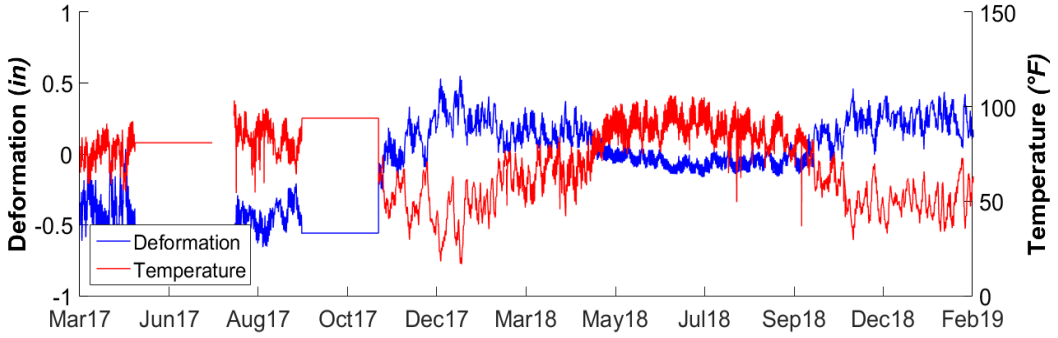

Span 19	Case: Fixed support (2 span)
Span 16	Case: Expansion support (2 span)

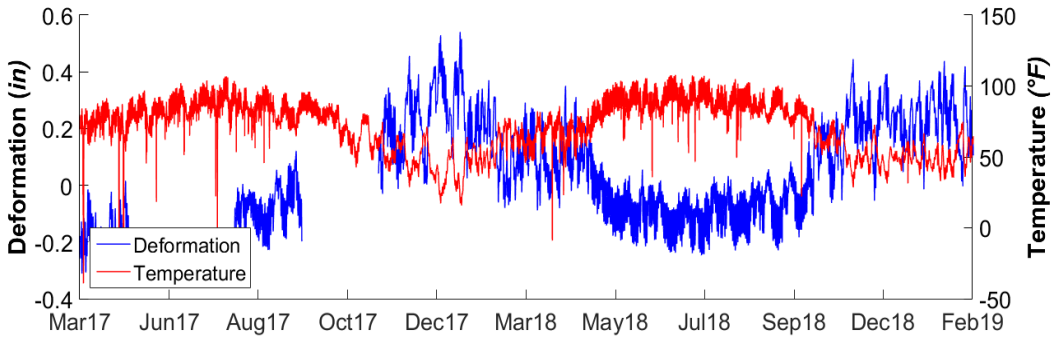

Girder End Displacement	Period: Full Range
Span 1	**Case: Expansion support (4 span)**

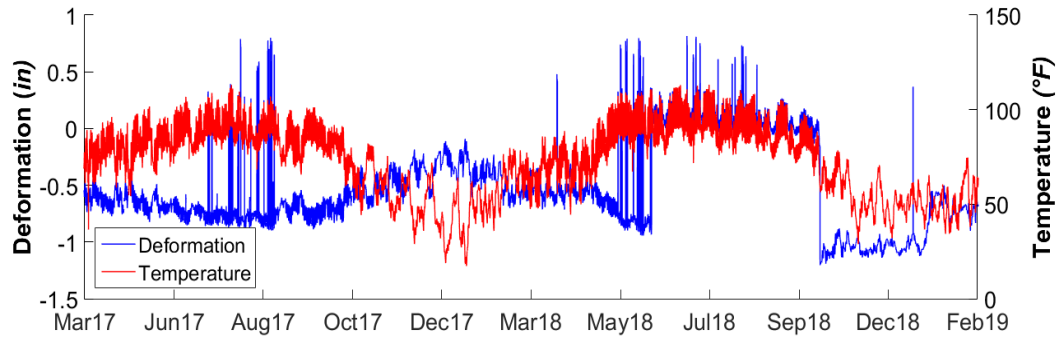

Span 2	Case: Expansion support (4 span)

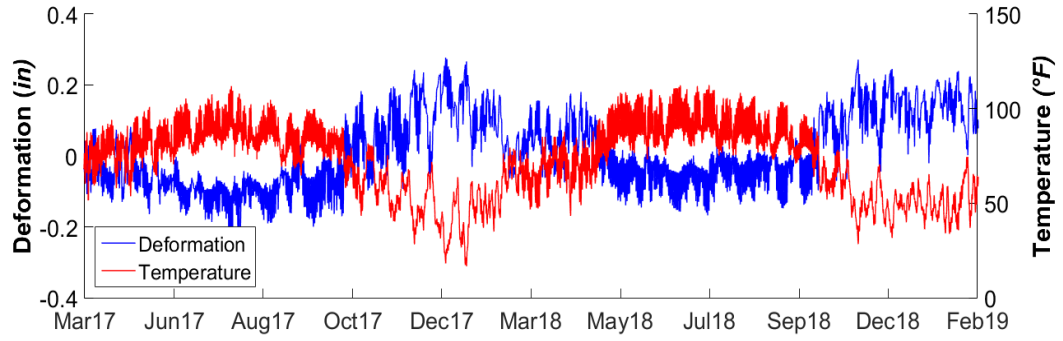

Span 3	Case: Expansion support (4 span)

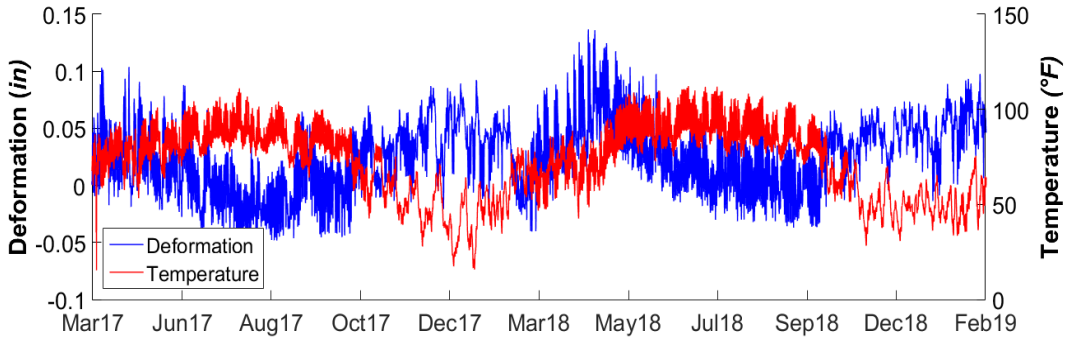

Span 4	Case: Expansion support (4 span)

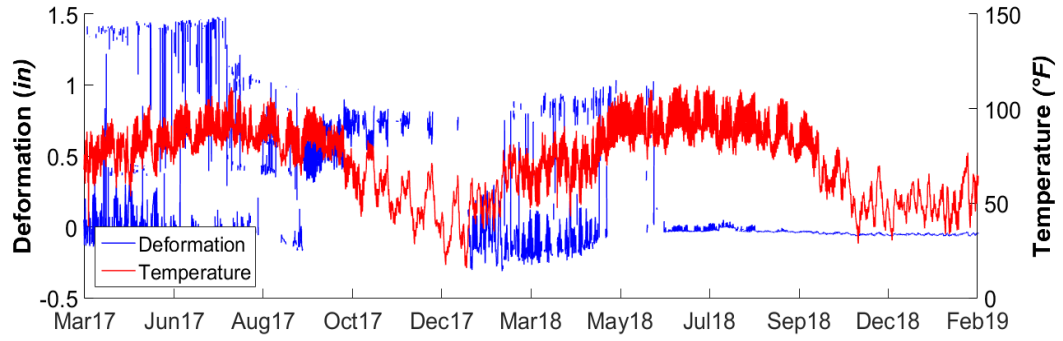

Girder 4	Baseline: Aug 1 2018 9:00
Segment A	**Case: 4-span segment**

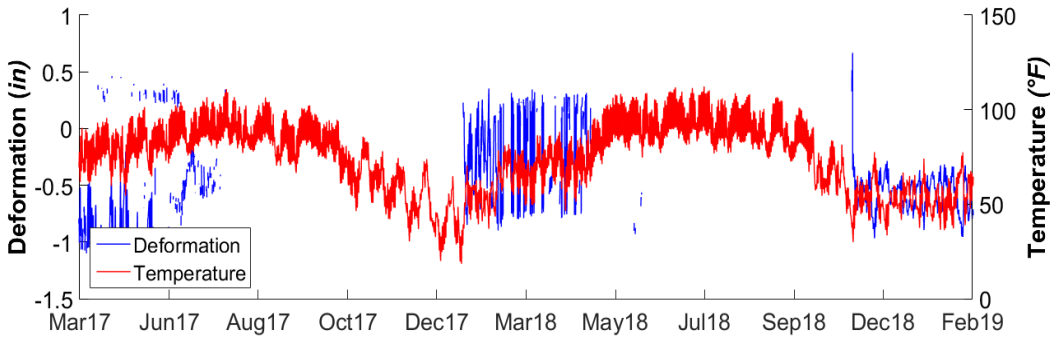

Segment B	Case: 2-span segment

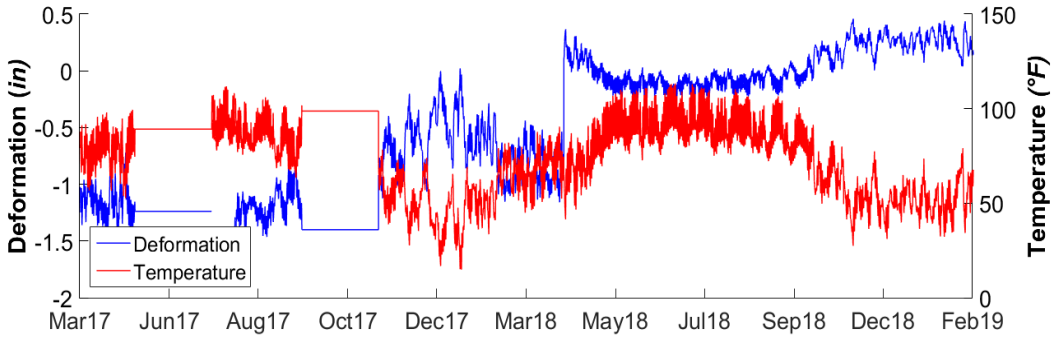

Span 19	Case: Fixed support (2 span)

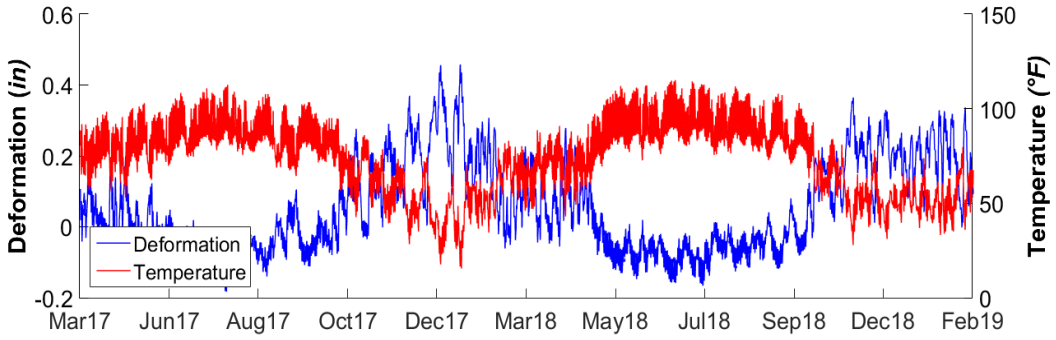

Span 16	Case: Expansion support (2 span)

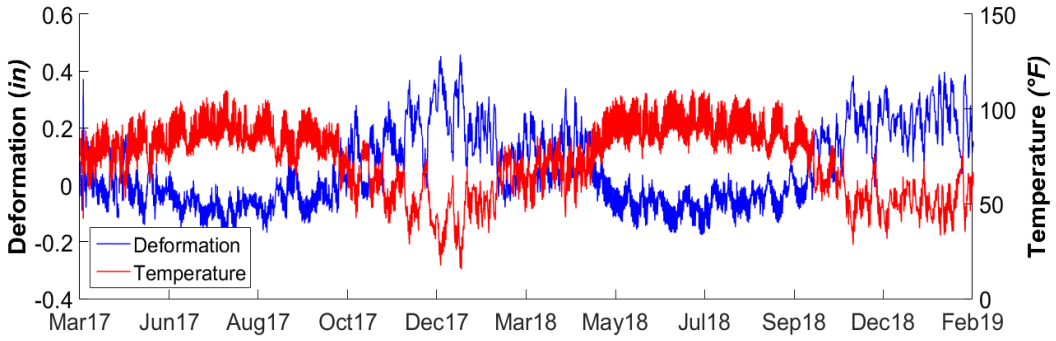

Girder 4	Baseline: Aug 1 2018 9:00
Span 1	**Case: Expansion support (4 span)**

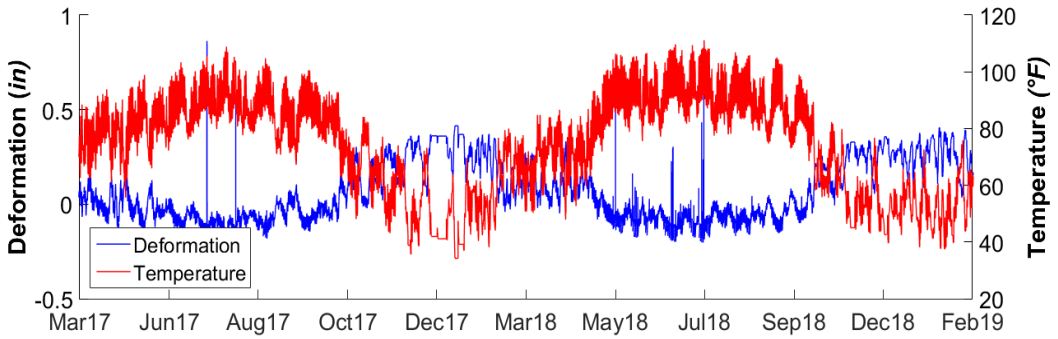

Span 2	Case: Expansion support (4 span)

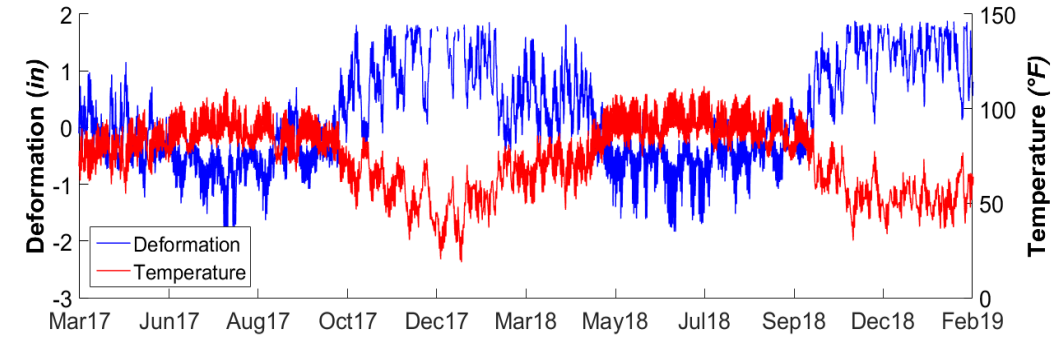

Span 3	Case: Expansion support (4 span)

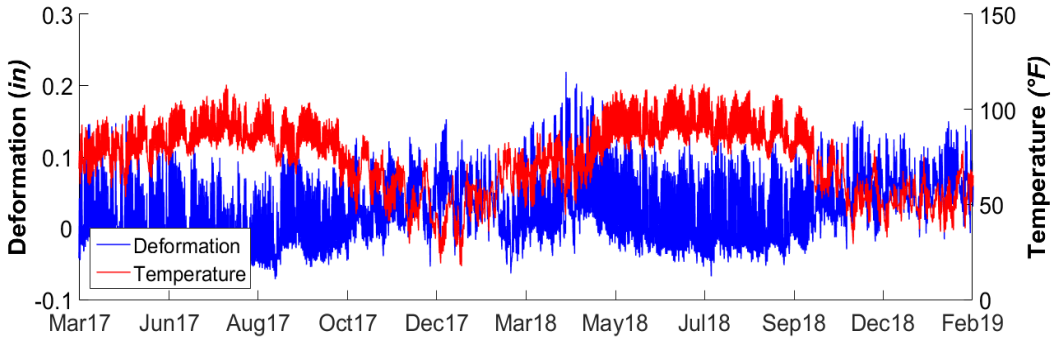

Span 4	Case: Expansion support (4 span)

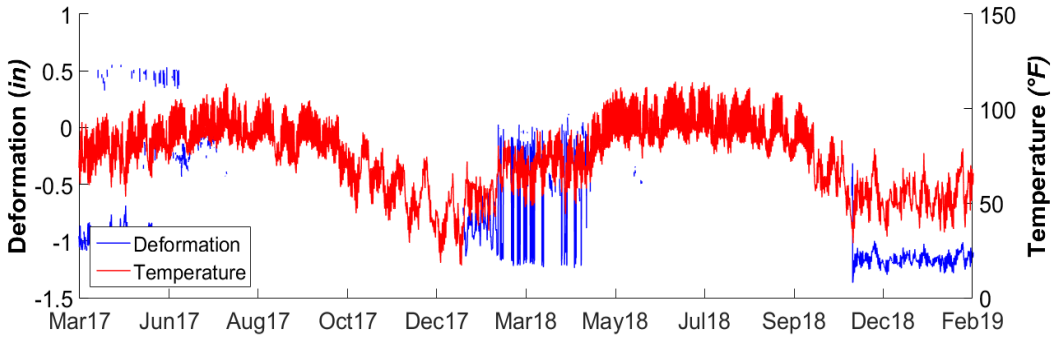

Girder End Displacement	Period: 24 hrs.
Beginning: Jun 19 2017 0:00	End: Jun 20 2017 0:00
Girder 7	Baseline : Jun 19 2017 9:00
Segment A	Case: 4-span segment

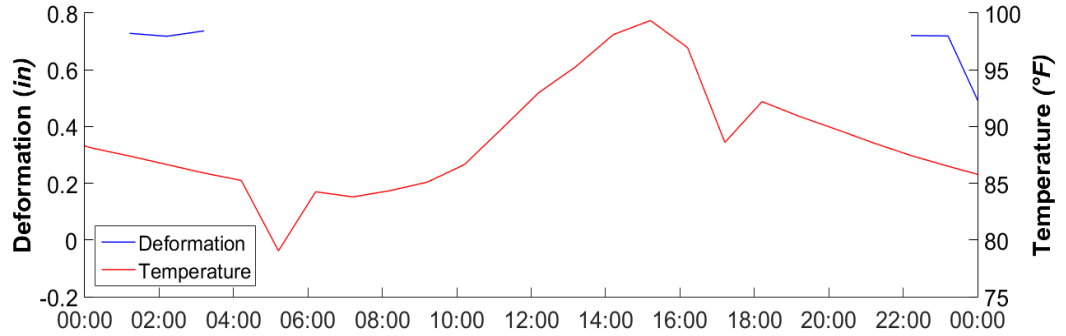

Segment B	Case: 2-span segment

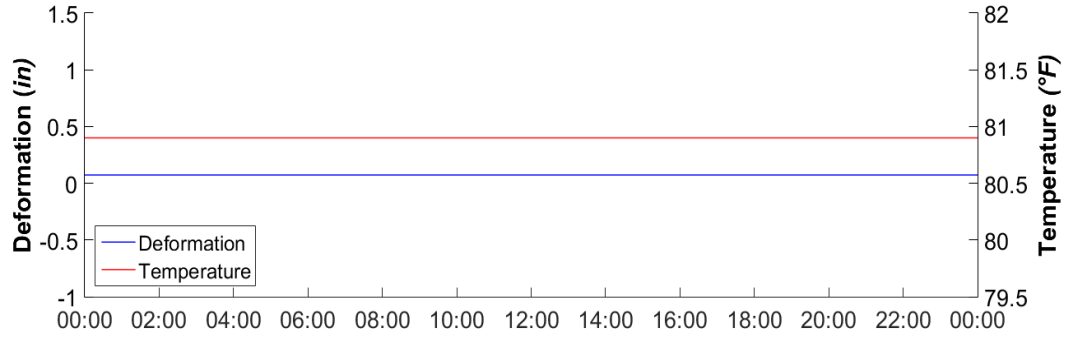

Span 19	Case: Fixed support (2 span)

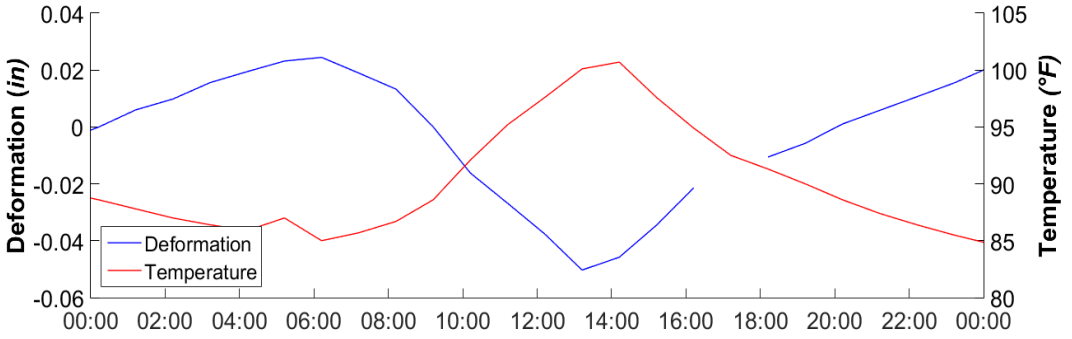

Girder End Displacement	Period: 24 hrs.
Span 16	**Case: Expansion support (2 span)**

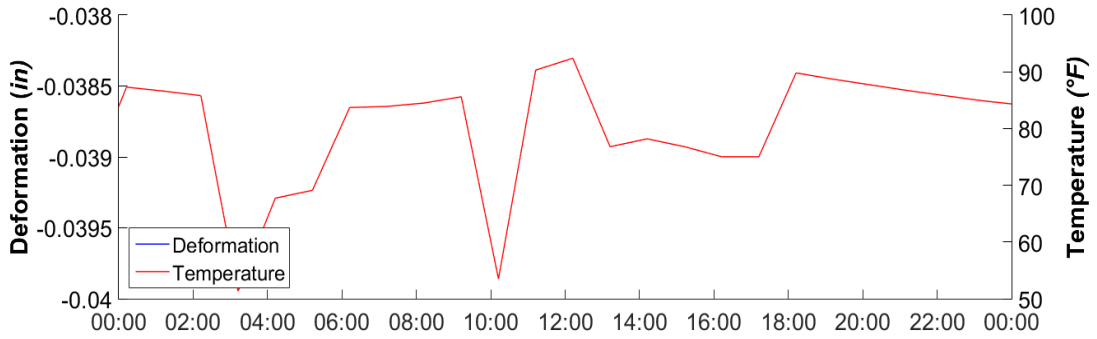

Span 1	Case: Expansion support (4 span)

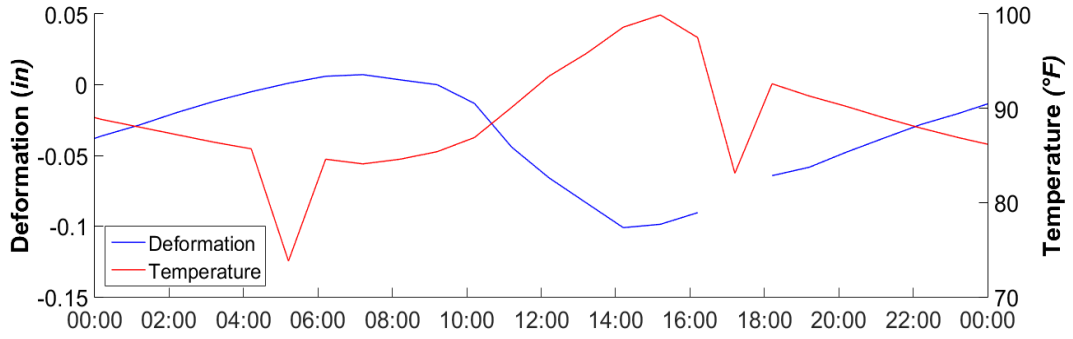

Girder 4	Baseline: Jun 19 2017 9:00
Segment A	**Case: 4-span segment**

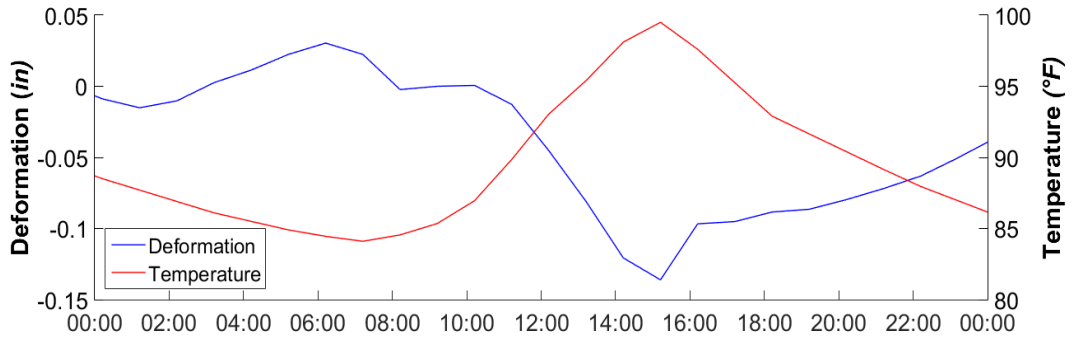

Segment B	Case: 2-span segment

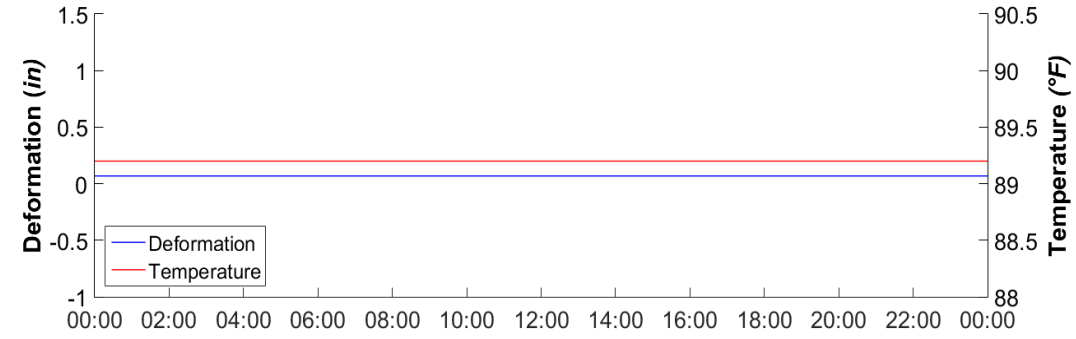

Span 19	Case: Fixed support (2 span)

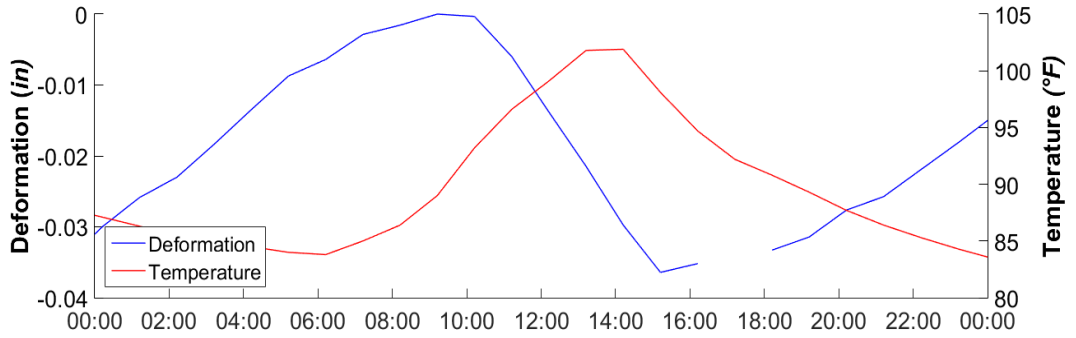

Span 16	Case: Expansion support (2 span)

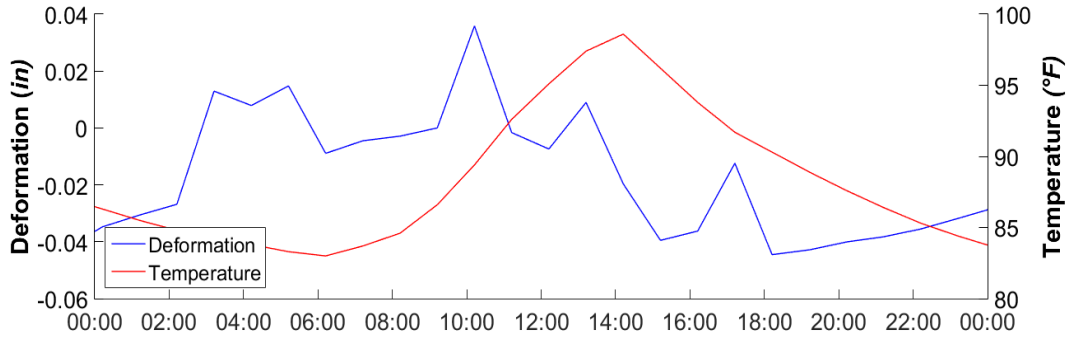

Girder 4	Baseline: Jun 19 2017 9:00
Span 1	Case: Expansion support (4 span)

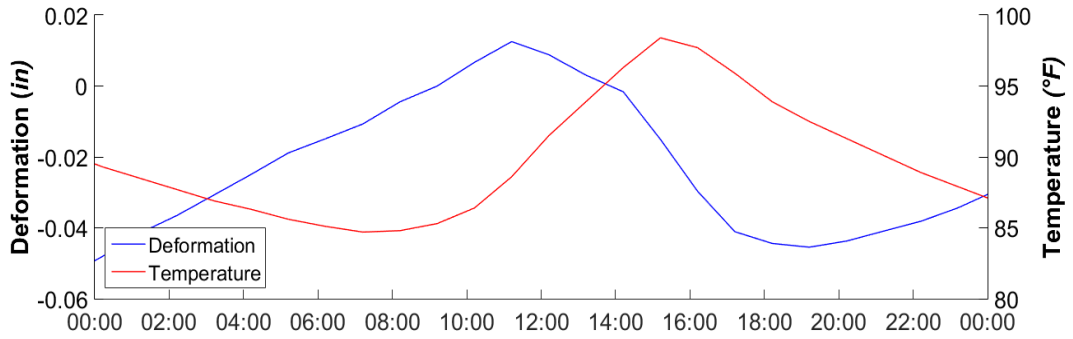

Girder End Displacement	Period: 24 hrs.
Beginning: Aug 1 2018 0:00	End: Aug 2 2018 0:00
Girder 7	Baseline : Aug 1 2018 9:00
Segment A	Case: 4-span segment

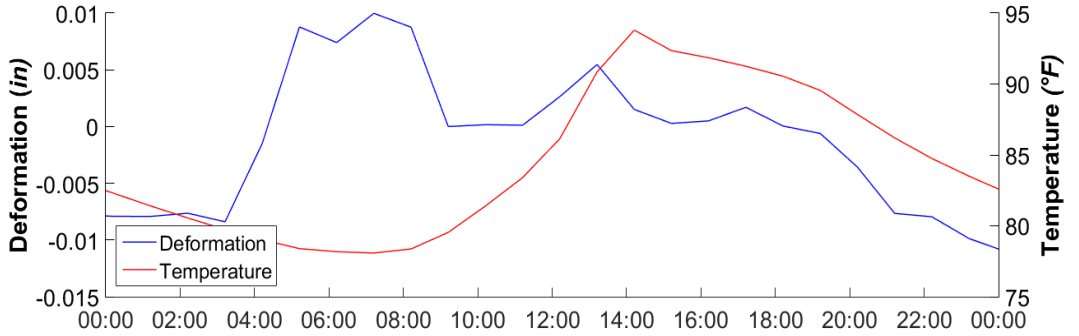

Segment B	Case: 2-span segment

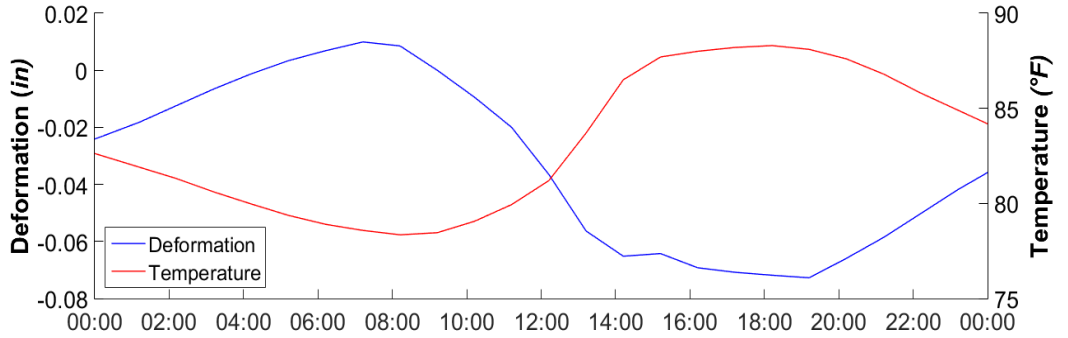

Span 19	Case: Fixed support (2 span)

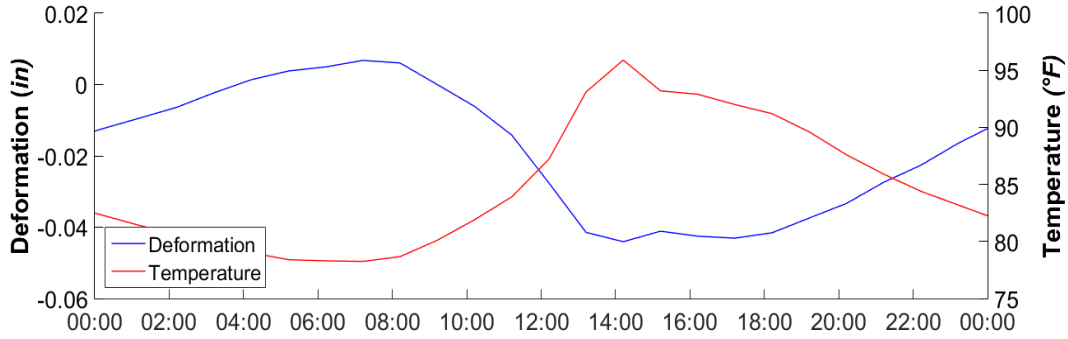

Girder End Displacement	Period: 24 hrs.
Span 16	**Case: Expansion support (2 span)**

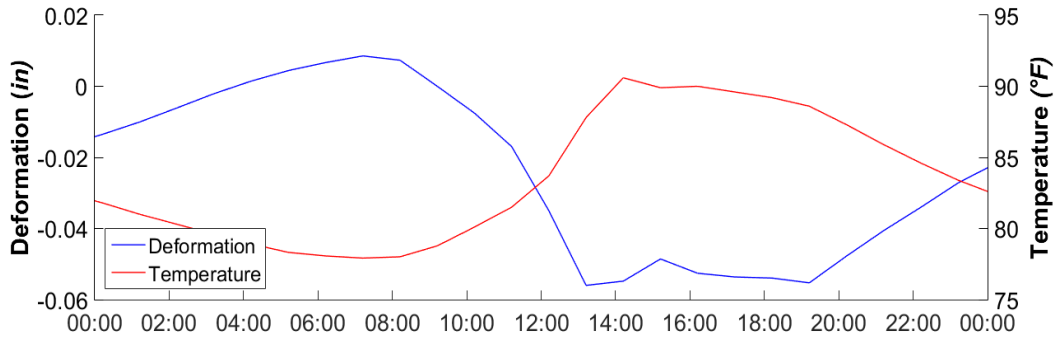

Span 1	Case: Expansion support (4 span)

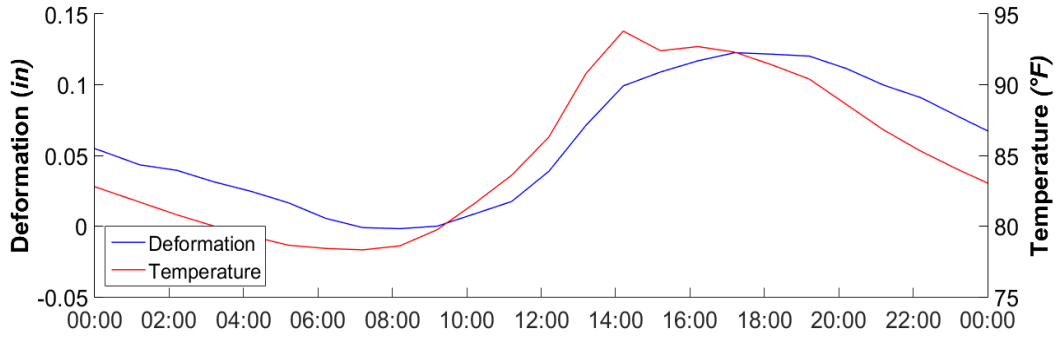

Girder 4	Baseline: Aug 1 2018 9:00
Segment A	**Case: 4-span segment**

N/A

Segment B	Case: 2-span segment

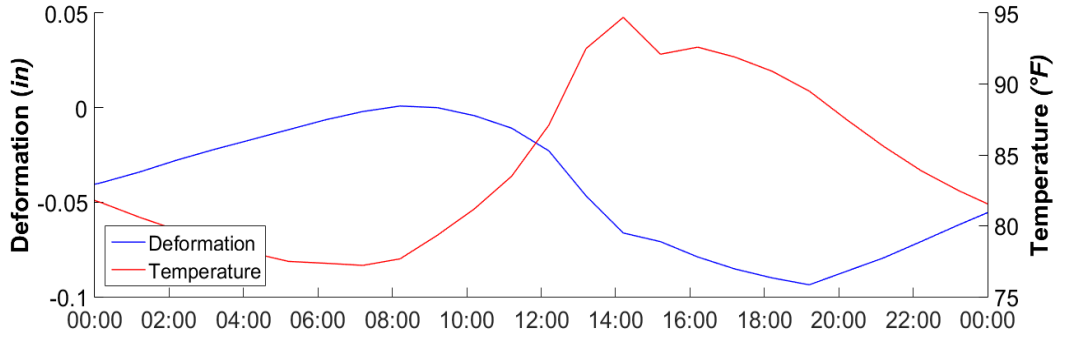

Span 19	Case: Fixed support (2 span)

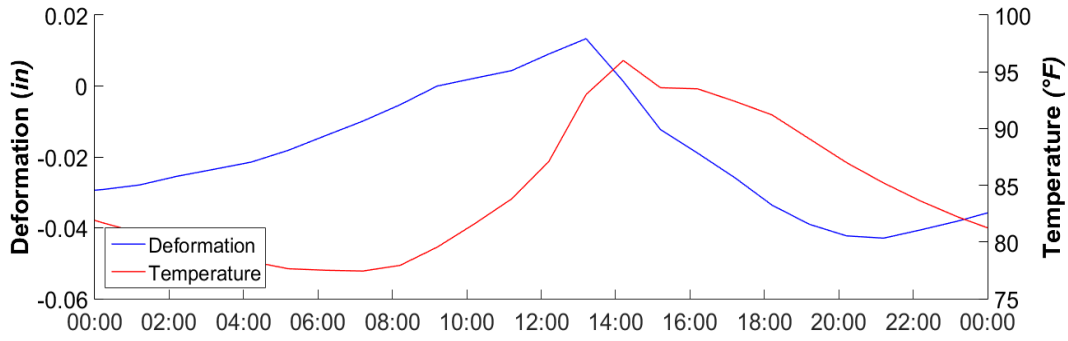

Span 16	Case: Expansion support (2 span)

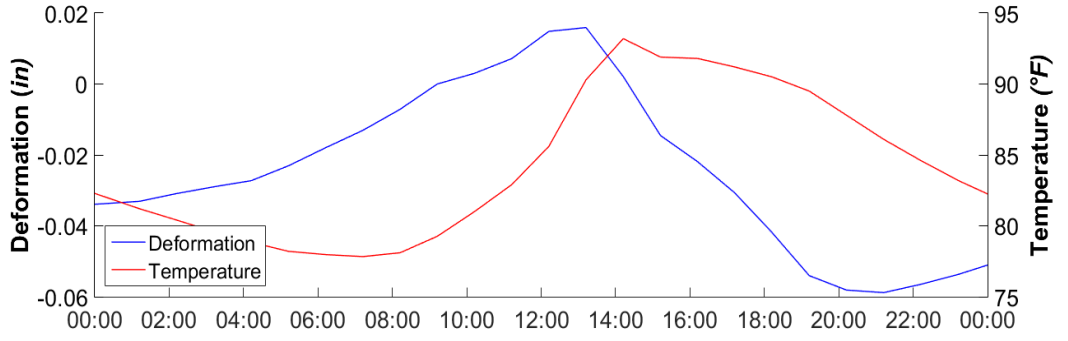

Girder 4	Baseline: Aug 1 2018 9:00
Span 1	Case: Expansion support (4 span)

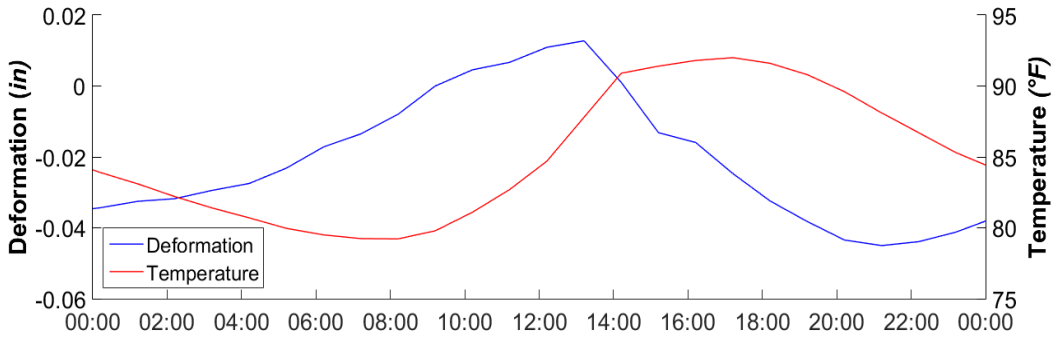

Forces (No Crack width)

Forces (no cracking)	Period: 30 day
Beginning: Jan 1 2018 0:00	End: Jan 31 2018 0:00
Girder 7	Baseline : Jan 2 2018 00:00
Bent 2	Case: Expansion support (4 span)

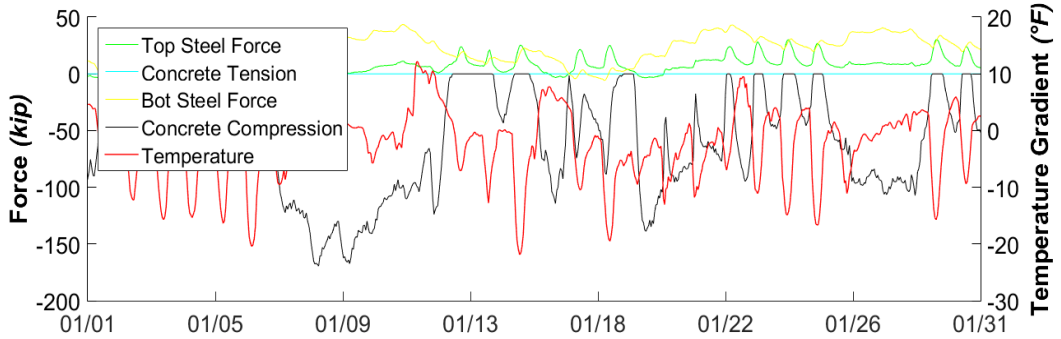

Bent 3	Case: Expansion support (4 span)

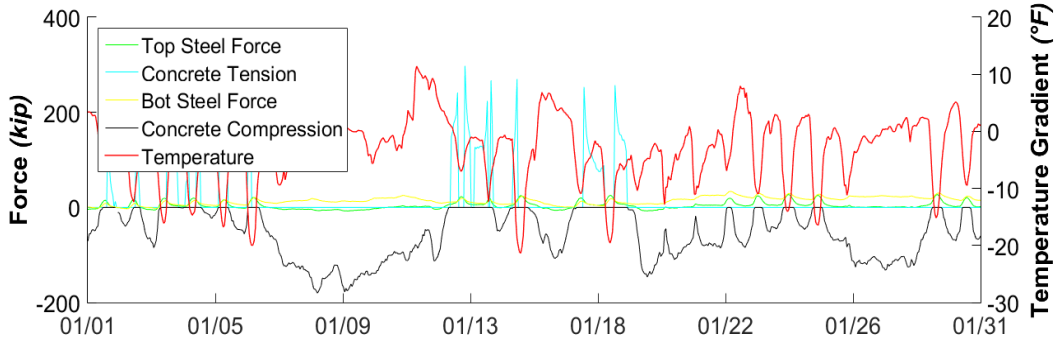

Bent 4	Case: Expansion support (4 span)

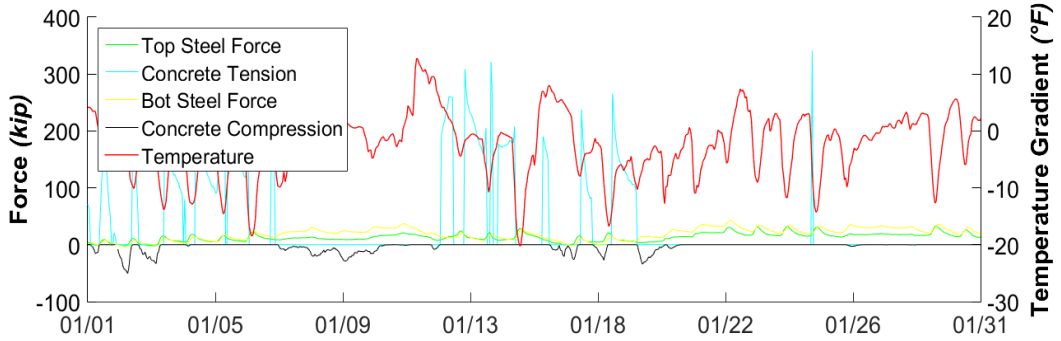

Forces (no cracking)	Period: 30 day
Bent 15	**Case: Expansion support (2 span)**

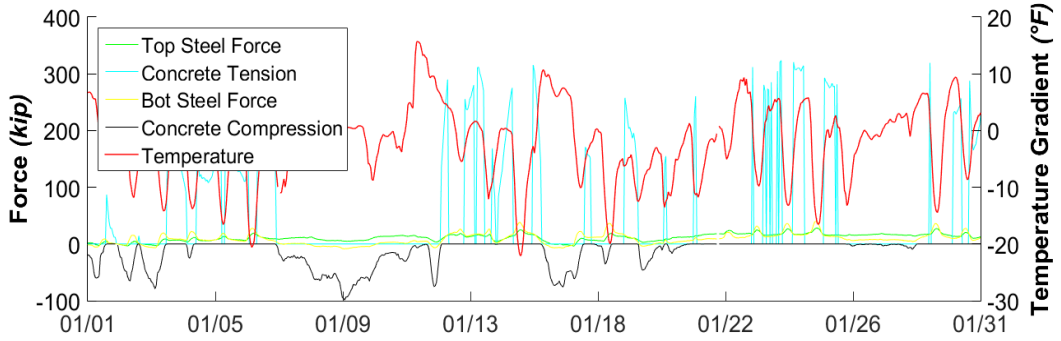

Bent 17	Case: Expansion support (2 span)

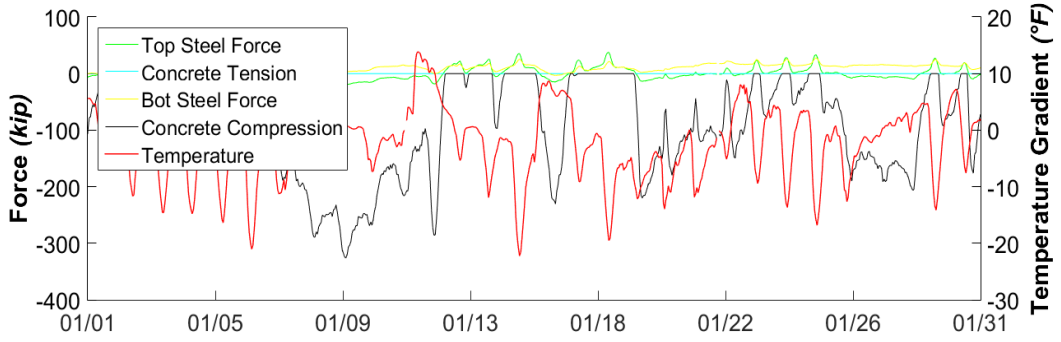

Bent 19	Case: Fixed support (2 span)

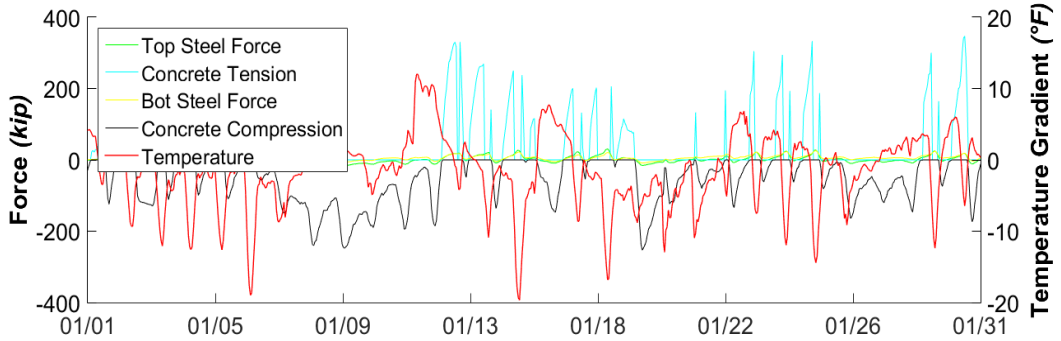

Girder 4	Baseline: Jan 2 2018 00:00
Bent 2	**Case: Expansion support (4 span)**

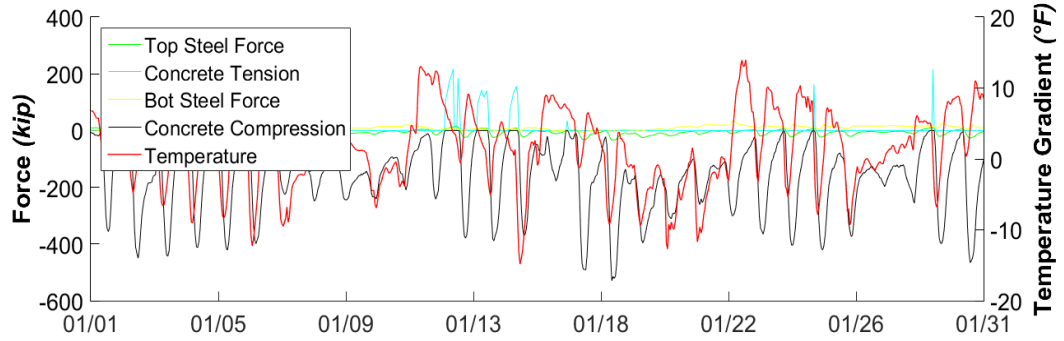

Bent 3	Case: Expansion support (4 span)

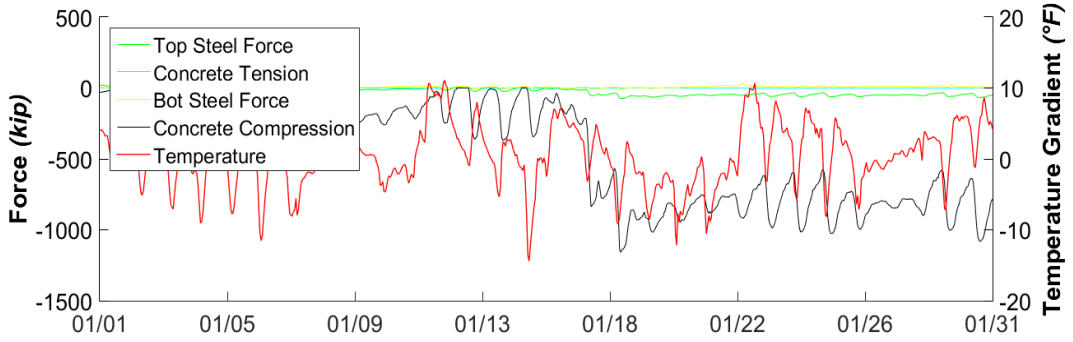

Bent 4	Case: Expansion support (4 span)

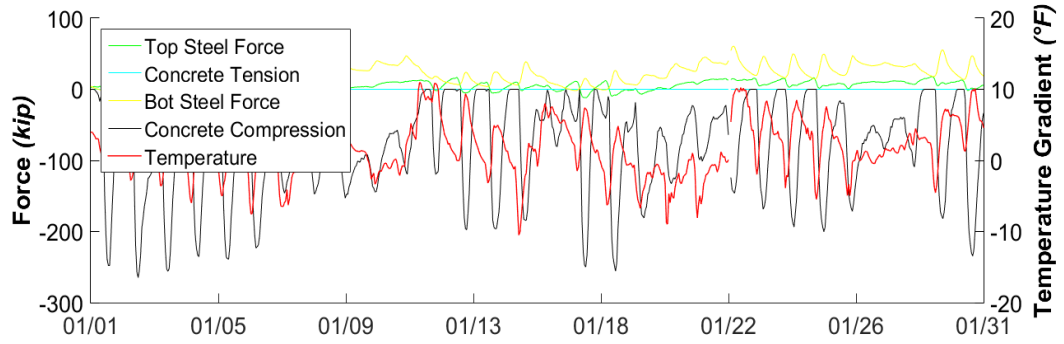

Bent 15	Case: Expansion support (2 span)

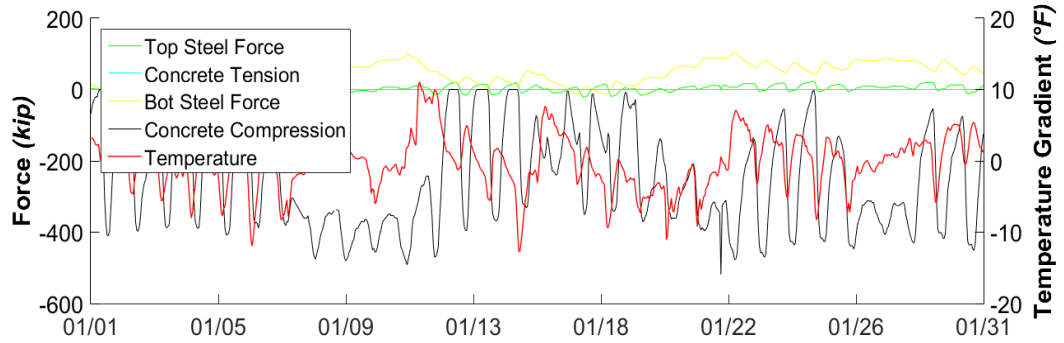

Girder 4	Baseline: Jan 2 2018 00:00
Bent 17	**Case: Expansion support (2 span)**

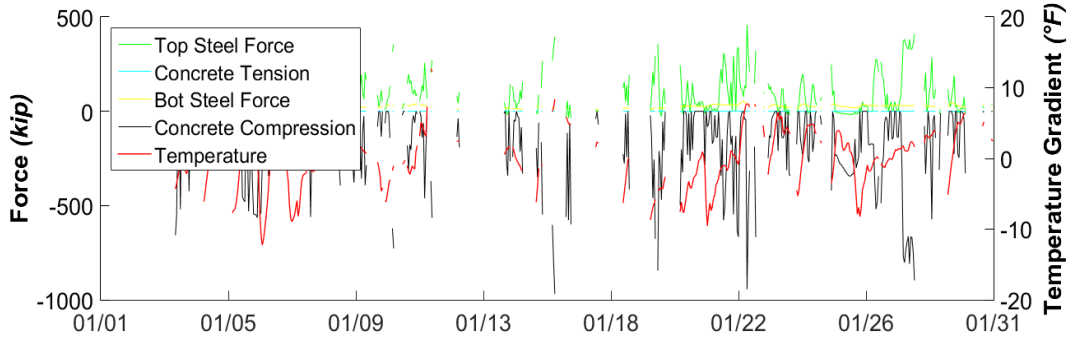

Bent 19	Case: Fixed support (2 span)

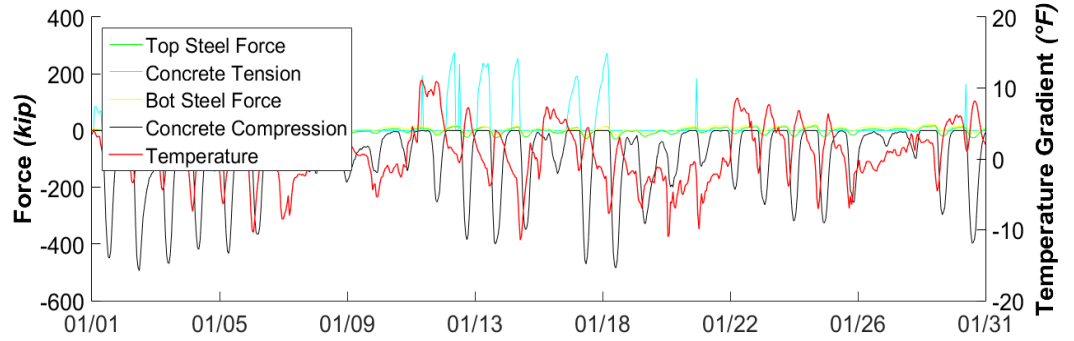

Forces (no cracking)	Period: 30 day
Beginning: Aug 1 2018 0:00	End: Aug 31 2018 0:00
Girder 7	Baseline : Aug 1 2018 09:00
Bent 2	Case: Expansion support (4 span)

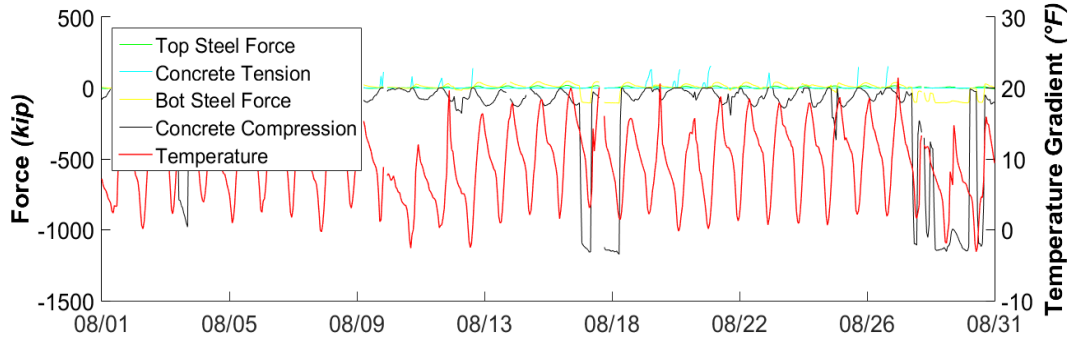

Bent 3	Case: Expansion support (4 span)

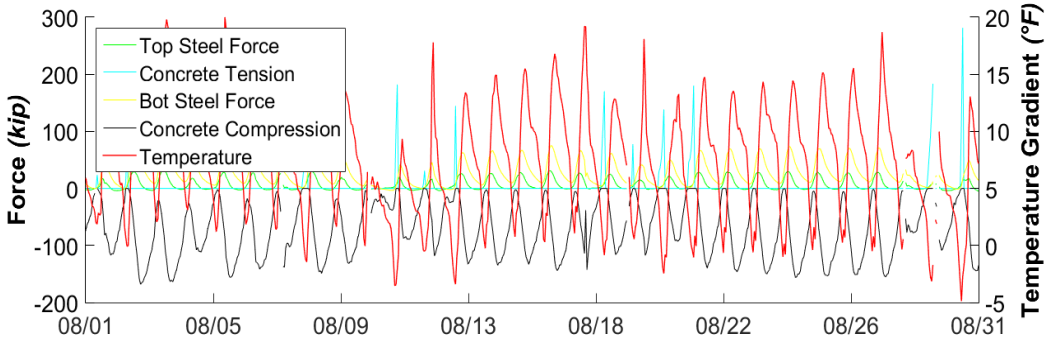

Bent 4	Case: Expansion support (4 span)

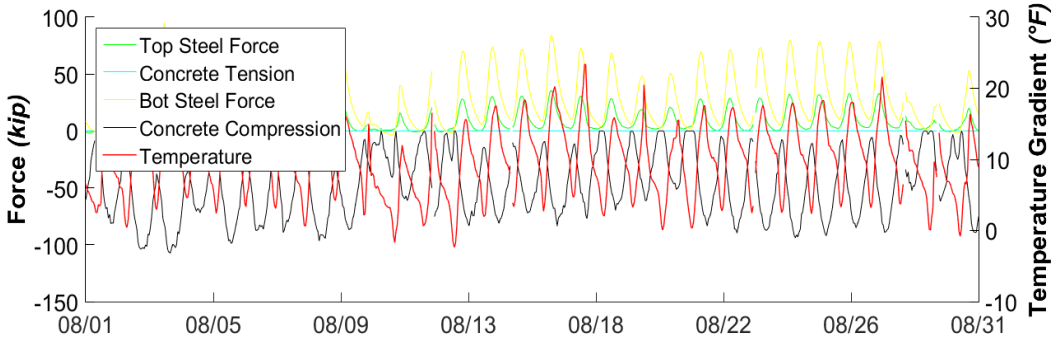

Forces (no cracking)	Period: 30 day
Bent 15	**Case: Expansion support (2 span)**

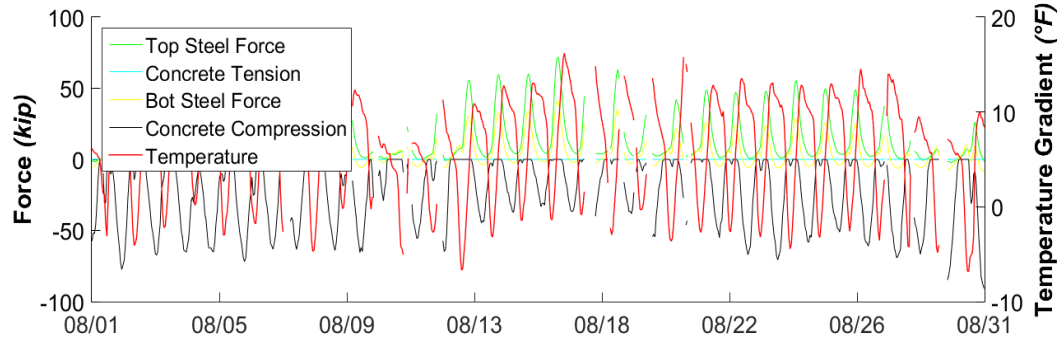

Bent 17	Case: Expansion support (2 span)

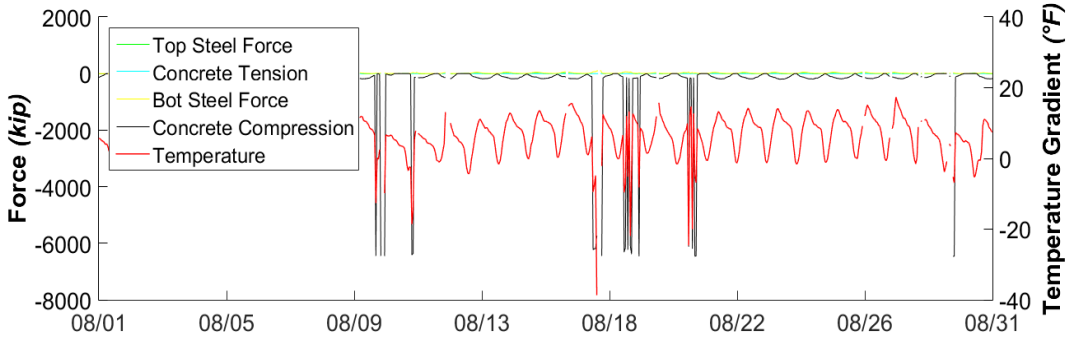

Bent 19	Case: Fixed support (2 span)

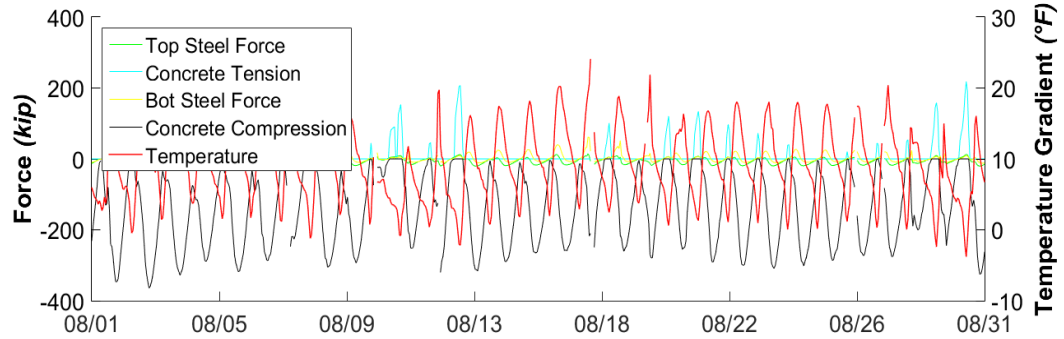

Girder 4	Baseline: Aug 1 2018 09:00
Bent 2	**Case: Expansion support (4 span)**

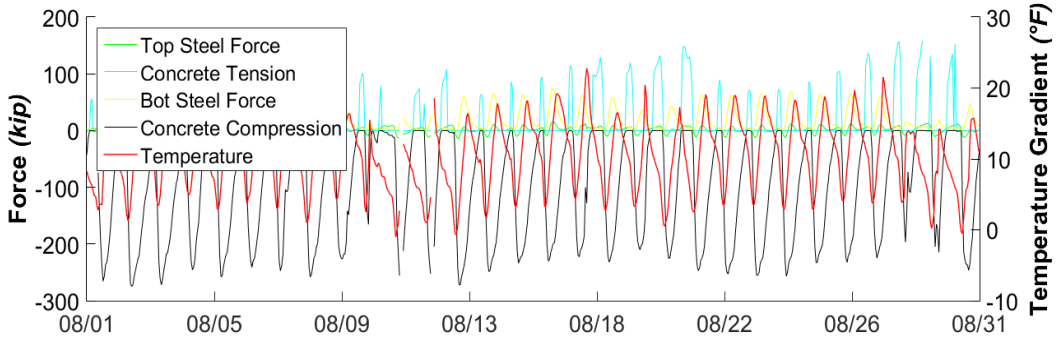

Bent 3	Case: Expansion support (4 span)

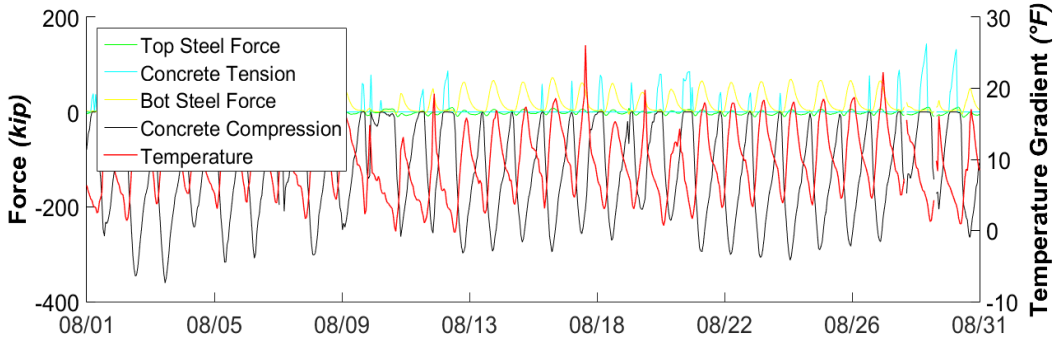

Bent 4	Case: Expansion support (4 span)

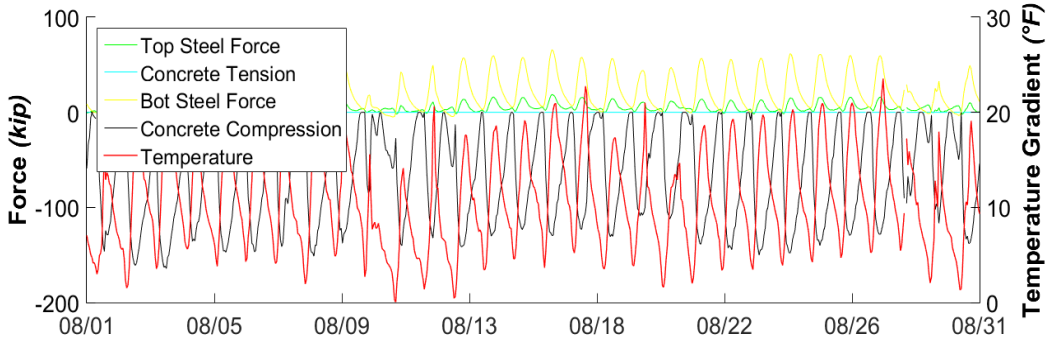

Bent 15	Case: Expansion support (2 span)

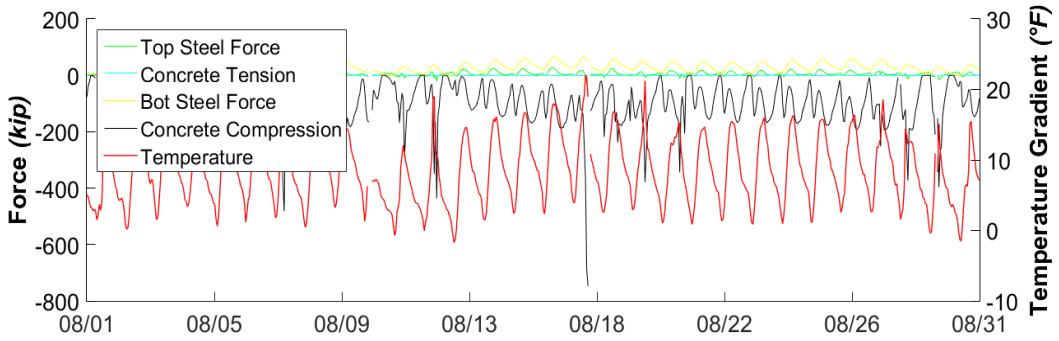

Girder 4	Baseline: Aug 1 2018 09:00
Bent 17	**Case: Expansion support (2 span)**

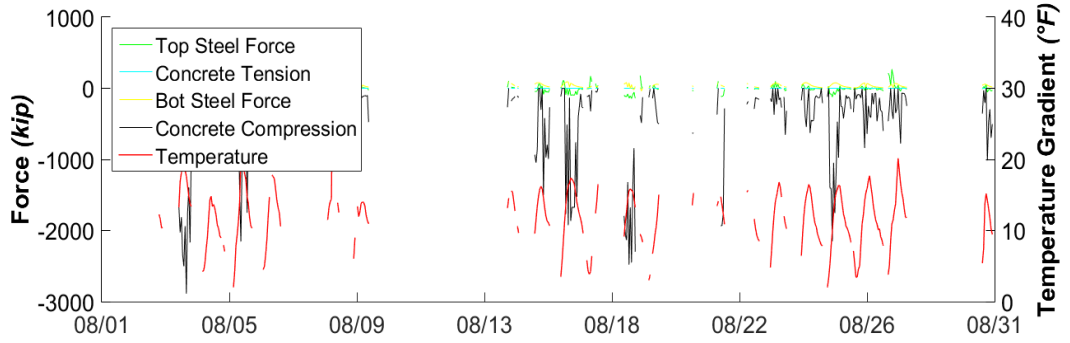

Bent 19	Case: Fixed support (2 span)

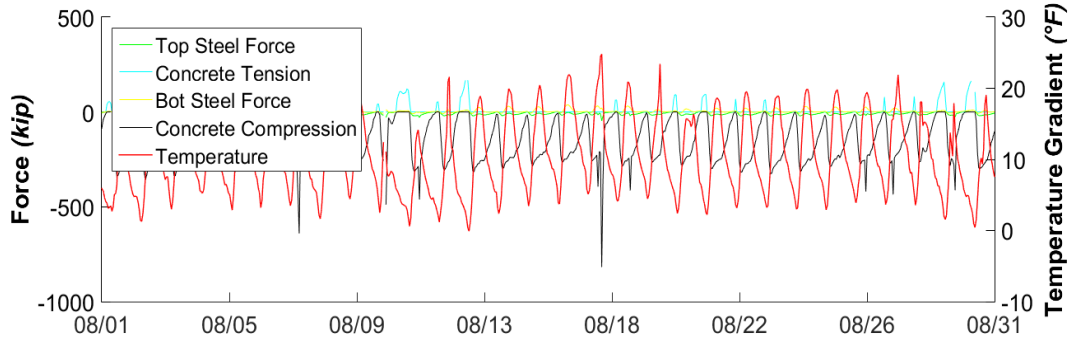

Link slab Force no CW	Period: 24 hrs.
Beginning: Aug 1 2018 0:00	End: Aug 2 2018 0:00
Girder 7	Baseline : Aug 1 2018 9:00
Bent 2	Case: Expansion support (4 span)

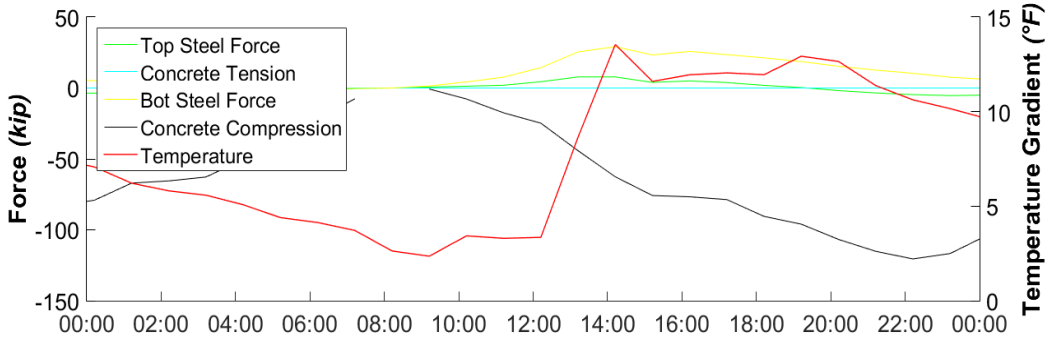

Bent 3	Case: Expansion support (4 span)

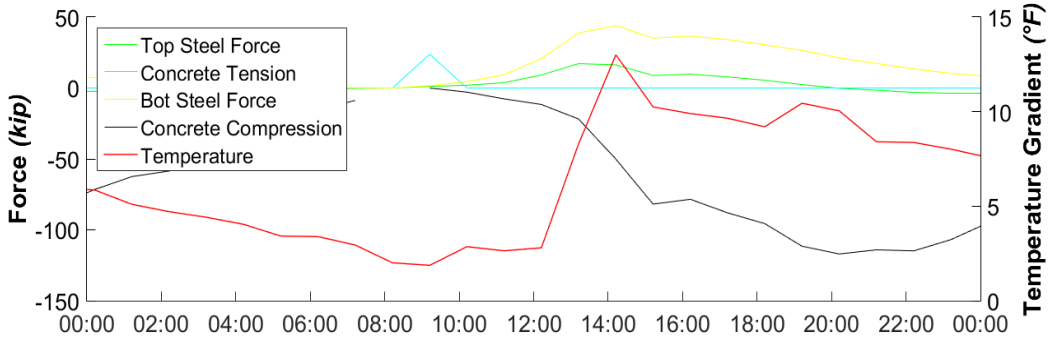

Bent 4	Case: Expansion support (4 span)

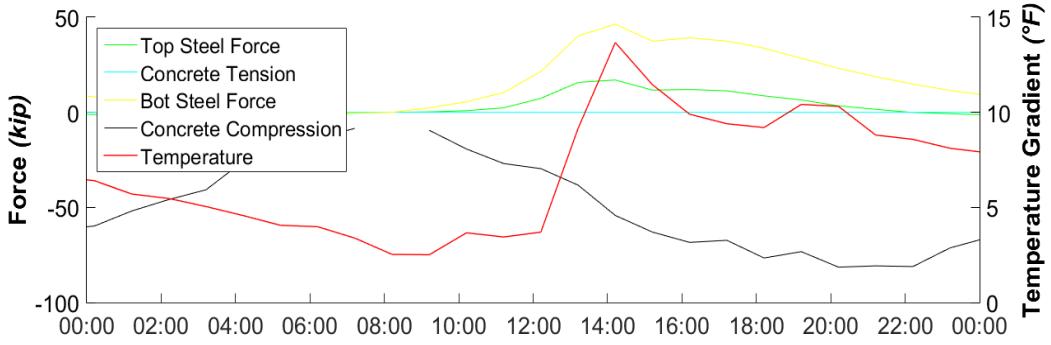

Link slab Force no CW	Period: 24 hrs.
Bent 15	**Case: Expansion support (2 span)**

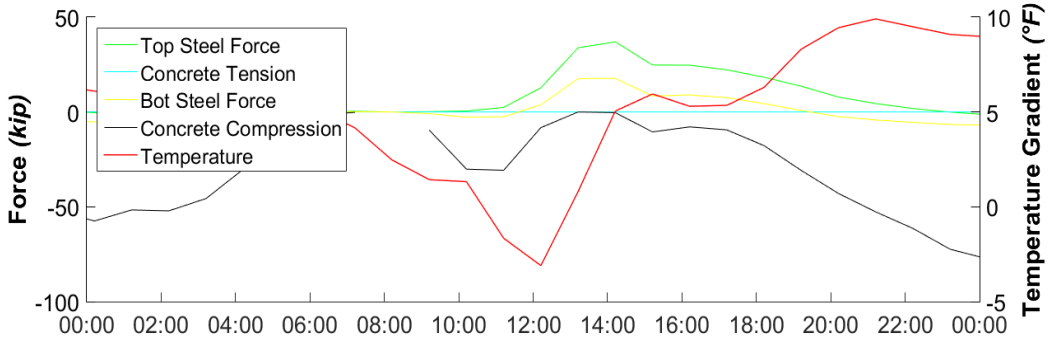

Bent 17	Case: Expansion support (2 span)

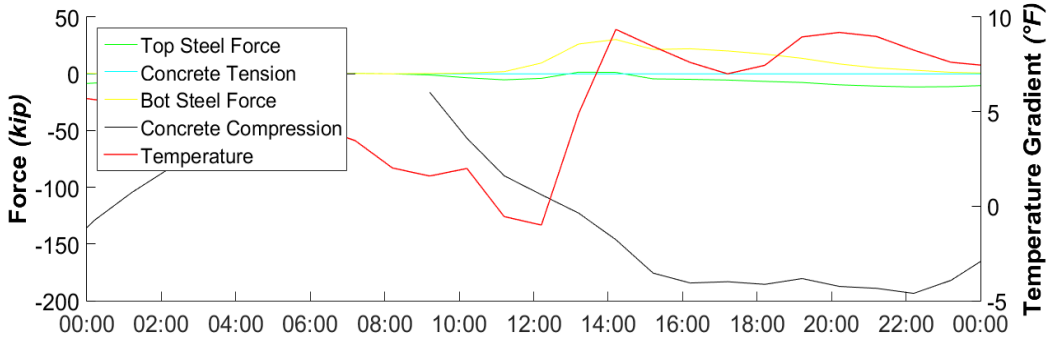

Bent 19	Case: Fixed support (2 span)

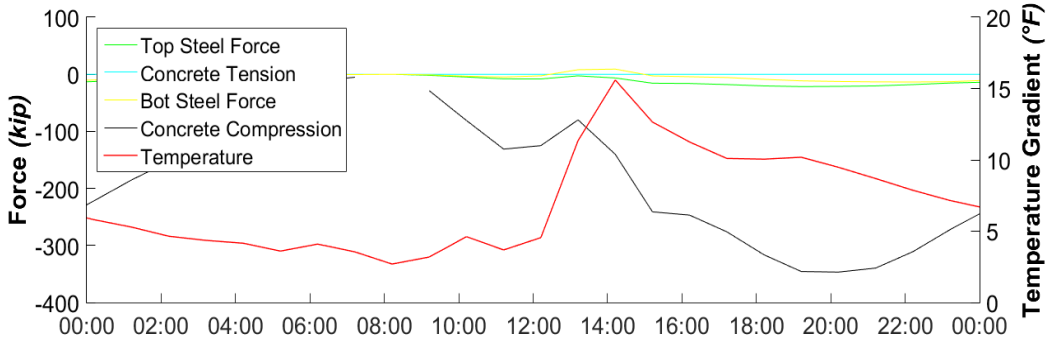

Girder 4	Baseline: Aug 1 2018 9:00
Bent 2	**Case: Expansion support (4 span)**

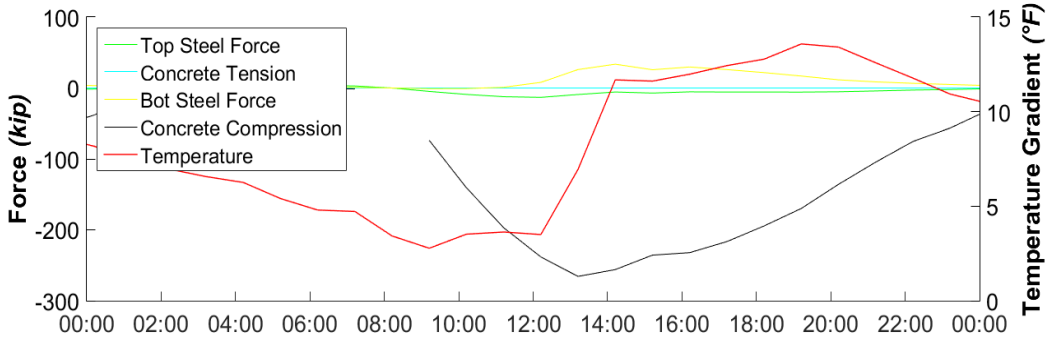

Bent 3	Case: Expansion support (4 span)

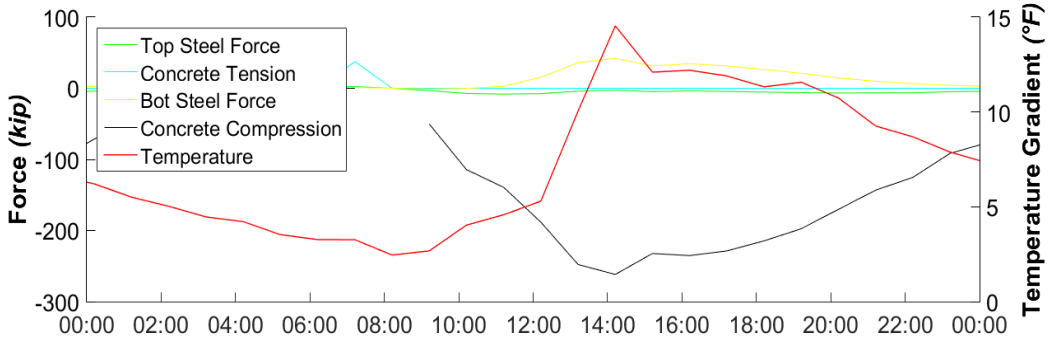

Bent 4	**Case: Expansion support (4 span)**

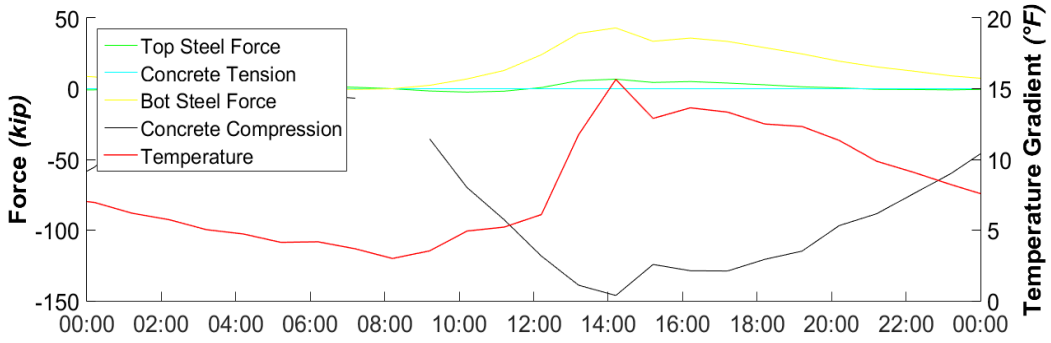

Bent 15	**Case: Expansion support (2 span)**

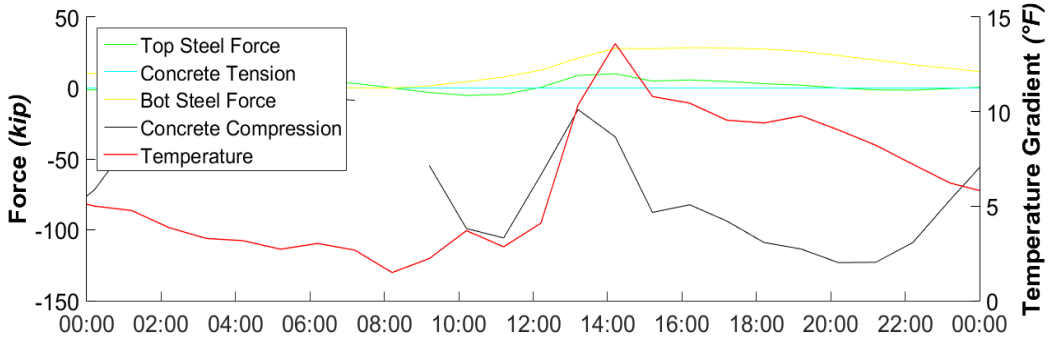

Girder 4	Baseline: Aug 1 2018 9:00
Bent 17	Case: Expansion support (2 span)

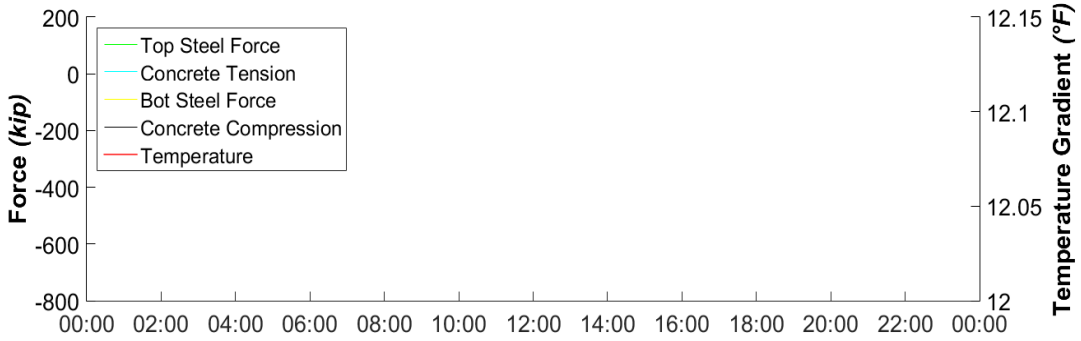

Bent 19	Case: Fixed support (2 span)

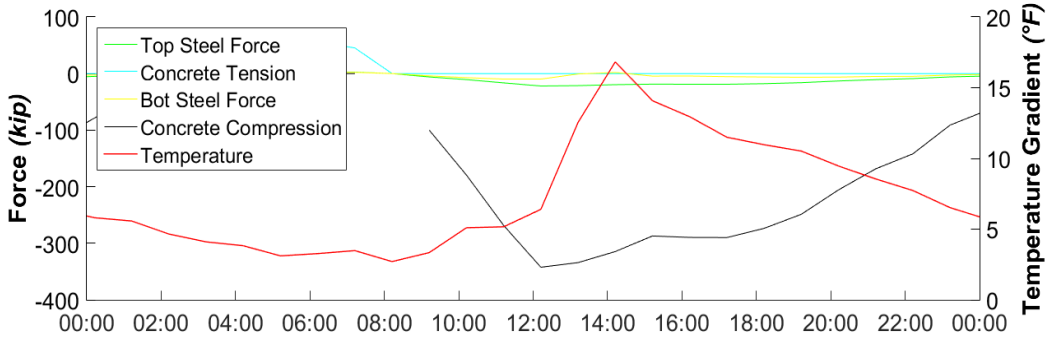

Forces (no cracking)	Period: 30 day
Beginning: Jan 1 2018 0:00	End: Jan 2 2018 0:00
Girder 7	Baseline : Jan 2 2018 00:00
Bent 2	Case: Expansion support (4 span)

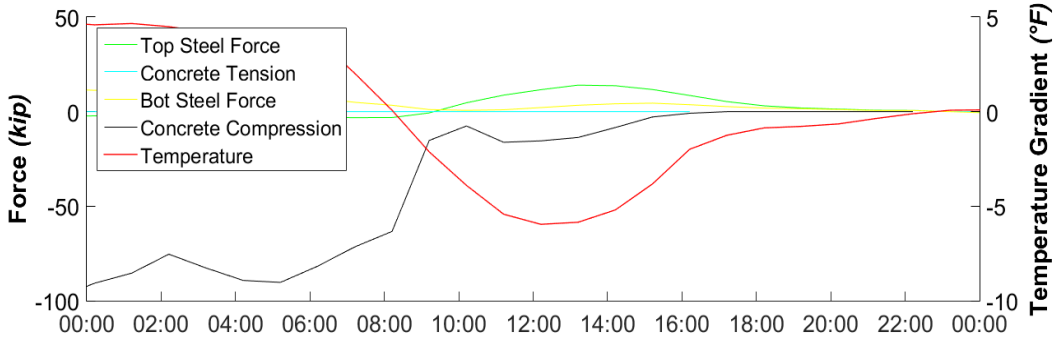

Bent 3	Case: Expansion support (4 span)

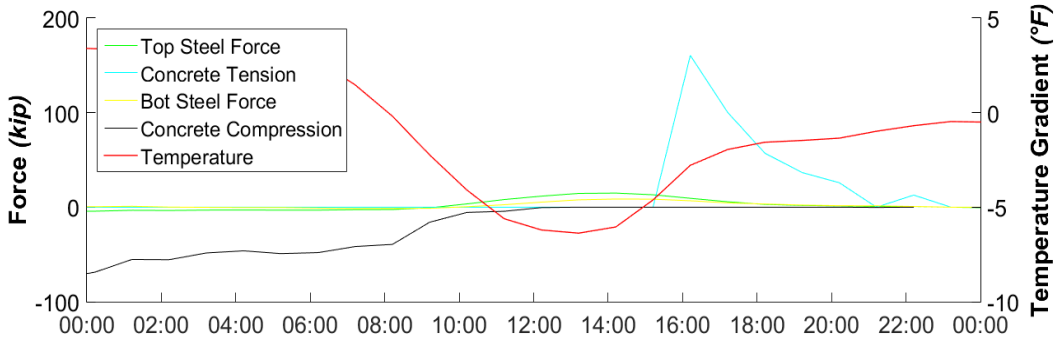

Bent 4	Case: Expansion support (4 span)

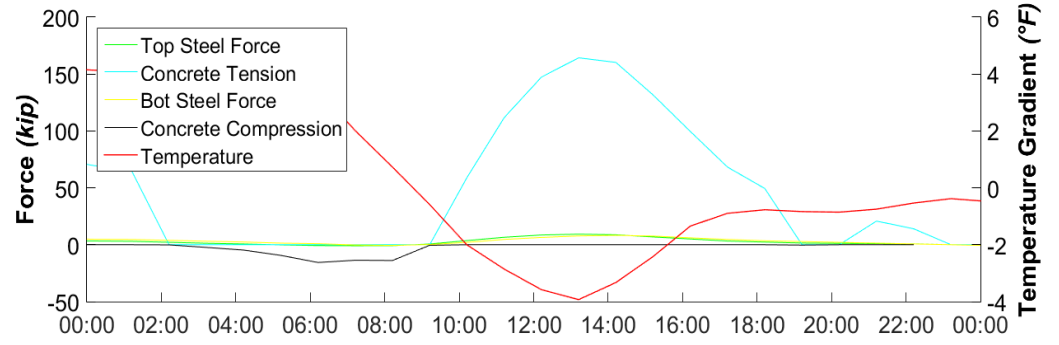

Forces (no cracking)	Period: 30 day
Bent 15	**Case: Expansion support (2 span)**

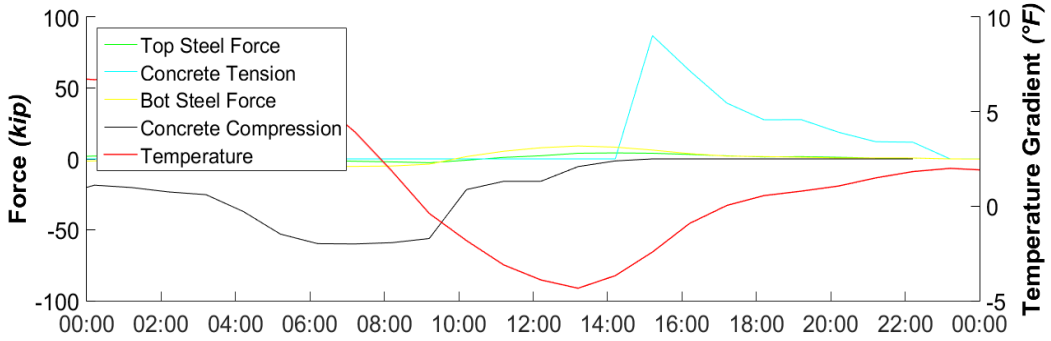

Bent 17	Case: Expansion support (2 span)

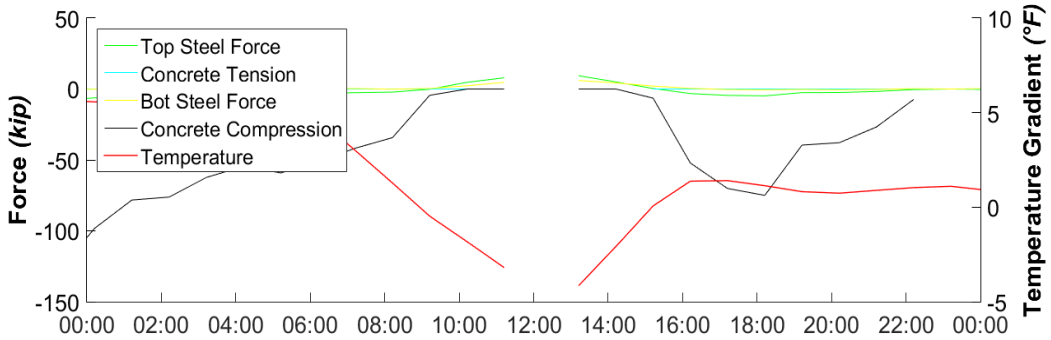

Bent 19	Case: Fixed support (2 span)

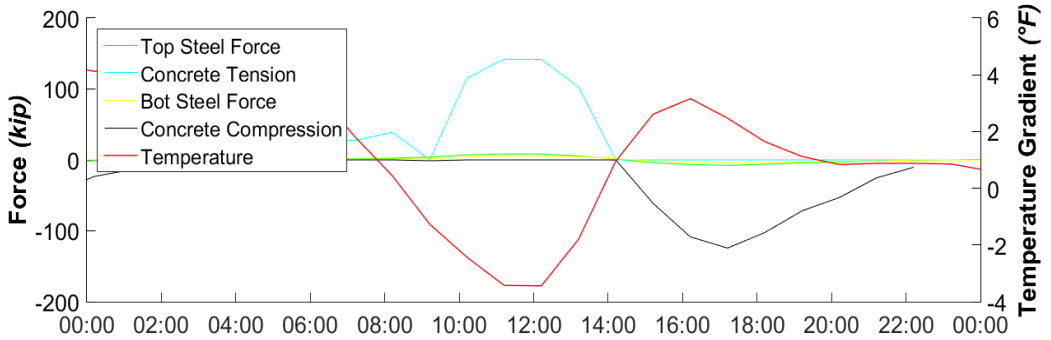

Girder 4	Baseline: Jan 2 2018 00:00
Bent 2	**Case: Expansion support (4 span)**

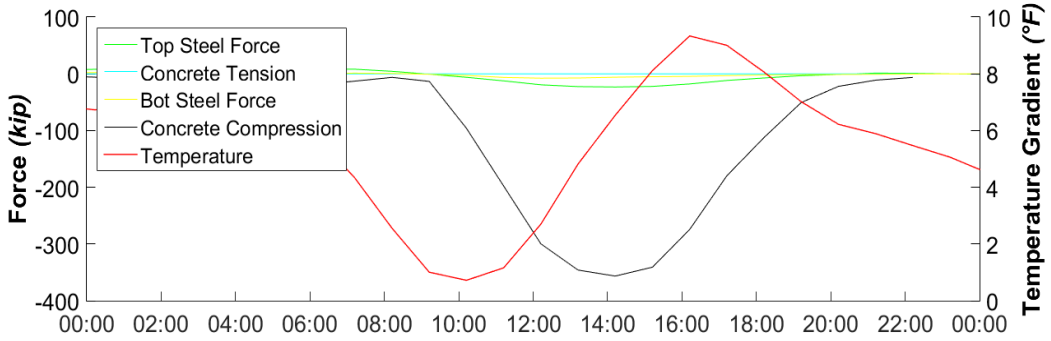

Bent 3	Case: Expansion support (4 span)

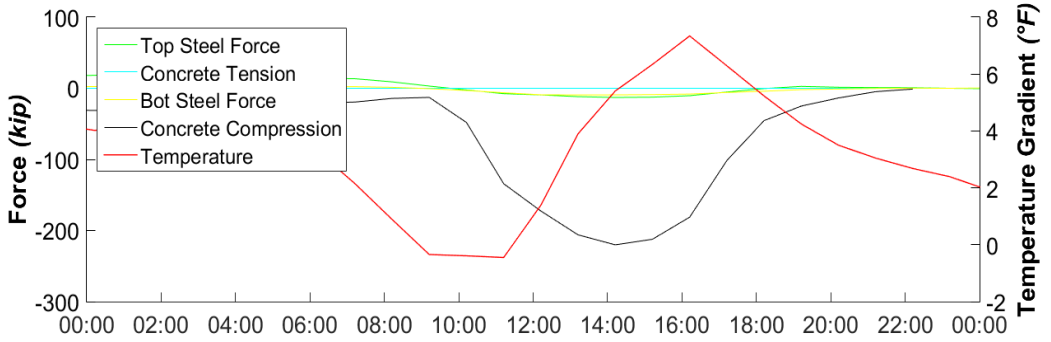

Bent 4	Case: Expansion support (4 span)

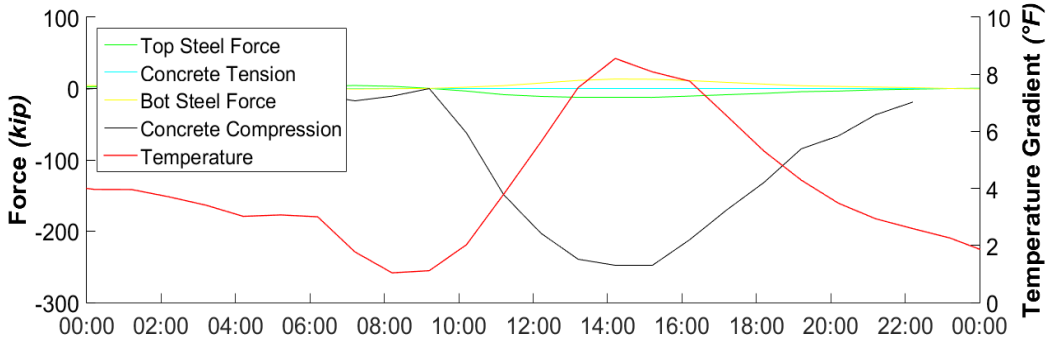

Bent 15	Case: Expansion support (2 span)

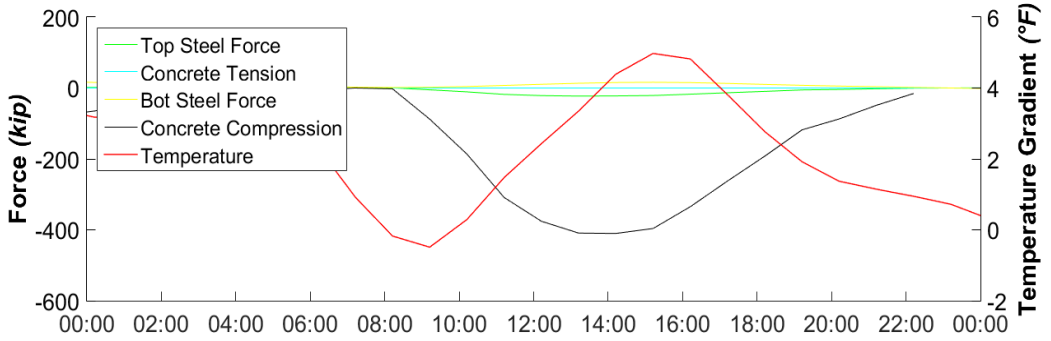

Girder 4	Baseline: Jan 2 2018 00:00
Bent 17	**Case: Expansion support (2 span)**

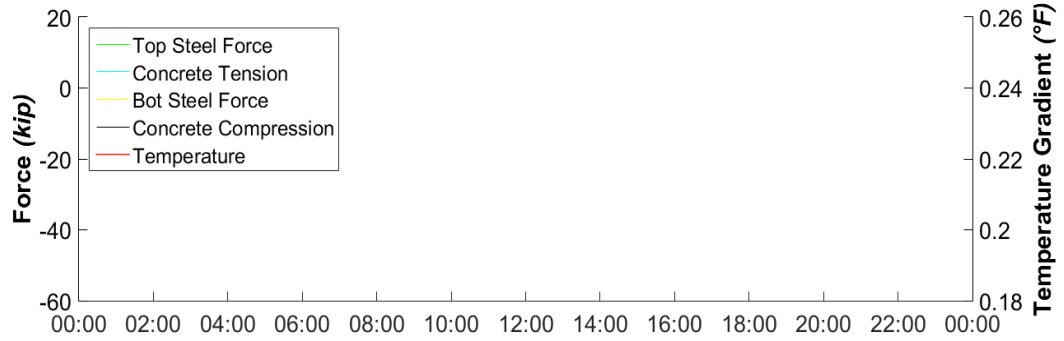

Bent 19	Case: Fixed support (2 span)

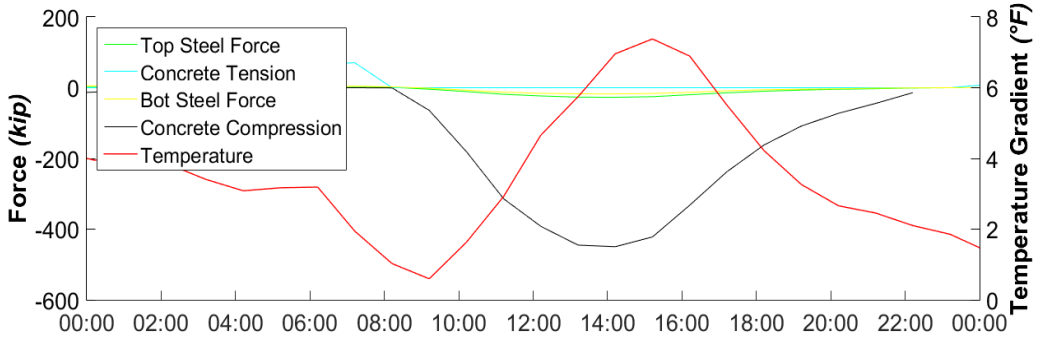

Forces (Crack Width)

Forces	Period: 30 day
Beginning: Jan 1 2018 0:00	End: Jan 31 2018 0:00
Girder 7	Baseline : Jan 2 2018 00:00
Bent 2	Case: Expansion support (4 span)

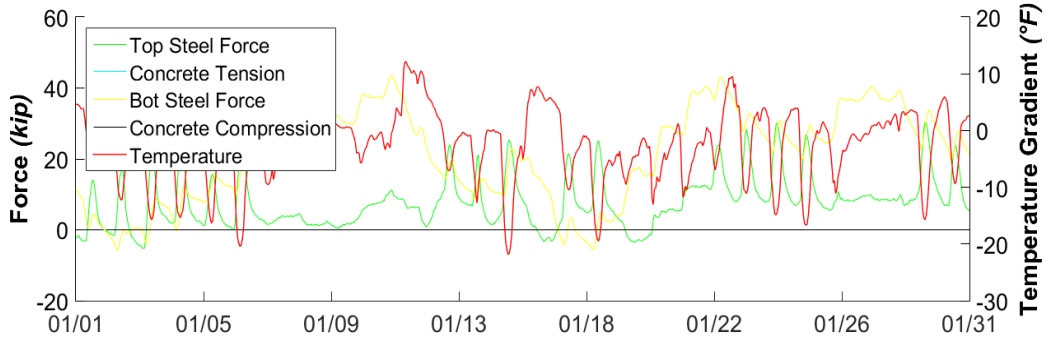

Bent 3	Case: Expansion support (4 span)

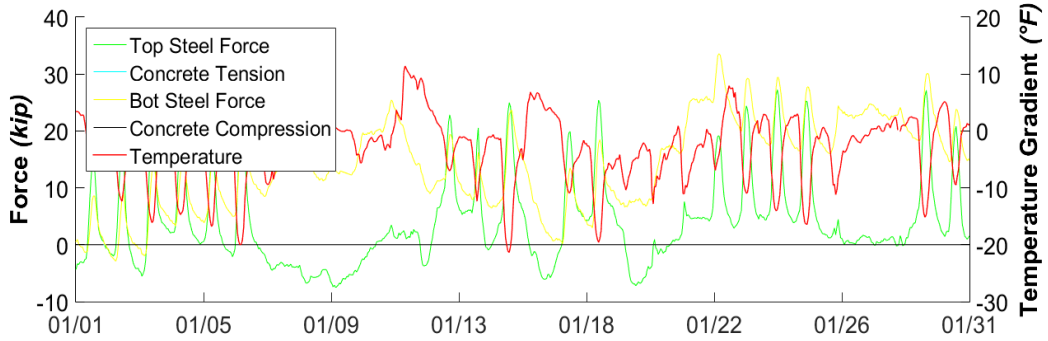

Bent 4	Case: Expansion support (4 span)

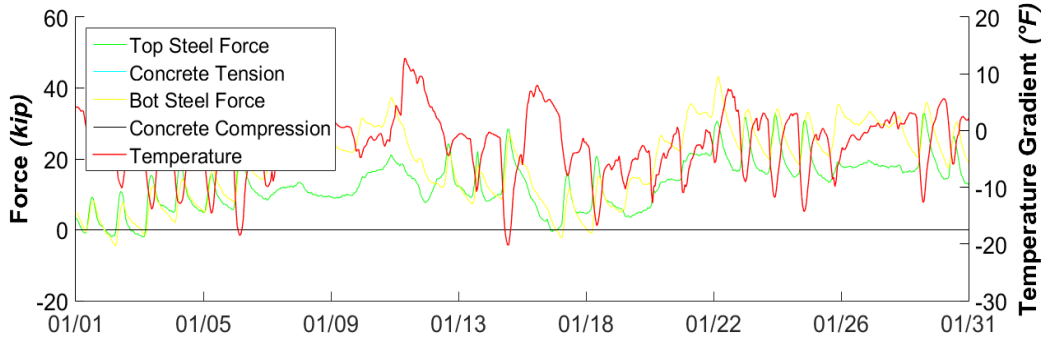

Forces	Period: 30 day
Bent 15	**Case: Expansion support (2 span)**

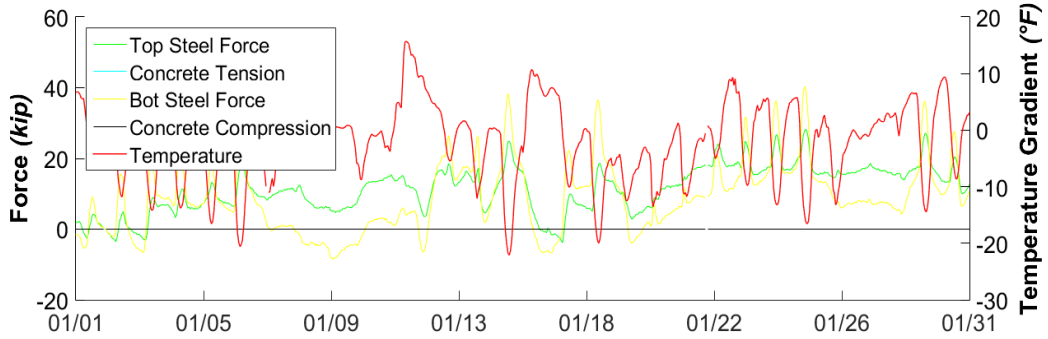

Bent 17	Case: Expansion support (2 span)

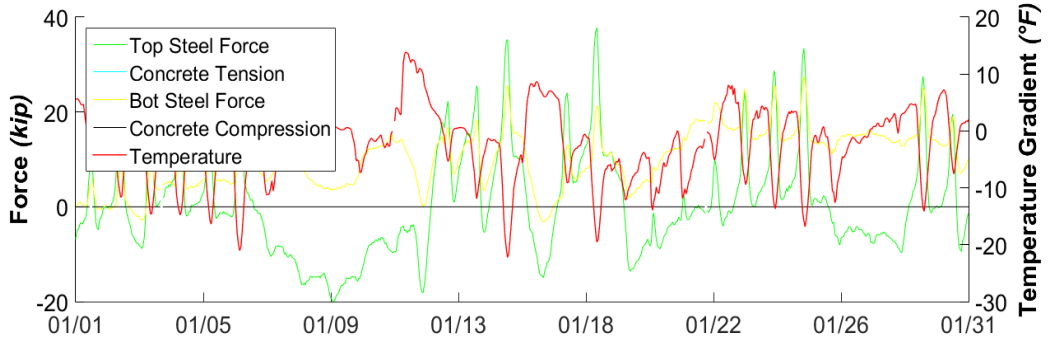

Bent 19	Case: Fixed support (2 span)

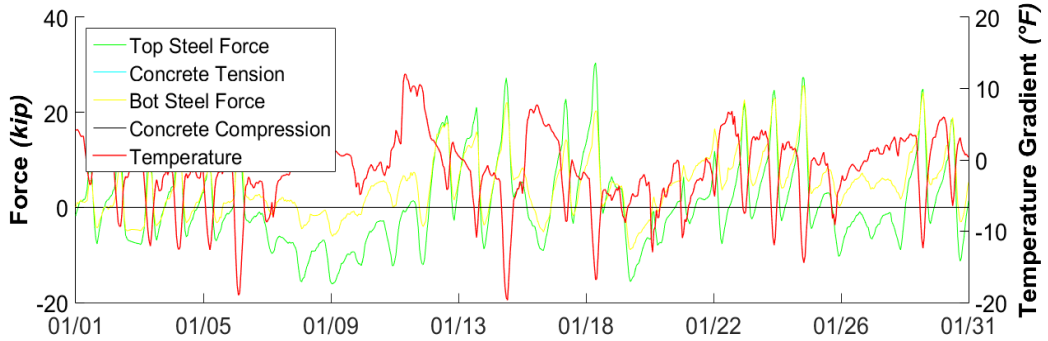

Girder 4	Baseline: Jan 2 2018 00:00
Bent 2	**Case: Expansion support (4 span)**

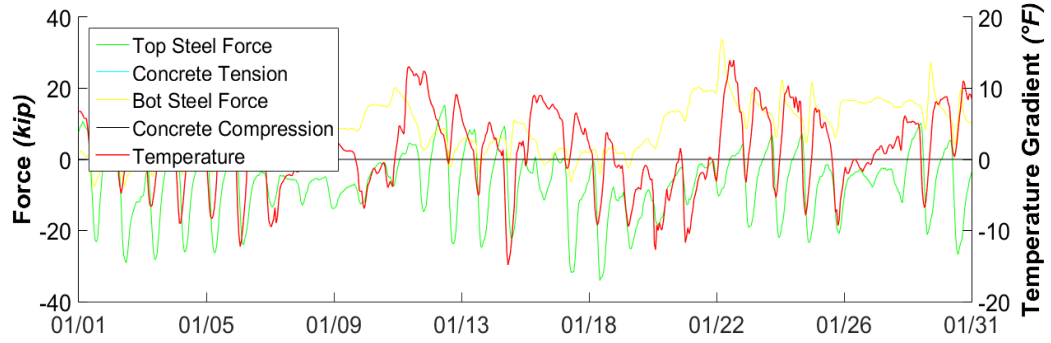

Bent 3	Case: Expansion support (4 span)

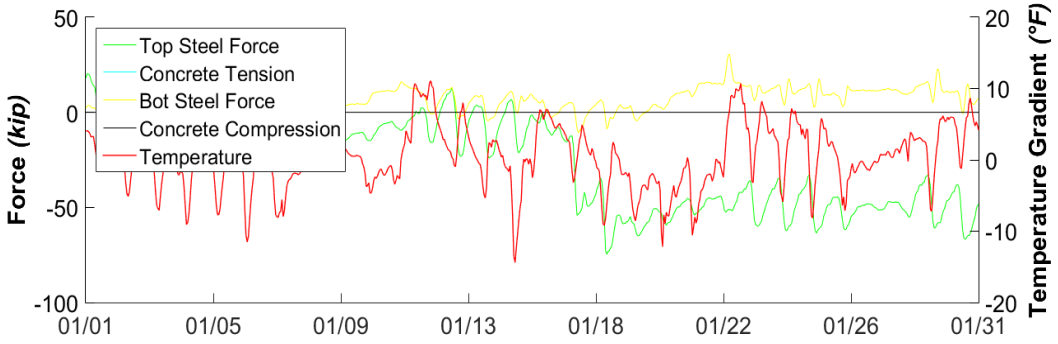

Bent 4	Case: Expansion support (4 span)

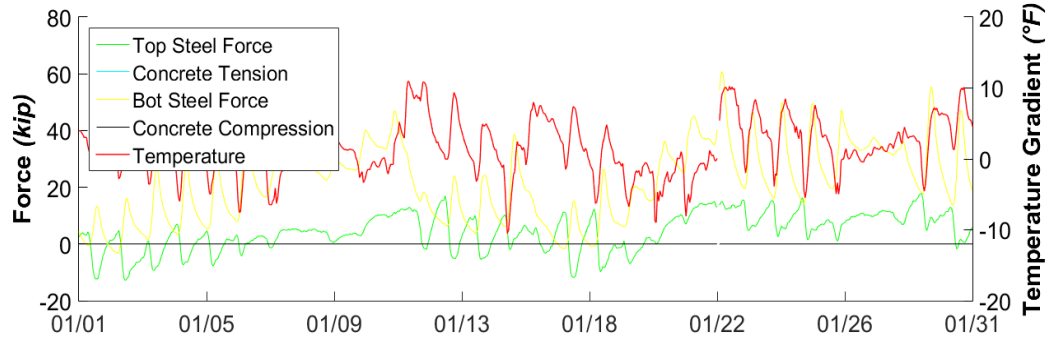

Bent 15	Case: Expansion support (2 span)

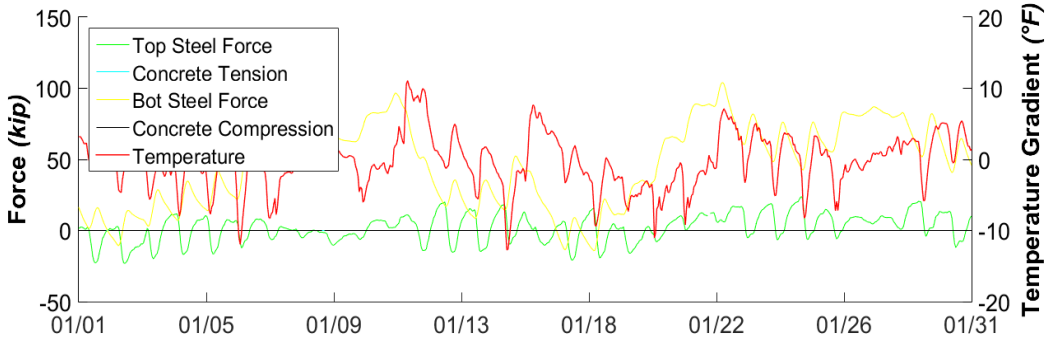

Girder 4	Baseline: Jan 2 2018 00:00
Bent 17	**Case: Expansion support (2 span)**

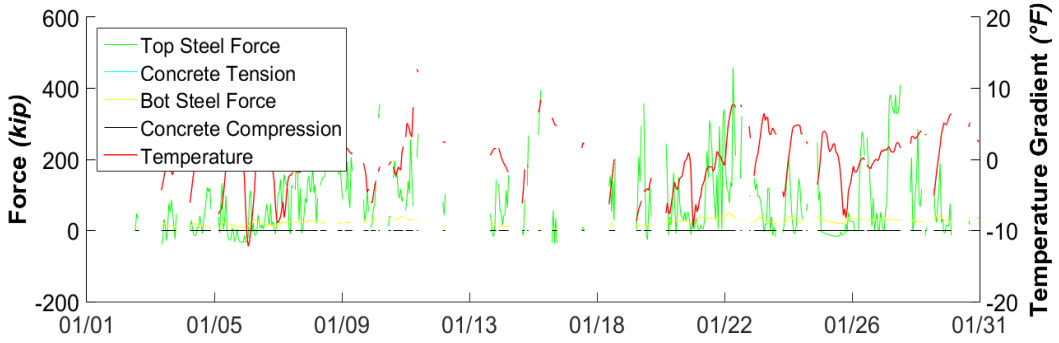

Bent 19	Case: Fixed support (2 span)

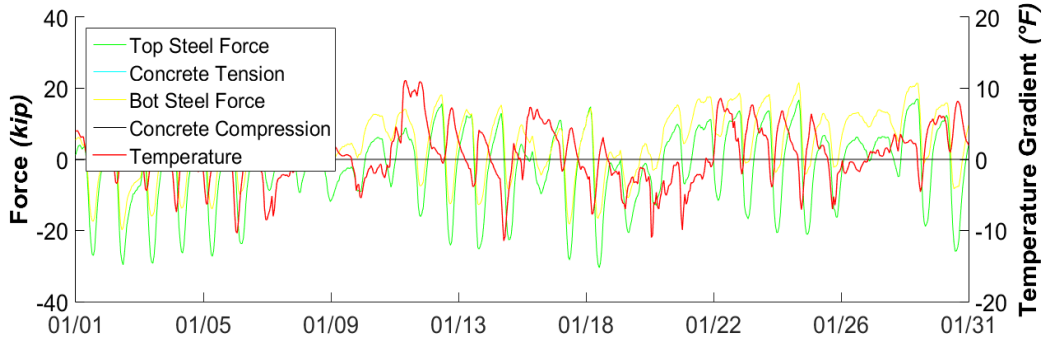

Forces	Period: 30 day
Beginning: Aug 1 2018 0:00	End: Aug 31 2018 0:00
Girder 7	Baseline : Aug 1 2018 09:00
Bent 2	Case: Expansion support (4 span)

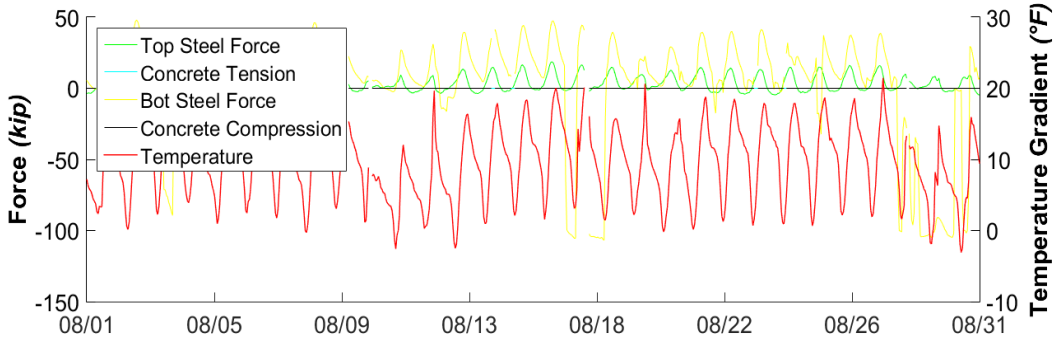

Bent 3	Case: Expansion support (4 span)

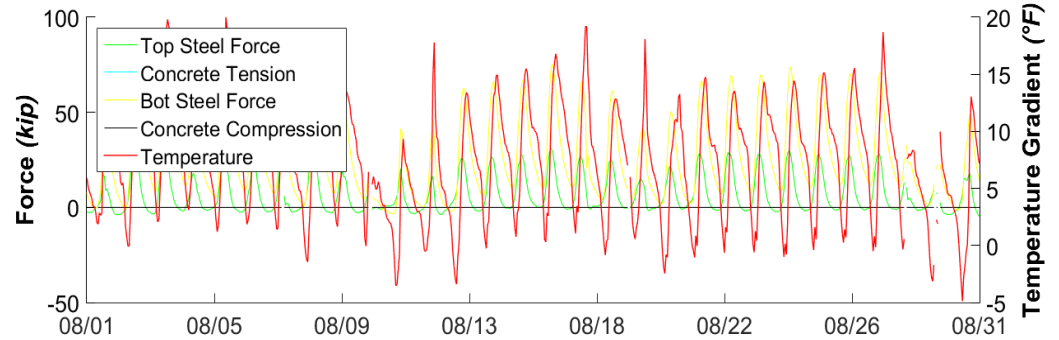

Bent 4	Case: Expansion support (4 span)

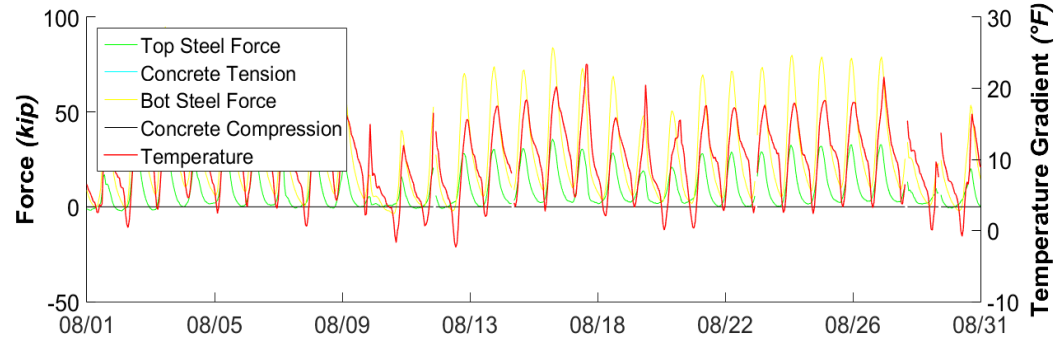

Forces	Period: 30 day
Bent 15	**Case: Expansion support (2 span)**

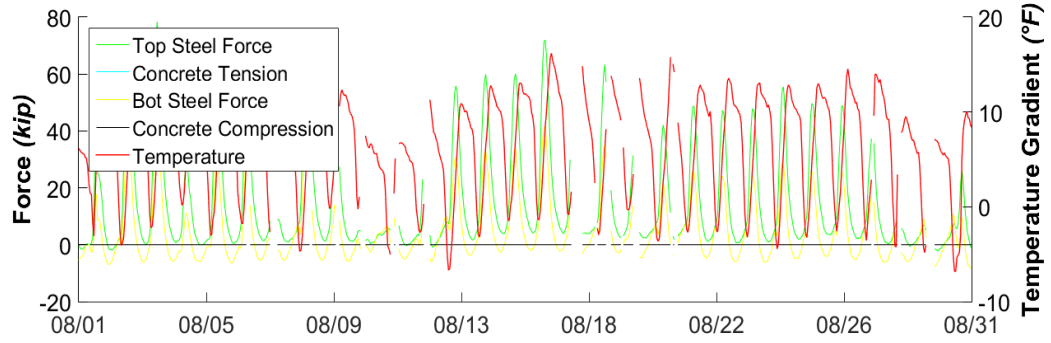

Bent 17	Case: Expansion support (2 span)

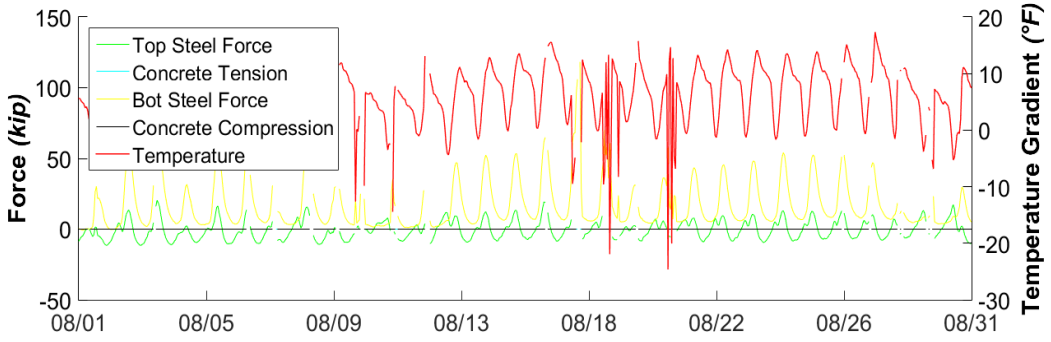

Bent 19	Case: Fixed support (2 span)

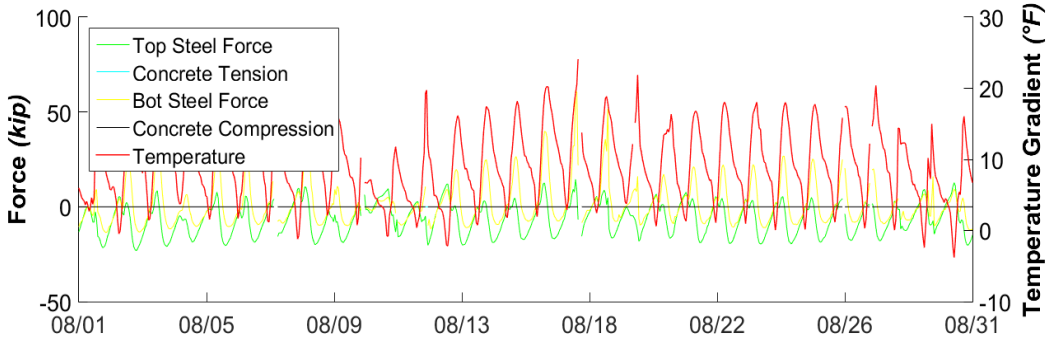

Girder 4	Baseline: Aug 1 2018 09:00
Bent 2	**Case: Expansion support (4 span)**

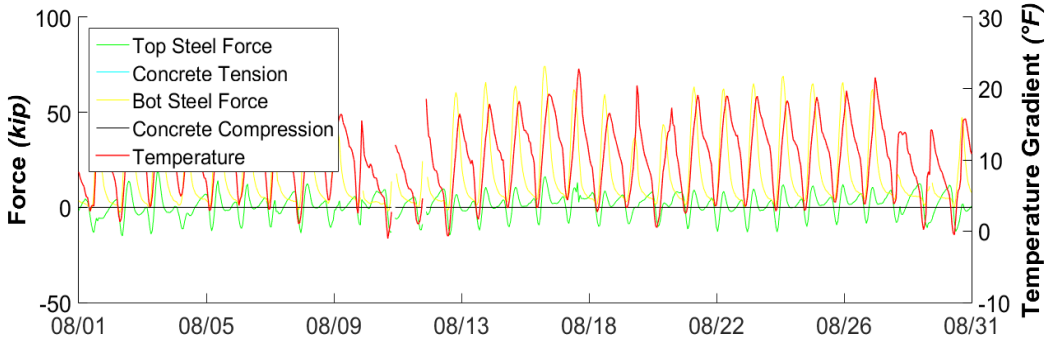

Bent 3	Case: Expansion support (4 span)

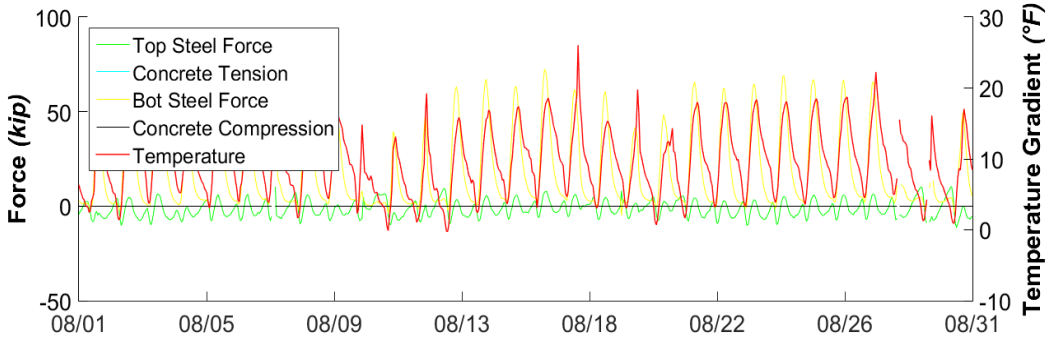

Bent 4	Case: Expansion support (4 span)

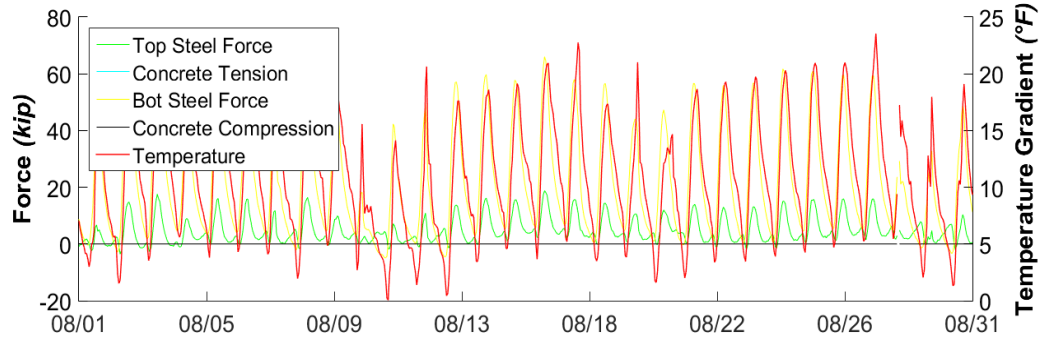

Bent 15	Case: Expansion support (2 span)

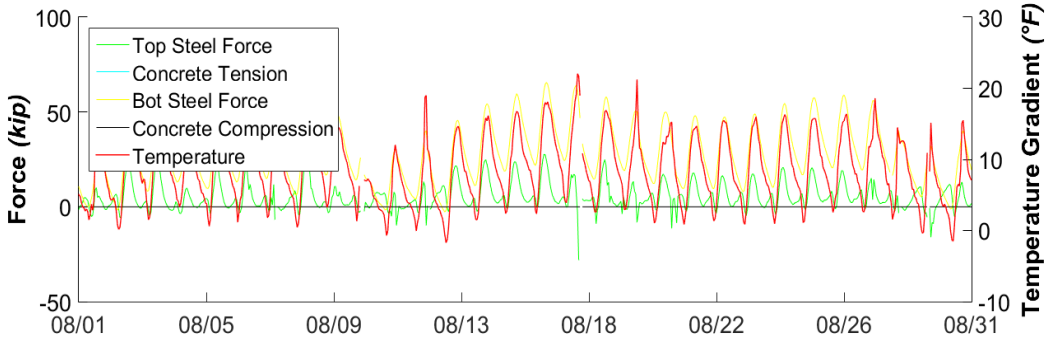

Girder 4	Baseline: Aug 1 2018 09:00
Bent 17	**Case: Expansion support (2 span)**

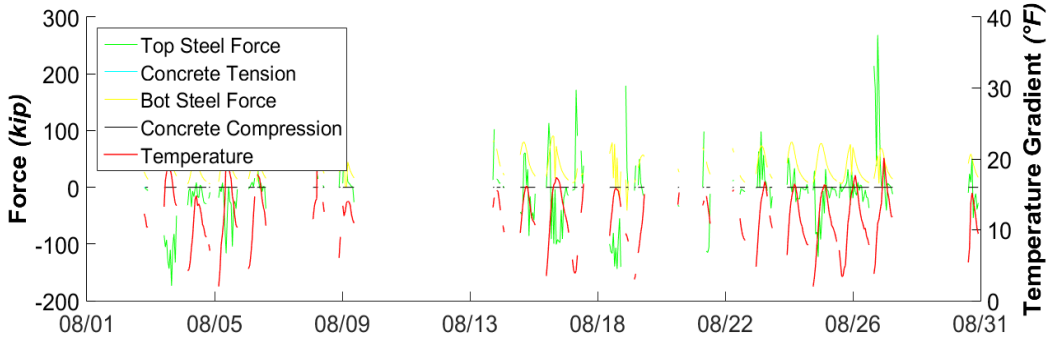

Bent 19	Case: Fixed support (2 span)

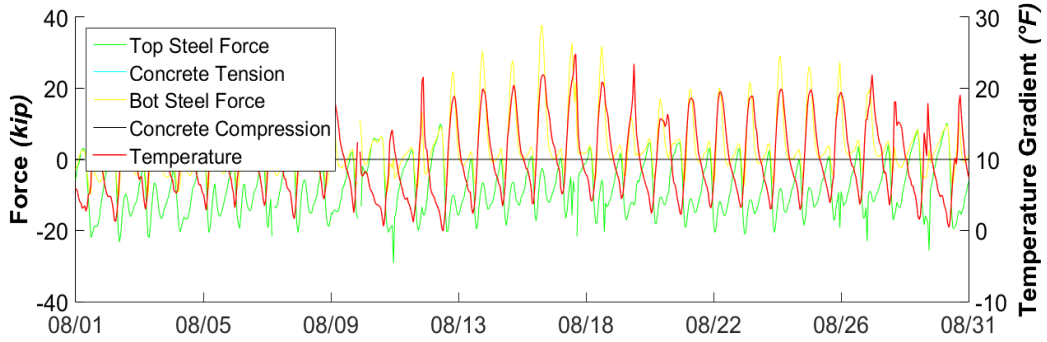

Forces	Period: 24 hrs.
Beginning: Jan 1 2018 0:00	End: Jan 2 2018 0:00
Girder 7	Baseline : Jan 2 2018 00:00
Bent 2	Case: Expansion support (4 span)

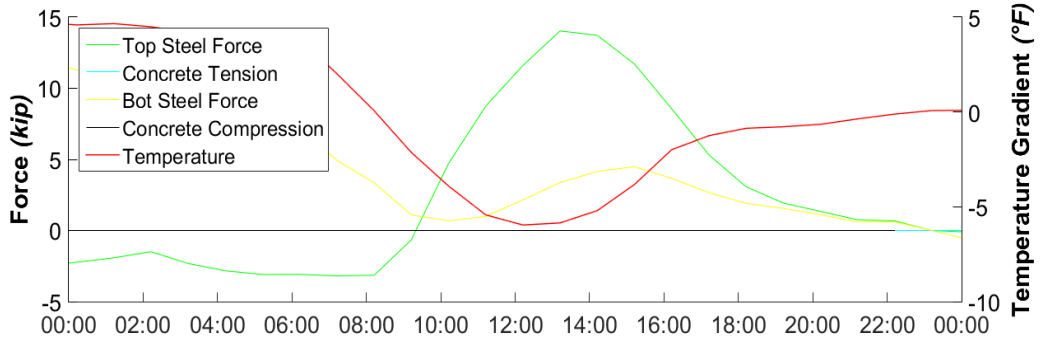

Bent 3	Case: Expansion support (4 span)

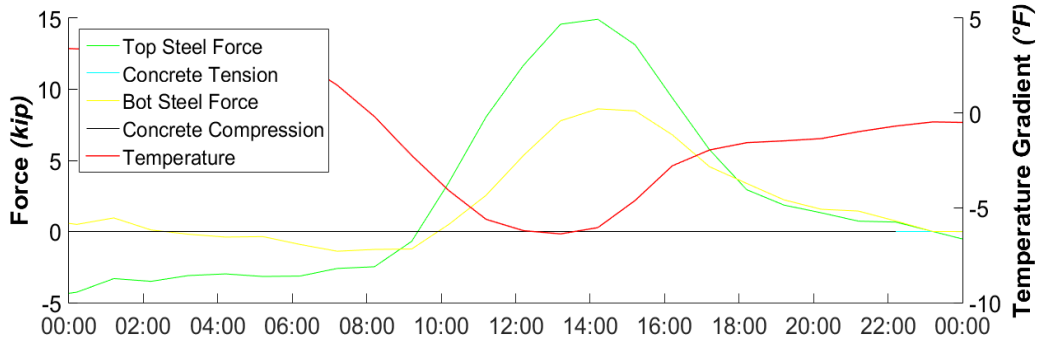

Bent 4	Case: Expansion support (4 span)

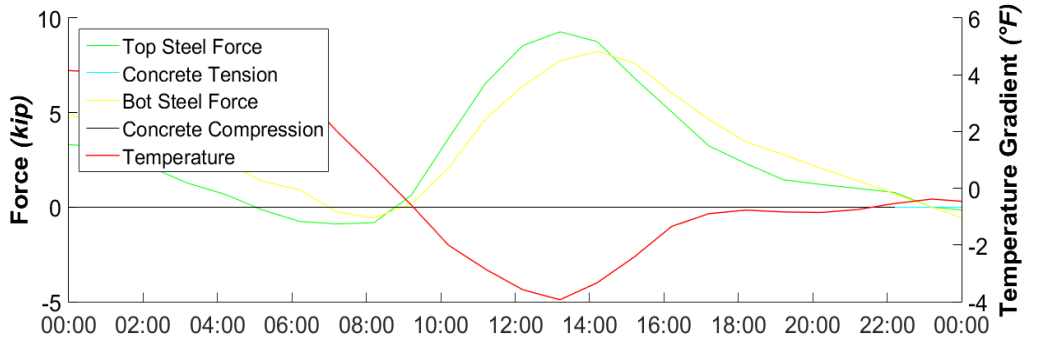

Forces	Period: 24 hrs.
Bent 15	**Case: Expansion support (2 span)**

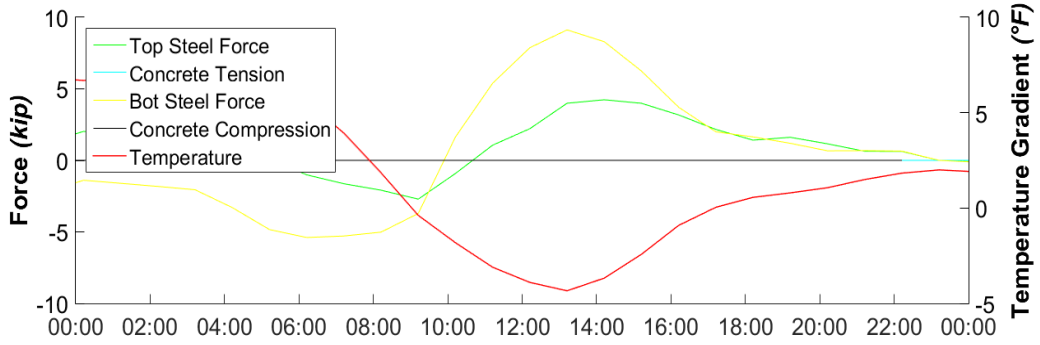

Bent 17	Case: Expansion support (2 span)

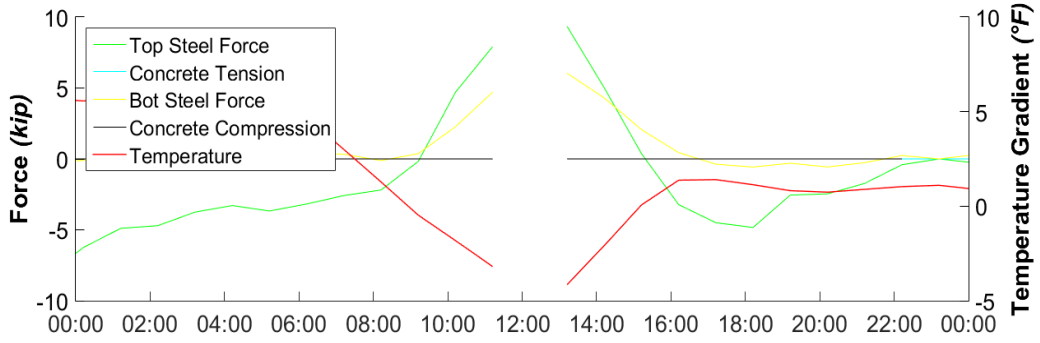

Bent 19	Case: Fixed support (2 span)

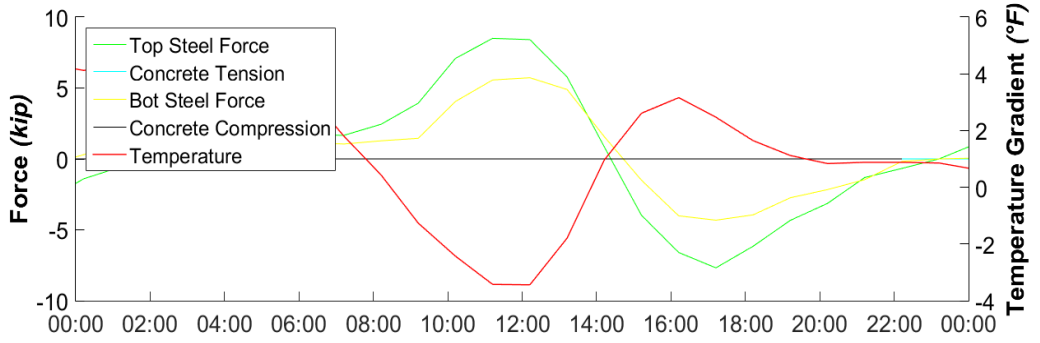

Girder 4	Baseline: Jan 2 2018 00:00
Bent 2	**Case: Expansion support (4 span)**

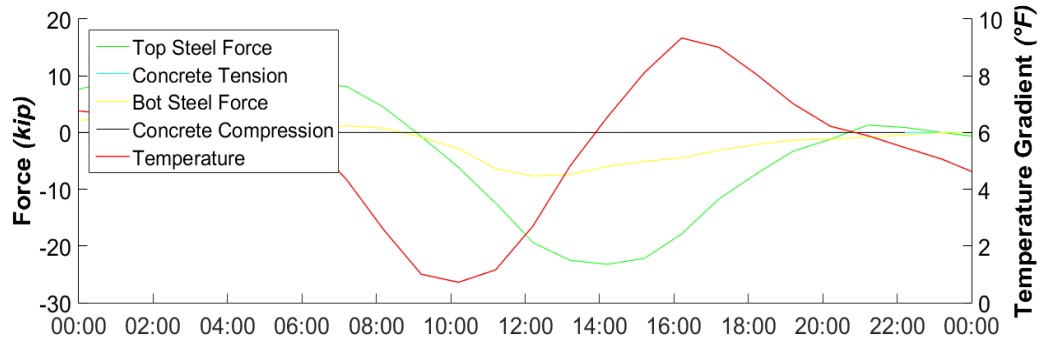

Bent 3	Case: Expansion support (4 span)

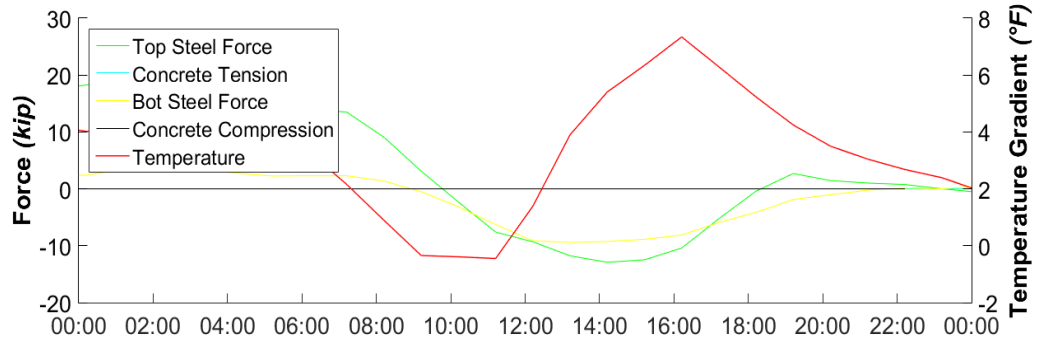

Bent 4	Case: Expansion support (4 span)

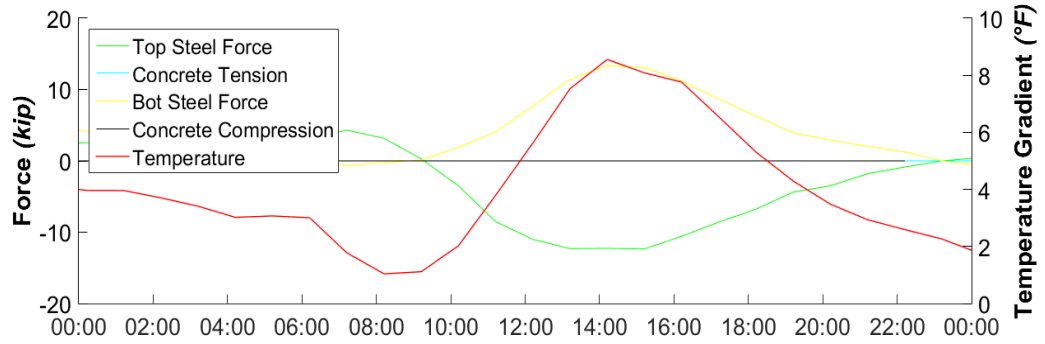

Bent 15	Case: Expansion support (2 span)

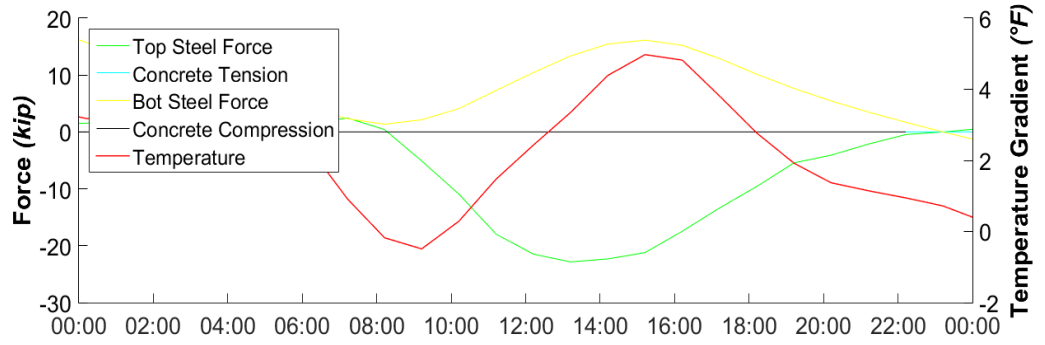

Girder 4	Baseline: Jan 2 2018 00:00
Bent 17	**Case: Expansion support (2 span)**

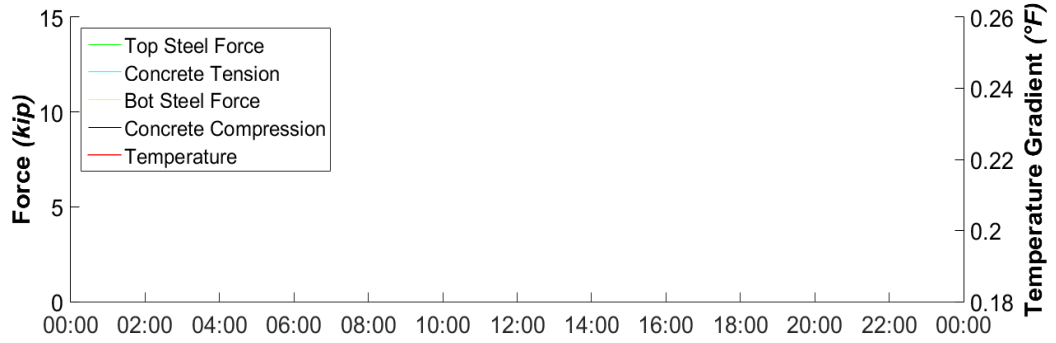

Bent 19	Case: Fixed support (2 span)

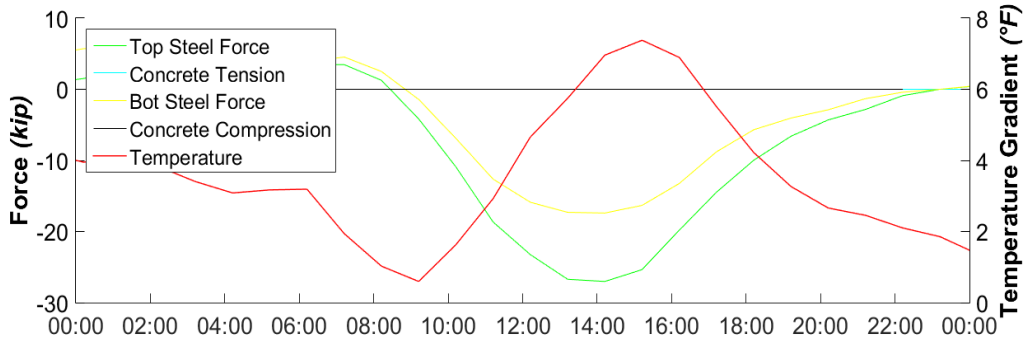

Link slab Force	Period: 24 hrs.
Beginning: Aug 1 2018 0:00	End: Aug 2 2018 0:00
Girder 7	Baseline : Aug 1 2018 9:00
Bent 2	Case: Expansion support (4 span)

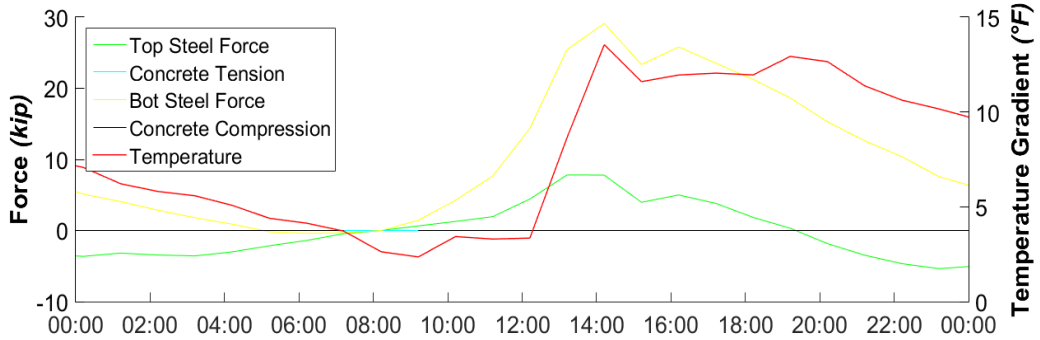

Bent 3	Case: Expansion support (4 span)

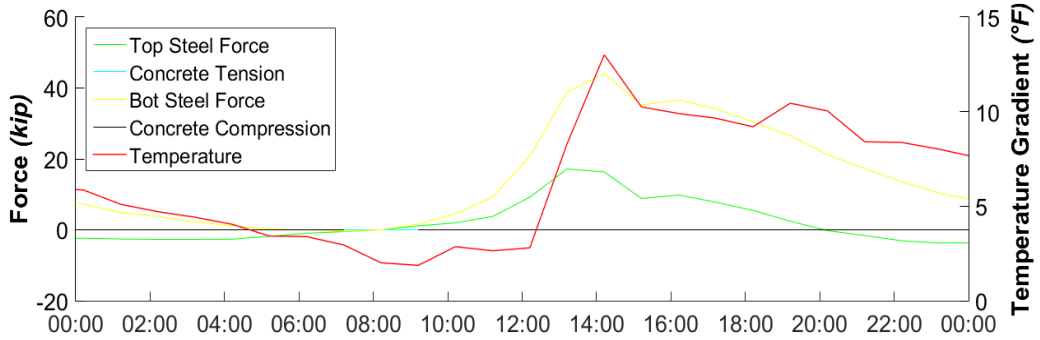

Bent 4	Case: Expansion support (4 span)

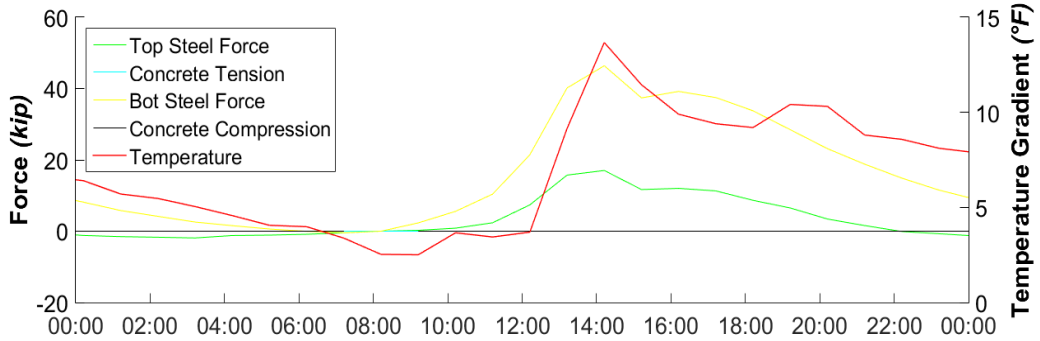

Link slab Force	Period: 24 hrs.
Bent 15	**Case: Expansion support (2 span)**

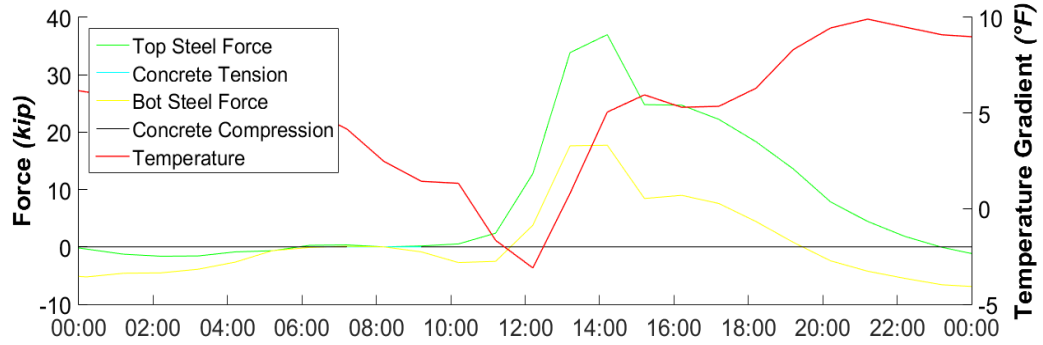

Bent 17	Case: Expansion support (2 span)

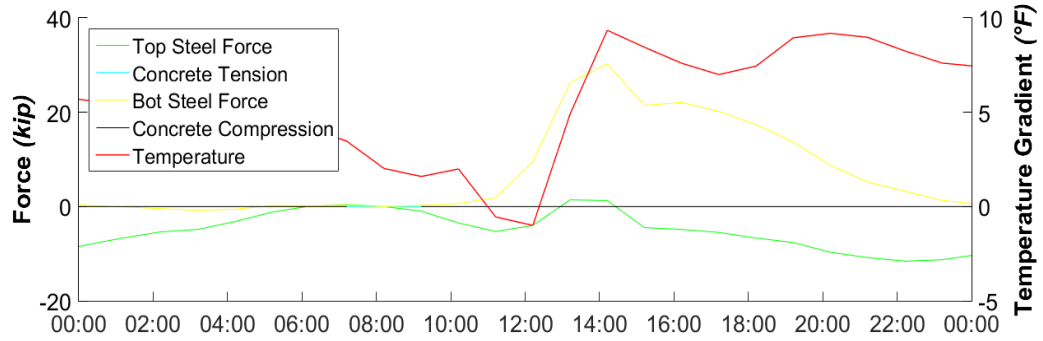

Bent 19	Case: Fixed support (2 span)

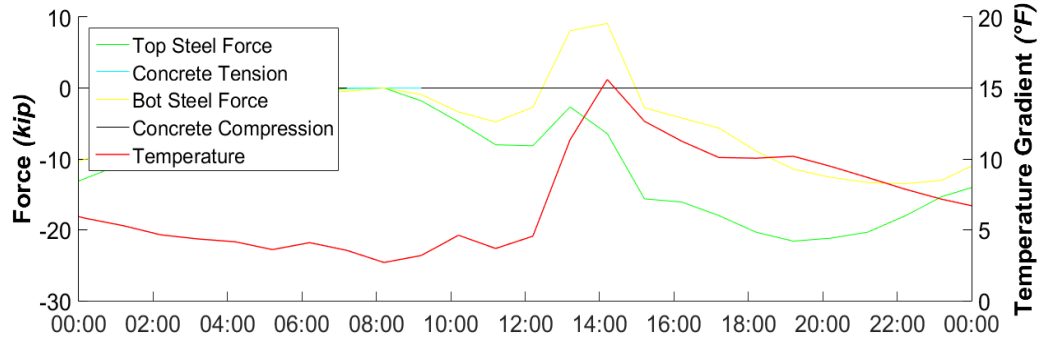

Girder 4	Baseline: Aug 1 2018 9:00
Bent 2	**Case: Expansion support (4 span)**

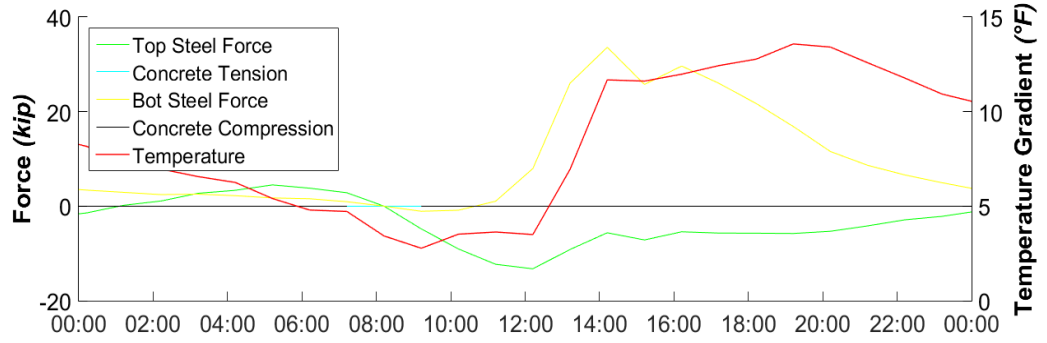

Bent 3	Case: Expansion support (4 span)

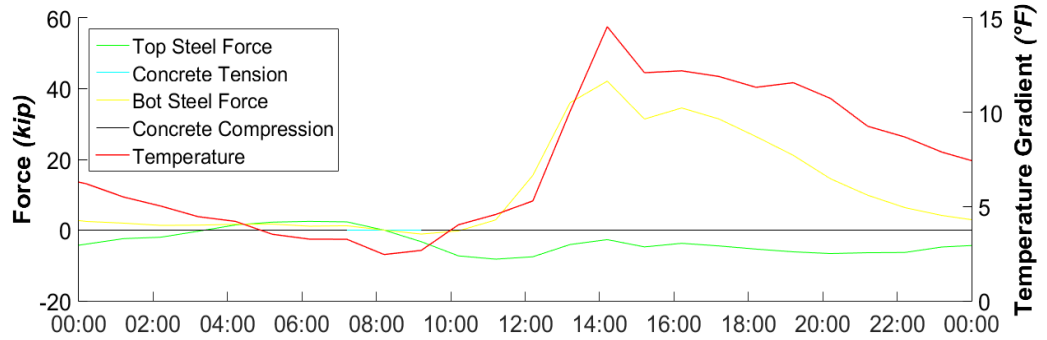

Bent 4	Case: Expansion support (4 span)

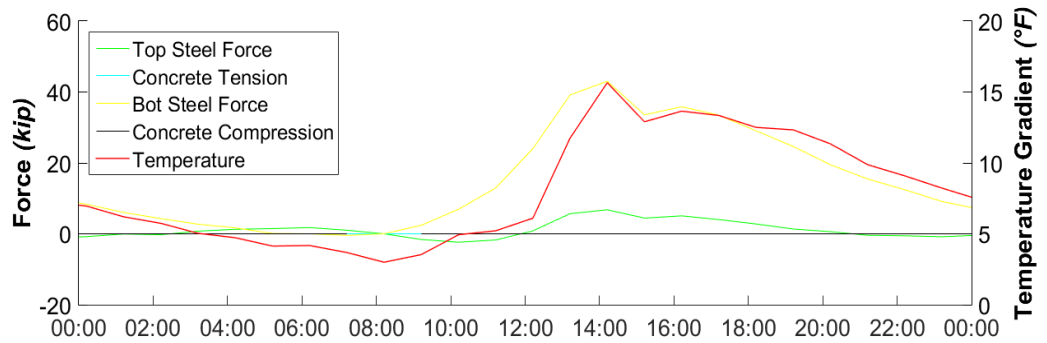

Bent 15	Case: Expansion support (2 span)

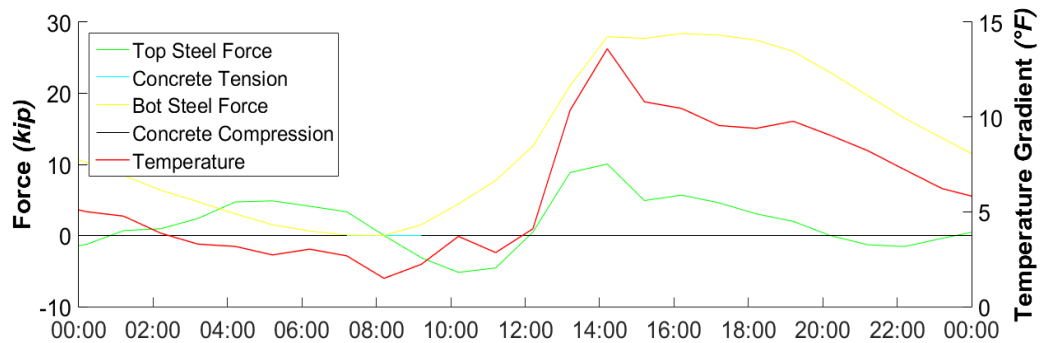

Girder 4	Baseline: Aug 1 2018 9:00
Bent 17	**Case: Expansion support (2 span)**

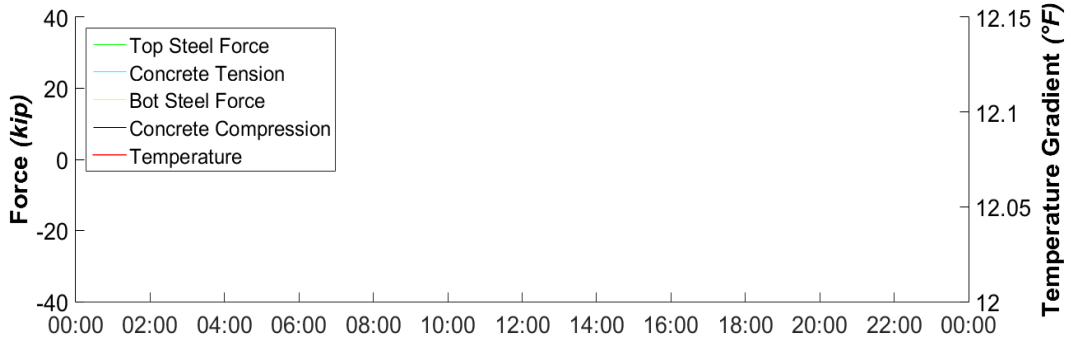

Bent 19	Case: Fixed support (2 span)

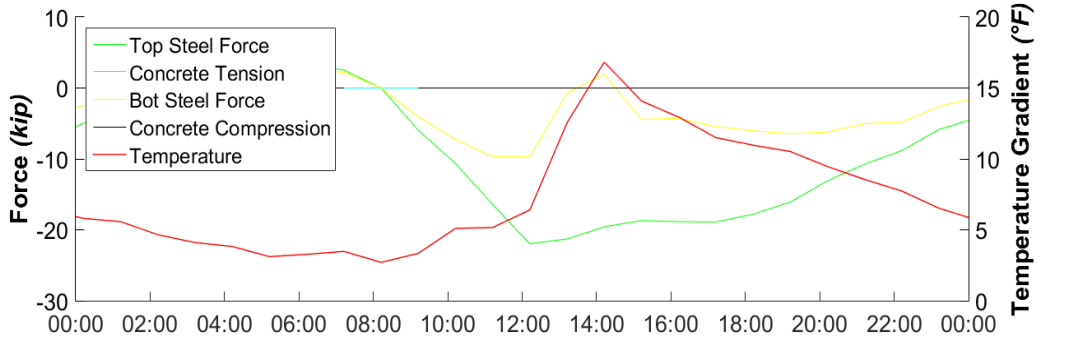

Link Slab Force

Link slab Force	**Period: Full Range**
Beginning: Pour Date	**End: Feb 15 2019**
Temperature	

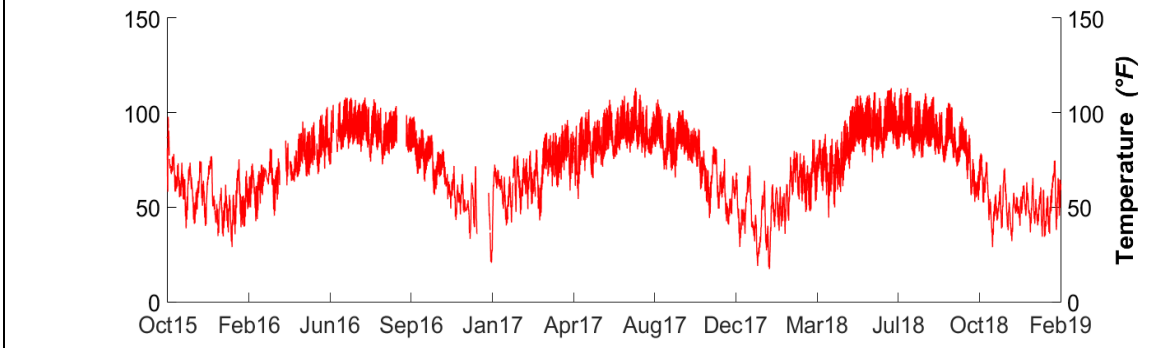

Girder 7	**Baseline : 108 Hrs after pour date**
Bent 2	**Case: Expansion support (4 span)**

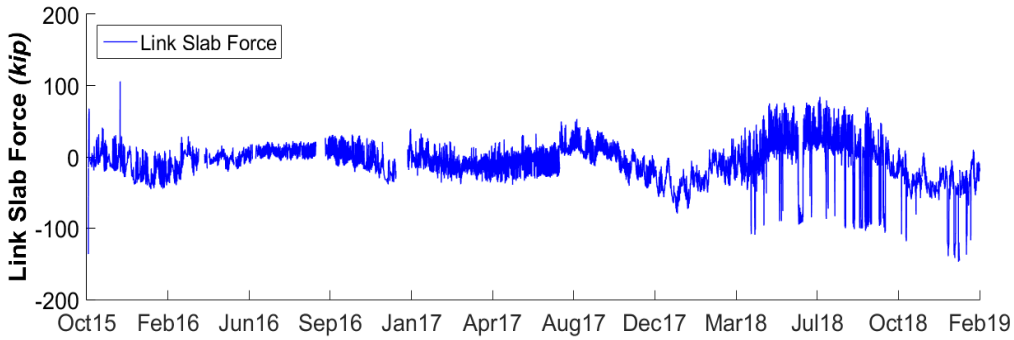

Bent 3	**Case: Expansion support (4 span)**

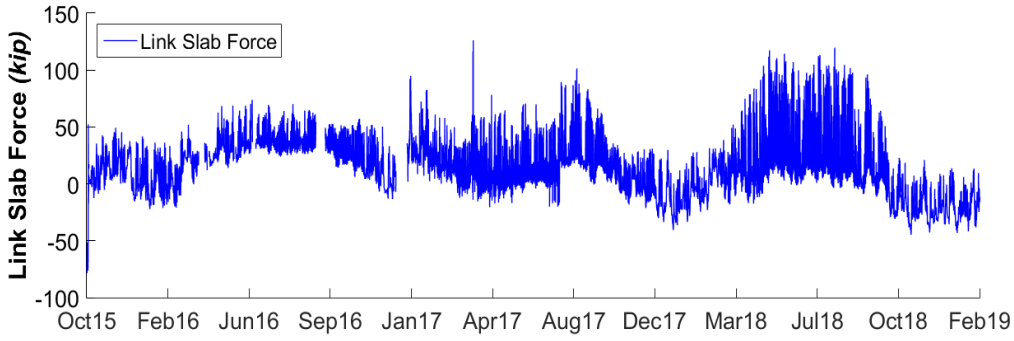

Link slab Force	Period: Full Range
Bent 4	**Case: Expansion support (4 span)**

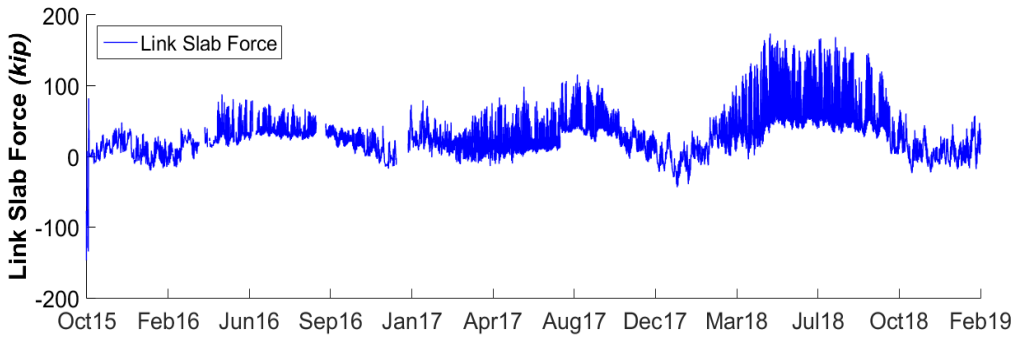

Bent 15	Case: Expansion support (2 span)

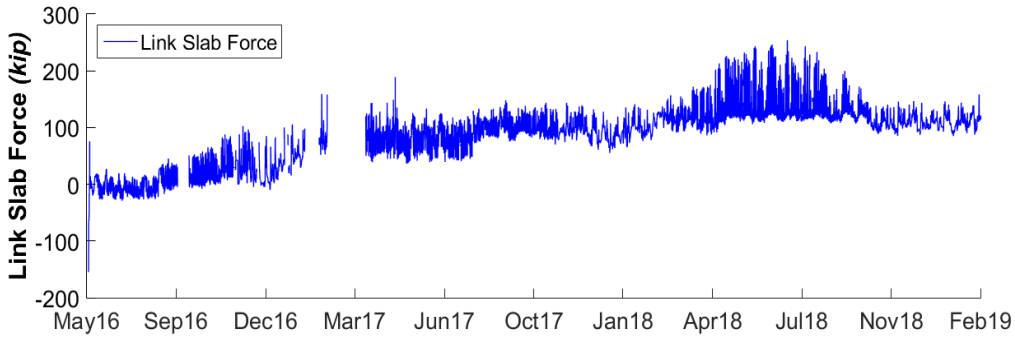

Bent 17	Case: Expansion support (2 span)

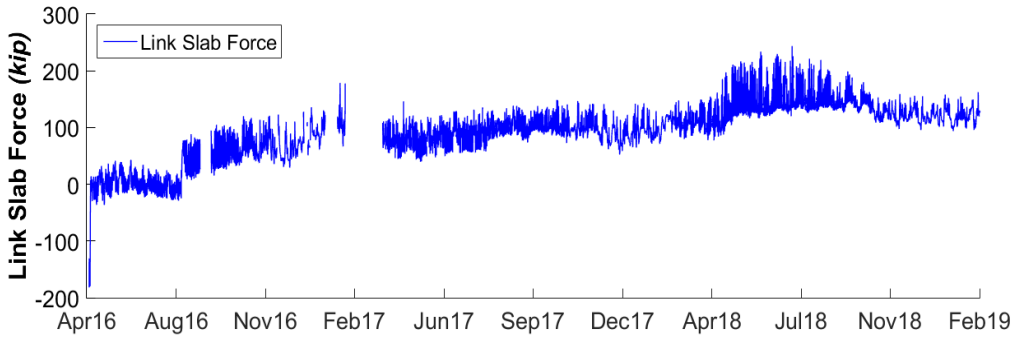

Bent 19	Case: Fixed support (2 span)

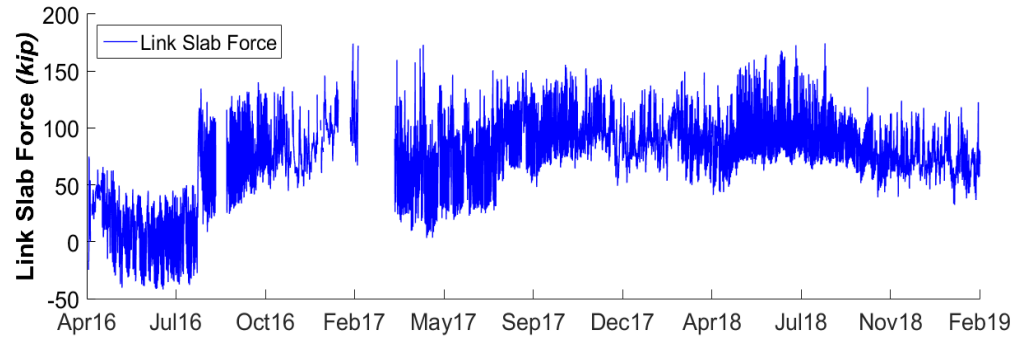

Girder 4	Baseline: 108 Hrs after pour date
Bent 2	**Case: Expansion support (4 span)**

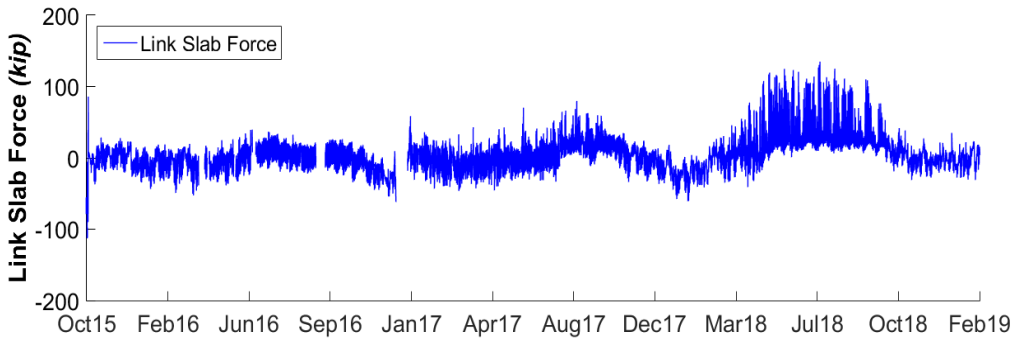

Bent 3	Case: Expansion support (4 span)

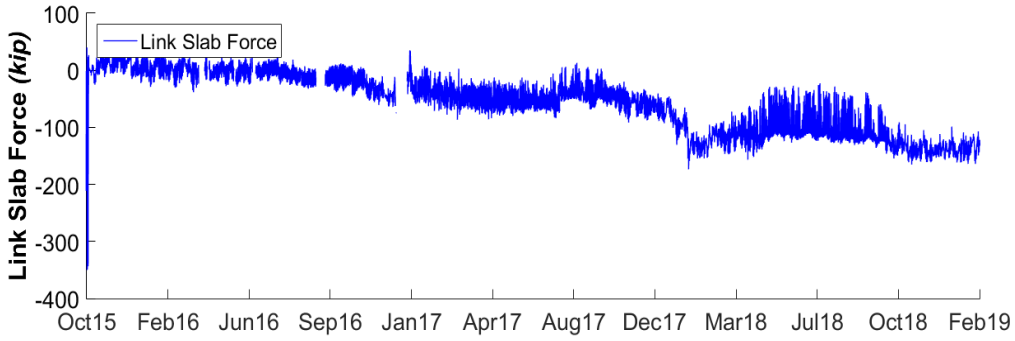

Bent 4	Case: Expansion support (4 span)

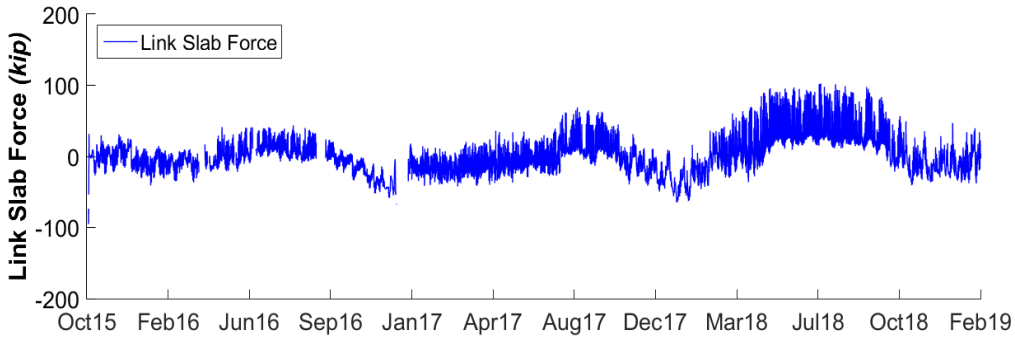

Bent 15	Case: Expansion support (2 span)

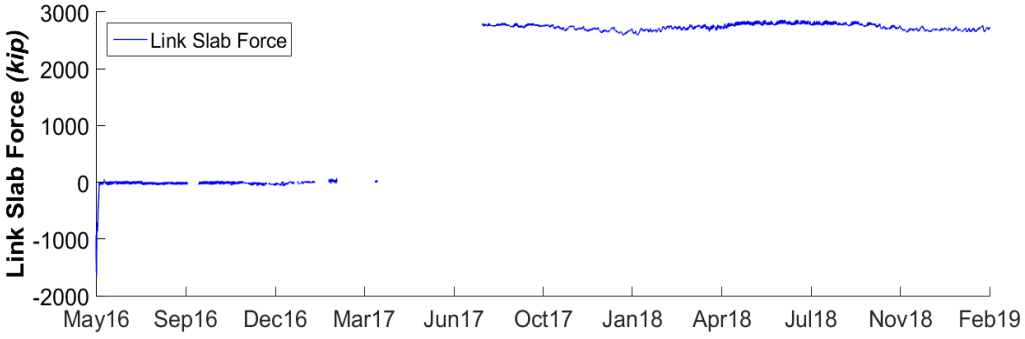

Girder 4	Baseline: 108 Hrs after pour date
Bent 17	**Case: Expansion support (2 span)**

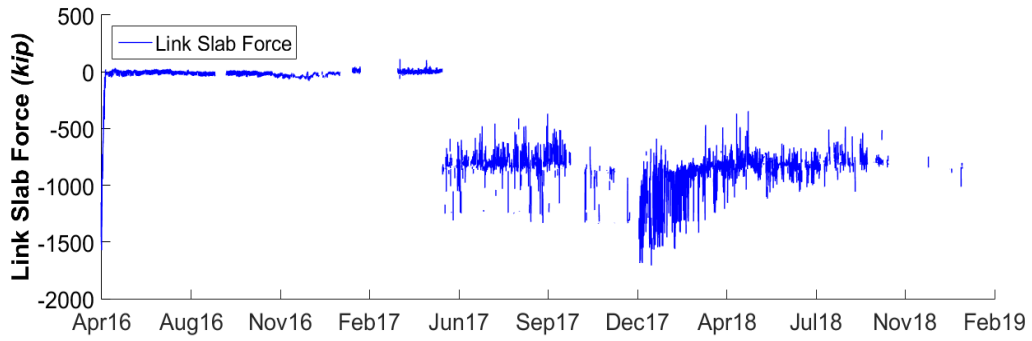

Bent 19	Case: Fixed support (2 span)

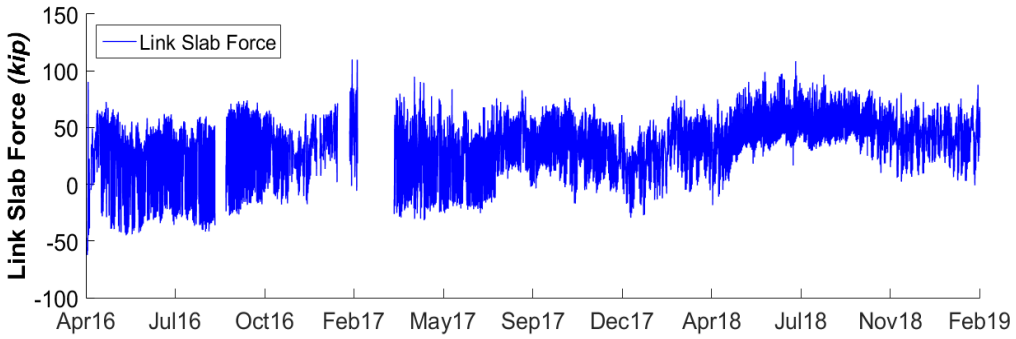

Link slab Force	**Period: 30 days**
Beginning: Aug 1 2018 0:00	**End: Aug 30 2018 0:00**
Girder 7	**Baseline : Aug 1 2018 9:00**
Bent 2	**Case: Expansion support (4 span)**

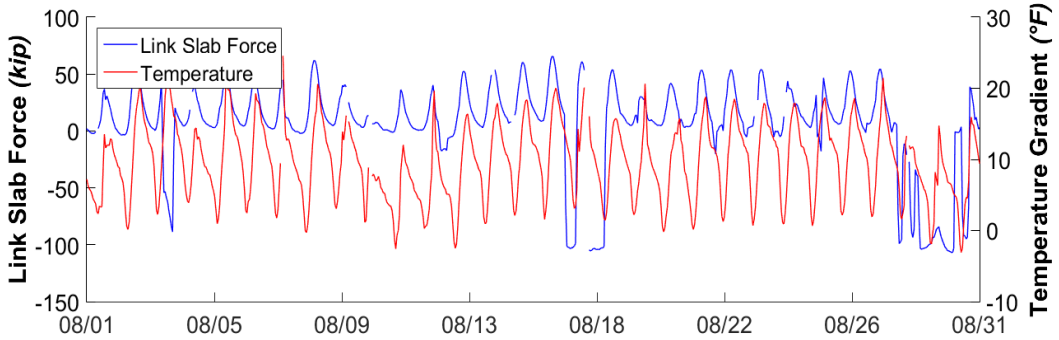

Bent 3	**Case: Expansion support (4 span)**

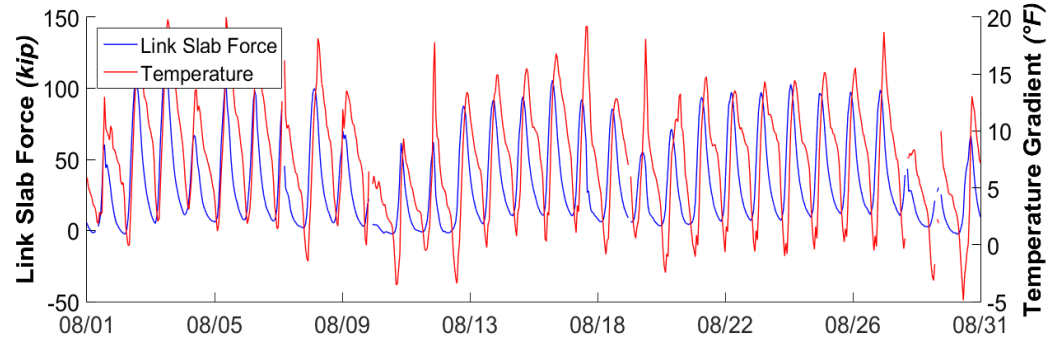

Bent 4	**Case: Expansion support (4 span)**

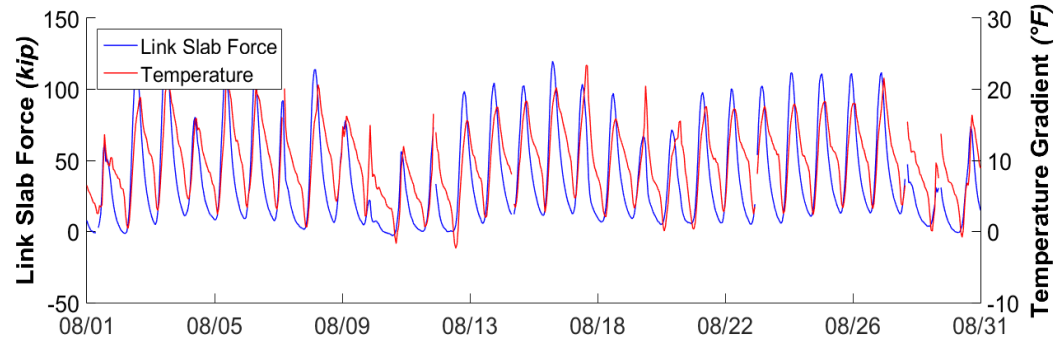

Link slab Force	Period: 30 days
Bent 15	**Case: Expansion support (2 span)**

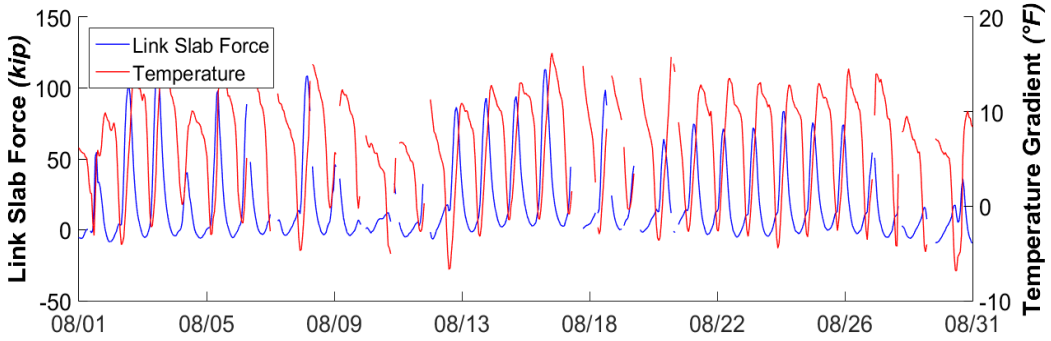

Bent 17	Case: Expansion support (2 span)

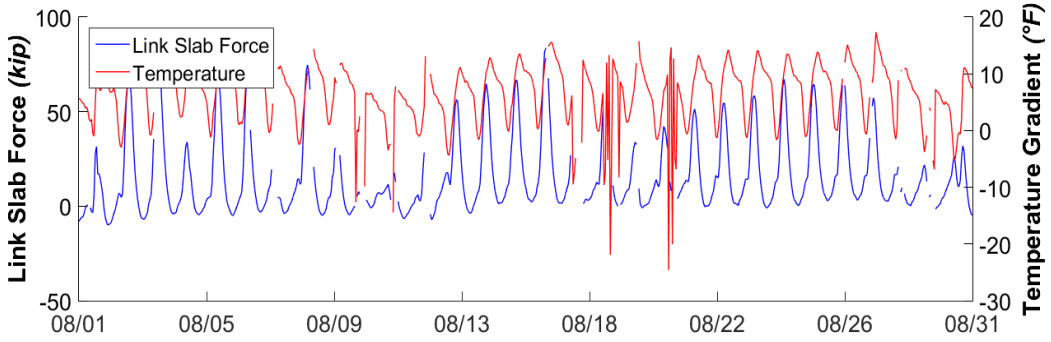

Bent 19	Case: Fixed support (2 span)

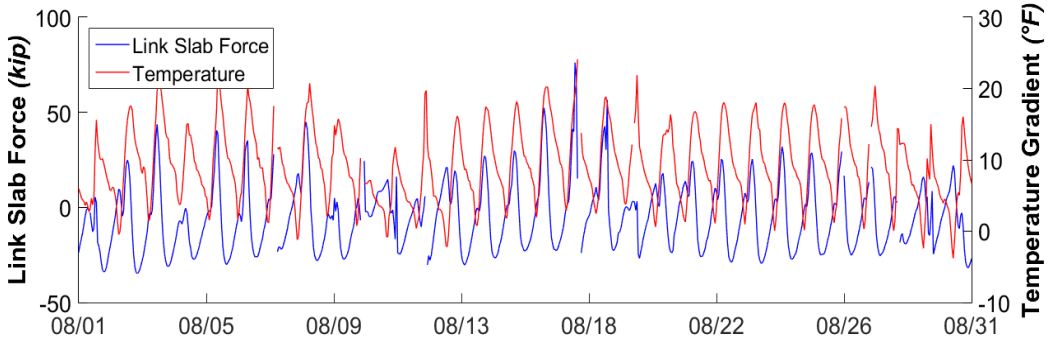

Girder 4	Baseline: Aug 1 2018 9:00
Bent 2	**Case: Expansion support (4 span)**

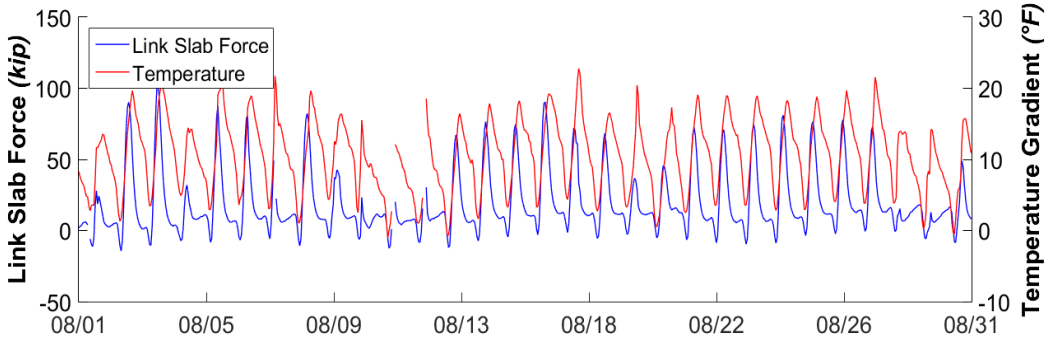

Bent 3	Case: Expansion support (4 span)

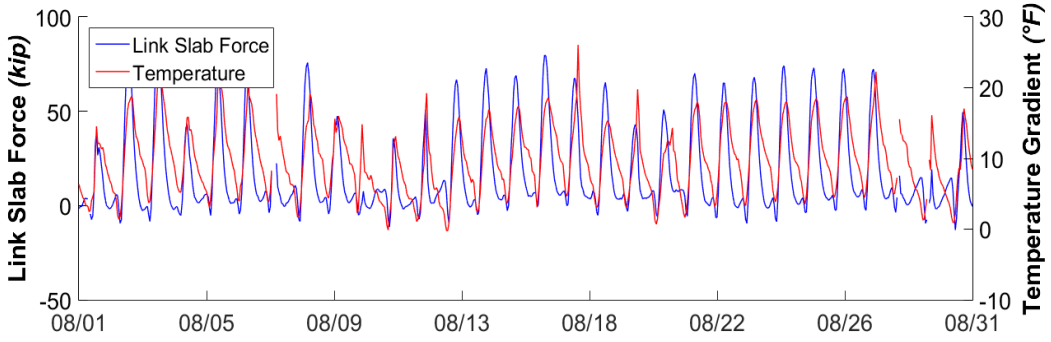

Bent 4	Case: Expansion support (4 span)

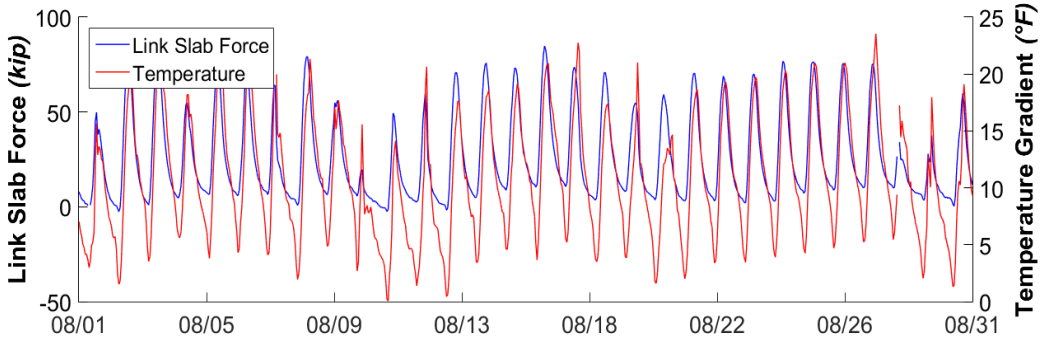

Bent 15	Case: Expansion support (2 span)

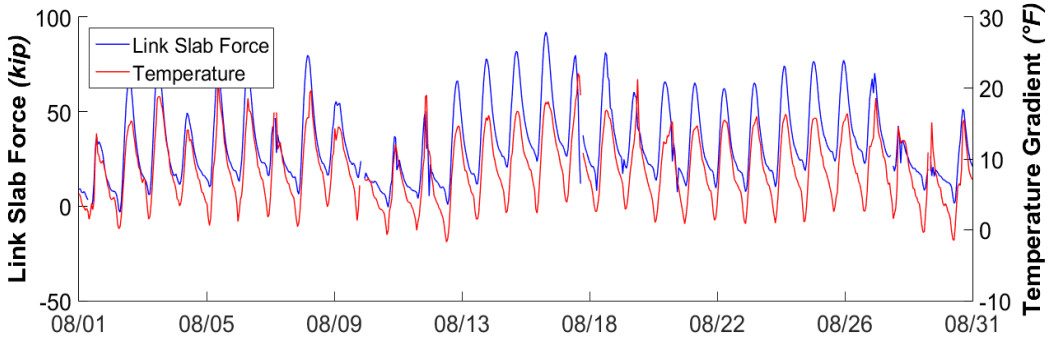

Girder 4	Baseline: Aug 1 2018 9:00
Bent 17	Case: Expansion support (2 span)

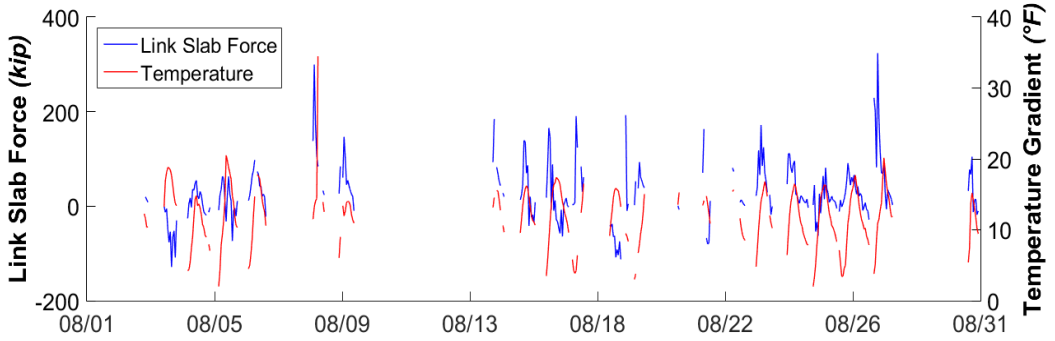

Bent 19	Case: Fixed support (2 span)

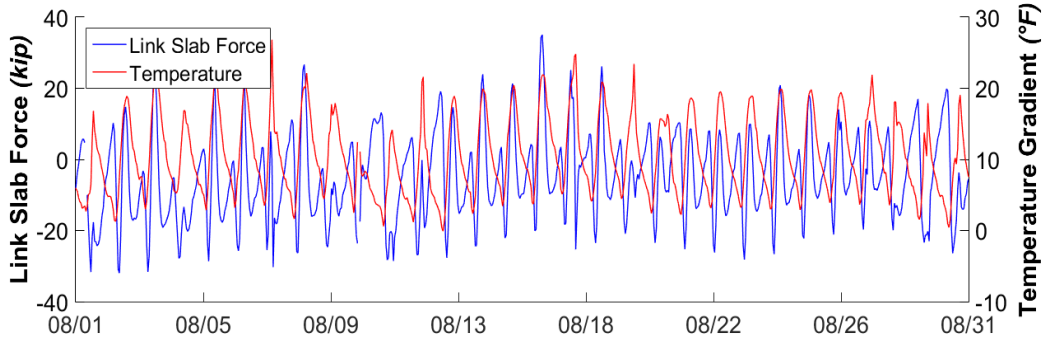

Link slab Force	Period: 30 days
Beginning: Jan 1 2018 0:00	End: Jan 31 2018 0:00
Girder 7	Baseline : Jan 2 2018 00:00
Bent 2	Case: Expansion support (4 span)

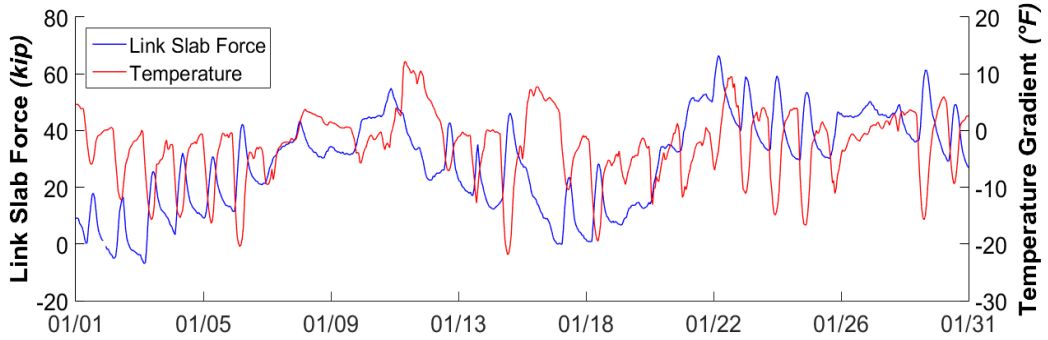

Bent 3	Case: Expansion support (4 span)

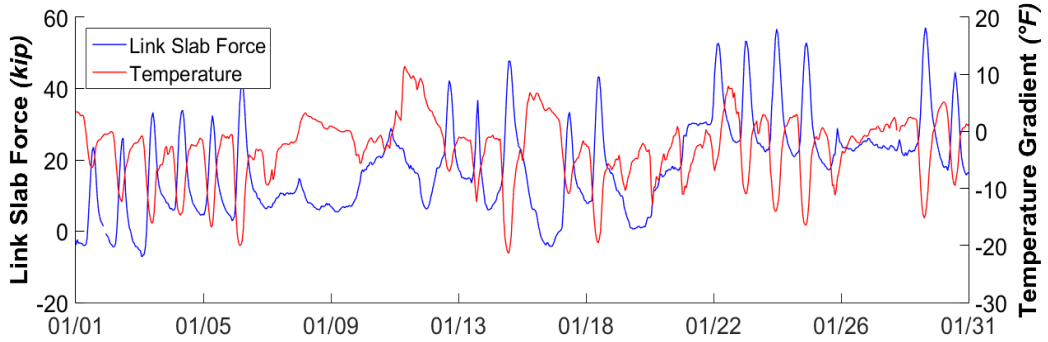

Bent 4	Case: Expansion support (4 span)

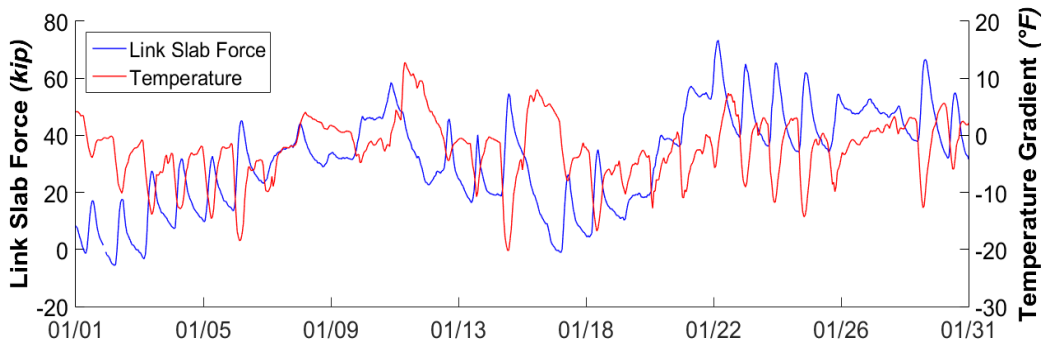

Link slab Force	Period: 30 days
Bent 15	**Case: Expansion support (2 span)**

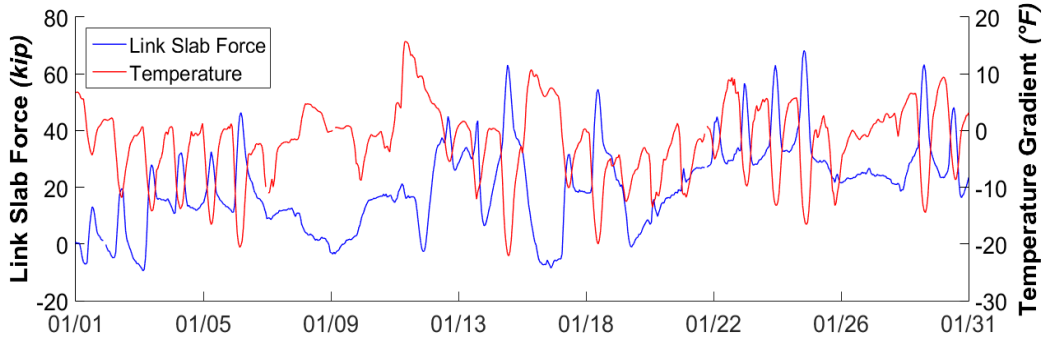

Bent 17	Case: Expansion support (2 span)

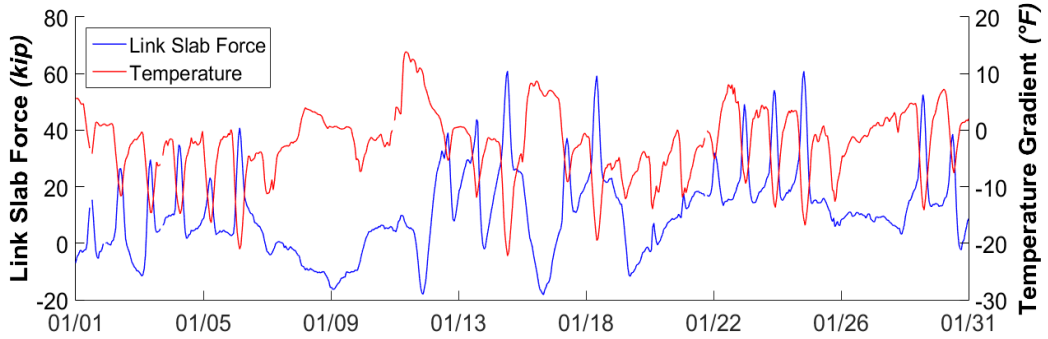

Bent 19	Case: Fixed support (2 span)

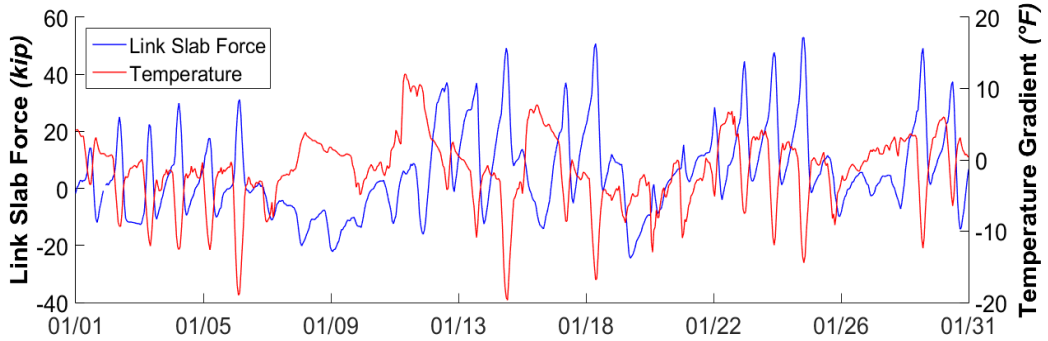

Girder 4	Baseline: Jan 2 2018 00:00
Bent 2	**Case: Expansion support (4 span)**

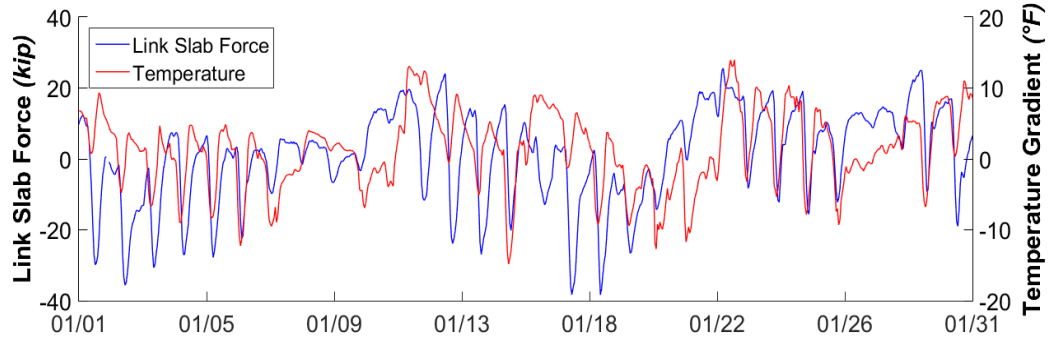

Bent 3	Case: Expansion support (4 span)

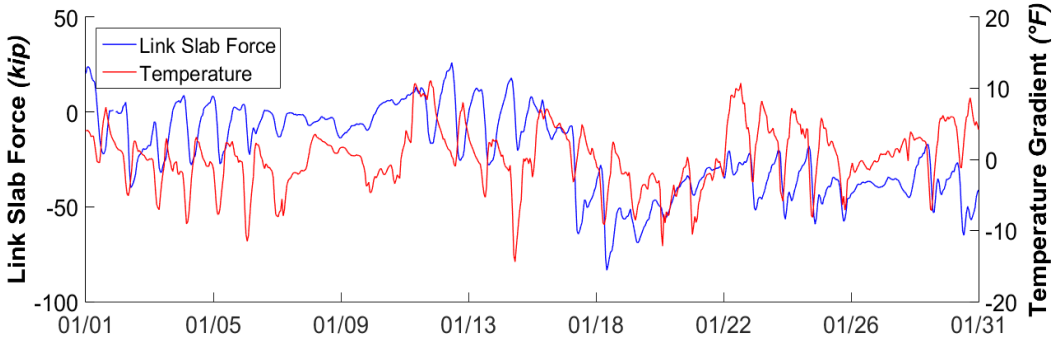

Bent 4	Case: Expansion support (4 span)

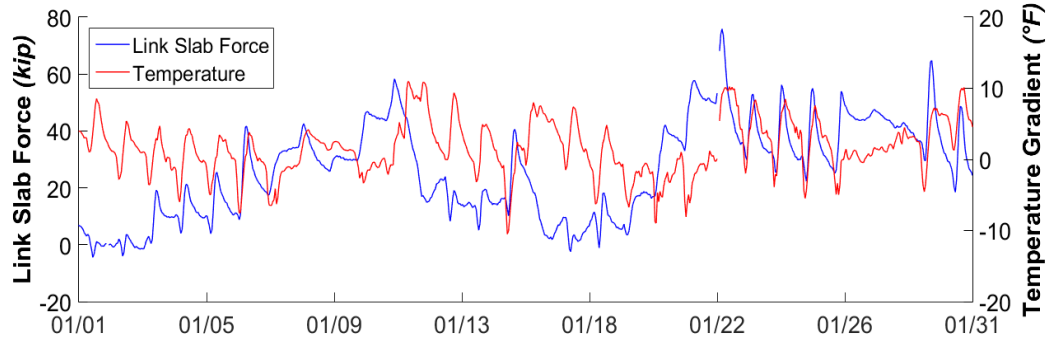

Bent 15	Case: Expansion support (2 span)

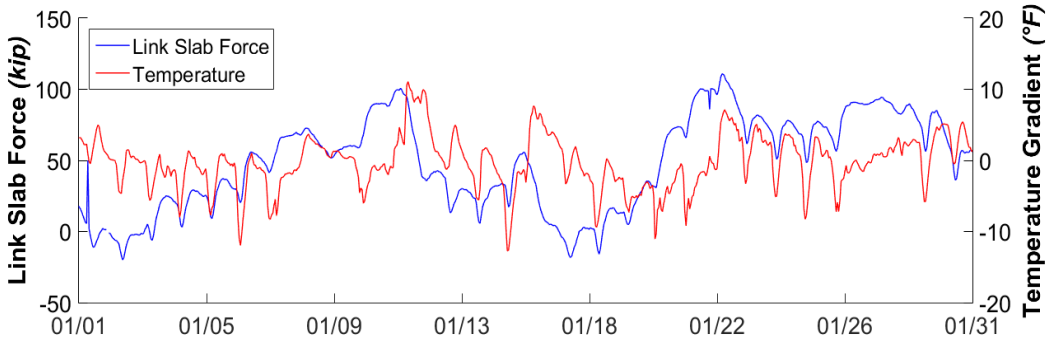

Girder 4	Baseline: Jan 2 2018 00:00
Bent 17	**Case: Expansion support (2 span)**

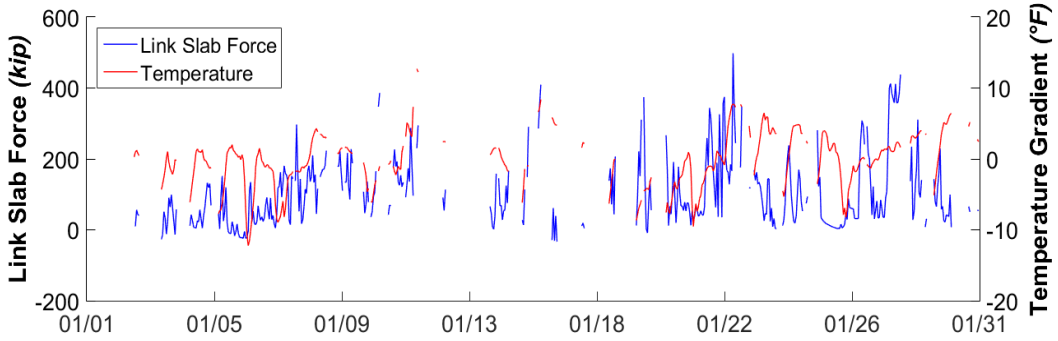

Bent 19	Case: Fixed support (2 span)

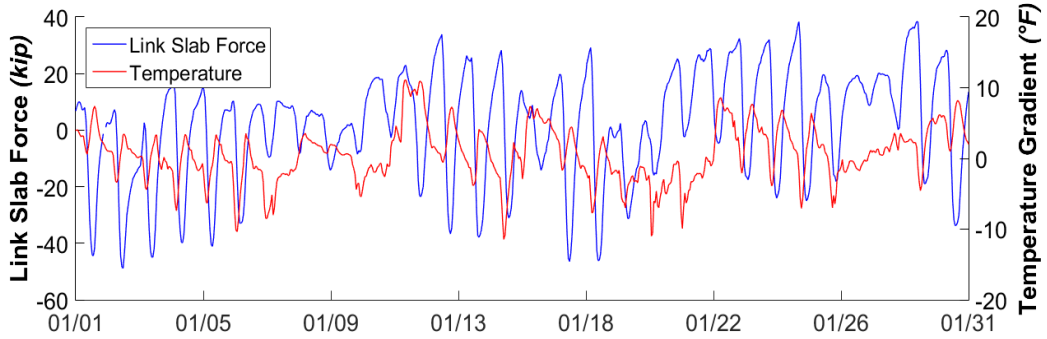

Link slab Force	Period: 24 hrs
Beginning: Jan 1 2018 0:00	End: Jan 2 2018 0:00
Girder 7	Baseline : Jan 2 2018 00:00
Bent 2	Case: Expansion support (4 span)

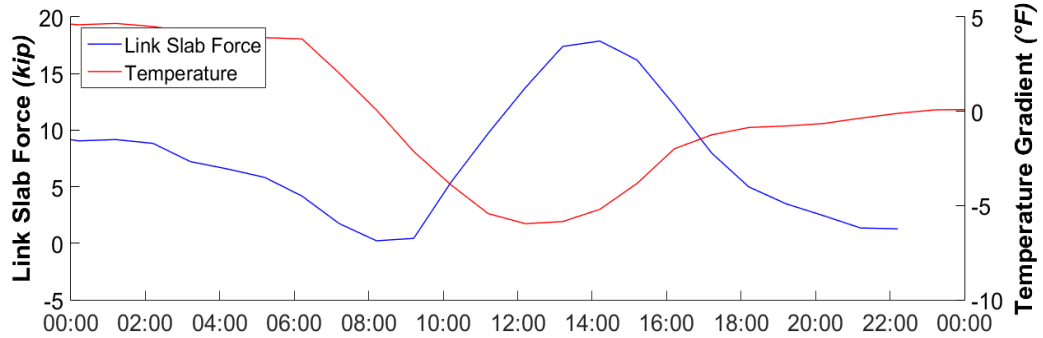

Bent 3	Case: Expansion support (4 span)

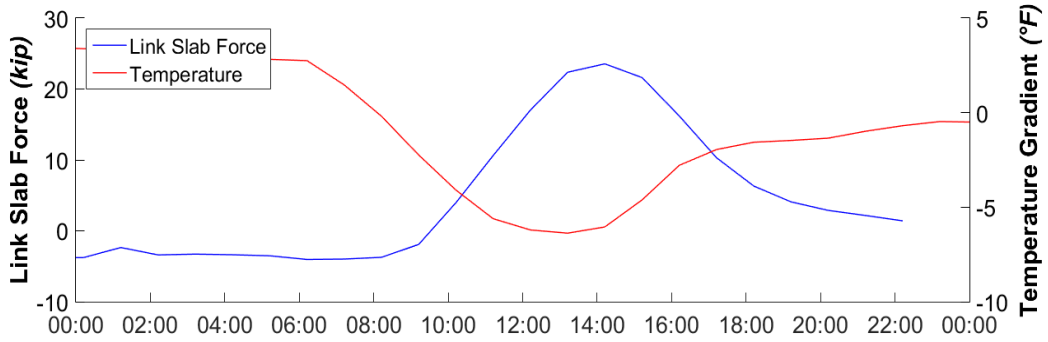

Bent 4	Case: Expansion support (4 span)

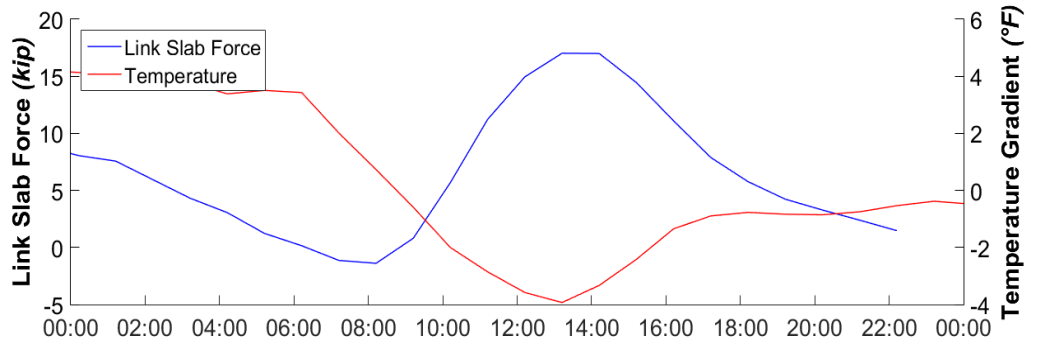

Link slab Force	Period: 24 hrs
Bent 15	**Case: Expansion support (2 span)**

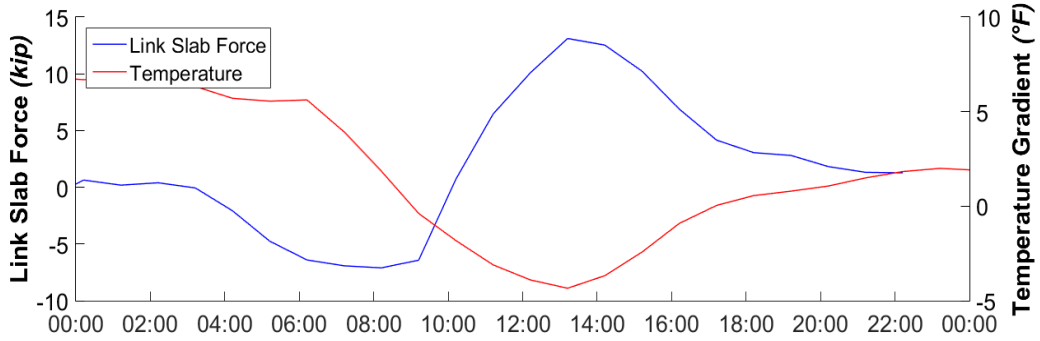

Bent 17	Case: Expansion support (2 span)

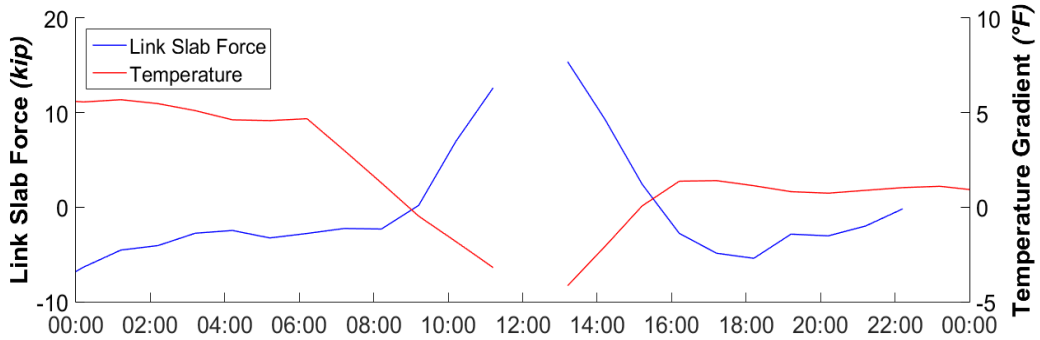

Bent 19	Case: Fixed support (2 span)

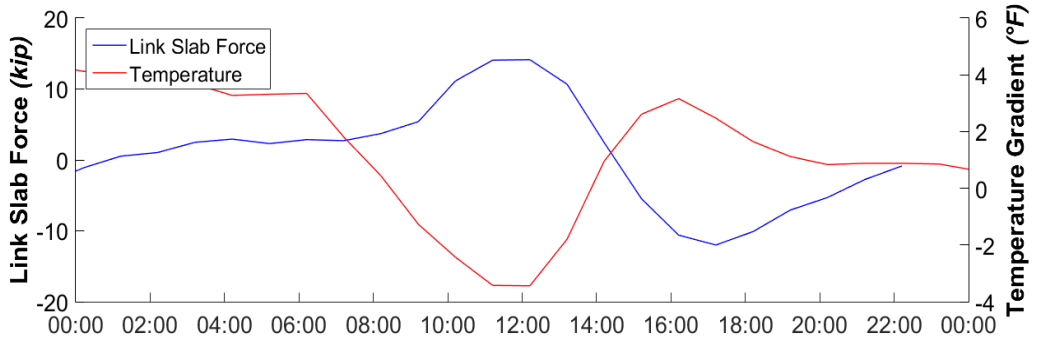

Girder 4	Baseline: Jan 2 2018 00:00
Bent 2	**Case: Expansion support (4 span)**

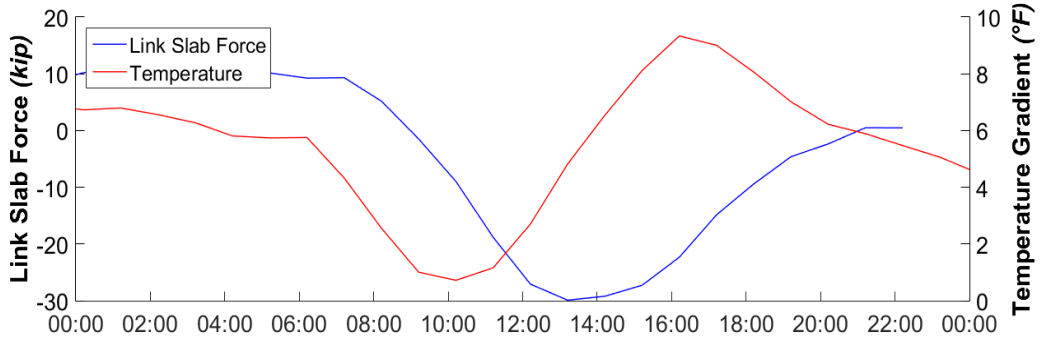

Bent 3	Case: Expansion support (4 span)

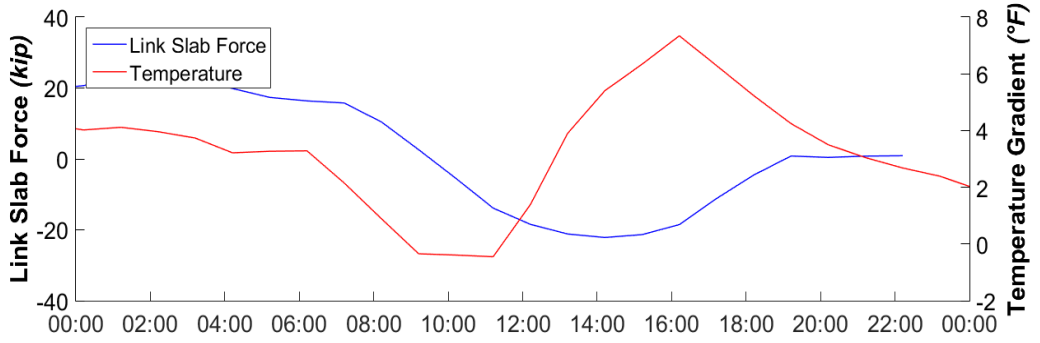

Bent 4	**Case: Expansion support (4 span)**

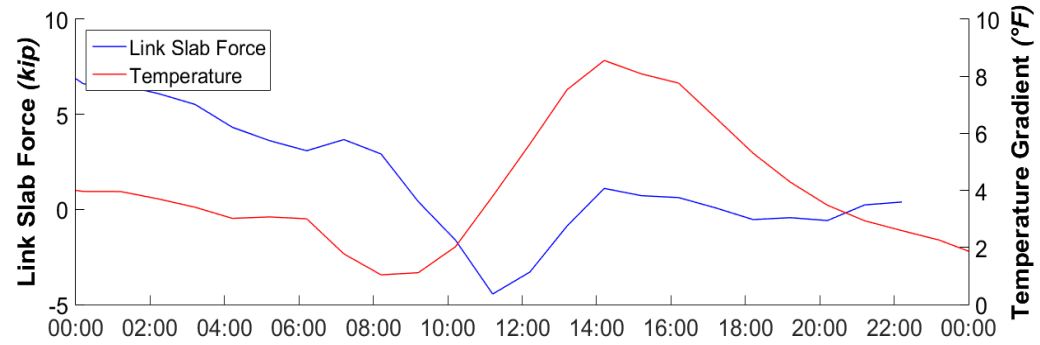

Bent 15	**Case: Expansion support (2 span)**

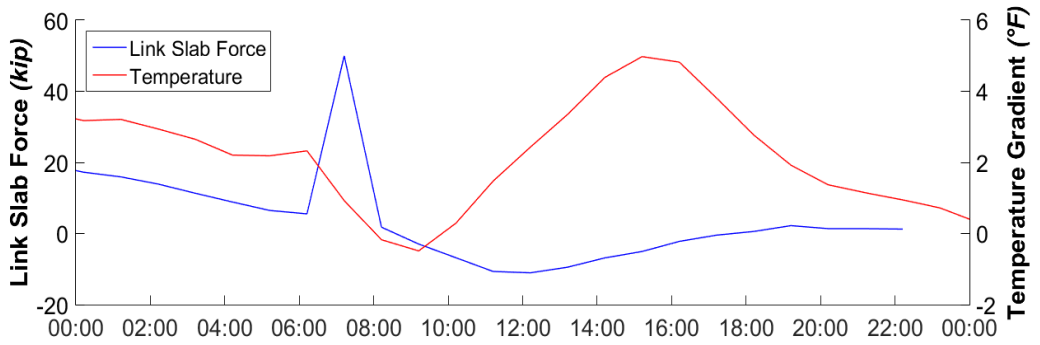

Girder 4	Baseline: Jan 2 2018 00:00
Bent 17	Case: Expansion support (2 span)

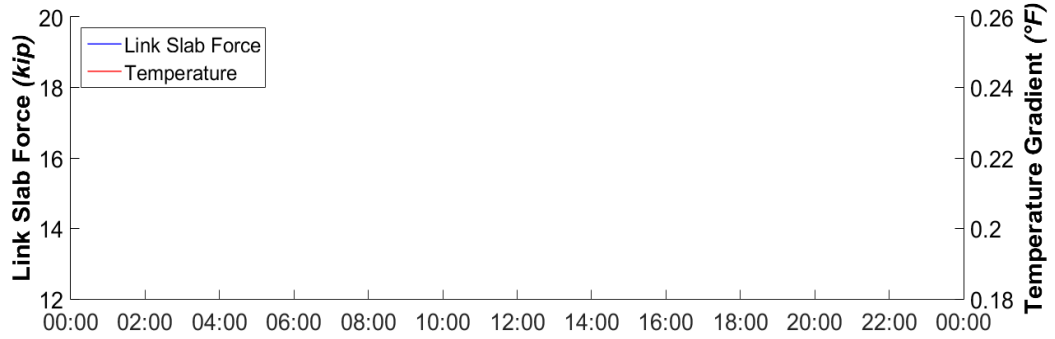

Bent 19	Case: Fixed support (2 span)

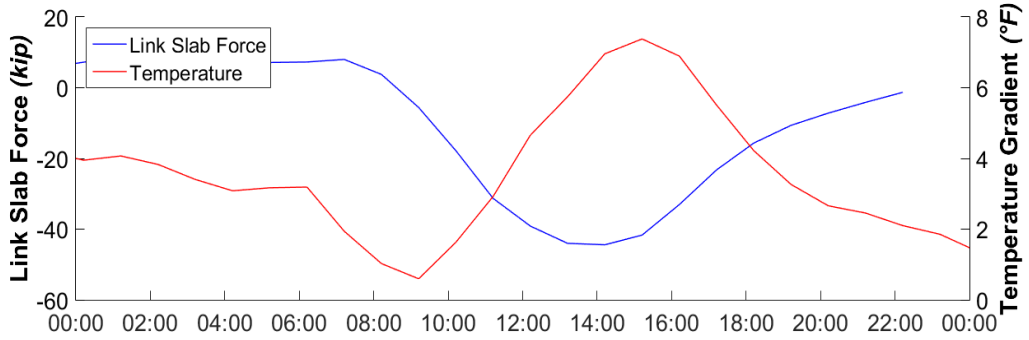

Link slab Force	Period: 24 hrs.
Beginning: Aug 1 2018 0:00	End: Aug 2 2018 0:00
Girder 7	Baseline : Aug 1 2018 9:00
Bent 2	Case: Expansion support (4 span)

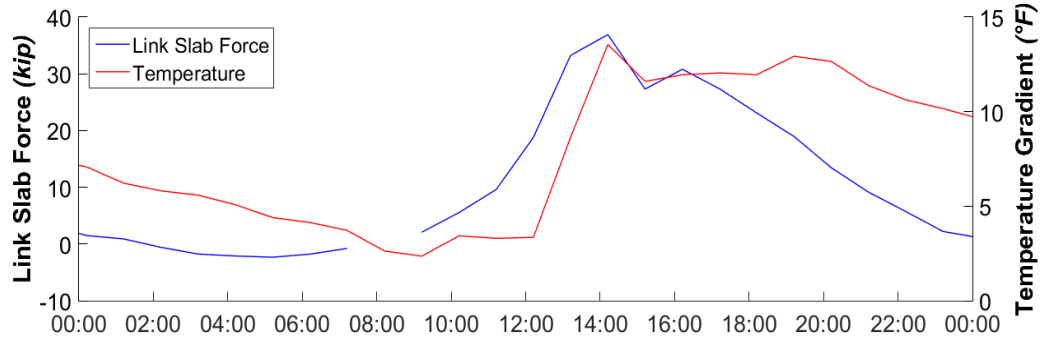

Bent 3	Case: Expansion support (4 span)

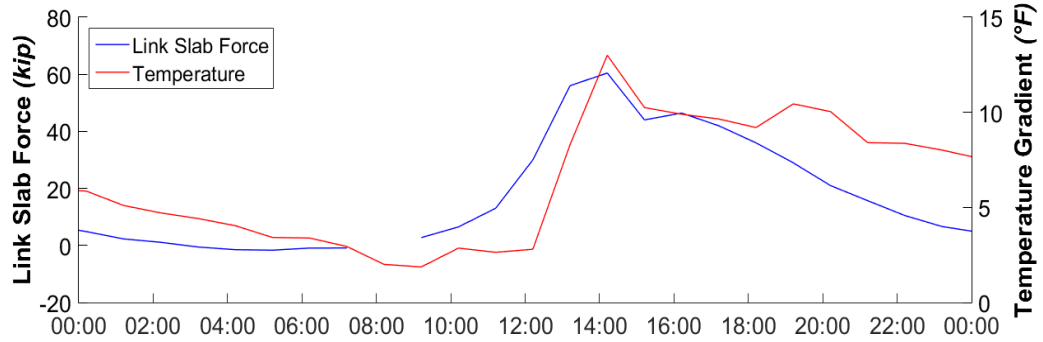

Bent 4	Case: Expansion support (4 span)

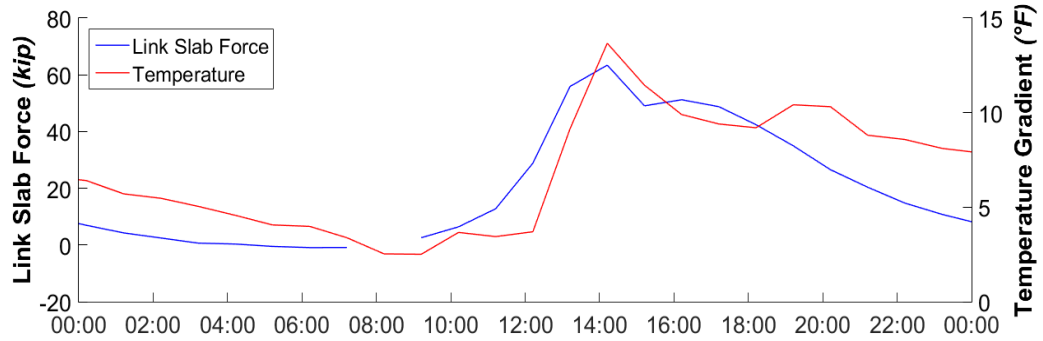

Link slab Force	Period: 24 hrs.
Bent 15	**Case: Expansion support (2 span)**

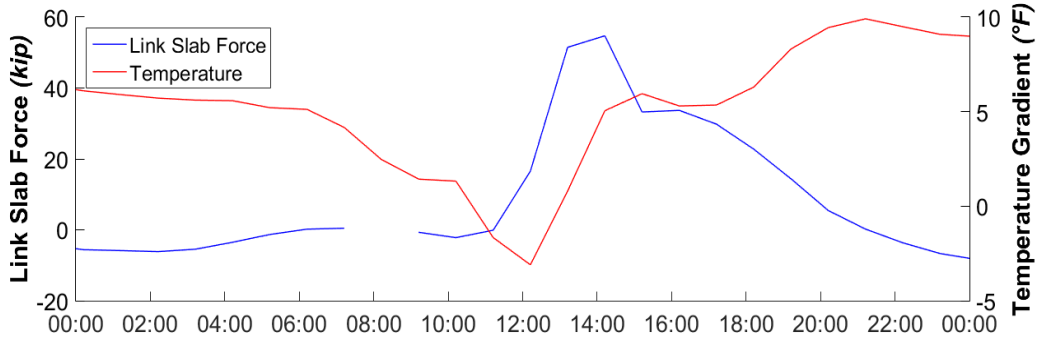

Bent 17	Case: Expansion support (2 span)

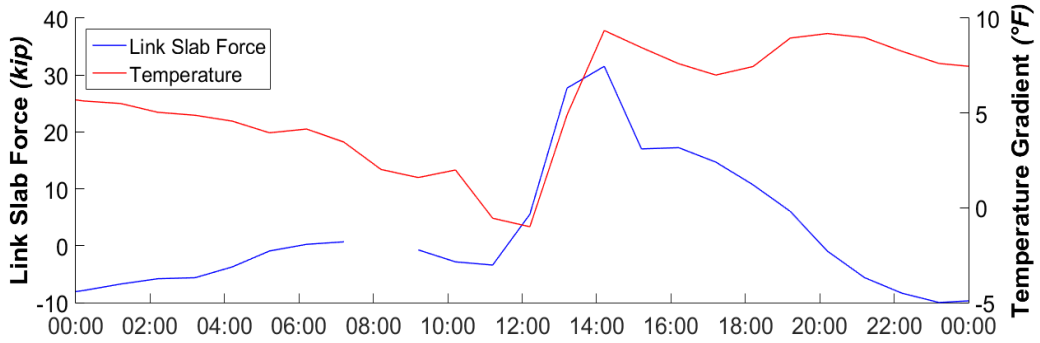

Bent 19	Case: Fixed support (2 span)

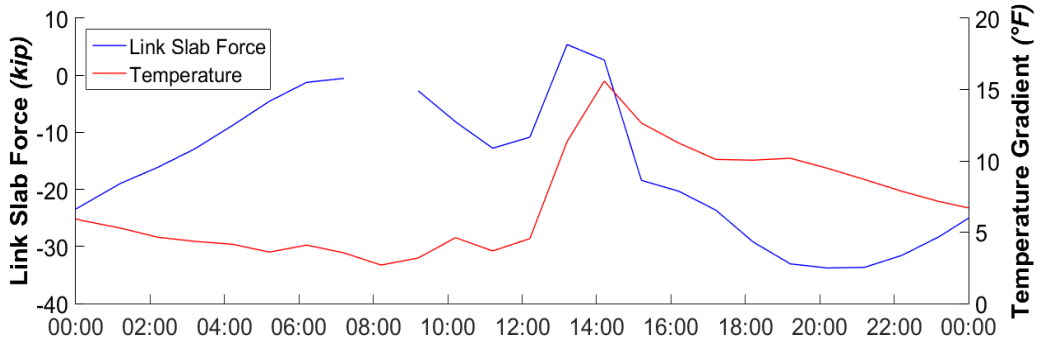

Girder 4	Baseline: Aug 1 2018 9:00
Bent 2	**Case: Expansion support (4 span)**

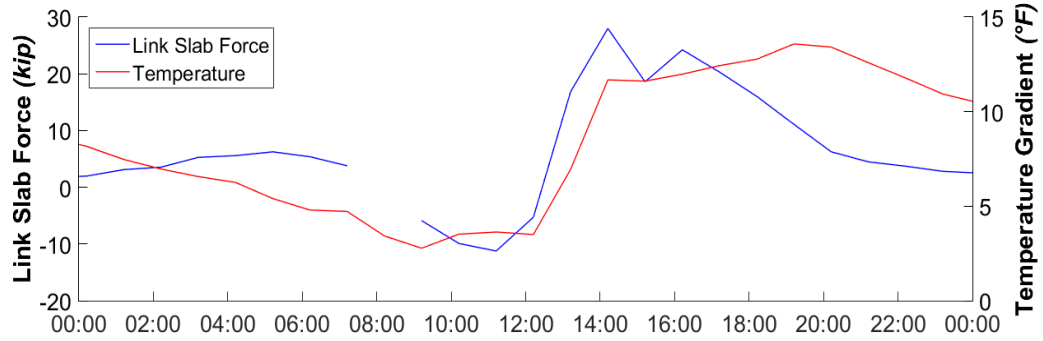

Bent 3	Case: Expansion support (4 span)

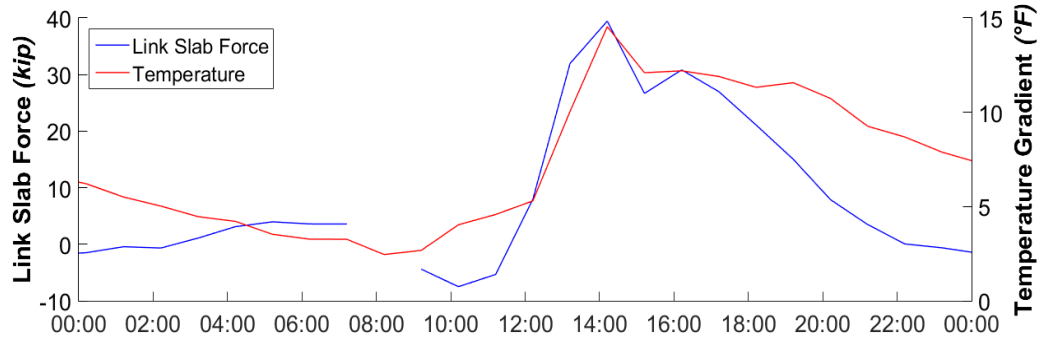

Bent 4	Case: Expansion support (4 span)

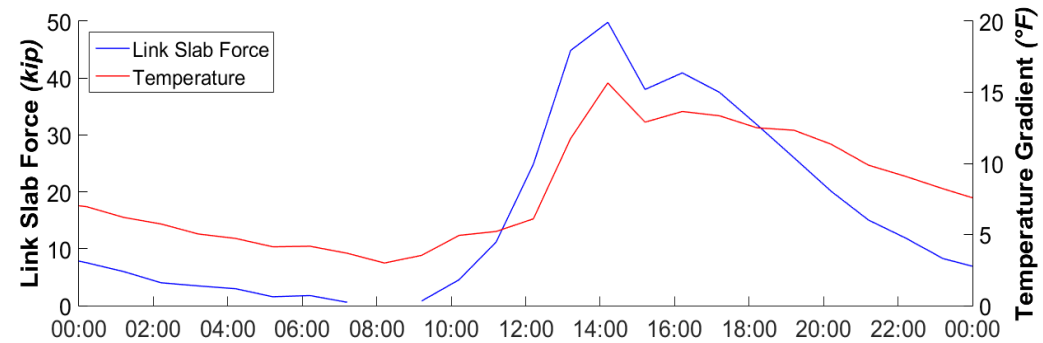

Bent 15	Case: Expansion support (2 span)

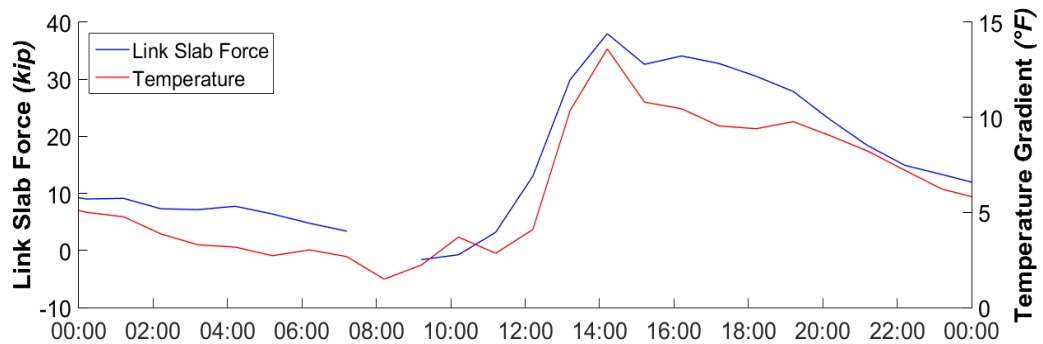

Girder 4	Baseline: Aug 1 2018 9:00
Bent 17	**Case: Expansion support (2 span)**
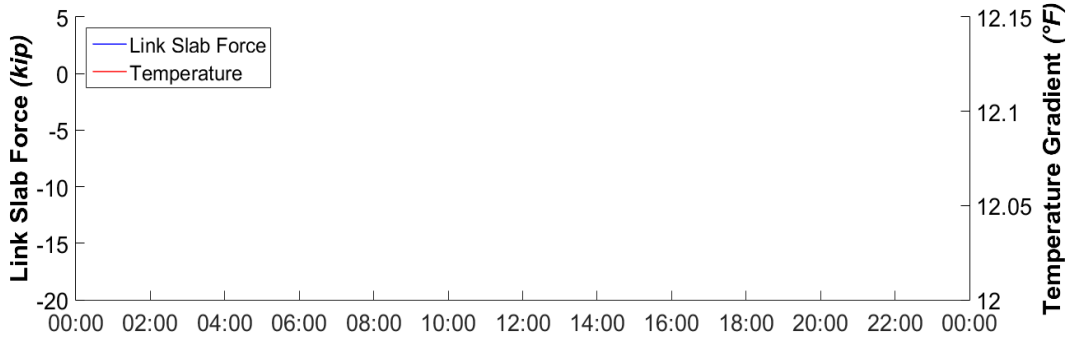	
Bent 19	**Case: Fixed support (2 span)**
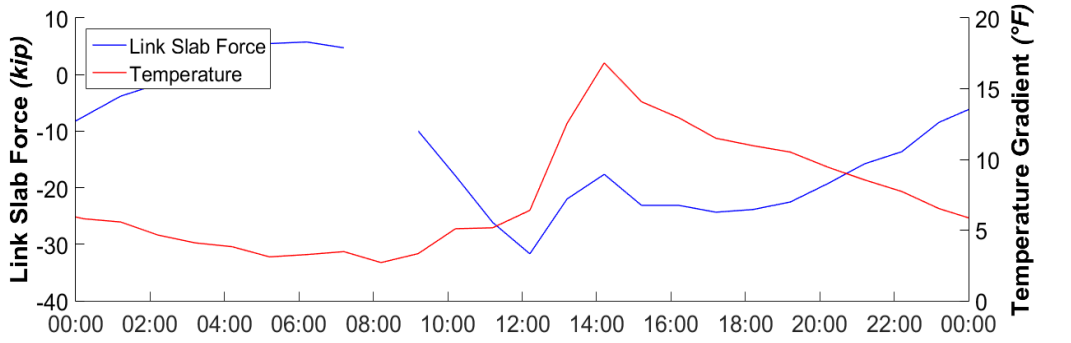	

Relative Angle

Relative Angle	Period: Full Range
Beginning: Sensor Install Date	End: Feb 15 2019
Temperature	

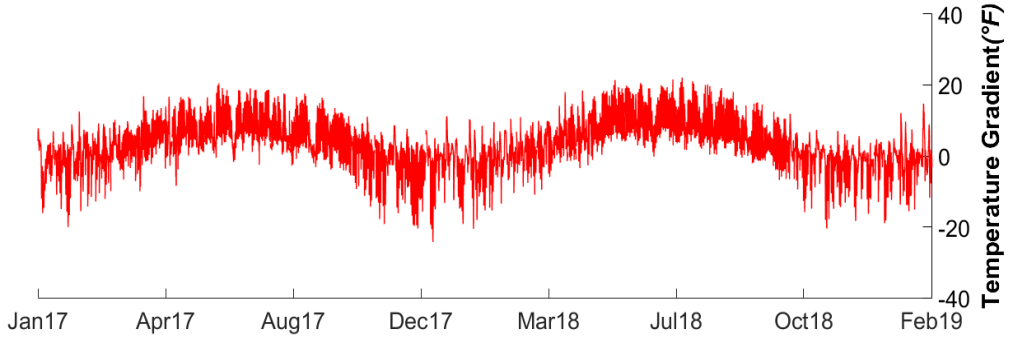

Girder 7	Baseline : at install date
Bent 2	Case: Expansion support (4 span)

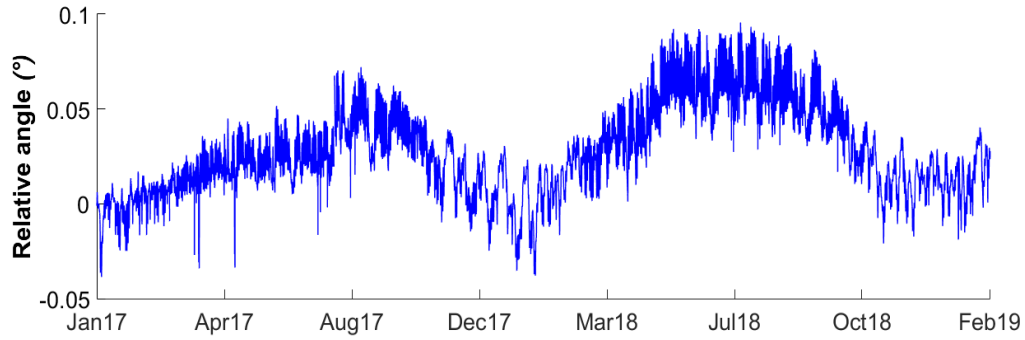

Bent 3	Case: Expansion support (4 span)

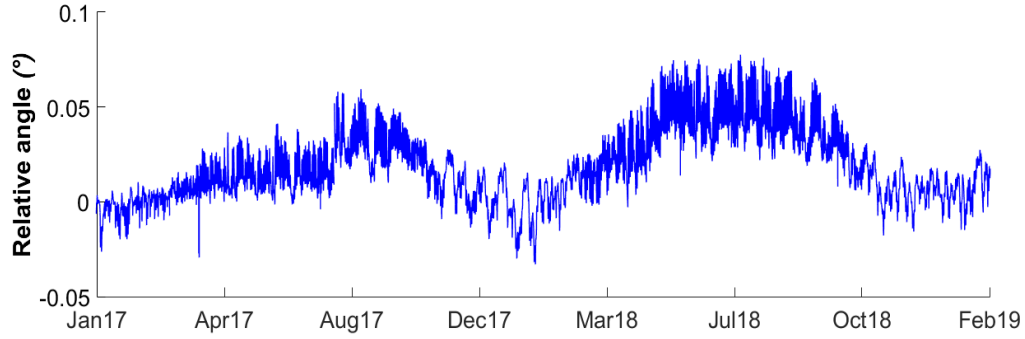

Relative Angle	Period: Full Range
Bent 4	**Case: Expansion support (4 span)**

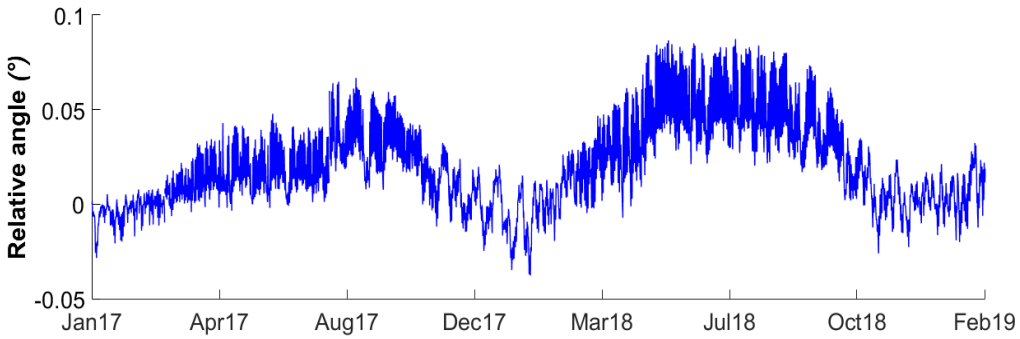

Bent 14	**Case: Expansion support (2 span) Exterior**

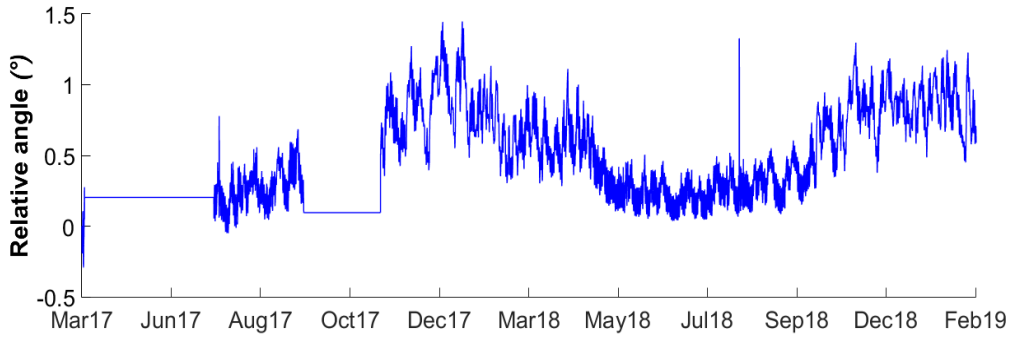

Bent 16	**Case: Expansion support (2 span) Exterior**

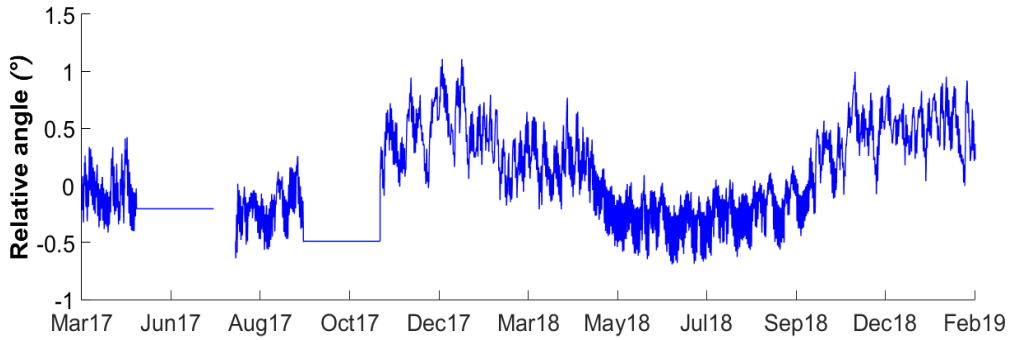

Bent 17	**Case: Expansion support (2 span)**

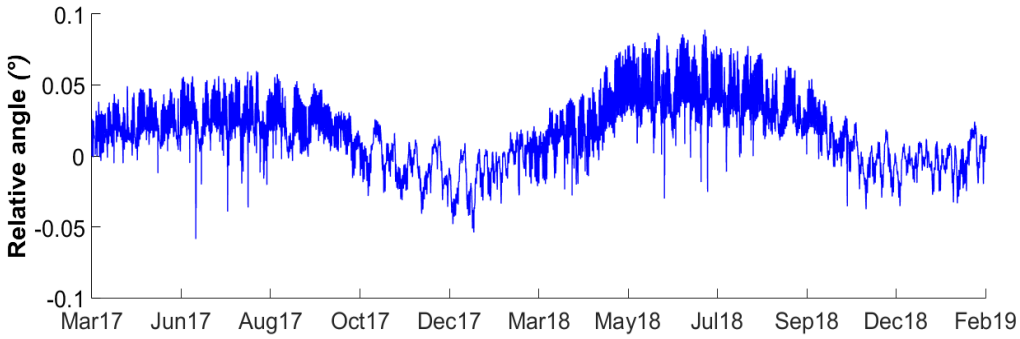

Relative Angle	Period: Full Range
Bent 19	Case: Fixed support (2 span)

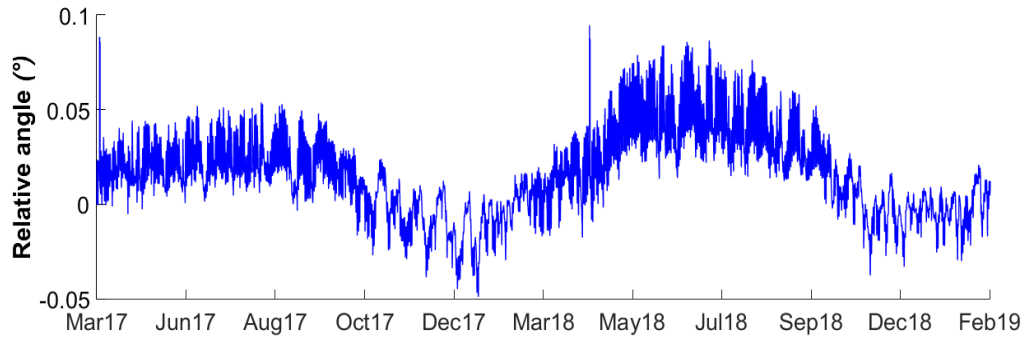

Girder 4	Baseline: 12 Hrs after pour date
Bent 2	Case: Expansion support (4 span)

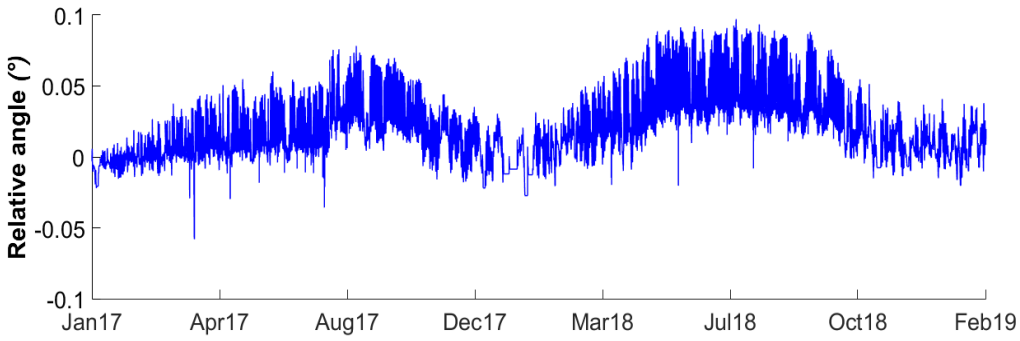

Bent 3	Case: Expansion support (4 span)

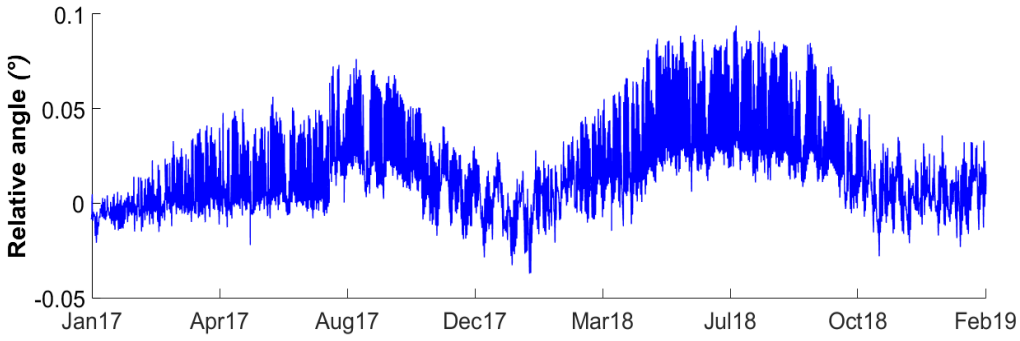

Bent 4	Case: Expansion support (4 span)

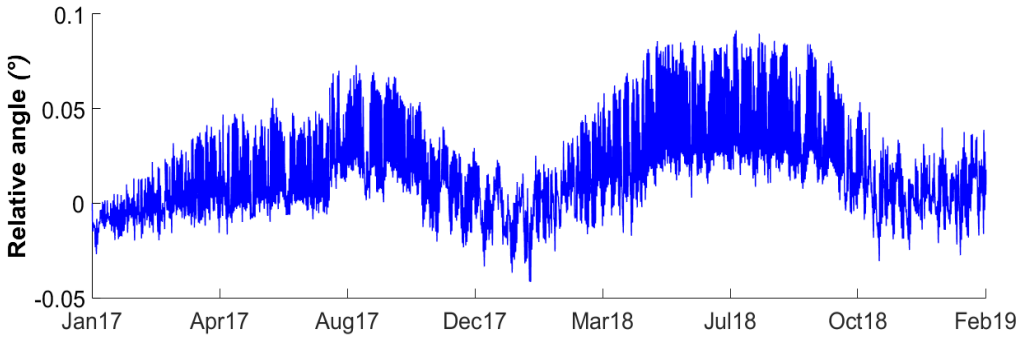

Bent 14	Case: Expansion support (2 span) Exterior

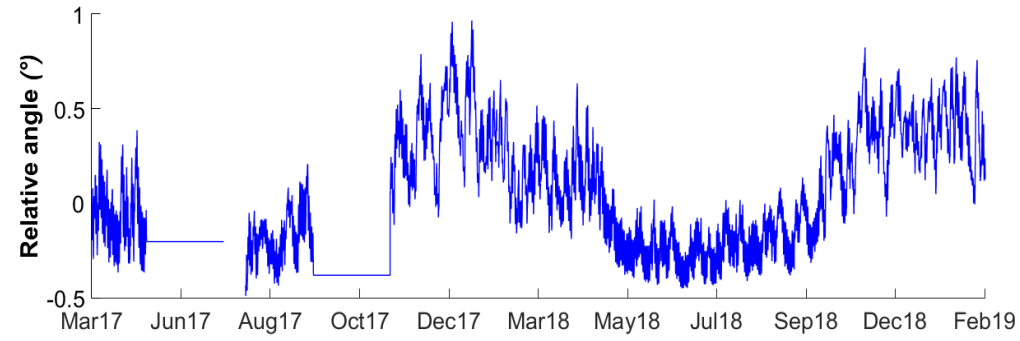

Girder 4	Baseline: 12 Hrs after pour date
Bent 16	Case: Expansion support (2 span) Exterior

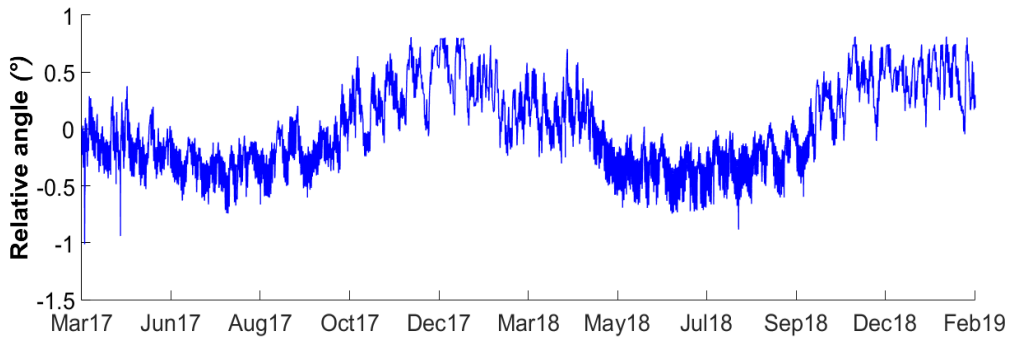

Bent 17	Case: Expansion support (2 span)

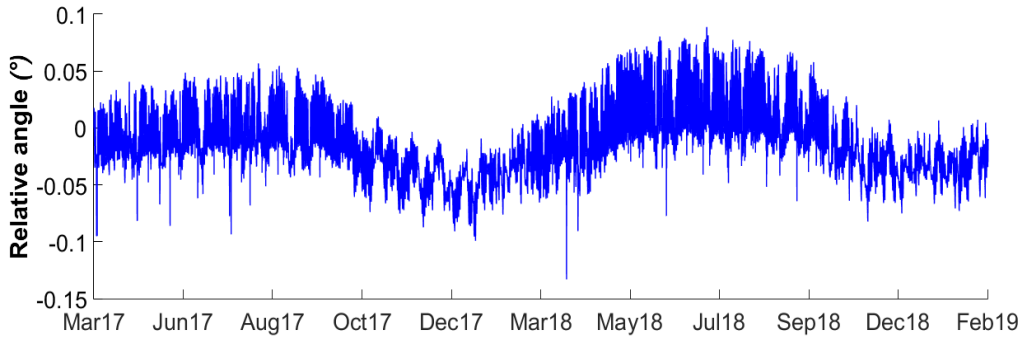

Bent 19	Case: Fixed support (2 span)

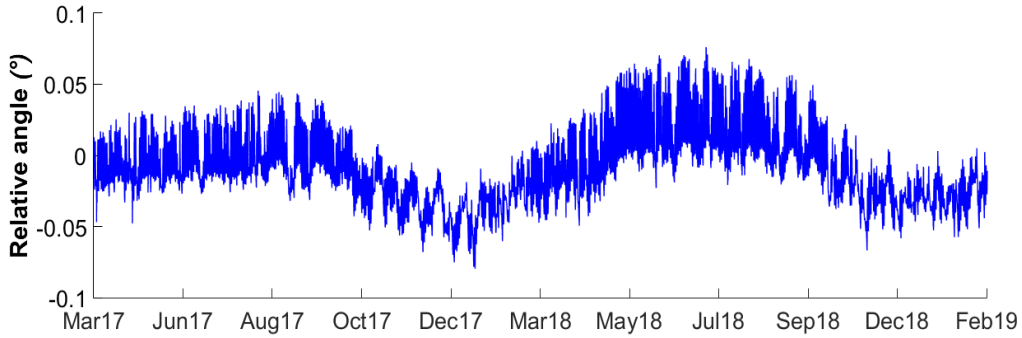

Relative Angle	Period: 30 days
Beginning: Jan 1 2018 0:00	End: Jan 31 2018 0:00
Girder 7	Baseline : Jan 2 2018 00:00
Bent 2	Case: Expansion support (4 span)

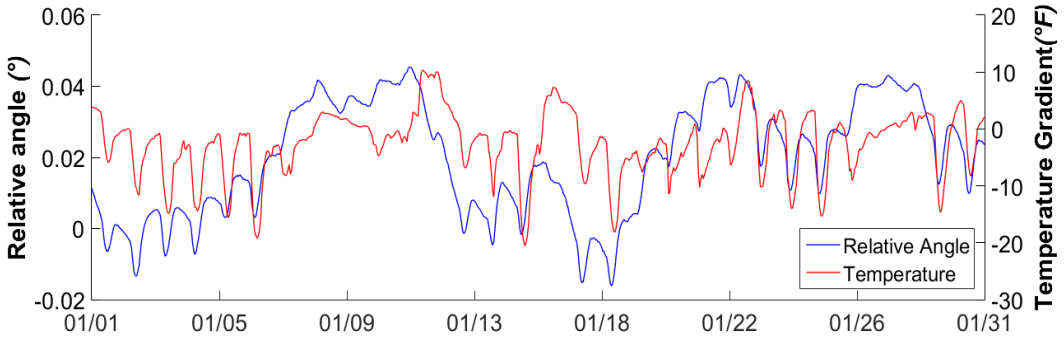

Bent 3	Case: Expansion support (4 span)

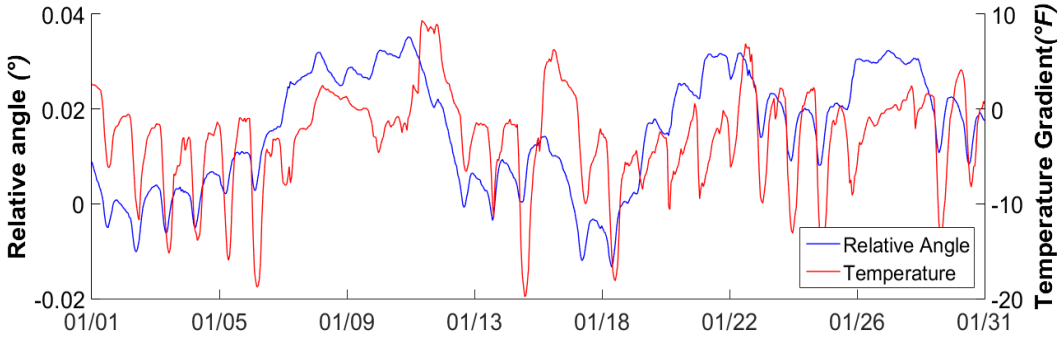

Bent 4	Case: Expansion support (4 span)

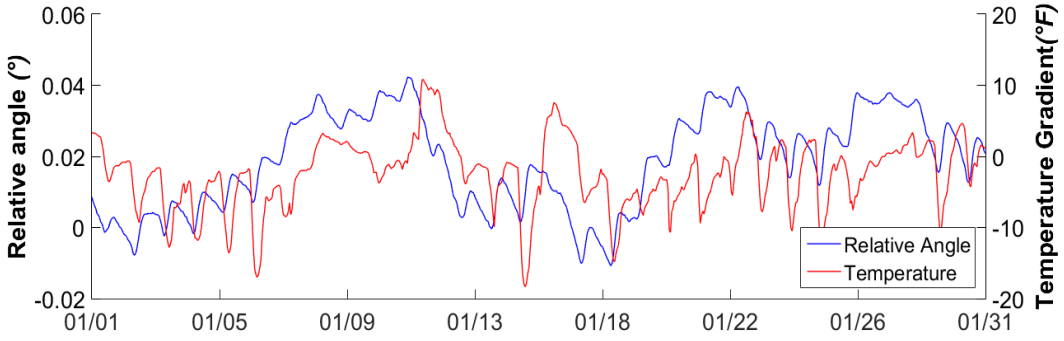

Relative Angle	Period: 30 days
Bent 14	**Case: Expansion support (2 span)**

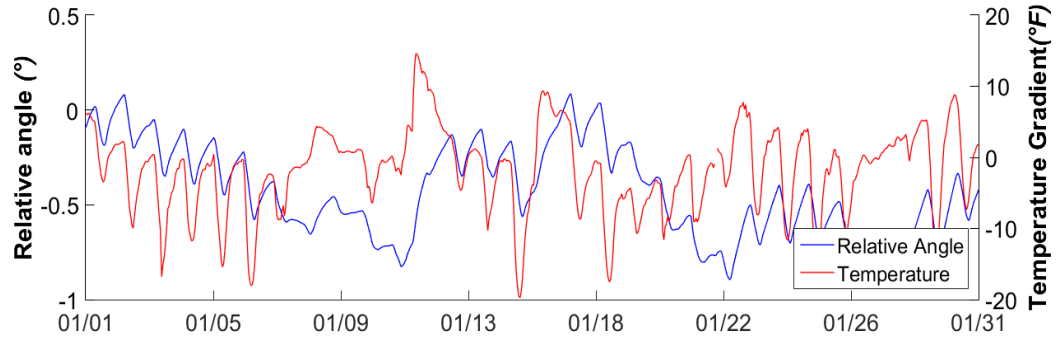

Bent 16	Case: Expansion support (2 span)

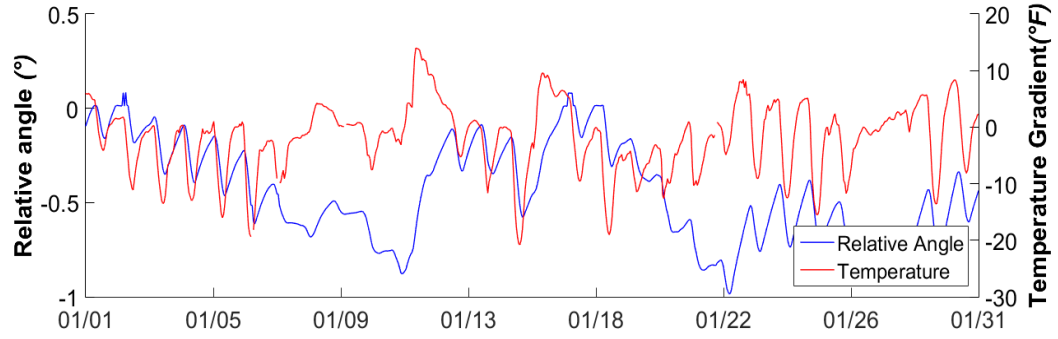

Bent 17	Case: Expansion support (2 span)

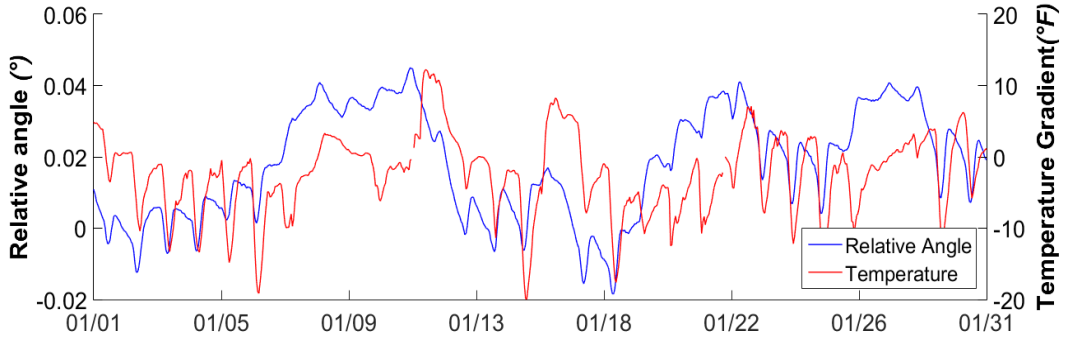

Bent 19	Case: Fixed support (2 span)

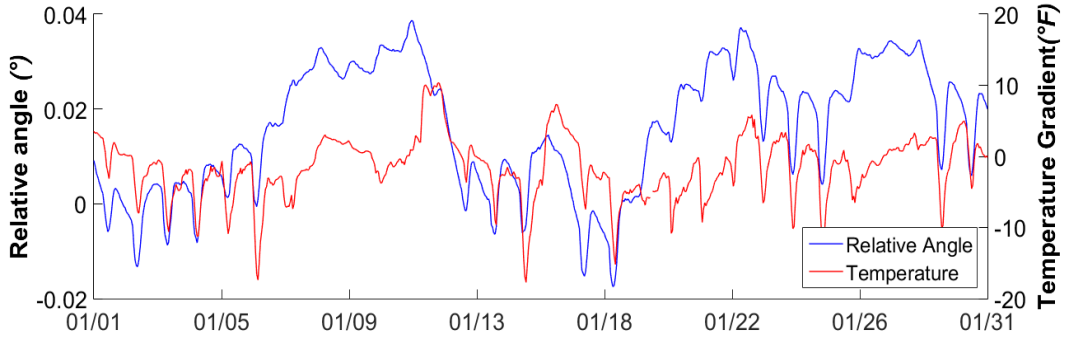

Girder 4	Baseline: Jan 2 2018 00:00
Bent 2	**Case: Expansion support (4 span)**

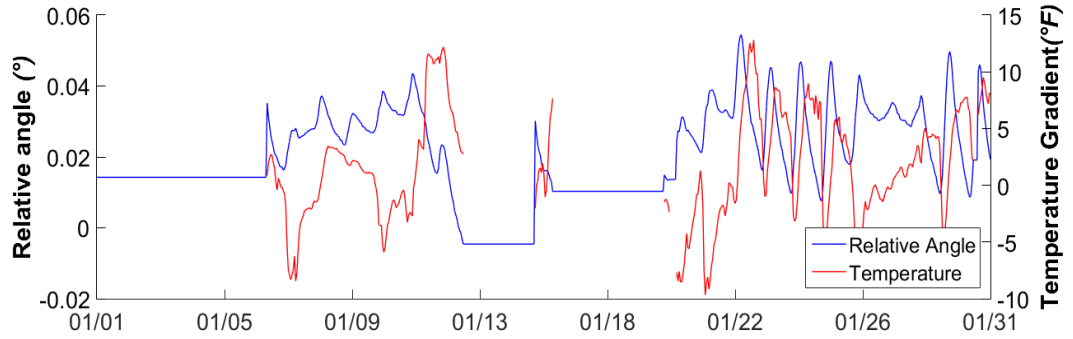

Bent 3	Case: Expansion support (4 span)

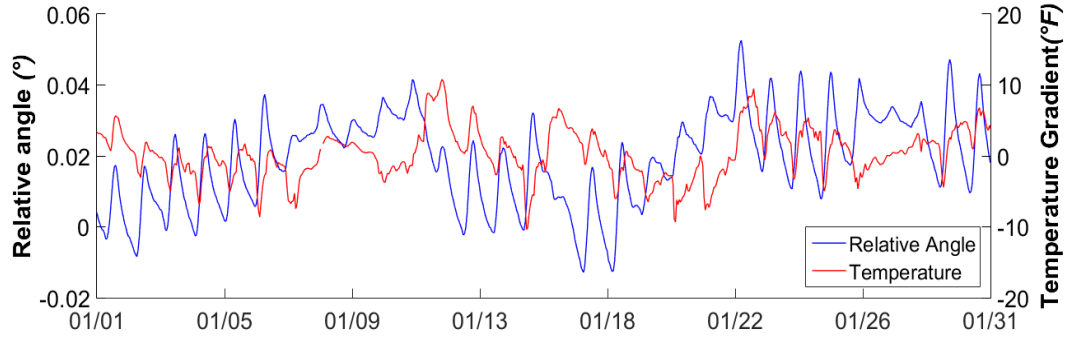

Bent 4	Case: Expansion support (4 span)

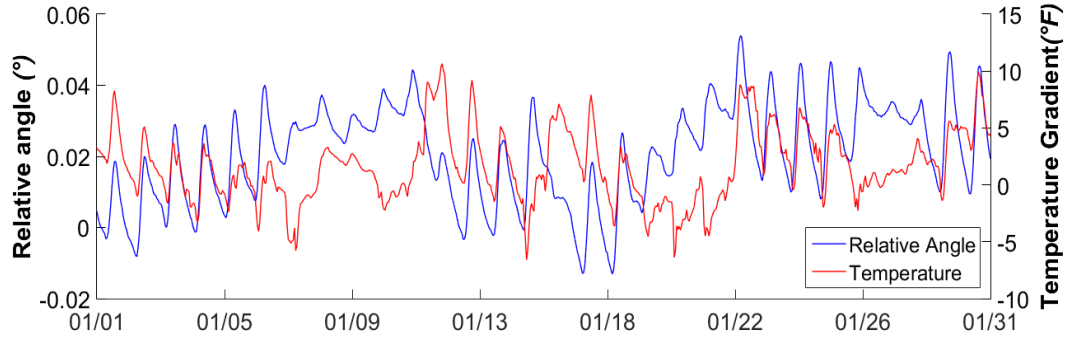

Bent 14	Case: Expansion support (2 span)

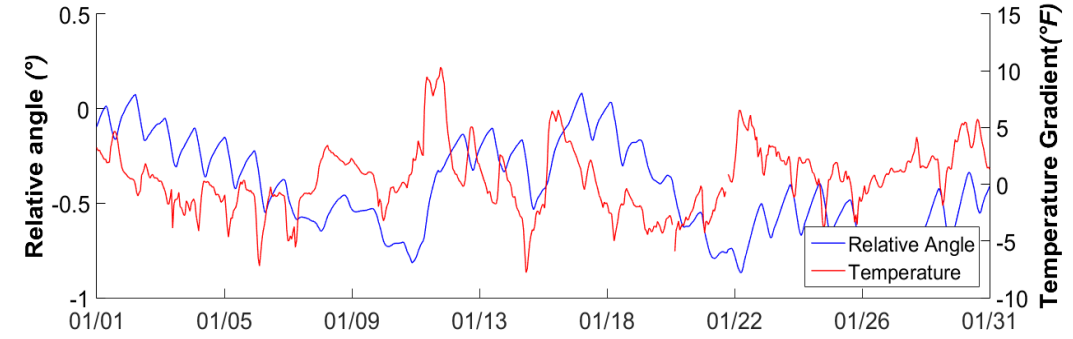

Girder 4	Baseline: Jan 2 2018 00:00
Bent 16	Case: Expansion support (2 span)

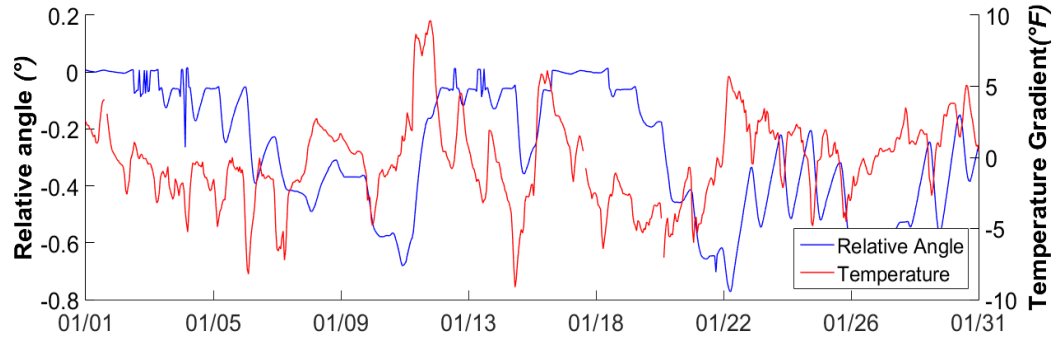

Bent 17	Case: Expansion support (2 span)

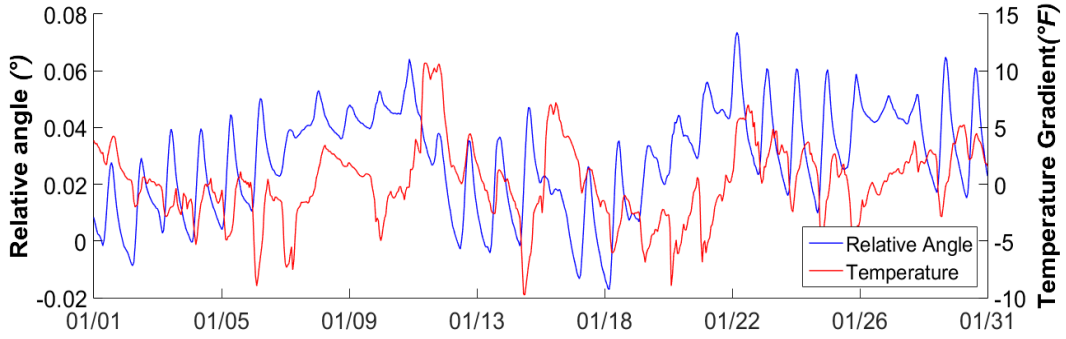

Bent 19	Case: Fixed support (2 span)

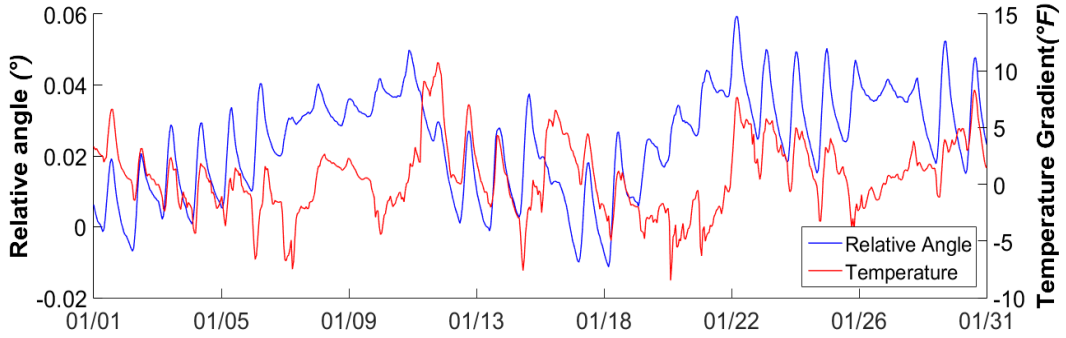

Relative Angle	Period: 30 days
Beginning: Aug 1 2018 0:00	End: Aug 31 2018 0:00
Girder 7	Baseline : Aug 1 2018 09:00
Bent 2	Case: Expansion support (4 span)

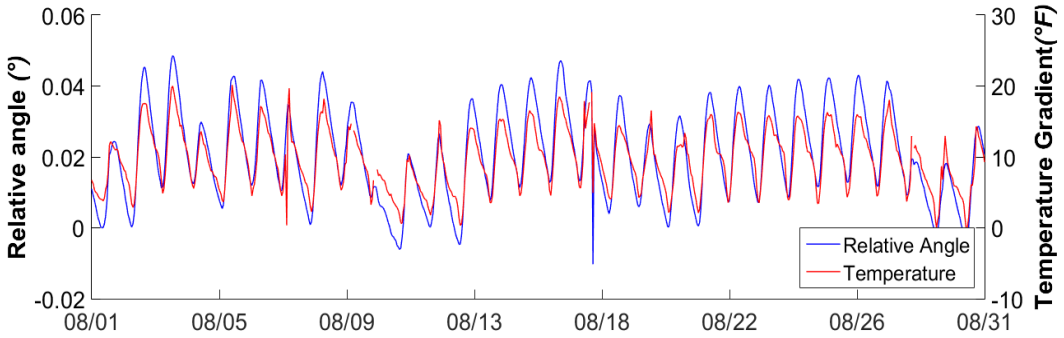

Bent 3	Case: Expansion support (4 span)

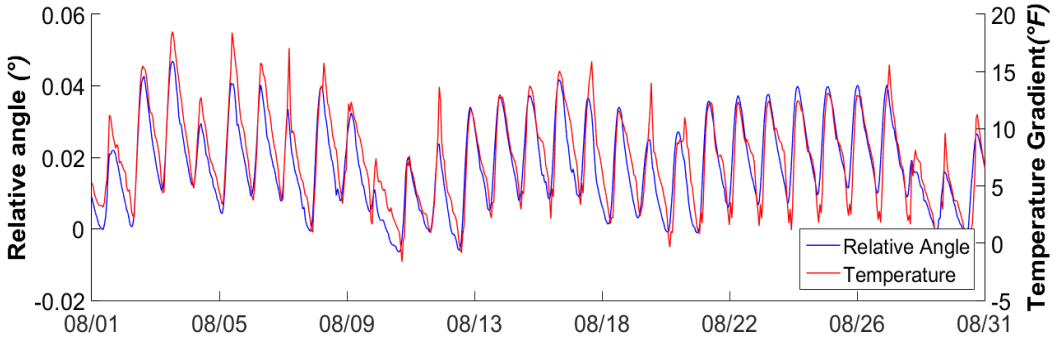

Bent 4	Case: Expansion support (4 span)

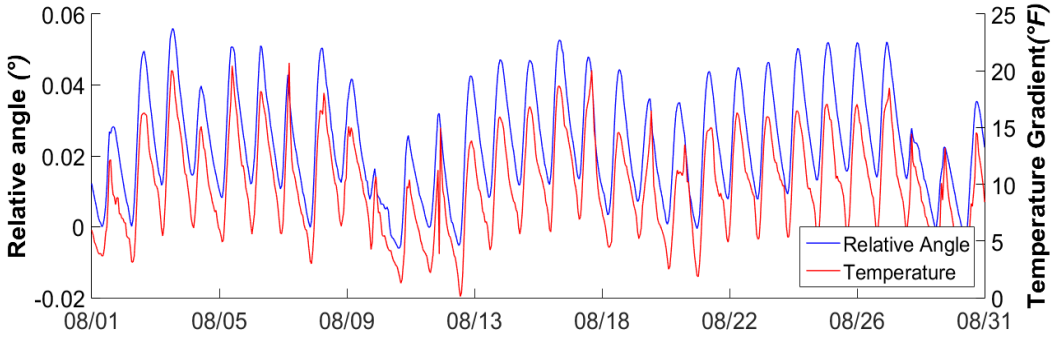

Relative Angle	Period: 30 days
Bent 14	**Case: Expansion support (2 span)**

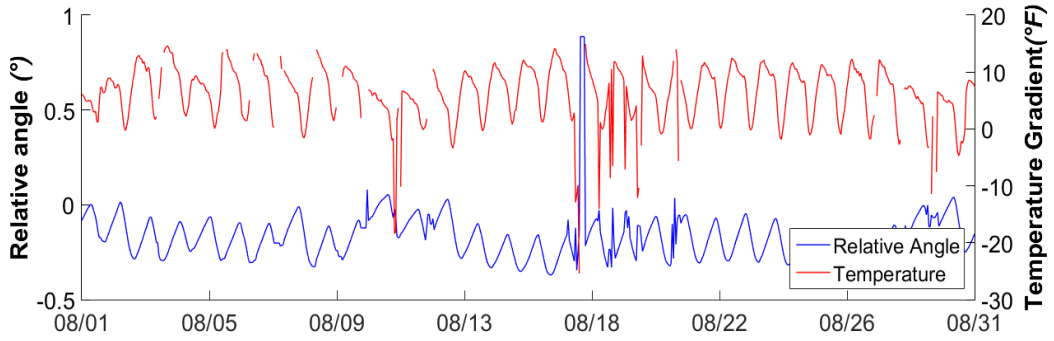

Bent 16	Case: Expansion support (2 span)

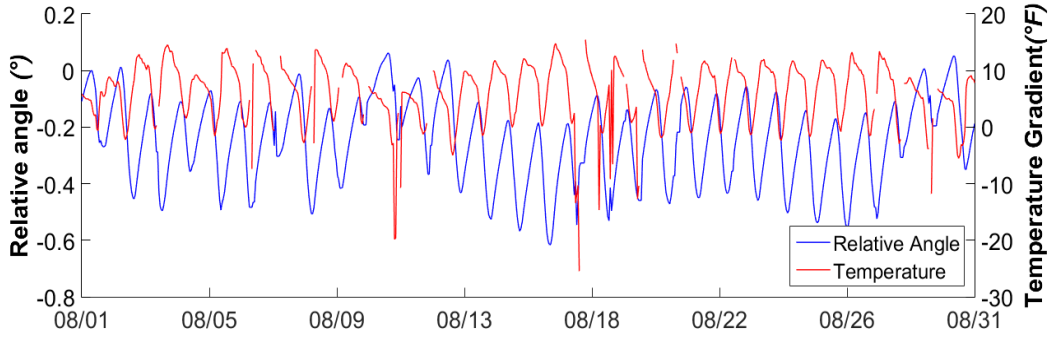

Bent 17	Case: Expansion support (2 span)

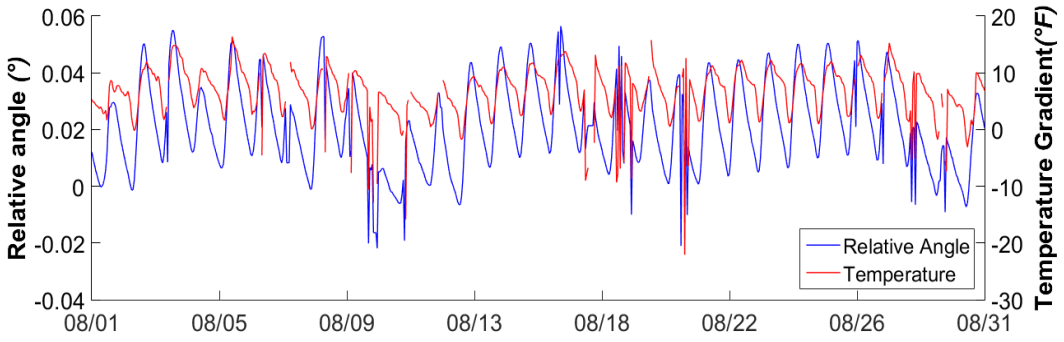

Bent 19	Case: Fixed support (2 span)

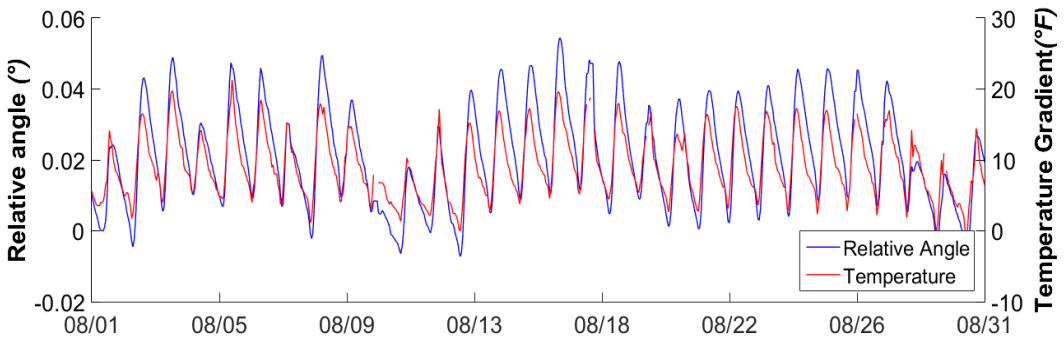

Girder 4	Baseline: Aug 1 2018 09:00
Bent 2	**Case: Expansion support (4 span)**

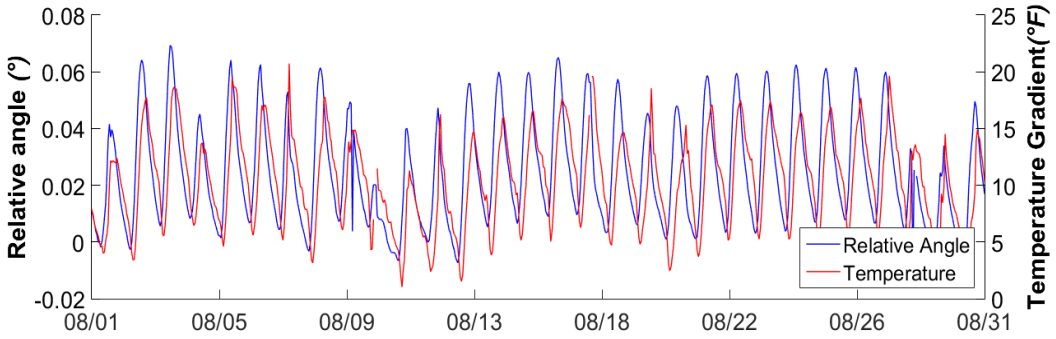

Bent 3	Case: Expansion support (4 span)

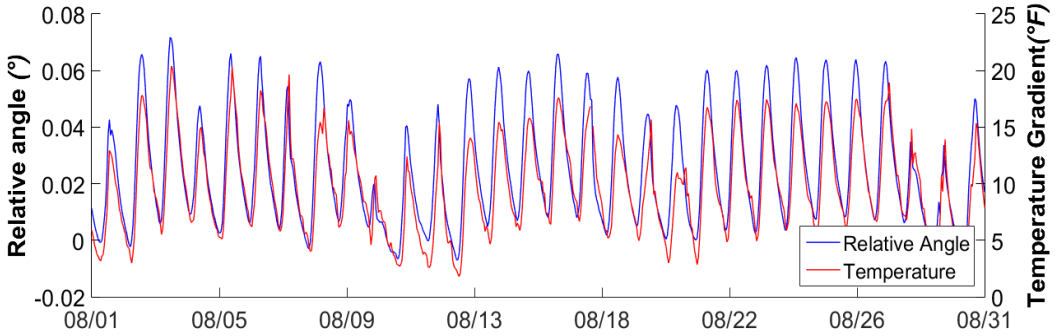

Bent 4	Case: Expansion support (4 span)

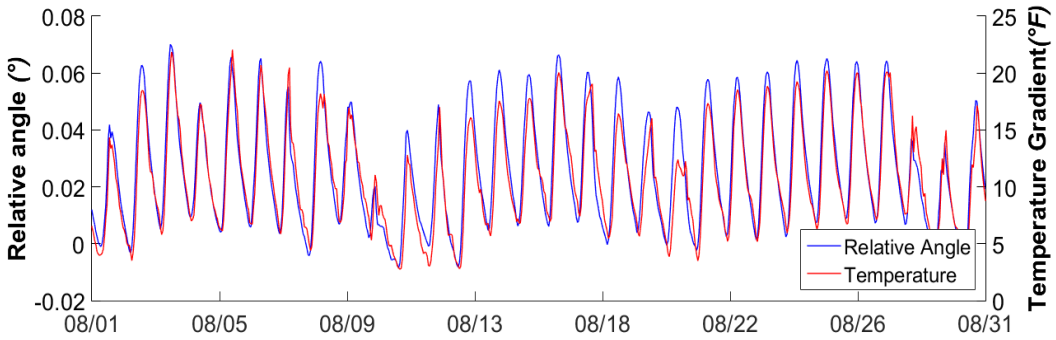

Bent 14	Case: Expansion support (2 span)

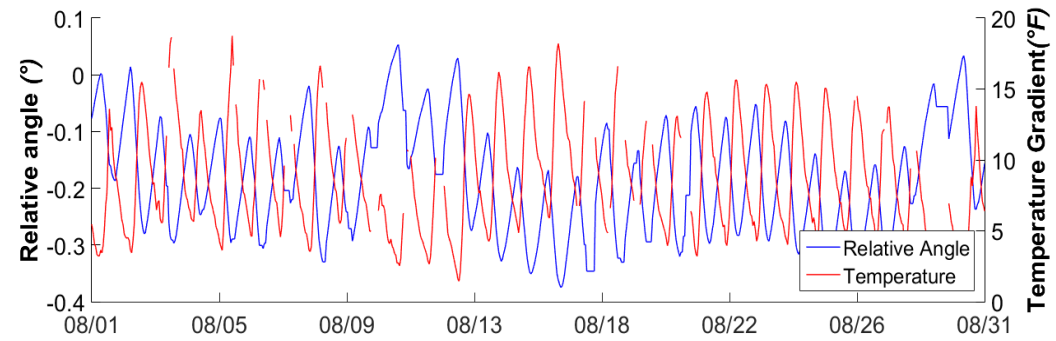

Girder 4	Baseline: Aug 1 2018 09:00
Bent 16	**Case: Expansion support (2 span)**

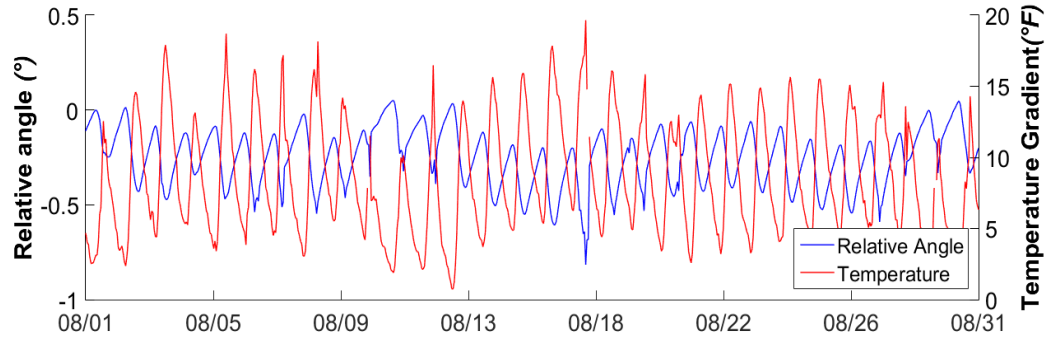

Bent 17	Case: Expansion support (2 span)

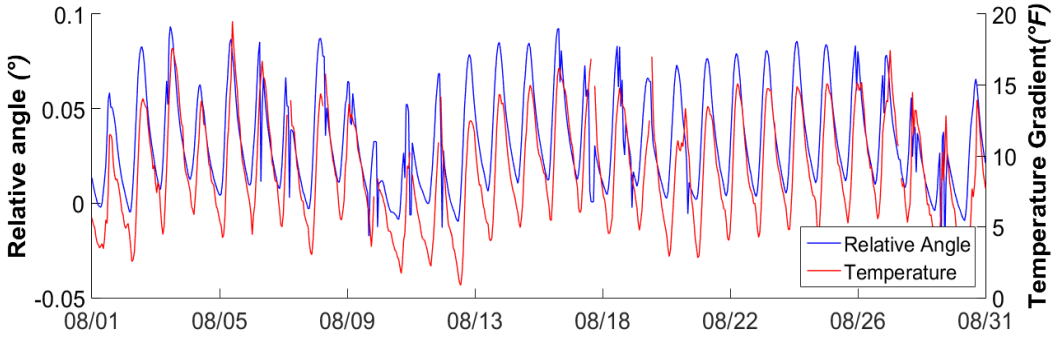

Bent 19	Case: Fixed support (2 span)

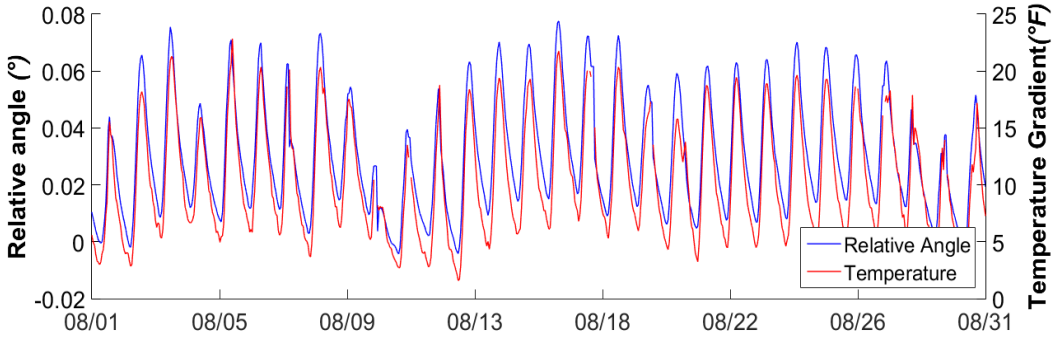

Relative Angle	Period: 24 hours
Beginning: Jan 1 2018 0:00	End: Jan 2 2018 0:00
Girder 7	Baseline : Jan 2 2018 00:00
Bent 2	Case: Expansion support (4 span)

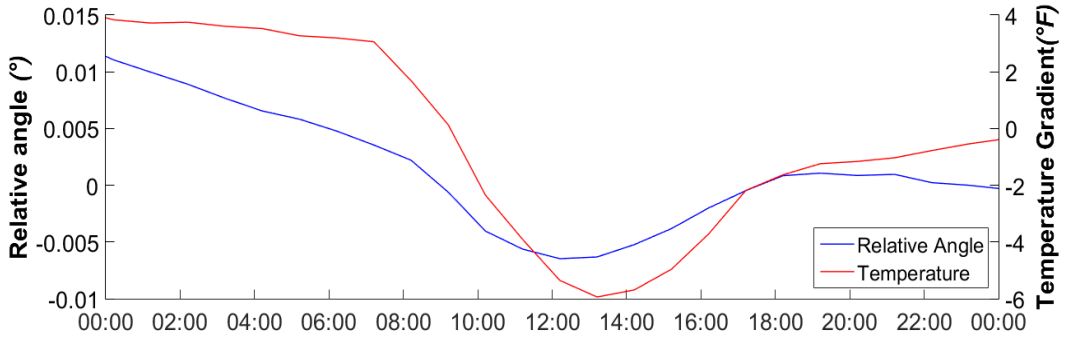

Bent 3	Case: Expansion support (4 span)

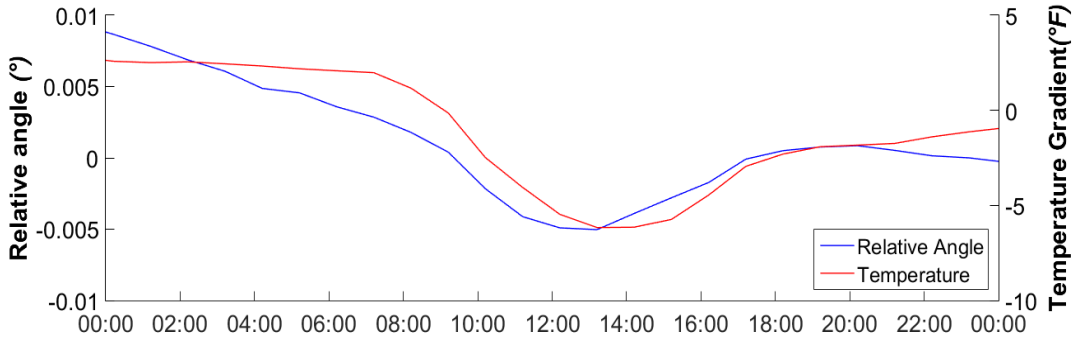

Bent 4	Case: Expansion support (4 span)

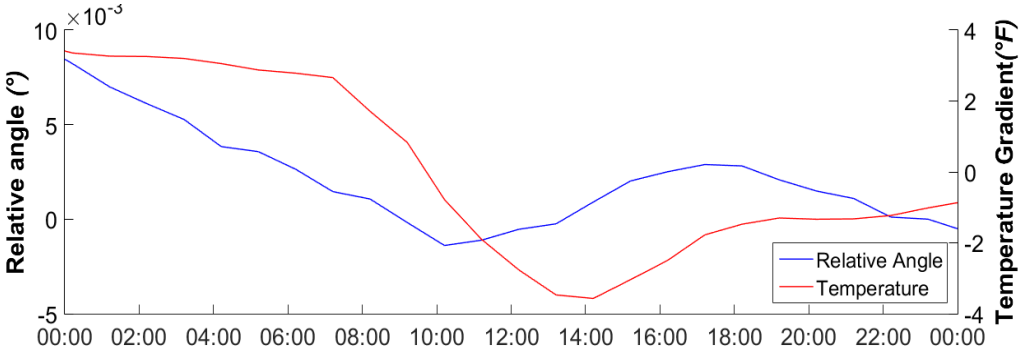

Relative Angle	Period: 24 hours
Bent 14	**Case: Expansion support (2 span)**

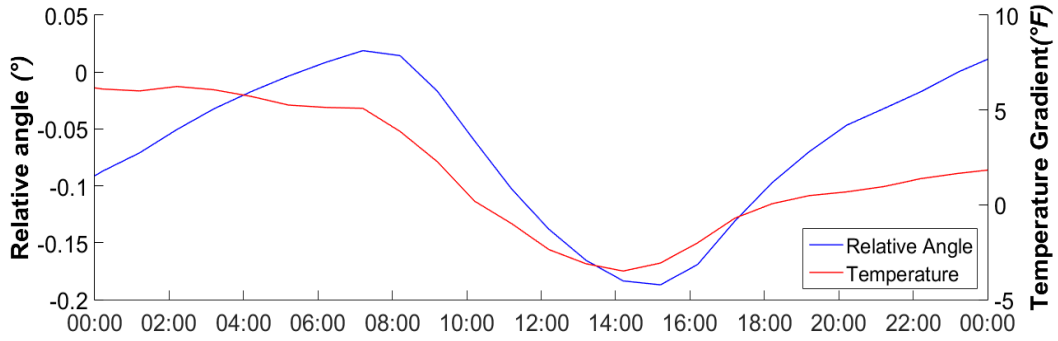

Bent 16	Case: Expansion support (2 span)

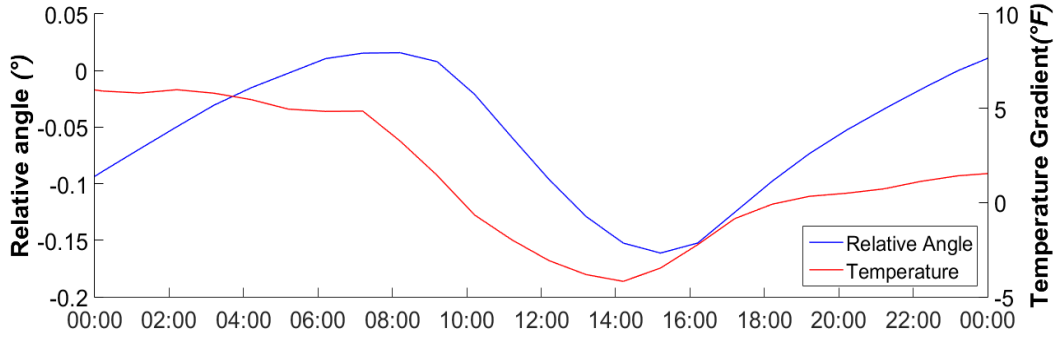

Bent 17	Case: Expansion support (2 span)

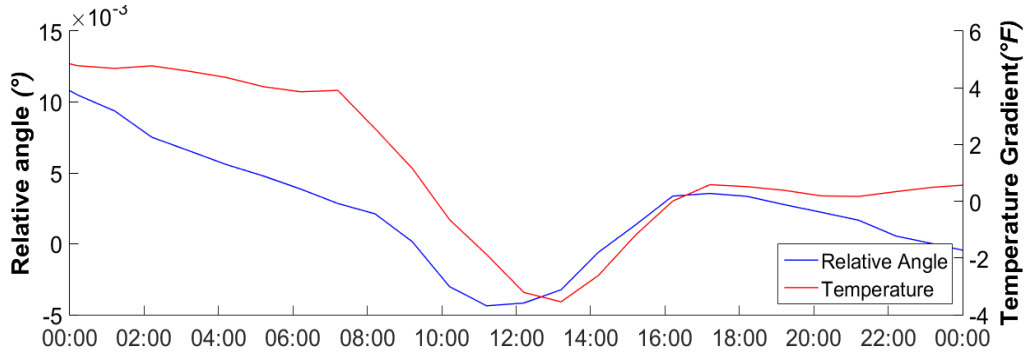

Bent 19	Case: Fixed support (2 span)

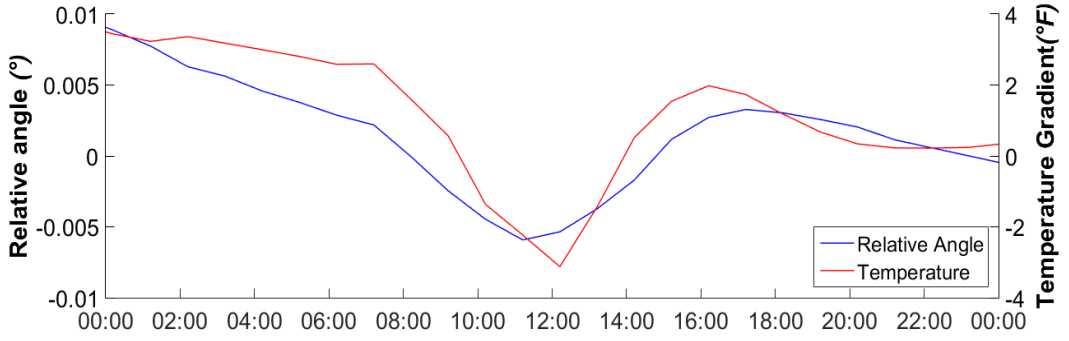

Girder 4	Baseline: Jan 2 2018 00:00
Bent 2	**Case: Expansion support (4 span)**

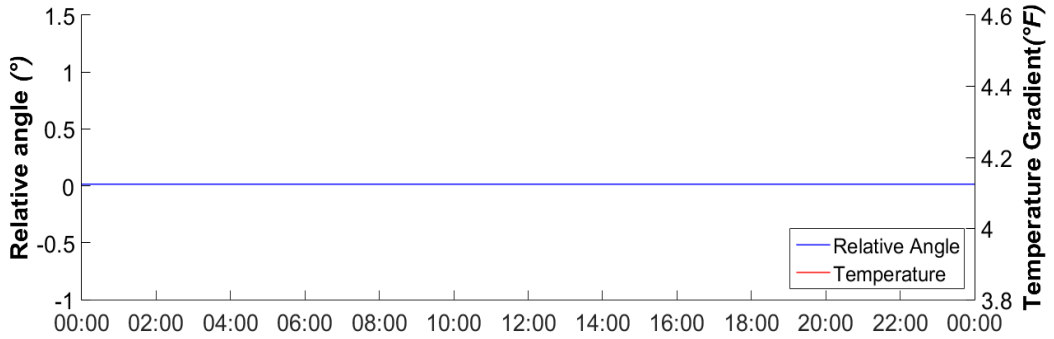

Bent 3	Case: Expansion support (4 span)

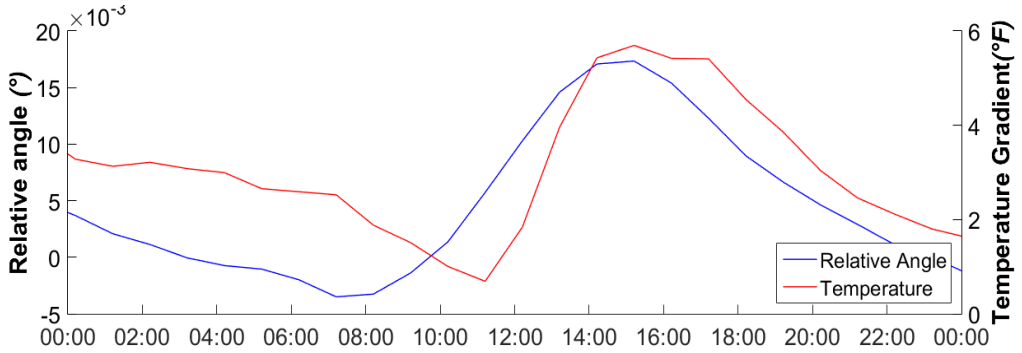

Bent 4	Case: Expansion support (4 span)

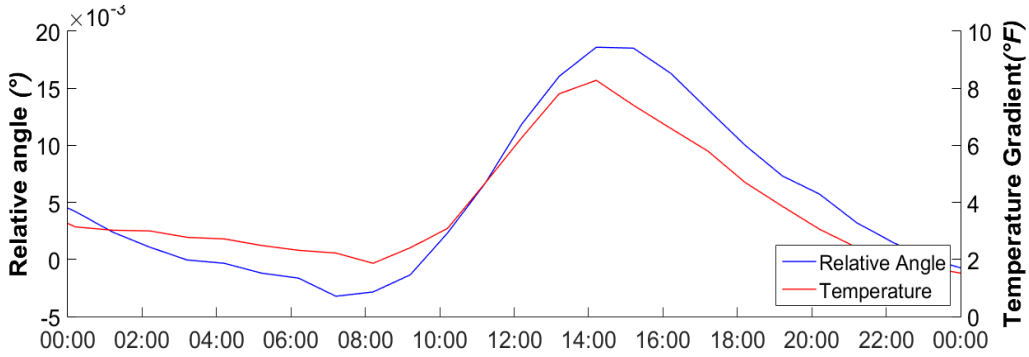

Bent 14	Case: Expansion support (2 span)

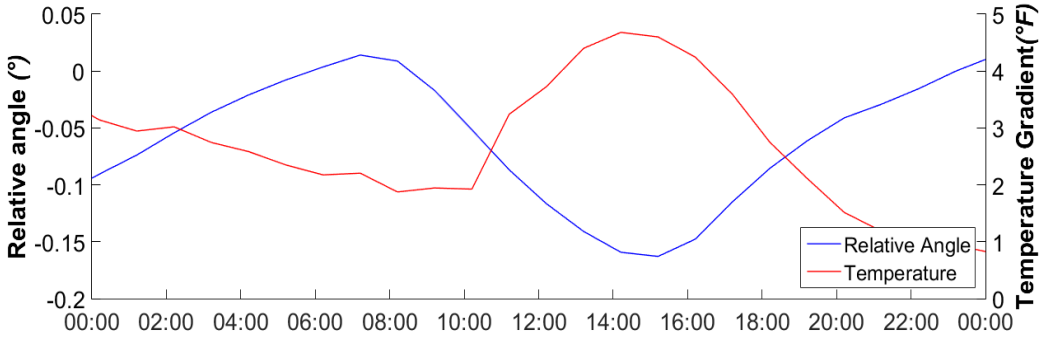

Girder 4	Baseline: Jan 2 2018 00:00
Bent 16	**Case: Expansion support (2 span)**

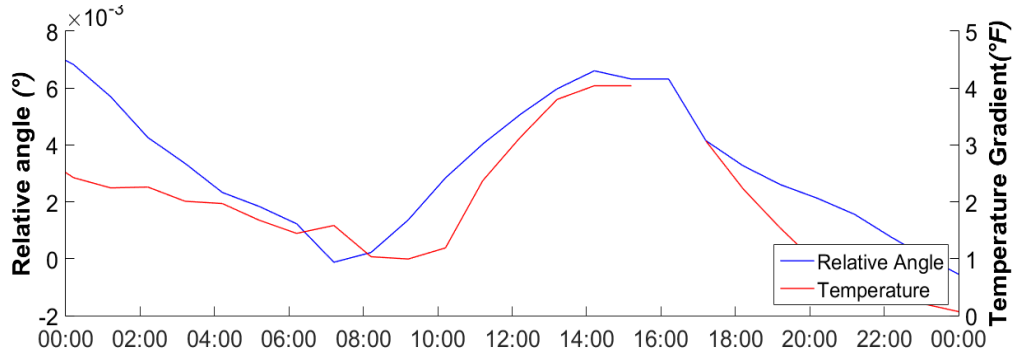

Bent 17	Case: Expansion support (2 span)

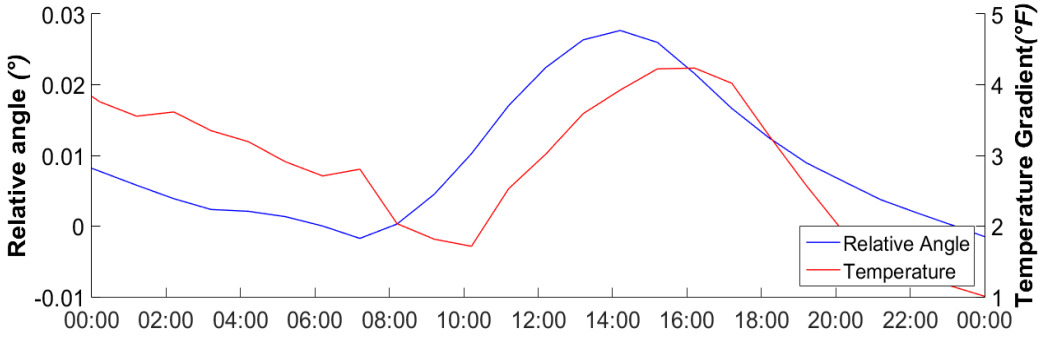

Bent 19	Case: Fixed support (2 span)

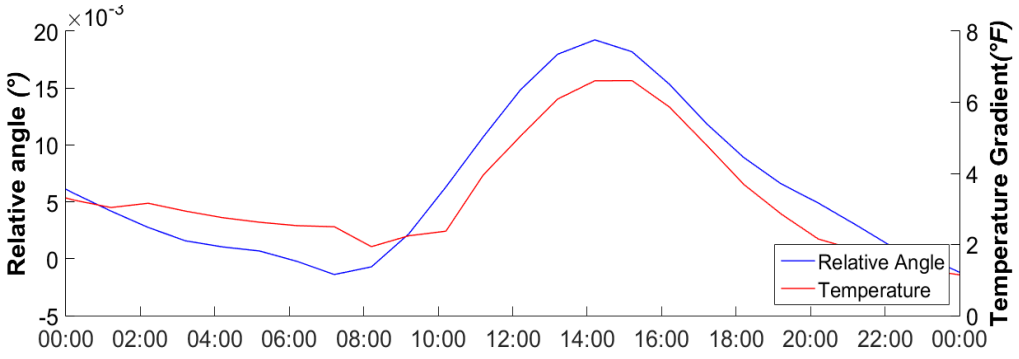

Relative Angle	Period: 30 days
Beginning: Aug 1 2018 0:00	End: Aug 2 2018 0:00
Girder 7	Baseline : Aug 1 2018 09:00
Bent 2	Case: Expansion support (4 span)

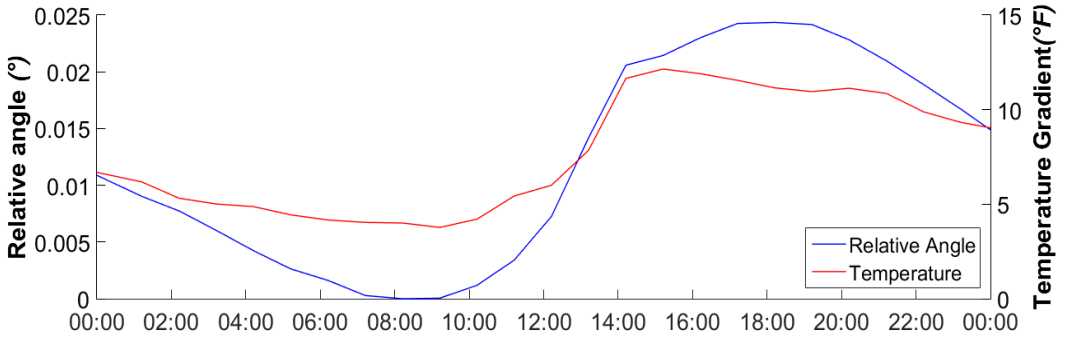

Bent 3	Case: Expansion support (4 span)

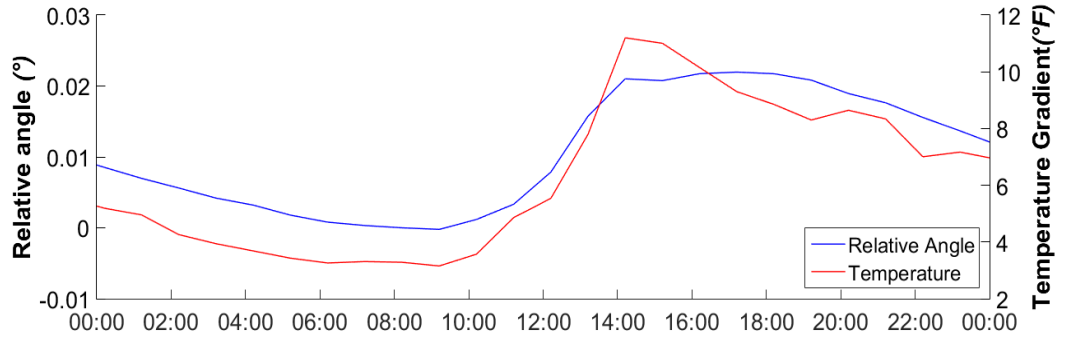

Bent 4	Case: Expansion support (4 span)

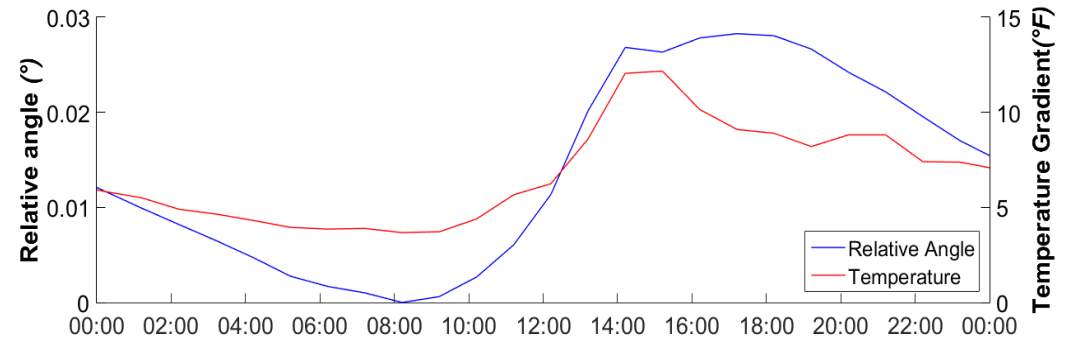

Relative Angle	Period: 30 days
Bent 14	**Case: Expansion support (2 span)**

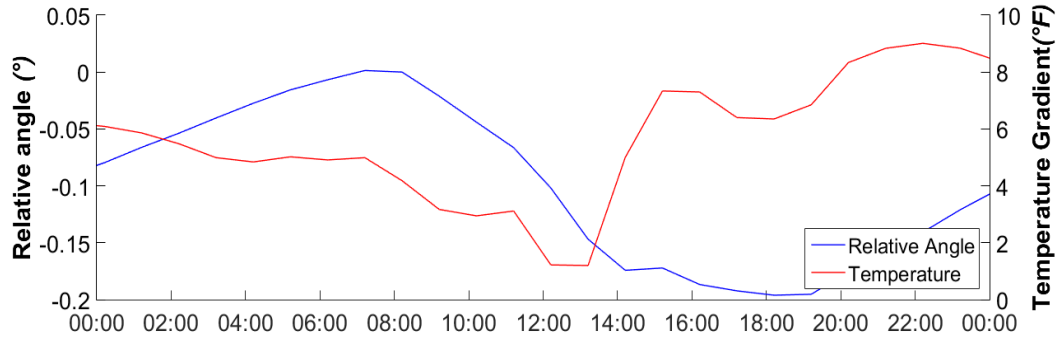

Bent 16	Case: Expansion support (2 span)

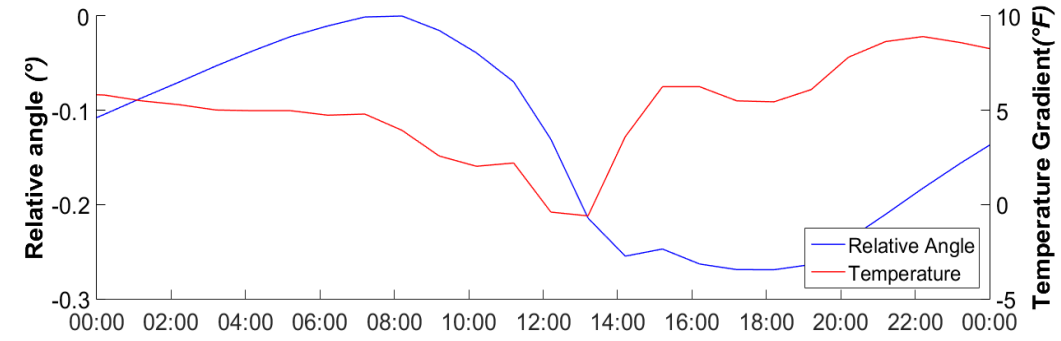

Bent 17	Case: Expansion support (2 span)

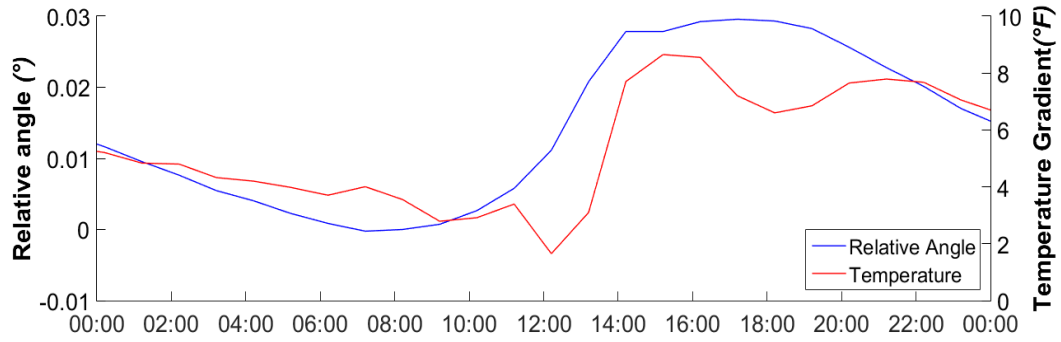

Bent 19	Case: Fixed support (2 span)

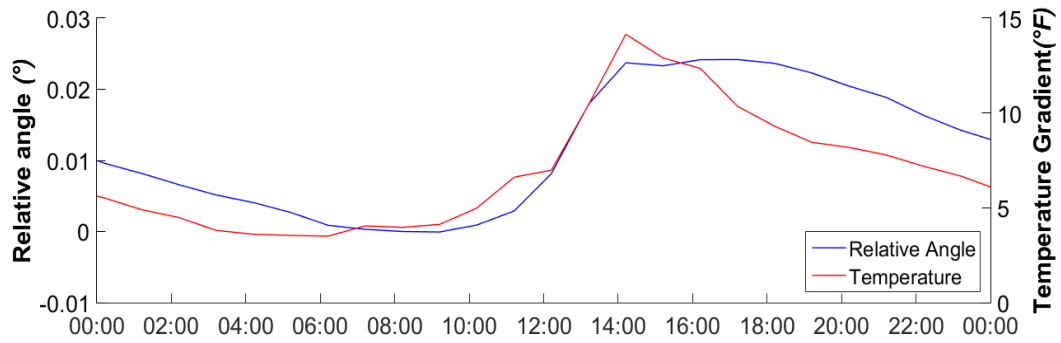

Girder 4	Baseline: Aug 1 2018 09:00
Bent 2	**Case: Expansion support (4 span)**

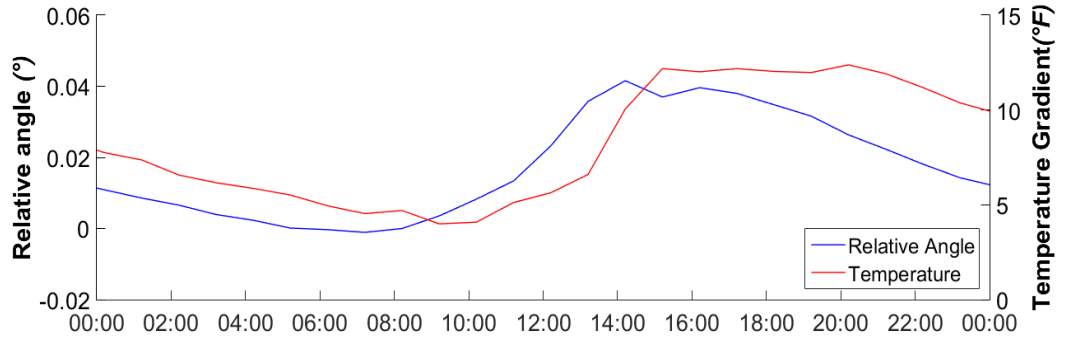

Bent 3	Case: Expansion support (4 span)

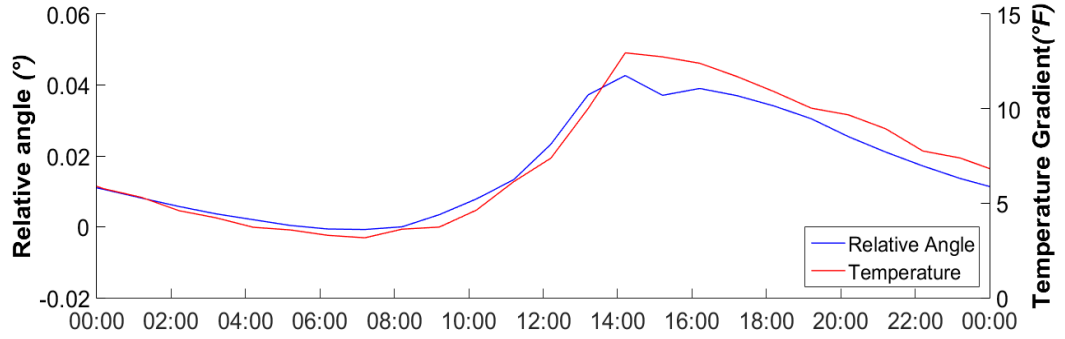

Bent 4	Case: Expansion support (4 span)

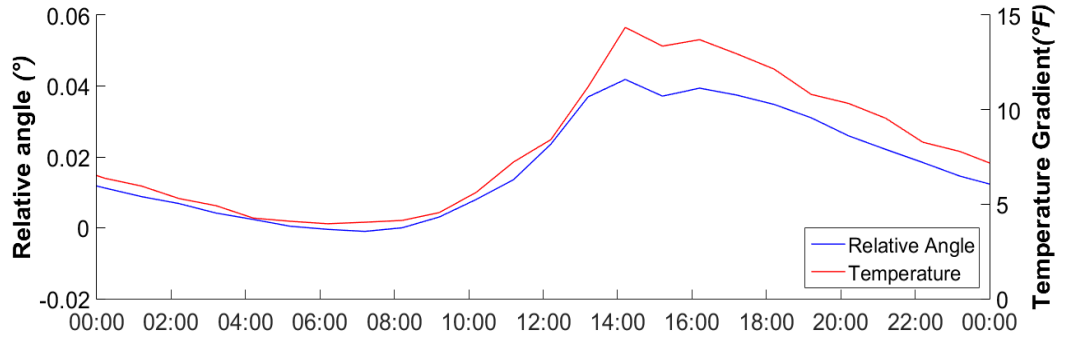

Bent 14	Case: Expansion support (2 span)

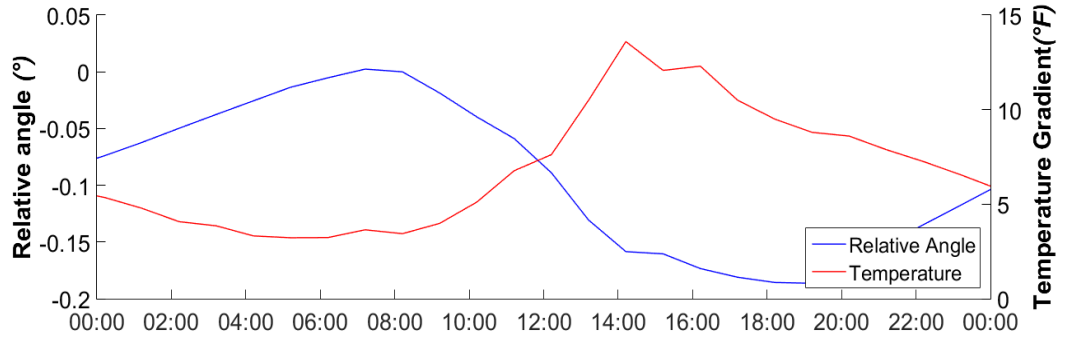

Girder 4	Baseline: Aug 1 2018 09:00
Bent 16	**Case: Expansion support (2 span)**

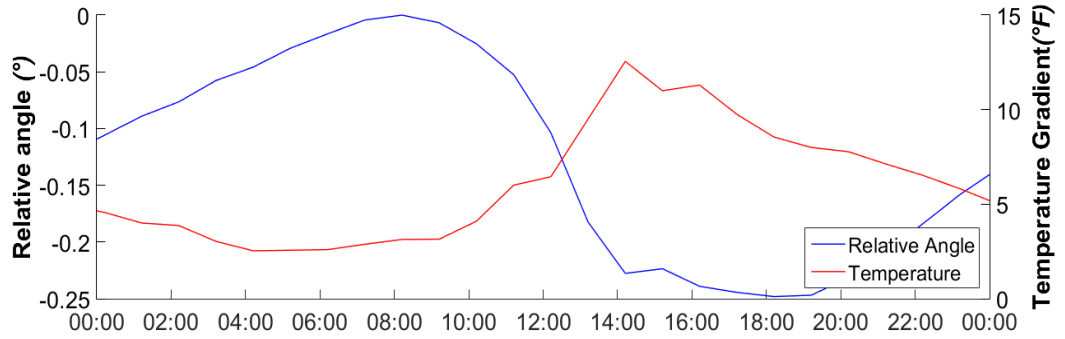

Bent 17	Case: Expansion support (2 span)

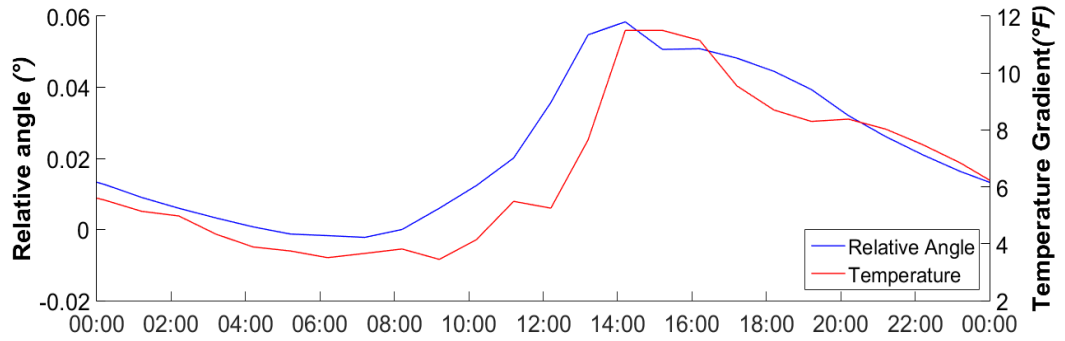

Bent 19	Case: Fixed support (2 span)

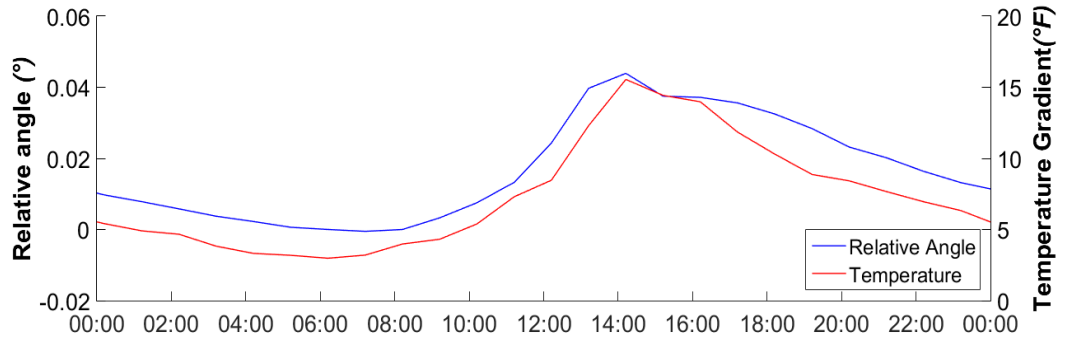

Link slab Force	Period: Live Load Test Duration
Beginning: Jul 11 2017 09:00/11:30	End: Jul 11 2017 12:00/15:30
Girder 7	Baseline : Jul 11 2017 09:00

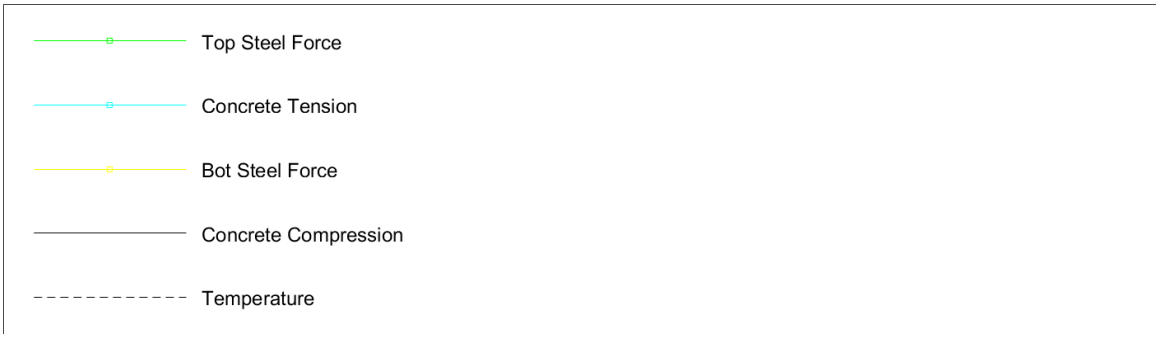

Bent 2	Case: Expansion support (4 span)

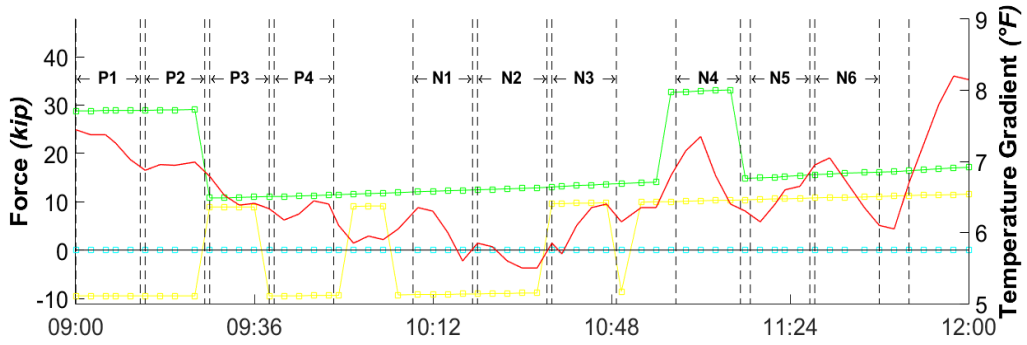

Bent 3	Case: Expansion support (4 span)

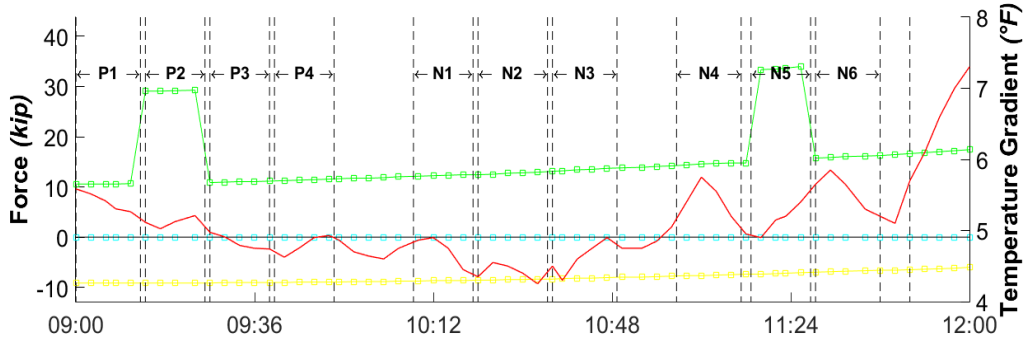

Bent 4	Case: Expansion support (4 span)

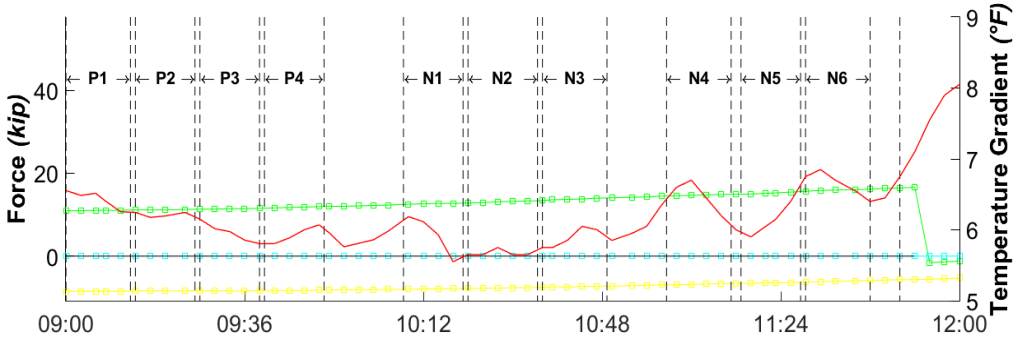

Link slab Force	Period: Live Load Test Duration
Bent 15	**Case: Expansion support (2 span)**

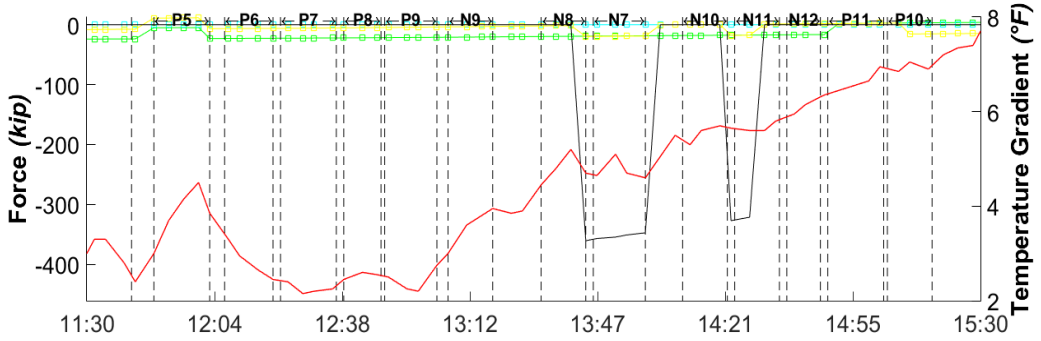

Bent 17	Case: Expansion support (2 span)

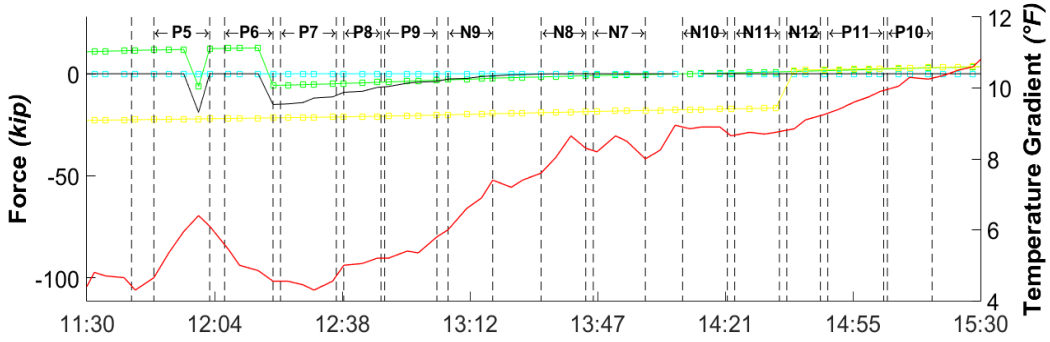

Bent 19	Case: Fixed support (2 span)

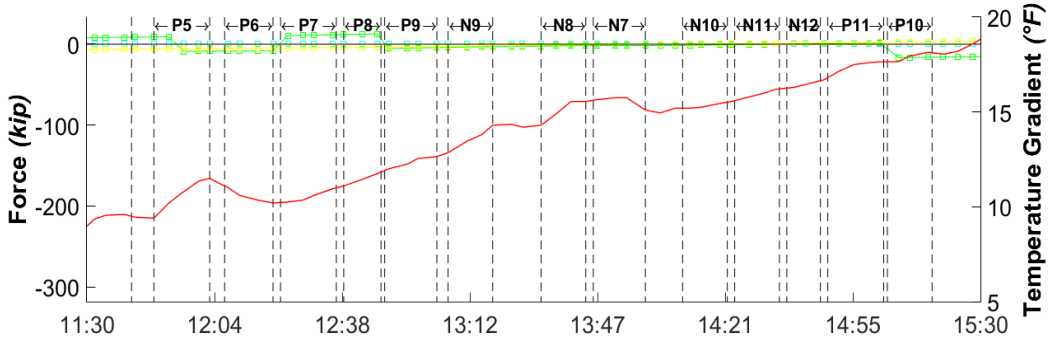

Girder 4	Baseline: Jul 11 2017 09:00
Bent 2	**Case: Expansion support (4 span)**

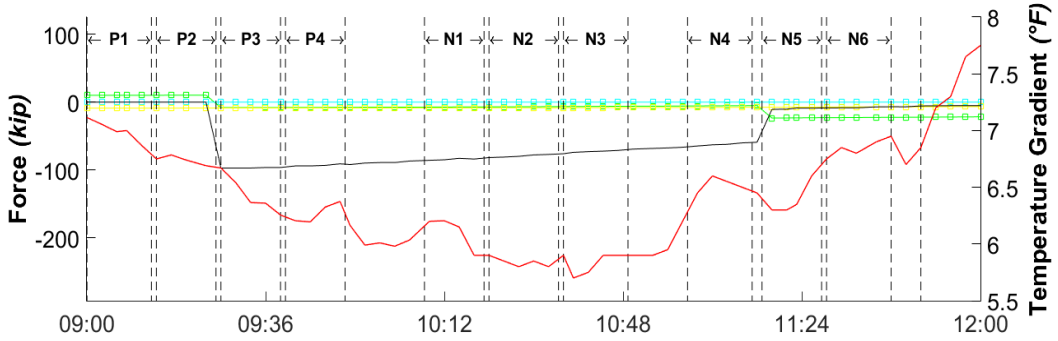

Bent 3	Case: Expansion support (4 span)

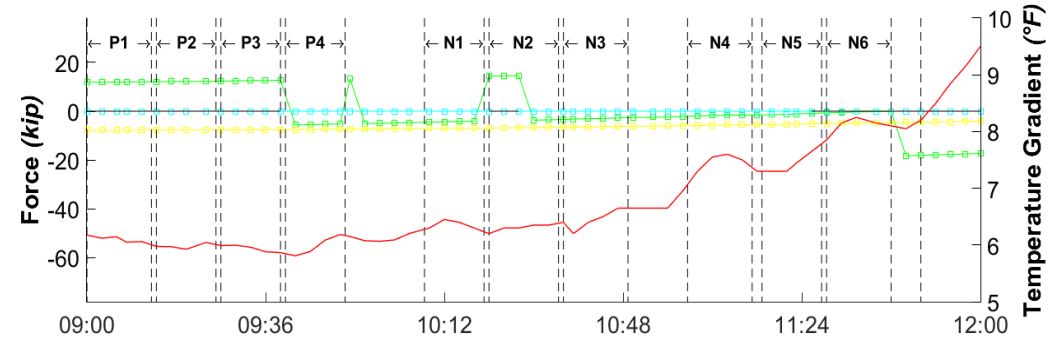

Bent 4	Case: Expansion support (4 span)

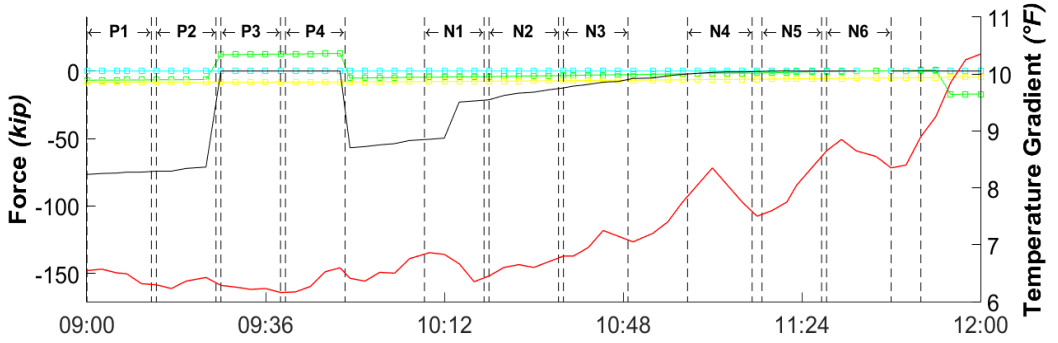

Bent 15	Case: Expansion support (2 span)

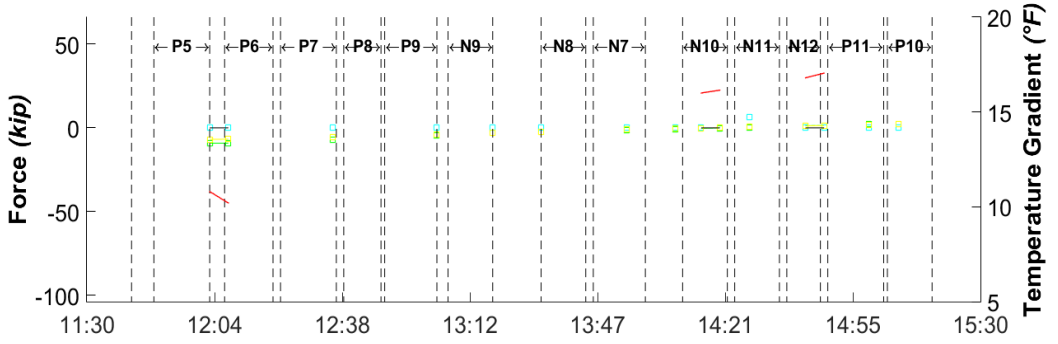

Girder 4	Baseline: Jul 11 2017 09:00
Bent 17	Case: Expansion support (2 span)

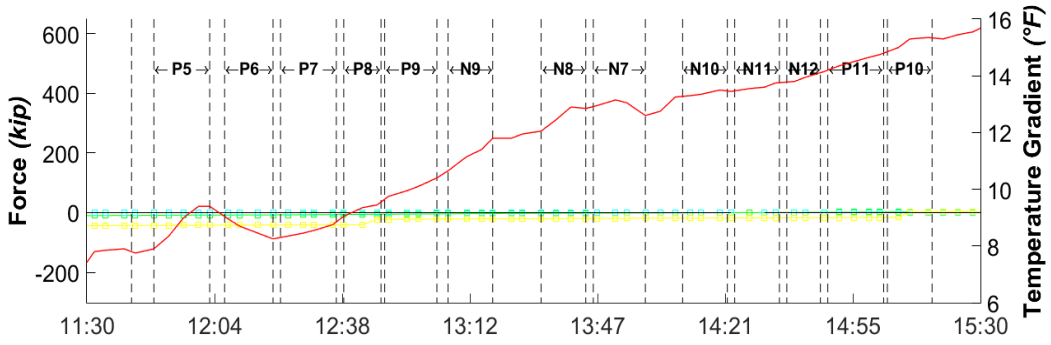

Bent 19	Case: Fixed support (2 span)

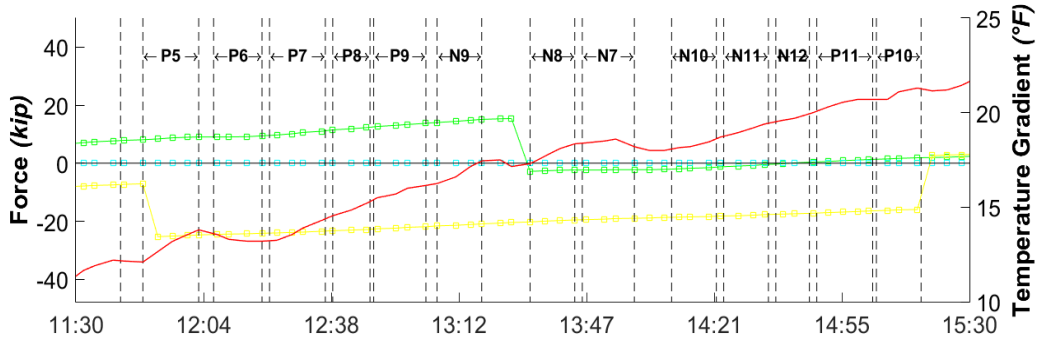

Girder End Displacement	Period: 24 hrs.
Beginning: Jul 11 2017 09:00/11:30	End: Jul 11 2017 12:00/15:30
Girder 7	Baseline : Jul 11 2017 09:00
Segment A	Case: 4-span segment

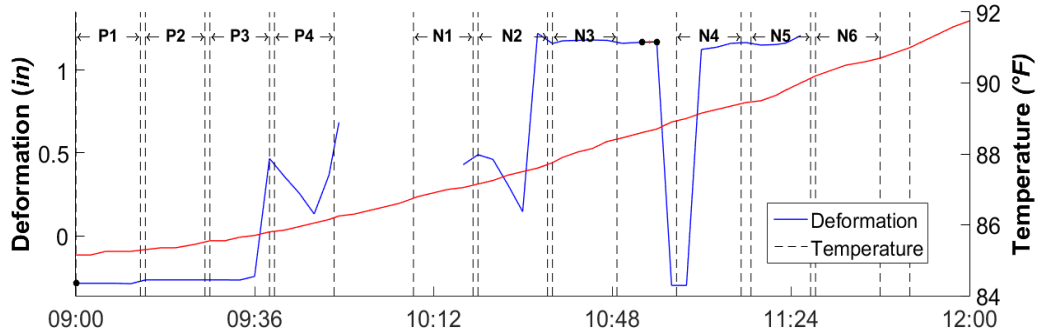

Segment B	Case: 2-span segment

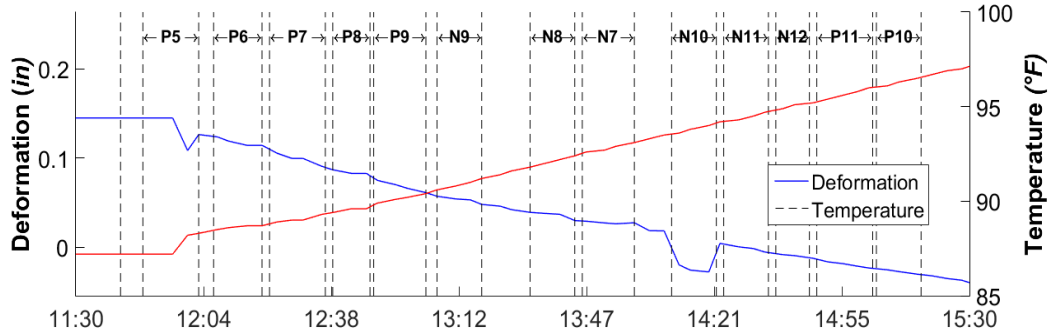

Span 19	Case: Fixed support (2 span)

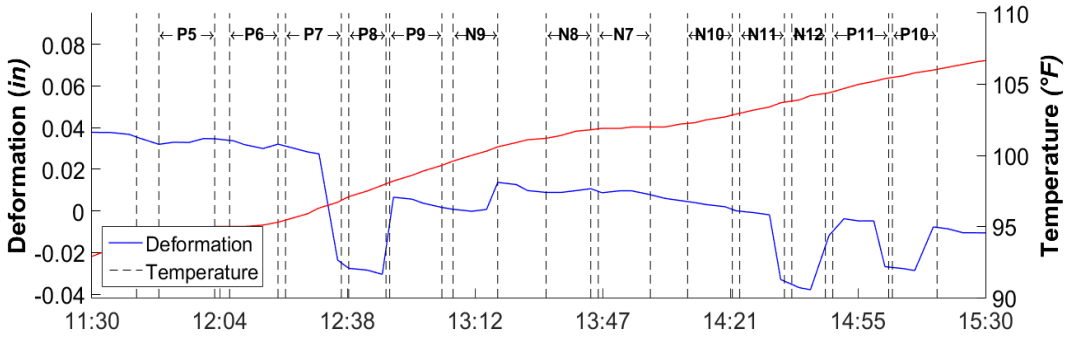

Girder End Displacement	Period: 24 hrs.
Span 16	Case: Expansion support (2 span)

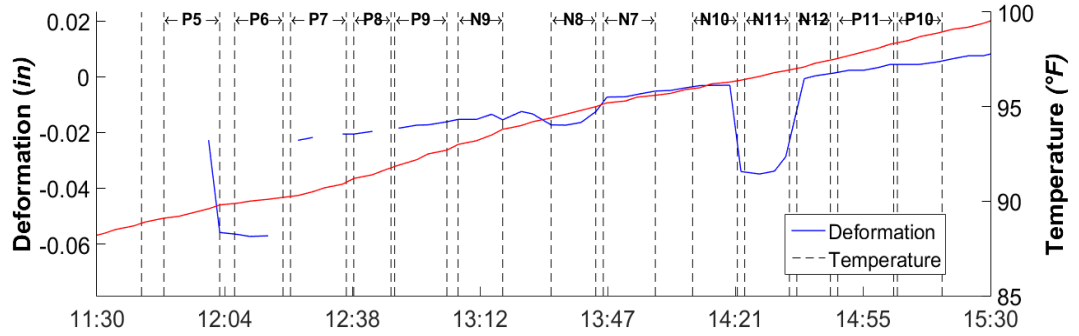

Span 1	Case: Expansion support (4 span)

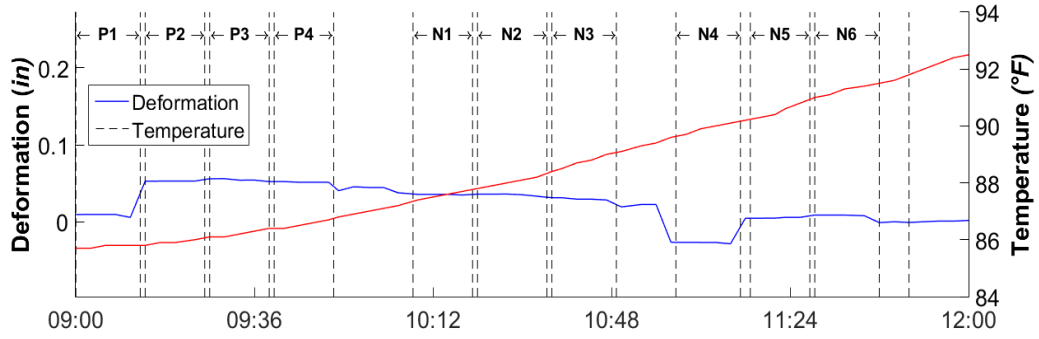

Girder 4	Baseline: Jul 11 2017 09:00
Segment A	**Case: 4-span segment**

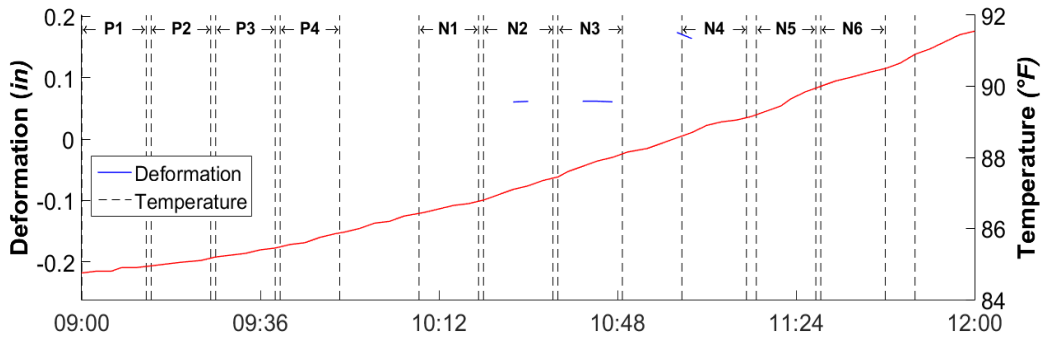

Segment B	Case: 2-span segment

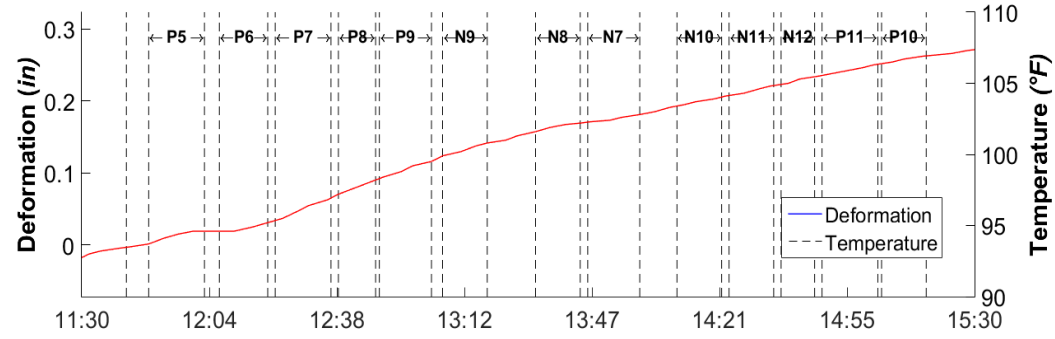

Span 19	Case: Fixed support (2 span)

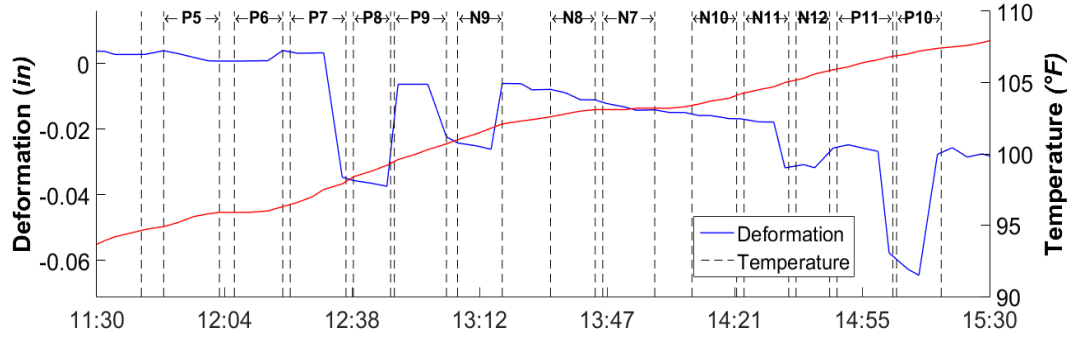

Span 16	Case: Expansion support (2 span)

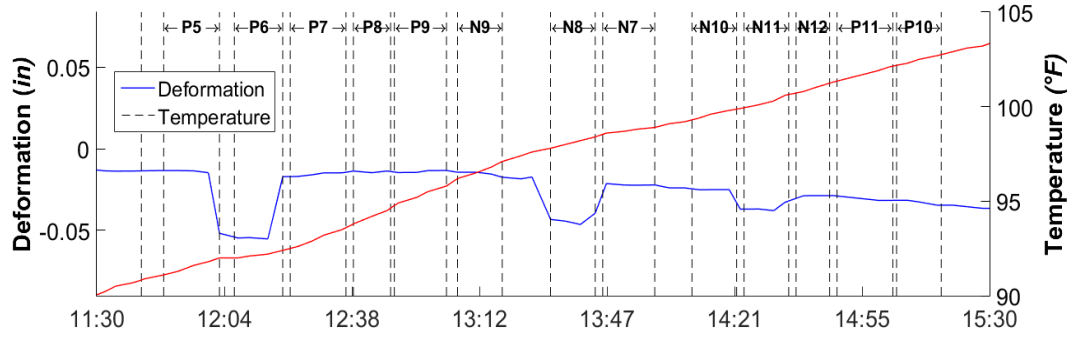

Girder 4	Baseline: Jul 11 2017 09:00
Span 1	Case: Expansion support (4 span)

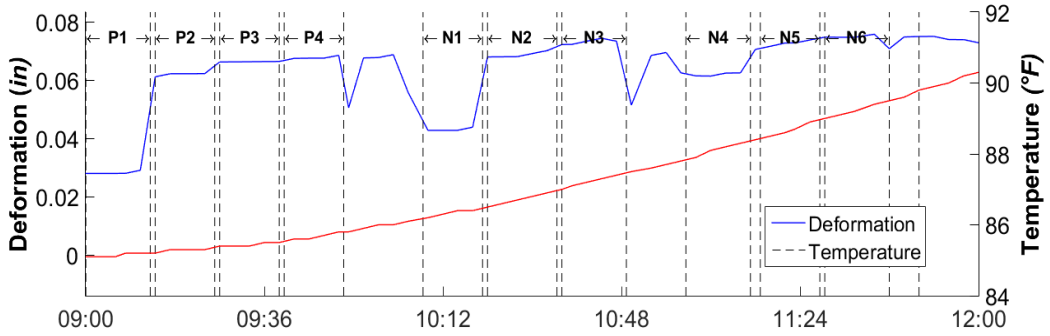

Link slab Force	Period: Live Load Test Duration
Beginning: Jul 11 2017 09:00/11:30	End: Jul 11 2017 12:00/15:30
Girder 7	Baseline : Jul 11 2017 09:00
Bent 2	Case: Expansion support (4 span)

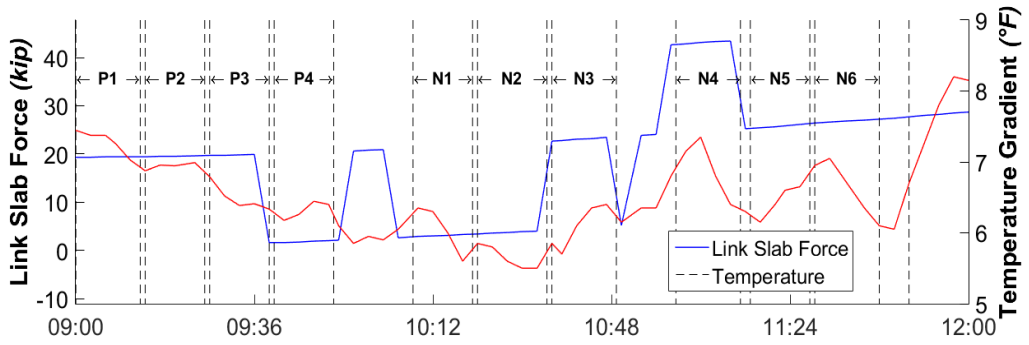

Bent 3	Case: Expansion support (4 span)

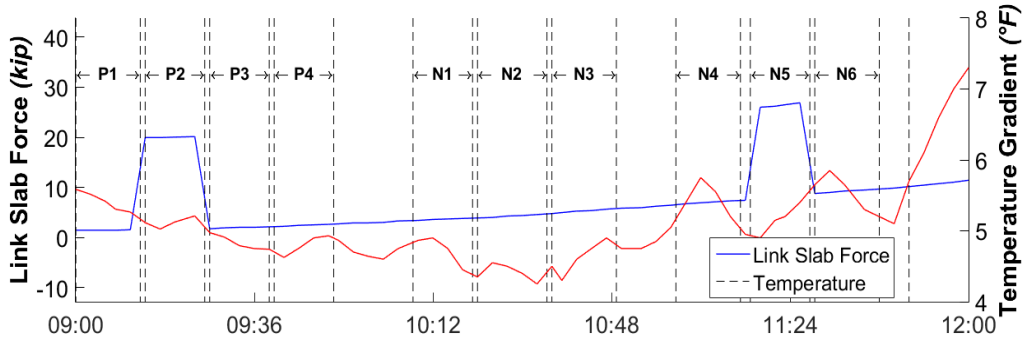

Bent 4	Case: Expansion support (4 span)

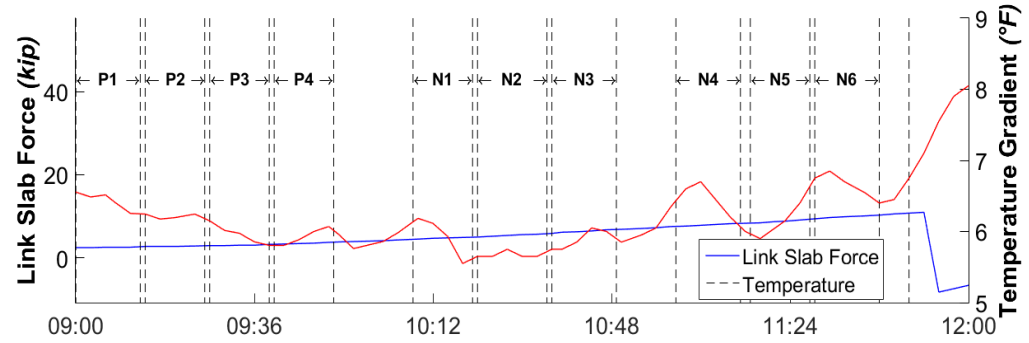

Link slab Force	Period: Live Load Test Duration
Bent 15	**Case: Expansion support (2 span)**

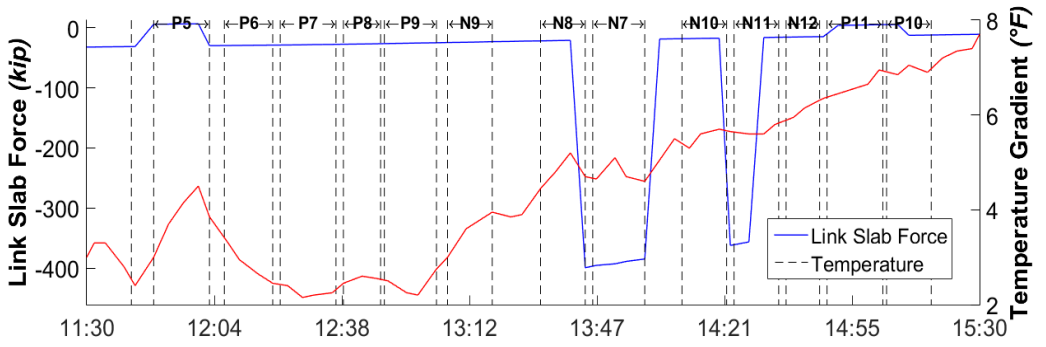

Bent 17	Case: Expansion support (2 span)

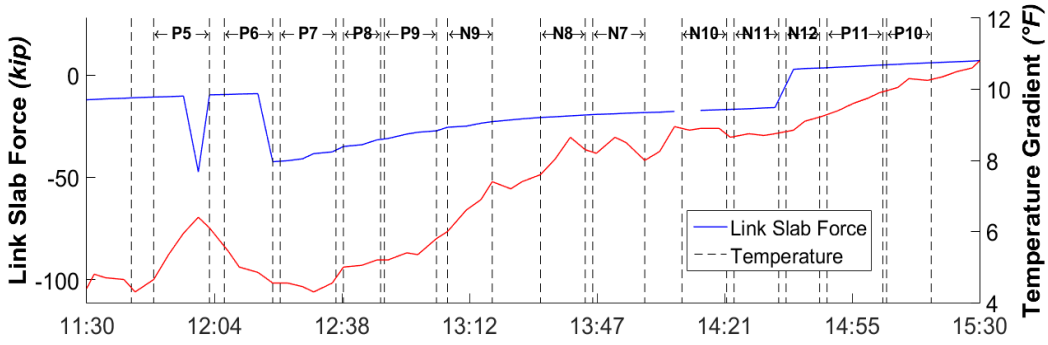

Bent 19	Case: Fixed support (2 span)

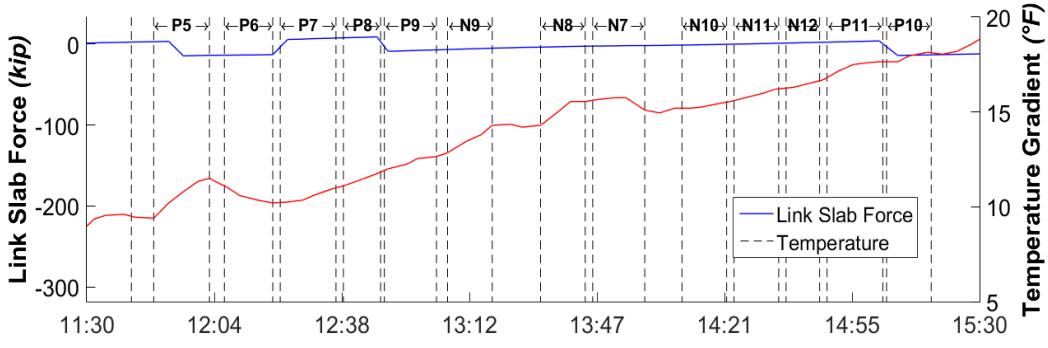

Girder 4	Baseline: Jul 11 2017 09:00
Bent 2	**Case: Expansion support (4 span)**

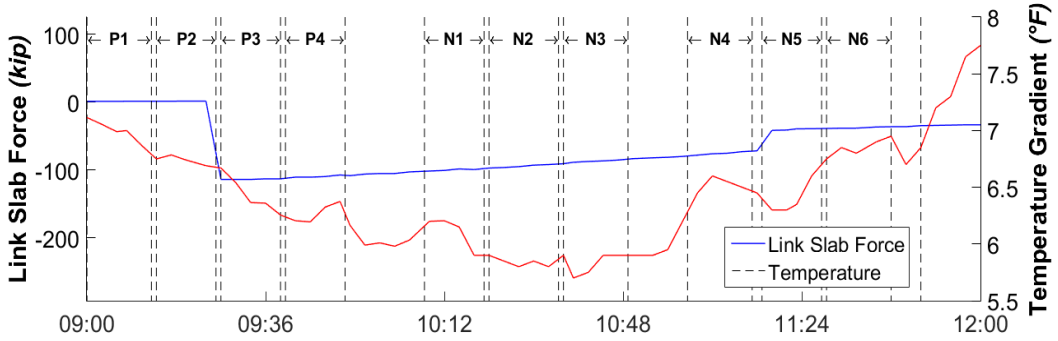

Bent 3	Case: Expansion support (4 span)

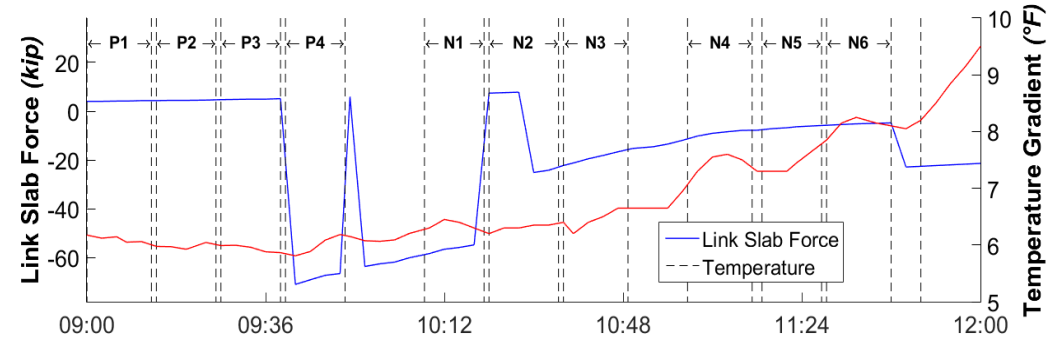

Bent 4	Case: Expansion support (4 span)

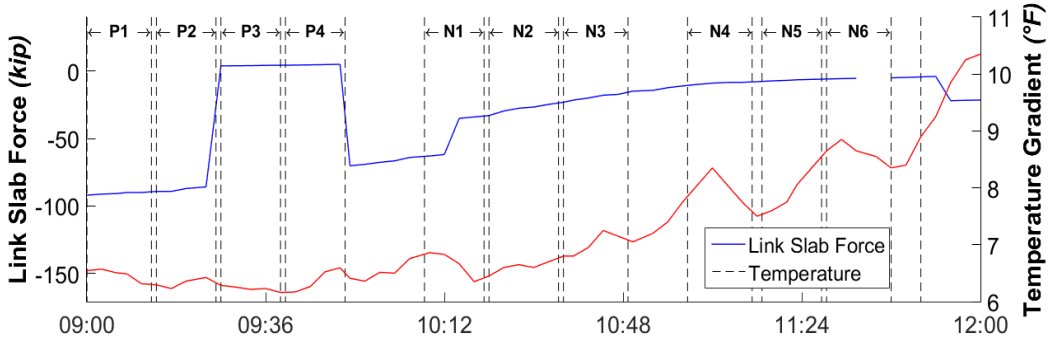

Bent 15	Case: Expansion support (2 span)

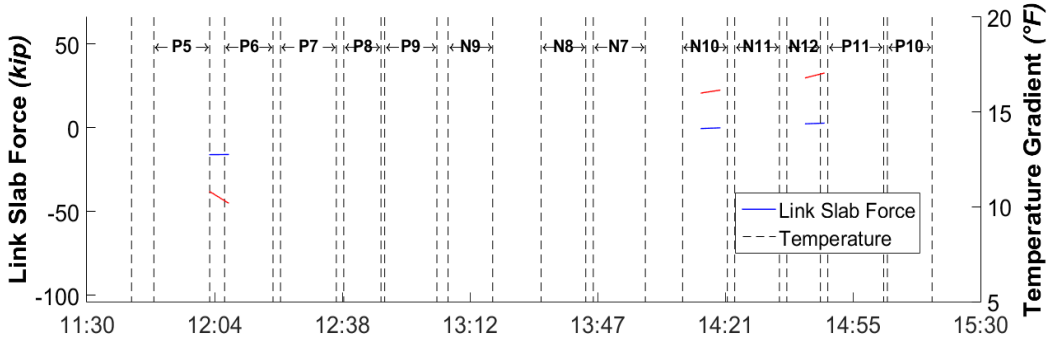

Girder 4	Baseline: Jul 11 2017 09:00
Bent 17	Case: Expansion support (2 span)

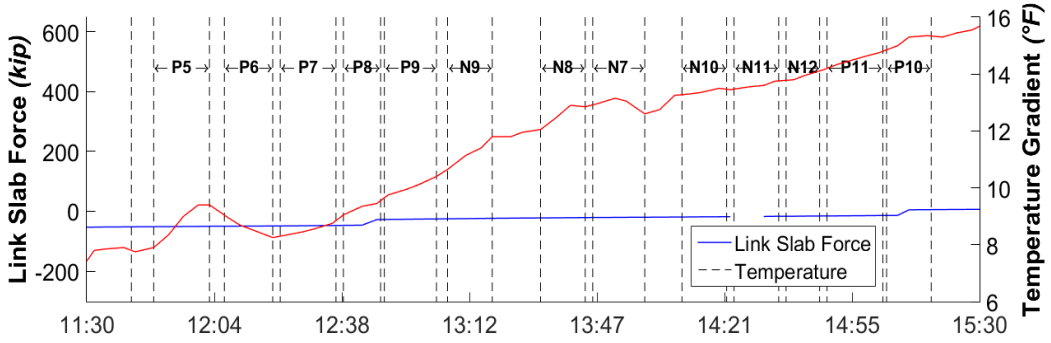

Bent 19	Case: Fixed support (2 span)

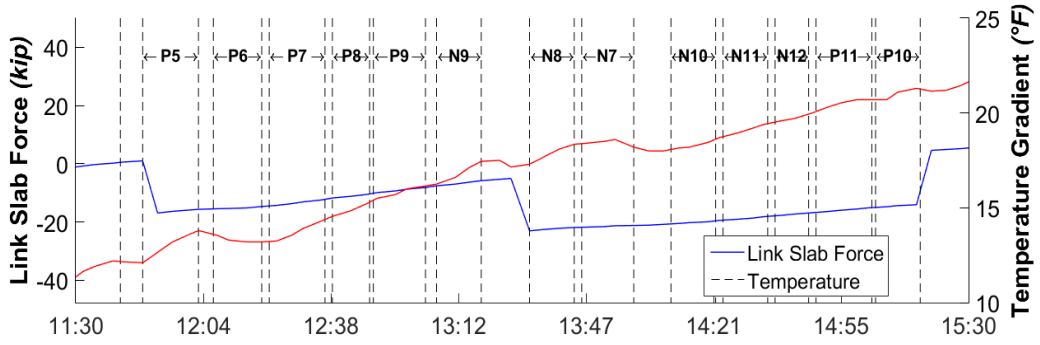

Relative Angle	Period: Live Load Test Duration
Beginning: Jul 11 2017 09:00/11:30	End: Jul 11 2017 12:00/15:30
Girder 7	Baseline : Jul 11 2017 09:00
Bent 2	Case: Expansion support (4 span)

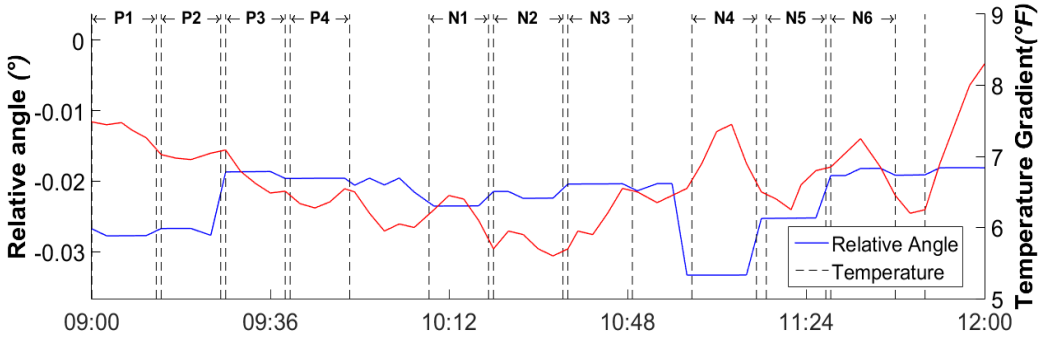

Bent 3	Case: Expansion support (4 span)

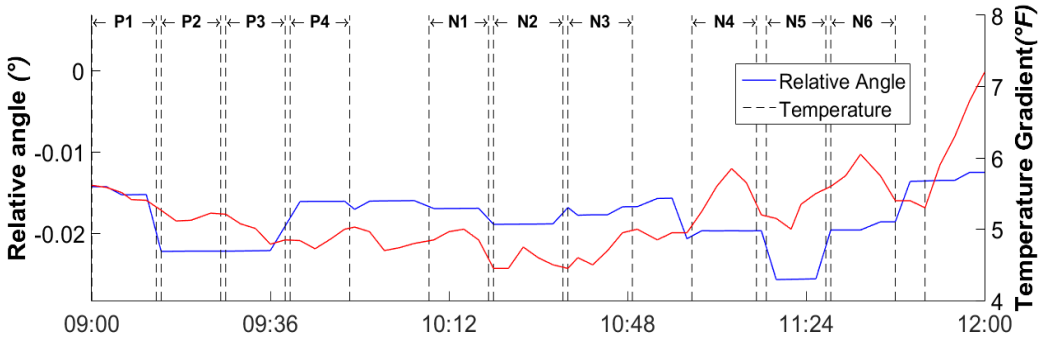

Bent 4	Case: Expansion support (4 span)

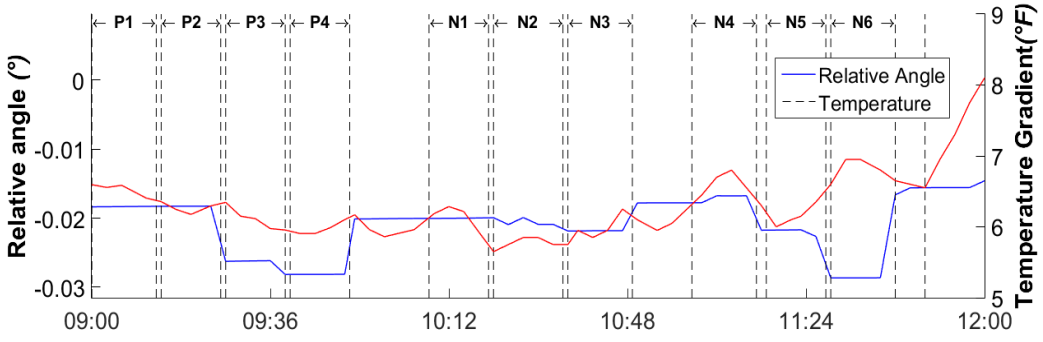

Relative Angle	Period: Live Load Test Duration
Bent 14	**Case: Expansion support (2 span)**

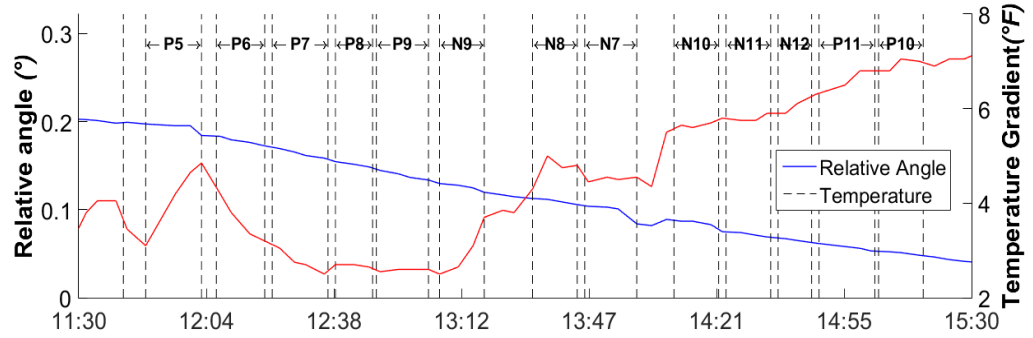

Bent 16	Case: Expansion support (2 span)

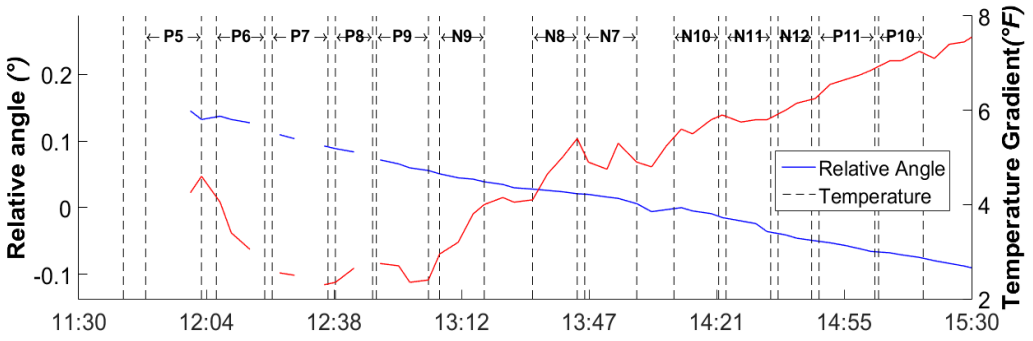

Bent 17	Case: Expansion support (2 span)

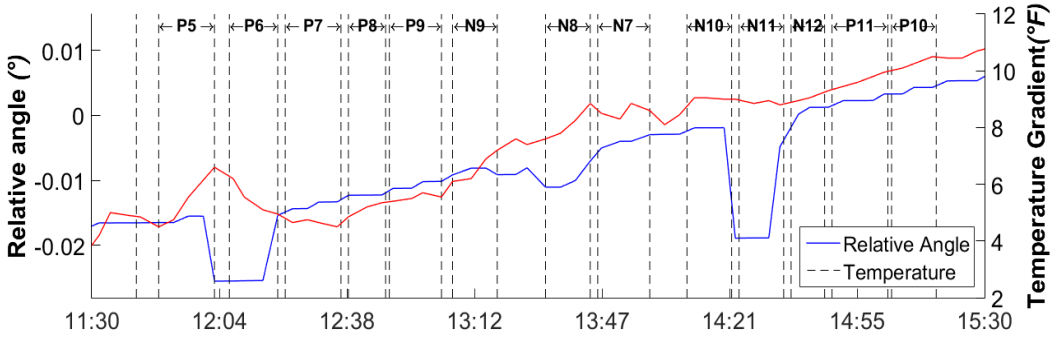

Bent 19	Case: Fixed support (2 span)

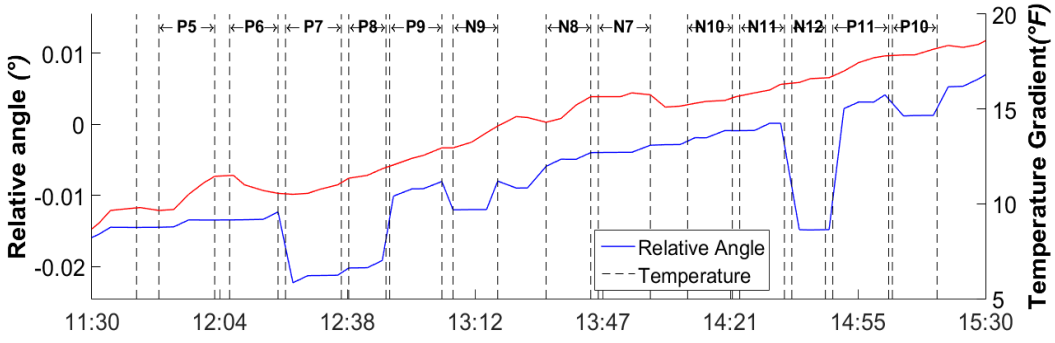

Girder 4	Baseline: Jul 11 2017 09:00
Bent 2	**Case: Expansion support (4 span)**

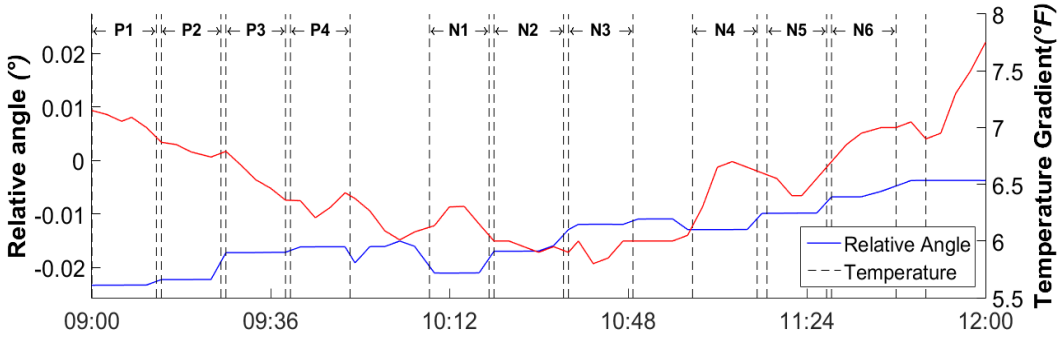

Bent 3	Case: Expansion support (4 span)

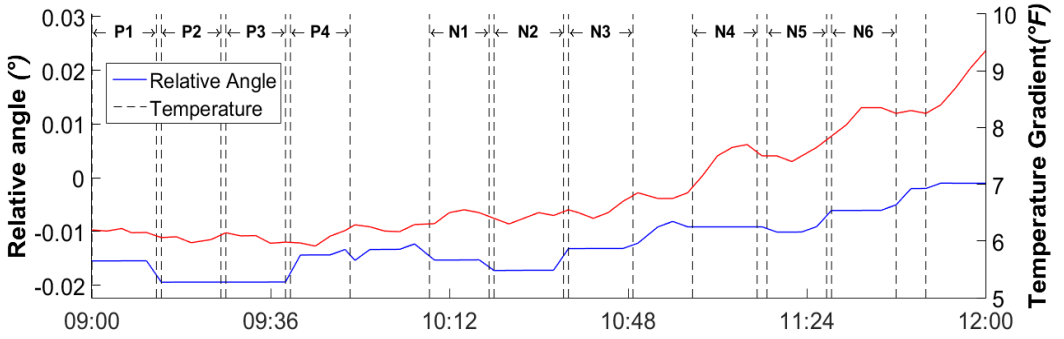

Bent 4	Case: Expansion support (4 span)

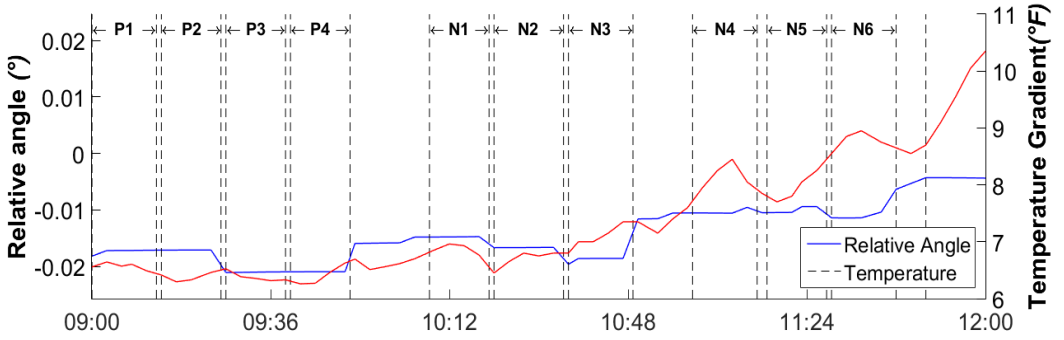

Bent 14	Case: Expansion support (2 span)

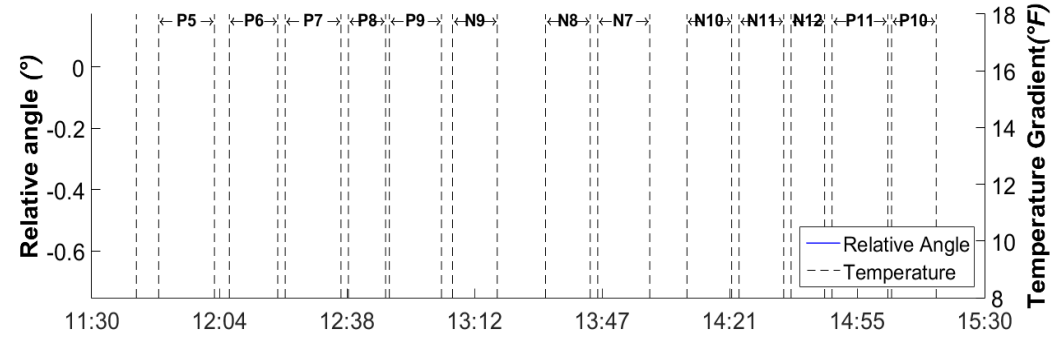

Girder 4	Baseline: Jul 11 2017 09:00
Bent 16	**Case: Expansion support (2 span)**

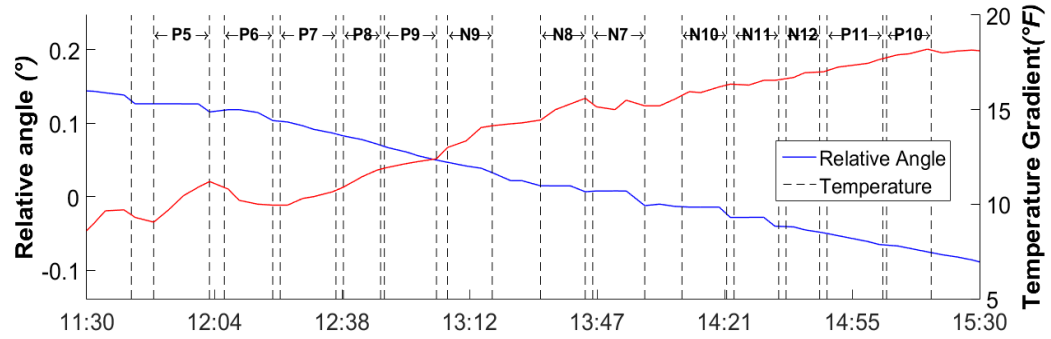

Bent 17	Case: Expansion support (2 span)

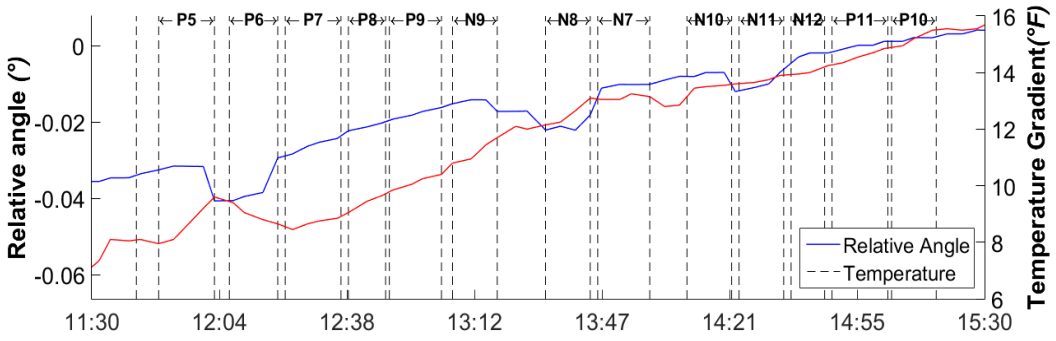

Bent 19	Case: Fixed support (2 span)

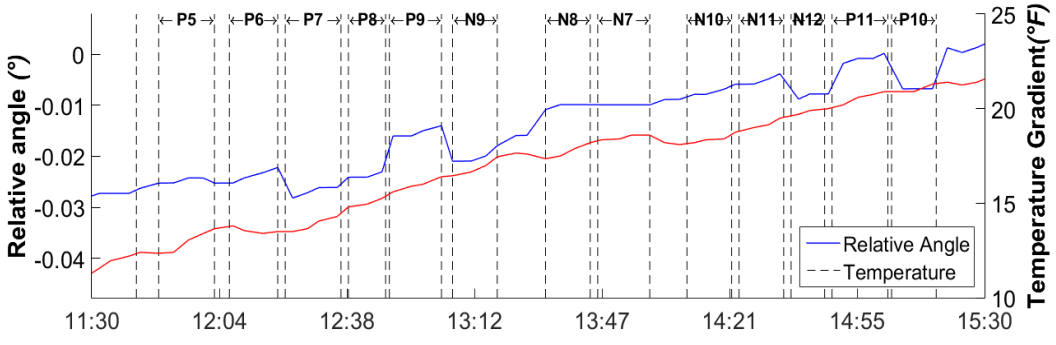

This public document is published at a total cost of $200.
29 copies of this public document were published in this first printing at a cost of $200. The total cost of all printings of this document including reprints is $200. This document was published by Louisiana Transportation Research Center to report and publish research findings as required in R.S. 48:105. This material was duplicated in accordance with standards for printing by state agencies established pursuant to R.S. 43:31. Printing of this material was purchased in accordance with the provisions of Title 43 of the Louisiana Revised Statutes.